Developments in Applied Phycology 10

Gabriel Cristóbal
Saúl Blanco
Gloria Bueno *Editors*

Modern Trends in Diatom Identification

Fundamentals and Applications

Springer

Developments in Applied Phycology 10

Series Editors

Michael A. Borowitzka, Algae R&D Centre, School of Veterinary and Life Sciences, Murdoch University, Murdoch, WA, Australia

Aims and Scope

Applied Phycology, the practical use of algae, encompasses a diverse range of fields including algal culture and seaweed farming, the use of algae to produce commercial products such as hydrocolloids, carotenoids and pharmaceuticals, algae as biofertilizers and soil conditioners, the application of algae in wastewater treatment, renewable energy production, algae as environmental indicators, environmental bioremediation and the management of algal blooms. The commercial production of seaweeds and microalgae and products derived there from is a large and well established industry and new algal species, products and processes are being continuously developed.

The aim of this book series, Developments in Applied Phycology, is to present state-of-the-art syntheses of research and development in the field. Volumes of the series will consist of reference books, subject-specific monographs, peer reviewed contributions from conferences, comprehensive evaluations of large-scale projects, and other book-length contributions to the science and practice of applied phycology.

Prospective authors and/or editors should consult the Series Editor or Publishing Editor for more details. Series Editor: Michael A. Borowitzka - M.Borowitzka@murdoch.edu.au Publishing Editor: Alexandrine Cheronet - alexandrine.cheronet@springer.com

More information about this series at http://www.springer.com/series/7591

Gabriel Cristóbal • Saúl Blanco • Gloria Bueno
Editors

Modern Trends in Diatom Identification

Fundamentals and Applications

Springer

Editors
Gabriel Cristóbal
Instituto de Optica (CSIC)
Madrid, Spain

Saúl Blanco
Facultad de Ciencias Biológicas y Ambientales
Departamento de Biodiversidad y Gestión Ambiental
Universidad de León
León, Spain

Laboratorio de diatomología y calidad de aguas
Instituto de Investigación de Medio Ambiente
Recursos Naturales y Biodiversidad
León, Spain

Gloria Bueno
VISILAB
Universidad de Castilla-La Mancha
Ciudad Real, Spain

Developments in Applied Phycology
ISBN 978-3-030-39211-6 ISBN 978-3-030-39212-3 (eBook)
https://doi.org/10.1007/978-3-030-39212-3

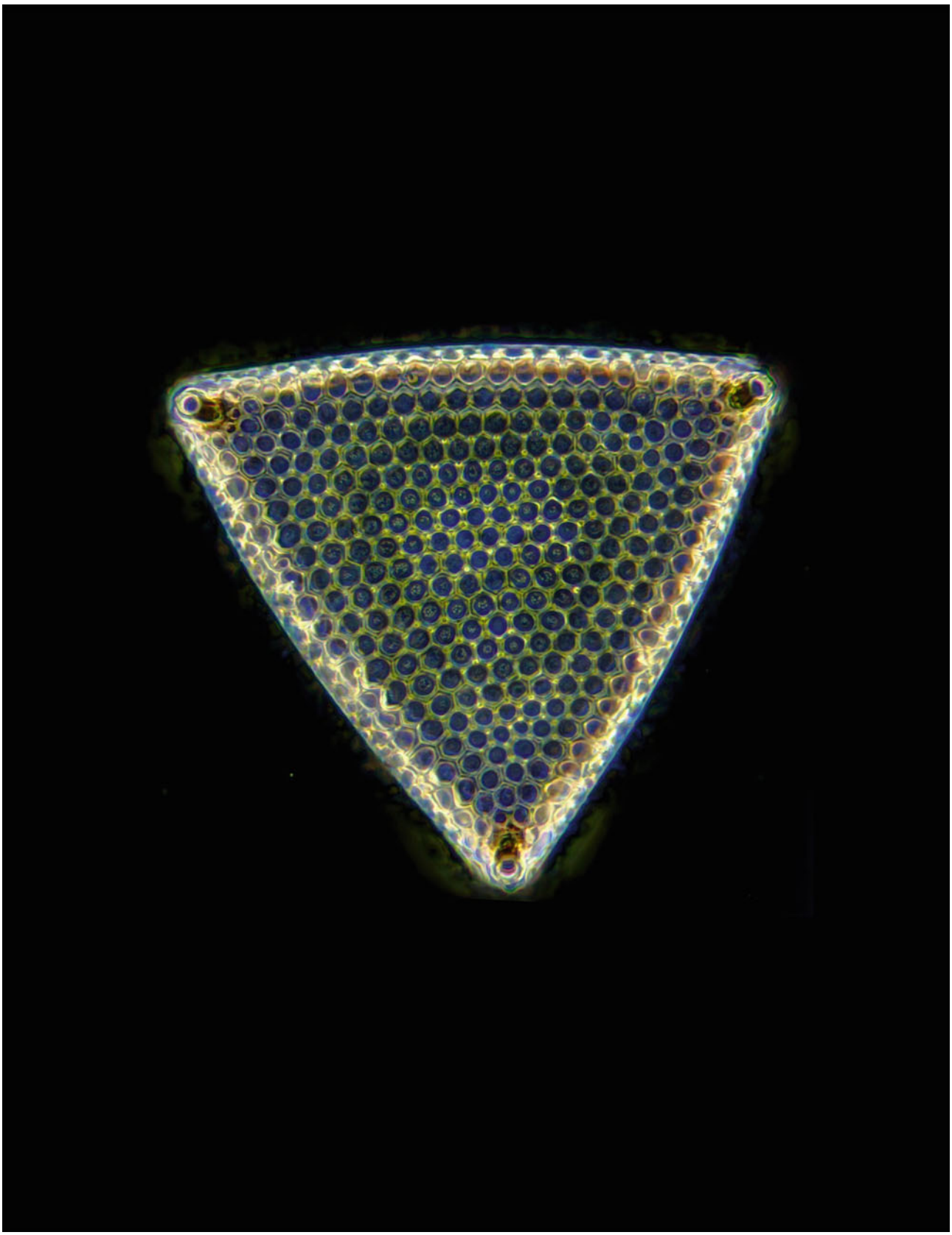

Photo picture of *Triceratium favus* observed with dark field illumination (60X, NA=0.85). Diatom microslide preparation by Klaus Kemp

This book is dedicated to Klaus Kemp one of the few contemporary diatomists that mastered the Victorian tradition, a beautiful mixture between art and science, and whose technique in the elaboration of microscopic preparations is unparalleled.

Credit: Snapshot of the film “The Diatomist” by Mattew Killip (http://tiny.cc/85pi7y). Photo courtesy of the author

Foreword

Identification of Diatoms: From Subjectivity to Objectivity

Diatoms are appreciated for the many ecological services they provide or contribute to, such as primary production, CO_2 sequestration, O_2 production, global cycling of silica and their presence at the interface of the abiotic and biotic worlds, being thus crucial in ecosystem functions. Their relatively short life cycles (dividing vegetatively 2–3 times/day [26]) allow them to respond quickly, together with their presence in the ecosystem 24 h a day, means that they can be sensitive sentinels regarding ecosystem change [46, 47]. In addition to these features, diatoms also have an immediate commercial value, with the fossil remains of their glass cell walls being sold as diatomite or diatomaceous earth [16], and products and by-products of their metabolic activities generating interest as nutraceuticals, pharmaceuticals, and renewal biofuels [45], and their potential for nanotechnology continues to interest both basic and applied researchers [29].

These unicellular organisms have 75,000 taxa already named [17], with many parts of the planet neither having been explored, nor inventoried. There is also a long history (greater than 300 years, since the first diatom was illustrated in the literature [1]—see Fig. 1) of study with light and electron microscopy. Thus, the determination of taxa (genera, species, subspecific units) relies on the accurate observation of discrete and continuous characters, mostly of the glass cell walls of diatoms. Correct taxon recognition is useful since names are

Fig. 1 First illustration of a diatom in the literature (a *Tabellaria* colony). After [1]

the currency we use to compare across studies. Discrete features like the presence/absence of a raphe system, fultoportulae, pore fields, and other valve and girdle band morphological features are important for identification. These discrete features may be present or absent between taxa, as well as within a taxon, depending upon life cycle stage or environmental conditions, sometimes producing teratological valves [21]. Because of the rigid, bipartite nature of their glass cell walls, a noted feature of the development of diatoms is that as cells divide vegetatively, the newly made cell walls must fit within the parent cell walls, meaning they must be smaller than the parent's walls. Over generations, this means that as populations "get older" they must "get smaller." This is known as the MacDonald–Pfitzer model [10, 32, 39] (see Chap. 4). Through this size diminution process, shape and morphological structures (e.g., density of striae) can change [12]. The way out of this physical predicament is through sexual reproduction, where meiosis-derived, haploid, non-siliceous gametes undergo syngamy to produce, at first, non-siliceous diploid zygotes, allowing the resulting cells to enlarge to maximum size. Then, the initial valves are produced ("Erstlingzellen"), which can look quite unlike the species as represented by smaller cells [15]. The dogma that "[...] most diatoms divide to produce valves that are virtually identical to the parent valves [...]" [26] (p. 84) may actually not be true for many parts of the life cycle of diatoms.

Species Identification

The identification of species is amazingly challenging, and there are many factors that may have influenced monographers and producers of floras in their determination and description of diatom species. The books and primary literature related to diatom taxonomy are found in a wide range of languages, in literature that serves either neontologists or palaeontologists, and can be focused on taxonomy, ecology, geography, limnology, or palaeontology. Given the limited audience size, the books seem to always have had high price tags, making their accessibility challenging, and offering power and influence to those with the largest libraries. Digitization and availability of historical works (e.g., Hathi Trust Digital Library), and new online floras such as Diatoms of North America (bit.ly/2v79OhF) or Diatoms of the Southern California Bight (bit.ly/2VBbcEr), together with other useful online tools (DiatomBase [17], AlgaeBase [13], ANSP [bit.ly/2V1Zlm9]) are helping to level the playing fields between labs in terms of access to resources.

Some of the factors influencing approaches to species recognition and identification relate to assumptions made regarding distributions over space, the ability of organisms with different morphologies to interbreed ("hybridize") and a sense that microscopic organisms should not be able to produce many species. For example, "everything is everywhere and the environment selects" is a well-known summary of lab- (not field!) based studies by the Dutch bacteriologist Baas Becking [2] that set the stage for assumptions about the ubiquity of single cell prokaryotes and eukaryotes. J.P. Lotsy [30] developed the concept of "syn-gameons" and applied it to groups of plant species that hybridize, and that idea has also been embraced by a few researchers for diatom species. Finally, late nineteenth century diatomists such as Van Heurck believed that diatom species descriptions were based on details that were part of the natural variation of taxa. He wrote [54, p. 100], "[...] true species are much less numerous than has been hitherto imagined." What is amazing about Van Heurck's statement is that he had previously been supporting Albert Grunow to document the diatom flora of The Netherlands and elsewhere. Grunow ended up describing over 900 diatom taxa, many of them at the level of species [17].

These concepts provided the theoretical underpinnings on which the Süsswasserflora von Mitteleuropa [23–26], perhaps the most consulted work on freshwater diatom identification ever produced, is based (see the section "Systema-tisches Konzept dieser Diatomeen-flora," pp. 74–78 in Krammer and Lange-Bertalot [23]). These authors used these ideas, which were derived in part by Bonik [5], Bonik and Lange-Bertalot [7], and Bonik et al. [6], to develop

species concepts and ideas on biogeography for their flora. This yielded an approach that included the "lumping" of many taxa, and the idea that they can occur widely in terms of geography and ecology. Some of the more extreme examples of this approach include taxa such as *Gomphonema parvulum* or *G. clavatum*.

The result of this approach, which is evident in the works by many diatomists, was summarized elegantly by Vanormelingen et al. [55, p. 394]: "According to advocates of the ubiquity hypothesis [...], the vast population sizes of microorganisms drive ubiquitous dispersal [...] and make local extinction virtually impossible. [...] Geographic isolation is therefore absent and as a result, allopatric speciation should be rare or nonexistent, which would explain the perceived low global morphospecies diversity of microbial eukaryotes [...]."

What had been known since the 1950s, and what we have learned more recently, is that diatoms do not appear to hybridize [26], they can have very limited distributions [19] and, in fact, even diatoms (and other groups of algae) that look very similar may be quite distinct in terms of molecular sequences [27, 31].

Challenges for the users of taxonomic references, should they be available, is whether the authors of these works had consistently applied concepts and names across large numbers of samples and geographic locations. For the practicing taxonomist, the situation is even more complicated when large-scale projects that, due to their size and complexity, require multiple, physically separated laboratories (with different libraries and staff with different backgrounds in training in terms of theory as well as technique). These many challenges have a tendency to give very different interpretations of taxa, making more difficult integrative studies such as ecology, biogeography, evolutionary history, and many others.

Discrete and Continuous Variables

We can evaluate diatom variation in terms of discrete features (presence/absence of structures in the frustule) and continuous variables (length, width, shape). For some discrete variables, differences between taxa may be expressed as the presence/absence of these features ("presence of a raphe system," "presence of costae") though there are examples where the extent of this variation is seen within a single taxon (*Sinoperonia*, for example, can have 0–2 raphe systems in frustules from the same populations [28]; different species of *Meridion* can have or lack costae, and cells with or without that feature can generate new valves with the opposite condition [18]). Presence/absence of a feature is relatively easy to evaluate/measure, as are metrics such as length, width, and stria density. More challenging, however, are some descriptors related to shape. For example, cells may have apices that are distinct, but those distinct attributes may change during size diminution. Thus, initial valves may have "broadly rounded" apices, but smaller valves of the same species may have apices that could be described as "capitate," "subcapitate," "pro-tracted," and, in the smallest cells, again "rounded." Use of these descriptive terms segmenting sections of a basically continuous variable (overall shape, shape of the apices) is difficult, since the definition and use of those terms may be highly subjective, between the authors from one text to another and from the users themselves.

Recognition, Identification, Classification

In the work of a taxonomist, we can define three separate but related aspects to the work. Taxonomists must recognize individuals to be a part of the same entity (taxon) and distinguish them from other entities. Both discrete and continuous variation must be considered, and as we have said with diatoms, understanding that variation at the same points in the life cycle and across the entire life cycle can be quite challenging. Once an individual or a set of individuals have been grouped together in some way, that group should get some

designation, either as a formal named entity or, perhaps, without a name. This is the process of identification. Identification is a process that need not be phylogenetic as its basis. For example, one could use a system for identification that can accurately identify things, but that system does not need to recognize groupings that have shared ancestry. There are many "artificial" systems for grouping biological entities. Classification is the process of recognizing and naming groups (species or higher levels of classification) that share ancestry and include the ancestor and all the descendents (the groups, at whatever level in a classification hierarchy, are monophyletic [22]). These practices are important elements of applying diatoms to a wide range of questions in ecology, monitoring, systematics, and many other fields. The classification piece of this set of activities ultimately allows for the comparison of entities with particular names, and the elements of shared ancestry may help explain the results of a particular study, such as groups of similar species having the propensity to produce higher volumes of oil [11] or common responses to environmental perturbations.

From Subjectivity to Objectivity

The practices of recognition and identification are seeking new ways to reduce or eliminate subjectivity and to find more objective and reproducible results. This is important if, for example, water quality monitoring points to unsafe or illegal practices and the data are to be used to justify legal actions. Some groups have worked on improving current approaches, by holding workshops, developing online tools, and other practices that yield more consistent results, and results that are correct in terms of identification and classification [20]. Some of these approaches involve molecular tools, but to date examples that demonstrate their applicability are more or less trivial (such as cases where there are few other taxa in the samples [43, 56]). Funding large-scale projects to develop libraries for the identification element of this molecular approach has not been forthcoming, and the search for the Holy Grail of the sequence(s) that can distinguish diatom taxa has been elusive [20, 14, 40]. There have been other ways to distinguish differences in diatom cell walls. Approaches such as Legendre polynomials, Fourier analysis, landmark analysis, morphometrics, and deep learning (e.g., [4, 8, 33, 35, 34, 36, 37, 38, 41, 42, 48, 49, 50, 51, 52, 53]) can all demonstrate high degrees of fidelity (reproducibility) and precision for the recognition of taxa based on shape or other features. The challenge of these approaches is the never-ending set of options and choices one can make, the general applicability of any one approach, and the search for interpretation beyond recognition of similar physical traits. Thus, the choice of approaches to yield more objectivity in the recognition and identification of diatoms can, in and of itself, be subjective [9]. As we see, the effects of human impacts, direct or indirect, across the globe, as the need for freshwater grows, and our reliance on harvestable food from marine and freshwaters also increases, the need to understand the changes in water quality, current conditions, and predict futures changes and relies heavily on monitoring [3]. The ability to process and evaluate these samples accurately, and in a way that is reproducible, is crucial to the success of this approach. The chapters in this book will help to provide the development of tools, and point to future directions, to help us achieve these lofty and important goals.

Boulder, CO, USA J. P. Kociolek

References

1. Anonymous: Two letters from a gentleman in the country, relating to Mr. Leeuwenhoek's letter in Transaction No. 283. Philos. Trans. (London) **288**, 1494–501 (1703)
2. Baas-Becking, L.G.M.: Geobiologie of inleiding tot de milieukunde. W.P. Van Stockum & Zoon, The Hague (1934)
3. Barton, P.S., et al.: Effects of environmental variation and livestock grazing on ant community structure in temperate eucalypt woodlands. Insect Conserv. Divers. **9**(2), 124–134 (2016)
4. Beszteri, B., Ács, É., Medlin, L.: Conventional and geometric morphometric studies of valve ultrastructural variation in two closely related Cyclotella species (Bacillariophyta). Eur. J. Phycol. **40**, 89–103 (2005)
5. Bonik, K.: Gibt et Arten bei Diatomeen? Eine evolutionsbiologische Deutung am Beispiel der Gattung Nitzschia. Senckenbergiana Biologische **62**, 413–434 (1982)
6. Bonik, K., Lange-Bertalot, H.: Strukturvariationen ökologisch wichtiger Kieselalgen – ein Beitrag zur Taxonomie der lanceolaten Nitzschien und kleinen Naviculaceen. Courier Forschungsinstitut Senckenberg **33**, 1–152 (1978)
7. Bonik, K., Gutmann, W.F., Lange-Bertalot, H.: Merkmale und Artabgrenzung: Die Vorrangigkeit Evolutionstheoretischer und biologisch-ökologischer Erklärung in der Taxonomie. Natur und Museum **108**, 33–43 (1978)
8. Bueno, G., et al.: Automated diatom classification (Part A): handcrafted feature approaches. Appl. Sci. **7**(8), 753 (2017)
9. Culverhouse, P.F., et al.: Do experts make mistakes? A comparison of human and machine identification of dinoflagellates. Mar. Ecol. Progr. Ser. **247**, 17–25 (2003)
10. Edlund, M.B., Stoermer, E.F.: Ecological, evolutionary and systematic significance of diatom life histories. J. Phycol. **33**, 897–918 (1997)
11. Fields, F.J., Kociolek, J.P.: An evolutionary perspective on selecting high lipid-content diatoms (Bacillariophyta) for commercial use. J. Appl. Phycol. (2015) https://doi.org/10.1007/s10811-014-0505-1
12. Geitler, L.: Der Formwechsel der pennaten Diatomeen (Kieselalgen). Archiv für Protistenkunde **78**, 1–226 (1932)
13. Guiry, M.D., Guiry, G.M.: AlgaeBase. World-wide electronic publication, National University of Ireland, Galway (2019). http://www.algaebase.org
14. Hamsher, S.E., et al.: Barcoding diatoms: exploring alternatives to COI-5P. Protist 162, pp. 405–422 (2011)
15. Hustedt, F.: Die Kieselalgen Deutschlands, Österreichs und der Schweiz unter Berücksichtigung der übrigen Länder Europas sowie der angrenzenden Meeresgebiete. In: Rabenhorst, L. (ed.) Kryptogamen Flora von Deutschland, Österreich und der Schweiz. Akademische Verlagsgesellschaft m.b.h. Leipzig. 7, pp. 273–464 (1928)
16. Ivanov, S.E., Belyakov, A.V.: Diatomite and its applications. Glass Ceram. **2**, 18–21 (2008)
17. Kociolek, J.P., et al.: DiatomBase (2019). Accessed at http://www.diatombase.org
18. Kociolek, J.P., Liu, Y., Wang, X.: Internal valves in populations of Meridion circulare (Greville) C.A. Agardh from the A'er Mountain region of northeastern China: implications for taxonomy and systematics. J. Syst. Evol. **49**, 486–494 (2011)
19. Kociolek, J.P., Spaulding, S.A.: Freshwater diatom biogeography. Nova Hedwigia **71**, 223–241 (2000)
20. Kociolek, J.P., Stoermer, E.F.: Taxonomy and ecology: a marriage of necessity. Diatom Res. **16**, 433–442 (2001)
21. Kociolek, J.P., Stoermer, E.F.: Variation and polymorphism in diatoms: the triple helix of development, genetics and environment and our understanding of diatom systematics. A review of the literature. Vie et Mileau **60**, 75–87 (2010)

22. Kociolek, J.P., Williams, D.M.: How to define a diatom genus? Notes on the creation and recognition of taxa, and a call for revisionary studies of diatoms. In: Proceedings of the 8th Central European Diatom Meeting, Zagreb. Acta Croatica Botanica **74**(2) (2015). https://doi.org/10.1515/botcro-2015-0018
23. Krammer, K., Lange-Bertalot, H.: Susswassflora von Mitteleuropa. Band 2/1. Bacillariophyceae. Naviculaceae, 876 p. Gustav Fischer, Stuttgart (1986)
24. Krammer, K., Lange-Bertalot, H.: Susswassflora von Mitteleuropa. Band 2/2. Bacillariophyceae. Bacillariaceae, Epithemiaceae, Surirellaceae, 596 p. Gustav Fischer, Stuttgart (1988)
25. Krammer, K., Lange-Bertalot, H.: Susswassflora von Mitteleuropa. Band 2/3. Bacillariophyceae. Centrales, Fragilariaceae, Eunotiaceae, 576 p. Gustav Fischer, Stuttgart (1991)
26. Krammer, K., Lange-Bertalot, H.: Susswassflora von Mitteleuropa. Band 2/4. Bacillariophyceae. Achnanthaceae. Kritische Ergänzungen zu Navicula (Lineolatae) und Gomphonema, 437 p. Gustav Fischer, Stuttgart (1991)
27. Leliaert, F., et al.: DNA-based species delimitation in algae. Eur. J. Phycol. **49**, 179–196 (2014)
28. Liu, Y., Kociolek, J.P., Fan, Y., Kulikovskiy, M.: A new genus of Eunotiales (Bacillariophyta, Bacillariophyceae: Peroniaceae) from southeast Asia, exhibiting remarkable phenotypic plasticity, and evidence for another lineage of monoraphid diatoms. Phycologia **57**, 147–158 (2018)
29. Lopez, P.J., et al.: Prospects in diatom research. Curr. Opin. Biotechnol. **16**(2), 180–186 (2005)
30. Lotsy, J.P.: Evolution by Means of Hybridization. Martinus, Nijhoff, The Hague (1916)
31. Lundholm, N., et al.: Cryptic and pseudo-cryptic diversity in diatoms with descriptions of *Pseudo-nitzschia hasleana sp.* nov. and *P. fryxelliana* sp. nov. J. Phycol. **48**, 436–454 (2012)
32. MacDonald, J.D.: On the structure of the diatomaceous frustule, and its genetic cycle. Ann. Mag. Nat. Hist. Ser. **4**(3), 1–8 (1869)
33. Mou, D., Stoermer, E.F.: Separating *Tabellaria* (Bacillariophyceae) shape groups based on Fourier descriptors. J. Phycol. **28**, 386–395 (1992)
34. Pappas, J.L.: Graph matching a skeletonized theoretical morphospace with a cladogram for gomphonemoid-cymbelloid diatoms (Bacillariophyta). J. Biol. Syst. **19**, 47–70 (2011)
35. Pappas, J.L., Kociolek, J.P., Stoermer, E.F.: Quantitative morphometric methods in diatom research. Nova Hedwigia Beihefte **143**, 281–306 (2014)
36. Pappas, J.L., Stoermer, E.F.: Legendre shape descriptors and shape group determination of specimens in the Cymbella cistula species complex. Phycologia **42**, 90–97 (2003)
37. Pappas, J.L., Fowler, G.W., Stoermer, E.F.: Calculating shape descriptors from Fourier analysis: shape analysis of *Asterionella* (Heterokontophyta, Bacillariophyceae). Phycologia **40**, 440–456 (2001)
38. Pedraza, A., et al.: Automated diatom classification (Part B): a deep learning approach. Appl. Sci. **7**(5), 460 (2017)
39. Pfitzer, E.: Untersuchungen über Bau und Entwicklung der Bacillariaceen (Diatomaceen). Botanische Abhandlungen **1**, 1–189 (1871)
40. Pogoda, C.S., et al.: Comparative analysis of the mitochondrial genomes of six newly sequenced diatoms reveals group II introns in the barcoding region of cox1. Mitochondrial DNA Part A (2018). https://doi.org/10.1080/24701394.2018.1450397
41. Potapova, M., Hamilton, P.B.: Morphological and ecological variation within the *Achnanthidium minutissimum* (Bacillariophyceae) species complex 1. J. Phycol. **43**(3), 561–575 (2007)
42. Rhode, K.M., Pappas, J.L., Stoermer, E.F.: Quantitative analysis of shape variation in type and modern populations of Meridion (Bacillariophyceae). J. Phycol. **37**(1), 175–183 (2001)

43. Rimet, F., et al.: The potential of high throughput sequencing (HTS) of natural samples as a source of primary taxonomic information for reference libraries of diatom barcodes. Fottea **18**(1), 37–54 (2018)
44. Round, F.E., Crawfors, R.M., Mann, D.G.: Diatoms: Biology and Morphology of the Genera. Cambridge University Press, Cambridge (2007)
45. Stephens, E., et al.: Future prospects of microalgal biofuel production systems. Trends Plant Sci. **15**(10), 554–564 (2010)
46. Stevenson, R.J., Bothwell, M.L., Lowe, R.L., Thorp, J.H.: Algal Ecology: Freshwater Benthic Ecosystem. Academic, San Diego (2011)
47. Stevenson, R.J., Pan, Y.: Assessing environmental conditions in rivers and streams with diatoms. In: Stoermer, E.F., Smol, J.P. (eds) The Diatoms: Applications for the Environmental and Earth Sciences. Cambridge University Press, Cambridge (1999)
48. Stoermer, E.: Further observations on *Gomphoneis*. In: Proceedings of the Eighth International Diatom Symposium, pp. 205–213 (1984)
49. Stoermer, E., Yu-Zao, Q., Ladewski, T.: A quantitative investigation of shape variation in *Didymosphenia* (Lyngbye) M. Schmidt (Bacillariophyta). Phycologia **25**(4), 494–502 (1986)
50. Theriot, E.: Principal component analysis of *Stephanodiscus*: observations on two new species from the *Stephanodiscus niagarae* complex. Bacillaria **7**, 37–58 (1984)
51. Theriot, E.: Principal component analysis of character variation in *Stephanodiscus niagarae Ehrenb.*: morphological variation related to lake trophic status. In: Proceedings of the 7th International Diatom Symposium, pp. 97–111. O. Koeltz, Koenigstein (1984)
52. Theriot, E.: Principal component analysis and taxonomic interpretation of environmentally related variation in silicification in *Stephanodiscus* (Bacillariophyceae). Br. Phycol. J. **22**(4), 359–373 (1987)
53. Theriot, E., Ladewski, T.B.: Morphometric analysis of shape of specimens from the neotype of *Tabellaria flocculosa* (Bacillariophyceae). Am. J. Bot. **73**(2), 224–229 (1986)
54. Van Heurck, H.F.: A Treatise on the Diatomaceae. Wesley & Son, London (1896)
55. Vanormelingen, P., Verleyen, E., Vyverman, W.: The diversity and distribution of diatoms: from cosmopolitanism to narrow endemism. Biodivers. Conserv. **17**, 393–405 (2008)
56. Vasselon, V., et al.: Assessing ecological status with diatoms DNA metabarcoding: scaling-up on a WFD monitoring network (Mayotte Island, France). Ecol. Indic. **82**, 1–12 (2017)

Preface

High resolution images of microbe cells such as diatoms or foraminifera can now be acquired by digital microscopes what facilitates automating the analysis and identification process of specimens. In the case of microalgae, these are useful for monitoring water quality, hence the importance of automating the analysis procedure. The conventional approach usually consists of identification and quantification by optical microscopy. However, manual image analysis of such systems is impractical due to the huge diversity of this group of microalgae and its great morphological plasticity. Therefore, there is a need for automated recognition techniques for diagnostic tools (networks of environmental monitoring, early warning systems) to facilitate proper management of water resources and decision-making processes. New image analysis systems offer a potentially advantageous compared to manual methods of counting and identification solution. This book will help to cover the lack of recent monographies to cover the entire workflow of a bioindicator system from capture, analysis, or identification to the determination of quality indices.

This book is a comprehensive yet thorough guide in the field of automatic classification of microalgae. The book provides a range of topics covering the main aspects of microalgae identification and water quality assessment and should thus not only appeal to those working in the field, but also many others who are interested in getting more involved in the area of microscopic feature identification. The book covers a wide range of topics from basic to more advanced topics along the different sections. This makes it a valuable book for undergraduates, students, and professional researchers alike by tackling in a single monograph information that is spread in different sources. The last part of the book will provide a review of some typical applications and the actual state of the art of research in the field.

Despite current research trends in biological systematics highlight the potential of DNA barcoding for species identification and delimitation, the application of molecular techniques for chromists and, particularly, for eucharyotic microalgae, has numerous pitfalls and limitations. It has been demonstrated that DNA barcoding has no discriminating success within species complexes, probably as a consequence of low variation rate at the plastid genome level.

The main purpose of this book is to serve as a practical monograph to be used by microscopists and diatom scientists, the core of the text being devoted to software applications, image analysis, and other applied issues. However, recent developments in microalgae science demanded an introductory overview focused to the audience not directly involved in biological studies, which is adequately covered in the first chapters. The original scope of the book has been broadened to cover also non-diatom microalgae to make the text eventually more attractive for a general audience, by including applications in other areas such as foraminifera with paleoenvironmental and restoration ecology implications. With the exception of foraminifera, the applications of the methods described for marine/terrestrial habitats is very limited at the present stage. On the contrary, the surveillance protocols for continental waters are highly developed and supported by standardized (ISO) protocols and international regulations and normatives, so that the outcoming results are comparable and reproducible over the long term. The current demand of automatic methods aiding identification/counting of microalgae covers almost entirely freshwater scenarios; therefore, it seems inadequate to expand the scope of the manuscript in this regard.

The key audience for this book are the many researchers, computer scientists, physicists, biologists, developers, practitioners, and students in academia and industry now working in microscopy imaging in the life sciences. However, the potential audience for this book is much broader than scientists, technicians, or students but also individuals from environmental authorities. The methods described will not imply the need of specialized hardware. On the contrary, we emphasize throughout the text the importance of cost-effective tools and open-source software. The "technical expertise" is precisely the aim that this book wants to cover in a single, updated monograph, overriding the need for the reader to look for different techniques in the literature. The book can also be used as a support textbook for classes at universities and colleges, mainly in Physics, Biology, and Electrical Engineering.

Madrid, Spain — Gabriel Cristóbal
León, Spain — Saúl Blanco
Ciudad Real, Spain — Gloria Bueno

Acknowledgements

We want to express our gratitude for the quality of the chapter provided by the authors and their efforts to maintain the size of the chapters within the specified limits. Without the valuable contributions made by a significant number of field experts from both academia and industry, this project would not have been achieved. We would like to thank everyone for your commitment to contribute to this important outcome. We would like to extend our gratitude to Alexandrine Cheronet, Judith Terpos, and Eva Loerinczi from Springer Nature to help us manage the project and to Justin Taberham for his advice and guidelines with the book proposal. The Spanish Government partially funded this work under the Aqualitas project (Ref. CTM2014-51907-C2-2-R-MINECO).

Finally, we are grateful to the following reviewers for their thoughtful comments and suggestions: María Borrego-Ramos (Univ. de Leon); Angela María da Silva Lehmkuhl. (Instituto de Botânica, São Paulo, Brazil); Adriana Olenici (Babes University, Romanía); Daiane Ruwer (Universidade Estadual de Maringá, Brazil); David Williams (The Natural History Museum, London); Patrick Kociolek (University of Colorado) and Saúl Blanco (Universidad de León).

Contents

Contributors

Călin Baciu Babes-Bolayi Univ., Cluj-Napoca, Romania

Cristina Beltran-Aroca Univ. Cordoba, Córdoba, Spain

Xavier Benito National Socio-Environmental Synthesis Center (SESYNC), University of Maryland, Annapolis, MD, USA

Saúl Blanco Facultad de Ciencias Biológicas y Ambientales, Departamento de Biodiversidad y Gestión Ambiental, Universidad de León, León, Spain

Laboratorio de diatomología y calidad de aguas, Instituto de Investigación de Medio Ambiente, Recursos Naturales y Biodiversidad, León, Spain

Gloria Bueno VISILAB, Universidad de Castilla-La Mancha, Ciudad Real, Spain

Gabriel Cristóbal Instituto de Optica (CSIC), Madrid, Spain

Oscar Deniz UCLM, Ciudad Real, Spain

José Luis Espinosa Aranda UCLM, Ciudad Real, Spain

M. Milagro Fernandez-Carrobles UCLM, Ciudad Real, Spain

Ecaterina Fodor Univ. Oradea, Oradea, Romania

Manuel G. Forero Faculty of Engineering, Univ. Ibague, Ibagué, Colombia

Herminia Garcia-Mozo Univ. Cordoba, Córdoba, Spain

Eloy Girela Univ. Cordoba, Córdoba, Spain

Alejandra Goldenberg CIMERA Estudios Aplicados S.L., Madrid, Spain

Instituto de Hidraulica Ambiental, Univ. Cantabria, Santander, Spain

Ovidiu I. Haruta University of Oradea, Oradea, Romania

Carlos A. Jacanamejoy Facultad Ciencias Naturales y Matemáticas, Univ. Ibague, Ibagué, Colombia

Cathy Kilroy National Institute of Water and Atmospheric Research Ltd., Christchurch, New Zealand

Patrick Kociolek Univ. Colorado, Boulder, CO, USA

Vinay Kumar ECE, Thapar Inst. of Engineering and Technology, Patiala, India

J. Alejandro Libreros Univ. del Valle, Cali, Colombia

Soizic Morin Unite de Researche EABX, IRSTEA, Cestas Cedex, France

Adriana Olenici Faculty of Environmental Science and Engineering, Babes-Bolyai University, Cluj-Napoca, Romania

Institute of Environment, Leon, Spain

Anibal Pedraza UCLM, Ciudad Real, Spain

Jorg Piper Laboratory for Applied Microscopy Research, Bullay, Germany

Timm Piper Laboratory for Applied Microscopy Research, Bullay, Germany

Victor Roldan CIMERA Estudios Aplicados S.L., Madrid, Spain

Jesús Ruiz-Santaquiteria Alegre UCLM, Ciudad Real, Spain

Jesús Salido UCLM, Ciudad Real, Spain

Carlos Sánchez Instituto de Optica, Madrid, Spain

Harbinder Singh ECE, Chandigarh Eng. College, Mohali, India

Robert Sturm Department of Materials Science and Physics, University of Salzburg, Salzburg, Austria

Noelia Vallez UCLM, Ciudad Real, Spain

David M. Williams National History Museum, London, UK

Part I

Fundamentals

Overview: Antecedents, Motivation and Necessity

1

Gabriel Cristóbal, Saúl Blanco, and Gloria Bueno

Abstract

This chapter introduces the antecedents, motivation, and necessity of the use of automatic identification methods in diatom taxonomy. Expert biologists have a repetitive and laborious identification mission. The principal taxonomic features used to describe and classify diatoms relate to the morphology and texture of frustule. Classical taxonomic diagnosis is carried out by means of identification keys or by visual comparison with respect to standard preparations or reference iconographies. Automatic diatom identification remains an open challenge because, for instance, many diatoms that have been known by the same species for decades have subsequently been split into different species, while on the other hand the emergence of new species is continuous. The very promising results of the new deep learning techniques together with the development of new optical devices in microscopy allow to predict a significant advance in the field.

1.1 Introduction

> "The diatoms are those microscopic algae that, to compensate for their smallness, show a siliceous livery where the ornamental spells of Indian art seem to have met with the elegant combinations of the decorative geometry of the Arabs. For these organisms the old adage seems to be written: in minimis perfectio. So great is the spell of such algae, which has managed to monopolize during the whole life the activity and ingenuity of many enlightened talents," Foreword of the book [6] by S. Ramon y Cajal, 1925.

Diatoms or Bacillariophyceae are a group of one-cell microalgae distributed throughout the world in a wide range of aquatic environments. Currently, more than 10,000 different species have been identified, each adapted to certain autoecological distributions so that a consistent association can be formed between the diatom community's composition and the physicochemical parameters of the environment in which they are developed

Diatoms or Bacillariophyceae are a category of single-cell algae scattered throughout the world in a wide range of aquatic habitats. A clear association between the diatom community's composition and the physicochemical parameters of the environment in which they are formed can be identified. It has been estimated that there are more than 200,000 different species [21]. Some researchers include 20,000 species as a more realistic number [16]. Thus, several works published since the 1970s of the last century demonstrate the effectiveness of water quality control methods based on the use of diatoms as bioindicators [1–5, 7]. Within phytobenthos, diatoms are the most representative group, gathering a series of particularities that make them ideal organisms for this purpose. The size of most diatom species ranges from 2 μm to 2 mm. Its silica skeleton gives great resistance to heat, acids, and putrefaction.

The main limiting factor for the consolidation of diatoms as ecological indicators lies in the difficulty of their taxonomic identification. The application of more generalized diatomological indexes frequently requires specific or subspecific level diagnosis, which implies important investments in optical equipment and expert training. Several intercalibration assays [23–25, 36] have shown that the results of the diatom-based biological indices are highly sensitive to the level of precision in taxonomic determinations. The main

G. Cristóbal (✉)
Instituto de Optica (CSIC), Madrid, Spain
e-mail: gabriel@optica.csic.es

S. Blanco
Facultad de Ciencias Biológicas y Ambientales, Departamento de Biodiversidad y Gestión Ambiental, Universidad de León, León, Spain

Laboratorio de diatomología y calidad de aguas, Instituto de Investigación de Medio Ambiente, Recursos Naturales y Biodiversidad, León, Spain
e-mail: sblal@unileon.es; degsbl@unileon.es

G. Bueno
VISILAB, Universidad de Castilla-La Mancha, Ciudad Real, Spain
e-mail: gloria.bueno@uclm.es

G. Cristóbal et al. (eds.), *Modern Trends in Diatom Identification*, Developments in Applied Phycology 10,
https://doi.org/10.1007/978-3-030-39212-3_1

taxonomic characters used in the identification and classification of diatoms refer to the morphology and ornamentation of frustule. The frustule is a siliceous cover formed by two elements (teak) that fit together enveloping the cell. In most pennate diatoms, each teak is traversed longitudinally by a groove (raphe) divided into two branches by a central area, where occasionally appear one or several slits (stigmas). Perpendicular to the raphe, there are numerous striations formed by the alignment of several pores or areolas.

Classical taxonomic diagnosis is carried out by means of identification keys or by visual comparison with respect to standard preparations or reference iconographies [32]. Nevertheless, there are currently many studies on the possibility of automating the process of identification by means of image analysis. For example, the ADIAC project: "Automatic Diatom Identification and Classification," http://rbg-web2.rbge.org.uk/ADIAC/, obtained satisfactory results through the application of data processing tools, images, and recognition of shapes in the identification of contour and ornamentation of each frustule and its subsequent identification [10]. The system that was developed in the ADIAC project has allowed 37 species to be identified with 97% accuracy. Nevertheless, considering the nature of the pilot study, ADIAC did not consider certain variables that could affect identification tasks such as species life cycle modeling and polymorphism.

The main difficulties faced by automated recognition methods are attributable not only to the high variety of species to be identified, but also to the broad similarities between them as well as morphological differences both at the individual level (polymorphism) and those related to the cycle of lifetime. The scanning and automatic focusing of microscopic preparations are in advanced stages of development. On the downside, to the identification of morphological microstructures close to the resolution limit and the discrimination of frustules of other elements in the sample (i.e., fragmented or overlapped cells) they are still to be resolved.

Automatic diatom identification is therefore an open challenge still under progress, as some diatoms, for example, have been considered for decades of the same species. They were subsequently divided into different species, while the appearance of new species is continuous. On the other hand, the identification process is a cumbersome and time consuming even for an expert biologist. In both counting and classification tasks, the design of automated analysis systems offers a beneficial approach compared to manual processing. The advantage provided by automated methods over manuals is a more robust taxonomic classification, avoiding the fatigue that occurs when repetitive tasks are performed. In this way, the automated classification processes of the most common taxa will be able to free taxonomists from these activities and thus focus on the most challenging identifications.

1.2 Organization of the Book Chapters

This book has been structured in four different parts and 15 chapters

- Part I: Fundamentals. This part is organized as follows:

  This chapter provides a comprehensive introduction and describes the organization of the book. It also includes a list of available resources related with diatom-research aspects.

  Chapter 2 discusses the quest for bigger, better, faster, and more accurate methods for diatom identification including the classical biological classification (natural classification) and the recent taxonomy-free and human-free molecular approaches.

  Chapter 3 describes the basis of the diatom taxonomy, providing an overview on diatom morphology. It includes the light microscopy keys to common extant nonfossil diatom genera.

  Chapter 4 describes the teratologies in algae, with special emphasis on diatoms. It includes a study of the intra- and inter-populational variations in diatom frustule and size. It discusses the effect of overriding diatom teratology on water quality diagnosis.
- Part II: Sensing. This part is organized as follows:

  Chapter 5 discusses the principles of microscope lighting techniques.

  Chapter 6 discusses the principles of microscope filtering techniques.

  Chapter 7 describes the basics of the main slide scanning strategies used in light microscopy. It includes also autofocusing and preprocessing techniques.
- Part III: Analysis. This part is organized as follows:

  Chapter 8 describes the main techniques used for diatom segmentation, including classical and deep learning approaches.

  Chapter 9 describes the main feature extraction and analysis techniques, using hand-crafted and deep learning approaches.

  Chapter 10 describes the main multifocus and multiexposure techniques. It provides tools for depth map and 3D visualization of the diatom frustules. It concludes including a discussion about fusion quality metrics performance.

  Chapter 11 describes the principles of 3D imaging in both light and electronic microscopy. It concludes with a discussion about the role of 3D imaging in diatom research.

  Chapter 12 describes the principles of geometric morphometrics applied to diatom analysis, mainly based on outline and landmark methods including quantitative techniques of shape variation.
- Part IV: Applications. This part is organized as follows:

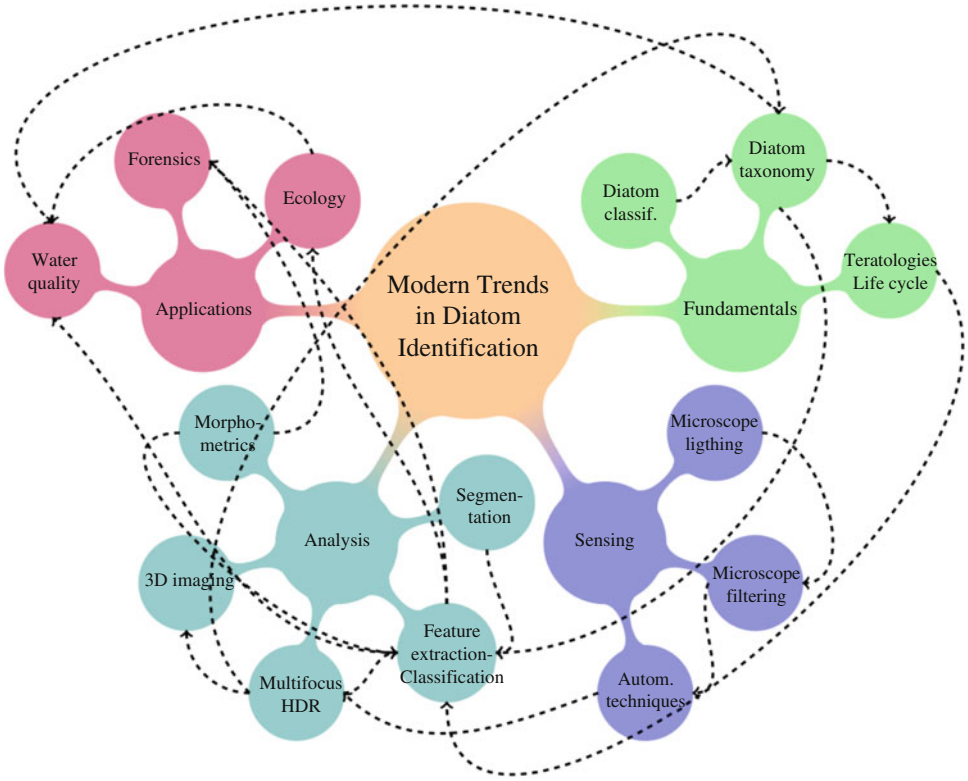

Fig. 1.1 Mind map of the book contents. Cross-links between chapters are shown as dashed lines. Credit: texsample.net

Chapter 13 describes the fundamentals of diatoms as biological indicators of pollution. It describes the sampling and analytical protocols as well as the diatom-based bioassessment tools.

Chapter 14 describes the use of diatoms in forensic analysis, from the sample preparation to the histological findings.

Chapter 15 describes the use of benthic foraminifera and diatoms as ecological indicators. It includes the sampling and foraminiferal analysis and its use as modern and past ecological indicator.

Figure 1.1 sketched the cross-links between the respective chapters. This book aims to provide an overview of automatic diatom classification which puts together the latest developments and applications in the field from the fundamentals. The three chapters chosen in the last part on water quality, forensics, and ecology are good representatives of three research domains where the techniques mentioned will be useful.

1.3 Other Diatom-Related Resources

1.3.1 Databases and Software

Table 1.1 refers the main image databases related with diatoms. Other microalgae of interest are the desmids: https://bit.ly/2UX9O0q and the cyanobacteria: https://bit.ly/39zm2BB.

Table 1.2 refers the main software packages related with diatoms.

1.3.2 Journals and Reference Books

- Journals: Diatom Research, Diatom, Phytotaxa, Fottea, Phycologia, European Journal of Phycology, Phycological Research, J. of Phycology, Algological Studies, Protist, International J. of Algae, The Amateur Diatomist, European J. of Taxonomy.
- The following general reference books can be cited: [10, 26, 31, 32]

1.3.3 Conferences/Societies

The following recent conferences and societies related with diatom research can be cited:

- Central European Diatom Meeting (CE-DiatoM). The 12th CE-DiatoM was organized by the Luxembourg Institute of Science and Technology (LIST) from 26 to 27 March 2019 in Belvaux
- 25th International Diatom Symposium was held in Berlin 25–30 June 2018

Table 1.1 Available diatom databases

Database	Description	Website
ADIAC	About 2300 images of 750 species	https://bit.ly/2WYBlOV
ANSP	Diatoms of USA freshwater rivers	https://bit.ly/2E4bH3R
Klaus Kemp	Over 15,000 species images	https://bit.ly/2V0oMkH
DIADIST	Diatom size reduction examples	https://bit.ly/2URyxBn
CAUP	1710 images of 1135 specimens	https://bit.ly/2IlCUn9
AlgaeBase	21,093 images of 154,501 species	https://bit.ly/2WWsspg
Diatom of UK and Ireland	2800 species	https://bit.ly/2N6hf0Y
Diatoms of North America	953 species	https://diatoms.org/
Diatoms of the Southern California Bight	Inc. Google Map	https://bit.ly/2VBbcEr
OMNIDIA	23,000 species with 800 genus	https://bit.ly/2I9B0ph
AQUALITAS	100 taxa with a minimum 100 specimens/taxon	http://bit.ly/2RUIKgH
Marine diatoms	Diverse list of taxa	https://bit.ly/2Eub1E5
Stidolph Atlas	Diverse list of taxa	https://on.doi.gov/2TcYIGl
AlgaTerra	Terrestrial and limnic microalgae	https://bit.ly/2C1YGqk
Phylogenies	Phylogenies of diatoms	https://bit.ly/2Xw8qSR
DiatomBase	2402 species; 31,2331 names	https://bit.ly/2Tc3h3L
R-Syst	Curated diatom barcode	http://www.rsyst.inra.fr/
WHOI-Plankton	Annotated Plankton Image Dataset	http://bit.ly/2IYZ2S2

Table 1.2 Image processing software

Software	Description	Website
OMNIDIA	Manage inventories and quality indices	https://omnidia.fr/en/
SHERPA	Identification and quantification of object outlines	https://bit.ly/2SxLE9z
SHAPE	Quantitative evaluation of shape	https://bit.ly/2BTZOfI
PlanktoVision	Identification workflow (open source)	https://bit.ly/2BVugWN
DIACURV	Diatom curvature analysis	https://bit.ly/2Ebibg8
PICOLAY	Focus stacking and 3D projections	https://bit.ly/2KGOQNx
PHOTOMATIX	High dynamic range (HDR) soft	https://bit.ly/2Vpq6gR
FIJI	Open source image processing	https://fiji.sc/
Phytobs	Phytoplankton counting tool	https://bit.ly/2NGWh94
WHOAS	Annotated plankton images	http://bit.ly/2IYZ2S2

- International Society for Diatom Research: http://www.isdr.org/
- North America Diatom Symposium 2019, Univ. Georgia, USA, July 31–August 4, 2019
- 35th Congress of the International Society of Limnology in Gwangju (Republic of Korea) from August 23–28, 2020
- Association des Diatomistes de Langue Francaise (ADLaF)
- The Japanese Society of Diatomology
- The British Phycological Society
- Phycological Society of America
- Federation of European Phycological Societies
- International Phycological Society
- Czech Phycological Society
- The Society for Freshwater Science. The society is offering a Taxonomic Certification Program to certify that trained and skilled people are proficient in aquatic identifications in North America (http://bit.ly/2OGnTgn). They also organize regular free and recorded webminars in the field (http://bit.ly/2vxqZw9).

1.3.4 Research Projects

The following recent research projects related with diatom research can be cited:

- German Barcode of Life Project Phase 2 (GBOL2)—Innovative, NGS-based tool to assess Water Framework Directive relevant diatoms, Lead of project: Regine Jahn- r.jahn@mbgbm.org (Botanisches Museum Berlin-Dahlem)

- Building a Global Registration and Index System for Scientific Names and Types of Algae. A joint project between the Research Group Diatoms and the Research Group Biodiversity Informatics is financed by the German Science Foundation (DFG)
- DNAqua-Net—Developing new genetic tools for bioassessment of aquatic ecosystems in Europe (EU COST Action CA15219)
- Antarctic Research with comparative investigations in Arctic ice areas, lead of project: Dr. Ulf Karsten
- AQUALITAS. Automatic taxonomic identification of diatoms and calculation of biotic indices. Website: http://aqualitas-retos.es/en/
- Hominin Sites and Paleolakes Drilling Project (HSPDP). Research on diatom-based paleoenvironmental/paleoclimatic issues. Website: https://hspdp.asu.edu/
- DIADIST project. Research on visual indexing of image diatoms and drawings. Website: https://bit.ly/2YzalX8
- SMIRES project. COST Action (CA 15113) addressing the science and management of intermittent rivers and ephemeral streams. Website: http://www.smires.eu/

1.3.5 Diatom Collections/Catalogs

The following collections/catalogs related with diatom research can be cited:

- Krammer, K. et al., Freshwater flora of Central Europe (1999), https://bit.ly/2Tj0c25
- Lange-Bertalot, H., "Iconographia Diatomologica," Koeltz Scientific Books, 1998
- Lange-Bertalot, H., "Diatoms of Europe," Gantner Verlag, 2000
- Various authors, Bibliotheca Diatomologica, Schweizerbart Sci. Publishers
- Witkowski, A. (ed.), Diatom Monographs, Gantner Verlag, 2014
- Various authors, "Bibliotheca Phycologica," Lubrecht & Cramer Ltd.
- Catalog of diatom names (62,000 names), https://bit.ly/2SIqLbr
- DiatomBase (31,229 species names including synonyms), https://bit.ly/2Tc3h3L
- HathiTrust Digital Library (historical works), https://www.hathitrust.org
- Open Archive (historical, not in copyright), https://archive.org
- OMNIDIA's diatom short list (species acronyms) [20], http://bit.ly/2WQ9dAu

1.4 Diatom Drawings

There is an extensive documentation of drawings made of diatoms by different scientists and microscopists over the last 200 years, which is a valuable tool in taxonomy. One of the most used diatom atlas due to the great diagnostic detail it provides is the Schmidt atlas [27] (see e.g. Fig. 1.2). It is available in open archives and a recent HTML tool has been developed that allows both the search by genus and by species [19]. Another great reference is the Hustedt's atlas and catalogue [28]. A fascinating collection of diatom plates originated by Horace Barber and annotated by H. Barber, J.R. Carter, and B. Hartley have been processed and compiled by S. Gill and S. Edgar. The drawings show an incomparable level of detail and constitute a very useful reference not only for the taxonomist but also for the amateur diatomist. These are available as electronic documents from [12–15]. About foraminifera, an interesting reference is the Heron-Allen' atlas [17] (see Fig. 1.3).

1.5 Social Impact/Educational Projects

The following list of social and/or educational aspects related with diatoms or microscopy can be referenced:

- Blogs. The following blogs are available on the topic [8, 18, 22, 33, 37]
- SimRiver: simulation software to study and understand diatoms easily [29]
- Diatom slide preparation (video) [34]
- Water drop simple microscope (video) [35]
- 3D-printer diatom models (.stl files) from the HSPDP project [9]. Website: https://bit.ly/2JT4l8t
- 3D-printer foraminifera models (.stl files) [11]. Website: https://bit.ly/2I57Yp7
- Citizen science (CS). A concept that is not new but has great application potential, thanks to new technologies. This concept implies the commitment and active participation of the general public in scientific research activities, obtaining new knowledge or skills as a kind of return for their voluntary contribution. An interesting initiative in the area of CS is AppEAR an Android application launched in 2016. AppEAR is an application that appeals to the collaboration of users of mobile devices in the collection of data that allow the study of aquatic ecosystems. Website: http://www.app-ear.com.ar/. CrowdWater is another app that facilitates the public involvement in hydrological observations. The collected data will be useful for developing hydrological models (http://bit.ly/2WTOFbi).

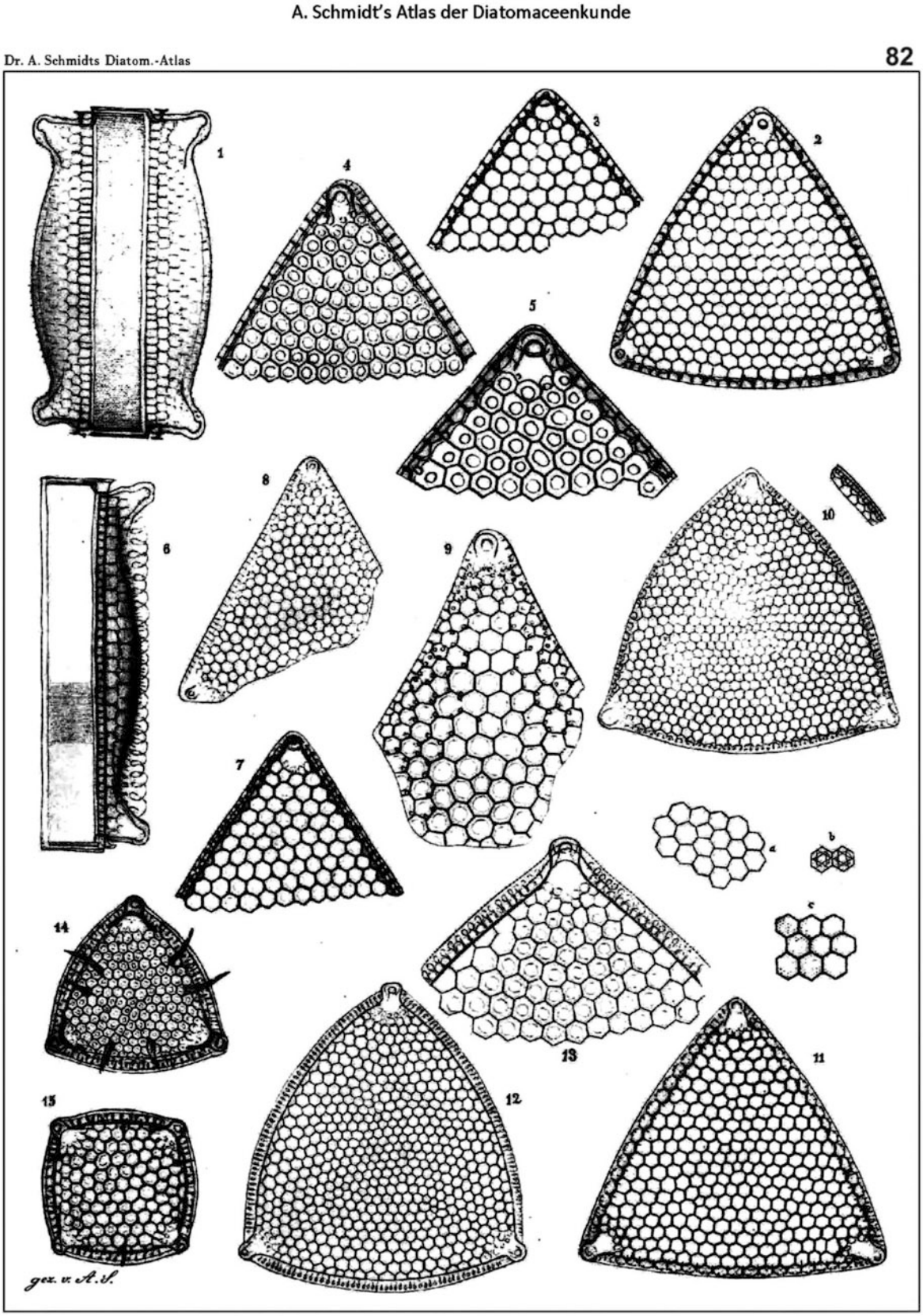

Fig. 1.2 Plate No. 82 of the Schmidt's atlas. Drawing 2 represents the *Triceratium favus* species whose photograph appears in the front matter of this book. Source [27]

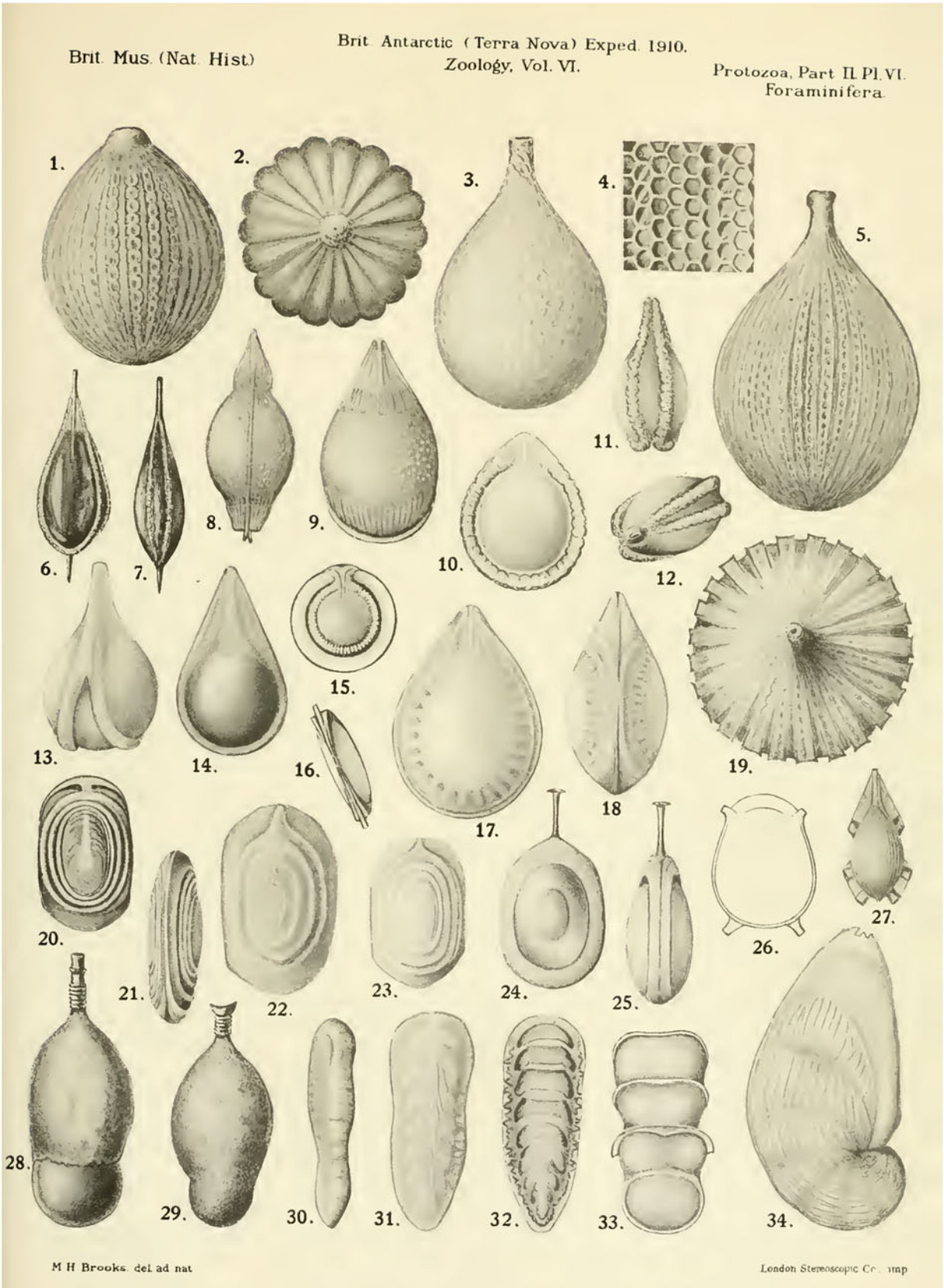

Fig. 1.3 Plate No. VI of the Heron-Allen and Earland's book of foraminifera. Source [17]

1.6 Conclusions

The automatic classification of diatoms is still an open challenge that however entails many advantages in comparison with the manual processes. One key aspect that will provide substantial progress in the field will be the availability of large public databases of annotated species (see Table 1.1), including morphological changes such as life cycle or teratological variations. This requirement is specially necessary in the case of deep learning techniques that require large datasets for training (see Chaps. 8 and 9). The development of new methods (including deep learning techniques) to create drawings of various diatom species at any point of their life cycle will be very useful for future references and comparisons in the field of taxonomy [30]. Another area for future development will be the use of 3D reconstruction techniques as an aid in taxonomy and visualization (see Chaps. 11 and 12). Finally, the very promising results of the new deep learning techniques (see Chaps 8 and 9) together with the development of new optical devices in microscopy (see Chaps. 5 and 6) allow to predict a significant advance in the field.

Acknowledgements This research was partially sponsored by the project CTM2014-51907 financed by the Spanish Ministry of Economy, Industry, and Competitiveness.

References

1. Blanco, S., Becares, E.: Are biotic indices sensitive to river toxicants? A comparison of metrics based on diatoms and macroinvertebrates. Chemosphere **79**, 18–25 (2010)
2. Blanco, S., Ector, L., Becares, E.: Epiphytic diatoms as water quality indicators in Spanish shallow lakes. Vie et milieu **54**, 71–79 (2004)
3. Blanco, S., et al.: Comparison of biotic indices for water quality diagnosis in the Duero Basin (Spain). Arch. Hydrobiol. Suppl. Large Rivers **17**, 267–286 (2007)
4. Blanco, S., et al.: Are diatom diversity indices reliable monitoring metrics? Hydrobiologia **695**, 199–206 (2012)
5. Blanco, S., et al.: Epiphytic diatoms along environmental gradients in Western European shallow lakes. Clean: Soil, Air, Water **42**, 229–235 (2014)
6. Caballero Bellido, E.: Tecnica de las preparaciones microscopicas sistematicas. Junta Ampliacion Estudios e Investigaciones Cientificas, Madrid (1925)
7. Cejudo-Figueiras, C., et al.: Nutrient monitoring in Spanish wetlands using epiphytic diatoms. Vie et milieu **60**, 89–94 (2010)
8. Diatoms online. Making the invisible visible. https://bit.ly/2GQHhF3. Accessed 1 Mar 2019
9. Diatom 3D models found in the HSPDP research project. https://bit.ly/2JT4l8t. Accessed 1 Apr 2019
10. du Buf, H., Bayer, M. (eds.): Automatic Diatom Identification. Series in Machine Perception and Artificial Intelligence, vol. 51. World Scientific, Singapore (2002)
11. Foraminifera 3D models of Elphidium spp. https://bit.ly/2JT4l8t. Accessed 1 Apr 2019
12. Gill, S. (ed.): Contributions to the Diatom Flora of Leicestershire. https://bit.ly/2YAHr9j. Accessed 1 Apr 2019
13. Gill, S. (ed.): An Account of the Diatom Flora of Nuneaton and some Outlying Districts. https://bit.ly/2I3B9Jl. Accessed 1 Apr 2019
14. Gill, S. (ed.): Some Further Works – Horace G. Barber. https://bit.ly/2Va0BAr. Accessed 1 Apr 2019
15. Gill, S., Edgar, S. (eds.): Horace George Barber's Miscellaneous Diatom Plates. https://bit.ly/2I3ALKT. Accessed 1 Apr 2019
16. Guiry, M.D.: How many species of algae are there? J. Psychol. **48**(5), 1057–1063 (2012)
17. Heron-Allen, E., Earland, A.: Zoology vol VI Foraminifera. The Trustees of the British Museum (1922)
18. Kelly, M.: Of Microscopes and monsters. https://bit.ly/2IazKSV. Accessed 12 Feb 2019
19. Lavigne, R.: The Schmidt's diatom atlas. HTML version. https://bit.ly/2GI0JTt. Accessed 12 Feb 2019
20. Lecointe, C., Coste, M., Prygiel, J., Ector, L.: Le logiciel OMNIDIA version 2, une puissante base de donnees pour les inventaires de diatomees et pour le calcul des indices diatomiques europeens. Cryptogam. Algol. **20**, 132–134 (1999)
21. Mann, D., Droop, S.: Biodiversity, biogeography and conservation of diatoms. In: Kristiansen, J. (ed.) Biogeography of Freshwater Algae. Developments in Hydrobiology, vol. 118, pp. 19–32. Dordrecht, Springer (1996)
22. Mikro-forum. https://bit.ly/2K555qW. Accessed 1 Apr 2019
23. Prygiel, J., Whitton, B.A., Bukowska, J. (eds.): Use of Algae for Monitoring Rivers III, Agence de l'Eau Artois-Picardie, France, ISBN: 2-9502083-5-5 (1999)
24. Round, F.E.. Diatoms in river water-monitoring studies. J. Appl. Physiol. **3**, 129–145 (1991)
25. Round, F.E.: A Review and Methods for the Use of Epilithic Diatoms for Detecting and Monitoring Changes in River Water Quality. H.M. Stationery Office, Richmond (1993)
26. Round, F.E., Crawford, R.M., Mann, D.G.: Diatoms: biology and morphology of the genera. Cambridge University Press, Cambridge (2007)
27. Schmidt, A.: Atlas der diatomaceenkunde. Forgesetzt durch M. Schmidt, F. Fricke, H. Heiden, O. Muller, F. Husted, O.R. Reisland, Leipzig, Germany (1874–1959)
28. Simonsen, R.: Atlas and catalogue of the diatom types of Friedrich Hustedt. Schweizerbart Publishers, Stuttgart (1987)
29. Simulation software to study diatoms. https://bit.ly/2JZ9XxY. Accessed 1 Apr 2019
30. Singh, H., Sanchez, C., Cristobal, G., Bueno G.: Pencil drawing of microscopic images through edge preserving filtering. In: Morales, A., Fierrez, J., Sánchez, J., Ribeiro B. (eds.) Pattern Recognition and Image Analysis. IbPRIA 2019. Lecture Notes in Computer Science, vol. 11868. Springer, Berlin (2019)
31. Smol, J.P., Stoermer, E.F.: The Diatoms: Applications for the Environmental and Earth Sciences. Cambridge University Press, Cambridge (2010)
32. Stoermer, E.F., Smol, J.P.: The Diatoms: Applications for the Environmental and Earth Sciences. Cambridge University Press, Cambridge (2001)
33. The Amateur Diatomist. http://www.diatoms.co.uk/. Accessed 1 Apr 2019
34. Video about slide preparation. https://bit.ly/2FP5kSY. Accessed 1 Apr 2019
35. Video about a water drop simple microscope. https://bit.ly/2FP5kSY. Accessed 1 Apr 2019
36. Whitton, B.A., Kelly, M.: Use of algae and other plants for monitoring rivers. Austral Ecol. **20**, 45–56 (1995)
37. Young ISDR. Early-career researchers and technicians group of the International Society of Diatom Research. http://youngisdr.blogspot.com/. Accessed 12 Feb 2019

Diatom Classifications: What Purpose Do They Serve?

2

David M. Williams

Abstract

Given it is now understood that there are up to 25,000 known diatom species, how is it possible for anyone, no matter how experienced and skilled that person might be, to identify correctly and consistently more than a small proportion of that total number? Even if a few gifted and well-trained individuals could manage a vast number of them, for the rest of us, we are left with a problem: How might the task of identifying diatoms be made more manageable? There are numerous diatom identification guides and floras available. Consulting them is the usual way forward. These now come in various formats, some easy to get, others less so; some easy to use, others less so. Many are focused on a particular region or area, others with a global coverage and some disregard regions altogether and focus on diatoms as a group (as a taxon). This still seems not to satisfy everybody and the quest for bigger and better, faster and more accurate methods of diatom identification is being explored, some embracing the idea that there could be a "Taxonomy-free molecular diatom index for high-throughput eDNA biomonitoring," or even a human-free approach. I want to discuss these issues and other related matters, from the perspective of classification, detailing the differences between identification guides and floras (for the most part artificial classifications) and biological classification (natural classification).

2.1 Introduction

> Why not consider taxa in general as units, and embrace the full measure of biodiversity? Although systematists routinely deal with taxa at all levels, ecologists and population biologists seemingly do not, as if real biology were to rise up the taxonomic hierarchy no further than the species (what is the biology of the genus, or family, after all?). A test of one's point of view is reading the above first paragraph. [We can] ponder why the 'biology of the species' should have meaning, whereas the 'biology of the genus', or 'family', should not. Extending one's vision of real biology beyond the species neither narrows nor dilutes the subject; rather it helps to discriminate actual species-level phenomena. ([1], p. 559)

> We need morphologically distinct entities that can be recognized any time and thus are suitable to be associated with certain ecological parameters that describe the state of a lake or river. For this purpose, *it does not really matter whether or not those taxa are true species*. ([2], pp. 1–2, emphasis mine)

For centuries biologists have sought to discover and document the biological diversity that exists now or had once existed but since passed into oblivion (bit.ly/2XrKD5N). Once discovered, that diversity is recognized by a system of names usually in a ranked hierarchy, with ranks such as Domain, Order, Family, and Genus, through to Species. A general understanding of this hierarchy is that an Order includes Families, a Family includes Genera, and Genera include Species; in short, biological diversity is recognized as a hierarchical classification.

Recognition of *what* is to be named (at whatever rank) is governed by *the science of taxonomy*, itself defined as the study of classification (from the Greek τάξις *taxis*, meaning "arrangement," and νομία *nomia*, meaning "method"). The *scientific* basis of taxonomy is discovery: "taxa are discovered through characters that are themselves discovered through *empirical investigation*" ([3], p. 442, emphasis mine). That is, taxonomy is a science that relates observations (evidence) to conclusions (taxa), first discussed in detail by Augustin Pyramus de Candolle (1778–1841) in 1813, of which more below. Assigning the correct name to each taxon so discovered (at whatever rank) is governed by the *laws of nomenclature*. Nomenclature is not a science but a system of rules captured in a Code that is revised every 5 years (the most recent is the *Shenzhen Code* [4]).

D. M. Williams (✉)
Department of Life Sciences, The Natural History Museum, London, UK
e-mail: d.m.williams@nhm.ac.uk

G. Cristóbal et al. (eds.), *Modern Trends in Diatom Identification*, Developments in Applied Phycology 10,
https://doi.org/10.1007/978-3-030-39212-3_2

Surprisingly, many still consider biological classification to be more an art-form rather than a science—mistakenly, it is understood as the relatively mundane task of assigning the names of man-made categories (Order, Family, Genus, etc.) to groups of entities that have been circumscribed by an array of characteristics thought to be typical for its included members. Those subscribing to this view usually—but not always—consider the species to be the only relevant (real) biological (rank) unit, perhaps believing it to be the only unit worthy of scientific study [5]. The two epigraphs above sit in stark contrast to one another: Nelson and Ladiges ask "Why not consider taxa in general as units, and embrace the full measure of biodiversity?" ([1], p. 559), capturing a view that sees classification in all its fullness, from "Domain to Species". This is contrasted with Lange-Bertalot and Ulrich, who believe "it does not really matter whether or not those taxa [we recognize] are true species," thus dismissing *any* relationship between our classifications and the world we live in, including species, except as a system of labels ([2], pp. 1–2).

Regardless of any particular biological classification, one might reasonably ask the following questions: What is its purpose? What is it designed for? Who is it for? Who will use it? I will attempt to answer these questions below from a consideration of diatom (Bacillariophyta) classification.

2.2 Diatoms

Diatoms are unicellular, microscopic eukaryotes that are primarily photosynthetic (hence once considered as "algae" and plants, e.g., [6]), although some live heterotrophically (e.g., [7]). Their phylogenetic relationships are amongst the Stramenopiles or Heterokonts [8], which includes a diverse array of organisms such as oomycetes, kelps, and a host of unicellular heterotrophic "protists" (a summary can be found in [9]). Although single-celled, diatoms can occur in colonies that are simple or branched, filamentous, with some enveloped in a gelatinous tube (for a review see [10, 11]). Of significance, the single cell is enclosed in a *frustule* made up of two *valves* that fit together by an expanding connective zone called the *girdle* [10, 11]. The entire frustule—the two valves and all its girdle elements—is made of silica. The valves are highly ornamented. Most—if not all—diatom taxonomy of the past is derived from the distinctive architecture found on the silica valves and girdle. As silica preserves extremely well, when diatom cells die their remains sink and become part of the sediment. Thus, diatoms have a reasonably dense fossil record and their diversity can be estimated with some accuracy for both the past and present [12], for the extinct and extant (still living) [10, 11].

Diatoms are *highly sensitive indicators of environmental change*, with their community composition altering when affected by changing environmental conditions [12]. As such they are used extensively in routine environmental monitoring of watercourses. Due to their excellent fossil record diatoms are also used extensively in reconstructing paleoclimates and past conditions, hence these organisms can be *used to model environmental change*. These factors make diatoms extremely useful organisms to study from the perspective of understanding past environments and monitoring their changes, as well as addressing questions concerning their evolution, distribution, and eventual extinction: *in short, diatoms are an extremely significant component of our biosphere*.

2.3 Scientific Classification

As noted above, the term taxonomy was first used by Candolle in his book *Théorie élémentaire de la botanique*: *ou, Exposition des principes de la classification naturelle et de l'art de décrire et d'étudier les végétaux* (Fig. 2.1), published over 200 years ago [13]—never properly translated into English, *Théorie élémentaire de la botanique* is still worth studying today (see commentary in, for example, [14–16]). The notion that taxonomy (systematics) involves at least two distinct (and contrasting) approaches has been known for some time, usually understood from the perspective of *artificial* and *natural* classifications. The distinction between the two goes back at least to Linnaeus but the first comprehensive account of the distinction is found in Candolle's *Théorie élémentaire* [13]. Candolle's argument is not particularly complex. The text in double quotations directly below is from Candolle's *Théorie élémentaire de la botanique* translated into English (by Williams and Ebach [17]). Following Candolle, first one needs to consider the properties of what he called a "rational classification" as only "Rational classifications have a real relation with the objects to which they apply" and "are the only ones that merit consideration." That is, a rational classification has *empirical content*; there is, or should be, a direct relationship between evidence, however conceived, and conclusions. Candolle recognized that there was a great diversity of classifications, which stemmed from "the special purpose for which each is proposed." Thus, when considering the task of *identification*, Candolle noted that they must have as their purpose to allow "persons who know nothing of the names of plants an easy way to discover the names by an inspection of the plant itself. These classifications have been given the name of *Artificial Methods*" (my emphasis). That is, artificial classifications allow anyone to find the name of any *known* plant by examining its key characteristics. This is its stated purpose.

The word "artificial" implies something inferior, as if any particular *artificial* classification is less worthy than a (or

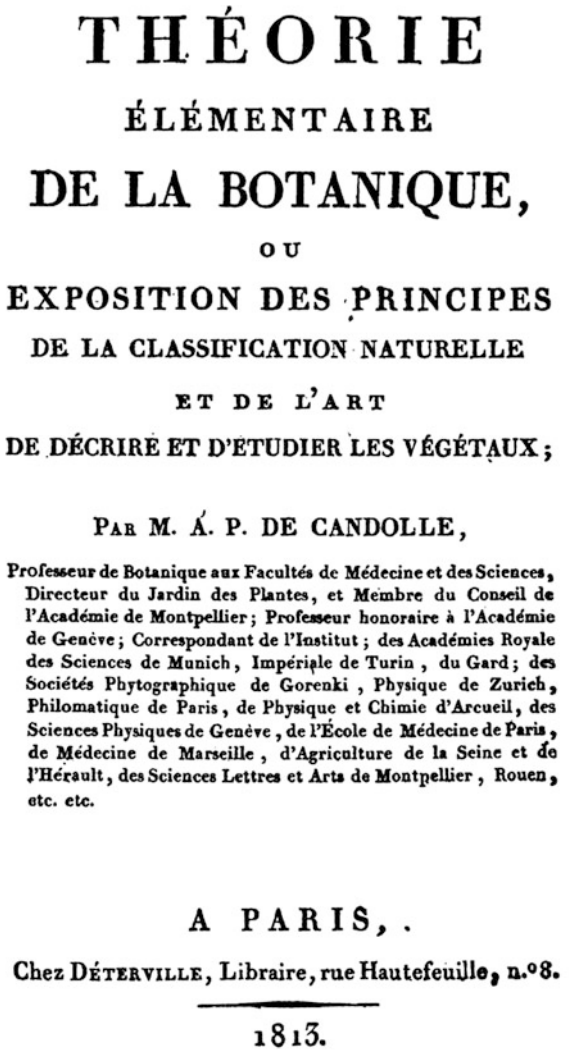
THÉORIE
ÉLÉMENTAIRE
DE LA BOTANIQUE,
OU
EXPOSITION DES PRINCIPES
DE LA CLASSIFICATION NATURELLE
ET DE L'ART
DE DÉCRIRE ET D'ÉTUDIER LES VÉGÉTAUX;
PAR M. A. P. DE CANDOLLE,
Professeur de Botanique aux Facultés de Médecine et des Sciences, Directeur du Jardin des Plantes, et Membre du Conseil de l'Académie de Montpellier; Professeur honoraire à l'Académie de Genève; Correspondant de l'Institut; des Académies Royale des Sciences de Munich, Impériale de Turin, du Gard; des Sociétés Phytographique de Gorenki, Physique de Zurich, Philomatique de Paris, de Physique et Chimie d'Arcueil, des Sciences Physiques de Genève, de l'École de Médecine de Paris, de Médecine de Marseille, d'Agriculture de la Seine et de l'Hérault, des Sciences Lettres et Arts de Montpellier, Rouen, etc. etc.
A PARIS,
Chez DÉTERVILLE, Libraire, rue Hautefeuille, n.°8.
1813.

Fig. 2.1 First edition of *Théorie élémentaire de la botanique*, by Candolle [13]

the) *natural* classification. But here artificial means "man-made" or *imposed*, as they have a particular purpose, such that Candolle noted that "For their unique purpose and their unique result, artificial classifications have, as we have seen, to make it possible to learn with more or less ease, the names of the species to which the system are applied."

Artificial classifications are all very well but organisms do have "real relations among themselves" and, as Candolle put it, "there are those persons who want to study plants, either in themselves, or in their real relations among themselves and to class them so that those plants most closely related in the order of nature are also those most closely related in our books. These classifications have received the name of *Natural Methods*" (my emphasis). This approach is for those who wish to study nature, to make *discoveries*—this is the basis of *natural classification*. This is what makes classification a science.

2.4 Diatoms: Classification and Identification

It is worth considering how one might approach the task of identification in the light of artificial and natural classifications. Given that there is now something in the order of 15,000–25,000 known species of diatoms, never mind how many might be left to discover, how is it possible for anyone, no matter how experienced and skilled, to identify correctly and consistently more than just a proportion of that number? Even if a few talented individuals could manage a relatively vast number, for the rest of us, we are left with a question: How might the task be made more manageable? By the task, I mean, when any single individual, or even any well-appointed laboratory for that matter, is faced with numerous samples, each with numerous diatom specimens, how might sense be made of them in some reasonable time?

At present there are many diatom identification guides, some provided in more than one format, some easy to obtain, others less so, some free, others not. Many of these identification guides are also considered to be floras and are focused on a particular region or area (a flora is usually considered to contain more information than a simple identification or field guide, the latter being created solely to name specimens found in the field). Several recent identification guides to freshwater taxa are discussed below, three having been randomly selected, three deliberately chosen. In contrast to these guides, there are a number of diatom classifications that are presented as summaries of diatom *relationships* rather than identification guides. I will discuss two of those. The first six items are considered artificial, the last two as natural.

2.5 Artificial Diatom Classifications

2.5.1 Three Randomly Selected Identification Guides

The first guide I briefly discuss is Taylor and Cocquyt's *Diatoms from the Congo and Zambezi Basins* [18], volume 16 of the journal *ABC Taxa*, that journal being "a series of peer-reviewed manuals dedicated to capacity building in zoological and botanical taxonomy, in collection management and in good practices in taxonomic and curatorial research" (www.abctaxa.be). The various issues of *ABC Taxa* are available as printed monographs (The prices of each vary, with Taylor and Cocquyt's monograph at 16€) or as free downloadable pdf files (364 pp.) (bit.ly/2Gy0Lgt). The stated aims of the diatom volume are twofold: "to encourage and facilitate the study of diatoms as a useful tool for water quality monitoring" and "to give an overview of the most common diatom genera which can be observed in the Congo and Zambezi basins" ([18], p. 4). Thus, it functions as a flora

and an identification guide. After just under 70 introductory pages, the rest is dedicated to describing and illustrating each genus that might be encountered in the Congo and Zambezi Basins (91 in all), some in more detail than others. The guide adopts the conventional approach to identification requiring the user to look at the specimens under the microscope and then compare them to the images in the book. Taylor and Cocquyt note that the "classification used is after Round et al. (1990) with some modifications when it concerns genera described after 1990" (p. 66). For example, in the family Stephanodiscaceae a total of five genera are included: *Cycostephanos* Round, *Stephanodiscus* Ehrenberg, *Cyclotella* Kützing ex Brébisson, *Discostella* Houk and Klee, and *Pantocsekiella* Kiss and Ács, the latter two described after 1990 and so were not in Round et al. [19].

The second guide is *Diatomeas del Canal de Panamá: Bioindicadores y otros estudios pioneros* (2012), which is an online resource, downloadable as a free pdf file (272 pp.), its aim being to document "Bioindicadores y otros estudios pioneros" (bit.ly/2Uqsx1K): "The work we present is the final part of an investigation that is related, in large part, to the biological component and, specifically, the diatoms. The field work was carried out during 2004–2006; and, the results of the physicochemical characteristics are published in the Water Quality Report of the Hydrographic Basin of the Panama Canal by the Water Quality Unit of the Panama Canal Authority 2003–2005" (first page, unnumbered, translated from Spanish). In this contribution, there are 55 pages of introductory matter followed by five Appendices of which the final two deal with "Morfometría de las diatomeas en ríos (Morphometry of diatoms in rivers)" and "Morfometría de las diatomeas en embalses (Morphometry of diatoms in reservoirs)," respectively. Each of the taxonomic appendices are arranged alphabetically first by genus name then by species, with 23 plates of light microscope images for the river diatoms and 25 plates of light microscope images for the reservoir diatoms. As the taxa are arranged alphabetically there is no need for any detailed classification. This guide also adopts the conventional approach of comparisons between specimens and images.

Finally, the six volumes of the *Atlas des diatomées des cours d'eau de la région Rhône-Alpes* ([20], bit.ly/2VRv4ni) are available as a set of printed monographs or as free downloadable pdf files. The stated purpose of this contribution is to enhance work with the EU Water Framework Directive ([21] bit.ly/1mKbUth). The six volumes total nearly 1400 printed pages, with numerous taxa illustrated with light micrographs, maps, and other details concerning their taxonomy and ecology. A classification is included, primarily designed to guide readers through the six volumes but also reflects, in part, diatom relationships (Table 2.2).

All three of these splendid contributions have as their primary purpose a guide to the *identification* of diatoms specifically for use with biomonitoring studies and only *secondarily* as a compendium for the species (taxon) diversity found in the area of interest: the Congo and Zambezi basins, the Panamá Canal and a broadly defined Europe, respectively. And all three rely on the simple direct comparison between specimens and images.

2.5.2 Three Non-Randomly Selected Identification Guides

The three deliberately selected guides are all exceedingly detailed; the first two in a state of continuous development as they are web-based online identification guides (no print version of either is available) and details are continuously added and modified.[1] The third is only available as a printed book.

The first guide I will discuss is the *Diatoms of the United States* (bit.ly/2Gs4vii), which aims "[. . .] to provide everyone with accurate information about diatoms of the United States" and "provide analysts with accurate information on taxonomy, nomenclature and ecology of diatoms to help federal and state agencies in the United States comply with the Clean Water Act"—effectively stating its twofold purpose as the others above have done. Interestingly, the classification used is (almost) entirely novel containing nine informal groups (Table 2.1).

The second guide reviewed is the *Diatom Flora of Britain and Ireland* (bit.ly/2DjZt6o), which has as its stated aim "to compile a web-based diatom flora and comprehensive taxonomic review of diatoms from freshwater, brackish and subaerial habitats in the British Isles." Similar to the *Diatomeas del Canal de Panamá* discussed above, no classification is provided as it is organized around a list of genera placed in alphabetical order.

Finally, the third guide reviewed is the *Freshwater Benthic Diatoms of Central Europe* [22], a massive 900+ page identification manual, a revised English language version of *Diatomeen im Süßwasser-Benthos von Mitteleuropa: Bestimmungsflora Kieselalgen für die Ökologische Praxis* ([23], a second edition was published in 2013), another exceptionally comprehensive work, available only in print. Its intention was to supersede the five volumes of the *Süßwasserflora von Mitteleuropa* ([24–27], some of the earlier volumes of that set were revised and reissued) and also aimed at those persons dealing with, or studying diatoms in the context of, WFD. Rather than a classification, there is a key, primarily to genus (some parts address families) but in some cases to species within a particular genus. The genus descriptions are listed alphabetically, as they are the species within each

[1] Here I must make a declaration of interest: I am an author/contributor to the two websites.

Table 2.1 Classification used in the *Diatoms of the United States* (2019) with the "nine *artificial* (not strictly evolutionary) categories to aid in identification"

"Taxon" [shape-group]	Number of inclusive genera
Centric	25
Araphid	23
Eunotioid	6
Symmetrical biraphid	59
Monoraphid	12
Asymmetrical biraphid	19
Epithemioid	2
Nitzschioid	2
Surirelloid	5

genus. In the Forward to the English Edition, the authors note that "These are exciting times for those interested in the phylogeny, biogeography and diversity of diatoms, but also hugely frustrating times for those concerned with the routine identification of diatoms for practical purposes" ([22], p. 9). How, then, to deal with taxonomic revisions undertaken since the publication of the *Süßwasserflora von Mitteleuropa* and the subsequent two versions of *Diatomeen im Süßwasser-Benthos von Mitteleuropa*? They continue: "Decisions on revisions were made following a very empirical criterion: all taxonomy and ecology papers of which we are aware [. . .] were considered and all genera and species [. . .] were included if they appeared to be recognized in the main online resources (in particular, 'Diatoms of the United States', 'Algaebase', etc. and by the community of diatomists)" ([22], p. 9).[2]

What can be said of these varying approaches? Consider for a moment the classification given in the *Diatoms of the United States*. The preamble to the website states that "For the purposes of a visual key, we group diatom shapes into nine *artificial* (not strictly evolutionary) categories to aid in identification" (emphasis mine) (Table 2.1).

Let us, then, imagine we have before us a specimen which we want to know the name. The specimen is circular. That would suggest the centric diatoms ("Centric") as a good place to start, as it corresponds to the first character given in the text: "Valves with radial symmetry (symmetric about a point)." We might then consider the second character: "Cells lack a raphe system and lack significant motility." We are now looking for something that is not there: the raphe (the idea we can observe its motility depends on whether we have a specimen that is still alive). Its third character, "Cells may possess fultoportulae and rimoportulae," requires us to examine our specimens in the electron microscope. The final character given, concerning sexual reproduction, requires not just a living specimen but a living specimen performing a function. Should we get this far and confirm that we do indeed have a "centric" diatom, we have another 25 options (genera) from which to choose.

Suppose we have no idea which of the 25 genera is relevant so we just pick one to start with, perhaps *Aulacoseira*. Here the guide usefully provides a further four characters of this genus we could look for, some illustrations of those characters and some text to explain what the characters actually are and look like (bit.ly/2VTBthU). There are 19 species to investigate in this genus (Although in total there are more than 100 known species)—the point here is that this set of instructions do, as Candolle suggested, help "persons who know nothing of the names of plants an easy way to discover the names by an inspection of the plant itself." The structure of the classification in *Diatoms of the United States* is similar to that of a key—and keys are the most common version of artificial classifications (see [28], also Chap. 4).

The *Diatoms of the United States* authors write in the introductory pages: "We agree that it would have been preferable to organize the navigation of this site based on biological relationships, rather than similar morphological features." I disagree. The classification in the *Diatoms of the United States* works extremely well—it would be reckless to change it. True, it tells us nothing about taxon relationships—but nor is it supposed to. Of course, one can *assume* that all the 19 included species of *Aulacoseira* are most closely related amongst themselves than they are to any other diatom, but beyond that, we learn little else. But its purpose—identification—is satisfied.

The same rationale applies to the classification in Bey and Ector [20] (see Table 2.2). For example, following on from the *Centriques* one is guided to 13 possible genera, each having a list of characters and illustrations. With this classification, one could assume a lot more about relationships than that given in the *Diatoms of the United States*, such that its hierarchical nature suggests, for example, that all *Biraphidées* are most closely related to each other than to anything else and within that taxon all members of *Rhopalodiacées* are most closely related to each other than to anything else. Of course, conclusions along these lines are obviously prone to misinform, such as *Araphidées*, which are clearly *not* all more closely related among themselves. Yet from the point of view of *identification*, to divide (artificially) the *Pennées* into *Araphidées* and all the various raphid diatoms groups helps enormously when sorting specimens. I make no further comment on the *Freshwater Benthic Diatoms of Central Europe* except to note that it is printed and expensive and when revisions are required a new book needs printing (see [29]).

[2]It should be noted that this is hardly empirical – it is more a method of consensus. To be empirical one needs to evaluate *the data* rather than a series of *opinions*.

Table 2.2 Classification in the *Atlas des diatomées des cours d'eau de la région Rhône-Alpes* [20]

Taxon					Tome no.
Centriques					1
	Pennées				1&6
		Araphidées			2
					1
					2
		Monoraphidées			6
		Brachyraphidées			
		Biraphidées	*Rhopalodiacées*		
			Bacillariacées		6
			Surirelliacées		6
			Naviculacées	*Cymbelloidées*	5
				Naviculoidées	3, 4
				Gomphonématoidées	5

2.6 Natural Diatom Classifications

> [. . .] exact classification of organisms will be achieved only through successive efforts of a large number of naturalists; it will be only painfully and very slowly achieved. ([30], pp. 1261–1262, *Elements of Physiology* par. 7, translated, after Nelson [30], p. 137).

2.6.1 Two Non-randomly Selected "Natural" Classifications

It is somewhat harder to discuss classifications that are not specifically intended for identification—that is, classifications that are not proposed as a way to orient a particular diatom identification guide, like those discussed above. I will discuss two classifications of this kind, simply because they are the most recent: Cox [32] and Mann (in [33]).

- *Cox's classification* [32]

A new diatom classification was included in the 13th edition of Engler's *Syllabus der Pflanzenfamilien* (as part of Part 2/1: Photoautotrophic eukaryotic Algae [34]). The aim of the first edition, published in 1892, was to document the organisms then recognized as part of the botanical kingdom—its primary aim was to be both *authoritative* and, following on from August Eichler's (1839–1887) classification ("Eichler's System"), to represent "phylogenetic relationships" instead of the "natural systems" of classification offered by a previous generation of botanists, in the hope of promoting a new and more significant post-Darwinian approach to systematics.

I have commented on this book in more detail elsewhere [29], but to summarize, in the Preface to the 13th edition it is noted that "... numerous molecular analyses led to new insights and a better understanding of the evolution and systematics of the lowermost groups." But it is also noted that "we are convinced that in the 'molecular times' there is an indispensable need to preserve the knowledge of the whole diversity and biology of organisms for the next generations" (p. v). One begins to detect a blurring of purpose.

In the diatom section of *Syllabus der Pflanzenfamilien*, Cox summarizes her approach to classification as follows: "The most recent comprehensive diatom classification was made by Round et al. (1990)[3], who treated the diatoms as a division with 3 classes and erected a large number of new families and orders. As mentioned above, this classification is primarily based on wall morphology and pre-dates the molecular phylogenetic studies. Because a relatively small number of diatoms have been included in molecular studies, many of the families erected by Round et al. (1990) have been retained for the time being, unless there is clear evidence to the contrary" ([32], p. 73). Thus, while no purpose is actually stated, one might possibly conclude that because there now exists "molecular phylogenetic studies" (even though limited), these data will yield a "phylogenetic classification," one which will be a better representation of actual taxon relationships, as if DNA = "phylogenetic classification" = natural classification. Alternatively, one might see this as a special purpose classification, reflecting only the relationships found with just one character: DNA [36, 37]. In any case, I doubt very much the general supposition that DNA *on its own* will fulfill the dream of a perfect (natural) classification. Consider one part of this classification, the Class Fragilariophyceae. This taxon is retained following Round et al. ([19], pp. 125, 127, Table 2.3, column 1), except where Round et al. had only one included subclass with 12 orders, Cox [32] eliminated the subclass and reduced the or-

[3] Actually, the most recent classification is that of Medlin and Kaczmarska [34].

ders to ten (six of these having only one family, the remaining four with two families apiece) (Table 2.3). The classification of Cox differs from Round et al. [19] as it includes the new Order Plagiogrammales (as a "nom. prov.;" validly published later by Gogorev and Stepanova [38], p. 82) but excludes Ardissoneales, Toxariales, and Climacospheniales, with these three combined into the Order Toxariales as part of the Class Mediophyceae, Subclass Biddulphiophycidae ([32], p. 80). Cox's classification differs from that in Round et al. [19] in some of its details but both Round et al. and Cox imply that the Class Fragilariophyceae is monophyletic by virtue of retaining it as a named taxon—otherwise, in the context of a "phylogenetic" (natural) classification, what is the meaning of the taxon? There is "clear evidence to the contrary" that Fragilariophyceae is not monophyletic as it has been consistently shown in the phylogenetic trees published by, for example, Medlin [34, 39, 40] and Theriot et al. [41], among others. As a consequence this part of the classification does not accurately reflect the phylogeny it is supposed to ([32], see figs. 7-8, 7-9).

Of further interest is Cox's order Fragilariales, which is more or less equivalent to Medlin's subclass Fragilariophycidae ([40], p. 123, Medlin's "core araphid" diatoms and the new (but invalid) family "Ulnariaceae" ([32], p. 87). Placed within an amended Licmophorales, "Ulnariaceae" is one of its two families, the other being Licmophoraceae ([32], p. 87). "Ulnariaceae" includes 15 genera removed from various orders in the Fragilariophyceae of Round et al. ([19], p. 127). According to the phylogenetic tree, the relationships of the families "Ulnariaceae" and Licmophoraceae differ from the classification ([32], p. 75, figs. 7-9), even though Cyclophorales are most closely related to the Licmophoraceae, they are placed in different families (see also [42, 43], fig. 10). There is, of course, no reason why the classification in Cox could not be a correct representation of relationships and the DNA cladograms incorrect, although Cox does not suggest that to be the case. The situation can only be judged on the basis of the evidence to hand irrespective of its source—and no evidence is presented. Thus, if the purpose of this classification is to represent natural relationships, then it fails in that respect.

- *Mann's classification* [33]

In a multiauthored account designed to present a revision of the "Classification, Nomenclature and Diversity of Eukaryotes" is another diatom classification (Mann in [33]). Although it is hard to divine any cogent scientific purpose to this revised classification (or, indeed, the earlier version [44]), a political motive is supplied: "This classification will serve as a primary starting reference for the taxonomic framework developed by UniEuk (unieuk.org; Berney et al. [45]), the Society supported, consensus-driven, community-based and expert-driven international initiative to maintain a universal taxonomy for, at least, microbial eukaryotes" ([33], p. 7)—which in attitude, if nothing else, harks back to Engler's *Syllabus der Pflanzenfamilien* in its desire to be *authoritative* rather than scientific. Be that as it may, what of the details? For the diatoms, of higher taxa there are eight sub-phyla (seven new), five families (three new) and ten subclasses (two new, eight revised from [19]). The explanation given for this is the following: "This revision reflects *numerous advances* in the phylogeny of the diatoms over the last decade. Due to our poor taxon sampling outside of the Mediophyceae and pennate diatom and the known and anticipated diversity of all diatoms, "many clades appear at a high classification level (and the higher level classification is rather flat)" (Mann in [33], p. 45, emphasis above mine). The classification reflects no particular study, thus, like Cox's, has no direct connection to any evidence whatsoever—just the vaguely worded promise of *numerous advances*. We might compare this classification with that of Cox. Let us consider Fragilariales (Family: Fragilariaceae) sensu Cox again and compare it with Fragilariophycidae. First, one has to consider its contents and then its definition. In Table 2.3 there is a list of included genera, 36 in Fragilariaceae (Cox), 14 in Fragilariophycidae (Mann), with only 7 in common.

For Cox, members of Fragilariaceae are defined (described) as "Cells elongate, often forming filaments held together by marginal spines. Apical pore fields and rimoportulae usually present" ([32], p. 85). This is somewhat problematic as although the word "usually" is included, none of the genera in "Staurosiraceae" (genera 1–9 in Table 2.3, those in subgroup D in Williams [46], pp. 27, 29, the "Staurosiroids" in Cox 2015, figs. 7-9 after Theriot et al. [41], fig. 2) has rimoportulae (*Martyana, Nanofrustulum, Pseudostaurosira, Punctastriata, Sarcophagodes, Stauroforma, Staurosira, and Staurosirella*) nor does *Porannulus* [47]; although the word "often" is used, neither *Fossula* nor *Porannulus* have spines [47, 48]; and it seems likely that *Frankophila* is an unusual raphid diatom related to *Hygroptera* [49–54]. With their removal from Fragilariaceae only three genera are left: *Centronella*, *Fragilaria*, and *Fragilarforma*.

In fact, scattered amongst the Fragilariales, most species have elongate cells (as perhaps all pennate diatoms do), many are "held together by marginal spines" and many have rimoportulae. There are, however, different kinds of apical pore fields and one in particular, the ocellulimbus, is present in *Centronella* and *Fragilaria* but not *Fragilarforma*.

"Ulnariaceae" is defined equally ambiguously: "Valves elongate, usually symmetrical and isopolar, occ. heteropolar or lunate; cells often attached to a surface or each other by a mucilage secreted through an apical pore field comprising round or elongated pores. Rimoportulae present" ([32], p. 87). Simplified, there are five characters: valve shape (elongate, symmetrical, isopolar/heteropolar/lunate); colony (cells attached via pore fields); pore field (elongated/round

Table 2.3 Comparison between Fragilariales Cox [32] and Fragilariophycidae Mann [33] at the level of genus

Order: Fragilariales Cox	Fragilariophycidae Mann
Family: Fragilariaceae	
Centronella	
Fossula	
Fragilaria	*Fragilaria*
Fragilarforma	
Frankophila	
Martyana	
Nanofrustulum	
Porannulus	
Pseudostaurosira	
Punctastriata	
Sarcophagodes	
Stauroforma	
Staurosira	*Staurosira*
Staurosirella	
Family: Tabellariaceae	
Asterionella	*Asterionella*
Diatoma	*Diatoma*
Distrionella	
Meridion	
Oxyneis	
Tabellaria	*Tabellaria*
Tetracyclus	
Family: Ulnariaceae	
Bleakeleya	Family: Urneidophycidae: *Bleakeleya*
Catacombas	
Ctenophora	
Falcula	
Hannaea	
Hyalosynedra	
Neosynedra	
Opephora	
Psammosynedra	
Pteroncola	
Synedra	*Synedra*
Tabularia	*Tabularia*
Thalassioneis	
Trachysphenia	
Ulnaria	
Other orders	*Grammatophora Cyclophora*
	Astrosyne
	Licmophora
	Rhabdonema
	Thalassionema

pores); rimoportulae. Again, the valve shape character(s) applies to (nearly) all pennate diatoms; colony formation is an epiphenomenon based on the mode of attachment, which relates to the possession of spines and pore fields, both reasonably widespread throughout diatoms; rimoportulae, as noted above, are also widely dispersed throughout diatoms. This appears, again, to leave the pore field as a defining character—but there is a simple pore field, where only the striae are reduced in size (*Bleakeleya*, *Pteroncola*, and *Thalassioneis*); or as a series of thin narrow slits (*Falcula, Neosynedra,* and *Psammosynedra*); or the ocellulimbus (*Catacombas, Ctenophora, Hannaea, Hyalosynedra, Neosynedra, Tabularia*, and *Ulnaria*). *Opephora* and *Trachysphenia* have been excluded as they are more likely members of the "Staurosiroids" and the name *Synedra* is problematic for nomenclatural reasons [55].

The Fragilariophycidae of Mann is equally ambiguously defined. Its inclusive genera are: *Fragilaria*, *Synedra*, *Tabellaria*, *Asterionella*, *Diatoma*, *Tabularia*, *Cyclophora*, *Astrosyne*, *Licmophora*, *Rhabdonema*, *Grammatophora*, *Staurosira*, and *Thalassionema* (see Table 2.3; "The genera are provided as examples only and are far from complete lists" [33]). The description is as follows: "Chain-forming or colonial (linked by pads or stalks, less often by valve spines) or solitary; valve outline bi- or multipolar, very rarely circular (with reduction of the sternum and secondary evolution of radial symmetry); valve structure usually simple; pore fields (rimmed or not) often present at the poles; rimoportulae present or absent, very variable in location but often polar; raphe absent; 'male' and 'female' gametes of equal or unequal size, amoeboid, or with 'male' gametes with non-cilium projections that generate movement; marine and freshwater." One need not dwell too long on this description to realize that most of the characters are found elsewhere in other diatoms ("Chain-forming or colonial"), are not really characters at all ("raphe absent") or are too vague to be of any use ("rimoportulae present or absent," "valve structure usually simple"). As noted above for Cox, this classification reflects no particular study and has no direct connection to *any evidence at all*. Although my desire is to avoid contentious words, these are both examples of what I refer to *authoritarian classifications*, one derived from authority—perhaps, even, examples of Candolle's *irrational* classifications. And both are built on the classification in [19], an earlier example of an authoritarian classification.

One might assume that rather than representing relationships, the two classifications are supposed to represent the sum total of our knowledge. This may, of course, be a stated purpose—but it was not stated as such in either of these classifications. One way or another, the two are supposed to be based on, or derived from, molecular data, in the form of one or another molecular cladogram (tree). Thus, *neither* can be representations of the sum total of our knowledge but only representations of the relationships expressed in one or another diagram (an excellent example of what *should* be concluded from such studies is [56]).

What, then, makes a natural classification? It seems generally agreed that synapomorphies (defining characters) constitute evidence and taxa (at whatever rank) are the conclusions. Synapomorphies fit to the "Tree of Life" at their appropriate level, known as *heterobathmy*, which literally means "different steps on a stair" (from the Greek *bathmos*, a step or stair, after [57], pp. 11, 13, [58], p. 227, see [59]).

Consider one last example, Cox's Eupodiscales ([32], p. 83, proposed as a provisional name only) and Mann's Odontellophycidae ([33], p. 46). These are (very) roughly equivalent. Cox's description is as follows: "Bi- to multipolar, porose or loculate valves with true ocelli; cells forming zig-zag or straight colonies, linked by mucilage and to other surfaces [. . .]." It includes 12 genera. Mann's Odontellophycidae is as follows: "Chain-forming (linked by mucilage pads) or solitary, generally large-celled and sometimes very robust; valve outline bi- or multipolar, rarely circular; valve pattern organized radially about a central circular or elongate annulus; valve structure simple or chambered; valve poles with well-defined pore fields ('ocelli') often surrounded by a thick rim; rimoportulae present (sometimes with long external tubes) or absent; exclusively marine." It includes eight genera. There is a great degree of overlap in characters between these two classifications, but, once again, most are applicable to a much broader group than intended by either author. Once those irrelevant characters are removed ["Chain-forming (linked by mucilage pads) or solitary, generally large-celled and sometimes very robust; valve outline bi- or multipolar, rarely circular; valve pattern organized radially about a central circular or elongate annulus; valve structure simple or chambered"], one synapomorphy is left: the ocelli (Sims et al. [60] present in detail the actual evidence, following on from a much earlier account in [61], with the synapomorphy recognized in that much earlier study). Unlike the artificial classifications above, neither of the natural classifications appears to work.

In summary, then, many of the artificial classifications in use are only as good as their stated purpose, with most working reasonably well. The classifications supposedly representing something natural are disconnected from the evidence that supports the conclusions. And it is natural classifications—ones supported by synapomorphies—that *discover* the entities that need *naming and identifying* by all those who use such classifications. Two final points: first, synapomorphies are not always useful for identification—the synapomorphy "closed girdle bands" found in all species of *Ulnaria* are not accessible if light microscopy only is used. Second, as natural classification is a science, the synapomorphies outlined are always considered provisional, such that more data might reveal them to be applicable to a larger group (marginal spines, for example) or define two unrelated groups, or some other conclusion. This, of course, conflicts with the desire for stability by those who are only interested in identification.

Candolle made a further significant point: "These sorts of classification [artificial and natural] follow entirely different laws and rules. However, they have often been and still are often confounded." It is of interest that our most recent natural diatom classifications yearn to be identification tools (artificial), while our artificial classifications yearn to be natural (phylogenetic). One of the taxonomist's tasks is to separate out these two endeavors and pursue them as guided by the appropriate rules.

2.7 Automatic Identification

Given that biological classification has at least two facets (artificial and natural classification), that it is a science, so it is constantly evolving, how might one rejuvenate the task of species (taxon) identification to satisfy those who require names before tackling their further interests?

With respect to the many diatom identification schemes created specifically with biomonitoring studies in mind, there is almost an *embarras de richesses*. Yet this seems not to be generally satisfactory and the quest for better, faster, "more accurate" methods of diatom identification is constantly being sought, perhaps beginning with [62] ("This paper describes a biomonitoring system, currently being developed, that employs coherent optical spatial filtering techniques to rapidly identify diatoms and process species-abundance information;" they concluded: "The primary value of this type of biomonitoring system is that, upon complete development, it should be able to provide a rapid, unbiased and economical analysis of a large number of diatom community samples").

There are a number of options available to choose from but they more or less fall into two kinds: Morphometric studies (see Chap. 12 and for a review see [63]), which are designed to deliver a more accurate account of diatom valve shapes; and molecular data, in some form of barcoding (e.g., [64–67] for single specimens), metabarcoding (e.g., [68, 69] for multiple specimens) or eDNA metabarcoding (e.g., [70] for environmental samples), the latter hoping for a "Taxonomy-free molecular diatom index" [70]. All of these methods are for *identification* rather than *discovery* (see [71] for an earlier review). We can briefly return to Candolle: the desire to have a classification, or method, to allow "persons who know nothing of the names of plants an easy way to discover the names by an inspection of the plant itself"—even if that inspection involves just a portion of its DNA. The key here is to *name a known taxon*. That is, taxa have to be *known* before such methodologies became useful. One example should suffice. An et al. studied the problem of *identifying* diatoms from "the eastern tidal flats of the Yellow Sea" [72]. They wrote in their abstract: "Based on the traditional morphological identification system, the 61 isolated strains were classified into 52 previously known taxa

from 13 genera. However, 17 strains could not be classified as known species by morphological analyses, suggesting a hidden diversity of benthic diatoms" ([72], p. 11). Here a method of identification is being used as a method of discovery (see also [66]). One might alternatively say that the molecular methods mislead. In short, one cannot identify what one does not yet know exists.

2.8 Numbers of Species

2.8.1 What Do We (Think We) Know?

As noted above, it is generally understood there are around 15,000–25,000 known species of diatoms—known meaning accepted as definable biological entities *at the rank of species* (Mann and Vanormelingen [73]: "The number of extant species of diatoms is estimated here to be at least 30,000 and probably ca. 100,000 . . .;" Guiry [74]: "12,000 described species of diatoms, with a further 8000 to be discovered;" "There are an estimated 20,000 to 2 million species of diatom on Earth" (bit.ly/1N2c8KL). While the numbers are impressive, it must be remembered that species are the only units being counted.

There are two figures of further interest, the first of little consequence, the second of some significance.

2.8.2 What Would We Like to Know?

The number of predicted species to account for all diatom diversity has been calculated at around 250,000 (e.g., [73], although they entertain various different numbers for the total and entertain various versions of the biological species concept, which will obviously affect the number). For comparison, there are ca. 7000 known species of mammals [75], ca. 450,000+ known species of flowering plants [76], and ca. 400,000+ known species of beetle [77]. The numbers for these three groups might be expected to increase, but maybe only by a relatively small amount. It might be argued that mammals, plants and beetles have been studied in greater detail than diatoms so their figures might be considered more accurate than those for diatoms.

Regardless, what, if anything, is the significance of any of these numbers, however accurate? What purpose does it serve to have these numbers? How would we learn of their accuracy without knowing the actual answer? And what might be the difference if, say, there was an estimated 1,000,000 diatom species, or an even a much greater number, say 10 million? Projecting into the unknown may be fun but it is ultimately pointless, of interest only to those who understand taxonomy as a task, one that, at some point in the future, will be complete and one that only takes into account one rank, the species (e.g., May [78]). For these persons, it is as if taxonomy is not a science but merely an exercise is searching for every living thing on the planet, giving it a name and handing over the data to those immersed in the "proper" experimental sciences to give meaning to this mass of data (May [78]: "Important though such considerations are, I think a more pressing and more basic utilitarian reason for studying and cataloguing diversity is because it is a prerequisite to understanding how biological systems work;" "Once you have finished counting [identifying] diatoms, the real fun begins" (Telford, bit.ly/2VW46Lt). With apologies to Hutchinson [79], Haldane [80], and Mann and Vanormelingen [73], whatever reasons the "creator" may have had for "An inordinate fondness for beetles," it is us humans who appear to have an unhealthy admiration for numbers and attribute to them a significance they may never have had or ever will.

2.8.3 What Do We Know?

Estimation of published diatom *binomial names* has been calculated at around 75,000 Kociolek, pers. comm. Although estimates vary widely concerning the number of published *names*, as opposed to the number of described *species*, many taxa described by legitimately published names have never been encountered a second time, not since their original description, nor do some have *any* representative specimens in *any* collection (an excellent non-diatom study on "the taxonomic significance of species that have only been observed once" is Thessen et al. [81]). Nevertheless, one could assume they have some empirical content as in most cases there must have been a reason to distinguish one species (taxon) from another. There are many examples, one will suffice: Consider *Fragilaria gieskesii* Cholnoky ([82], p. 168, pl. 25, fig. 31). Known only from its type description, although specimens (as slides) were sent to various museums ([83], p. 38), it has never been encountered or studied since its description (Karthick et al. in prep.). Searching for the name using any search engine yields less than a handful of results, most as records in databases.

Alternatively, there are a number of binomial names that act as an umbrella for an undescribed diversity, usually common species. Consider the taxon *Fragilariforma virescens*, normally thought of as a cosmopolitan species recorded from many localities and appears in many regional floras from around the world. A Google search (1/2/2019) of the name yielded over 7000 hits; an alternative search using its older name of *Fragilaria virescens* yielded a further 11,000+ hits. It would appear that, if nothing else, many are able to identify this species as specimens get the name. Related to the

name are in excess of 80 varieties and forms. Resolution is achieved by the inspection of *actual specimens*, including the types of each of these 80 names. Doing so suggests that for *Fragilariforma virescens* there are at least 12 species hidden under that name (Williams in prep.). Thus, in the fullness of time, what was once considered just one species will be many—and the many will have significant distributions. Hidden diversity, then, may be lurking in collections that already exist in our museums [84].

Finally, many of the recorded names may simply be errors. For example, the diatom name "*Synedra bipes*" is attributed to a person called Roll in the online catalog *Diatombase* (bit.ly/2Pnxzvd): the author is Yakiv V. Roll (1887–1961, www.ipni.org). What is "*Synedra bipes*?" The name first appeared on page 560 of the catalog of names in Gollerbach and Krasavina [85]. It apparently appears as a taxon name in the Roll publication. The German title of Roll's paper was included in the printed version of VanLandingham's index (Roll [86] in VanLandingham [87], p. 4223) but no page was indicated for the name "*Synedra bipes*" ([87] p. 3903). Inspection of Roll's paper in the *Archives Russes de Protistologie* yielded the following information: on pages 14, 15, 19, and 40 the name "*Synedra bipes*" does indeed appear, but it is attributed to William Smith ("W. Sm.") and thus it is most likely a spelling error for *Synedra biceps* W. Smith ([88], p. 69, pl. 11, fig. 83). It becomes more complicated. Smith's *Synedra biceps* really belongs in the genus *Eunotia*. There is an earlier use of the name *Synedra biceps* by Kützing, which belongs in *Ulnaria*. So, although the name "*Synedra bipes*" does appear in print it is an obvious spelling error but it is still not clear what it is without a specimen (see below): it needs deleting from the record as no such species exists for that name, nor, as far as is known, are there any specimens attached to the name. Technically, the name should be referred to as a *designation* (from the glossary of the current Code: "the term used for what appears to be a name but that (1) has not been validly published and hence is not a name in the sense of the *Code* (Art. 6.3) or (2) is not to be regarded as a name (Art. 20.4 and 23.6)," Turland et al. [4]). Interestingly, a Google search (1/2/2019) for "*Synedra bipes*" yields roughly 8 hits. Of those, two refer to the *Diatombase* entry, three form part of the GBIF (Global Biodiversity Information Facility) record, and the remaining three records have the same spelling error for *Synedra biceps* (e.g., Lilitskaya [89], p. 272). Both *Diatombase* [90, 91] and GBIF ("the Global Biodiversity Information Facility is an international network and research infrastructure funded by the world's governments and aimed at providing anyone, anywhere, open access to data about all types of life on Earth," www.gbif.org) are standard references for those wishing to learn of taxon diversity. GBIF is linked to *Diatombase*. "*Synedra bipes*" has been assigned a DOI in GBIF (see bit.ly/2UxE9jz) and an *lsid* (Life Science Identifier[4]) (bit.ly/2PkbPAu) in *Diatombase*.

Thus, many names remain in circulation simply for a lack of any specific knowledge concerning their validity—and these names are harvested for Big Data projects. It seems to be of some importance, then, to at least attempt to deal with this abundance of names in the literature now entering into significant databases.

2.9 Specimens

> Fundamental to DNA barcoding is a sound knowledge base where the DNA sequence is anchored to a known species that has been identified using classical morphology (voucher specimen) [92].

It seems obvious that the *only* important factor is to have specimens, which may be of various kinds, the most well-known being *type specimens* and *voucher specimens*. As Theresa Culley notes of voucher specimens: "As a *preserved* specimen of an *identified* taxon deposited in a permanent and accessible storage facility, the voucher serves as the *supporting material* for published studies of the taxon and ensures that the *science is repeatable*" (Culley [93] all emphasis mine; see also Robinson [94]). Type specimens, on the other hand, are more about anchoring names to an object:

> A name, therefore, has a type and a type belongs to a taxon, thus a taxon does not have a type but may *include* one. Be aware that a type is not necessarily that most typical (i.e., normal) or adequate example of a taxon, even though ideally it should be if it is to provide the link between name and taxon [95].

Consider one large diatom specimen collection housed in the NHM (bit.ly/2yMSu0S). It contains over 350,000 slides. Of those, at least 12,000 are types. Yet, with respect to the collection as a whole, in the last 20 years, roughly 65% of the specimens have never been looked at since their deposition. In a very crucial sense, *all* specimens should be considered voucher specimens.

Any particular species concept is based on a varying number of specimens from $n = 1$ to $n = \geq 1$. Voucher specimens are but one kind from whatever n happens to be; type specimens are but one kind from whatever $n =$ happens to be, but supply the name. In short, *all* specimens are voucher specimens; some might be named correctly, others not—but none should be neglected. And without them, we have literally nothing (see the "*Synedra bipes*" example above).

[4] "The LSID concept introduces a straightforward approach to naming and identifying data resources stored in multiple, distributed data stores in a manner that overcomes the limitations of naming schemes in use today," www.lsid.info

All of these details deal with *taxon discovery*. For identification, one deals with specimens collected in the here and now. Yet, rather than, or in addition to, quests for new technology or perfect data to solve outstanding problems, one might profitably turn to the large collections around the world, specimens designed for taxonomic research, utilize the concept of synapomorphy to *define* taxa (at all ranks) and then *describe* taxa with a view to determining a process of identification. It may not increase the speed of the endeavor, it may not satisfy all the apparent "users" of taxonomy but it will increase accuracy and, more crucially, will increase our knowledge of the world we live in.

2.10 Conclusions

After decades of neglect, taxonomy appears to be changing, adopting new technology and new ideas, enabling the creation of new interactive, illustrated, and online taxonomies ([96], for diatoms see *Diatoms of North America* and *Freshwater Diatom Flora of Britain and Ireland*). While the revolution in taxonomy gains momentum, simultaneously the current biodiversity crisis threatens many of the world's species with imminent extinction. What we fail to get right the first time will be lost forever: the advance of taxonomic knowledge must be accelerated [97]. Yet, there is little appreciation of past achievements, such as that of Candolle, who teased apart artificial and natural classifications, alongside the work of countless individuals who have collected, preserved, and studied a veritable avalanche of specimens, many ending up in museum collections. With respect to identification, there seems to be numerous useful tools, new technologies, and new kinds of data. With respect to discovery, finding a natural classification requires more thought. In time honored fashion, classifications emerge from various sources, by various persons (or groups), the most recent being understood as the most up to date and hence the most modern, regardless of how it was determined, or what its relationship to evidence might be—one "system" preferred over another for no good reason than preference for one authority over another, a form of bookkeeping [29]. These authoritarian classifications serve no purpose. The equation for taxon discovery is simple: evidence (characters, synapomorphies) yield conclusions (taxa). Diversity is captured in a classification, in its entirety, not just at the species rank: "Extending one's vision of real biology beyond the species neither narrows nor dilutes the subject; rather it helps to discriminate actual species-level phenomena" ([1], p. 559). And identification can only follow discovery.

References

1. Nelson, G., Ladiges, P.: Biodiversity and biogeography. J. Biogeogr. **30**, 1285–1296 (2003)
2. Lange-Bertalot, H., Ulrich, S.: Contributions to the taxonomy of needle-shaped Fragilaria and Ulnaria species. Lauterbornia. **78**, 1–73 (2014)
3. Nelson, G., Patterson, C.: Cladistics, sociology and success: a comment on Donoghue's critique of David Hull. Biol. Philos. **8**(4), 441–443 (1993)
4. Turland, N.J., et al.: International Code of Nomenclature for Algae, Fung and Plants (Shenzhen Code), Adopted by the Nineteenth International Botanical Congress Shenzhen, China, July 2017 (2018)
5. Sigwart, J.D.: What Species Mean: A User's Guide to the Units of Biodiversity. CRC Press, Boca Raton (2018)
6. Bessey, C.E.: The modern conception of the structure and classification of desmids: with a revision of the tribe and a rearrangement of the North American genera. Trans. Am. Microsc. Soc. **22**, 89–98 (1901)
7. Frankovich, T.A., Ashworth, M.P., Sullivan, M.J., Theriot, E.C., Stacy, N.I.: Epizoic and apochlorotic *Tursiocola* species (Bacillariophyta) from the skin of Florida manatees (*Trichechus manatus latirostris*). Protist. **169**(4), 539–568 (2018)
8. Leipe, D., et al.: The stramenopiles from a molecular perspective: 16S-like rRNA sequences from *Labyrinthuloides minuta* and *Cafeteria roenbergensis*. Phycologia. **33**(5), 369–377 (1994)
9. Ruggiero, M.A., et al.: A higher level classification of all living organisms. PLoS One. **10**(4), e0119248 (2015)
10. Julius, M.L., Theriot, E.C.: The diatoms: a primer. In: Smol, J.P., Stoermer, E.F. (eds.) The Diatoms: Applications for the Environmental and Earth Sciences, pp. 23–54 (2010)
11. Theriot, E.C.: Diatoms. In: eLS. Wiley, New York (2001)
12. Smol, J.P., Stoermer, E.F.: The Diatoms: Applications for the Environmental and Earth Sciences. Cambridge University Press, Cambridge (2010)
13. de Candolle, A.P.: Théorie élémentaire de la botanique, ou, Exposition des principes de la classification naturelle et de l'art de décrire et d'étudier les végétaux. Deterville, Paris (1819)
14. Drouin, J.-M.: Classification des sciences et classification des plantes chez Augustin-Pyramus de Candolle. Rev. Synth. **115**(1–2), 149–165 (1994)
15. Drouin, J.-M.: Un Botaniste Philosophe: Augustin-Pyramus de Candolle (1778-1841). Actes du colloque «Voyages en botanique» des 16 et 17 juin 2005 à Besançon, 1–9 (2006)
16. Drouin-Hans, A.-M., Drouin, J.-M.: Les idées pédagogiques d'Augustin-Pyramus et d'Alphonse de Candolle. Rev. Hist. Sci. **51**, 507–534 (1998)
17. Williams, D.M., Ebach, M.: Cladistics: A Guide to Biological Classification. Cambridge University Press, Cambridge (2020)
18. Taylor, J.C., Cocquyt, C.: Diatoms from the Congo and Zambezi basins-Methodologies and identification of the genera. ABC Taxa. **16**, 1–353 (2019)
19. Round, F.E., Crawford, R.M., Mann, D.G.: Diatoms: Biology and Morphology of the Genera. Cambridge University Press, Cambridge (1990)
20. Bey, M., Ector, L.: Atlas des diatomées des cours d'eau de la région Rhône-Alpes, Tomes 1-6. DREAL Rhône-Alpes (2013)
21. European Commission, 2000. Directive 2000/60/EC of the European Parliament and of the Council of 23 October 2000 establishing a framework for community action in the field of water policy. Off. J. Eur. Communities 2000

22. Cantonati, M., Kelly, M., Lange-Bertalot, H.: Freshwater Benthic Diatoms of Central Europe. Koeltz Botanical Books, Schmitten-Obereifenberg (2018)
23. Hofmann, G., Werum, M., Lange-Bertalot, H.: Diatomeen im Süsswasser-Benthos von Mitteleuropa: Bestimmungsflora Kieselalgen für die ökologische Praxis; über 700 der häufigsten Arten und ihrer Ökologie. Gantner (2011)
24. Krammer, K., Lange-Bertalot, H.: Bacillariophyceae 1. Teil: Naviculaceae. Süsswasserflora von Mitteleuropa, 2/1, Gustav Fischer Verlag, Stuttgart (1986)
25. Krammer, K., Lange-Bertalot, H.: Bacillariophyceae 3. Teil: Centrales, Fragilariaceae, Eunotiaceae. Süsswasserflora von Mitteleuropa, 2/3, Gustav Fischer Verlag, Stuttgart (1991)
26. Krammer, K., Lange-Bertalot, H.: Bacillariophyceae 4. Teil: Achnanthaceae. Kritische Ergänzungen zu *Navicula* (Lineolatae) und *Gomphonema*. Süsswasserflora von Mitteleuropa, 2/4, Gustav Fischer Verlag, Stuttgart (1991)
27. Lange-Bertalot, H., Krammer, K.: Bacillariophyceae 2. Teil:Bacillariaceae, Epithemiaceae, Surirellaceae. Süsswasserflora von Mitteleuropa, 2/2, Gustav Fischer Verlag, Stuttgart (1988)
28. Griffing, L.R.: Who invented the dichotomous key? Richard Waller's watercolors of the herbs of Britain. Am. J. Bot. **98**(12), 1911–1923 (2011)
29. Williams, D.M.: Book review. Willdenowia. **47**(3), 341–343 (2017)
30. Diderot, D.: Œuvres, tome I, Philosophie. Laurent Versini, Paris (1994)
31. Nelson, G.: Resemblance as evidence of ancestry. Zootaxa. **2946**, 137–141 (2011)
32. Cox, E.: Coscinodiscophyceae, Mediophyceae, Fragilariophyceae, Bacillariophyceae (Diatoms). Syllabus of Plant Families. Adolf Engler's Syllabus der Pflanzenfamilien Part 2/1, 64–103 (2015)
33. Adl, S.M., et al.: Revisions to the classification, nomenclature and diversity of eukaryotes. J. Eukaryot. Microbiol. **66**(1), 4–119 (2019)
34. Frey, W.: Syllabus of Plant Families-A. Engler's Syllabus der Pflanzenfamilien Part 2/1: Photoautotrophic Eukaryotic Algae. Wolfgang Frey, Schweizerbart (2015)
35. Medlin, L.K., Kaczmarska, I.: Evolution of the diatoms: V. Morphological and cytological support for the major clades and a taxonomic revision. Phycologia. **43**(3), 245–270 (2004)
36. Doyle, J.J.: Gene trees and species trees: molecular systematics as one-character taxonomy. Syst. Bot. **17**, 144–163 (1992)
37. Doyle, J.J., Davis, J.I.: Homology in molecular phylogenetics: a parsimony perspective. In: Molecular Systematics of Plants 2, pp. 101–131. Columbia University Press, New York (1998)
38. Stepanova, V., Gogorev, R.: Sistema klassa Fragilariophyceae Round emend. Gogorev et Stepanova (Bacillariophyta). Novosti Sistematiki Nizshih Rasteniy. **49**, 75–91 (2015)
39. Medlin, L.K.: Opinion: can coalescent models explain deep divergences in the diatoms and argue for the acceptance of paraphyletic taxa at all taxonomic hierarchies? Nova Hedwigia. **102**(1–2), 107–128 (2016)
40. Medlin, L.K.: Evolution of the diatoms: major steps in their evolution and a review of the supporting molecular and morphological evidence. Phycologia. **55**(1), 79–103 (2016)
41. Theriot, E.C., Ashworth, M., Ruck, E., Nakov, T., Jansen, R.K.: A preliminary multigene phylogeny of the diatoms (Bacillariophyta): challenges for future research. Plant Ecol. Evol. **143**(3), 278–296 (2010)
42. Li, C.L., et al.: New insights into *Plagiogrammaceae* (Bacillariophyta) based on multigene phylogenies and morphological characteristics with the description of a new genus and three new species. PloS One. **10**(10), e0139300 (1995)
43. Lobban, C.S., Ashworth, M.P., Car, A., Herwig, W., Ulanova, A.: *Licmosphenia* revisited: transfer to *Licmophora*, redescription of *L. clevei* Mereschkowsky and descriptions of three new species. Diatom Res. **30**(3), 227–236 (2015)
44. Adl, S.M., et al.: The revised classification of eukaryotes. J. Eukaryot. Microbiol. **59**(5), 429–514 (2012)
45. Berney, C., et al.: UniEuk: time to speak a common language in protistology! J. Eukaryot. Microbiol. **64**, 407–411 (2017). https://doi.org/10.1111/jeu.12414
46. Williams, D.M.: Some notes on the classification of *Fragilaria*, *Synedra* and their sub-groups. Nova Hedwig. Beih. **130**, 17 (2006)
47. Hamilton, P.B., Poulin, M., Yang, J.-R., Klöser, H.: A new diatom genus, *Porannulus* (Bacillariophyta), associated with marine sponges around King George Island, South Shetland Islands, Antarctica. Diatom Res. **12**(2), 229–242 (1997)
48. Hasle, G.R., Syvertsen, E.E., von Quillfeldt, C.H.: *Fossula arctica* gen. nov., spec. nov., a marine Arctic araphid diatom. Diatom Res. **11**(2), 261–272 (1996)
49. Furey, P.C., Mayama, S., Lowe, R.L., Catenazzi, A.: *Frankophila wayqechae* sp. nov., a new aerophilic diatom species from the Peruvian Andes, South America. Diatom Res. **27**(3), 165–175 (2012)
50. Lange-Bertalot, H.: *Frankophila*, *Mayamaea* und *Fistulifera*: drei neue gattungen der klasse Bacillariophyceae. Arch. Protistenkd. **148**(1–2), 65–76 (1997)
51. Lowe, R.L., Morales, E., Kilroy, C.: *Frankophila biggsii* (Bacillariophyceae), a new diatom species from New Zealand. N. Z. J. Bot. **44**(1), 41–46 (2006)
52. Mayama, S., Idei, M.: Fine structure of two *Hygropetra* species, *Hygropetra gelasina* sp. nov. and *Hygropetra balfouriana* (Bacillariophyceae) and the taxonomic position of the genus with special reference to *Frankophila*. Phycol. Res. **57**(4), 290–298 (2009)
53. Rivera, P., Cruces, F.: *Frankophila sudamericana* sp. nov., a new diatom species (Bacillariophyta) found in Salar de Aguas Calientes and Salar de Huasco, high altitude Andean localities in northern Chile. Gayana Bot. **72**(2), 373 (2015)
54. Rumrich, U., Lange-Bertalot, H., Rumrich, M.: Diatomeen der Anden: Von Venezuela bis Patagonien/Feuerland und zwei weitere Beiträge. Iconographia Diatomol. **9**, 1–673 (2000)
55. Williams, D.M.: *Synedra, Ulnaria*: definitions and descriptions—a partial resolution. Diatom Res. **26**(2), 149–153 (2011)
56. Thomas, E.W., Stepanek, J.G., Kociolek, J.P.: Historical and current perspectives on the systematics of the 'enigmatic' diatom genus *Rhoicosphenia* (Bacillariophyta), with single and multimolecular marker and morphological analyses and discussion on the monophyly of 'monoraphid' diatoms. PLoS One. **11**(4), e0152797 (2016)
57. Takhtadzhian, A.L.: Die evolution der angiospermen. Fischer, Jena (1959)
58. Takhtadzhian, A.L.: Evolutionary Trends in Flowering Plants. Columbia University Press, New York (1991)
59. Williams, D.M.: Spines and homologues in 'araphid' diatoms. Plant Ecol. Evol. **152**(2), 150–162 (2019). https://doi.org/10.5091/plecevo.2019.1597
60. Sims, P.A., Williams, D.M., Ashworth, M.: Examination of type specimens for the genera *Odontella* and *Zygoceros* (Bacillariophyceae) with evidence for the new family Odontellaceae and a description of three new genera. Phytotaxa. **382**(1), 1–56 (2018)
61. Ross, R.: Generic limits in the Biddulphiaceae as indicated by the scanning electron microscope. In: Scanning Electron Microscopy: Systematic and Evolutionary Applications, pp. 155–177. Academic, London (1971)
62. Cairns, J., Dickson, K., Slocomb, J.: The ABC's of diatom identification using laser holography. Hydrobiologia. **54**(1), 7–16 (1977)

63. Pappas, J., Kociolek, P., Stoermer, E.F.: Quantitative morphometric methods in diatom research. Nova Hedwig. Beih. **143**, 281–306 (2014)
64. Evans, K.M., Mann, D.G.: A proposed protocol for nomenclaturally effective DNA barcoding of microalgae. Phycologia. **48**, 70–74 (2009)
65. Hamsher, S.E., Evans, K.M., Mann, D.G., Poulíčková, A., Saunders, G.W.: Barcoding diatoms: exploring alternatives to COI-5P. Protist. **162**(3), 405–422 (2011)
66. Rimet, F., et al.: The potential of high throughput sequencing (HTS) of natural samples as a source of primary taxonomic information for reference libraries of diatom barcodes. Fottea. **18**(1), 37–54 (2018)
67. Rimet, F., et al.: R-Syst:: diatom: an open-access and curated barcode database for diatoms and freshwater monitoring. Database. **2016**, baw016 (2016)
68. Piredda, R., et al.: Diatom diversity through HTS-metabarcoding in coastal European seas. Sci. Rep. **8**(1), 18059 (2018)
69. Vasselon, V., Rimet, F., Tapolczai, K., Bouchez, A.: Assessing ecological status with diatoms DNA metabarcoding: scaling-up on a WFD monitoring network (Mayotte island, France). Ecol. Indic. **82**, 1–12 (2017)
70. Apothéloz-Perret-Gentil, L., Cordonier, A., Straub, F., Iseli, J., Esling, P., Pawlowski, J.: Taxonomy-free molecular diatom index for high-throughput eDNA biomonitoring. Mol. Ecol. Resour. **17**(6), 1231–1242 (2017)
71. du Buf, H., Bayer, M.M.: Automatic diatom identification. World Scientific, Singapore (2002)
72. An, S.M., Choi, D.H., Lee, J.H., Lee, H., Noh, J.H.: Identification of benthic diatoms isolated from the eastern tidal flats of the Yellow Sea: comparison between morphological and molecular approaches. PLoS One. **12**(6), e0179422 (2017)
73. Mann, D.G., Vanormelingen, P.: An inordinate fondness? The number, distribution. And origins of diatom species. J. Eukaryot. Microbiol. **60**(4), 414–420 (2013)
74. Guiry, M.D.: How many species of algae are there? J. Phycol. **48**(5), 1057–1063 (2012)
75. Burgin, C.J., Colella, J.P., Kahn, P.L., Upham, N.S.: How many species of mammals are there? J. Mammal. **99**(1), 1–14 (2018)
76. Pimm, S.L., Joppa, L.N.: How many plant species are there, where are the. And at what rate are they going extinct? Ann. Mo. Bot. Gard. **100**(3), 170–177 (2015)
77. Stork, N.E., McBroom, J., Gely, C., Hamilton, A.J.: New approaches narrow global species estimates for beetles, insect and terrestrial arthropods. Proc. Natl. Acad. Sci. U.S.A. **112**(24), 7519–7523 (2015)
78. May, R.M.: Taxonomy as destiny. Nature. **347**(6289), 129–130 (1990)
79. Hutchinson, G.E.: Homage to Santa Rosalia or why are there so many kinds of animals? Am. Nat. **93**(870), 145–159 (1959)
80. Haldane, J.B.S.: What Is Life? Lindsay Drummond, London (1949)
81. Thessen, A.E., Patterson, D.J., Murray, S.A.: The taxonomic significance of species that have only been observed once: the genus *Gymnodinium* (Dinoflagellata) as an example. PLoS One. **7**(8), e44015 (2012)
82. Cholnoky, B.J.: Ein Beitrag zur Kenntnis der Diatomeenflora von Hollandisch-Neuguinea. Nova Hedwigia. **5**, 157–198 (1963)
83. Schoeman, F.R.: The B.J. Cholnoky Diatom Slide Collection. Council for Scientific and Industrial Research, Pretoria (1981)
84. Bebber, D.P., et al.: Herbaria are a major frontier for species discovery. Proc. Natl. Acad. Sci. U.S.A. **107**(51), 22169–22171 (2010)
85. Gollerbakh, M.M., Krasavina, L.K.: Vodorosli: svodnyi ukazatel'k otechestvennym bibliografiiam po vodorosliam za 1737-1960 gg. BAN, Leningrad (1971)
86. Roll, J.: Untersuchungen am Phytoplankton der Binnengewasser in Ukraina. Arch. Russ. Protistol. **5**, 1–44 (1926)
87. VanLandingham, S.L.: Catalogue of the Fossil and Recent Genera and Species of Diatoms and Their Synonyms: Part VII: *Rhoicosphenia* Through *Zygoceros.* J. Cramer, Vaduz (1979)
88. Smith, W., West, T.: A Synopsis of the British Diatomaceae: With Remarks on Their Structure, Functions and Distribution; and Instructions for Collecting and Preserving Specimens. Smith and Beck, Van Voorst (1853)
89. Lilitskaya, G.: Bacillariophyta of Small Water Bodies of Kiev (Ukraine). 2. Araphid Diatoms: *Fragilariaceae*, *Diatomacea* and *Tabellariaceae*. Int. J. Algae. **18**(3), 225–246 (2016)
90. Kociolek, J., et al.: DiatomBase. http://www.diatombase.org
91. Vandepitte, L., et al.: A decade of the World Register of Marine Species–general insights and experiences from the Data Management Team: where are we, what have we learned and how can we continue? PLoS One. **13**(4), e0194599 (2018)
92. Kelly, M., et al.: A DNA Based Diatom Metabarcoding Approach for Water Framework Directive Classification of Rivers. SC140024/R. Environment Agency, Bristol (2018)
93. Culley, T.M.: Why vouchers matter in botanical research. Appl. Plant Sci. **1**(11), 1300076 (2013)
94. Robinson, W.H.: Type specimens vs. voucher specimens. Syst. Biol. **24**(1), 110–111 (1975)
95. Turland, N.J.: The Code Decoded: A User's Guide to the International Code of Nomenclature for Algae, Fung, and Plants. Koeltz Scientific Books, Königstein (2013)
96. Wheeler, Q.D.: Taxonomic triage and the poverty of phylogeny. Philos. Trans. R. Soc. Lond. B Biol. Sci. **359**(1444), 571–583 (2004)
97. Kolbert, E.: The Sixth Extinction: An Unnatural History. Henry Holt and Company, New York (2014)

Diatom Taxonomy and Identification Keys

3

Saúl Blanco

Abstract

Correct identification of diatom taxa is indispensable for diatom-based water quality studies, as well as for biotechnological applications. Biological applications of taxonomy include the identification of taxa from particular specimens. In this regard, identification keys, that use a predetermined set of characters to identify a given individual, are not commonly employed by diatom specialists due to the extreme biological diversity found in this group of microalgae. This chapter reviews previous attempts of using taxonomic keys for diatom identification, highlighting the pros and cons of the use of this and similar methods. The main morphological features found in common freshwater diatom genera are briefly presented, together with an account of the historical development of technologies used for species description.

3.1 The Value of Taxonomic Keys for Applied Diatomology

Until the apparition of modern identification methods (numerical taxonomy, electron microscopy, metabarcoding, etc.), taxonomy has not been regarded as an attractive research topic in Biological Sciences [1]. Traditional taxonomy was based on intuitive or subjective decisions concerning similarity, which depend mostly on experience and trained skills [2]. Despite identification keys have long played a fundamental part with regard to practical biological identification [3], their use in diatomology is not as spread as in other fields of Botany. Within microalgae, diagnosis is often based on the "general appearance" of the specimen [4] or on some critical characters [5], by means of visual comparison with reference floras, trying to match specimens with illustrations [6, 7]. This approach, however, quickly becomes intractable when the number of taxa grows exponentially, as in the case of diatoms. Given there may be tens of different species in a common freshwater sample, the "classical" identification procedure requires large amounts of work to spot diagnostic characters, which evidently possess a big job for diatomists [8].

Keys to plants and animals were constructed by biologists more than two centuries ago, and methods of constructing them were discussed much earlier [6]. Keys provide basically a sequence of questions ("tests") about the features exhibited by the organism to be identified, with alternative choices that depend upon the results of previous answers. The use of keys, in contrast to visual matching, ensures that relevant characters are fully considered, thus making the identification process substantially more objective [9]. Diatomists usually design their keys manually, although algorithms for the automated creation of identification keys are provided in the literature [10, 11]. The use of computers leads to optimal identification keys which minimize the number of tests [2, 12], but few tools can help to generate identification keys without expert's supervision [8].

The process usually starts with the elaboration of a data matrix (X taxa × Y characters), entries in each cell consisting of the value that the character takes for a given taxon [4]. Choosing adequate diagnostic characters is a critical step. The ideal character should combine ease of observation and high information content (the ability to separate taxa, see [13]), that is, characters that have the highest consistency

S. Blanco (✉)
Facultad de Ciencias Biológicas y Ambientales, Departamento de Biodiversidad y Gestión Ambiental, Universidad de León, León, Spain

Laboratorio de diatomología y calidad de aguas, Instituto de Investigación de Medio Ambiente, Recursos Naturales y Biodiversidad, León, Spain
e-mail: degsbl@unileon.es; sblal@unileon.es

G. Cristóbal et al. (eds.), *Modern Trends in Diatom Identification*, Developments in Applied Phycology 10,
https://doi.org/10.1007/978-3-030-39212-3_3

within taxa, but separate the set of taxa under consideration into approximately equal halves [2]. Characters combining both features should be placed in the first steps of the key [10]. Qualitative characters (particularly valve outline) in the case of diatoms are difficult to define and are more likely to confuse, but on the other hand quantitative characters (valve size, stria density) exhibit continuous variation [9], which are difficult to deal with taxonomically [13, 14]. Other desirable properties of diagnostic characters include (1) permanence throughout the life cycle, (2) presence in all the individuals, and (3) independence of the status of other characters [9]. In this regard, diatom identification is often impaired by the presence of debris, incomplete individuals or very small populations that prevent the observation of size ranges or different perspectives (valve/connective views). The typology of colonies, with taxonomic relevance, is also frequently lost during slide preparation.

Authors of keys should bear in mind their eventual users, with probably different degrees of experience in diatom taxonomy. Most diatom keys usually start separating the "pennate" and "centric" groups, and this initial distinction may not be evident for certain taxa, e.g., *Cycotella austriaca* (a putative centric with bilateral symmetry) or *Cavinula pseudoscutiformis* (a pennate diatom with a roundish shape in valve view). The presence of a raphe, a distinctive character that separates "araphids," "monoraphids," and "biraphids" in the first steps of most keys, is hard to spot at first glance for the dilettante within the Bacillariaceae or the Eunotiaceae. It is therefore advisable to use reliable characters which can be easily observed to be included in the first steps of the key, considering not only the division criteria but also the future receptors of the keys [10, 13]. On the contrary, important characters visible to the user (e.g., the occurrence of the frustules in colonial filaments) may not feature in the key until a relatively late stage.

In diatomology, taxonomic identification presents particular problems. As a general rule, species-level determinations cannot be achieved from isolated individuals (valves or frustules), observing a whole population is often necessary to account for the whole morphologic/morphometric variability of the taxon, which has taxonomic relevancy (see in this chapter). Some keys handle the presence of quantitative characters by assigning a single representative value (e.g., the mean or the median) to such varying character, with an inherent loss of information [15]. Moreover, the occurrence of individuals in different perspectives (valve/connective view) may be imperative for certain species. Identification in this group is also impaired by the common presence of "species complexes" [16] or "cryptic taxa" which are difficult to disentangle even for the specialists. If any of the species included in a key are doubtfully distinct, then they will emerge as being difficult to identify by this or any other method, thus lowering the identification success rate [3]. In these cases, when a test is particularly troublesome, it is often necessary to follow the trail both ways, adding to the confusion [3]. When such key tests have uncertain outcomes, full identification cannot be guaranteed, as it is possible for several species to produce the same result [11]. If identification with certainty is impossible, either because too many characters are variable within taxa or because all assessments of character states are subject to error, probabilistic identification methods may be used [2]. These keys can compute a probability value for each determination, based on how often particular character states occur in taxa and, in some cases, the relative rates of occurrence of the taxa themselves [9].

The probability of a right determination is almost always improved by changing the structure of the key to make it as short as possible [17]. This is why, in extremely specious groups such as algae, key-based identification may be impractical. Prescott's famous key to identify 558 common freshwater genera [18] needs hundreds of steps to complete in the worst cases. Evidently, the more species in a key, the longer the average number of steps to an answer, and the more likely the user of the key strays from the path [5]. For instance, if the chance of answering correctly each test is, e.g., 0.9, when the key path length exceeds only six steps, the chances of getting a right answer fall below 50% [13]. Adding "reticulations" or alternative identification paths through the key usually improves the determination of certain species, but may diminish the overall probability of correct determination averaged over all taxa [17]. Additionally, if there exist taxa which are notably different from the others, it is often convenient to dispose of these first, at or near the beginning of the key [13].

A further difficulty is that taxonomic keys for algae are typically regional, and the degree to which such keys can be applied to larger or more distant geographic areas is always uncertain [19]. Due to the aforementioned reasons, taxonomic keys are relatively scarce in modern diatom literature. Most volumes in the collections *Bibliotheca diatomologica* and *Iconographia diatomologica* lack of them. *Diatoms of Europe,* which include a comprehensive account of known taxa arranged by genera—not only from Europe but also from other regions of the world—present useful "visual keys" aiding at the first delimitation of morphological groups. Published three decades ago, the second volume of the *Susswasserflora von Mitteleuropa* is still the most widely used taxonomic reference for diatoms, containing a detailed artificial key to the species level which was translated to English and French in 2000 [20]. At the genus level, the most accurate reference is the "tentative key for the determination of freshwater diatom genera" by the late P. Compère, available at bit.ly/2VnHXFC. Table 3.1 summarizes other widely used keys in phycological research (see also Chap. 1). Annex contains a friendly, visual key for the most important diatom genera found in world freshwaters.

Since 1960s to present, artificial intelligent technologies such as expert systems, decision trees, automatic learning,

Table 3.1 Taxonomic keys about or including diatoms. Keys dealing with specific taxonomic groups were excluded

References	Scope	Level
[21]	Freshwater algae	Mostly genera
[22]	Marine planktonic diatoms	Genera
[23]	Australian coastal diatoms	Species
[24]	Freshwater diatoms	Genera
[25]	Marine planktonic diatoms	Species
[26]	European freshwater benthic diatoms	Genera
[27]	Plankton diatoms of the west coast of North America	Species
[28]	Freshwater diatoms	Genera
[29]	British coastal diatoms	Genera
[30]	Freshwater algae common in water supplies and polluted waters	Genera
[31]	British freshwater diatoms	Genera
[32]	Diatoms from live material	Species
[33]	European freshwater benthic diatoms	Genera
[34]	River diatoms	Species
[35]	River periphytic microalgae	Genera
[36]	Algae of the western Great Lakes Area	Genera
[37]	Freshwater algae of North America	Genera
[38]	Algae of Korea	Species
[39]	Diatoms	Species

or multilayer perceptrons have led to the development of electronic, interactive, and online keys [40, 41]. Neural networks are also useful for practical botanical keys [3]. Calvo-Flores et al. [10] review available tools for generating interactive keys. In the field of diatomology, it is worth to mention in this regard the key to "Antarctic marine diatoms" (bit.ly/2P1ClhW), based on LUCID technology, and the key to "Common freshwater diatoms of Britain and Ireland" [42], that covers taxa most likely to be encountered in routine monitoring.

3.2 Overview on Diatom Morphology

Diatoms are a highly diversified group of microscopic algae with a wide distribution in both marine and freshwater aquatic ecosystems. About 400 new species are described every year, but 80% of newly erected taxa are only known from their respective type localities. The application of electron microscopy techniques since the 1950s explains to a certain extent such remarkable proliferation of new taxa, especially at the generic level, resulting in a nomenclatural instability due to the frequent and not always justified intergeneric transfers of certain species. As in the case of many other algal groups, the lack of genetic or physiological

Fig. 3.1 A living *Navicula* cell showing internal organelles

data leads to adopting a "morphological" species concept [43], this approach being followed by most diatomists. In this regard, the systematics and phylogeny of this group have been widely debated in recent years, particularly as a result of molecular studies that propose evolutionary relationships between taxa sometimes different to those inferred only from morphological data.

Silica (SiO_2) is the main constituent of diatoms, diatom cell is protected by a silica shell called *frustule* that gives it great hardness and strength. The frustules are composed of two halves that fit together, called *thecae*, the upper (*epitheca*) is always larger and partially envelops the lower (*hypotheca*). Each of these units is formed by a *valve* (respectively *epi-* and *hypovalve*) and a *cingulum* (*epi-* and *hypocingulum*). Different ornamentations are developed in the valve surface, allowing taxonomic identification. Longitudinally, in many species the valve is crossed by a thin furrow called *raphe*, which crosses the theca down to the protoplast (Fig. 3.1). Cell locomotion is possible thanks to the presence of a ribbon-shaped organelle formed by fibrils, which contracts rhythmically. Perpendicular to the raphe there is often a series of lines of perforations called *areole*, the succession of these in each line forms *striae*. Joining the two thecae is a cingulum formed by a variable amount of *copulae* that envelops the cell.

The protoplast fills the entire space delimited by the siliceous cell wall. The nucleus is commonly located in the central part of the cell and the chloroplasts are often marginal, usually one or two in the raphe-bearing diatoms and numerous and discoid in the araphid and centric diatoms. Four different pigment types are normally found within chloroplasts: chlorophyll, carotenes, carotenoids, and xanthophylls [44]. On the sides of the central plasma bridge, there are two large or several small vacuoles. The assimilation products are oils, accumulated forming drops that confer buoyancy to planktonic diatoms.

Figures 3.2, 3.3, 3.4, 3.5, and 3.6 synthesize the basic concepts of general diatom morphology (see also the Glossary). More detailed information is available in classic reference works such as Barber and Haworth [31] or Round et al. [45].

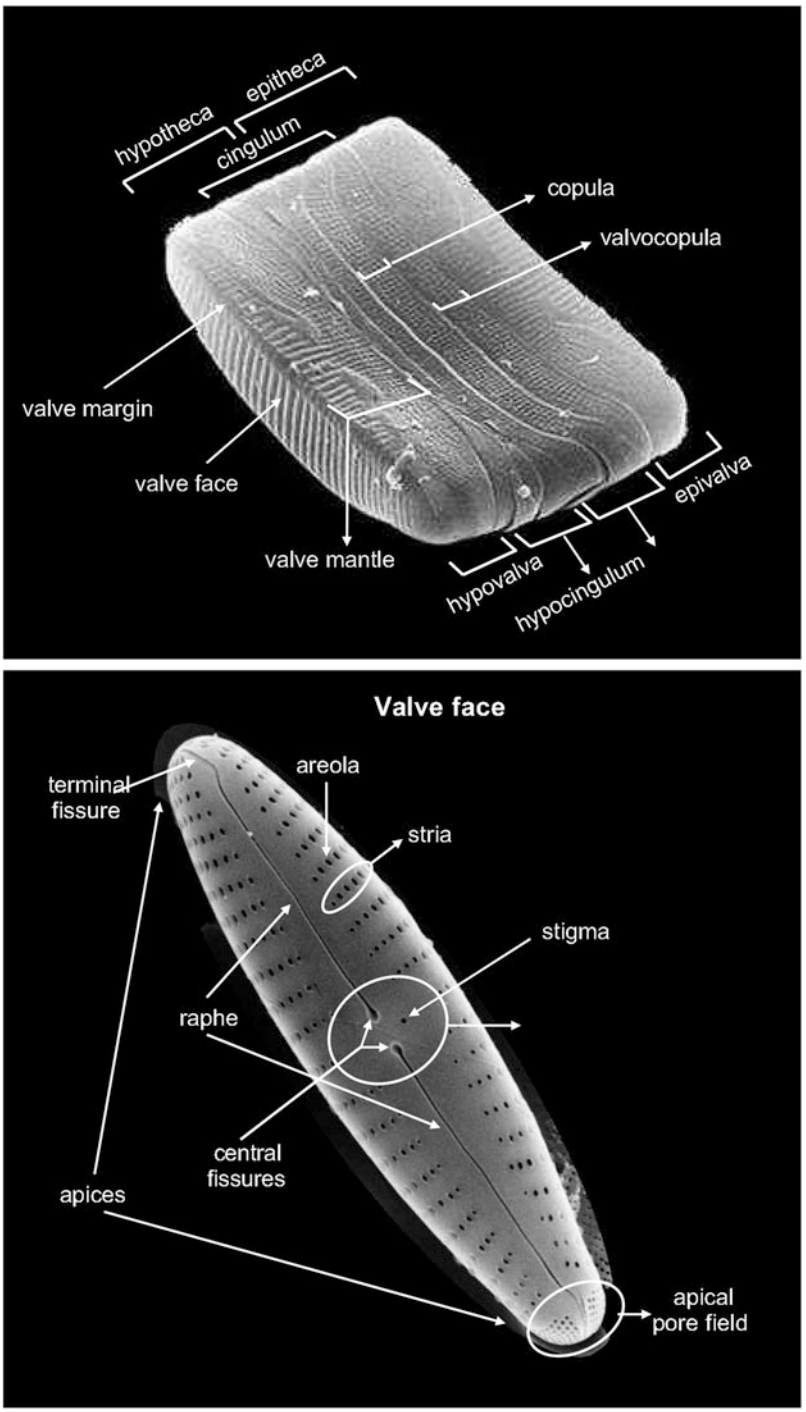

Fig. 3.2 Main morphological features observed in common freshwater diatoms

3.3 Diatom Illustrations: From Drawings to Electron Microscopy

Obtaining accurate, good quality illustrations is a key step in any taxonomic study. Since diatoms were recognized as a distinct class of aquatic microbes, phycologists have used illustrations to characterize virtually all described taxa. Illustrations have not only morphological or esthetic interest but they also serve to account for the differential details that allow species discrimination and provide a basis to evidence the morphologic/morphometric variability of studied populations. In Botany, illustrations are described as any "work of art or a photograph depicting a feature or features of an organism" [46], including drawings and microscopic photographs ("micrographs"). In order to be validly published, new diatom taxa must be accompanied by an illustration showing their distinctive morphological features. Moreover, until 1907 these illustrations sufficed to publish new diatoms, even with no accompanying descriptive texts. Illustrations

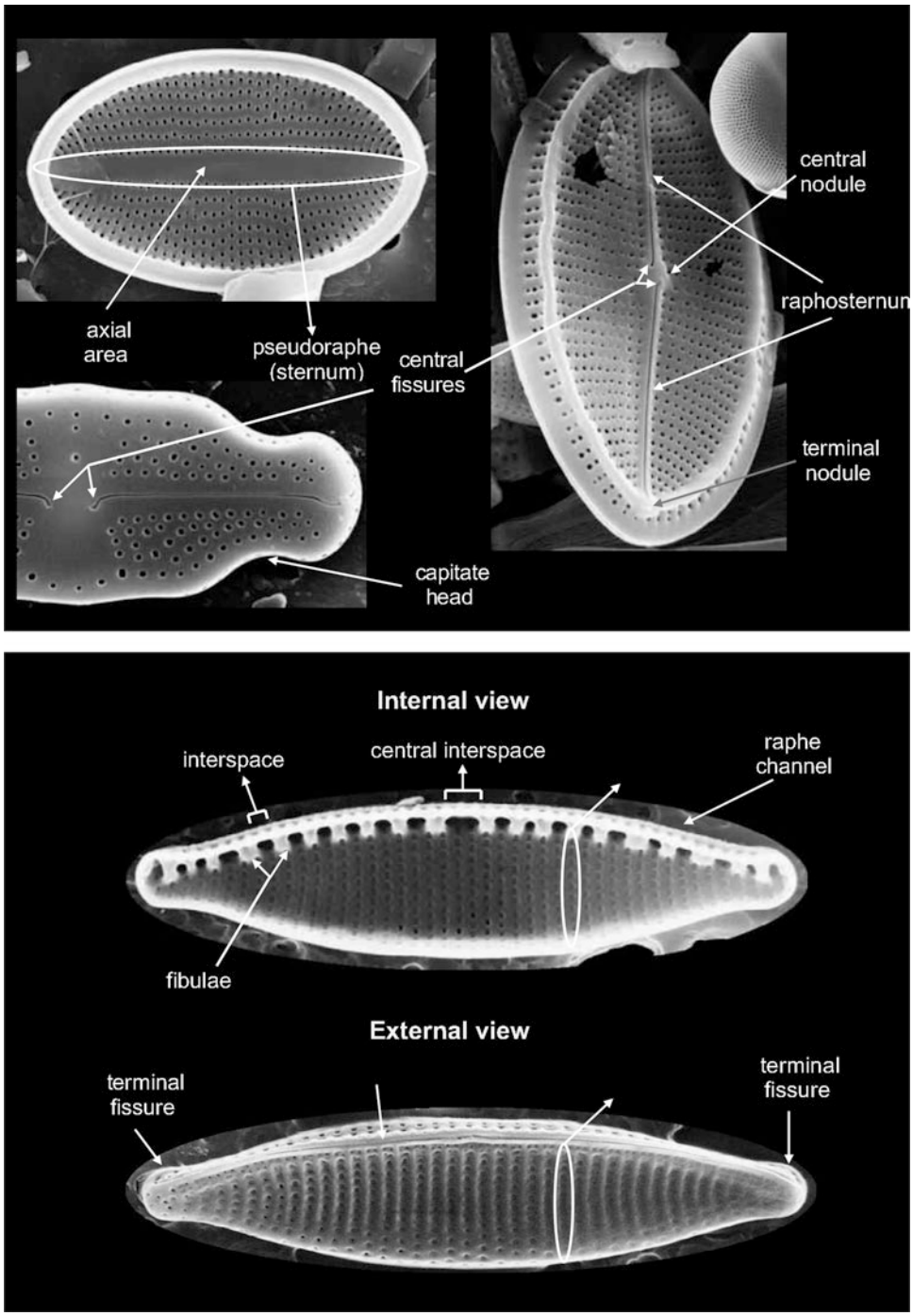

Fig. 3.3 Main morphological features observed in common freshwater diatoms (cont.)

served also to typify names, that is, to provide element(s) to which the species name is permanently attached; as of 2007 this provision only affects microalgae that are difficult to preserve in standard collections, which certainly is not the case of diatoms. These rules are based on the fact that diatom illustrations, contrary to other organisms, "may substantiate and visually reinforce the description of the diatom, even to the extent of practically standing alone for that purpose," as acknowledged by the famous microscopist Robert B. McLaughlin [47].

Diatom diagnoses should be illustrated with multiple images so that the user can form an adequate concept of the taxon [48]. Traditionally, diatoms are illustrated in the specialized literature by presenting several (usually >5) individuals (valves or frustules) forming "diminution series" and arranged in plates at 1500×. It must be noted, however, that if these illustrations constitute a nomenclatural type, all the organisms depicted must come from the same population, that is, they should have been collected by the same

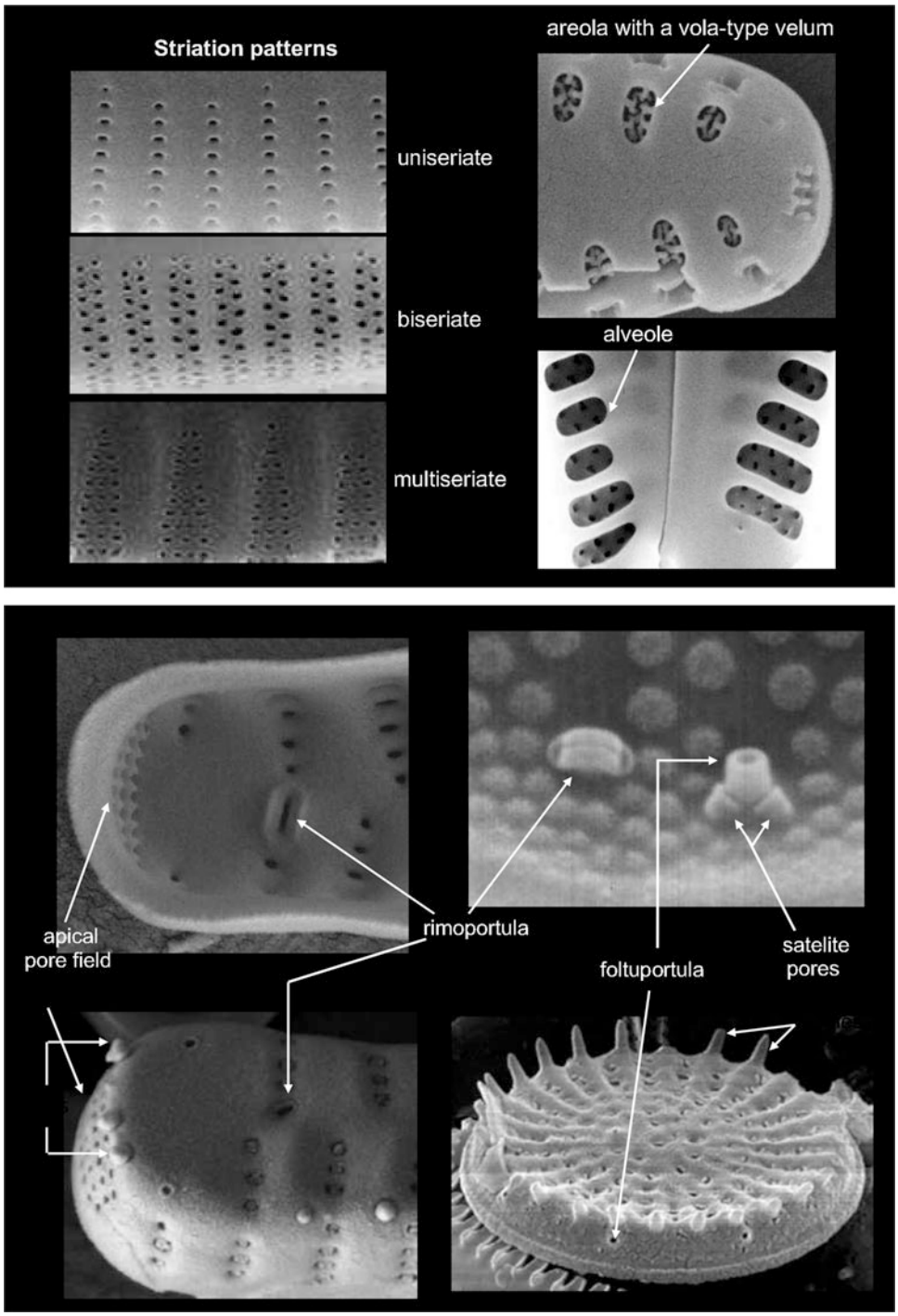

Fig. 3.4 Main morphological features observed in common freshwater diatoms (cont.)

collector(s), at the same place, and the same time. Blanco [49] explains how to deal in cases where these assumptions are not met.

Already in 1896 the diatomists Henri van Heurck noted in his notable *Treatise on the Diatomaceae* [39] that "a careful determination of any diatom is impossible without previously taking a good drawing of it." Drawings have traditionally been the most important medium for botanical illustration [41] because they are often better at representing a typical example than are photographs, which must necessarily represent the state in a specific individual [48]. In the context of taxonomic descriptions, drawings have several advantages over photographs, since (1) they can combine images from different focal planes, (2) they highlight certain diagnostic details, and (3) illustrate the specimen in a "standard elevation," thus facilitating comparison [50]. Besides, drawings can be easily idealized, leaving out some unimportant parts [41] (Fig. 3.7).

Diatom drawings contain mainly the salient information required for identification and thus may serve for typifi-

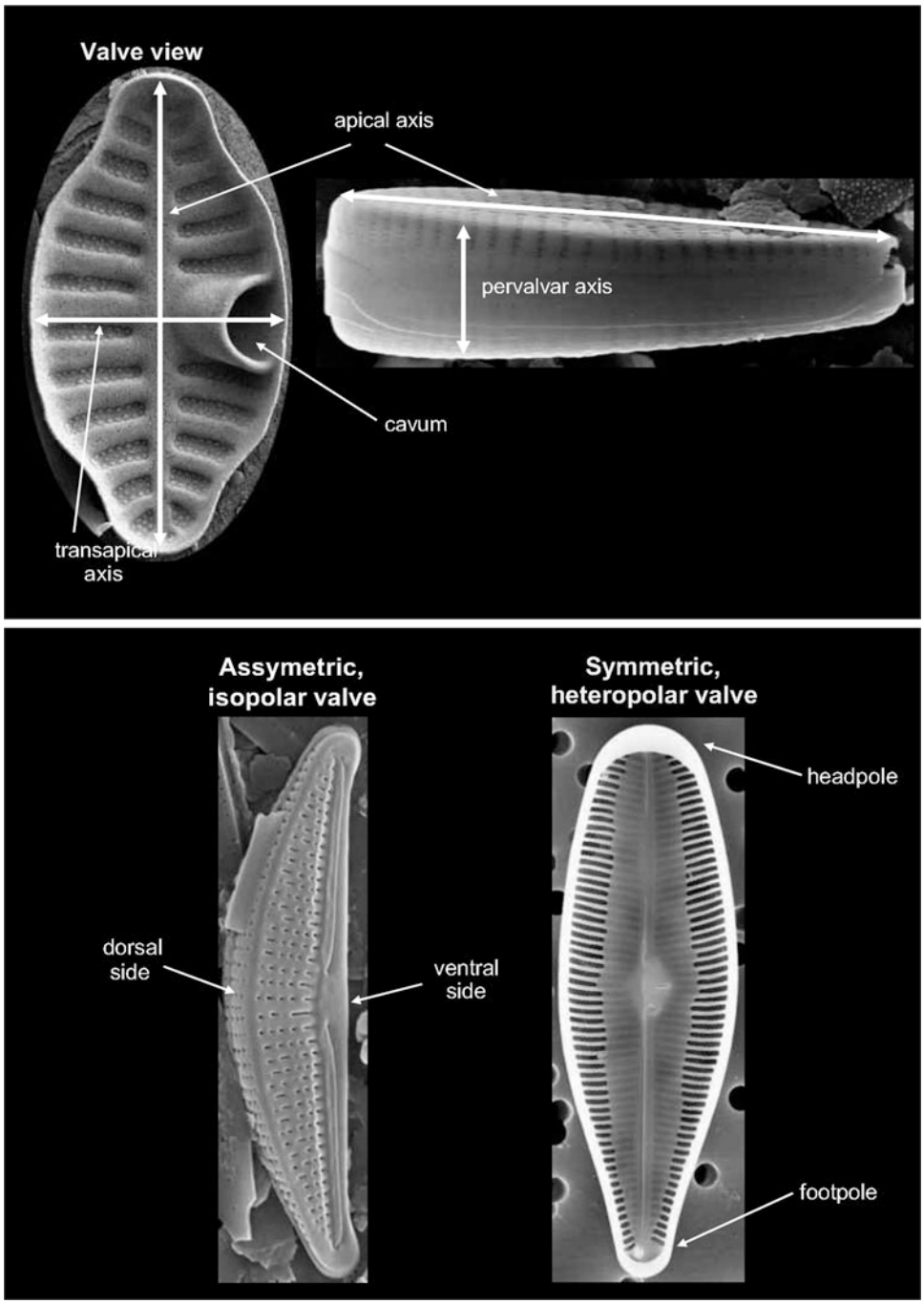

Fig. 3.5 Main morphological features observed in common freshwater diatoms (cont.)

cation purposes [52]. Type drawings often synthesize in a single (or few) figures the morphological characteristics found in many individuals or populations [53]. Actually, drawings have been continuously used by diatomists since the eighteenth century and even long after microphotography became available, e.g., the extensive North American diatom flora published by Ruth Patrick and Charles W. Reimer between 1966 and 1975 [54, 55] is still illustrated with excellent line drawings. Other widely used references which are based entirely on drawings are Schmidt's *Atlas der Diatomaceenkunde* [56] (the quality of the images it contains has not been surpassed to date); *Die Kieselalgen* by Friedrich Hustedt [57] (the 7th volume of Dr. Rabenhorst's *Kryptogamenflora von Deutschland, Osterreich und der Schweiz*); or the S*ynopsis des Diatomees de Belgique* by Henri Van Heurck [58], which contains 141 illustrated plates. Special mention deserves the extensive work by Horace G. Barber, who made thousands of finely illustrated plates which have been recently made publicly available (e.g., bit.ly/2PGebK6, bit.ly/2YAHr9j, bit.ly/2Va0BAr).

However, it is generally insufficient to assume that the diatom viewed under a light microscope can be identified by comparison to published drawings since the literature often lacks these observations for comparison [59]. This

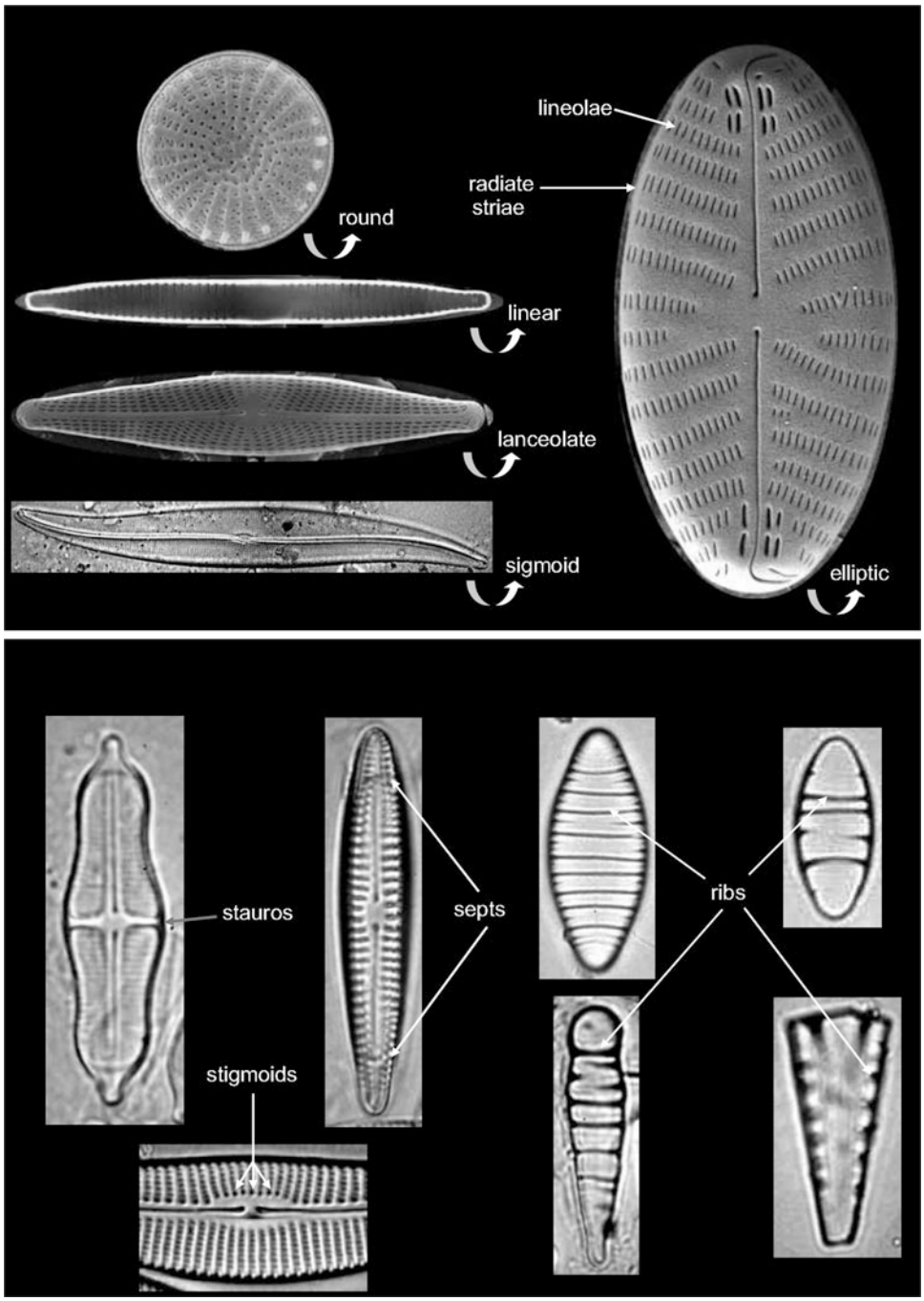

Fig. 3.6 Main morphological features observed in common freshwater diatoms (cont.)

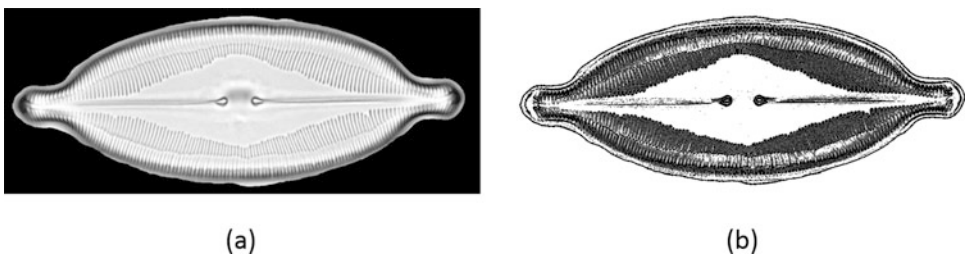

Fig. 3.7 Example of pencil drawing generated automatically. (**a**) Original gray level image (*Caloneis amphisbaena*); (**b**) Black and white drawing [51]

explains the frequent use of good quality light micrographs in conjunction with schematic drawings, which has done much in the last decades to improve descriptions [60]. Optical aberrations, which hampered early microscopy [61], were partially corrected by the mid-nineteenth century with the introduction of Lister and Amici achromatic objectives

that reduced chromatic aberration and raised numerical apertures. The subsequent apparition of better microscopical techniques, such as the use of differential interference contrast or Nomarski (DIC) optics, and scanning electron microscopy (SEM), was crucial not only in the process of taxonomic description but also in the development of the current species concept in diatoms [62]. Discrimination of small-celled taxa (fragilarioid genera, small Sellaphoraceae and Achnanthidiaceae, etc.) has been possible only by the availability of these methods.

Whereas brightfield light microscopy has been useful for conventional applications [e.g., 63] (routine countings), it is of limited use in detailed taxonomic studies. In this regard, several methods have been proposed to artificially increase the contrast and/or resolution of the images obtained. Darkfield microscopy is the oldest and simplest method of increasing the contrast of microscopic specimens [64], allowing the detection of weak diffracted light signals, and may be the method of choice for viewing fine structural details [65] such as those present in diatom frustules. Physicist Georges Nomarski authored a new contrast-generating microscopy technique in 1955 commonly referred to as Nomarski interference microscopy [61] that, along with phase contrast, has allowed more precise observations of valve features. More recently, interference reflection contrast has been successfully used for the examination of diatoms [66], being regarded as a method that significantly improves the resolution of structural details.

New microscopes generally are digital in nature and result in images with higher extractable information content [67]. Bayer et al. [68] review digital imaging in general and in the field of microalgal research in particular, presenting a number of imaging techniques that are critical for image acquisition and optimization, advances in digital imaging and analysis have also enabled microscopists to acquire quantitative measurements quickly and efficiently on specimens [61]. However, it is to the electron microscope that much of the recent progress is due, particularly with respect to small species [60]. Recently [69], atomic force microscopy (AFM) has been successfully used also to image the topography of the diatom frustule at the nanometer range scale. Other modern microscope techniques, briefly discussed in [67] include second harmonic imaging microscopy, 4 pi microscopy, stimulated emission depletion (STED), or near-field scanning optical microscopy (NSOM).

3.4 Conclusions

This chapter reviewed previous attempts of using taxonomic keys for diatom identification, highlighting the pros and cons of the use of this and similar methods. Drawings have not only morphological or aesthetic interest. They serve to highlight the differential details allowing species discrimination. New diatom taxa need to be accompanied by an illustration showing the morphological differentiation. The main morphological features found in common freshwater diatom genera are briefly presented, together with an account of the historical development of technologies used for species description. Although algorithms for the automated creation of identification keys, few of them can help to generate identification keys without the expert's supervision. Taxonomy is the science and art of species classification and has his roots back to Aristotle who was the first to create hierarchical structures based on similarities. Later, Linnaeus (God's registrar [70]) in the eighteenth century, developed the first universal taxonomy system to organize living specimens. Taxonomy is a tool that provides knowledge about organisms. Scientists working in the area of natural sciences recognize the importance of taxonomy. However, due to a number of reasons, taxonomy is an endangered work, even more than the species themselves [70]. It is important that the different research agencies and evaluators recognize and appreciate the importance of these tasks as well as favoring not only the consolidation of the few existing groups but also the training of young research personnel. An interesting aspect to be considered is the participation of amateur diatomists taking into account the limited number of professionals in diatom research, the limitation of funding sources and the extent of the species to be explored. The participation of amateurs goes back to the end of the eighteenth century at the beginning of the discipline. With a modest team (or even without equipment in some cases), amateurs can contribute to the preparation of collections as well as collaborating with professionals [71]. In any case, what is important is to have free and readily accessible online identification resources like those mentioned in this chapter and Chap. 1 of this book.

Acknowledgments We thank Cathy Kilroy from the National Institute of Water and Atmospheric Research (NIWA), New Zealand, for providing us the Quick Guide to diatoms included in the Annex. I. Álvarez is thanked for her help in figure elaboration.

A.1 Annex

A.1.1 Quick Guide to Common Diatom Genera in Freshwaters

Cathy Kilroy[1]

This guide can be used as a teaching aid for courses on algae identification for nonspecialists and it is available from the provider website: http://bit.ly/30Zj7iy

[1]National Institute of Water and Atmospheric Research Ltd., Christchurch, New Zealand

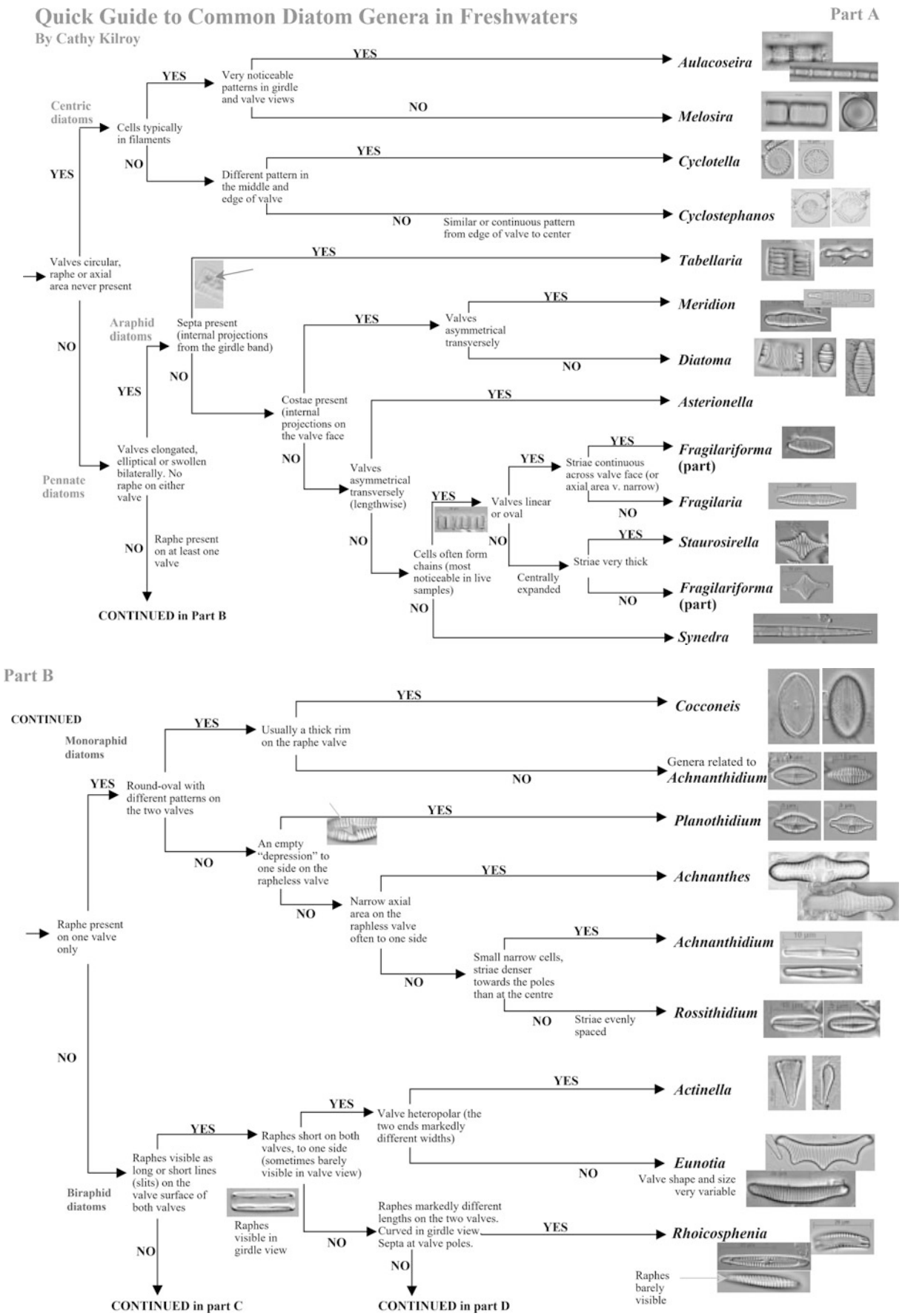
Quick Guide to Common Diatom Genera in Freshwaters
Part A
By Cathy Kilroy
Centric diatoms
Cells typically in filaments
Very noticeable patterns in girdle and valve views
Different pattern in the middle and edge of valve
Similar or continuous pattern from edge of valve to center
Aulacoseira
Melosira
Cyclotella
Cyclostephanos
Valves circular, raphe or axial area never present
Tabellaria
Araphid diatoms
Septa present (internal projections from the girdle band)
Meridion
Valves asymmetrical transversely
Diatoma
Costae present (internal projections on the valve face
Asterionella
Pennate diatoms
Valves elongated, elliptical or swollen bilaterally. No raphe on either valve
Valves asymmetrical transversely (lengthwise)
Striae continuous across valve face (or axial area v. narrow)
Fragilariforma (part)
Fragilaria
Valves linear or oval
Cells often form chains (most noticeable in live samples)
Staurosirella
Striae very thick
Centrally expanded
Fragilariforma (part)
Raphe present on at least one valve
Synedra
CONTINUED in Part B
Part B
CONTINUED
Monoraphid diatoms
Usually a thick rim on the raphe valve
Cocconeis
Genera related to Achnanthidium
Round-oval with different patterns on the two valves
Planothidium
An empty "depression" to one side on the rapheless valve
Achnanthes
Raphe present on one valve only
Narrow axial area on the raphless valve often to one side
Achnanthidium
Small narrow cells, striae denser towards the poles than at the centre
Rossithidium
Striae evenly spaced
Actinella
Valve heteropolar (the two ends markedly different widths)
Raphes short on both valves, to one side (sometimes barely visible in valve view)
Eunotia
Valve shape and size very variable
Biraphid diatoms
Raphes visible as long or short lines (slits) on the valve surface of both valves
Raphes visible in girdle view
Raphes markedly different lengths on the two valves. Curved in girdle view. Septa at valve poles.
Rhoicosphenia
Raphes barely visible
CONTINUED in part C
CONTINUED in part D

Part C

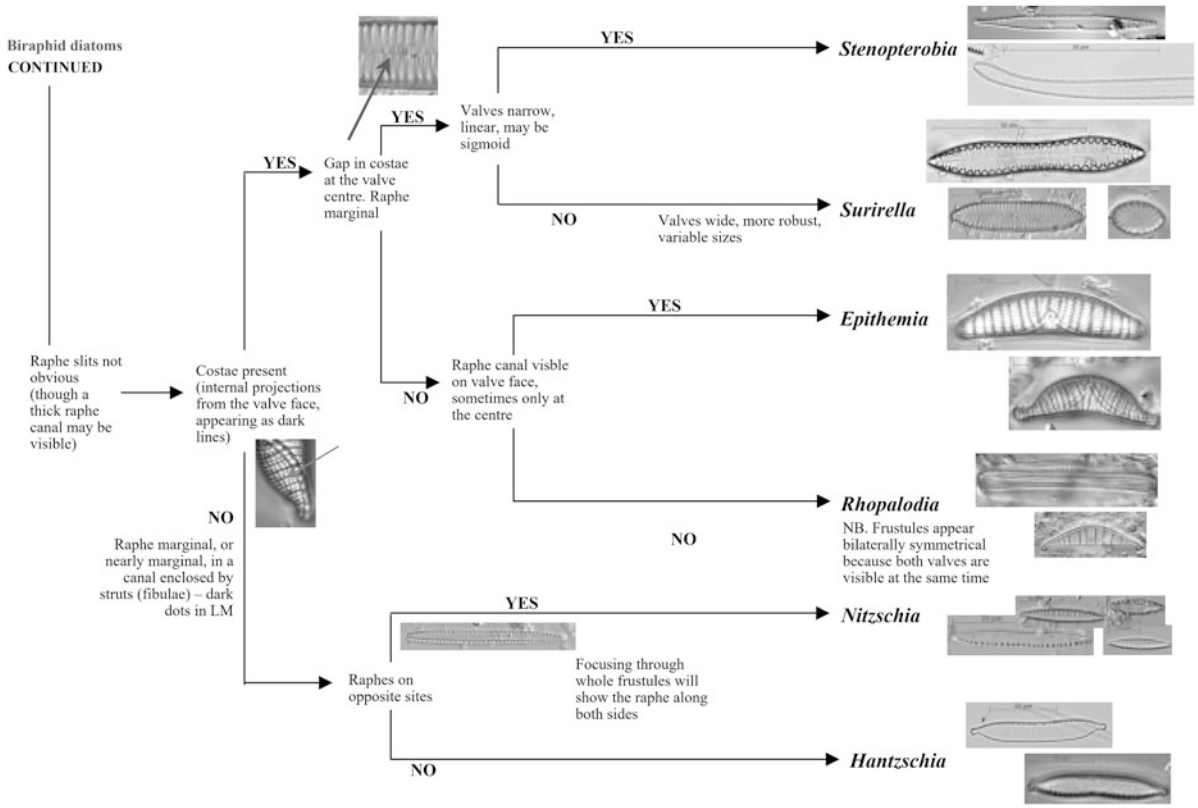
Biraphid diatoms
CONTINUED
Raphe slits not obvious (though a thick raphe canal may be visible)
Costae present (internal projections from the valve face, appearing as dark lines)
Raphe marginal, or nearly marginal, in a canal enclosed by struts (fibulae) – dark dots in LM
Raphes on opposite sites
Gap in costae at the valve centre. Raphe marginal
Valves narrow, linear, may be sigmoid
Valves wide, more robust, variable sizes
Raphe canal visble on valve face, sometimes only at the centre
Focusing through whole frustules will show the raphe along both sides
YES
NO
Stenopterobia
Surirella
Epithemia
Rhopalodia
NB. Frustules appear bilaterally symmetrical because both valves are visible at the same time
Nitzschia
Hantzschia

Part D

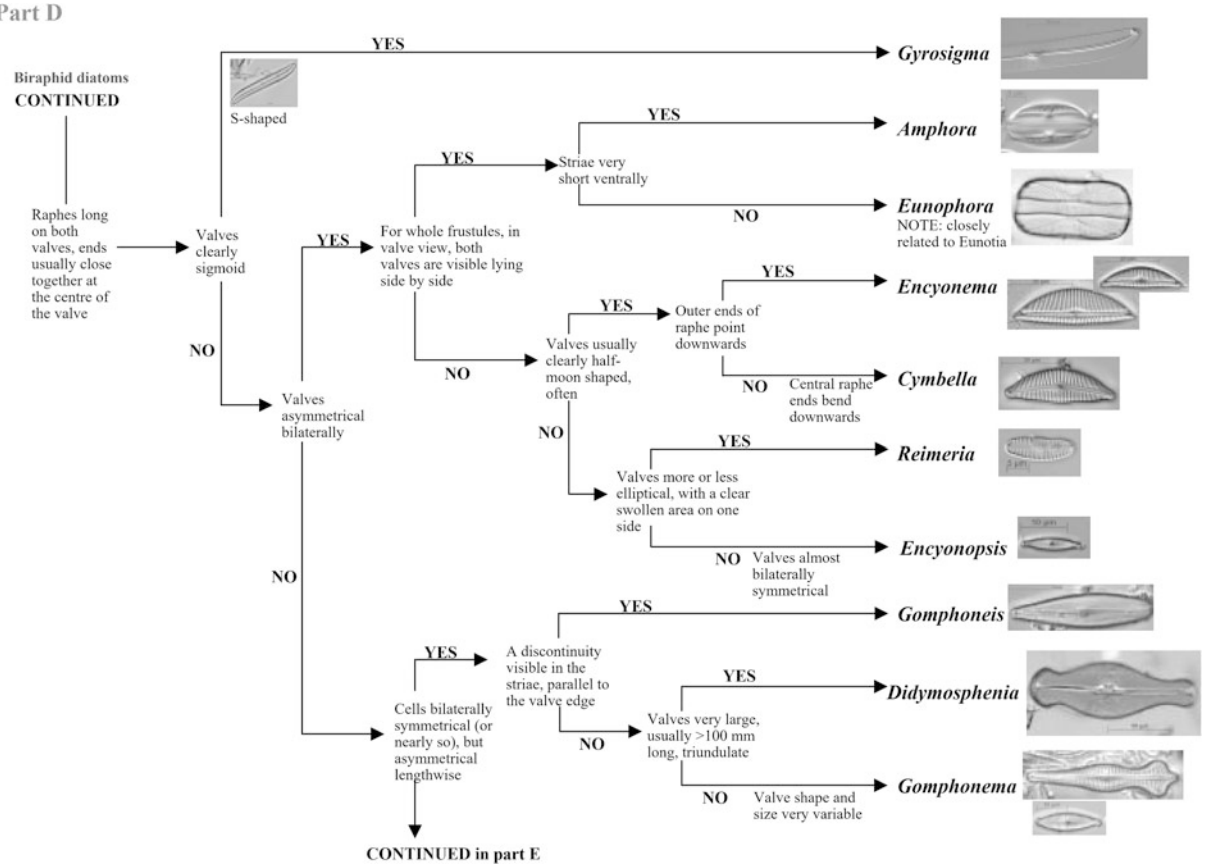
Biraphid diatoms
CONTINUED
Raphes long on both valves, ends usually close together at the centre of the valve
Valves clearly sigmoid
S-shaped
Valves asymmetrical bilaterally
For whole frustules, in valve view, both valves are visible lying side by side
Striae very short ventrally
Valves usually clearly half-moon shaped, often
Outer ends of raphe point downwards
Central raphe ends bend downwards
Valves more or less elliptical, with a clear swollen area on one side
Valves almost bilaterally symmetrical
A discontinuity visible in the striae, parallel to the valve edge
Valves very large, usually >100 mm long, triundulate
Valve shape and size very variable
Cells bilaterally symmetrical (or nearly so), but asymmetrical lengthwise
CONTINUED in part E
YES
NO
Gyrosigma
Amphora
Eunophora
NOTE: closely related to Eunotia
Encyonema
Cymbella
Reimeria
Encyonopsis
Gomphoneis
Didymosphenia
Gomphonema

Part E

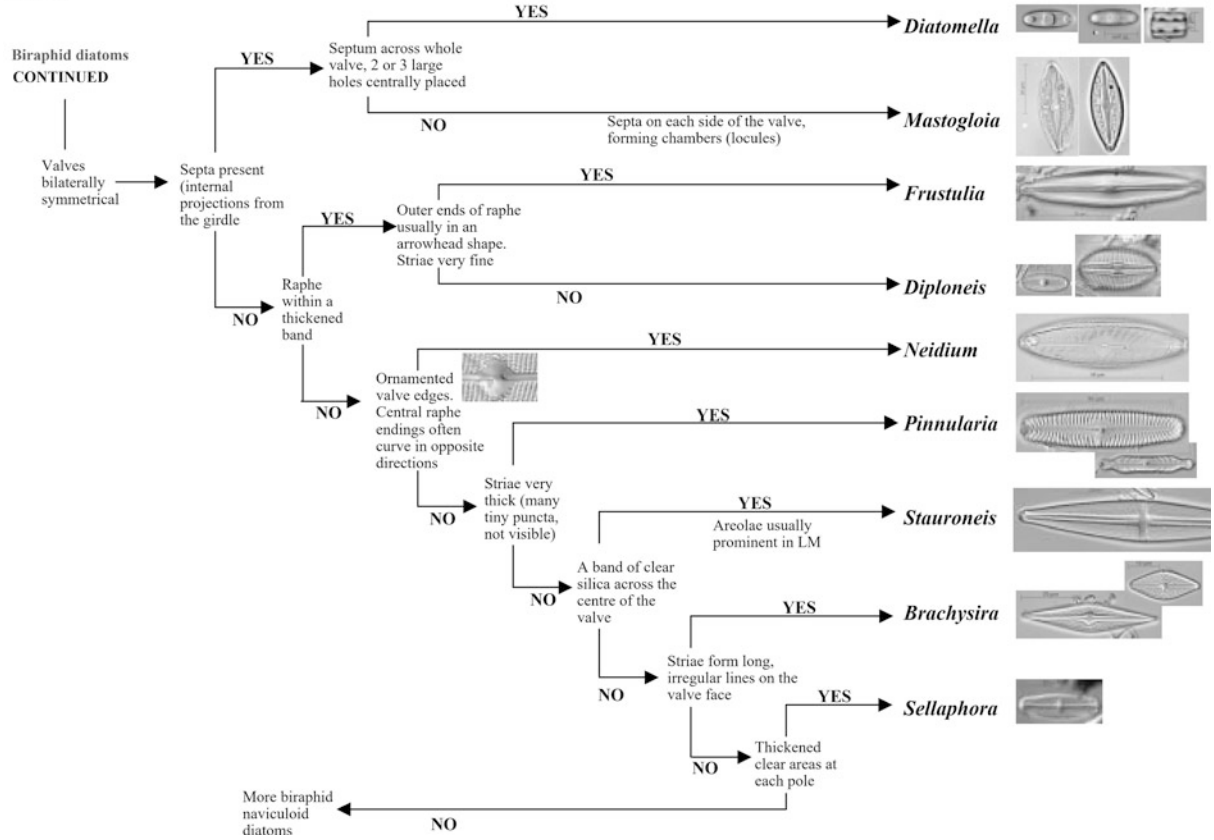

Part F

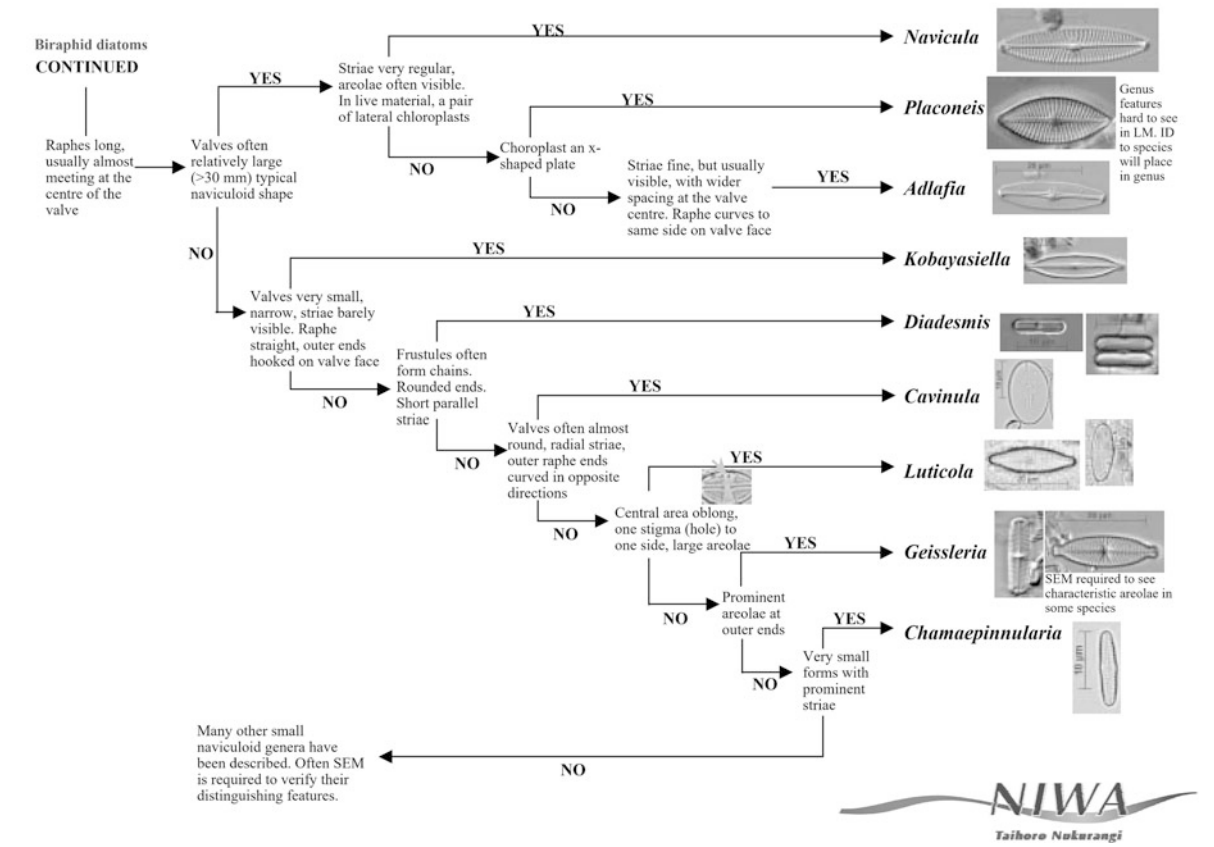

NIWA
Taihoro Nukurangi

References

1. Leuschner, D., Sviridov, A.: The mathematical theory of taxonomic keys. Biom. J. **28**(1), 109–113 (1986)
2. Dunn, G., Everitt, B.S.: An Introduction to Mathematical Taxonomy. Courier Corporation, Massachusetts (2004)
3. Clark, J.Y., Warwick, K.: Artificial keys for botanical identification using a multilayer perceptron neural network (MLP). In: Panigrahi, S., Ting, K.C. (eds.) Artificial Intelligence for Biology and Agriculture, pp. 95–115. Springer, Dordrecht (1998)
4. Dallwitz, M.: A comparison of matrix-based taxonomic identification systems with rule-based systems. In: Proceedings of IFAC Workshop on Expert Systems in Agriculture, pp. 215–218. International Academic Publishers, Beijing (1992)
5. Walter, D.E., Winterton, S.: Keys and the crisis in taxonomy: extinction or reinvention? Annu. Rev. Entomol. **52**, 193–208 (2007)
6. Lobanov, A.: Keys to beetles and biological diagnostics. http://www.zin.ru/Animalia/Coleoptera/eng/syst8.htm
7. Walter, D.E., Proctor, H.C.: Mites: Ecology, Evolution and Behaviour. Springer, Dordrecht (1999)
8. Zhang, X., Chen, X., Cheng, J.: SIKey: a tool to generate secondary identification keys for targeted diagnosis. Expert Syst. Appl. **34**(4), 2812–2818 (2008)
9. Tilling, S.: Keys to biological identification: their role and construction. J. Biol. Educ. **18**(4), 293–304 (1984)
10. Calvo-Flores, M.D., Contreras, W.F., Galindo, E.G., Pérez-Pérez, R.: XKey: a tool for the generation of identification keys. Expert Syst. Appl. **30**(2), 337–351 (2006)
11. Reynolds, A.P., et al.: Algorithms for identification key generation and optimization with application to yeast identification. Workshops on Applications of Evolutionary Computation, pp. 107–118. Springer (2003)
12. Payne, R., Preece, D.: Identification keys and diagnostic tables: a review. J. R. Stat. Soc. Series A. **143**(3), 253–282 (1980)
13. Pankhurst, R.J., et al.: Biological Identification: The Principles and Practice of Identification Methods in Biology. Edward Arnold, London (1978)
14. Talent, N., Dickinson, R.B., Dickinson, T.A.: Character selection during interactive taxonomic identification: 'best characters'. Biodivers. Inform. **9**, 1–12 (2014)
15. McNeill, J.: The handling of character variation in numerical taxonomy. Taxon. **23**, 699–705 (1974)
16. Blanco, S., Borrego-Ramos, M., Olenici, A.: Disentangling diatom species complexes: does morphometry suffice? PeerJ. **5**, e4159 (2017)
17. Osborne, D.V.: Some aspects of the theory of dichotomous keys. New Phytol. **62**(2), 144–160 (1963)
18. Prescott, G.W.: How to Know the Freshwater Algae. Brown Company, Dubuque (1975)
19. Graham, L., Wilcox, L.: Algae. Prentice Hall, Upper Saddle River, NJ (2000)
20. Krammer, K.: Bacillariophyceae. 5. English and French translation of the keys. SuBwasserflora Von Mitteleuropa. **2**, 2–12 (2000)
21. Bellinger, E.G., Sigee, D.C.: Freshwater Algae: Identification and Use as Bioindicators. Wiley, Chichester (2010)
22. Ricard, M.: Diatomophycées. Atlas du Phytoplankton Marin. **2**, 1–297 (1987)
23. Wood, E.F., Crosby, L., Cassie, V.: Studies on Australian and New Zealand diatoms, Part VI. Trans. R. Soc. N. Z. **2**(15), 189–218 (1965)
24. AWWA: Algae: Source to Treatment. American Water Works Association, Denver (2010)
25. Tomas, C.R.: Identifying Marine Phytoplankton. Elsevier, Oxford (1997)
26. Lange-Bertalot, H., Hofmann, G., Werum, M., Cantonati, M., Kelly, M.G.: Freshwater Benthic Diatoms of Central Europe: Over 800 Common Species Used in Ecological Assessment. Koeltz Botanical Books, Schmitten-Oberreifenberg (2017)
27. Cupp, E.E.: Marine Plankton Diatoms of the West Coast of North America. University of California Press, La Jolla (1943)
28. Prygiel, J., Coste, M.: Guide méthodologique pour la mise en oeuvre de l'Indice Biologique Diatomées, Agences de l'Eau, Ministiére de l'Amnagement du Territoire et de l'Environment, Direction de l'Eau & CEMAGREF, Paris (2000)
29. Hendey, N.I.: An Introductory Account of the Smaller algae of British Coastal Waters, Fishery Investigation Series, vol. 5, pp. 1–317. Her Majesty's Stationery Office, London (1964)
30. APHA: Standard Methods for the Examination of Water and Wastewater. American Public Health Association, Washington (2018)
31. Barber, H.G., Haworth, E.Y.: A Guide to the Morphology of the Diatom Frustule: With a Key to the British Freshwater Genera, vol. 44, pp. 1–111. Freshwater Biological Association Scientific Publication, Ambleside (1981)
32. Cox, E.J.: Identification of Freshwater Diatoms from Live Material. Chapman & Hall, London (1996)
33. Rumeau, A., Coste, M.: Initiation à la systématique des diatomées d'eau douce. Pour l'utilisation pratique d'un indice diatomique générique. Bull. Fr. Peche Piscic. **309**, 1–69 (1988)
34. John, J.: A guide to diatoms as indicators of urban stream health. LWRRDC Occasional Paper 14/99, pp. 1–91 (2000)
35. Biggs, B., Kilroy, C.: Stream Periphyton Monitoring Manual. Niwa, Christchurch (2000)
36. Prescott, G.W., et al.: Algae of the Western Great Lakes Area, with an Illustrated Key to the Genera of Desmids and Freshwater Diatoms. Brown Company, Dubuque (1982)
37. Wehr, J.D., Sheath, R.G., Kociolek, J.P.: Freshwater Algae of North America: Ecology and Classification. Elsevier, San Digo (2015)
38. Joh, G., Lee, J.H., Lee, K., Yoon, S.-K.: Algal Flora of Korea. National Institute of Biological Resources, Incheon (2010)
39. Van Heurck, H.: A Treatise on the Diatomaceae: Containing Introductory Remarks on the Structure, Life History, Collection, Cultivation and Preparation of Diatoms, and a Description and Figure Typical of Every Known Genus, as Well as a Description and Figure of Every Species Found in the North Sea and Countries Bordering It, Including Great Britain, Belgium, & c. William Wesley, London (1896)
40. Chakaravarthy, V.T., Pandit, V., Roy, S., Awasthi, P., Mohania, M.: Decision trees for entity identification: approximation algorithms and hardness results. In: Proceedings of the Twenty-sixth ACM SIGMOD-SIGACT-SIGART Symposium on Principles of Database Systems, ACM, pp. 53–62 (2007)
41. Hawthorne, W., Lawrence, A.: Plant Identification: Creating User-Friendly Field Guides for Biodiversity Management. Routledge, London (2012)
42. Kelly, M., et al.: Common Freshwater Diatoms of Britain and Ireland: an Interactive Key. Environment Agency, Bristol (2005)
43. Mann, D.G.: The species concept in diatoms. Phycologia. **38**(6), 437–495 (1999)
44. Hoek, C., Van den Hoeck, H., Mann, D., Jahns, H.: Algae: An Introduction to Phycology. Cambridge University Press, Cambridge (1995)
45. Round, F.E., Crawford, R.M., Mann, D.G.: Diatoms: Biology and Morphology of the Genera. Cambridge University Press, Cambridge (1990)
46. Turland, N.J., et al.: International code of nomenclature for algae, fungi, and plants (Shenzhen code) adopted by the Nineteenth International Botanical Congress Shenzhen, China, July 2017, IAPT, Shenzhen (2018)
47. McLaughlin, R.B., An introduction to the microscopical study of diatoms, http://www.microscopy-uk.eu/diatomist/rbm_US_Royal.pdf (2012)

48. Leggett, R., Kirchoff, B.K., Image Use in Field Guides and Identification Keys: Review and Recommendations, AoB Plants, plr004 (2011)
49. Blanco, S.: On the misuse of lectotypification in diatom taxonomy. Phycologia. **56**(1), 108–113 (2016)
50. Mann, D.G., et al.: New methods for preparing, imaging and typifying desmids (Chlorophyta, Zygnematophyceae), including extended depth of focus and 3-D reconstruction. Phycologia. **46**, 29–45 (2007)
51. Singh, H., Sánchez, C., Cristobal, G.: Pencil drawing of microscopic images through edge preserving filtering. In: Morales, A., Fierrez, J., Sánchez, J., Ribeiro, B. (eds.) Pattern Recognition and Image Analysis, IbPRIA, Lecture Notes in Computer Science, vol. 11868. Springer, Cham (2019)
52. Hicks, Y.A., Marshall, A.D., Martin, R.R., Rosin, P.L., Droop, S.J., Mann, D.G.: Building shape and texture models of diatoms for analysis and synthesis of drawings and identification. Proceedings of the Irish Machine Vision and Image Processing Conference, Trinity College, Dublin. pp. 26–33 (2004)
53. Wittmann, B.: Outlining species: drawing as a research technique in contemporary biology. Sci. Context. **26**(2), 363–391 (2013)
54. Patrick, R., Reimer, C.: The diatoms of the United States (exclusive of Alaska and Hawaii). Volume 2: Systematic descriptions of diatoms of the taxonomic orders Navicuales (families Entomoneidaceae, Cymbellaceae, and Gomphonemaceae), and Epithemiales Monograph 13, The Academy of Natural Sciences, Philadelphia (1975).
55. Patrick, R., Reimer, C.: The Diatoms of the United States: Exclusive of Alaska and Hawaii: Fragilariaceae, Eunotiaceae, Achnanthaceae, Naviculaceae. Academy of Natural Sciences, Philadelphia (1975)
56. Schmidt, A.: Atlas der Diatomaceenkunde. Reisland, Leipzig (1874–1959)
57. Hustedt, F.: Die Kieselalgen: Deutschlands, Österreichs und der Schweiz unter Berücksichtigung der übrigen Länder Europas sowie der angrenzenden Meeresgebiete. O. Koeltz Science Publishers, Koenigstein (1977)
58. Van Heurck, H.: Synopsis des Diatomees de Belgique. Henri Van Heurck, Anvers (1881)
59. Lobban, C., et al.: Diatoms on coral reefs and in tropical marine lakes. In: Stoermer, E.F., Smol, J.P. (eds.) The Diatoms: Applications for the Environmental and Earth Sciences, 2nd edn, pp. 346–356. Cambridge University Press, Cambridge (2010)
60. Werner, D.: The Biology of Diatoms, Botanical Monographs, vol. 13, pp. 1–498. Blackwell Scientific, Oxford (1977)
61. Davidson, M.W., Abramowitz, M.: Optical microscopy: encyclopedia of imaging. Sci. Technol. **2**, 1106–1140 (2002)
62. Van de Vijver, B.: 'Diatom taxonomy in the 21st century' in honour of Henri Van Heurck (1838–1909). Plant. Ecol. Evol. **143**(3), 249–250 (2010)
63. Siver, P.A., Baskette, G.: A morphological examination of *Frustulia* (Bacillariophyceae) from the Ocala National Forest, Florida, USA. Can. J. Bot. **82**(5), 629–644 (2004)
64. Delly, J.G.: Basic contrast methods in light microscopy. Microsc. Microanal. **12**(S02), 222–223 (2006)
65. Murphy, D.B.: Fundamentals of Light Microscopy and Electronic Imaging. Wiley, New York (2002)
66. Siver, P.A., Hinsch, J.: The use of interference reflection contrast in the examination of diatom valves. J. Phycol. **36**(3), 616–620 (2000)
67. Lawrence, J.R., Neu, T.R.: Modern microscopic techniques for studies in aquatic microbial ecology. SIL News. **45**, 1–3 (2005)
68. Bayer, M.M., Droop, S.J., Mann, D.G.: Digital microscopy in phycological research, with special reference to microalgae. Phycol. Res. **49**(4), 263–274 (2001)
69. Gebeshuber, I.C.: Atomic force microscopy study of living diatoms in ambient conditions. J. Microsc. **212**(3), 292–299 (2003)
70. Pisupati, B.: Taxonomy–the science and art of species. Curr. Sci. **108**(12), 2149–2150 (2015)
71. Bahls, L.: The role of amateurs in modern diatom research. Diatom Res. **30**(2), 209–210 (2015)

4 Naturally and Environmentally Driven Variations in Diatom Morphology: Implications for Diatom-Based Assessment of Water Quality

Adriana Olenici, Călin Baciu, Saúl Blanco, and Soizic Morin

Abstract

Diatom identification must consider the large variability in both morphological and morphometric features, characteristic of this group of microorganisms. This chapter describes variations in shape/size observed in diatom populations either as a consequence of their particular asexual reproductive cycle or induced by environmental conditions. Concerning this latter, teratological diatoms are commonly associated with a variety of environmental stressors, particularly the presence of micropollutants in the aquatic ecosystem, such as heavy metals. We evidence an overestimation of water quality conditions caused by overriding deformed individuals in diatom-based biomonitoring studies. It can be shown that normal and aberrant forms of the same taxon differ in autecological preferences. Finally, we advise on a critical issue in the description of diatom specimens, that is, the sample size on which morphometric ranges should be provided. The section concludes with some recommendations in this regard.

A. Olenici (✉)
Faculty of Environmental Science and Engineering, Babes-Bolyai University, Cluj-Napoca, Romania

Institute of Environment, Leon, Spain
e-mail: aole@unileon.es

C. Baciu
Faculty of Environmental Science and Engineering, Babes-Bolyai University, Cluj-Napoca, Romania

S. Blanco
Facultad de Ciencias Biológicas y Ambientales, Departamento de Biodiversidad y Gestión Ambiental, Universidad de León, León, Spain

Laboratorio de diatomología y calidad de aguas, Instituto de Investigación de Medio Ambiente, Recursos Naturales y Biodiversidad, León, Spain

S. Morin
Unité de Recherche EABX, Irstea, Cestas Cedex, France

4.1 Teratology in Algae, with a Special Focus on Diatoms

The occurrence of teratological (aberrant) forms within natural microalgal populations has been long documented in the psychological literature. Teratological forms are nonadaptive phenotypic abnormalities caused by various environmental stresses [1] and, whereas the study of teratology within unicellular algae has been mostly focused on freshwater diatoms, some studies record aberrant cells in other algal groups, e.g., teratological *Pediastrum duplex* var. *rugulosum* colonies (Chlorophyceae) were illustrated in Lenarczyk et al. [2], and Barinova [3] found aberrant forms in *Microcystis* and *Woronichinia* (Cyanobacteria) with enlarged cell sizes and/or losses of gas vesicles. In marine waters, high abundances of teratological forms are also commonly observed in locations with a high degree of environmental stress [4].

The first systematic approach to diatom teratology was provided by Falasco et al. [5] who reviewed the causes leading to the apparition of aberrant diatoms in freshwaters, proposing a tentative classification of the alterations recorded in previous studies: deformities in valve (type I), striae (type II), raphe (type III), and mixed types (type IV) (Figs. 4.1 and 4.2). Olenici et al. [6] recently described a fifth type concerning frustule cingulum. Teratology has been observed both infield and laboratory studies, and can be induced in diatom cultures (e.g., the effect of concanamycin A on the outline of *Phaeodactylum tricornutum* [7]). In natural habitats, valve deformations are caused by a small number of variables, basically metals and acid conditions [8, 9], but some authors suggest additional causes, such as high concentrations of phosphorus and ammonium nitrogen [10, 11], artificial growth conditions [1], mechanical stress, or parasitism [3].

Although the association between teratological valves and metal contamination has been largely demonstrated, the underlying causal biochemical mechanisms are still poorly known. Metals interfere with biochemical and cellular processes triggering a dysfunctioning that reduces growth and

G. Cristóbal et al. (eds.), *Modern Trends in Diatom Identification*, Developments in Applied Phycology 10,
https://doi.org/10.1007/978-3-030-39212-3_4

Fig. 4.1 A teratological *Gyrosigma* cell (deformed outline) in Ulló River, Vilaboa, Spain. Courtesy of Diego Muñoz

may ultimately lead to cell death [12]. The effect of Cd on valve morphogenesis in *Planothidium frequentissimum* was studied in detail by Arini et al. [13]. These authors observed that Cd firstly generated striae and mixed teratologies, then affected the central area and the valves. Actually, pollutants not only alter valve features but are responsible also for nuclear anomalies, alteration in photosynthetic apparatus, and lipid bodies [14], changes that are commonly neglected in diatom-based biomonitoring studies. Changes in carotenoid/chlorophyll *a* ratios and in cell motility were also observed by Pandey and Bergey [15] at severely polluted (Cu, Zn) sites. Besides, the expression of genes involved in the regulation of mitochondrial metabolism, photosynthesis, oxidative stress, and silica metabolism is affected by the exposure to heavy metals [16]. Recent advances [17] have even linked specific contaminants to particular aberrations found in diatom frustules, e.g., raphe modifications are more frequent in the case of Cu exposure, while abnormalities in striations and mixed deformities were more prevalent in diatoms exposed to Zn or Pb.

Teratology is only one aspect of the general response of phytobenthos to metal pollution. Morin et al. [18] review these effects from community (succession toward the dominance of tolerant taxa, loss of diversity) to the individual level. In this regard, apart from morphological abnormalities, cell size diminution is another commonly observed trend, both at the intraspecific level (e.g., [19]) or with a dominance of small-sized diatoms in polluted streams [20, 21]. Additionally, metals do not only reduce diatom abundance and richness: a direct relationship between the degree of valve deformity and pollutant contamination has been recently described [22, 23]. These changes provide insights into the use of teratological diatoms to assess ecosystem impairment in water bodies [24].

4.2 The Effect of Overriding Diatom Teratology on Water Quality Diagnosis

Diatoms constitute an ideal group to study global biodiversity patterns and to understand the factors controlling ecological processes in freshwater habitats. Their community structure can be affected by high levels of micropollutants and in particular by metals (Sect. 4.1), which are often found in rivers in mining areas. Based on the current literature, the presence of deformities in contaminated environments is considered a clear indication of stress. Diatom deformities are good indicators providing warnings that water quality measurements are required at a site [24]. There are countless studies that show that diatoms need to adapt to the stress generated by the heavy metals and acidity in order to survive, and such stress determines which diatoms can grow. For instance, in areas affected by acid mine drainage (AMD)

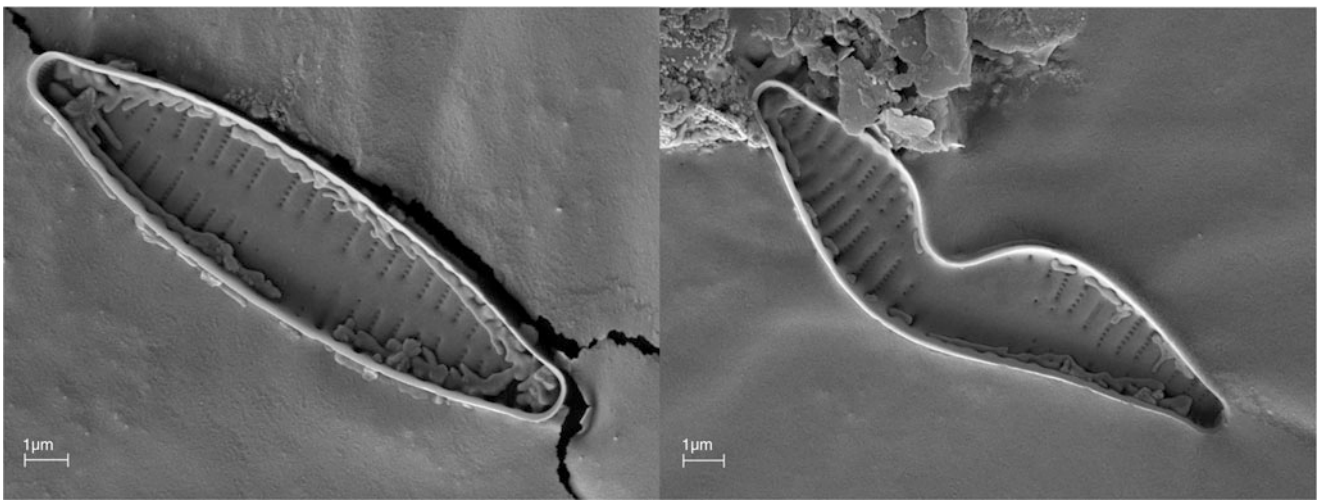

Fig. 4.2 A normal (left) and a teratological (right) *Fragilaria* valve showing a deformed outline and alterations in the striation pattern

sensitive species are replaced by tolerant ones [25], together with changes in size, shape, and occurrence of morphological deformities [18].

Lavoie et al. [24] stress the fact that diatom-based indices have not been settled to directly assess toxic pollutants and that contaminant-related stress on biota is difficult to assess when lethal impacts are not observed. Diatoms, by displaying deviations from normal shape or ornamentation, have the potential to reflect sublethal responses to environmental stressors. Among commonly used diatom-based water quality indices (see Chap. 10), the use of specific pollution index (SPI) is quite common for the assessment of ecosystem health both in lotic and in lentic systems, not only in Europe but also elsewhere. In general, statistically significant correlations have been found in the literature between SPI scores and different stressors, this metric being known to be sensitive to micropollutants such as Cd and Zn [26] (but see [27]). The accuracy of diatom indices depends both on the number of taxa considered for their computation and on the autecological parameters assigned to each of these taxa [28], and SPI is the only metric based on the ecological profiles of virtually all known taxa at species or sub-specific levels, including teratological forms as distinct taxa whose occurrence downweights the final score of this metric. However, it must be noted that (a) standard protocols [29] do not warn about the necessity of recording these abnormal values in routine counts, and (b) only ca. 1% of the taxa considered for SPI computation are teratological forms [30]. Therefore, it can be hypothesized that neglecting the apparition of deformed diatoms can lead to unrealistic water quality diagnoses.

In order to explore this idea, a sampling survey took place in Roșia Montană, Romania (46°18′22″N 23°07′49″E), one of the most representative gold deposits in Europe, with a long history of mining, spanning over the last two millennia. The damage to the environment produced by all the years of mining is significant. The landscape has been considerably modified, especially by the open pit works. The main source of pollution is AMD produced by the exposed rock surfaces in underground galleries and in open pits. Important sources of acidic waters are also the waste dumps and the tailings management facilities. Epilithic diatoms were collected on the Abrud River, upstream and downstream the confluence with tributaries polluted with mining waters. Samples were taken, processed and analyzed following standard protocols, more details are available in Olenici et al. [23]. The physico-chemical characteristics were analyzed using a portable multiparameter probe (350i/SET WTW), an ion chromatograph Dionex ICS-1500 and an atomic absorption spectrometer ZeEnit700. SPI was calculated with OMNIDIA software [30], either pooling normal and teratological forms of the same taxon, or separating abnormal valves as different taxa. The analysis focused on the dominant taxa *Achnanthidium minutissimum*, *A. macrocephalum*, and *Fragilaria rumpens*,

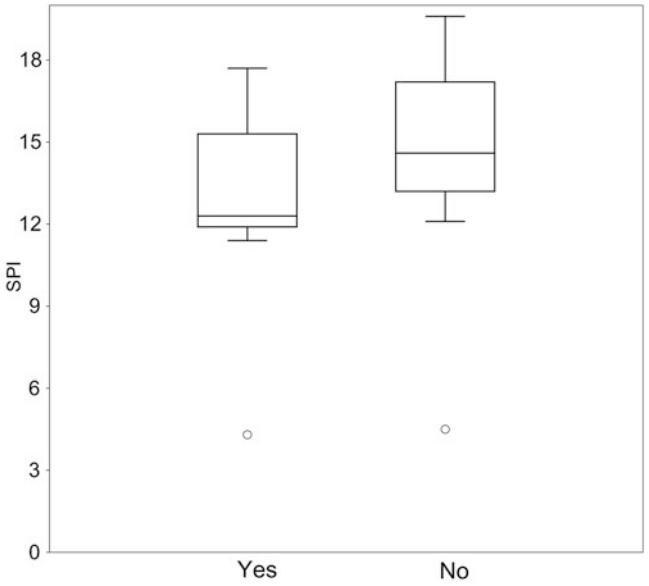

Fig. 4.3 Boxplot of SPI values computed segregating (left) or pooling (right) teratological individuals in an AMD-polluted river

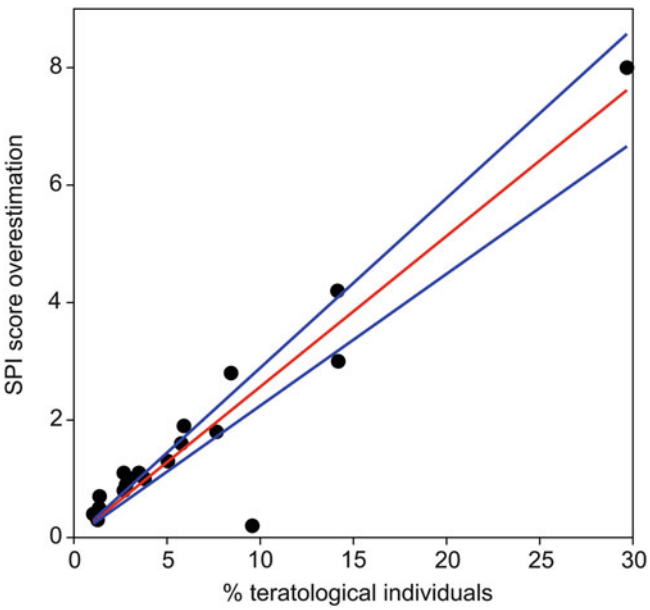

Fig. 4.4 SPI overestimation as a consequence of overriding teratology in routine diatom counts

all of them commonly observed in habitats with high concentrations of heavy metals [23, 31]. Methodological details are available in [23].

SPI values computed segregating abnormal valves were significantly lower, as shown in Fig. 4.3 (Wilcoxon test, $W = 210$, $p < 0.001$). In samples where teratological diatoms were particularly abundant (30% of counted individuals), SPI overestimation can reach up to 8 units (Fig. 4.4), so that water impairment in these locations may remain hidden. It can be evidenced that normal and teratological forms of the same taxon have different ecological profiles with respect

Table 4.1 Autecological parameters (optima ± tolerances) for the dominant diatom taxa found in Abrud River. Values computed according to ter Braak and Van Dam [32]. "–": Not computed due to lack of fit. a: Teratological

	A. minutissimum	*A. minutissimum*[a]	*A. macrocephalum*	*A. macrocephalum*[a]	*F. rumpens*	*F. rumpens*[a]
T (°C)	–	19.5 ± 0.6	–	19.5 ± 0.6	17.9 ± 0.2	17.9 ± 0.2
pH	6.6 ± 1.4	7.8 ± 0.1	–	7.8 ± 0.1	6.4 ± 0.1	6.49 ± 0.5
Conductivity ($\mu S\ cm^{-1}$)	871.1 ± 323.7	556.0 ± 4.1	557.5 ± 144.9	555.8 ± 3.7	1664.5 ± 231.7	1442.3 ± 198.7
$[O_2]$ (ppm)	–	8.3 ± 5.6	8.8 ± 1.5	10.2 ± 1.5	–	–
Turbidity (NTU)	17.5 ± 31.8	9.2 ± 2.6	16.6 ± 31.4	13.1 ± 1.3	24.1 ± 25.1	28.9 ± 0.2
$\left[NO_3^-\right]$ (ppm)	3.6 ± 1.4	3.8 ± 0.9	4.4 ± 2.2	3.9 ± 1.1	14.3 ± 6.1	15.8 ± 6.7
$\left[SO_4^{2-}\right]$ (ppm)	181.1 ± 166.0	199.5 ± 30.9	202.8 ± 92.5	201.1 ± 19.6	249.8 ± 4.7	266.5 ± 8.4

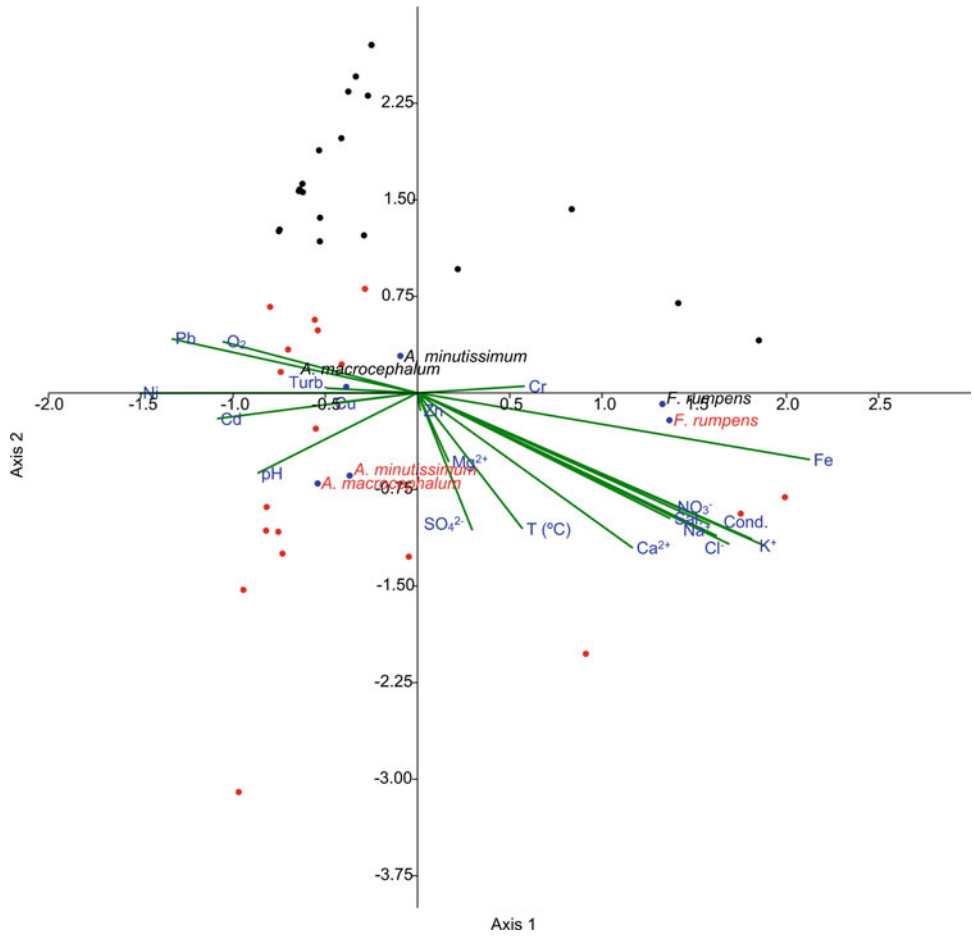

Fig. 4.5 CCA triplot showing the autecological differences between normal (black) and teratological (red) specimens of three diatom species found in Abrud River, Romania. Black dots: Control stations. Red dots: Metal-contaminated stations

to main limnological variables (Table 4.1, Fig. 4.5). This is in agreement with Coste et al. [33] and Fernandez et al. [25] where the teratological forms have a different ecological profile than the normal ones. As expected, the canonical correspondence analysis (CCA) plot shows that teratological occurrences of both *Achnanthidium* taxa are related to acidity and Cd and Cu levels. This stresses the need for assigning different autecological parameters to teratological forms in order to better reflect water conditions in polluted areas.

4.3 Intra- and Interpopulational Variations in Diatom Frustule Size and Shape

Basic morphometric insights are of fundamental importance to diatom taxonomy [34]. Since the early 1960s, numerical techniques have produced a wide variety of methods to suggest classifications of organisms based on quantitative measurements [35]. However, although morpholog-

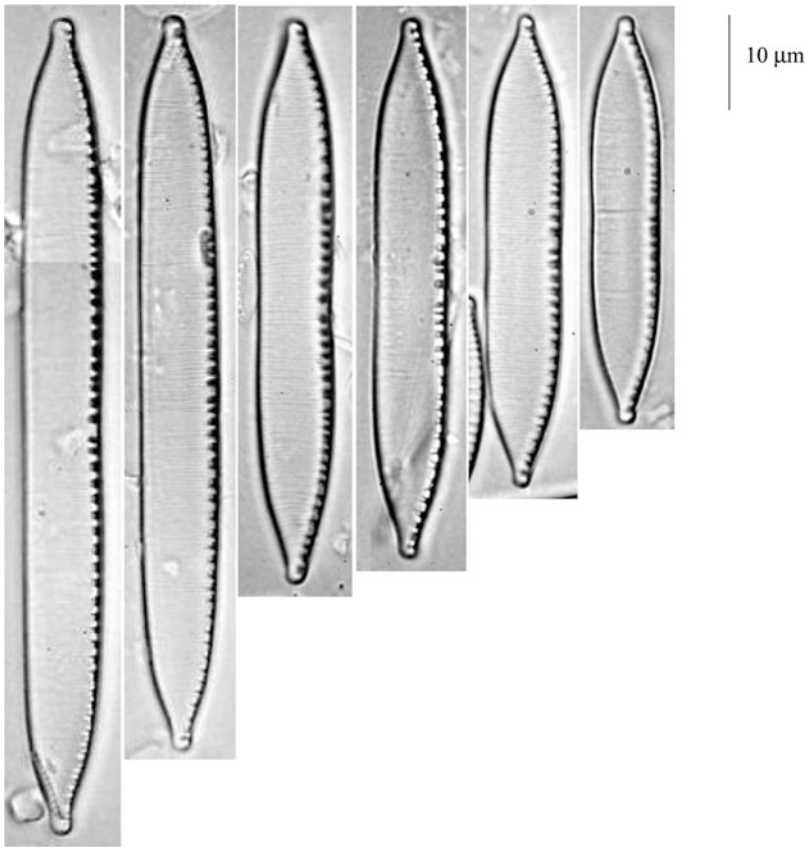

Fig. 4.6 Size diminution series of *Nitzschia umbonata* collected at Ovieco River, Spain, in September 2004. After Blanco et al. [38]

ical discontinuity is considered important [36], the use of quantitative approaches in diatom systematics is relatively rare. In contrast with other microscopic objects (e.g., pollen grains), human-based or automated identification of diatoms using light microscopy is impaired by the extreme morphological/morphometric plasticity shown within species and even within populations [37] (Fig. 4.6). This is a consequence of the "size reduction" process that occurs during the particular asexual reproduction cycle present in most species, first described with some detail independently by MacDonald [39] and Pfitzer [40] in the nineteenth century (Fig. 4.7), and fully documented in the extensive work by the Austrian algologist Lothar Geitler (1899–1990) during the 1930s. According to this model, diatoms must become reduced in size by half the frustule thickness at each cell division, leading to a continuous decrease in the average cell size down to a point when auxospores may be formed, allowing the re-establishment of maximum size [41]. The size of the cells that trigger the formation of auxospores seems to be commonly above halfway between the maximum and the minimum possible values [42]. New valves must conform more or less to the pattern of the parent cell, but once the parent frustule is discarded the naked cell is free to rehabilitate itself with a frustule whose outline may not necessarily conform to that of the pre-auxospore generation, but only preserving its basic design [41]. However, as cell size decreases from subsequent cell divisions, the general frustule outline is preserved within a given species [43]. As a consequence, valve shape remains relatively stable on a large chronological scale [44] and can thus be employed as a main diagnostic character.

The tendency to decrease in valve size after several generations is commonly accepted to characterize many diatom lineages, although confirmatory studies in natural populations are still scarce [45]. For instance, whereas smaller valves usually correspond with higher abundances following successive vegetative reproduction [46], some exceptions have been recently documented in the literature (e.g., *Didymosphenia geminata* [47]). Moreover, the size of the post-auxospore frustules can be altered by external factors after auxospore formation has been initiated [42], so that initial cells may also exhibit size ranges [48].

Variability in valve shape/size may not reflect merely the reproductive cycle of diatoms, since population density and distribution of individual's influence also the degree of variation in these features [49]. Soudek and Robinson [50] observed that cyclical change in frustule length can also vary up to 60 µm between different ecotypes in the diatom *Asterionella formosa*. Intensive morphometric studies on the marine species *Fragilariopsis kerguelensis* [51] evidence that the average costae length decreases toward the north in a latitudinal gradient.

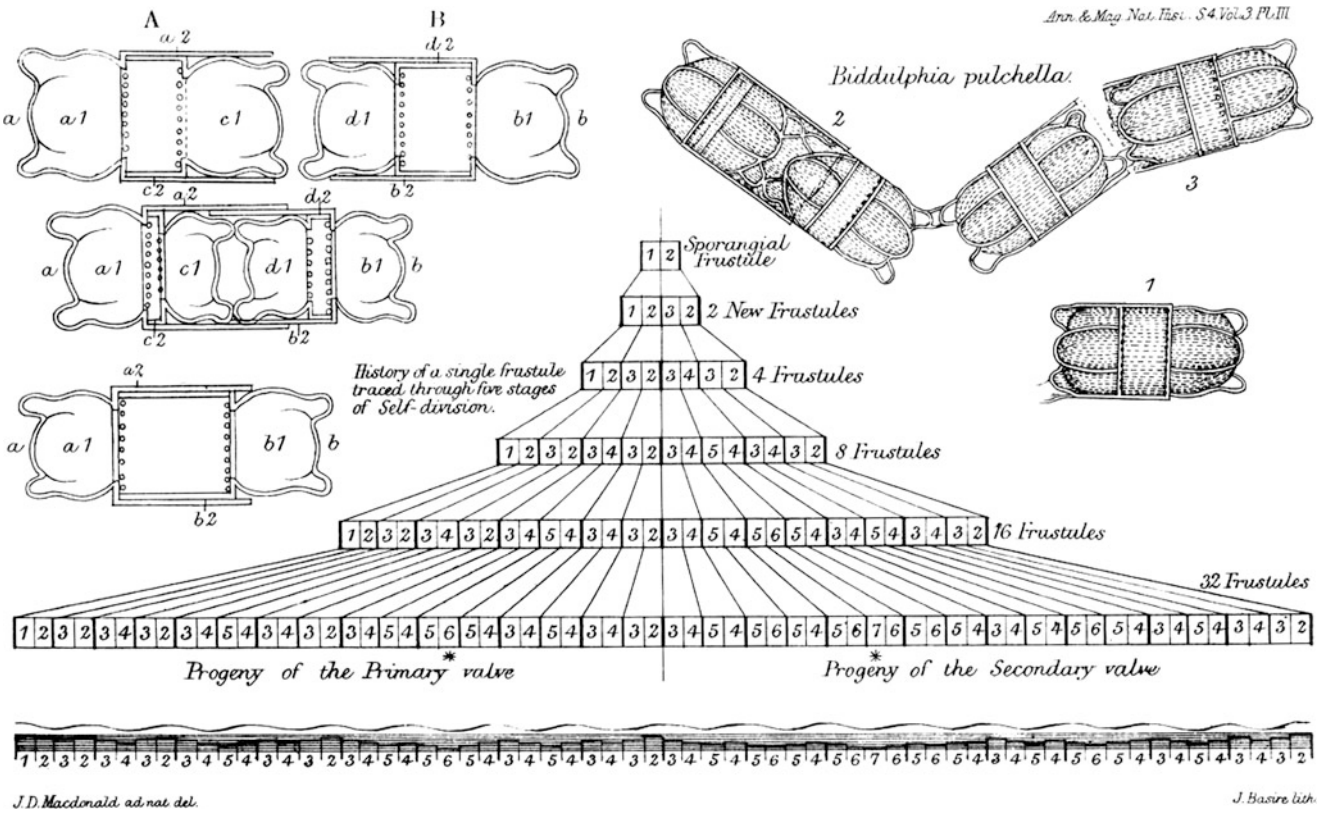

Fig. 4.7 First description of the reduction in frustule size along the asexual reproductive cycle of diatoms, by MacDonald [39]

Environmental factors are known to alter both size distribution within diatom assemblages (the dominance of different species according to their average sizes) and within diatom populations (the prevalence of certain size classes) [52]. Alterations in diatom cell dimensions and corresponding changes in cell volume are commonly observed in response to a variety of abiotic stressors [53]. Actually, modern ecological investigations have revealed consistent morphotypes associated with particular geographical ecological conditions [44, 54], and changes in valve size may provide clues over a variety of ecological processes which are difficult to trace otherwise [51]. For instance, in the marine fossil record [33] smaller valves are usually associated with lower dissolved silicon and iron concentrations. At shorter scales, average valve length experiments also seasonal fluctuations, with smaller sizes during autumn and winter, which indicates higher cellular activity [51, 55]. These habitat features may not affect valve length/width but other morphometric parameters such as stria density [56] or surface-to-volume ratios [57].

The effect of environmental drivers on diatom length/shape has been particularly well studied in planktonic communities, where diatom size affects physiological rates and ecological functions [58]. In these ecosystems, size mediates intraspecific as well as interspecific interactions [49], e.g., larger cells may outcompete smaller ones in resource competition, and exhibit adaptative advantages against predation [51], larger cells being additionally more heavily silicified than smaller ones [59]. Diatom size has also the potential to impose fundamental constraints on the rate of acquiring and processing energy and materials from the environment [58], e.g., this explains the usual finding [60] of smaller diatom sizes being more speciose in the plankton and larger sizes in the benthos.

Size decrease along a diatom life cycle is often accompanied by an allometric change in valve proportions because shortening of the apical axis occurs faster than that of the transapical axis [61, 62]. Thus, valve outline invariably changes, shorter valves appearing relatively wider than longer ones and many shapes become more rounded [56]. Consequently, most of the shape descriptors, when obtained for morphologically similar diatom taxa, are highly correlated with valve length [63]. In general, allometric variation involves a rate of change in a taxonomic feature that is not proportional to the rate of change in size [64]. Lund [42] summarized additional allometric trends observed in most pennate diatoms: (1) in girdle view, smaller cells are relatively wider than the larger cells, (2) valve outline is less complex in smaller cells, this simplification sometimes leading to considerable difficulties in separating the smallest

cells of different species, e.g., the case of the species complex around *Nitzschia inconspicua* [65], (3) changes in stria orientation may happen along the size diminution series, and (4) density of frustular ornamentations remain, though, almost constant within a species (but see [66] for centric diatoms). In the green alga *Micrasterias rotata*, allometric variation has been also related to patterns of symmetric and asymmetric shape variation [67]. Besides, allometric changes have not only taxonomic but also physiological consequences, since biomass decreases allometrically with the log of body size [68]. Size reduction also allows diatoms to increase their surface area in relation to cell volume and decrease the diffusive boundary layer thickness, thus maximizing the number of nutrient transporter sites [69].

When taxonomic discrimination based on shape is not feasible, other morphometric parameters such as valve length and width, and stria and areola densities, may be used [43]. The most popular ratio in diatom taxonomy involves length and width (as *L*/*W*), this ratio being often size dependent, as evidenced by Theriot [66]. However, it can be shown that the slope of the *L*/*W* ratio is not genus dependent for the most abundant pennate diatoms (Fig. 4.8). Particularly, although stria density is often considered inadequate to distinguish between species due to its poor statistical behavior [66, 70]; it is actually the less variable morphometric parameter (Fig. 4.9), as previously suggested by Genkal [71], known to vary little with changing valve length [56].

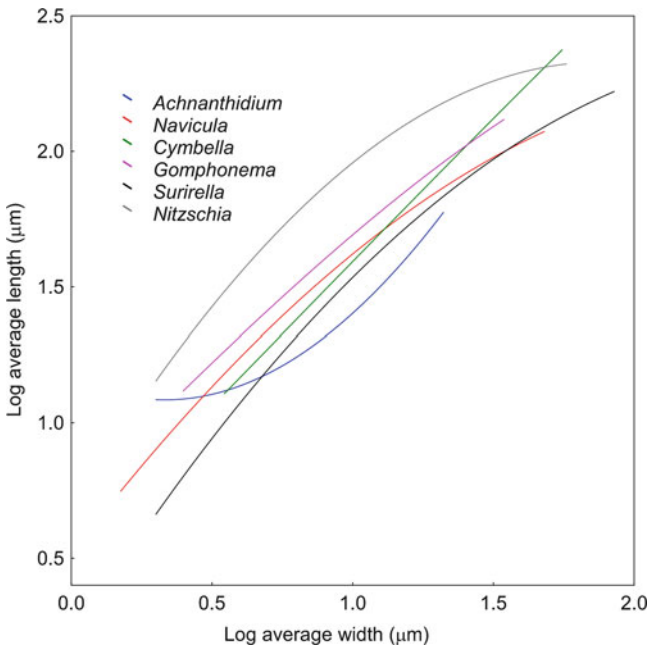

Fig. 4.8 Length/width relationship for 1500 diatom species of six representative pennate genera. Data (omitted) fitted to least-squares curves. Data from Lecointe et al. [30]

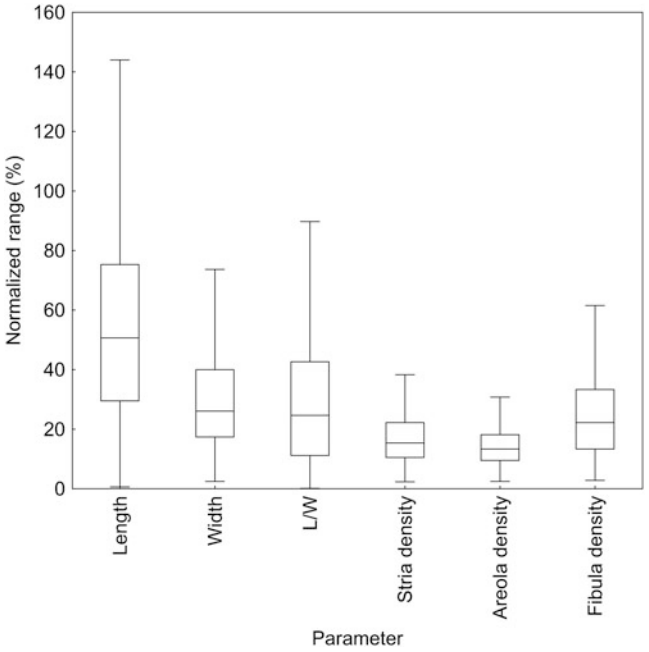

Fig. 4.9 Ranges observed for the main morphometric parameters in 4623 diatom taxa available in Lecointe et al. [30]

4.4 The Sample Size of Type Populations: Implications for Taxonomic Diagnoses

The biological relevance of the morphological distinctness of samples of diatom valves depends on whether the differences can be explained simply by size differences [34]. Blanco et al. [72] recently showed that morphometry does not suffice for disentangling closely related species, so that valve shape should also be considered. In this regard, formal shape analysis (see Chap. 10) allows distinction of groups that have different size ranges but vary only subtly in other characters [44]. Numerical characterization of the valve outline is understood to be representative of a feature that can be used to determine species status [43]. However, as aforementioned, diatom taxa show a large morphometric plasticity; during routine counts, microscopists usually find "average" individuals, but also initial or subinitial cells (those formed after sexual reproduction, being the largest within the population) that can double in size terminal or senescent cells, as a consequence of the peculiar decrease in size along the reproduction cycle. If insufficient numbers of specimens are examined, extremes of sizes may be mistaken for different varieties or even species [42]. Besides, it is well-known that the size and morphology of a species also depend on environmental conditions [73], so that specimens should be chosen from as wide as possible a range of habitats and localities [74]. However, type specimens (those used to

fix the names concerned according to the rules of botanical nomenclature) must have been collected from a single locality [75]. In the diagnosis of new taxa, the range of each morphometric (valve length/width) and meristic (density of striae and areolae) parameters observed by the author in the type population are determined. The ranges provided in most works suggest that the usual aim is to give the "normal" range [74], i.e., the interval between which 95% of values of the population fall into so that 2.5% of the individuals will be less/larger than the lower/upper limits, respectively, but the actual meaning of these intervals is unclear in most cases. Subsequent studies may correct (emend) or broaden these ranges, but identification at a specific level of these organisms is usually based on these parameters, so that many taxonomic identification keys (see Chap. 3) lead to the identification of species based only on these criteria [74]. For instance, according to the protologue [76] the only difference between *Cymbella vulgata* var. *vulgata* and *C. vulgata* var. *plitvicensis* lies in valve width (greater or less than 7.8 μm, respectively); however, both taxa are characteristic of very different environmental conditions.

Obviously, the range of each parameter increases along with the observed sample size, although many diagnoses do not specify the number of individuals on which they are based, or this is a clearly insufficient number, so that they do not reflect the natural variability of the species. Some diagnoses are based on a single individual, with no further records elsewhere, as is the case for many new species introduced by Friedrich Hustedt (e.g., *Navicula brehmioides* [77], the so-called pseudotaxa by Lange-Bertalot [78]). This can lead to incorrect identification of some diatoms and, consequently, to an inaccurate estimation of water quality during biomonitoring studies. For instance, only 18% of papers dealing with descriptions or morphological studies of diatoms published in *Diatom Research* between 1986 and 2013 specified sample sizes (pers. obs.).

In 1935, the botanist Edgar Anderson encouraged collectors to gather and deposit in herbaria "at least twenty-five" individuals to allow biometric studies [79]. In the case of diatoms, Kitton had already stated in 1867 that "no new species should be published until a copious gathering has been obtained" [80]. Hendey [41] noted again that "it is necessary to examine, not merely a few specimens, but many carefully prepared strewn slides, in order to ascertain the general overall appearance of the entire population." Since then, the determination of the minimal sample size (MSS) required for the characterization of a population is a classic topic of biostatistics. It must be noted that few diatom morphometric parameters follow normal distributions, smaller individuals being more abundant than larger ones [76] (but see [47]). Moreover, in many taxa only a small proportion of cells in a population reproduce sexually at the same time; such species display a multimodal distribution in cell length [47]. For nonparametrically distributed variables, a specially useful approach is the determination of its "tolerance interval," i.e., the range of values that contain, with a certain probability, a specified interpercentile. Nonparametric tolerance intervals offer a simple, robust tool for assessing the probable sample set coverage [81]. It has been shown that, for any continuously distributed variable, the minimal sample size (N) needed to account for $100\beta\%$ of the individuals with a probability P is given by the formula [82]:

$$N = \left\lceil \frac{\log(1-P)}{\log(\beta)} \right\rceil \tag{4.1}$$

For instance, in the case of diatom length, to obtain a range of values such that only 2.5% of the largest and 2.5% of the smallest valves are excluded ($\beta = 0.95$), with an $\alpha = 0.05$, $N = 59$ individuals should be measured. A more conservative approach following the algorithm first proposed by Wilks [83] suggest that the MSS, in this case, should be $N = 93$ [84, 85]; if the variable can be proven to be at least symmetrically distributed, this number can be reduced to 59 [86].

To assess experimentally, the MSS required to obtain a 90% tolerance interval for valve length and width, we measured 1000 individuals of the following common diatom species: *Cocconeis lineata*, *Cymbella compacta*, *Diatoma vulgaris*, *Didymosphenia geminata*, *Eolimna minima*, *Gomphoneis minuta*, *Gomphonema pumilum*, *Gomphonema rhombicum*, *Navicula cryptotenella*, and *Nitzschia palea*. Measurements were taken with ImageJ software [87] on digital LM images obtained from slides stored in the IMARENABIO-D collection (bit.ly/2GVAI4S) by selecting random microscope fields. For each species, the $N = 100$ measurements were bootstrapped 10 times to simulate random inspections of each population. MSS values obtained varied between 3 and 58 individuals for both parameters, with an average of 22 valves to be measured. Noticeably, MSS was not correlated with the absolute value of the parameter or with its variation coefficient (Fig. 4.10), that is, larger species or intrinsically more variable taxa do not need larger MSS to account for a 90% tolerance interval in valve dimensions. For the case of *D. geminata*'s valve length, we used the $>10^5$ valve length measurements available in [88]. Best-fit curve describing the increase of valve length with increasing N is a saturation function that follows Michaelis–Menten equation (Fig. 4.11):

$$y = \frac{a + x}{bx} \tag{4.2}$$

where a is the asymptotic maximum value expected for the variable (in this case, 177.55 μm). When $y(P_{0.95}) = 142$ μm,

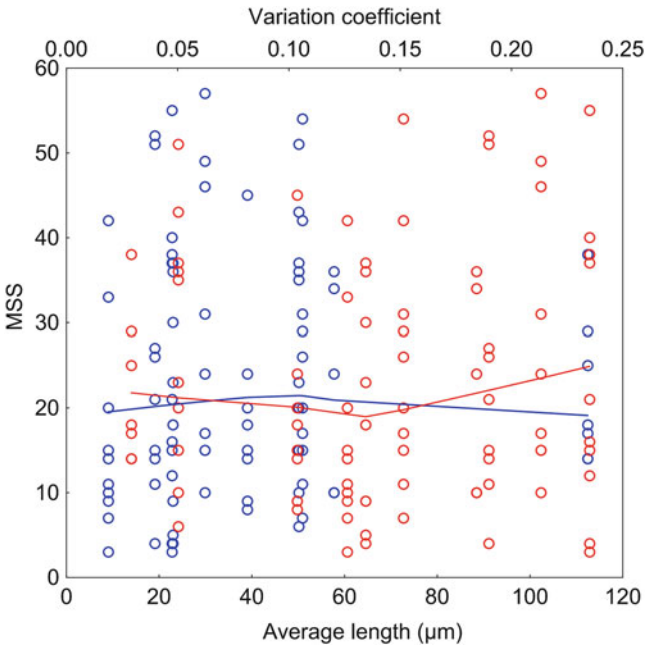

Fig. 4.10 Relationship between the minimum sample size (MSS) needed to observe a 90% tolerance interval in different diatom populations, and valve size (average length in blue, variation coefficient in red). Data fitted to LOESS smoothers

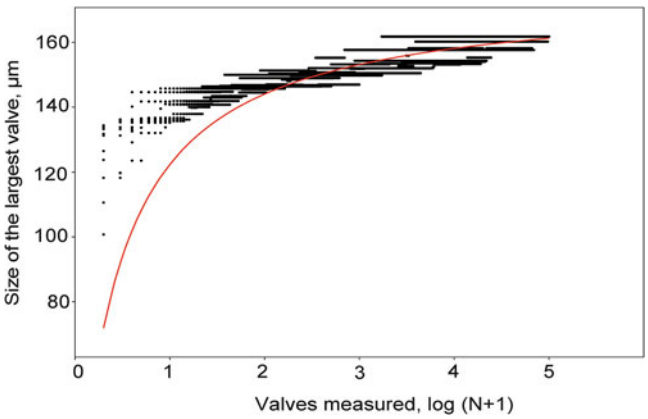

Fig. 4.11 Size of the largest *D. geminata* valve recorded after N individuals are observed. Data from [88], randomized after 10 bootstrap replications

$\lceil x \rceil = 28$ measurements suffice to observe the $P_{0.95}$ largest individual within the population.

It must be noted, however, that if the decision of ascribing a given individual to a certain taxon depends on several measurements, the probability of a false negative increase, and the use of multivariate tolerance regions [89] becomes advisable.

As aforementioned, diatom morphometric data are commonly provided by a mere reference to the maximum and minimum values observed in a population, measured in an often unknown number of individuals. Recent studies tend to inform also about the average, although the median and the quartiles (or the 0.05 and 0.95 percentiles) would be much more informative for skewed data [74, 90], as it is the case in many diatom morphometric parameters. When quantitative attributes have to be used in diagnostic keys it is particularly important to have such information [74]. If the range (a, b), the mean $(\bar{X})$ and the sample size (N) are provided, it is possible to estimate the sample median (m) using Hozo et al.'s [91] formula:

$$m \simeq \frac{\left(aN + a + bN + b - 4\overline{X}\right)}{2\left(N - 1\right)} \tag{4.3}$$

or, more accurately [92]:

$$m \simeq \frac{\left(-2a - 2b + \left(N^{0.75} + 4\right)\overline{X}\right)}{N^{0.75}} \tag{4.4}$$

and the interquartile range (IQR) as estimated in [93]:

$$\mathrm{IQR} \simeq 1.35S \tag{4.5}$$

where the sample variance (S^2) would be [92]:

$$S^2 \simeq \frac{1}{N-1}\left(a^2 + m^2 + b^2 + \frac{(N-3)}{2}\frac{(a+m)^2 + (m+b)^2}{4} - \frac{N(N+2m+b)^2}{16}\right) \tag{4.6}$$

To sum up, we recommend: (1) to inform about the sample size used for the morphometric characterization of diatom populations, especially type populations, (2) to use >59 individuals for such characterizations, and (3) to provide the median and the percentiles for each variable rather than the mean and the range.

4.5 Conclusions

Morphological variations in diatoms care related to their peculiar life cycle or to the impact of environmental factors that can modify the morphometrics or induce teratologies. The organisms exhibiting the latter impairments have different environmental preferenda, compared to their "normal" congeners, making their use promising in a biomonitoring framework. While the percentage of teratologies can easily be included in the calculation of diatom indices to better assess water quality degradation, disentangling the "normal" variability and the environmentally driven changes require appropriate approaches, such as geometric morphometry. However, to well account for subtle variations in morphol-

ogy, large amounts of morphological data are necessary, with the objective of correctly characterizing the natural range of frustule variability within a species and then efficiently discriminate the affected individuals.

Current descriptions of species are based on average dimensions of too low numbers of individuals, it is therefore recommended to increase the number of specimens measured and provide the range of values that can be found in normal population, to constitute a reference set of measurements that can be further used for comparisons and improvement of diatom-based water quality assessment.

Acknowledgments The present contribution was financially supported by a grant of the Romanian National Authority for Scientific Research, CCCDI—UEFISCDI, project 3-005 Tools for sustainable gold mining in EU (SUSMIN). A. González kindly helped us in Sect. 4.4.

References

1. Falasco, E., Bona, F., Ginepro, M., Hlúbiková, D., Hoffmann, L., Ector, L.: Morphological abnormalities of diatom silica walls in relation to heavy metal contamination and artificial growth conditions. Water SA. **35**(5), 595–606 (2009)
2. Lenarczyk, J., et al.: Palaeoecological implications of the subfossil *Pediastrum argentinense*-type in Europe. Rev. Palaeobot. Palynol. **222**, 129–138 (2015)
3. Barinova, S.: Aberrant forms of algae and bioindication of aquatic ecosystem state. Int. J. Oceanogr. Aquac. **1**(3), 1–7 (2017)
4. Munnecke, A., Delabroye, A., Servais, T., Vandenbroucke, T.R., Vecoli, M.: Systematic occurrences of malformed (teratological) acritarchs in the run-up of Early Palaeozoic δ13C isotope excursions. Palaeogeogr. Palaeoclimatol. Palaeoecol. **367**, 137–146 (2012)
5. Falasco, E., Bona, F., Badino, G., Hoffmann, L., Ector, L.: Diatom teratological forms and environmental alterations: a review. Hydrobiologia. **623**(1), 1–35 (2009)
6. Olenici, A., Blanco, S., Borrego-Ramos, M., Jiménez-Gómez, F., Guerrero, F., Momeu, L., Baciu, C.: A new diatom teratology driven by metal pollution in a temperate river (Roșia Montană, Romania). Ann. Bot. **9**, 113–118 (2019)
7. Vartanian, M., Desclés, J., Quinet, M., Douady, S., Lopez, P.J.: Plasticity and robustness of pattern formation in the model diatom *Phaeodactylum tricornutum*. New Phytol. **182**(2), 429–442 (2009)
8. Leguay, S., Lavoie, I., Levy, J.L., Fortin, C.: Using biofilms for monitoring metal contamination in lotic ecosystems: the protective effects of hardness and pH on metal bioaccumulation. Environ. Toxicol. Chem. **35**(6), 1489–1501 (2016)
9. da Silva, E.F., et al.: Heavy metal pollution downstream the abandoned Coval da Mó mine (Portugal) and associated effects on epilithic diatom communities. Sci. Total Environ. **407**(21), 5620–5636 (2009)
10. Koreneva, T., Latkovskaya, E.: Teratological forms of diatomic algae in alga-flora of the Lake Teletskoye (Russian Altai). Water Chem. Ecol. **10**, 112–119 (2013)
11. Majewska, R., Zgrundo, A., Lemke, P., De Stefano, M.: Benthic diatoms of the Vistula River estuary (Northern Poland): seasonality, substrata preferences and the influence of water chemistry. Phycol. Res. **60**(1), 1–19 (2012)
12. Masmoudi, S., et al.: Cadmium, copper, sodium and zinc effects on diatoms: from heaven to hell—a review. Cryptogam. Algol. **34**(2), 185–225 (2013)
13. Arini, A., Durant, F., Coste, M., Delmas, F., Feurtet-Mazel, A.: Cadmium decontamination and reversal potential of teratological forms of the diatom *Planothidium frequentissimum* (Bacillariophyceae) after experimental contamination. J. Phycol. **49**(2), 361–370 (2013)
14. Pandey, L.K., et al.: The use of diatoms in ecotoxicology and bioassessment: insights, advances and challenges. Water Res. **118**, 39–58 (2017)
15. Pandey, L.K., Bergey, E.A.: Exploring the status of motility, lipid bodies, deformities and size reduction in periphytic diatom community from chronically metal (Cu, Zn) polluted waterbodies as a biomonitoring tool. Sci. Total Environ. **550**, 372–381 (2016)
16. Tiam, S.K., Lavoie, I., Doose, C., Hamilton, P.B., Fortin, C.: Morphological, physiological and molecular responses of *Nitzschia palea* under cadmium stress. Ecotoxicology. **27**(6), 675–688 (2018)
17. Pandey, L.K., Kumar, D., Yadav, A., Rai, J., Gaur, J.: Morphological abnormalities in periphytic diatoms as a tool for biomonitoring of heavy metal pollution in a river. Ecol. Indic. **36**, 272–279 (2014)
18. Morin, S., et al.: Consistency in diatom response to metal-contaminated environments. In: Emerging and Priority Pollutants in Rivers, pp. 117–146. Springer, Berlin (2006)
19. Luís, A.T., Teixeira, P., Almeida, S.F.P., Matos, J.X., da Silva, E.F.: Environmental impact of mining activities in the Lousal area (Portugal): chemical and diatom characterization of metal-contaminated stream sediments and surface water of Corona stream. Sci. Total Environ. **409**(20), 4312–4325 (2011)
20. Barral-Fraga, L., Morin, S., Rovira, M.D., Urrea, G., Magellan, K., Guasch, H.: Short-term arsenic exposure reduces diatom cell size in biofilm communities. Environ. Sci. Pollut. Res. **23**(5), 4257–4270 (2016)
21. Pandey, L.K., et al.: River water quality assessment based on a multi-descriptor approach including chemistry, diatom assemblage structure and non-taxonomical diatom metrics. Ecol. Indic. **84**, 140–151 (2018)
22. Cerisier, A., Vedrenne, J., Lavoie, I., Morin, S.: Assessing the severity of diatom deformities using geometric morphometry. Bot. Lett. **166**(1), 32–40 (2019)
23. Olenici, A., Blanco, S., Borrego-Ramos, M., Momeu, L., Baciu, C.: Exploring the effects of acid mine drainage on diatom teratology using geometric morphometry. Ecotoxicology. **26**(8), 1018–1030 (2017)
24. Lavoie, I., et al.: Diatom teratologies as biomarkers of contamination: are all deformities ecologically meaningful? Ecol. Indic. **82**, 539–550 (2017)
25. Fernández, M., et al.: Design and testing of a new diatom-based index for heavy metal pollution. Arch. Environ. Contam. Toxicol. **74**(1), 170–192 (2018)
26. Morin, S., et al.: Long-term survey of heavy-metal pollution, biofilm contamination and diatom community structure in the Riou Mort watershed, South-West France. Environ. Pollut. **151**(3), 532–542 (2008)
27. Blanco, S., Bécares, E.: Are biotic indices sensitive to river toxicants? A comparison of metrics based on diatoms and macroinvertebrates. Chemosphere. **79**(1), 18–25 (2010)
28. Blanco, S., Bécares, E., Cauchle, H.-M., Hoffmann, L., Ector, L.: Comparison of biotic indices tor water quality diagnosis in the Duero Basin (Spain). Arch. Hydrobiol. Suppl. Large Rivers. **161**, 3–4 (2007)
29. CEN: Water Quality–Guidance Standard for the Identification, Enumeration and Interpretation of Benthic Diatom Samples from Running Waters. EN 14407: 2004, Comité Européen de Normalisation, Geneva (2004)
30. Lecointe, C., Coste, M., Prygiel, J.: 'Omnidia': software for taxonomy, calculation of diatom indices and inventories management. Hydrobiologia. **269**(1), 509–513 (1993)

31. Cattaneo, A., Couillard, Y., Wunsam, S., Courcelles, M.: Diatom taxonomic and morphological changes as indicators of metal pollution and recovery in Lac Dufault (Québec, Canada). J. Paleolimnol. **32**(2), 163–175 (2004)
32. ter Braak, C.J., van Dam, H.: Inferring pH from diatoms: a comparison of old and new calibration methods. Hydrobiologia. **178**(3), 209–223 (1989)
33. Coste, M., Boutry, S., Tison-Rosebery, J., Delmas, F.: Improvements of the biological diatom index (BDI): description and efficiency of the new version (BDI-2006). Ecol. Indic. **9**(4), 621–650 (2009)
34. Beszteri, B., Ács, É., Medlin, L.: Conventional and geometric morphometric studies of valve ultrastructural variation in two closely related *Cyclotella* species (Bacillariophyta). Eur. J. Phycol. **40**(1), 89–103 (2005)
35. Julius, M., Estabrook, G., Edlund, M., Stoermer, E.: Recognition of taxonomically significant clusters near the species level, using computationally intense methods, with examples from the *Stephanodiscus niagarae* complex (Bacillariophyceae). J. Phycol. **33**, 1049–1054 (1997)
36. Beszteri, B.: Morphometric and Molecular Investigations of Species Limits in *Cyclotella meneghiniana* (Bacillariophyceae) and Closely Related Species. Doctoral Dissertation, Verlag nicht ermittelbar (2005)
37. Cox, E.J.: Diatom systematics—a review of past and present practice and a personal vision for future development. Beih. Nova Hedwig. **106**, 1–20 (1993)
38. Blanco, S., Cejudo-Figueiras, C., Álvarez-Blanco, I., Bécares, E., Hoffmann, L., Ector, L.: Atlas de las Diatomeas de la Cuenca del Duero-Diatom Atlas of the Duero Basin. Área de Publicaciones, Universidad de León, León (2011)
39. Macdonald, J.D.: On the structure of the Diatomaceous frustule and its genetic cycle. J. Nat. Hist. **3**(13), 1–8 (1869)
40. Pfitzer, E.H.H.: Untersuchungen über Bau und Entwicklung der Bacillariaceen (Diatomaceen). Marcus, Bonn (1871)
41. Hendey, N.I.: Littoral diatoms op Chichester harbour with special reference to fouling. J. R. Microsc. Soc. **71**(1), 1–86 (1951)
42. Lund, J.: Observations on soil algae. 1. The ecology, size and taxonomy of British soil diatoms. New Phytol. **45**(1), 56–110 (1946)
43. Kingston, J., Pappas, J.L.: Quantitative shape analysis as a diagnostic and prescriptive tool in determining *Fragilariforma* (Bacillariophyta) taxon status. Nova Hedwig. Beih. **135**, 103–119 (2009)
44. Mou, D., Stoermer, E.F.: Separating *Tabellaria* (Bacillariophyceae) shape groups based on Fourier descriptors 1. J. Phycol. **28**(3), 386–395 (1992)
45. Round, F.E., Crawford, R.M., Mann, D.G.: Diatoms: Biology and Morphology of the Genera. Cambridge University Press, Cambridge (1990)
46. Shukla, S.K., Romero, O.E.: Glacial valve size variation of the Southern Ocean diatom *Fragilariopsis kerguelensis* preserved in the Benguela Upwelling System, Southeastern Atlantic. Palaeogeogr. Palaeoclimatol. Palaeoecol. **499**, 112–122 (2018)
47. Bishop, I.W., Spaulding, S.A.: Life cycle size dynamics in *Didymosphenia geminata* (Bacillariophyceae). J. Phycol. **53**(3), 652–663 (2017)
48. Meyer, B., Wulf, M., Håkansson, H.: Phenotypic variation of life-cycle stages in clones of three similar *Cyclotella* species after induced auxospore production. Diatom Res. **16**(2), 343–361 (2001)
49. Pfister, C.A., Stevens, F.R.: The genesis of size variability in plants and animals. Ecology. **83**(1), 59–72 (2002)
50. Soudek Jr., D., Robinson, G.: Electrophoretic analysis of the species and population structure of the diatom *Asterionella formosa*. Can. J. Bot. **61**(2), 418–433 (1983)
51. Cortese, G., Gersonde, R.: Morphometric variability in the diatom *Fragilariopsis kerguelensis*: implications for Southern Ocean paleoceanography. Earth Planet. Sci. Lett. **257**(3–4), 526–544 (2007)
52. Kerrigan, E.A., Irwin, A.J., Finkel, Z.V.: Community-and population-level changes in diatom size structure in a subarctic lake over the last two centuries. PeerJ. **3**, e1074 (2015)
53. Marchetti, A., Cassar, N.: Diatom elemental and morphological changes in response to iron limitation: a brief review with potential paleoceanographic applications. Geobiology. **7**(4), 419–431 (2009)
54. Trobajo Pujadas, R.: Ecological Analysis of Periphytic Diatoms in Mediterranean Coastal Wetlands (Empordà Wetlands, NE Spain). ARG Gantner Verlag, Ruggell (2010)
55. Gari, E., Corigliano, M.: Spatial and temporal variations of *Cocconeis placentula* var. *euglypta* (Ehrenb.) 1854 Grunow, 1884 in drift and periphyton. Braz. J. Biol. **67**(4), 587–595 (2007)
56. Cox, E.J.: Morphogenetic information and the selection of taxonomic characters for raphid diatom systematics. Plant Ecol. Evol. **143**(3), 271–277 (2010)
57. Pappas, J.L., Stoermer, E.F.: Multidimensional analysis of diatom morphologic and morphometric phenotypic variation and relation to niche. Ecoscience. **2**(4), 357–367 (1995)
58. Finkel, Z.V., Beardall, J., Flynn, K.J., Quigg, A., Rees, T.A.V., Raven, J.A.: Phytoplankton in a changing world: cell size and elemental stoichiometry. J. Plankton Res. **32**(1), 119–137 (2009)
59. Pappas, J.L., Stoermer, E.F.: Morphometric comparison of the neotype of Asterionella formosa Hassall (Heterokontophyta, Bacillariophyceae) with Asterionella edlundii s p. nov. from Lake Hovsgol, Mongolia. Diatom. **19**, 55–65 (2003)
60. Passy, S.I.: Differential cell size optimization strategies produce distinct diatom richness–body size relationships in stream benthos and plankton. J. Ecol. **95**(4), 745–754 (2007)
61. Kociolek, J.P., Williams, D.M.: Unicell ontogeny and phylogeny: examples from the diatoms. Cladistics. **3**(3), 274–284 (1987)
62. Schmid, A.-M.M.: Aspects of morphogenesis and function of diatom cell walls with implications for taxonomy. In: The Protistan Cell Surface, pp. 43–60. Springer, Berlin (1994)
63. Potapova, M., Hamilton, P.B.: Morphological and ecological variation within the *Achnanthidium minutissimum* (Bacillariophyceae) species complex 1. J. Phycol. **43**(3), 561–575 (2007)
64. Kling, H.J.: Ecology, Ontogeny and Morphometry of the Freshwater Centric Diatom Species Complex *Cyclotella bodanica/radiosa*. Master thesis, University of Manitoba, Winnipeg (1997)
65. Trobajo, R., Rovira, L., Ector, L., Wetzel, C.E., Kelly, M., Mann, D.G.: Morphology and identity of some ecologically important small *Nitzschia* species. Diatom Res. **28**(1), 37–59 (2013)
66. Theriot, E.: An empirically based model of variation in rotational elements in centric diatoms with comments on ratios in phycology 1. J. Phycol. **24**(3), 400–407 (1988)
67. Savriama, Y., Neustupa, J., Klingenberg, C.P.: Geometric morphometrics of symmetry and allometry in *Micrasterias rotata* (Zygnemophyceae, Viridiplantae). Nova Hedwig. Suppl. **136**, 43–54 (2010)
68. Quinones, R.A., Platt, T., Rodríguez, J.: Patterns of biomass-size spectra from oligotrophic waters of the Northwest Atlantic. Prog. Oceanogr. **57**(3–4), 405–427 (2003)
69. Marchetti, A., Maldonado, M.T., Lane, E.S., Harrison, P.J.: Iron requirements of the pennate diatom *Pseudo-nitzschia*: comparison of oceanic (high-nitrate, low-chlorophyll waters) and coastal species. Limnol. Oceanogr. **51**(5), 2092–2101 (2006)
70. Paull, T.M., Hamilton, P.B., Gajewski, K., LeBlanc, M.: Numerical analysis of small Arctic diatoms (Bacillariophyceae) representing the *Staurosira* and *Staurosirella* species complexes. Phycologia. **47**(2), 213–224 (2008)

71. Genkal, S.: Morphological variability and taxonomy of *Diatoma tenue* Ag. (Bacillariophyta). Int. J. Algae. **6**(4), 319–330 (2004)
72. Blanco, S., Borrego-Ramos, M., Olenici, A.: Disentangling diatom species complexes: does morphometry suffice? PeerJ. **5**, e4159 (2017)
73. Smol, J.P., Stoermer, E.F.: The Diatoms: Applications for the Environmental and Earth Sciences. Cambridge University Press, Cambridge (2010)
74. Jardine, N., Sibson, R.: Quantitative attributes in taxonomic descriptions. Taxon. **19**, 862–870 (1970)
75. Turland, N., et al.: International code of nomenclature for algae, fungi and plants. Regnum Veg. **159**, 1–254 (2018)
76. Krammer, K.: Diatoms of Europe. Diatoms of the European Inland Waters and Comparable Habitats. Vol. 3. *Cymbella*. ARG Gantner Verlag KG, Ruggell (2002)
77. Tusset, E.A., Tremarin, P.I., Straube, A., Ludwig, T.A.: Morphology of *Adlafia* taxa (Bacillariophyta, Cymbellaceae), with proposition of two new species from Brazil. Phytotaxa. **306**(4), 259–274 (2017)
78. Lange-Bertalot, H.: As a practical diatomist, how does one deal with the flood of new names? Diatom. **13**, 9–12 (1997)
79. Anderson, E., Turrill, W.B.: Biometrical studies on herbarium material. Nature. **136**(3451), 986 (1935)
80. Kitton, F.: Remarks on the publication of new genera and species from insufficient material. J. Cell Sci. **2**(26), 118–121 (1897)
81. Barnes, R.J.: Bounding the required sample size for geologic site characterization. Math. Geol. **20**(5), 477–490 (1988)
82. Mood, A.M.: Introduction to the Theory of Statistics. McGraw-Hill, New York (1974)
83. Wilks, S.S.: Determination of sample sizes for setting tolerance limits. Ann. Math. Stat. **12**(1), 91–96 (1941)
84. Hahn, G.J., Meeker, W.Q.: Statistical Intervals: A Guide for Practitioners. Wiley, New York (1991)
85. Somerville, P.N.: Tables for obtaining non-parametric tolerance limits. Ann. Math. Stat. **29**(2), 599–601 (1958)
86. Walsh, J.E.: Distribution-free tolerance intervals for continuous symmetrical populations. Ann. Math. Stat. **33**, 1167–1174 (1962)
87. Schneider, C.A., Rasband, W.S., Eliceiri, K.W.: NIH Image to ImageJ: 25 years of image analysis. Nat. Methods. **9**(7), 671 (2012)
88. Bishop, I.W., Spaulding, S.A.: Data from: "Life Cycle Size Dynamics in *Didymosphenia geminata* (Bacillariophytceae)", Dryad Digital Repository. bit.ly/2K5f6DU
89. Abt, K.: Scale-independent non-parametric multivariate tolerance regions and their application in medicine. Biom. J. **24**(1), 27–48 (1982)
90. Lang, T.A., Altman, D.G.: Basic statistical reporting for articles published in biomedical journals: the 'Statistical Analyses and Methods in the Published Literature' or the SAMPL guidelines. Eur. Assoc. Sci. Ed. **256**, 256 (2013)
91. Hozo, S.P., Djulbegovic, B., Hozo, I.: Estimating the mean and variance from the median, range and the size of a sample. BMC Med. Res. Methodol. **13**, 1–10 (2005)
92. Luo, D., Wan, X., Liu, J., Tong, T.: Optimally estimating the sample mean from the sample size, median, mid-range, and/or mid-quartile range. Stat. Methods Med. Res. **27**(6), 1785–1805 (2018)
93. Dietz, T., Kalof, L.: Introduction to Social Statistics: The Logic of Statistical Reasoning. John Wiley & Sons, New York (2009)

Part II

Sensing

Microscopic Modalities and Illumination Techniques

5

J. Piper and T. Piper

Abstract

This chapter gives an introduction to basic optical principles and components of a light microscope (light source, condenser, objective [finite and infinite systems], tube lens, and eyepiece). Light microscope imaging of complex structured, three-dimensional objects having a high thickness and low contrast due to a lack of intrinsic color, presents a number of challenges for conventional types of illumination. Several technical modifications and additional alternative techniques have been presented and evaluated in the following sections.

5.1 Introduction

Compound light microscopes can be regarded as basic equipment for examination of diatoms and other specimens in life sciences. Although most diatomists may be familiar with light microscopy, a short review of historical roots, principles, and optical components of light microscopes is given in the first section, followed by short descriptions of the most important and widely used illumination modes established in routine. Each of these illumination techniques is characterized by specific advantages and disadvantages and affected with typical limitations and artifacts which are relevant for practice.

In particular, light microscope imaging of complex structured, three-dimensional objects having a high thickness and low contrast due to a lack of intrinsic color presents a number of challenges for conventional types of illumination. This also applies to the imaging of objects with large differences in regional densities as well as phase shifting and light absorbing details. If they have a low density, such problematic objects have low contrast in standard bright-field illumination. Fine internal structures may be hidden from the observer. Closing the aperture diaphragm increases the depth of field and leads to enhancements of contrast but lowers the resolution. However, one advantage of this method is that it is based on the zeroth-order diffraction maximum and is almost free from artifacts, as long as the apertures of the illuminating and imaging components remain adequate. In dark-field, the object shows its intrinsic color; however, the image may be affected by edge blooming caused by scattered light. Furthermore, the depth of field cannot be increased by closing the aperture diaphragm. In phase contrast, thin objects with low contrast can be visualized with superior quality; however, "thick" or optically dense objects often appear with broad marginal contours caused by undesirable halo artifacts. Moreover, in standard phase contrast, the spatial depth cannot be enhanced by closing the aperture diaphragm. Interference contrast is characterized by relief effects which are only real in regions of constant optical density and refractive index. Otherwise, pseudo-relief effects will occur. Structures of very low density may be imaged with a lower contrast when compared with phase contrast. In standard fluorescence microscopy, only fluorescent structures are selectively visualized so that their nonfluorescent environment remains invisible.

In view of these issues, several technical modifications and additional alternative techniques have been evaluated that combine the advantages of the aforementioned methods and also offer improved imagery. These techniques recently developed are presented in the following sections. Moreover, even in some biological probes, such as diatom frustules, for instance, incident light may contribute further visual information, especially when combined with transmitted light microscopy. Thus, our contribution also deals with these practical aspects.

J. Piper (✉) · T. Piper
Laboratory for Applied Microscopy Research, Bullay, Germany
e-mail: lab-appl-microscopy-research@t-online.de

G. Cristóbal et al. (eds.), *Modern Trends in Diatom Identification*, Developments in Applied Phycology 10,
https://doi.org/10.1007/978-3-030-39212-3_5

5.2 Principles and Optical Basics in Light Microscopy

In this chapter, fundamental principles of light microscopy are described in the first section, followed by explanations of the most commonly used light sources and illumination techniques established for routine tasks. Additionally, several new methods are described based on modifications of standard techniques or multimodal microscopy, i.e., combination of two or more illumination techniques which are simultaneously carried out. With the help of these methods recently developed, especially "problematic" specimens characterized by high ranges of local thickness and density, ultra-low density or complex three-dimensional architecture can be revealed in superior clarity and precision.

5.2.1 Light Pathway of a Compound Microscope

Modern light microscopes are built up as so-called compound microscopes. The objective generates a real intermediate image which is projected into the tube. This intermediate image leads to a magnified image of the specimen. The grade of magnification corresponds with the objective's magnification factor (Fig. 5.1). The distance between the back focal plane of the objective and the plane of the intermediate image is called "optical tube length" (Fig. 5.1). The intermediate image is magnified further by the eyepiece, and the grade of post-magnification is determined by the magnification factor of the eyepiece as well. Thus, the eyepiece generates a magnified virtual image of the intermediate image. This image is projected to the retina of the human eye (Fig. 5.2). Subsidiary, the final image can be detected by a camera sensor or a photographic film instead of the retina. All in all, the specimen is magnified in two steps, firstly by the objective, secondly by the eyepiece. The total magnification can be calculated by multiplying the magnification factors of the objective and eyepiece. Example: A circular diatom frustule, diameter: 0.1 mm, is observed with a 40-fold magnifying objective combined with a 10-fold magnifying eyepiece. In this case, the total magnification is $40 \times 10 = 400\times$. In visual observation, the diatom now appears at a virtual size of $0.1 \times 400 = 40$ mm.

Historical Annotation:
Robert Hooke (1635–1703), a famous pioneer of light microscopy, worked with a simply constructed compound mi-

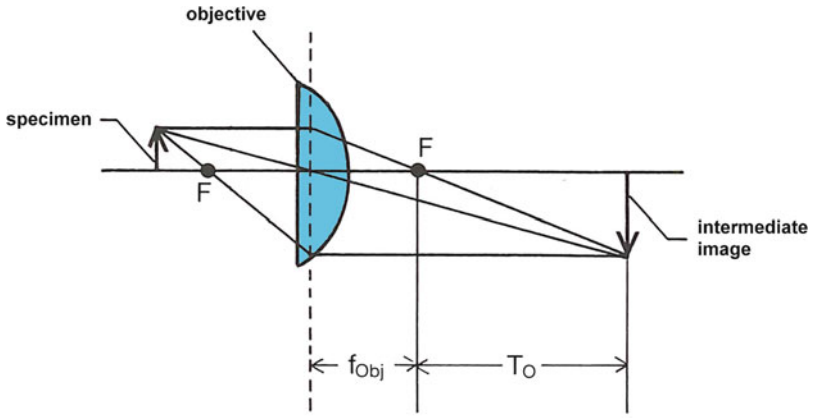

Fig. 5.1 Simplified principle of a microscope objective (here: single lens), f_{Obj} = focal length of the objective, T_O = optical tube length

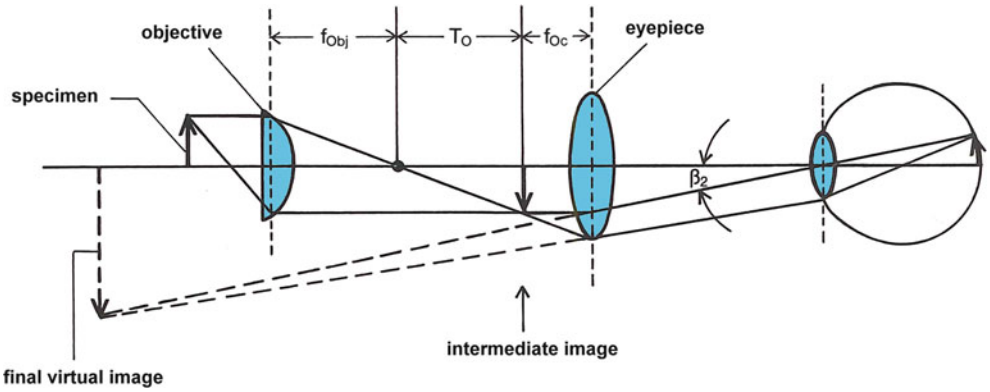

Fig. 5.2 Simplified principle of a compound microscope, f_{Obj} = focal length of the objective, T_O = optical tube length, f_{Oc} = focal length of ocular (eyepiece). Annotation: objective's magnification shown here: circa 1×

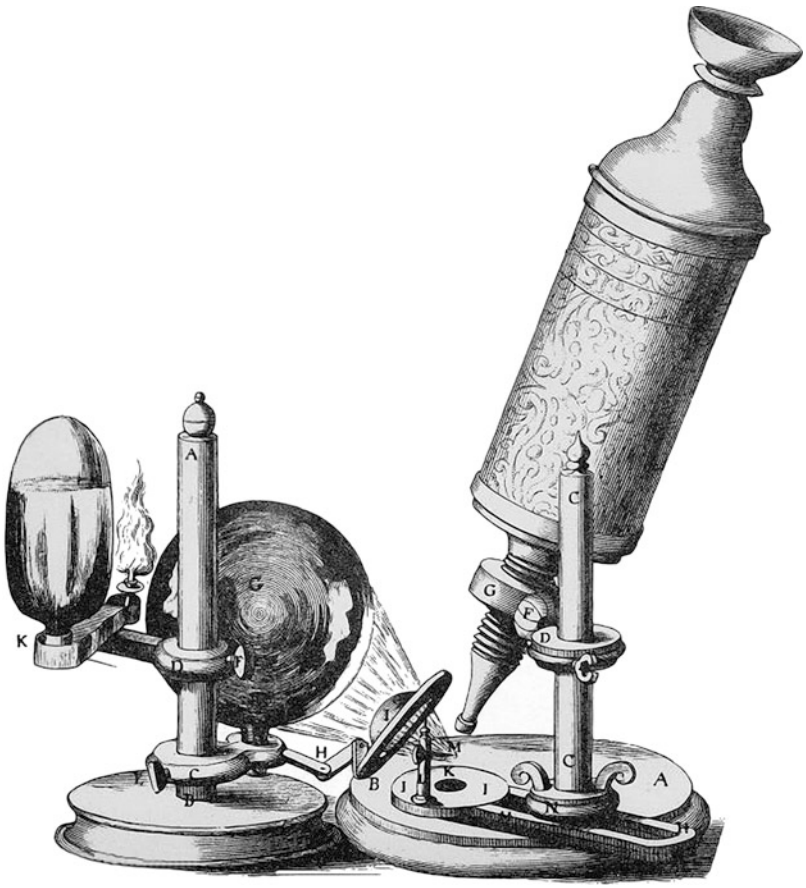

Fig. 5.3 Historical microscope of Robert Hooke (modified from "Micrographia", 1665)

croscope (Fig. 5.3). The ancient glass lenses were affected with severe optical aberrations which were multiplied by the succeeding post-magnification achieved by the eyepiece. Thus, the total magnification of this instrument was limited to circa 50×.

Antony van Leeuwenhoek (1632–1723), however, worked with a more simple type of microscope consisting of only one single lens (Fig. 5.4, modified from [1]) which led to a much higher magnification (about 270×). While Hooke used incident light (see Fig. 5.3), Leeuwenhoek's observations were based on transmitted light. Thus, he could describe several small transparent objects such as human erythrocytes and bacteria from the oral mucosa (Fig. 5.5).

5.2.2 Optical Components in General

Each sort of light microscope consists of several typical components which can be regarded as elementary and fundamental parts.

5.2.2.1 Light Source

In biology, medicine, and other life sciences microscopic examinations of transparent specimens are commonly carried out with transmitted light. The light source is integrated into the microscope stand, or external light sources—in most cases implemented in so-called lamp housings—are coupled with the respective stand. In other disciplines, opaque specimens are observed with incident light. In the latter case, external light sources can be used, fitted with swan neck fibers, for instance, or special illuminators designed for incident light are integrated into the microscope.

Bulb

Bulb or halogen light is the traditional solution for illumination being independent of sunshine or daylight. A typical light spectrum of a halogen bulb is shown in Fig. 5.6a. These light sources are characterized by continuous light spectra and low color temperature (circa 2500 K), so that the light emitted can be described as "warm." Color images taken with unfiltered bulb light are affected with a typical red, orange, or yellowish hue. The lower the intensity of light, the lower the color temperature will be. On the other hand, the range of colors and color tunes is maximized, because no wavelengths are excluded from the light spectrum.

LED

Many up-to-date microscopes are fitted with light emitting diodes (LED). A typical light spectrum of a 6000 K LED is presented in Fig. 5.6b. All in all, a high wide variety of LEDs is available being different in color temperature and light spectra. In most cases, the color temperatures of LEDs used

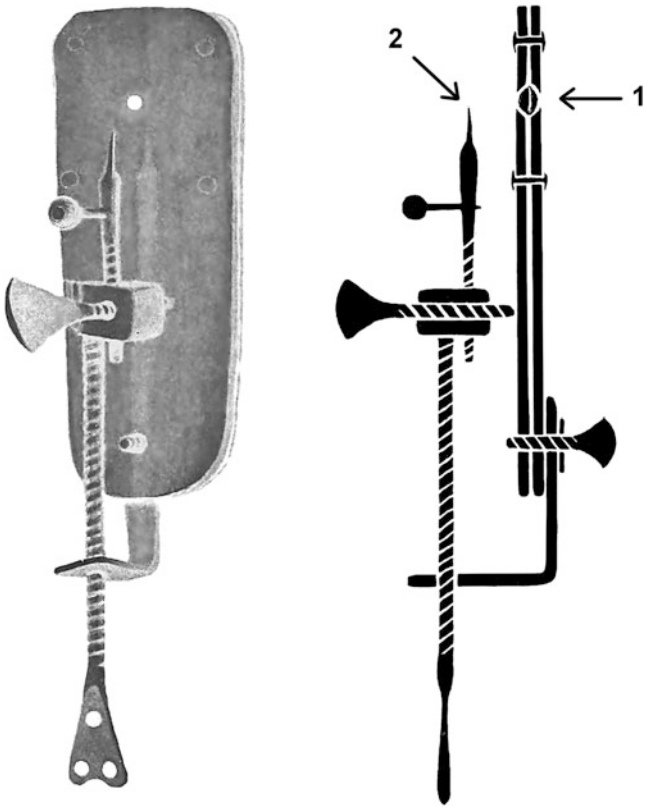

Fig. 5.4 Historical microscope of Antony van Leeuwenhoek (modified from Dobell [1]), biconvex single lens (1), specimen holder (2)

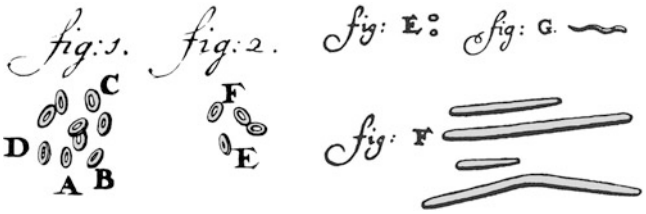

Fig. 5.5 Human erythrocytes (left and center) and bacteria from the oral mucosa (right), historical drawing from A. van Leeuwenhoek (1632–1723)

in light microscopy are significantly higher than in traditional bulb light; they normally range from 4500 to 6000 K. Some of them lead to "neutral" colorization of microscope images, others may have a slight green or blue taint. In many LEDs, especially red tones appear somewhat suppressed, or original red colors may be converted to violet. Moreover, the range and differentiation of colors may be lower than in bulb light, because most LEDs do not have a continuous light spectrum comparable with natural light. In contrast to blub light, the color temperature of an LED remains nearly constant over the full range of intensity, and the duration of life is significantly higher than in each sort of bulb. All in all, it may be influenced by the specific microscopic task and the personal preference of the user whether bulb or LED light is preferred.

Flash

A flash can be used for taking photomicrographs of motile specimens. Thus, any indistinctness caused by locomotion can be avoided. The color temperature of a flash is circa 6500 K so that a slight bluish hue may be visible. This dominance of blue can be mitigated by appropriate filters. Of course, the flash has to be appropriately integrated into the pathway of the illuminating light. Some examples of technical solutions are shown in Figs. 5.7, 5.8, and 5.9. The exposure of photomicrographs taken with a flash can be varied by gray filters or—in some cases—with the help of automatic metering systems.

5.2.2.2 Condenser

Condensers are optical systems used for forming and modulating the illuminating light. Divergent light beams emitted by the light source are at first parallelized by the so-called collector which is integrated into the microscope stand. Collectors mostly consist of a single lens (Fig. 5.10a), or they are designed as a double lens system (Fig. 5.10b, c). After passing the collector, the parallelized illuminating light beams run to the condenser (Fig. 5.10b, c). By the condenser lens system, the illuminating light beams are focused on the specimen plane, by closing the aperture diaphragm the light

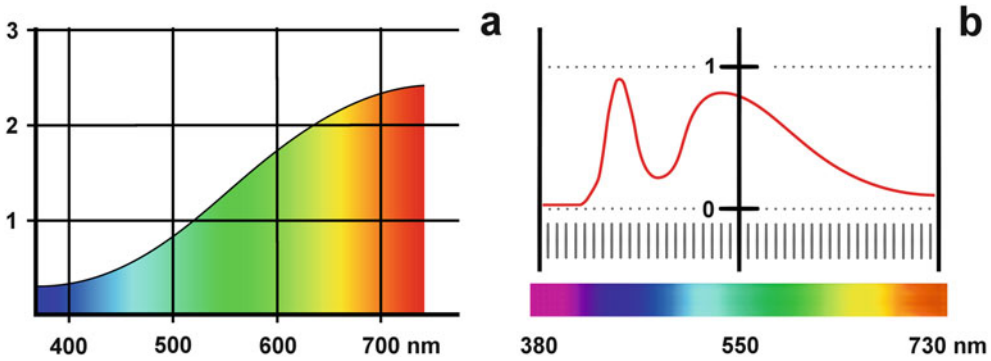

Fig. 5.6 Light spectra of a halogen bulb (**a**) and 6000 K LED (**b**)

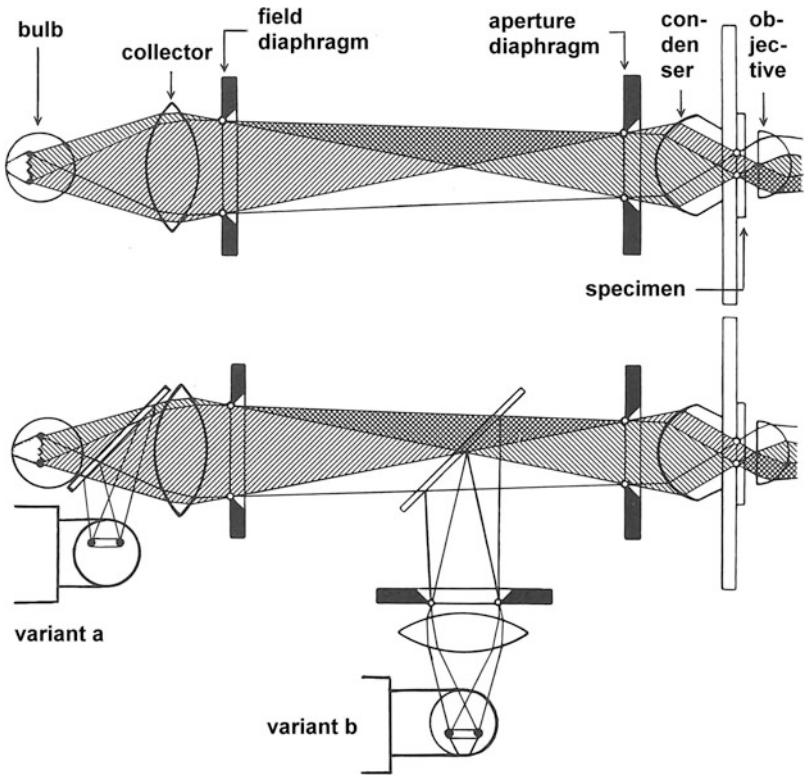

Fig. 5.7 Technical suggestions for integration of a flash used for photomicrography

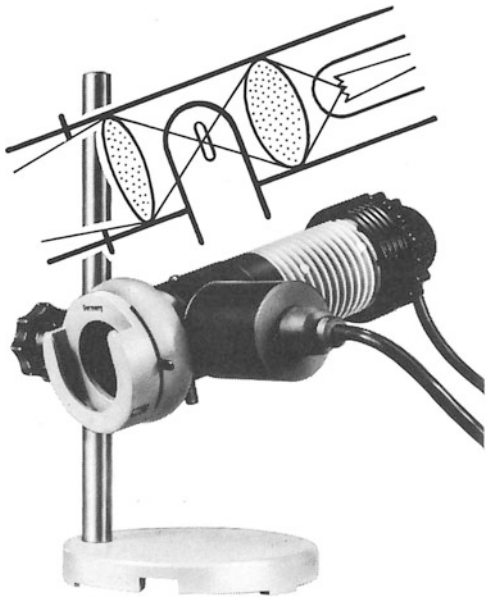

Fig. 5.8 Example of "variant b" from Fig. 5.7

beams can be collimated so that contrast and depth of field are enhanced, whereas the condenser aperture and lateral resolution are reduced.

Various illumination techniques such as dark-field, phase contrast, and differential interference contrast (DIC) are achieved by special sorts of condensers which are described in separate sections.

5.2.2.3 Objective

The objective is the "heart" of the imaging system, which—in first line—determinates the image quality, in particular, lateral and vertical resolution, purity of colors, contrast, distinctness, and planarity of field. Categories of quality are defined by the grade of correction regarding the chromatic aberration (achromatic, semi apochromatic and apochromatic systems, Fig. 5.11) and the spherical aberration (standard lenses vs. plane objectives). Basic parameters of each objective are the magnification factor and the numerical aperture (NA). The lateral resolution, i.e., the smallest distance "*d*" of structures which can be revealed, is approximately calculated as follows: $d = 0.6\,\lambda/\mathrm{NA}$ (Rayleigh criterion). The smaller is the wavelength λ of the illuminating light and the higher is the NA of the imaging system, the smaller is this distance "*d*." Thus, for maximizing the lateral resolution, the wavelength has to be as short and the numerical aperture as high as possible. In normal circumstances, the lateral resolution achievable with a standard light microscope is restricted to circa 0.2 μm.

In so-called dry systems the maximum limit of NA is ≤0.9. For a higher NA, the objective has to be designed as an "immersion system" (water immersion: NA ≤ 1.2, glycerin immersion: NA ≤ 1.3, oil immersion: NA ≤ 1.4). Figure 5.12 demonstrates the influence of immersion oil on the numerical aperture. While light beam 1, as shown in Fig. 5.12, cannot contribute to the final image in dry immersion as it is bent or even reflected at the upper side of the specimen slide, it can enter the objective in oil immersion due to a refractive index higher than air.

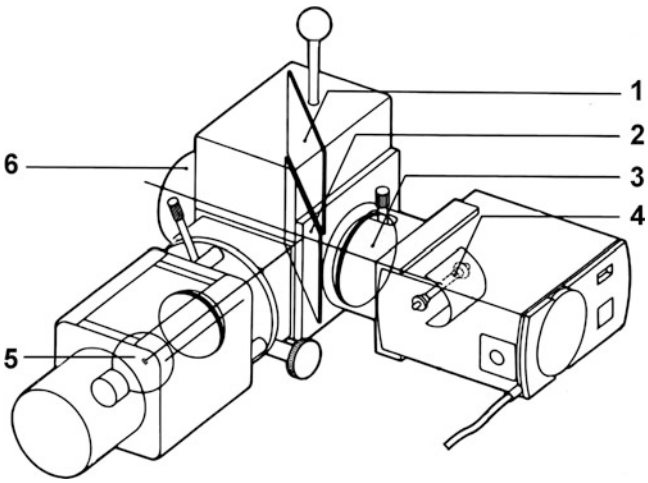

Fig. 5.9 "Micro flash" device from E. Leitz/Leica Wetzlar, consisting of semi permeable mirrors (1, 2), collector lens (3), flash (4), (halogen) bulb/pilot light (5), bayonet (6)

The working distance, i.e., the distance between the objective's front lens and the specimen or coverslip, and also the depth of field are reverse to the grades of magnification and numerical aperture. Thus, an "ideal" universal objective does not exist so that the selection of an objective should correspond with the specific microscopic task.

Systems for Finite Tube Length ("Finite Systems")

In the course of technical history, light microscopes were firstly designed as finite systems according to the schematic light path shown in Fig. 5.2. In this optical design, the objective generates the intermediate image as a standalone system so that only two components are needed for generating the final microscope image: the objective and the eyepiece. In most microscopes of this sort, the intermediate image is not completely purified from optical artifacts. Thus, the optical design of the eyepiece is adapted to the corresponding objective so that these remaining artifacts are compensated by the eyepiece used. For this reason, such eyepieces are

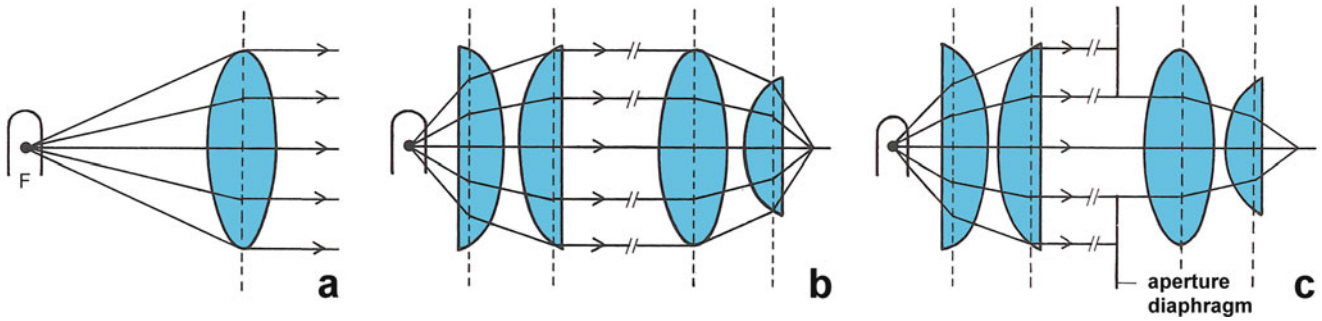

Fig. 5.10 Principles of single (**a**) and double (**b**, **c**) collector lenses interacting with a condenser (**b**, **c**) fitted with an aperture diaphragm (**c**)

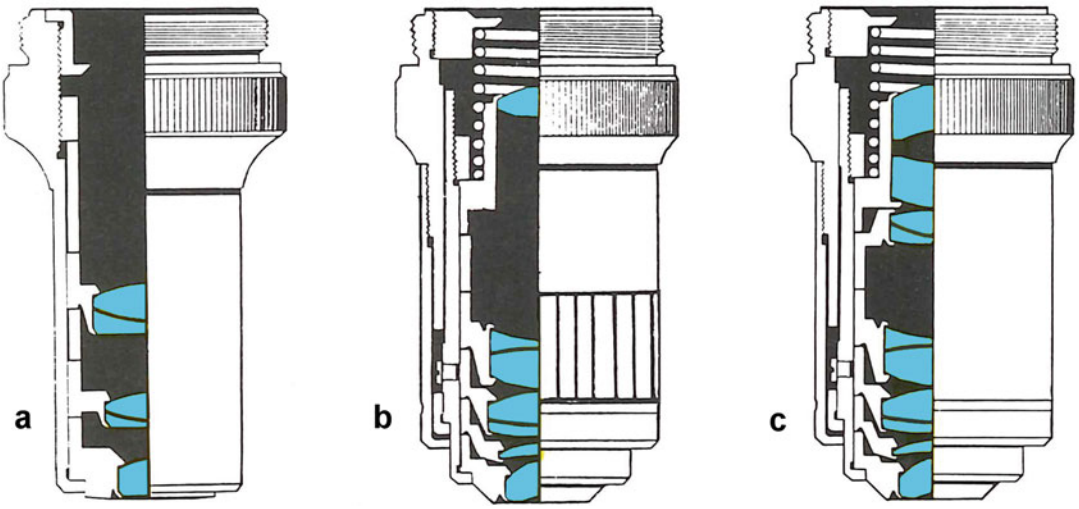

Fig. 5.11 Achromatic (**a**) semi apochromatic (**b**) and apochromatic (**c**) objectives

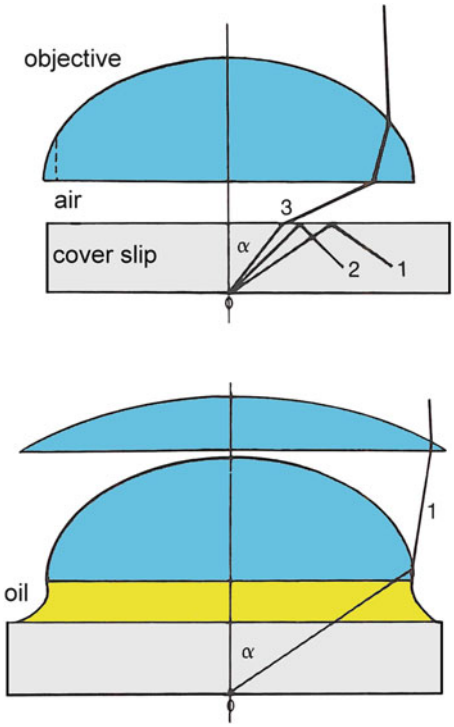

Fig. 5.12 Comparison of a dry (top) and oil immersion lens (bottom)

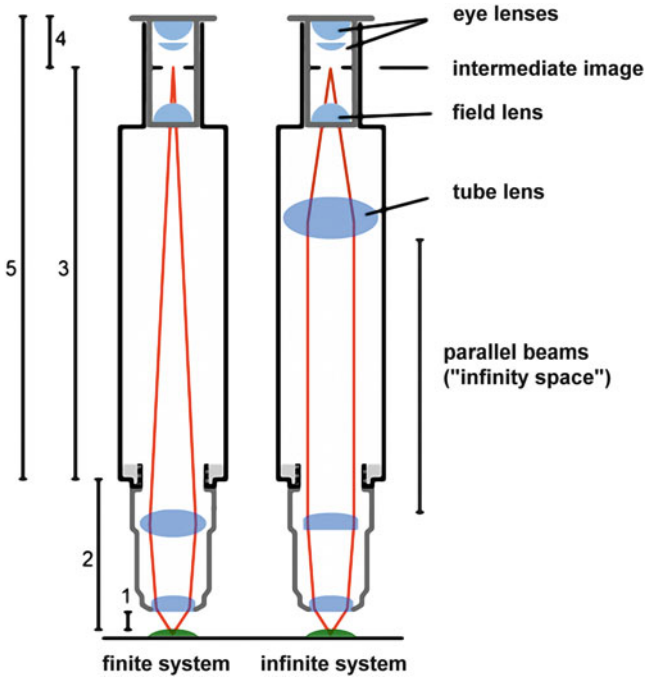

Fig. 5.13 Comparison of a finite and infinite system (modified and redrawn from [2]). 1 = working distance, 2 = adjustment length, 3 = image distance of the objective, 4 = intermediate image distance of the ocular, 5 = mechanical tube length

called "compensating oculars." When the original eyepiece designed for the finite objective used is replaced by another one constructed by another manufacturer the quality of the final image observed may be reduced in the case that remaining aberrations of the intermediate image are no longer completely eliminated. Beside the optical tube length already mentioned (see Fig. 5.2) a "mechanical tube length" can be defined as the distance of the objective's barrel and the external lens of the eyepiece. In most finite systems this mechanical tube length is standardized to 160 or 170 mm. In each finite microscope, the mechanical tube length remains constant for all combinations of objectives and eyepieces designed for the respective instrument.

Systems for Infinite Tube Length ("Infinite Systems")

Circa at the beginning of the 1990s, the leading "big four" manufacturers of microscopes (Zeiss, Leitz/Leica, Olympus, and Nikon) developed new generations of standard microscopes based on infinite optics. The principles and differences of infinite and finite systems are demonstrated in Fig. 5.13 (modified from [2]). In infinite objectives, the image generating light beams running to and being inside of the tube are parallelized. Thus, the final image is not influenced by the mechanical tube length as long as the light beams remain parallel. In theory, the proportion of the tube passed by these parallel beams could have an infinite length. In order to collimate these parallel beams, a tube lens is necessary as an additional and obligatory optical component which generates the intermediate image in the usual plane, beneath the eye lens of the eyepiece. Thus, the intermediate image is formed by two coactive components, the objective, and the tube lens. These both components are optically adjusted to each other so that the intermediate image is free from remaining aberrations or artifacts. Consequently, the eyepieces of an infinite microscope do not work as "compensating" systems, but as so-called non-compensating oculars. Therefore, compensating oculars from finite instruments should not be used with an infinite system and vice versa. Moreover, infinite objectives are strictly designed for their coactive tube lens so that objectives from one defined manufacturer should not be combined with microscopes and tube lenses of another one.

5.2.2.4 Tube Lens

As described above, tube lenses are obligatory components in infinite microscopes. Moreover, some finite microscopes can also be fitted with facultative tube lenses for specific tasks. Some microscopes of this sort may contain 0.8 or 1.25× tube lenses, for instance, so that the magnification factor of the objectives used can be varied. In this case, a 10-fold magnifying objective can also be used as an 80- or 125-fold one. Additionally, tube lenses are necessary for finite systems when illuminators for incident light have to be integrated into standard microscopes so that the distance between objective and eyepiece is greater than in normal circumstances. In this case, the tube lens is used for optical compensation of the resulting enlargement of the tube length.

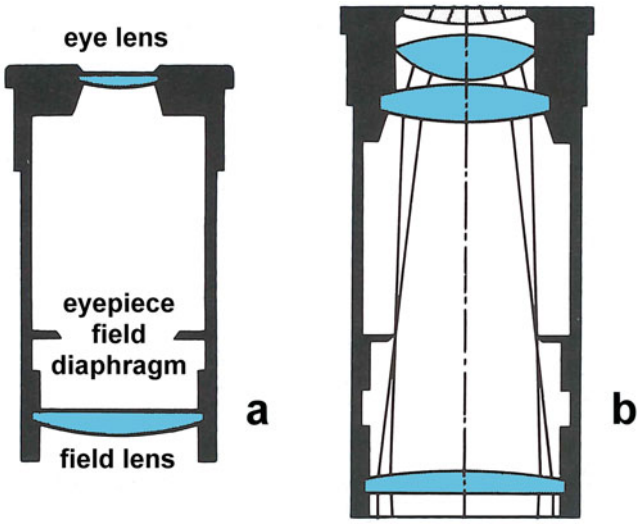

Fig. 5.14 Huygens (**a**) and wide field (**b**) ocular (eyepiece)

5.2.2.5 Eyepiece

Eyepieces (oculars) are used for magnification of the intermediate image—in finite and infinite microscopes. Simply constructed so-called Huygens oculars consist of two lenses, the "eye lens" and the "field lens" (Fig. 5.14a). The eye lens is used for magnifying the intermediate image, whereas the field lens leads to an enlargement of the field observable. The circular margin of the field observed results from the eyepiece's field diaphragm (Fig. 5.14). Figure 5.15 demonstrates the effects of both lenses mentioned.

For high-end objectives, eyepieces have been developed further so that more complex lens systems interact as eye and field lenses (Fig. 5.14b). In particular, so-called wide field oculars are designed in this manner. They interact with compatible wide field objectives. Such eyepieces are a special advantage when an overview of a great field is desired which can directly be observed without moving the specimen or specimen slide.

5.3 Standard Illumination Techniques

In this chapter, typical standard techniques are described which are commonly be used in several routine tasks. The following descriptions are focused on practical aspects. For further theoretical explanations, special literature is recommended.

5.3.1 Bright-Field

Bright-field is the "classical" basic illumination mode firstly used in microscopic observations of transparent specimens. In principle, even Antony van Leeuwenhoek used bright-field illumination when examining blood cells, bacteria, protozoa, sperm, and other transparent probes with his special single lens instrument. In standard bright-field techniques, specimens are illuminated with transmitted light formed to a homogeneous light cone which nearly runs perpendicularly through the specimen. The area of this light cone is as great as (or greater than) the specimen field observed. In this technique, structures can be revealed which absorb a sufficient proportion of light so that they appear darker than the bright background. When transparent structures are colorized, their natural color can be seen, too. Specimens of this sort are called "absorption specimens." They are characterized by a medium or high optical density. Structures of very low density which do not absorb the light transmitted in a sufficient manner (colorless native cells, for instance) remain barely visible or invisible in bright-field. These structures are called "phase specimens." Lastly, very dense and opaque specimens which absorb nearly the whole light transmitted appear as dark silhouettes so that no internal structures can be seen. Figure 5.16 demonstrates the different appearance of low-, medium-, and high-density specimens in bright-field illumination. Additionally it shows the same preparation in dark-field. It is clear to see that both illumination modes give complementary visual information.

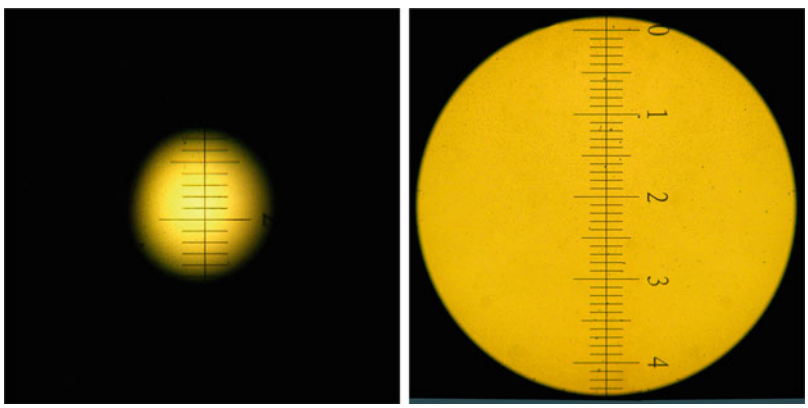

Fig. 5.15 Optical effects of eye lens (left) and field lens (right)

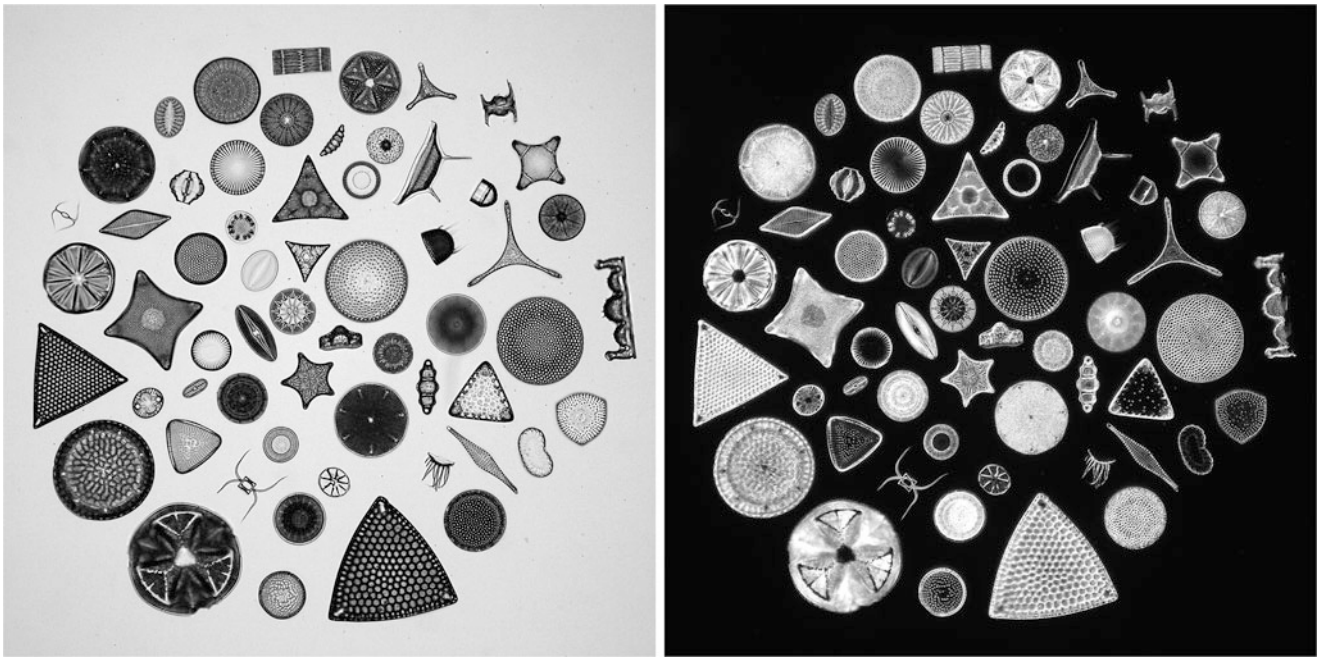

Fig. 5.16 Diatoms of different optical density, arranged slide, diameter of the whole arrangement: 0.9 mm, bright-field (left), dark-field (right)

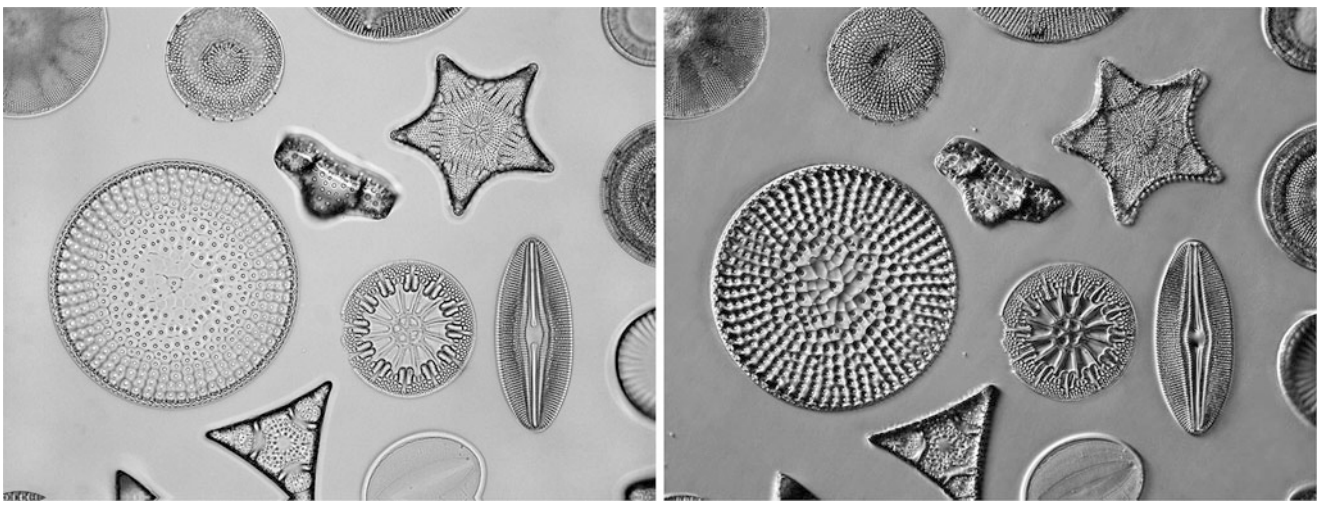

Fig. 5.17 Diatoms (arranged slide), horizontal field width (HFW): 0.34 mm, standard bright-field (left), oblique light (right)

5.3.2 Eccentric Oblique Bright-Field

When bright-field illumination is carried out with oblique light, running to the specimen from a definite direction, the lateral resolution can be enhanced. Moreover, the plasticity of three-dimensional structures can be accentuated (pseudo-relief-effects). An example of this modification is given in Fig. 5.17. This effect can be achieved when the incoming light is covered from one side, or the light outlet of a condenser is turned in an eccentric position.

5.3.3 Concentric Oblique Bright-Field (Circular Oblique Lighting)

In this variant of bright-field illumination, the illuminating light cone is modified so that its internal (central) area is faded out. Now, the specimen is only illuminated by the remaining concentric oblique annular light. In order to achieve this, an annular light mask can be integrated into a bright-field condenser so that all illuminating light beams running to the specimen and passing the objective come from

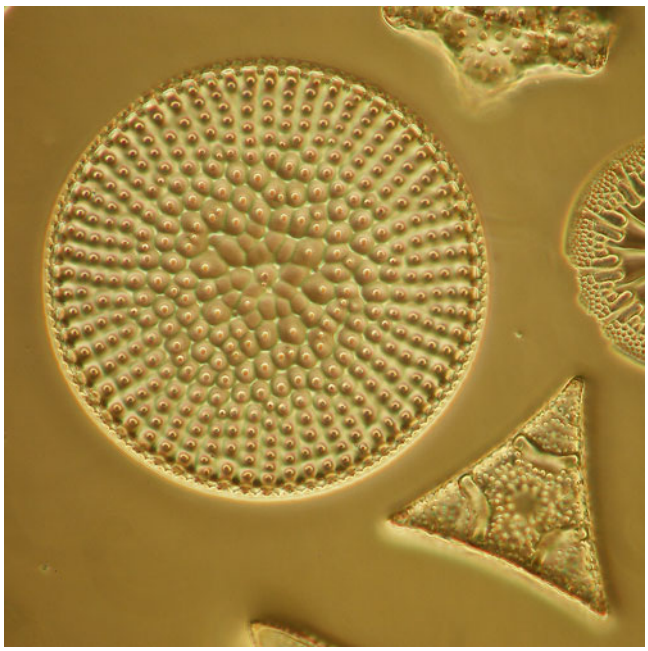

Fig. 5.18 Diatoms (arranged slide), (HFW): 0.18 mm, circular oblique lighting (COL)

the periphery of the field. The optical arrangement of this technique can be observed with a phase telescope focused on the back focal plane of the objective. The illuminating light annulus is projected into the periphery of the visible field. An example of practical use is given in Fig. 5.18.

5.3.4 Dark-Field

In dark-field techniques, specimens are brightly illuminated on a dark or black background. The most commonly used variant of dark-field is based on peripheral light, whereas axial or central light can be used for dark-field illumination in some rare and special assemblies. In dark-field images, lateral resolution is maximized so that even very small particles can be revealed sized beyond the normal resolution limit of the optical system used (Tyndall effect). Low-density specimens including bacteria can also be observed without being stained. On the other hand, the zeroth-order diffraction maximum does not contribute to the image so that the object trueness may be reduced [3]. Figure 5.19 shows a typical dark-field view of diatom frustules arranged to a circle and

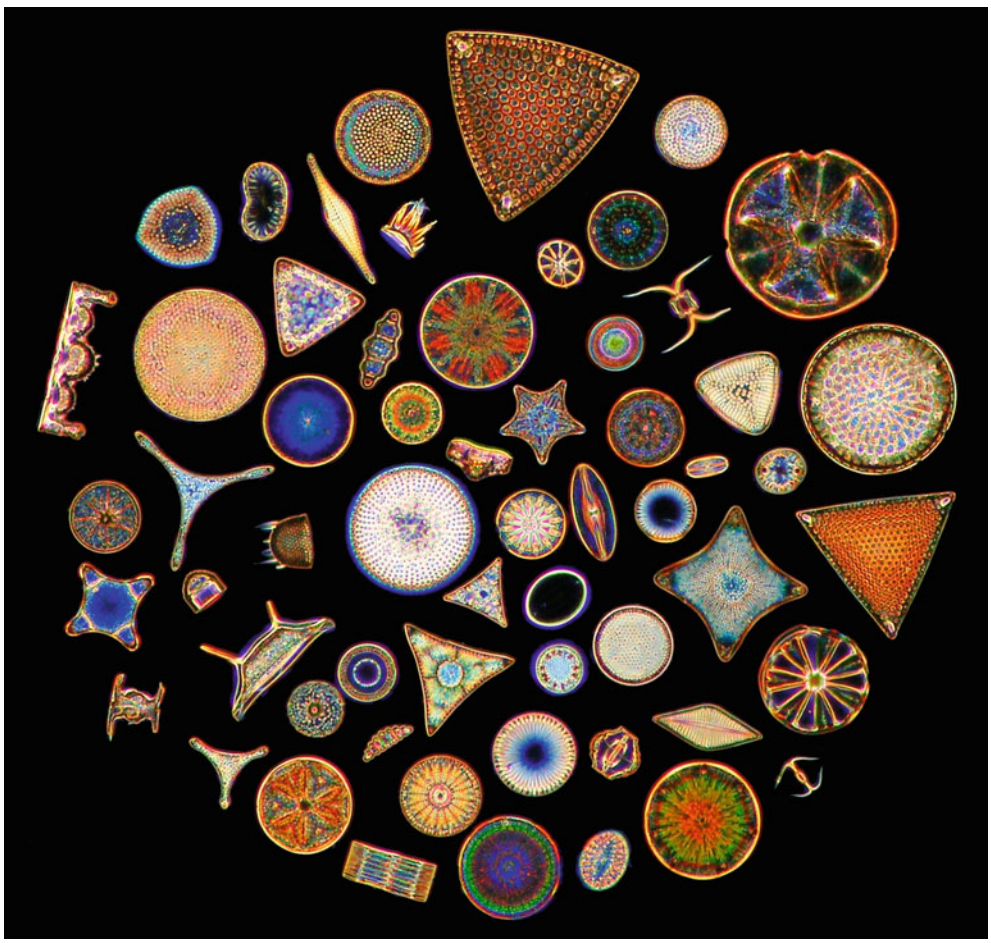

Fig. 5.19 Diatoms (arranged slide from Fig. 5.16), color image taken in dark-field, interference colors

taken in color. Various interference colors can appear in dark-field illumination of such specimens, especially at low magnification.

5.3.4.1 Dark-Field Based on Peripheral Light

To achieve this standard method for dark-field illumination a bright-field condenser can be modified or replaced by a special dark-field condenser (mirror system). The easiest way leading to dark-field is an appropriately sized circular black and opaque disc which has to be mounted inside of or beneath a bright-field condenser. Thus, all illuminating light passing the objective is blocked so that the specimen is only illuminated by the remaining peripheral oblique light beams which hit the specimen without reaching the objective. In professional so-called universal condensers, annular light masks are integrated in the same manner as described for circular oblique lighting (COL), but their diameters are greater than in COL. Thus, the respective light rings are projected outside of the objective's cross-section area, i.e., outside of the visible field observable with a phase telescope. Alternatively, a special dark-field condenser can be used designed as a dry system (for low magnifying objectives) or designed for immersion. In all variants, the numerical aperture (NA) of the objective must be lower than the condenser's one. Dark-field condensers with NA 0.9 can be combined with objectives up to NA 0.65 or 0.7, and immersion condensers with NA 1.2 or 1.4 can be used with objectives up to NA 0.9 or 1.0. Immersion lenses of higher NA (Oil 100/1.3, for instance) must be fitted with an (iris) diaphragm for reducing the aperture. Figure 5.20 shows the principle of a bright-field condenser modified for dark-field, and Fig. 5.21 demonstrates the construction of a special dark-field condenser (mirror system).

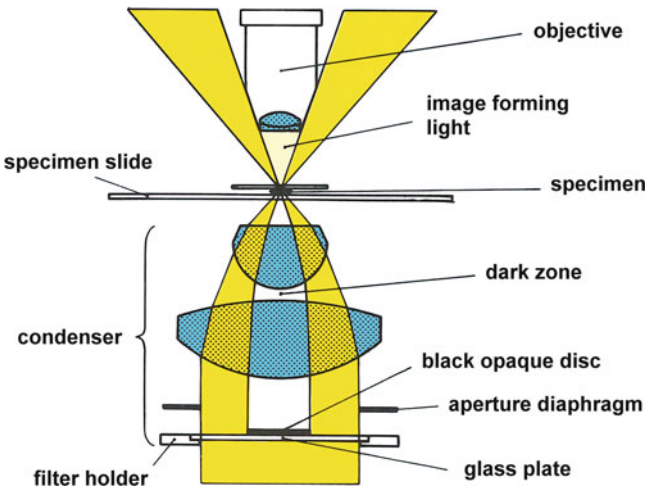

Fig. 5.20 Modification of a bright-field condenser for dark-field illumination

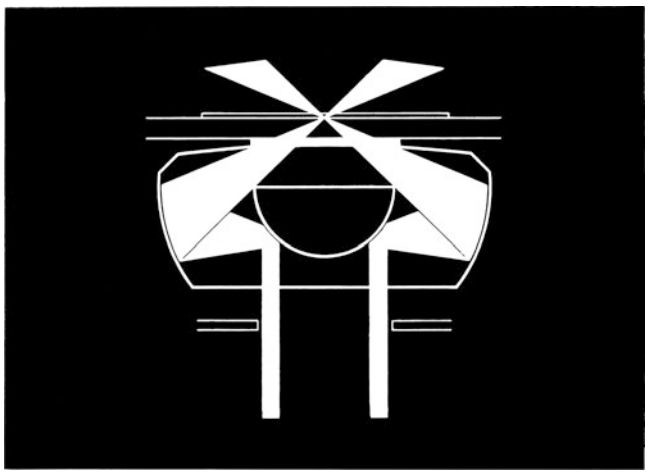

Fig. 5.21 Principle of a special dark-field condenser (dry system)

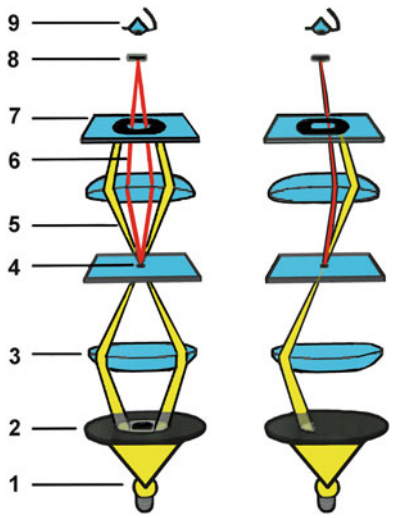

Fig. 5.22 Simplified light pathway of central dark-field, concentric (left), oblique/eccentric variant (right), light source (1), condenser light mask (2), condenser lens (3), specimen slide (4), illuminating light (5), image forming light (6), modified "phase plate" with an annular light stop (7), intermediate image (8), eye (9)

5.3.4.2 Dark-Field Based on Central Light

In this variant, the illuminating light is formed to an annular light cone, and a light stop is mounted above the objective being in optical congruence with the illuminating light (Fig. 5.22). In this variant, the specimen is illuminated by central light passing the objective and being stopped on its further pathway. The image forming light bent by the specimen runs beside the light stop and generates the intermediate image. Dark-field images achieved in this way are different from corresponding images generated with standard dark-field, because the specimen is illuminated at a much steeper angle of incidence.

5.3.5 Rheinberg Illumination

In this variant of dark-field illumination, the black and opaque disc inside of the condenser is replaced by a high-density color filter, and the peripheral light annulus can be fitted with facultative color filters as well. Thus, specimens appear in a dark-field-like manner, but the background is colorized and the specimen can be highlighted in one or more other colors so that bi- or multicolor effects can be achieved. Figure 5.23 gives an example of Rheinberg illumination.

5.3.6 Phase Contrast

So-called phase specimens (unstained living cells, for instance) are characterized by a very low optical density so that transmitted light is barely absorbed when passing such specimens. For this reason, phase specimens are nearly invisible in bright-field. On the other hand, the phase of light is roundabout shifted by a quarter wavelength (−90°) when it passes a phase specimen. This phase shift can neither be seen with the eye nor detected by a camera sensor or a photographic film. In phase contrast microscopy, the background light is usually retarded by a phase shift of three-quarter wavelengths (−270°). Now, the resulting phase difference of the specimen light and the background light will be a half wavelength (180°) so that the specimen is contrasted by destructive interference. Moreover, the background light is dimmed by circa 70–90% for augmentation of the final contrast. The basic principle of a phase contrast microscope is demonstrated in Fig. 5.24 (modified from [4]). The condenser is fitted with a light annulus so that the specimen is illuminated by a light cone passing the objective. The objective is fitted with a phase plate containing a phase ring localized in the objective's back focal plane. The light annulus is projected into the phase ring so that both components are congruent with each other. Their proper alignment can be observed with a phase telescope (Fig. 5.25).

Fig. 5.23 Radiolarian, Rheinberg illumination, HFW: 0.2 mm, bicolor contrast, background light filtered in blue, illuminating dark-field light filtered in red. Photomicrograph taken by Frank Fox, Trier, Germany

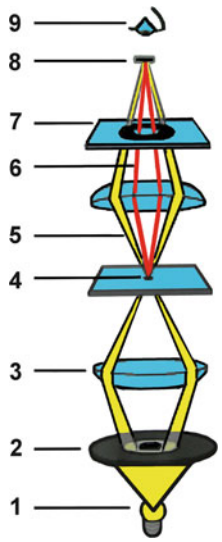

Fig. 5.24 Simplified light pathway of phase contrast, light source (1), condenser light mask (2), condenser lens (3), specimen slide (4), illuminating light (5), image forming light (6), phase plate with phase ring (7), intermediate image (8), eye (9). Figure redrawn and modified from nobel-prize.org

The optical design described leads to the so-called positive phase contrast. This is the most commonly used variant. Phase specimens appear darker than the background. They are surrounded by bright haloing. In negative phase contrast, the phase difference between specimen and background light is 360° so that the specimen is highlighted by constructive interference. Now, it appears bright on a dark background and is surrounded by dark haloing. In the rare colorized phase contrast (developed by Carl Zeiss Jena), the phase specimen is colorized by interference colors that mark regions of a particular density. Thus, zones of the same density appear in the same color and changes of density correspond with changes in colorization. Figure 5.26 gives examples of positive, negative, and colorized phase contrast.

5.3.7 Polarized Light Microscopy

In polarized light, anisotropic material can be selectively highlighted. When polarized light passes anisotropic material, the plane of vibration is varied. Thus, such material appears bright on a dark background, when the probe is situated between a pair of rotatable polarizing filters turned in a crossed position. This principle is demonstrated in Fig. 5.27. The incoming illuminating light is polarized by the

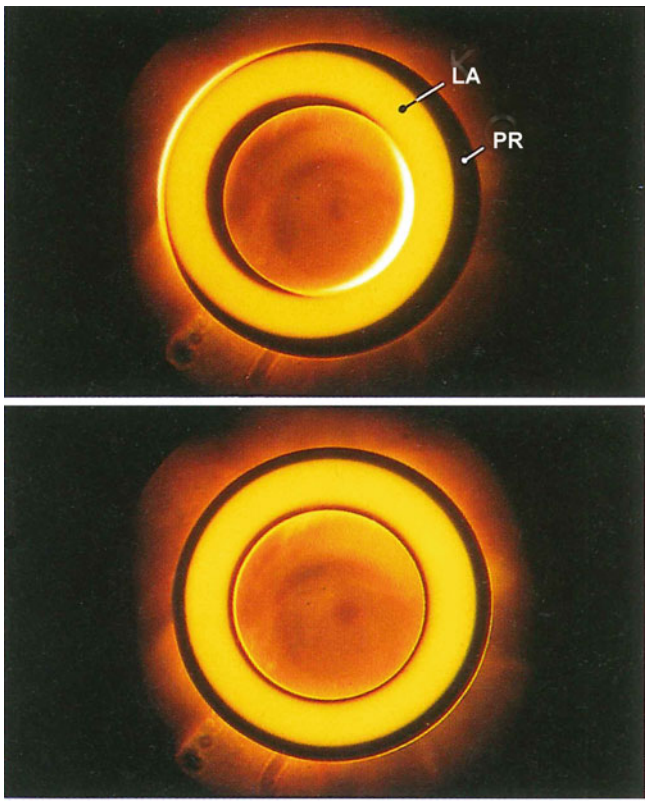

Fig. 5.25 Alignment of condenser light annulus (LA) and phase ring (PR), controlled with a phase telescope, slight misalignment (top), proper alignment (bottom)

first polarizing filter, called "polarizer." This polarized light runs to the second polarizing filter, called "analyzer." When the analyzer is turned in a crossed position, all incoming polarized light is blocked so that the background will be dark or black. On the other hand, those polarized light beams which pass the anisotropic specimen vibrate in an aberrant plane so that it can selectively pass the analyzer. Now, this specimen is brightly contrasted on a dark or black background. By turning the polarizer the background can be brightened in tiny steps. Additional color contrast can

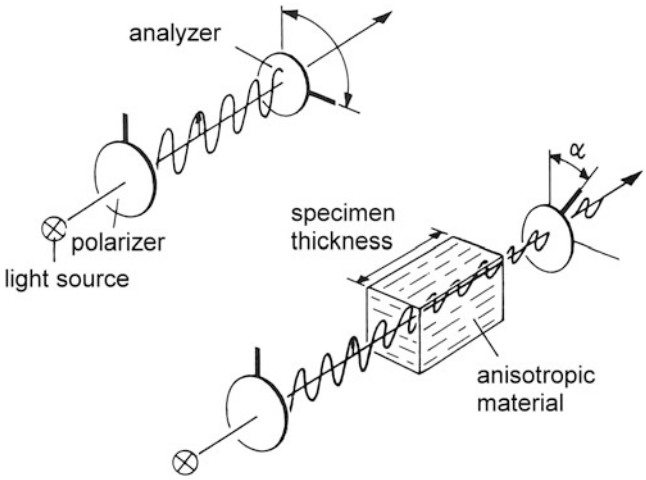

Fig. 5.27 Principle of polarized light microscopy, selective visualization of an anisotropic probe situated between crossed polarizing filters

be achieved when a (rotatable) compensator (λ-compensator, for instance) is inserted between polarizer and specimen (example in Fig. 5.28).

5.3.8 Differential Interference Contrast

In life sciences, this method is an alternative sophisticated technique for the examination of phase specimens. The general principle of interference contrast is shown in Fig. 5.29. A polarized illuminating light beam is divided by the first DIC prism (Wollaston prism) to a couple of two separate parallel rays running on two different polarization planes forming an angle of 90° to each other. Their distance is beyond the resolution limit of the optical system. This couple of light beams passes the specimen at different points. When having passed the objective both light beams are rejoined by the second DIC prism (Wollaston prism) and converted to one polarized composite beam by a second polarizer (analyzer). As both beams pass the specimen at different points, their

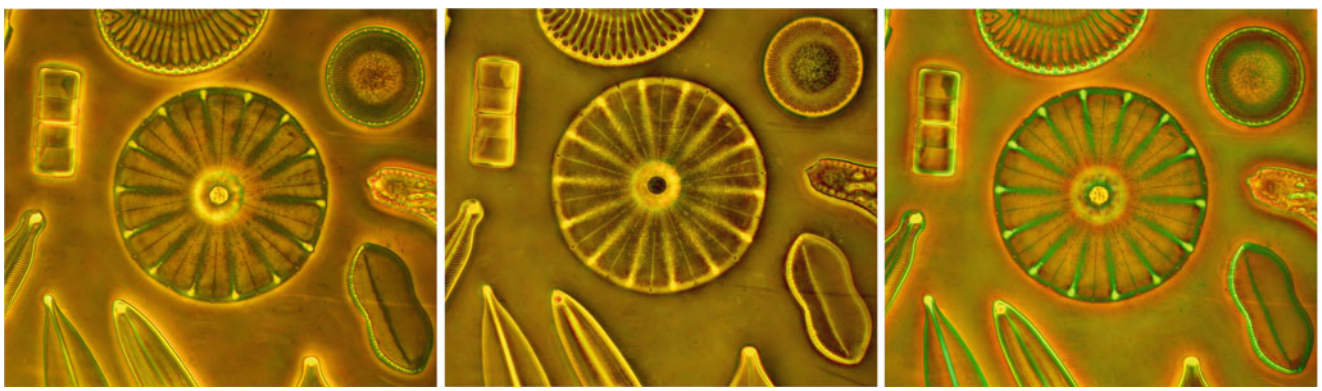

Fig. 5.26 Low-density diatoms, HFW: 0.14 mm, positive (left), negative (center), colorized (right) phase contrast

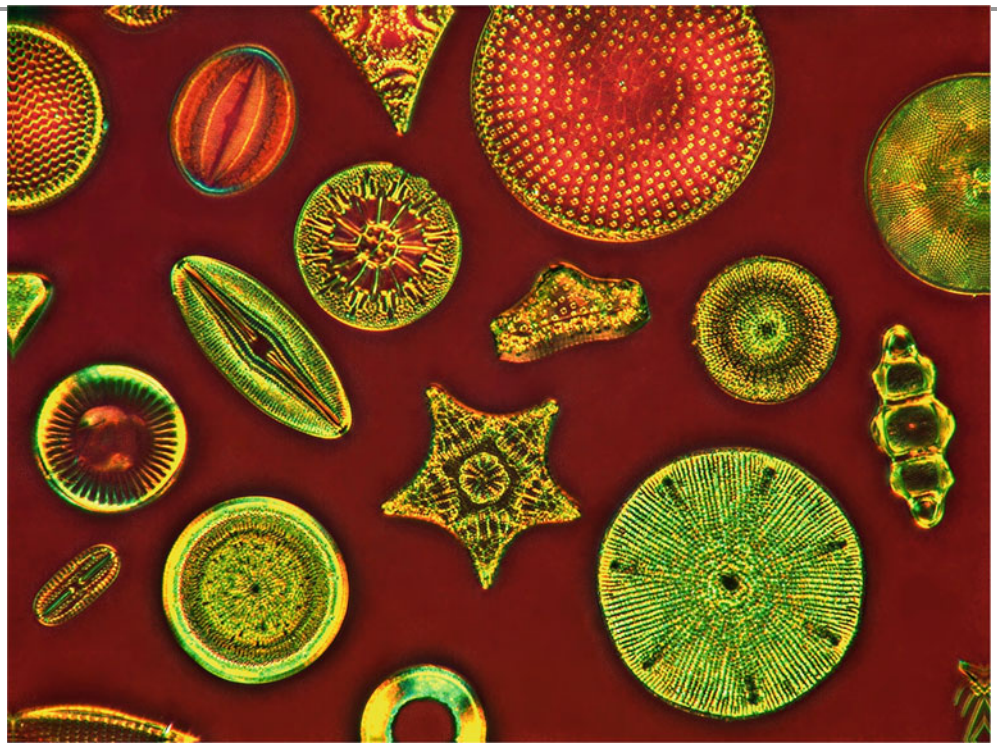

Fig. 5.28 Diatoms, arranged slide, polarized light, Lambda compensator. HFW: 0.5 mm

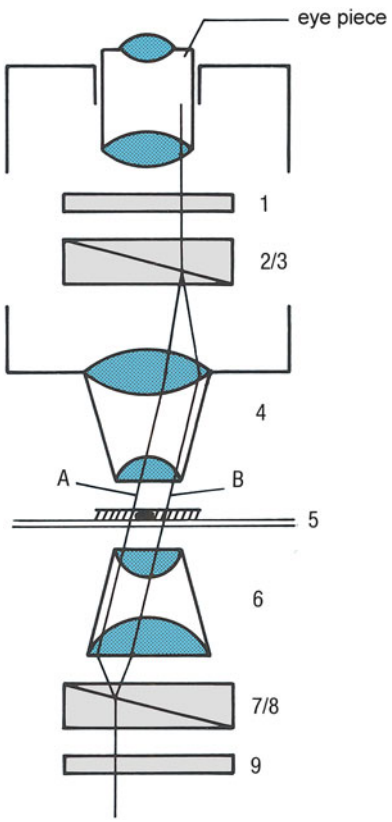

Fig. 5.29 Principle of differential interference contrast (DIC), Analyzer (1), DIC prism (2/3), objective (4), specimen slide (5), splitting of light beams (A, B), condenser (6), DIC prisms (7/8), polarizer (9)

phase is different, too. This phase difference is visualized by interference when both beams are recombined. Images resulting from this technique are characterized by a three-dimensional relief effect, loss of haloing and a low grade of indistinctness ("optical sections"). As long as the refractive index remains constant, visible reliefs correspond with the real texture of the specimen. On the other hand, regional changes in density lead to pseudo-relief effects. Figure 5.30 gives an example of interference contrast. Various technical modifications or variations of interference contrast have been developed in light microscopy, according to Nomarski, Smith, Jamin-Lebedeff, Mach–Zehnder, Beyer & Schöppe (Interphako) and others. Beyond morphological imaging of biological structures, especially the Mach–Zehnder and Interphako methods can also be used for measurements of local thickness, refractive index and dry mass. Figure 5.31 demonstrates the principle of measurements based on interferometry carried out with an unstained human erythrocyte examined by use of a Mach–Zehnder microscope. The maximum thickness at the erythrocyte's margin is 992 nm, the minimum thickness in the middle of this blood cell is 744 nm, and the refractive index of the erythrocyte is 1.4.

5.3.9 Fluorescence Microscopy

When fluorescent material is illuminated with high energy excitation light of an appropriate wavelength, fluorescent

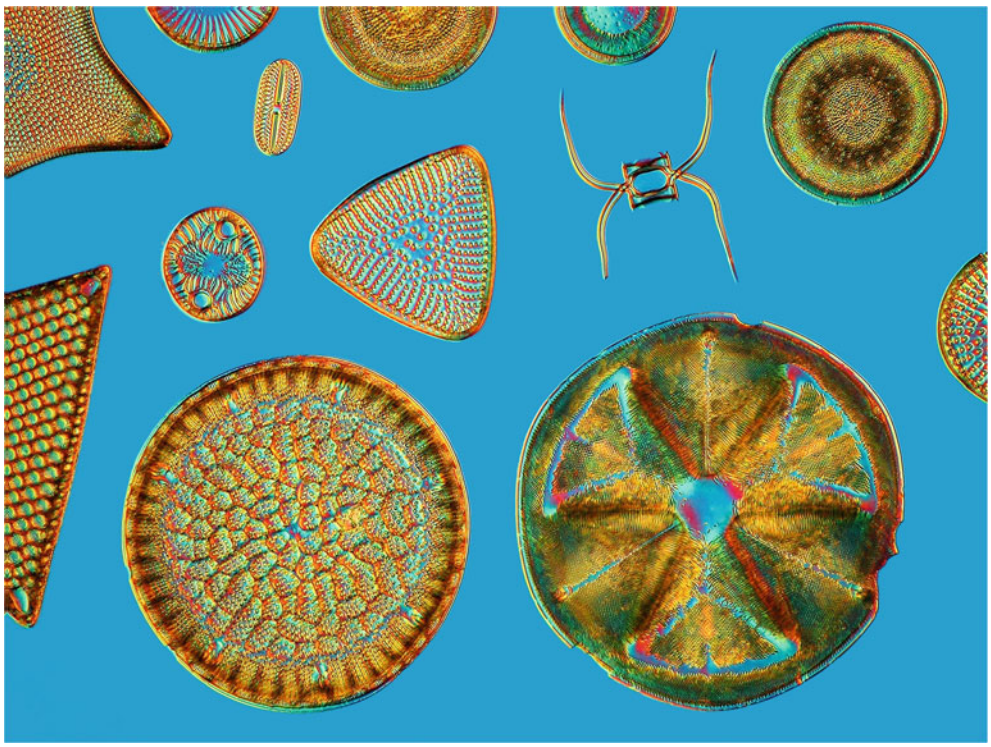

Fig. 5.30 Diatoms, arranged slide, HFW: 0.52 mm, DIC technique

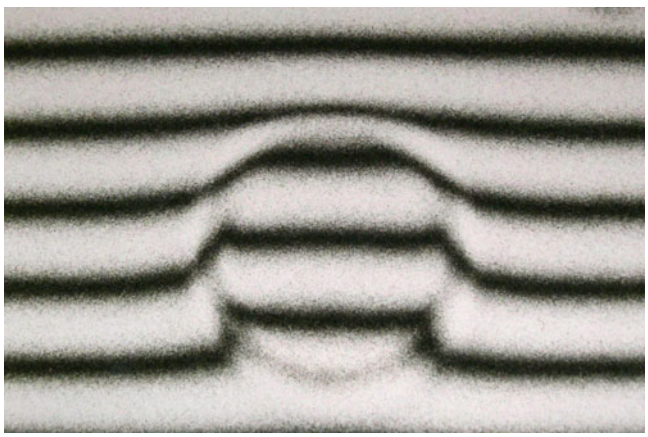

Fig. 5.31 Use of a Mach–Zehnder microscope for measurements of regional thickness carried out with an unstained human erythrocyte taken from a blood smear. The grade of deviation within the interference stripes corresponds with the local thickness. HFW: 0.02 mm

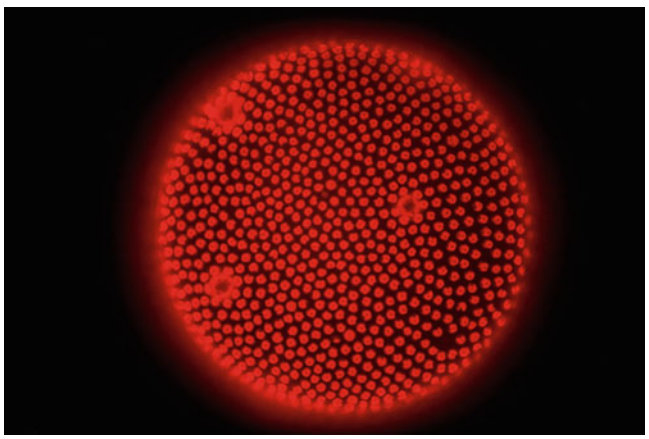

Fig. 5.32 *Volvox* sp., fluorescence, blue excitation light, red autofluorescence of chlorophyll. Specimen diameter: 0.7 mm. Photomicrograph taken by Frank Fox, Trier, Germany

light is emitted which has lower energy and a longer wavelength than the incoming excitation light. Some natural material can produce fluorescent light when it comes in contact with appropriate excitation light (autofluorescence, see Fig. 5.32). Other material can be stained with special fluorescent dyes in order to generate images based on fluorescence. Chlorophyll is characterized by a red autofluorescence when illuminated with blue excitation light. DNA, for instance, can be dyed with DAPI so that it is imaged by blue fluorescence light when illuminated with violet excitation light. In all cases described, the low energy fluorescent light can only be visualized when the high energy excitation light

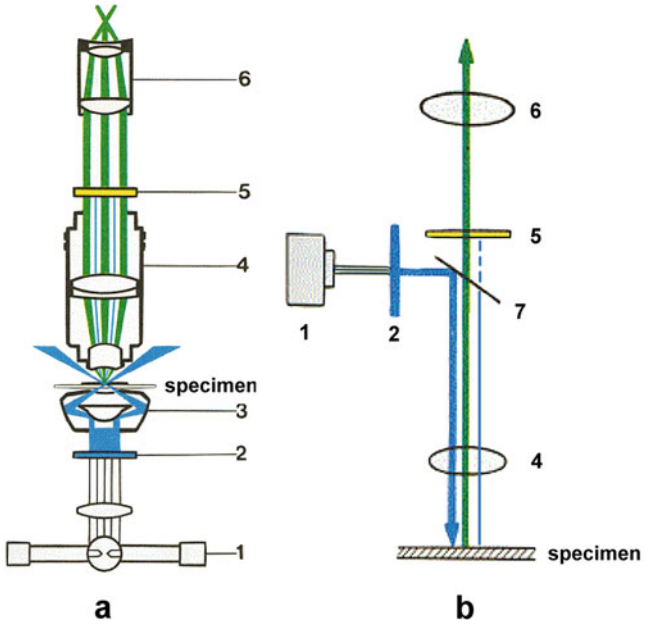

Fig. 5.33 Principles of fluorescence microscopes based on transmitted (**a**) and incident (**b**) light, excitation light: blue, fluorescence light emitted: green, 1 = light source, 2 = excitation filter, 3 = (dark-field) condenser, 4 = objective, 5 = emission filter, 6 = eye piece, 7 = dichroic mirror

is filtered out by an emission filter. The basic principle of a fluorescence microscope is shown in Fig. 5.33. Fluorescence microscopes first developed were based on transmitted light (Fig. 5.33a). The excitation light was lead to a dark-field or a bright-field condenser fitted with the excitation filter (blue, for instance). The proportion of excitation light running through the specimen was blocked by the emission filter so that only the fluorescence light emitted (green, for instance) could pass the eyepiece and generate the image observed. Modern fluorescence microscopes, however, are designed for incident light (Fig. 5.33b). Excitation and emission filters are combined with a dichroic mirror and joined to a filter cube. The excitation light (blue) is reflected by the mirror and runs through the objective to the specimen. The fluorescence light emitted (green) passes the objective, the dichroic mirror, and the emission filter so that it can generate an image. In such assemblies the lenses of the objective act as "condenser" for the excitation light and as an image forming system for the fluorescence light emitted by the specimen.

Various technical variants were developed further leading to superior distinctness and resolution (confocal fluorescence microscopy, Airy scan, light sheet microscopy, STED, PALM/STORM, and MINFLUX).

Moreover, fluorescence microscopy can be combined with complementary illumination modes so that fluorescent structures can be simultaneously revealed together with their nonfluorescent environment (example in Fig. 5.34).

5.3.10 Incident Light Microscopy (Epi-illumination)

Incident light is preferably used for illumination of opaque specimens. Use of an external light source (swan neck fiber, for instance) is the most simple way for epi-illumination. Special illuminators for incident light are the more sophisticated variant (Fig. 5.35). For epi-dark-field (Fig. 5.35a), objectives are needed consisting of two separate light corridors: an external annular light corridor for the illumination light and an internal light corridor containing the objective lenses for the image forming light. In epi-bright-field illumination (Fig. 5.35b) the illuminating and the image forming light run through the same lens system. Therefore, the latter illumination technique is only suitable for observation of highly reflective material.

Nevertheless, incident light can accentuate fine superficial structures also in several biological probes. Such specimens can also be well observed when incident light is combined with transmitted light. Figure 5.36 shows diatom frustules taken in incident light (epi-dark-field). When dark-filed is simultaneously carried out with incident and transmitted light, both light components can be filtered at different colors (example in Fig. 5.37). Moreover, dark-field based on incident light can be combined with bright-field in transmitted, preferably monochromatic light (example in Fig. 5.38).

Lastly, reflection contrast can be mentioned as a very special illumination technique developed by E. Leitz Wetzlar in the 1970s. By this method, ultra-fine biological structures can be revealed and three-dimensional measurements of transparent specimens can be carried out based on interferometry. In analogy to epi-bright-field, the incident illuminating light is led through the objective as well as the reflected light coming from the specimen. In contrast to epi-bright-field, the illuminating light is selectively filtered out by polarizing techniques so that only the specimen light contributes to the image. Thus, ultrafine specimens are highly contrasted against a black background. As the illuminating light is directed at an angle of 45°, interference patterns can be apparent which can be used for three-dimensional measurements. Examples of practical use are given in Figs. 5.39 and 5.40. Distances of interference lines correspond

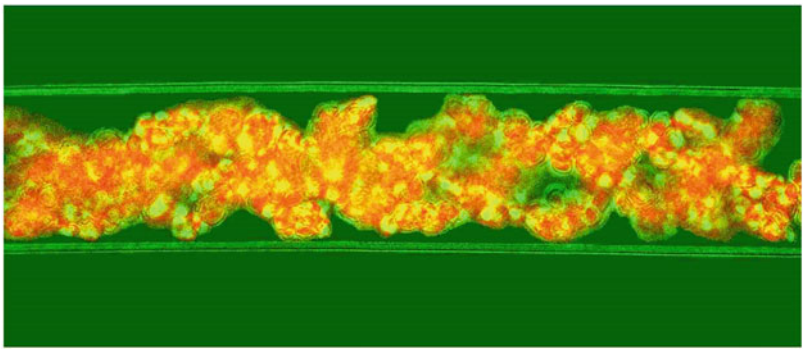

Fig. 5.34 Visualization of algae using fluorescence blue excitation light, combined with monochromatic green transmitted light and red autofluorescence of chlorophyll. Additional visualization of nonfluorescent structures in green. HFW: 0.2 mm

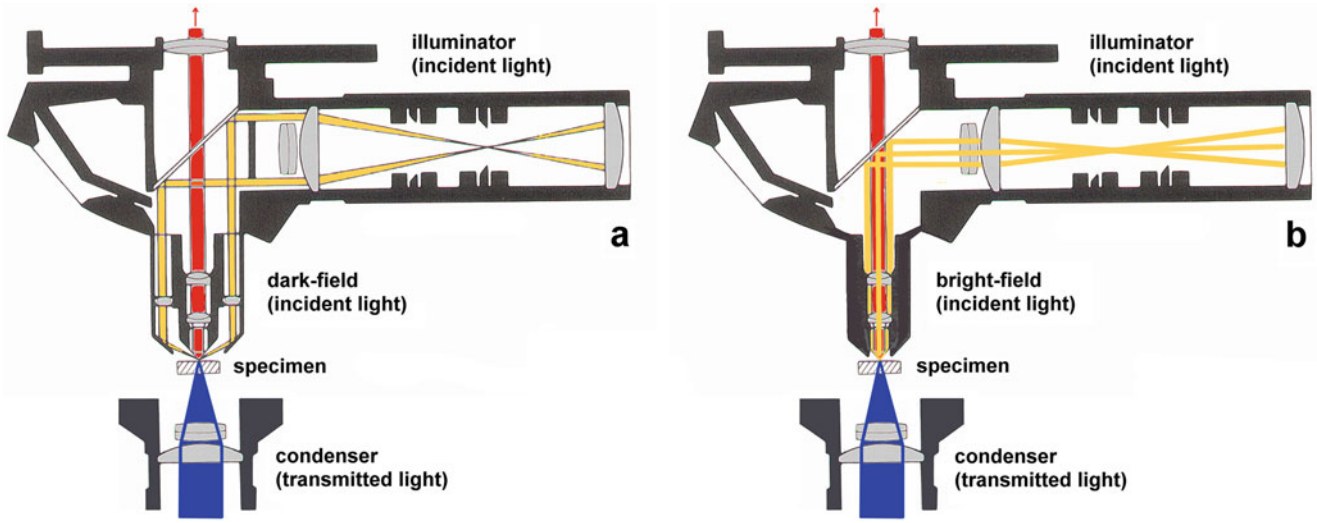

Fig. 5.35 Principle of an illuminator for incident light, equipment for epi-dark-field (**a**) and epi-bright-field (**b**). Facultative transmitted light can be added

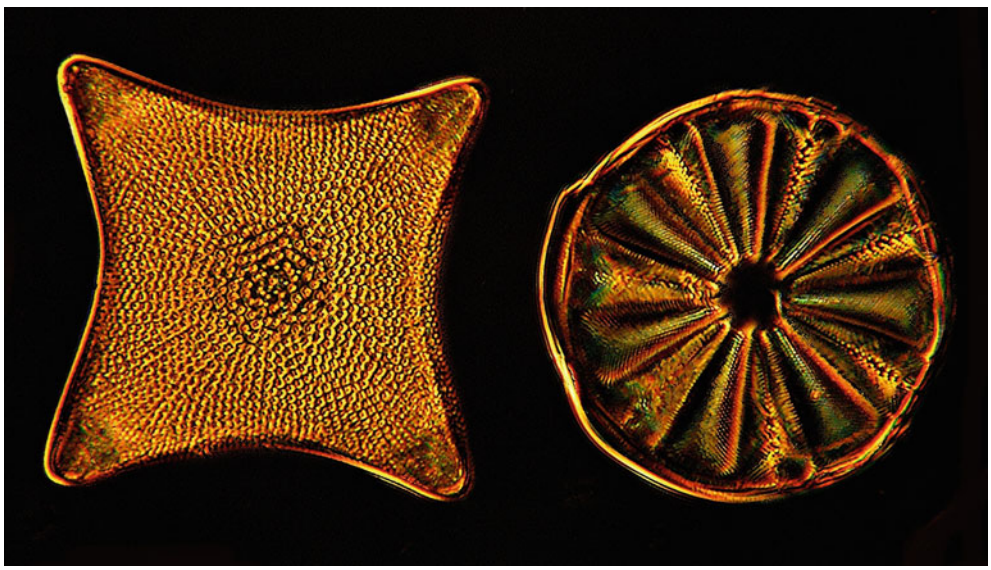

Fig. 5.36 Diatoms taken with incident light (epi-dark-field, achieved with an illuminator according to Fig. 5.35a). HFW: 0.3 mm. Left: *Stictodiscus* sp., right: *Actinoptychus* sp.

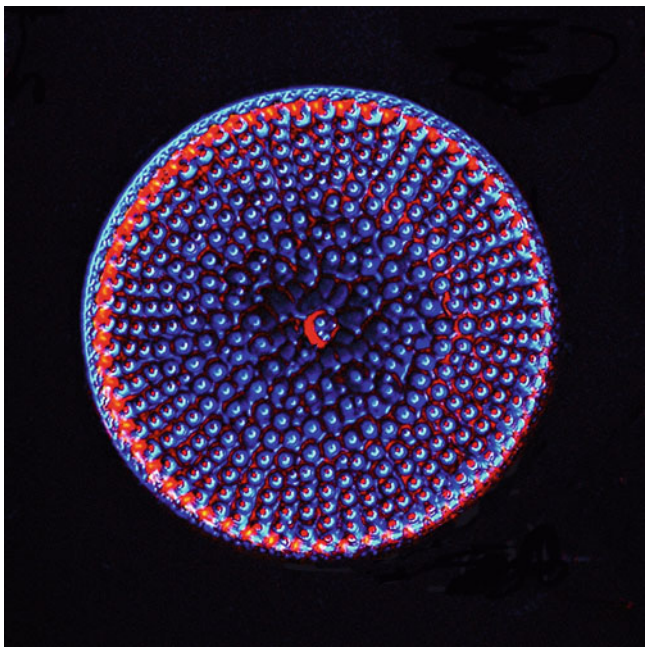

Fig. 5.37 Diatom (diameter: 0.12 mm). Composite image taken in dark-field carried out with transmitted blue light and incident red light

with differences in thickness of 226 nm so that superficial reliefs of cells can be quantified and three-dimensional reconstructions can be derived.

A concurrent method ("immersion contrast") developed by Zeiss came on the marked circa 1 year later. In this variant, the incident light is directed to the specimen at 90° (angle of incidence) so that the specimen is illuminated by perpendicular light. Beyond this mean, the optical design is the same as in reflection contrast.

5.4 Modifications of Standard Illumination Techniques and Variable Multimodal Techniques

All of the standard techniques described above lead to complementary visual information. They are characterized by specific advantages and disadvantages. Several optical limitations are prevalent in these methods, especially when "problematic" transparent specimens have to be examined which are characterized by strong marginal contours, fine internal structures, high ranges in local thickness and a complex three-dimensional architecture consisting of high-density light absorbing and low-density phase shifting components. Some of these given limitations can be overcome, when the optical design of the respective method is modified or several complementary methods are combined with each other and simultaneously carried out.

5.4.1 Apodized Phase Contrast

In this variant of phase contrast, the phase ring (light absorption: ca. 75%) situated on a phase plate inside of the phase contrast objective is surrounded by two additional light

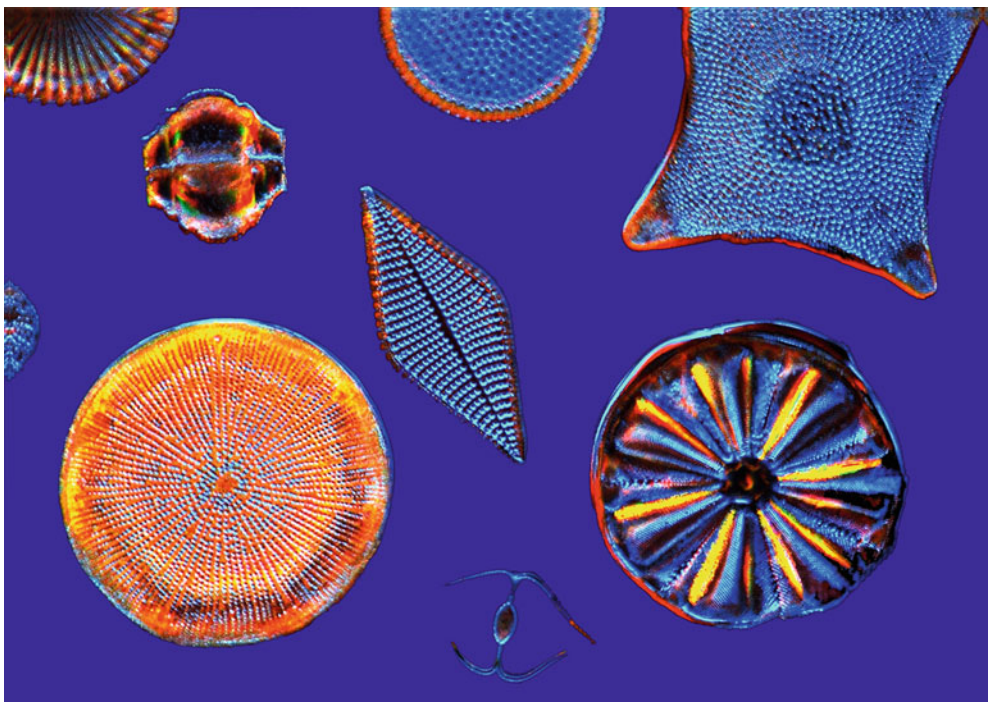

Fig. 5.38 Diatoms, arranged slide, composite image, optical superimposition of incident dark-field (bulb light) and bright-field carried out with transmitted monochromatic blue light. HFW: 0.35 mm

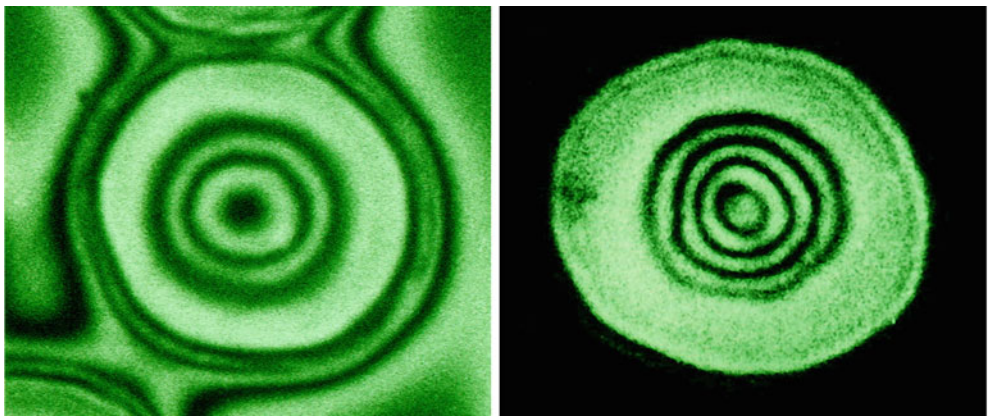

Fig. 5.39 Interference patterns in human erythrocytes, unstained (left), stained according to Pappenheim (right), reflection contrast [5, 6]. The interference lines mark regions of constant thickness. Neighboring interference minima (black) or maxima (bright) correspond with a 226 nm difference in local thickness. HFW: 0.01 mm

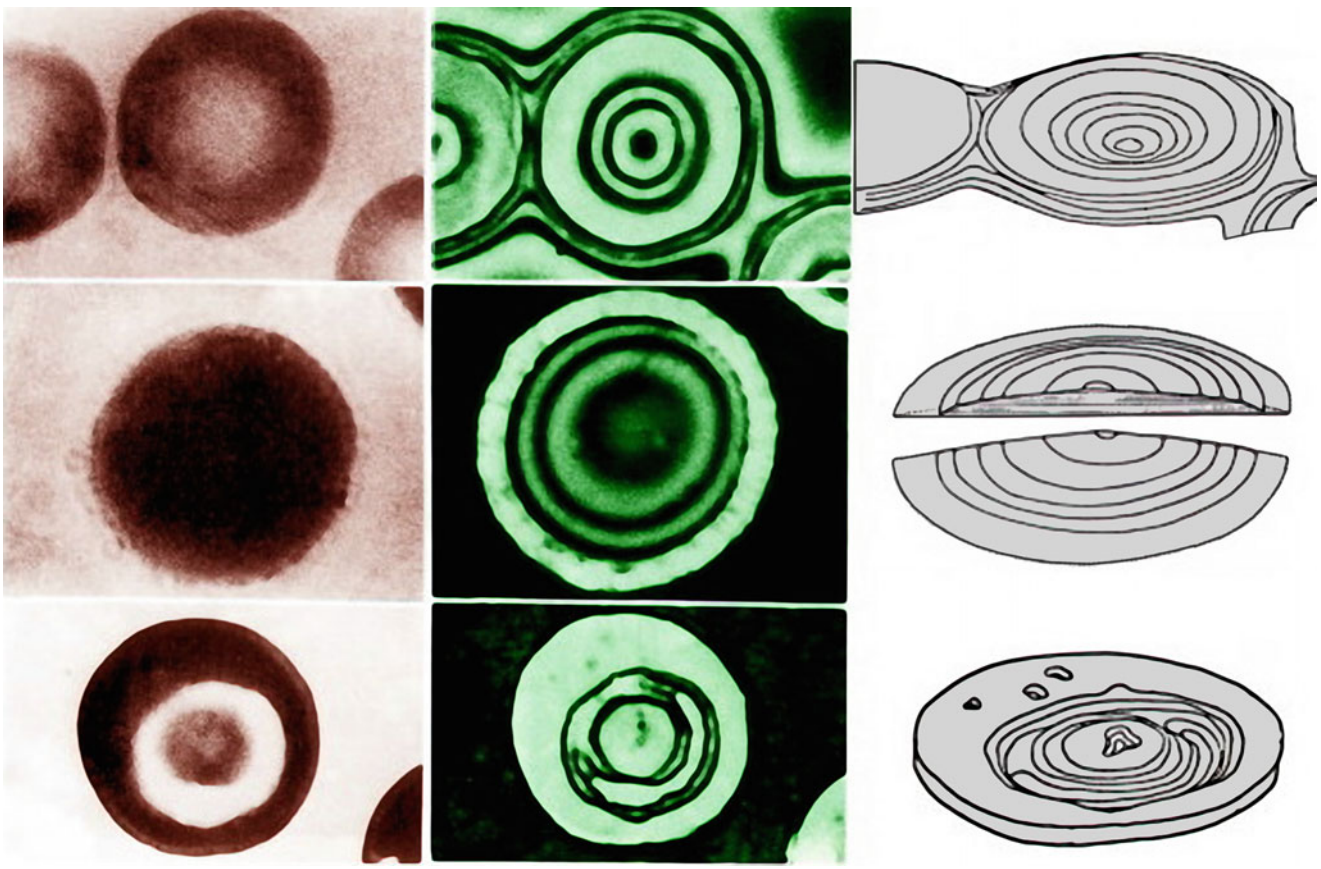

Fig. 5.40 Three-dimensional reconstructions based on reflection contrast imaging, normocytosis (top), spherocytosis (center), target cell/thalassemia major (bottom). HFW: 0.01 mm

absorbing films of higher transmission (light absorption: ca. 50%), which are adjacent to the external and internal margins of the phase ring. Each of these three separate films has the same breadth. Both semitransparent annular zones surrounding the phase ring reduce the intensity of light diffracted from the specimen at small angles. This special design leads to enhanced clarity of fine structures, improved contrast, and reduced halo artifacts [7]. The condenser light annulus is designed as usual, i.e., it is only congruent with the genuine phase ring situated between both annular zones added at the phase plate. Figure 5.41 demonstrates visible differences between standard and apodized phase contrast (reconstructed from a digital animation).

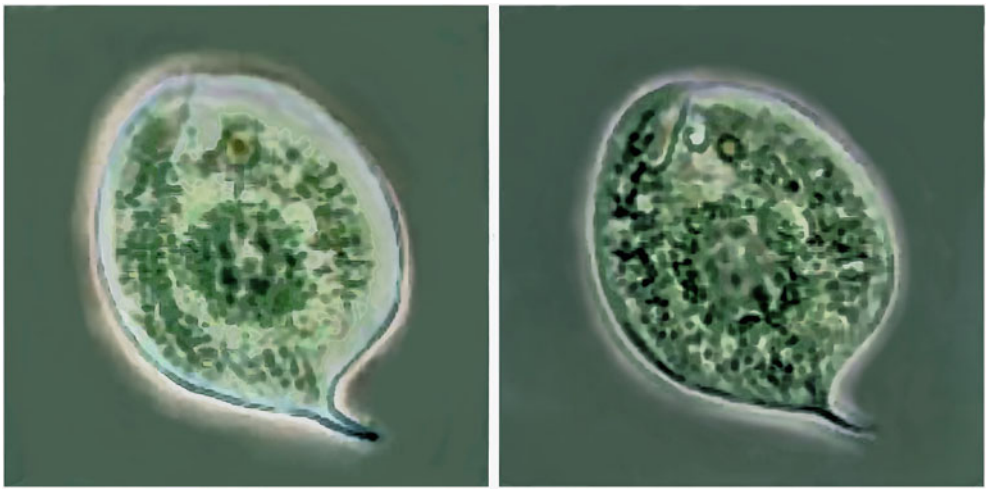

Fig. 5.41 *Euglena* sp., standard (left) and apodized (right) phase contrast, based on a simulation of Nikon Comp. HFW: 0.13 mm

5.4.2 Relief Phase Contrast

In this variant of phase contrast, the condenser light mask is modified so that the circular light annulus is replaced by a light segment being congruent with a corresponding segment of the phase ring inside of the phase contrast objective. Thus, the specimen is no longer illuminated concentrically by a circular light cone, but the illuminating light comes from one defined direction so that an oblique illumination is achieved. Figure 5.42 shows the principle of this arrangement and Fig. 5.43 gives an example of practical use taken from epithelial cells with a simple achromatic lens. When compared with standard phase contrast, image contrast and focal depth are enhanced, the planarity of field can be improved and haloing reduced. Moreover, relief effects are generated by the oblique illumination achieved [8].

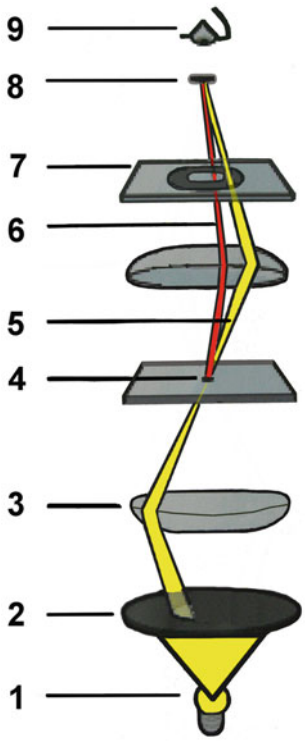

Fig. 5.42 Simplified light pathway of relief phase contrast, light source (1), condenser light mask (2), condenser lens (3), specimen slide (4), illuminating light (5), image forming light (6), phase plate with phase ring (7), intermediate image (8), eye (9)

5.4.3 Aperture Reduction Phase Contrast

Based on a variant optical design, a condenser for phase contrast can be fitted with an aperture diaphragm which is no longer be projected into the objective's back focal plane, but into an intermediate plane situated between this back focal plane and the specimen plane. The light annulus, however, is still projected into the back focal plane of the objective, i.e., into the phase ring situated there. By this modification, the projection planes of light annulus and aperture diaphragm are separated from each other. The aperture diaphragm can now be used in the same manner as usual in bright-field-illumination so that contrast and spatial depth can be enhanced when this diaphragm is appropriately closed. In contrast to the standard design, in this technical variant, the phase contrast image is not compromised by closing the aperture diaphragm, but it can be significantly improved [9].

Figure 5.44 shows the principle of optical modification, and Fig. 5.45 gives an example of practical use.

5.4.4 Aperture Reduction Dark-Field

In a lens-based condenser designed as described above, the light annulus needed for phase contrast can be replaced by a greater light annulus suited for dark-field illumination. Now, the aperture diaphragm can also be closed in dark-field without compromising the image observed. Not only

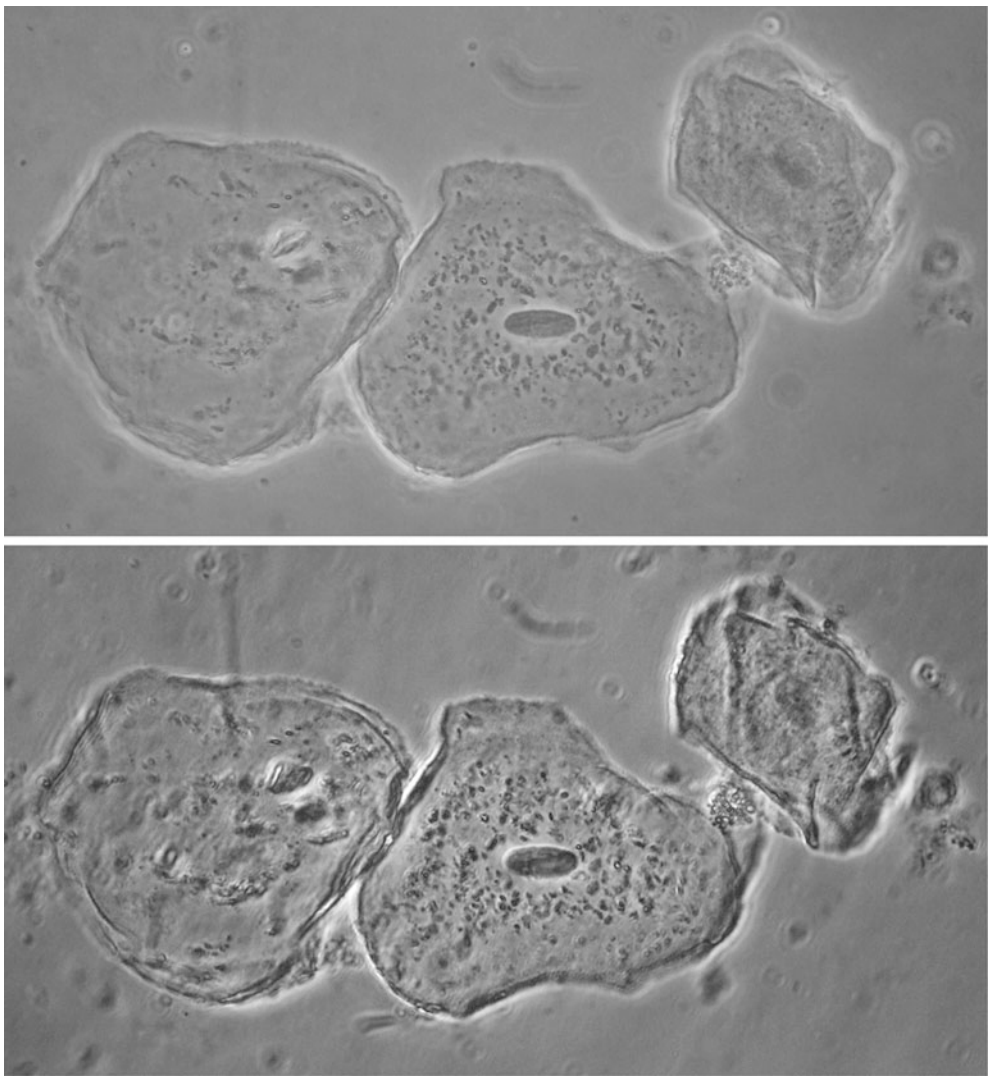

Fig. 5.43 Epithelial cells from the oral mucosa taken with an achromatic phase contrast lens, standard phase contrast (top), relief phase contrast (bottom). HFW: 0.1 mm

the depth of field can be enhanced, but—in particular—marginal irradiation and scattering, which are often apparent in standard dark-field examinations, can be successfully reduced or eliminated [9]. The improvements achievable are demonstrated in Fig. 5.46.

5.4.5 Digital Dark-Field

Fine details taken in bright-field can often be visualized in superior clarity when the bright-field image is inverted to a dark-field-like appearance by digital post-processing. Appropriate algorithms are implemented in each sort of standard-software for image processing [10]. By this procedure, the genuine bright background is converted to a dark tone, and fine structures are revealed in a higher grade of contrast and differentiation. Such digital dark-field images are different from dark-field illumination achieved by optical means. As the zeroth-order diffraction maximum contributes to the image, the object trueness may be enhanced. The depth of field may be greater because the aperture diaphragm can be used for varying the effective condenser aperture. Digital dark-field images are purified from blooming and scattering so that fine structures appear in higher precision. In contrast to standard bright-field, small details and low differences in density can be detected in higher sensitivity against a black background. Figure 5.47 gives an example of practical use.

5.4.6 Digital Phase Contrast

By ultrahigh contrast amplification phase specimens can also be visualized in bright-field illumination, although they are only barely visible or invisible in normal circumstances

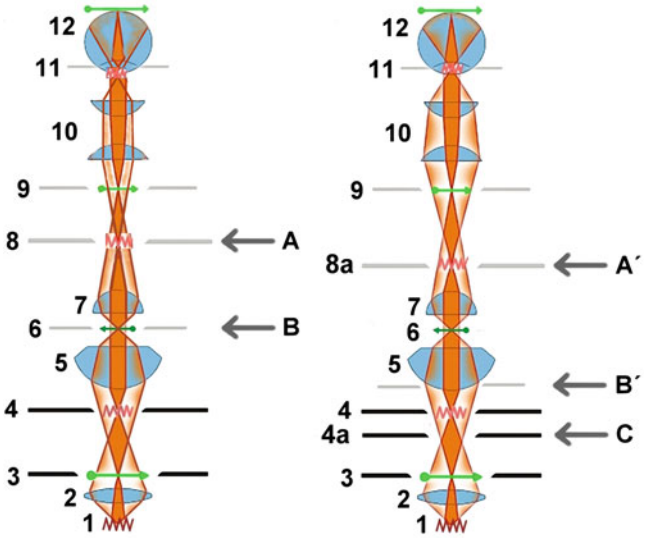

Fig. 5.44 Fundamental light pathways and projection planes on standard equipment (left) and optical variants modified for aperture reduction imaging (right), light source (1), collector lens (2), field diaphragm (3), condenser aperture diaphragm (4), facultative additional iris diaphragm (4a), condenser lens (5), specimen (6), objective lens (7), back focal plane of objective (8), intermediate image (9), eyepiece (10), back focal plane of the eyepiece (11), eye (12), A = projection plane of the condenser aperture diaphragm in conventional equipment, A′ = projection plane of the condenser aperture diaphragm in equipment modified for aperture reduction techniques, B = projection plane of the field diaphragm in conventional equipment, B′ = projection plane of the field diaphragm in equipment modified for aperture reduction techniques, C = position of a facultative second iris diaphragm for enhanced contrast and relief effects

when examined in bright-field. This enhancement of contrast can be achieved by multistep post-processing [11]. At first, several images have to be taken at a different exposure. The first image is taken in standard exposure, and the following images have to be successively underexposed. In the next step, this series of images differently exposed have to be rendered with the same algorithms as used for high dynamic range rendering (HDR) so that the original low differences in brightness and density are accentuated further without increasing the noise level. Lastly, contrast and gray level gradation have to be amplified in the so-generated HDR image by use of standard algorithms developed for single shot images.

For several reasons, digital phase imaging based on ultrahigh contrast amplification of bright-field images may lead to superior results when compared with standard phase contrast. Normal bright-field lenses can be used so that the optical quality of the objective is not degraded by a phase ring. The full aperture of a bright-field condenser can be used for illumination because the condenser's aperture is not reduced by a light annulus. The condenser's aperture diaphragm can be used in the same way as in traditional bright-field imaging if necessary. Thus, the depth and planarity of field, the contour sharpness of linear structures, and the optical contrast in low-density specimens can be enhanced. Lastly, the final image contrast can be optimally adjusted to the properties of the specimen examined. Images generated in this way are not affected with haloing and shade-off which are typical artifacts in standard phase contrast imaging.

The multi-step image processing described could be implemented in digital microscopes so that digital phase contrast could also be used for life observations. The capacity of this method is demonstrated by Fig. 5.48.

5.4.7 Luminance Contrast

In luminance contrast, the specimen is illuminated by a very small axial light beam, which is congruent with the optical axis. When passing the objective, this central beam

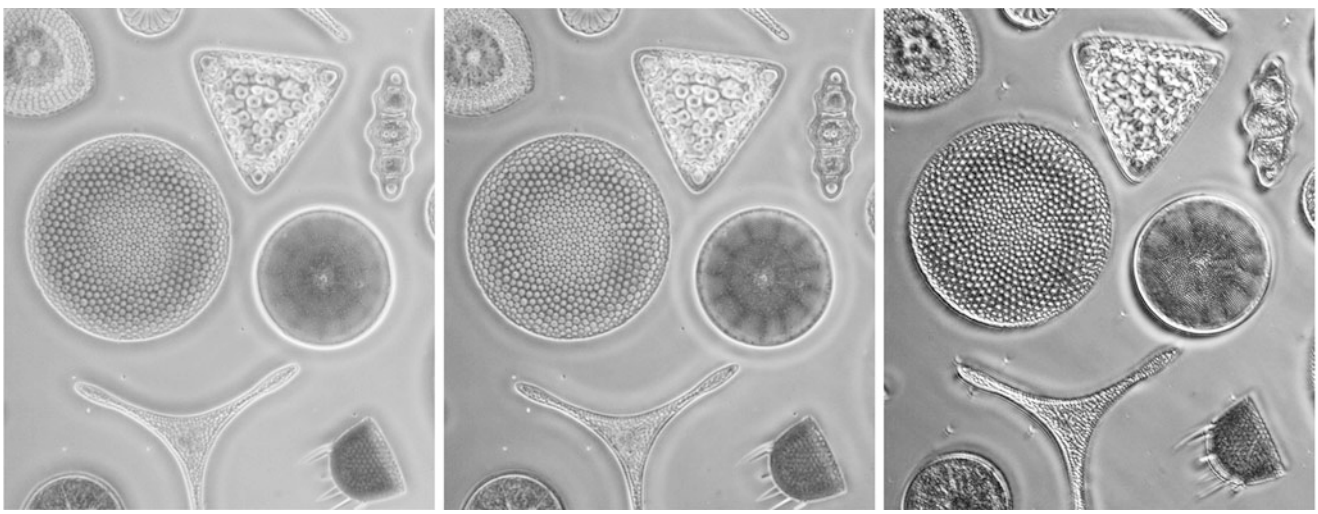

Fig. 5.45 Diatoms, arranged slide, conventional phase contrast (left), aperture reduction phase contrast (center), variant with facultative second diaphragm (right). HFW: 0.27 mm

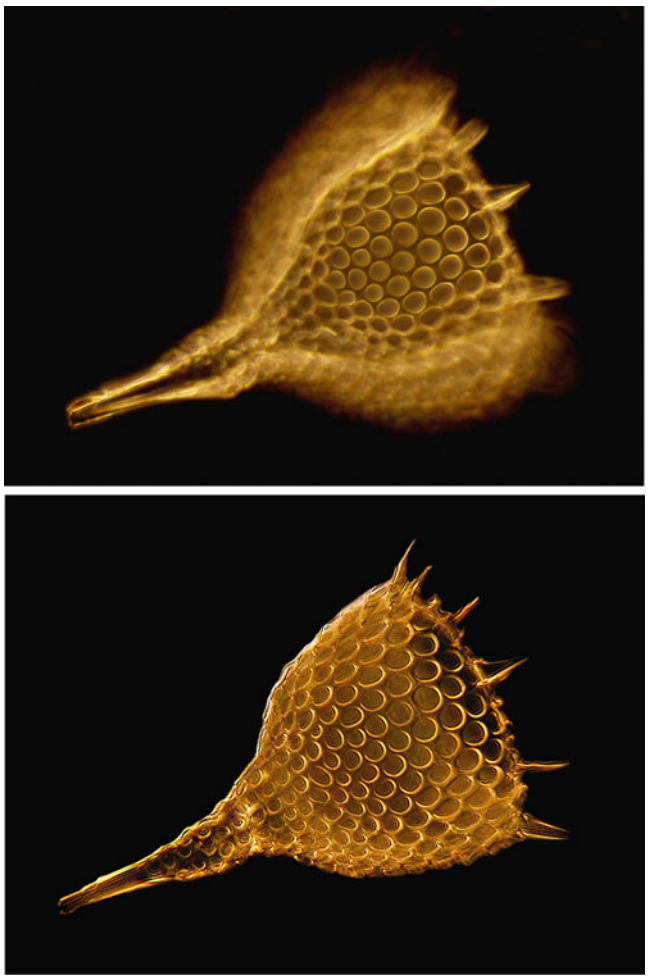

Fig. 5.46 Radiolarian, conventional dark-field (top), aperture reduction dark-field (bottom). Specimen length: 0.24 mm

is blocked by a light stop situated in the back focal plane of the objective used. The light stop area should be about 10 or 20% of the objective's internal cross-section area.

Instead of glass lenses modified as described above, mirror objectives can preferably be used for luminance contrast, constructed as catoptric systems according to the Cassegrain-/Schwarzschild-type or designed as catadioptric mirror-glass lenses. In such objectives, the backside of the centric convex or plane mirror can act as a light stop. In contrast to a glass lens modified, the light stop is no "foreign body," but an essential optical component according to the specific design of a mirror lens. Moreover, mirror lenses are characterized by several typical advantages: loss of chromatic and spherical aberration, great visual field, very long working distance [12]. Figure 5.49 shows the principle of luminance contrast generated with mirror lenses and a glass lens fitted with a centric light stop. When the illuminating central beam is completely covered by the light stop, as shown in Fig. 5.49, axial dark-field can be achieved. The specimen is illuminated by perpendicular light so that even fine internal structures are visible in high contrast. Axial light can be generated with a bright-field condenser when the condenser aperture diaphragm is maximally closed.

When the aperture diaphragm is opened in tiny steps, a small peripheral component of the central light beam is no longer covered by the light stop so that it can pass the objective. A moderate brightening of the background results from this. Moreover, this background light interferes with the specimen light, and fine phase differences are contrasted similar to negative phase contrast. By digital inversion, the image can be converted to a positive phase contrast-like appearance. The respective phase images are free from haloing (Fig. 5.50). Even bacterial cells can be revealed in superior precision by use of luminance contrast when compared with concurrent standard techniques (Fig. 5.51). When a phase contrast condenser is available instead of a bright-field condenser, the illuminating effects described can also be achieved with appropriately designed light masks.

When compared with standard techniques, luminance contrast promises several advantages [13, 14]. Spatial depth and lateral resolution can be significantly enhanced—nearly doubled—and even structures of very low density can be maximally contrasted. As specimens are illuminated by a small and maximally collimated perpendicular axial light beam of high coherency, also very small structures sized beyond the optical resolution limit can be revealed; they appear like self-luminous bodies. Blooming and scattering are significantly reduced when compared with standard dark-field. Examples of high-resolution images taken in luminance contrast (axial dark-field) are given in Figs. 5.52 and 5.53.

5.4.8 Fluorescence Luminance Contrast

Luminance contrast can be combined with fluorescence imaging in order to reveal fluorescent structures in context with their nonfluorescent environment. In this variant, the transmitted light generating the luminance contrast image should be monochromatic. Of course, this monochrome light must be able to pass the emission filter. The fluorescence image is generated with incident excitation light in the usual manner. The objective must be fitted with a light stop as described, or a mirror objective can be used. As nonfluorescent structures are contrasted on a dark background in high precision and as any irradiation or scattering of light is maximally reduced, the fluorescence image is not compromised by the luminance contrast image superimposed. Figure 5.54 gives an example of practical use.

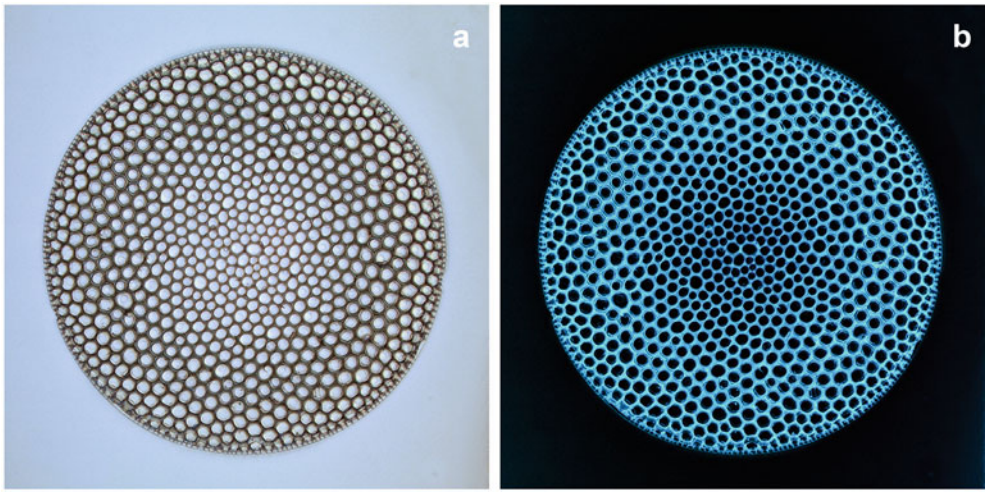

Fig. 5.47 Diatom (*Coscinodiscus* sp.), diameter: 0.13 mm, conventional bright-field (**a**), digital inversion (**b**)

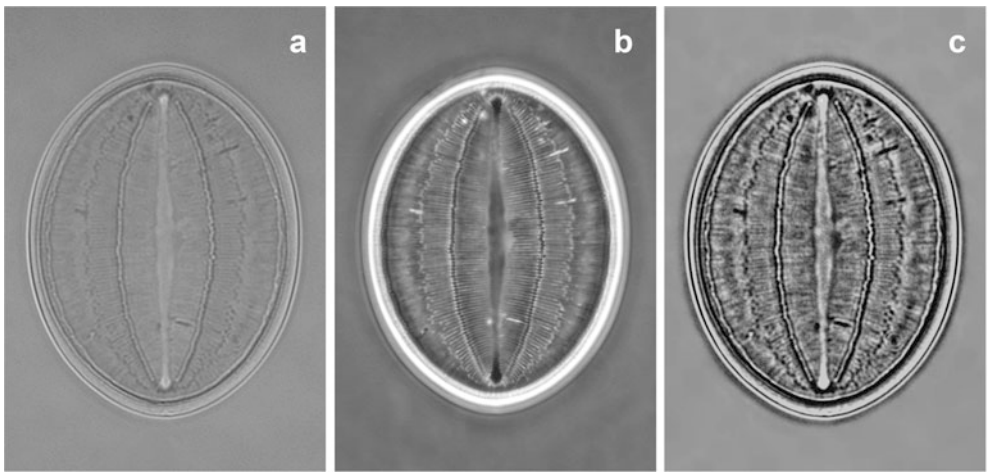

Fig. 5.48 Low-density diatom (*Cocconeis* sp.), bright-field (**a**), phase contrast (**b**), digital phase contrast (**c**). Specimen length: 0.06 mm

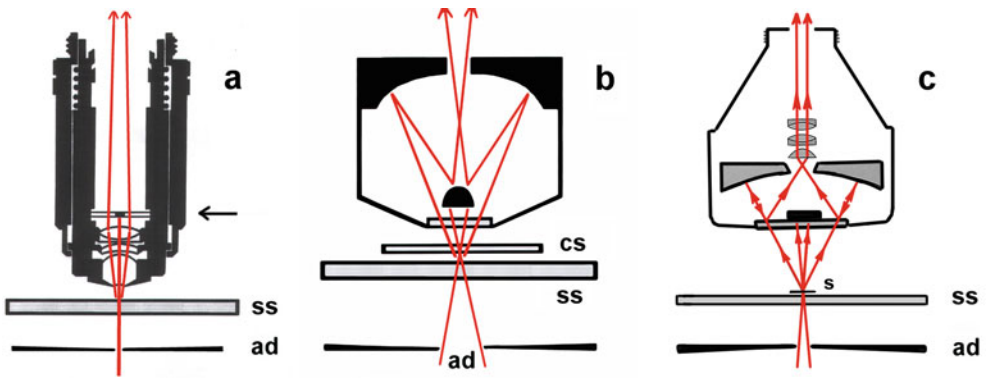

Fig. 5.49 Principle of luminance contrast (axial dark-field), achieved with a modified glass lens (**a**), a catoptric (**b**) and catadioptric (**c**) mirror lens, ad = aperture diaphragm, ss = specimen slide, cs = cover slip

5.4.9 Variable Bright-Dark-Field Contrast

In variable bright-dark-field contrast (VBDC) the specimen is simultaneously illuminated by two different components of transmitted light which create two partial images based on one bright- and dark-field image. These partial images are optically superimposed and interfere with each other. Their intensity and brightness can be separately regulated by the

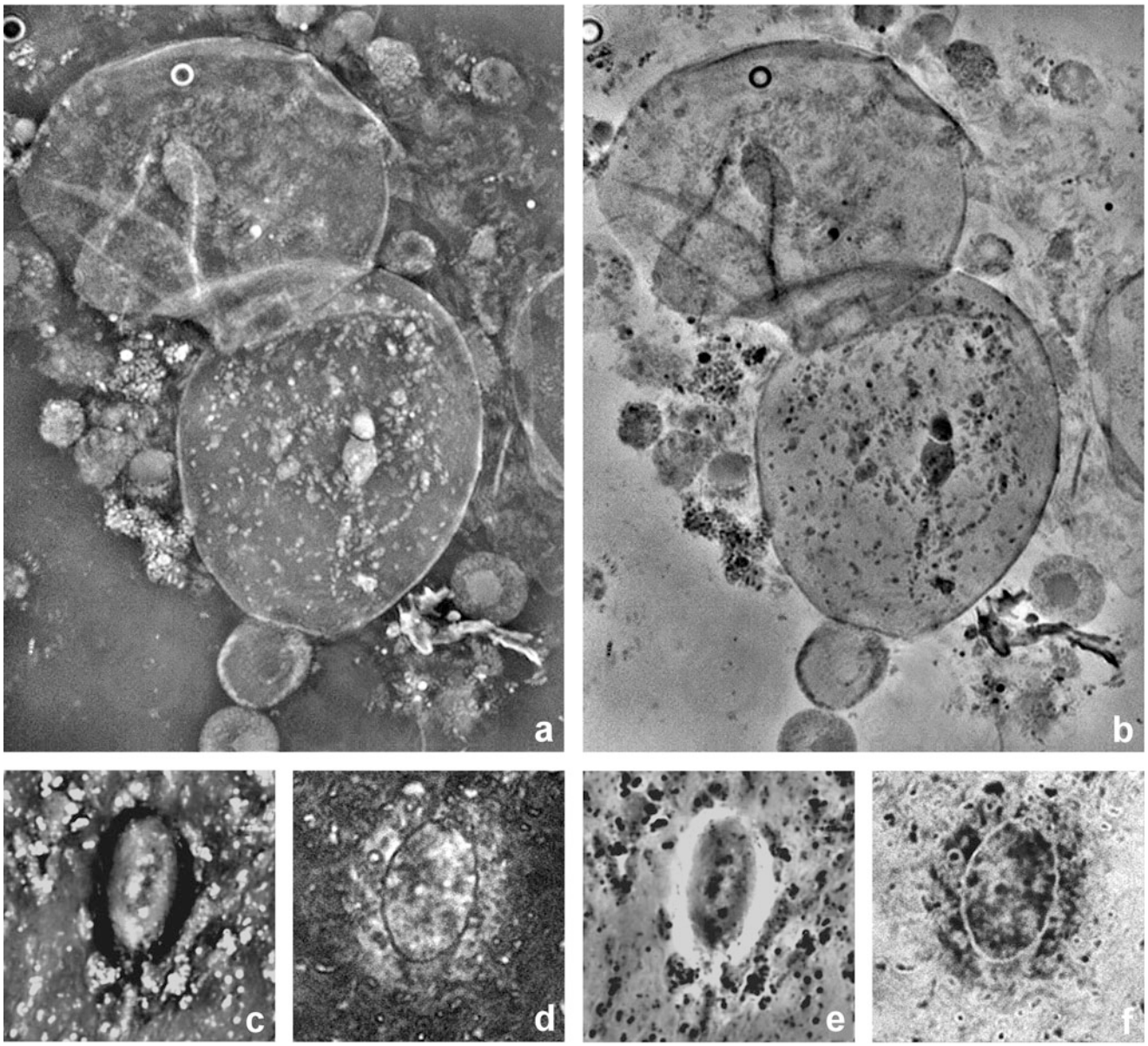

Fig. 5.50 Epithelial cells from the oral mucosa, phase contrast-like imaging achieved with luminance contrast ("luminance phase contrast"), purified from haloing, compared with conventional phase contrast, negative (**a**, **d**) and positive (**b**, **f**) "luminance phase contrast", conventional negative (**c**) and positive (**e**) phase contrast. HFW: 0.15 mm (top), 0.015 mm (bottom)

user. In this way, the character of optical contrast can be modified in tiny steps, and the appearance of the resulting image can be continuously changed from a bright-field-like aspect via overlapping images with medium background brightness, up to a dark-field-like appearance.

This illumination can be achieved when a universal condenser for phase contrast is modified so that the original light annuli are replaced by a set of appropriately designed larger sized annuli. The inner diameter of the respective light annulus has to be somewhat smaller and its external diameter has to be somewhat larger than the diameter of the corresponding objective's internal cross-section area. In this way, the specimen is concentrically illuminated in a bright-field-like manner according to COL by transmitted light beams which come from the internal section of the light annulus and run through the peripheral zones of the objective lenses. Additionally, the specimen is also illuminated in a dark-field-like manner by concentric light beams from the external section of the light annulus which run in an oblique direction without reaching the objective lenses. The corresponding light path is demonstrated in Fig. 5.55. By use of a phase telescope, the alignment of the light annulus can be visually controlled (Fig. 5.56). The internal zone of the light annulus is projected into the marginal periphery of the

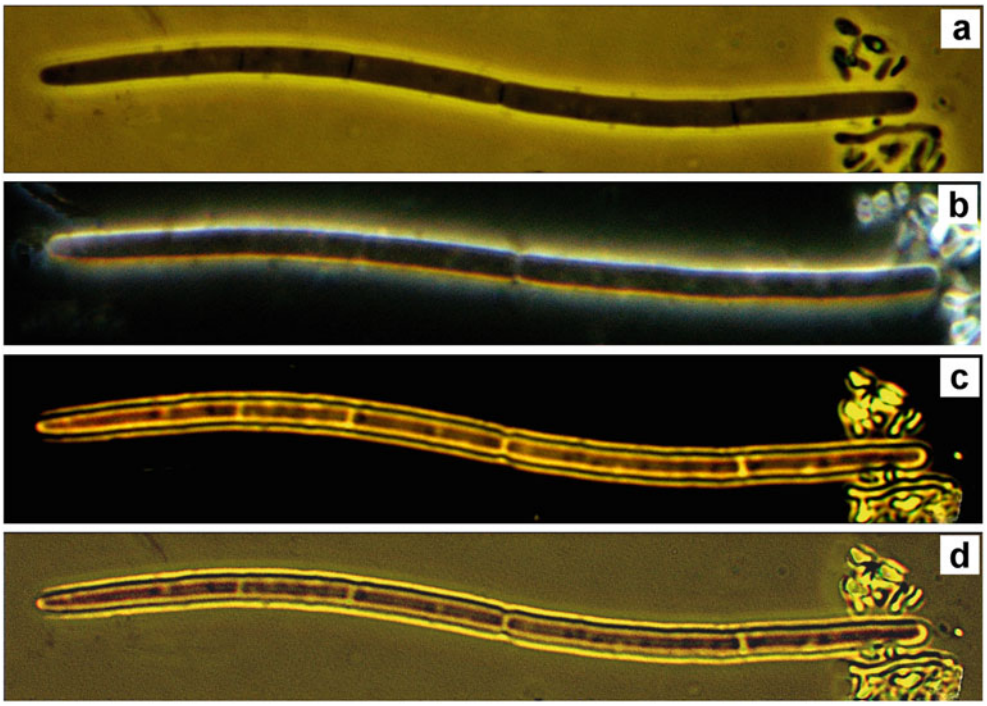

Fig. 5.51 Native bacillus from the oral mucosa, HFW: 0.06 mm, phase contrast (**a**), dark-field (**b**), luminance contrast, central dark-field (**c**), moderate background-brightening (**d**)

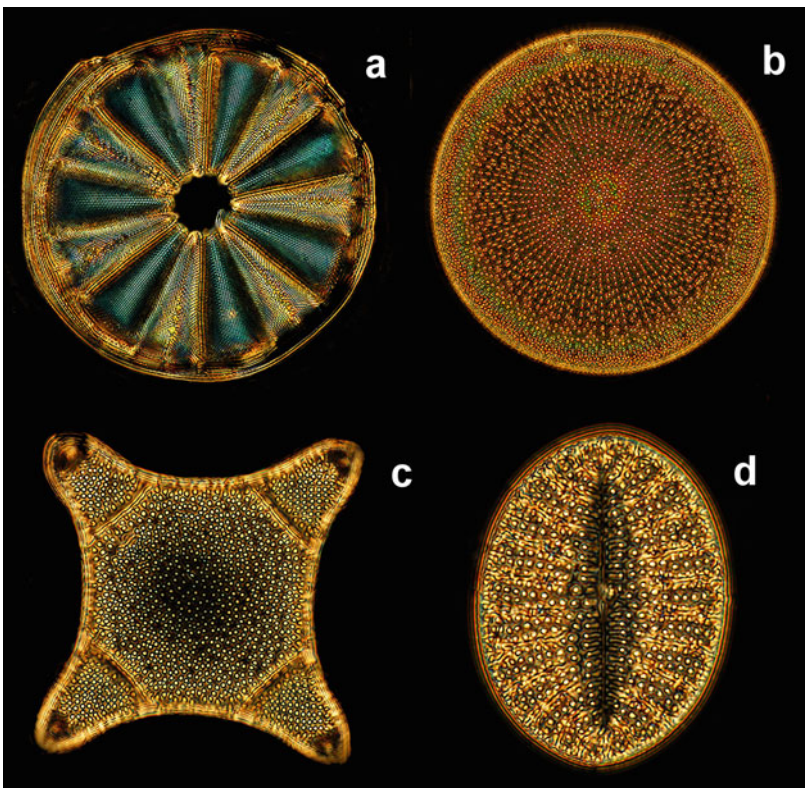

Fig. 5.52 Diatoms frustules of different sizes mounted to a table (maximal lengths: (**a**) 0.11 mm, (**b**, **c**) 0.10 mm, (**d**) 0.05 mm). Luminance contrast (axial dark-field) carried out with a mirror lens

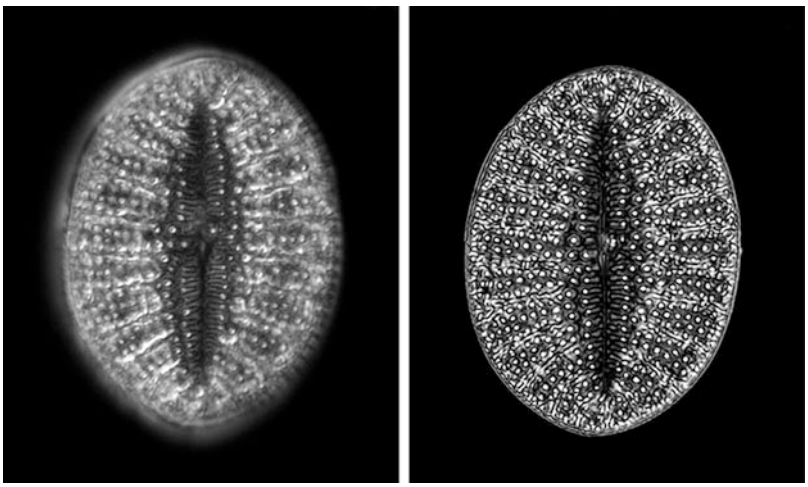

Fig. 5.53 Specimen from Fig. 5.52d (*Coscinodiscus* sp.), conventional dark-field (left) versus luminance contrast (right). Specimen length: 0.05 mm

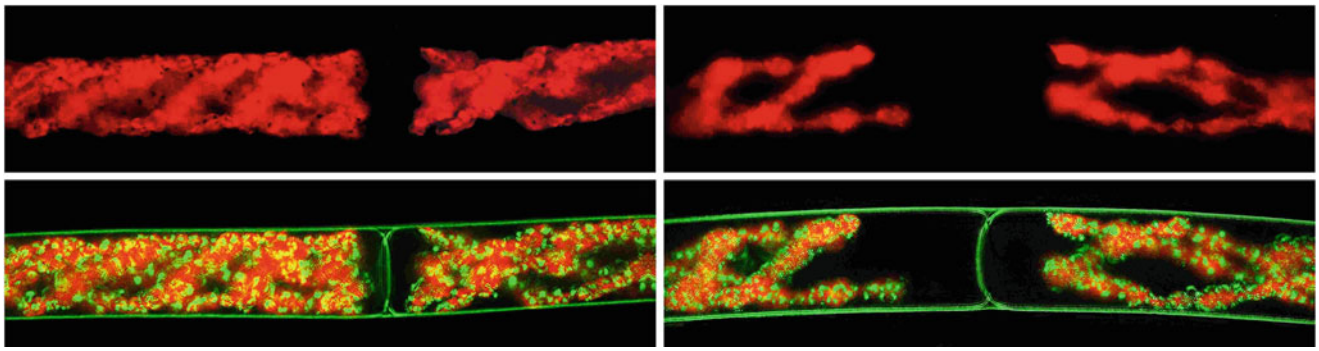

Fig. 5.54 Alga (*Spirogyra*), fluorescence, blue excitation light, autofluorescence of chlorophyll (top), addition of luminance contrast (axial dark-field) achieved with monochromatic green light, $\lambda = 540$ nm (bottom). HFW: 0.25 mm

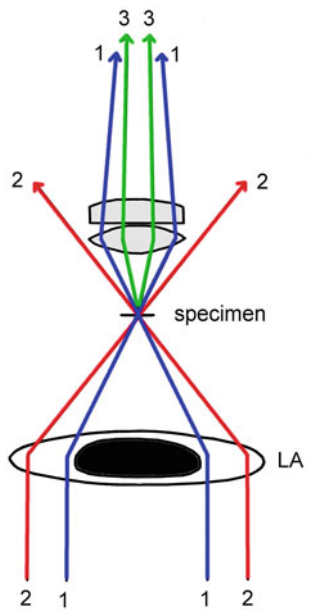

Fig. 5.55 Principle of variable bright-dark-field contrast (VBDC), illuminating light for bright-field (1) and dark-field (2), image forming light (3), light annulus (LA)

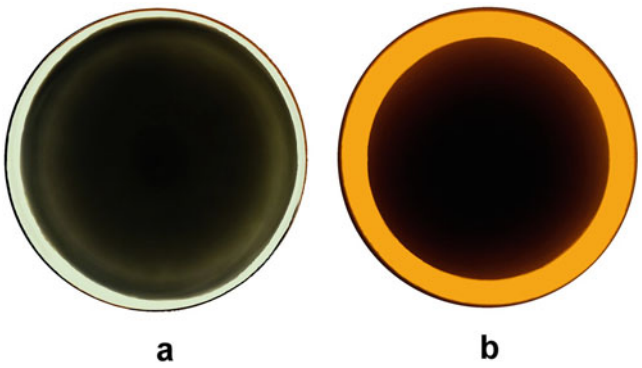

Fig. 5.56 Projections of a light annulus for VBDC, controlled with a phase telescope, examples of dark-field dominated (**a**) and bright-field dominated adjustment (**b**)

objective's cross-section area, whereas the external zone of the light annulus is not visible as it is situated outside the territory of the objective. When the internal zone of the light annulus is very small, the final image will be dominated by the dark-field component (Fig. 5.56a), and the bright-field illumination will be dominant when the broadness of the internal illuminating zone is increased (Fig. 5.56b).

The breadth of the external zone which corresponds with the dark-field-like image can be reduced with the help of the condenser aperture diaphragm if necessary. When the objective is fitted with an iris diaphragm mounted in its back focal plane, the objective's cross-section area can also be reduced on demand. The projection size of the condenser annulus and the path of the illuminating light components can be modified and adjusted in tiny steps when the condenser is shifted up and down. Alternatively, the condenser can be designed as a zoom system so that the projection size of the light annulus can be continuously changed.

Instead of using peripheral light, VBDC can also be carried out with central light, when an annular light stop is integrated which is conjugate with an appropriately sized condenser light annulus. Central dark-field can be superimposed with bright-field, when a small proportion of the illuminating light cone runs beside the light stop. In analogy to relief phase contrast, oblique illumination can be achieved from a defined direction when a sector of the illuminating light annulus is covered.

VBDC is characterized by a significant increase of axial resolution so that the focal depth (depth of field) is significantly enhanced. Especially in thick and complex textured specimens, the three-dimensional architecture can be visualized much better than in concurrent methods. Although the axial resolution is enhanced, lateral resolution is not diminished, but enhanced, too. Also small structures inside transparent specimens, fine textures at the specimen's surface and three-dimensional reliefs are often visualized with superior clarity. In low-density specimens, existing low differences in the optical density can also be visualized by VBDC in a phase or interference contrast-like manner. When the illuminating light components leading to bright- and dark-field are filtered at different colors, additional color contrast can be achieved [15–17]. Examples of practical use are given in Figs. 5.57 and 5.58.

5.4.10 Variable Phase-Dark-Field Contrast

In this variant, phase contrast and dark-field are simultaneously carried out, and both partial images superimposed interfere with each other. The amplitude of both illuminating light components and thus also the intensity and brightness

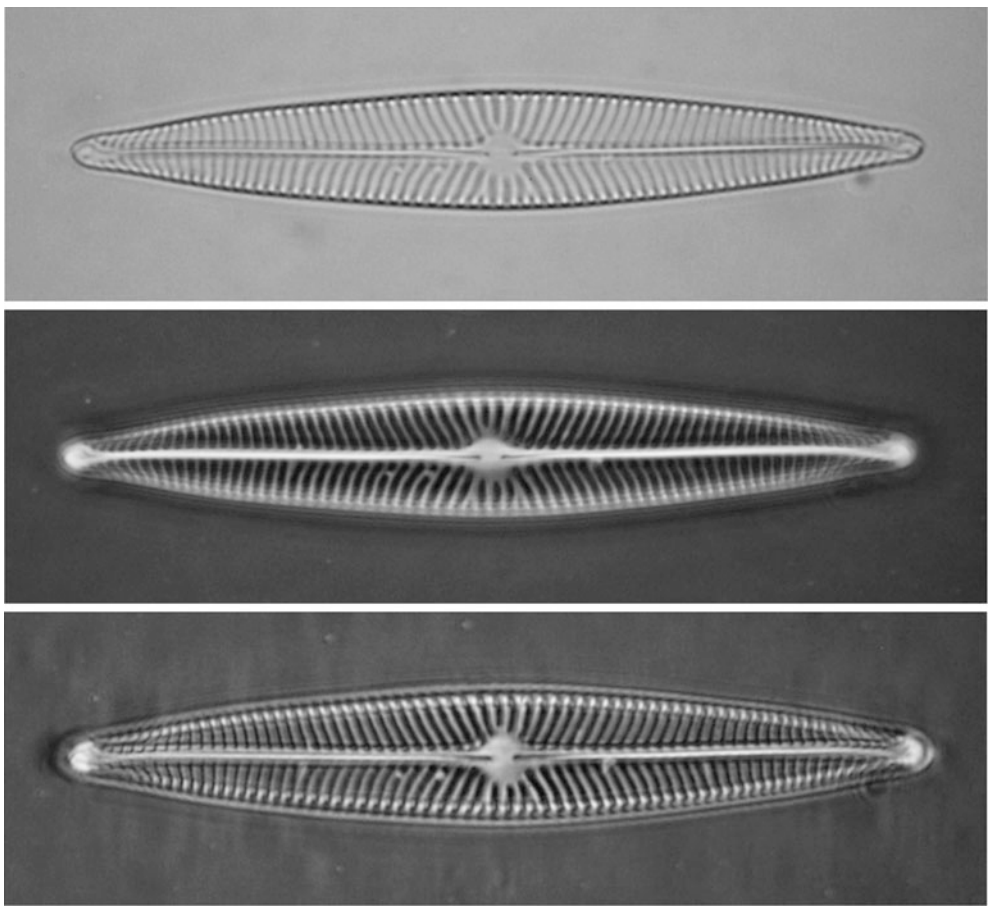

Fig. 5.57 Diatom (*Navicula* sp.) taken in bright-field (top), phase contrast (center) and VBDC (bottom). Specimen length: 0.05 mm

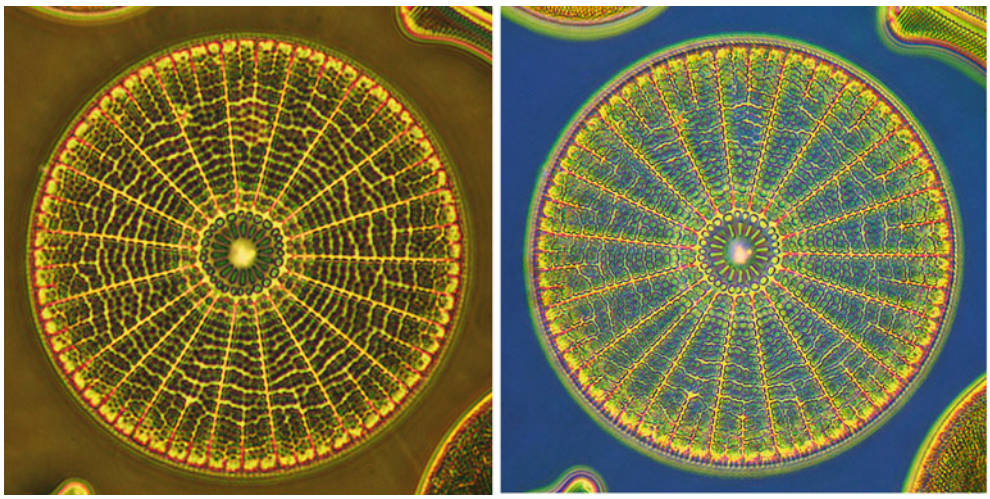

Fig. 5.58 Diatom (*Arachnodiscus* sp.), diameter: 0.1 mm, taken in phase contrast (left) and colorized VBDC (right)

Fig. 5.59 Condenser light mask modified for variable phase-dark-field contrast (VPDC)

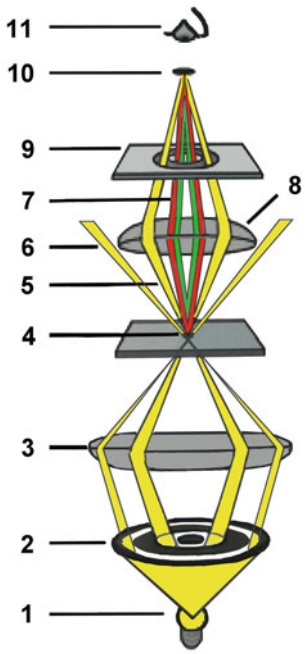

Fig. 5.60 Simplified light pathway of variable phase-dark-field contrast VPDC, light source (1), condenser light mask (2), condenser lens (3), specimen slide (4), illuminating light for phase contrast (5) and dark-field (6), image forming light, two components (7), objective lens (8), phase plate with phase ring (9), intermediate image (10), eye (11)

of the partial images can be separately regulated by the user in tiny steps. In this way, the appearance of the resulting composite image can be continuously changed from a dark-field-dominated to a phase contrast-dominated image. Parts of the illuminating light beams can be covered by a facultative light stop if oblique illumination is required. In order to achieve variable phase-dark-field contrast (VPDC), condensers used for phase contrast have to be equipped with modified light masks consisting of a pair of concentric light annuli (Fig. 5.59): one internal light annulus for phase contrast illumination which has to be conjugate with the phase ring within the objective and another larger sized external light annulus for dark-field illumination. The inner diameter of the latter annulus has to be somewhat larger than the diameter of the corresponding objective's internal cross-section area so that it is projected outside the objective. In this way, the specimen is concentrically illuminated in a phase contrast- and dark-field-like manner. In both so-generated partial images, the specimen is illuminated by concentric light cones at different angles of incidence, i.e., different steepness. The corresponding light path is demonstrated in Fig. 5.60.

The total light flow in the internal light annulus corresponding with phase contrast has to be much smaller than in the external dark-field producing annulus. Otherwise, the dark-field image will be superseded by the phase contrast image. To achieve a well balanced proportion of these different partial images, special light masks can be created fitted with a few small internal perforations instead of the circular phase contrast producing light annulus normally used. Alternatively, according to Fig. 5.59, this light annulus can be covered with a light absorbing (gray) filter or a polarizing filter. In the latter case, the intensity of light can be regulated with a rotatable second polarizer situated beneath the condenser. The breadth of the dark-field-producing external light annulus and thus the intensity of the dark-field

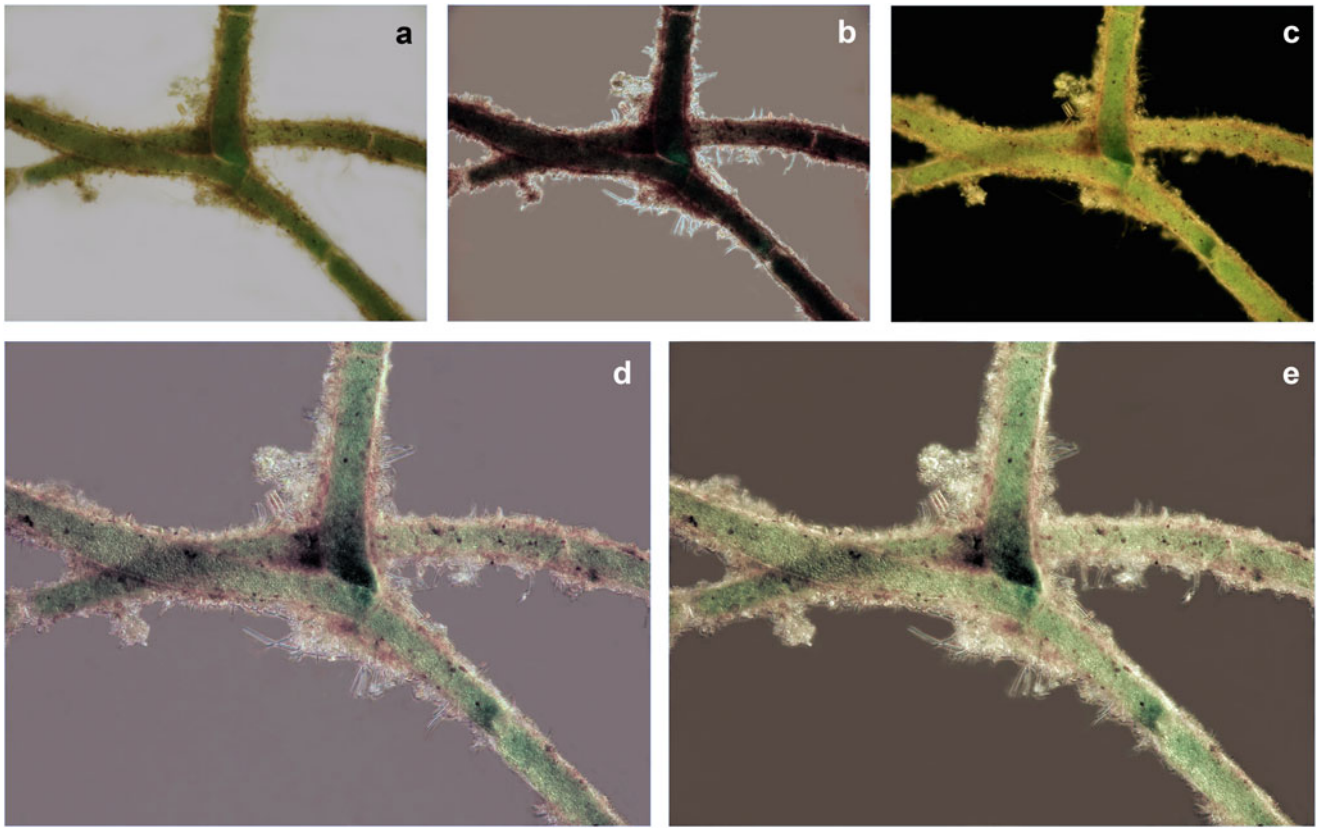

Fig. 5.61 Algae and detritus, bright-field (**a**), phase contrast (**b**), dark-field (**c**), VBDC, dominance of bright-field (**d**) and dark-field (**e**). HFW: 0.8 mm

image can be regulated by the condenser aperture diaphragm. When this diaphragm is wide open, the final image can be dominated by the dark-field component, and phase contrast illumination will be dominant when the broadness of the external light annulus is decreased.

When dark-field and phase contrast illumination are appropriately balanced, the background is moderately brightened, and preexisting ultrahigh ranges in brightness and contrast appear more equalized. By use of special phase contrast objectives fitted with an additional iris diaphragm, the objective's aperture can be regulated in the same manner as well known in standard dark-field microscopy so that potentially blooming and scattering can be mitigated and the depth of field can be enhanced. Also in this variant oblique illumination can be achieved when parts of the illuminating light are covered.

In low-density specimens (phase specimens), existing low differences of the optical density remain visualized by VPDC in a phase contrast-like manner, but haloing can be reduced, and more fine details can be detected in suitable specimens because of the additional dark-field component. In medium- or high-density specimens (absorption specimens), however, natural colors and existing fine details can appear in higher clarity than achievable by use of bright-field, phase, and interference contrast [18]. Some examples of practical use are given in Figs. 5.61 and 5.62.

5.4.11 Axial Phase-Dark-Field Contrast

The light path in axial VPDC achieved with a modified phase contrast microscope is schematically shown in Fig. 5.63 together with a detail view of a modified phase plate fitted with a central light stop and a modified light mask. In axial VPDC, luminance contrast is combined with phase contrast. The specimen is illuminated first by a small axial light beam which is congruent with the optical axis. This beam is covered within the objective by a small light stop situated in the middle of the objective's cross-section area, i.e., in the center of the phase ring, near, or in the back focal plane. The specimen is illuminated further by a concentric light cone which passes the phase ring mounted within the objective according to the common technical standard.

In order to achieve axial phase-dark-field contrast (APDC), phase contrast objectives containing normal phase rings have additionally to be fitted with a discoid light stop in a centered position (i.e., in the middle of the phase ring). The condenser's light mask has also to be modified and

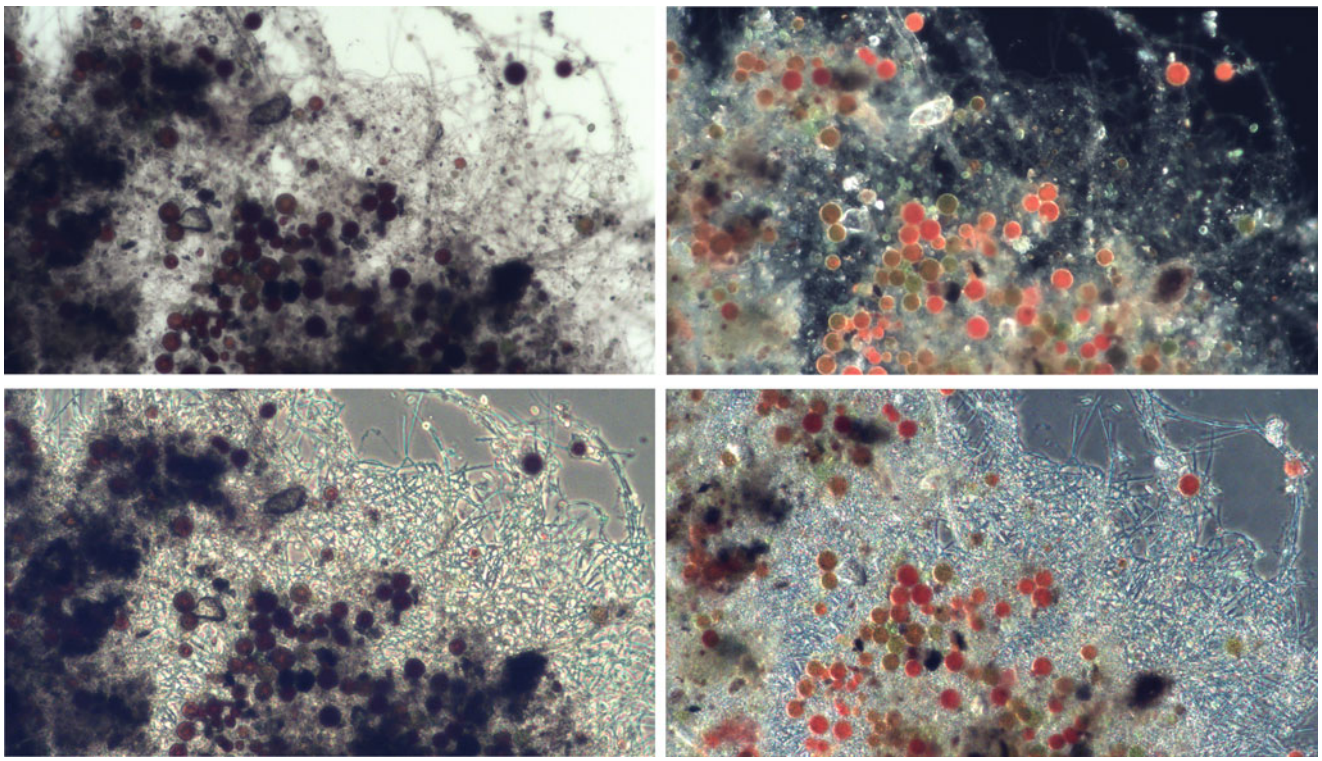

Fig. 5.62 Red colored algae (*Haematococcus pluvialis*) surrounded by low-density blue-green algae and detritus, bright- and dark-field (top), phase contrast and VPDC (bottom). HFW: 0.8 mm

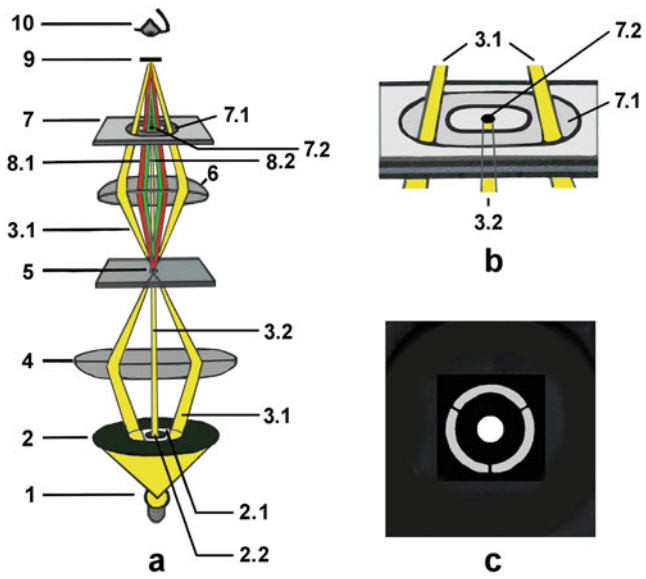

Fig. 5.63 Simplified light pathway of axial phase dark-field contrast (APDC), overview (**a**), modified phase plate (**b**), modified light mask (**c**), light source (1), condenser light mask (2), light outlet for phase contrast (2.1) and axial dark-field (2.2), illuminating light for phase contrast (3.1) and axial dark-field (3.2), condenser lens (4), specimen slide (5), objective lens (6), phase plate (7) with phase ring (7.1) and central light stop (7.2), image forming light for phase contrast (8.1) and axial dark-field (8.2), intermediate image (9), eye (10)

fitted with an additional small central perforation situated in the middle of the respective light annulus designed for phase contrast. This central perforation has to be congruent with the objective's light stop. In normal circumstances, the intensity of illuminating light needed for adequate image brightness is much higher in dark-field illumination than in phase contrast examinations. Thus, the phase contrast and dark-field partial images have both to be equalized in APDC with regard to their brightness. To achieve this, the light flow in the phase contrast producing condenser annulus can be mitigated in the ways described above, preferably by appropriate closing of the condenser aperture diaphragm.

The alignment of the light outlets in the condenser's light mask and the objective's light stopper and phase ring can be controlled by a phase telescope. When the phase contrast producing annulus is completely covered by the maximum closed aperture diaphragm, the specimen is only illuminated by the remaining central axial light so that it appears in axial dark-field illumination. When the aperture diaphragm is moderately opened, the transparent area of the condenser annulus is enhanced in tiny steps so that a phase contrast image is added and superimposed with the axial dark-field image. The intensity of the phase contrast partial image can be continuously regulated so that the appearance of the

resulting APDC-image can be changed from a dark-field-dominated to a phase contrast-dominated image in tiny steps. Instead of glass lenses, mirror lenses can be used for APDC which have to be equipped with an additional phase ring. Parts of the illuminating light beams can be covered on demand if oblique illumination is desired.

Also in APDC, axial and lateral resolutions are increased as pre-described for luminance contrast. Especially in thick and complex textured specimens, the three-dimensional architecture, small internal structures, and fine textures at the specimen's surface can often be visualized better than in concurrent methods. In low-density specimens (phase specimens), existing low differences in the optical density remain visualized in a phase contrast-like manner, but haloing can be reduced, and additional fine details can be contributed by the axial dark-field component. Natural colors are accentuated in a similar manner as achievable with VPDC [19]. Examples of practical use are shown in Figs. 5.64 and 5.65.

5.4.12 Variable Phase-Bright-Field Contrast

In variable phase-bright-field contrast (VPBC), the specimen is simultaneously illuminated in phase contrast and bright-field each filtered in different colors. The illuminating light beams leading to bright-field and phase contrast are separated from each other and also different with regard to their intensities and angles of incidence. In this way, two partial images are optically superimposed and interfere with each other—one phase contrast and one bright-field image. The brightness of both different images and so the weighting of the phase contrast and bright-field illumination can be continuously regulated by the user. Thus, the appearance of resulting images can be modulated from phase contrast-dominated or equalized (balanced) to bright-field dominated images. In phase contrast, the specimen is illuminated by a light cone in the same manner as usual in standard technique. Bright-field illumination can be generated based on axial or

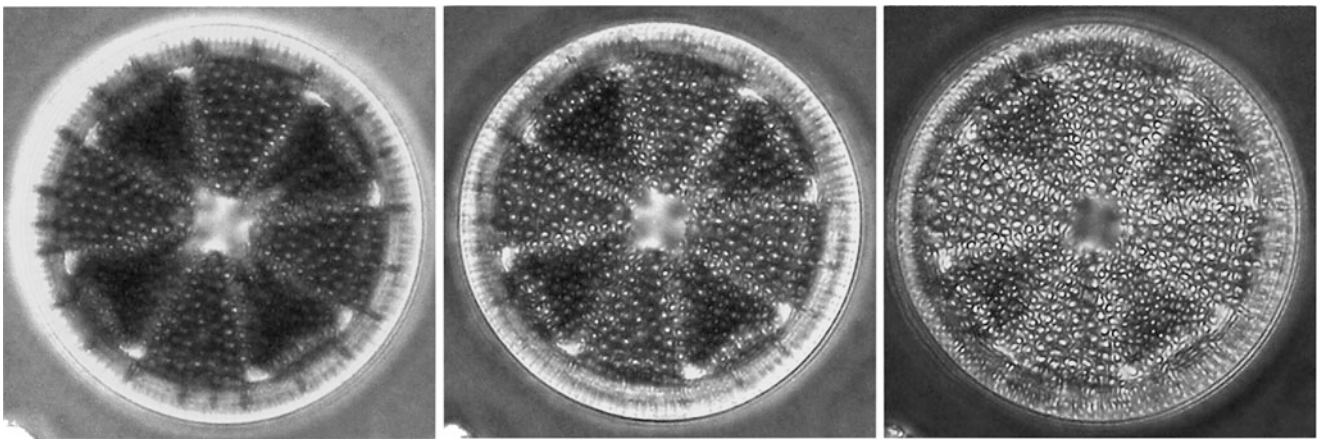

Fig. 5.64 Diatom (diameter: 0.1 mm) taken in phase contrast (left) and APDC dominated by phase contrast (center) and dark-field (right)

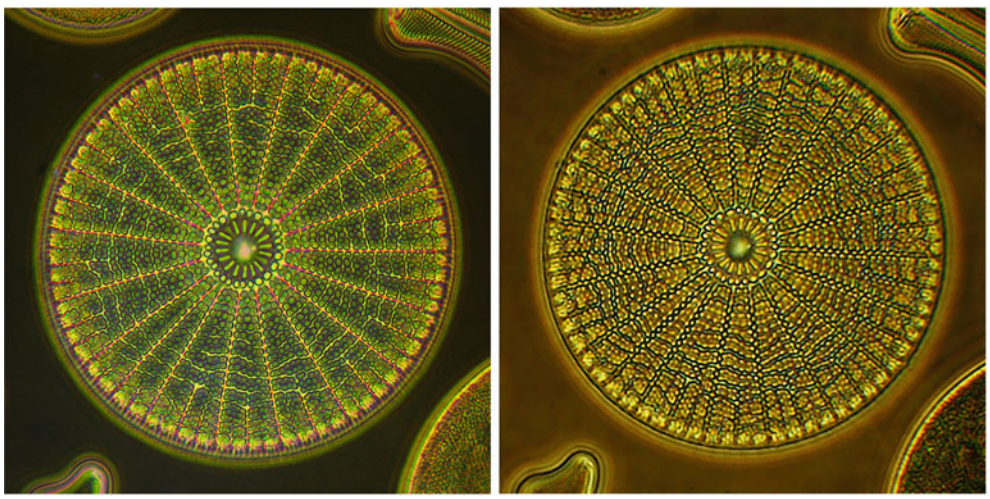

Fig. 5.65 Diatom from Fig. 5.58, taken with a mirror lens fitted with a facultative phase ring, axial dark-field (left), APDC (right). Specimen diameter: 0.1 mm

peripheral light. In the latter case, phase contrast is combined with COL.

VPBC can be carried out with normal phase contrast objectives equipped with a phase plate and a phase ring. The light mask within a phase contrast condenser fitted with an appropriately sized light annulus for phase contrast illumination has to be modified for VPBC so that an additional bright-field image is generated based on axial or concentric peripheral light. For axial bright-field illumination (axial VPBC), a small centric perforation has to be added in the middle (center point) of the light annulus being congruent with the optical axis. Alternatively, the light mask can be fitted with an additional larger sized peripheral (external) light annulus which is concentric with the smaller internal light annulus for phase contrast. Instead of transparent light segments, the external light outlet can also consist of small perforations. The illuminating light pathway for axial and peripheral VPBC and corresponding bicolor light masks are schematically shown in Fig. 5.66. The imaging light which is diffracted by the specimen runs the same way as in normal bright-field and phase contrast and is therefore not shown in these light paths. In all variants of light masks, the light transmitting area of the external light outlet can be varied with the aperture diaphragm, and the internal light outlet can preferably be covered with a polarizer and regulated with an additional rotatable polarizing filter situated beneath the condenser.

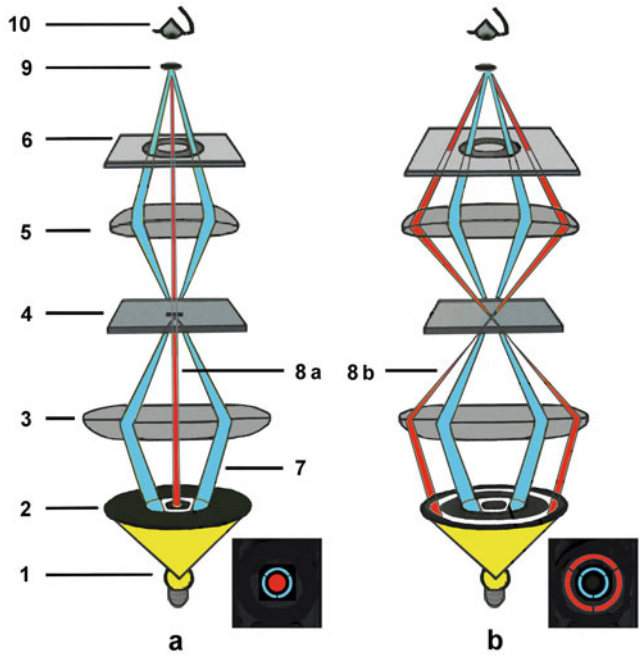

Fig. 5.66 Simplified light pathway of variable phase bright-field contrast (VPBC), based on axial (**a**) and circular oblique (**b**) bright-field, light source (1), condenser light mask (2), condenser lens (3), specimen slide (4), objective lens (5), phase plate with phase ring (6), illuminating light for phase contrast (7) and bright-field (8a and b), intermediate image (9), eye (10)

Prototypes of light masks designed for axial and peripheral VPBC are presented in Fig. 5.66. In the examples shown here, the phase contrast producing light annuli are filtered in blue and the light outlets necessary for simultaneous bright-field illumination are filtered in red. It is essential for well-balanced results that the areas of the light outlets associated with phase contrast and bright-field are similar or equal so that the intensities of the respective partial images are well balanced. The proper alignment of so-modified light masks can be visually controlled by use of a phase telescope in the same manner as usual in normal phase contrast microscopy. When the diameter of the aperture diaphragm is moderately reduced, depth of field, global contrast and accentuation of marginal contours can also be enhanced, i.e., comparable with normal bright-field examinations. To obtain oblique illumination, parts of the illumination light can be covered.

By the optical means described, high-density light absorbing and low-density phase shifting structures can be simultaneously visualized. As the illuminating light components leading to bright-field and phase contrast are filtered at different colors, and as they are separated from each other and run to the specimen at different angles of incidence, the phase contrast image is not "disturbed" by the bright-field image superimposed and the clarity of the bright-field image is not reduced by the phase contrast image simultaneously generated. Halo artifacts and shade-off are significantly reduced in the composite image so that fine details and marginal contours are visualized with greater precision even in low-density phase specimens. In thick specimens, the accuracy of fine and small structures can be significantly enhanced by use of VPBC when compared with corresponding standard applications. In thin specimens, additional contrast effects can be obtained when both partial images interfere with each other. The 3D appearance and the plasticity of the specimen can be improved and the depth of focus enhanced because the aperture diaphragm can be used for modulations of the image's appearance and the illuminating light components associated with bright-field and phase contrast are different with regard to their angles of incidence. Haloing apparent in phase contrast may be reduced by the bright-field light added so that fine linear and punctual structures may be revealed at higher precision [20].

As the final image can be continuously modulated from a phase contrast-dominated to a bright-field-dominated character, the illumination can be adapted to the average or prevalent optical density of the specimen. Photomicrographs taken in VPBC are well suited for converting to black and white. In particular, all immanent fine details and structures can be highly accentuated when the color channels for red and blue are separately regulated with regard to their dominance and gradation while the conversion into B&W is carried out. Some examples of VPBC are shown in Figs. 5.67 and 5.68.

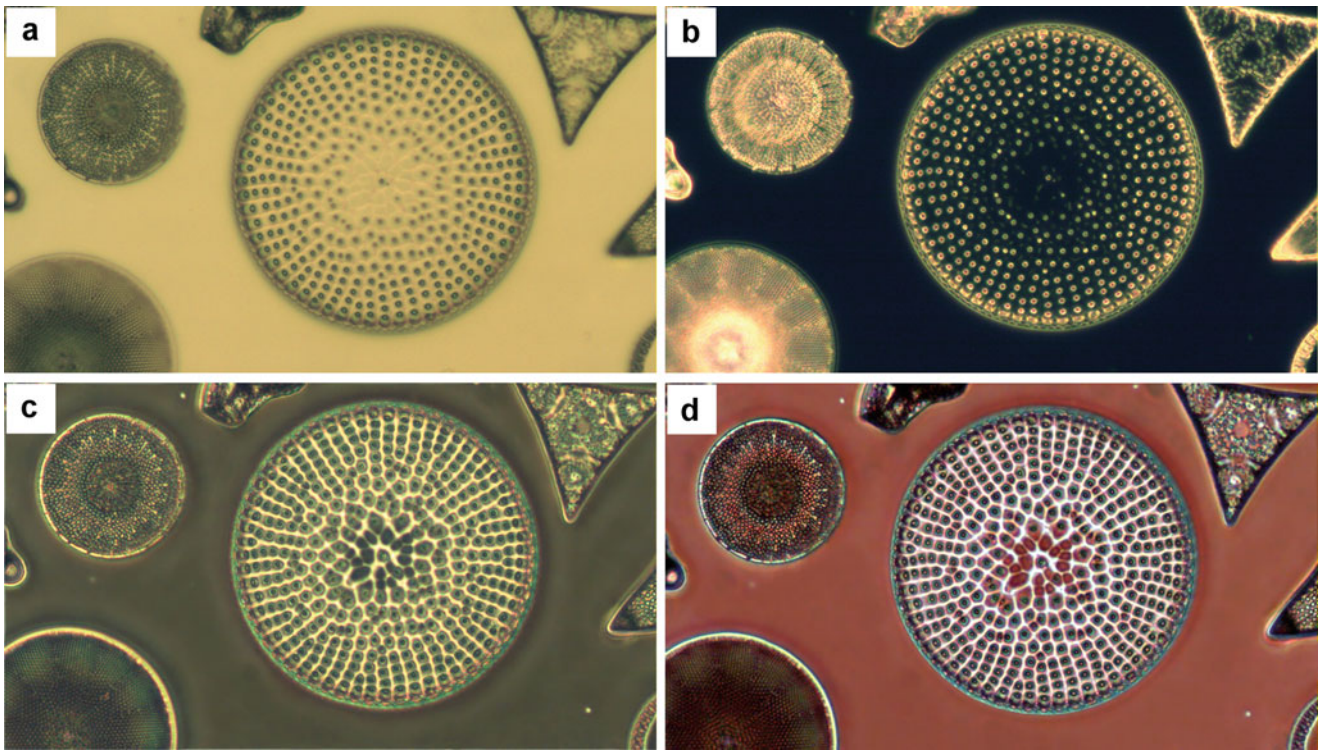

Fig. 5.67 Diatoms, arranged slide, bright-field (**a**), dark-field (**b**), phase contrast (**c**), VPBC (**d**). HFW: 0.26 mm

5.4.13 Variable Combinations of DIC with Phase Contrast and Dark-Field

High grades of visual information can also be obtained when differential interference contrast (DIC) is combined with phase contrast or dark-field illumination. Optical assemblies suited for this task can be created in different ways [21].

5.4.13.1 Variable Interference-Phase Contrast

When DIC is carried out according to the Nomarski method, a standard objective for phase contrast can be used, and the illumination apparatus has to be fitted with an additional light annulus (Fig. 5.69). When DIC is carried out according to the Smith's variant,[1] a special objective was designed for interference contrast containing an integrated DIC prism. In this case, the phase plate and phase ring can be integrated into a special tube which duplicates the objective's back focal plane as well as the intermediate image (Fig. 5.70). In both variants, the specimen is solely illuminated by a light cone which is optically congruent with the phase ring so that a phase contrast image is generated in the usual manner. A DIC image is added by the usual set of DIC prisms and polarizing elements. The dominance of interference contrast can be enhanced in the composite image when an additional proportion of illuminating light is led beside of the phase ring.

5.4.13.2 Variable Interference-Dark-Field Contrast

When the phase ring is replaced by an opaque annular light stop, central dark-field is generated instead of phase contrast in the assemblies described. A DIC image is added, when an additional part of illuminating light passes the light stop. In order to achieve this, the condenser light annulus can be slightly turned into an off-centered position, or the projection size of the light annulus deviates from that of the annular light stop so that a small proportion of the annular light runs beside the light stop. Thus, the proportion of both partial images superimposed—the dark-field and the interference contrast image—can be influenced by the position and projection size of the light annulus. The more light runs beside the light stop, the more the interference contrast image will be dominant.

When a small circular light stop is placed in axial position instead of an annular light stopper, axial dark-field illumination can be added instead of central (paraxial) dark-field. In this case, the condenser light annulus has to be replaced by a small axial light outlet conjugate with the light stopper. In all variants described, the correct alignment of the condenser light outlet and the phase ring or light stop can be controlled with a phase telescope.

[1] Francis Smith patented a difference contrast microscope in the 1930s, approximately 30 years before Nomarski developed DIC.

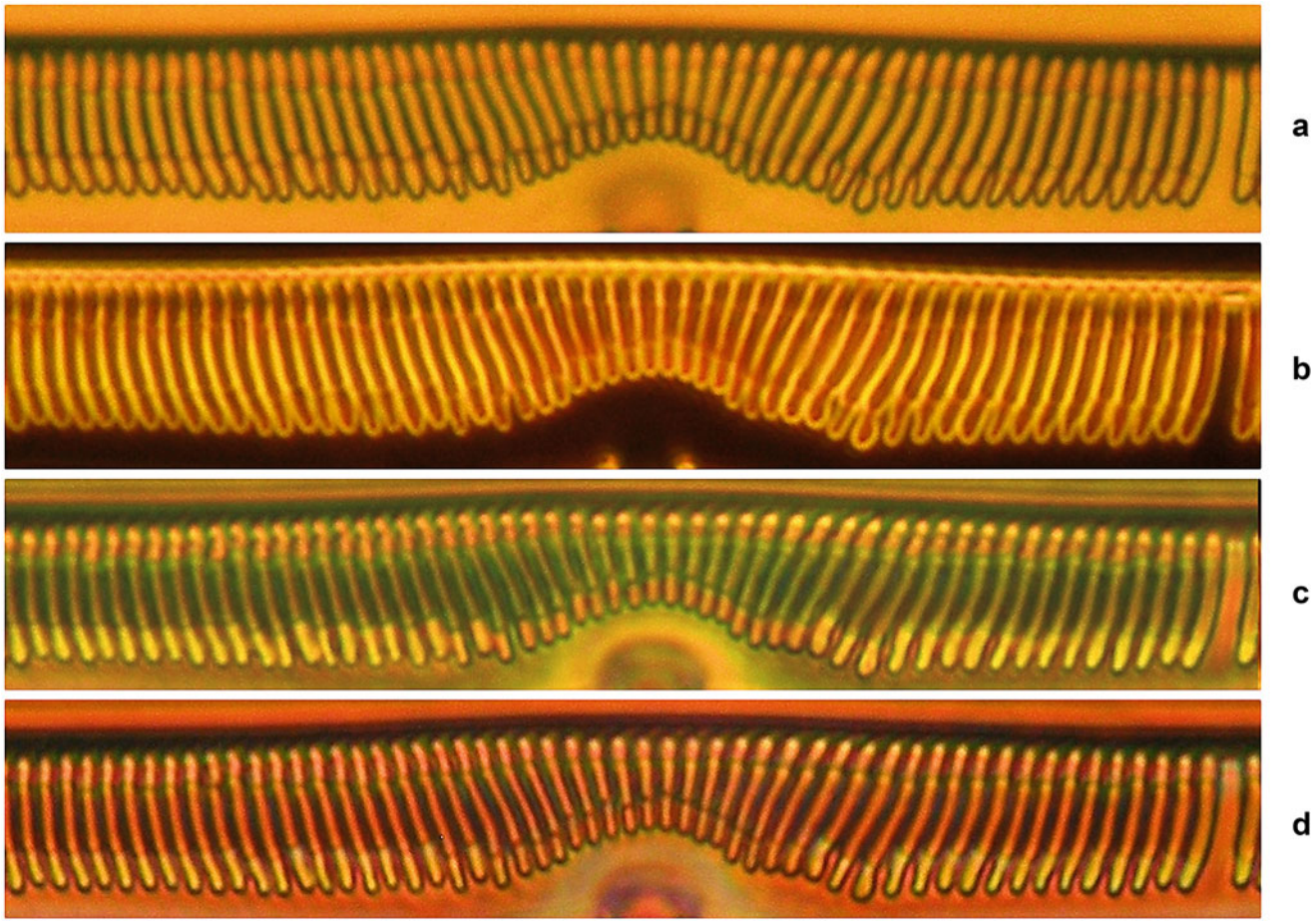

Fig. 5.68 Lamellate structures of diatom frustules, bright-field (**a**), dark-field (**b**), phase contrast (**c**), VPBC (**d**). HFW: 0.12 mm, distances of lamellae: 2 μm

In the assemblies shown in Figs. 5.69 and 5.70, interference contrast and phase contrast (or central/axial dark-field) are both generated on the same axis, i.e., in the same light corridor. Thus, the light components associated with both partial images superimposed are not separated from each other. For this reason, the intensity of interference contrast illumination cannot be selectively reduced on its own when combined with phase contrast. This limitation can be overcome when the contrast tube is designed for a couple of light corridors (Fig. 5.71). In this variant, the incoming light is divided by a splitting prism into two components which run through the special tube in two separate light corridors. Thus, one light corridor can be used for generating interference contrast and the other for achievement of phase contrast (or central/axial dark-field). Consequently, in the light corridor provided for interference contrast, a second DIC prism is inserted in the back focal plane duplicated (back focal plane 2), and in the other light corridor, light modulators (phase rings or light stoppers) can be inserted at the corresponding plane so that phase contrast or central/axial dark-field can be added. Both so-created partial images are reunited by a joining prism so that the partial images generated in both light corridors are optically superimposed. In this arrangement, each light corridor can be fitted with rotatable double polarizers (P_1 and P_2) so that the intensities of the partial images superimposed can be regulated independently from each other over the full range of brightness and darkness. Of course, variable gray filter sets could also be used for analogous regulations of these intensities instead of double polarizers. In this way, variable transitions between interference contrast and phase contrast (or dark-field/bright-field) can be achieved so that the specimen can be illuminated in pure interference contrast, pure phase contrast (or dark-field) or both coactive illumination techniques contributing to the final composite image in variable proportions, which can be continuously regulated. Figure 5.72 shows the results of the superimposition of phase and interference contrast, and Fig. 5.73 corresponding images resulting from the superimposi-

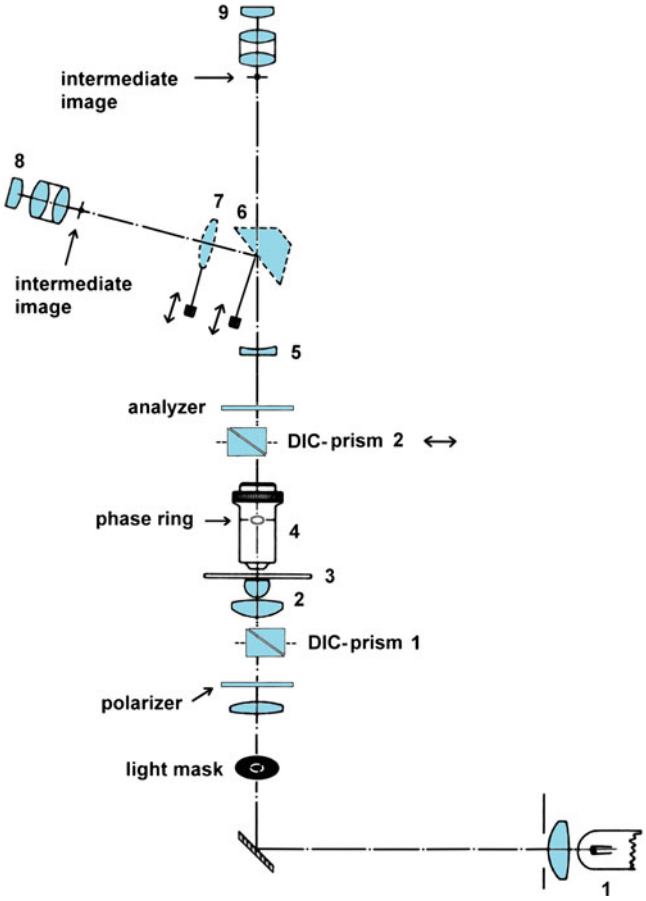

Fig. 5.69 Assembly for variable interference phase contrast (VIPC) based on Nomarski, light source (1), condenser (2), specimen (3), objective (4), tube lens (5), tube prism (6), Bertrand lens (7), eyepieces (8, 9)

tion of central dark-field and interference contrast. Figure 5.74 gives comparisons of resolution cropped from Figs. 5.72 and 5.73. It can be clearly seen that resolution is enhanced in the compound images, especially when DIC is combined with the central dark-field.

This enhancement of resolution is caused by several reasons:

- The partial images superimposed interfere with each other, so that additional visual information can become apparent.
- In axial and central dark-field, specimens are hit by nearly perpendicular axial or paraxial light beams so that fine internal structures within the specimen observed are not excluded from illumination. This is a significant difference to standard dark-field which is based on oblique peripheral light. Thus, even very small structures can be detected by slight light components which are bent and reflected by the specimen so that even very small structures sized at the resolution limit appear in a similar manner as self-luminous or fluorescent bodies.
- The coherency of illuminating light is higher than in concurrent techniques, especially in axial dark-field. Further optical aspects are discussed in [13, 14].

5.5 Conclusions

This chapter provided an introduction to basic optical principles and components of a light microscope (light source, condenser, objective [finite and infinite systems], tube lens, and eyepiece). Standard techniques of illumination have been shortly described (bright-field, circular oblique lighting/COL, dark-field, Rheinberg illumination, phase contrast, polarized light microscopy, differential interference contrast/DIC, fluorescence, and incident light microscopy). Moreover, several additional illumination techniques recently developed have been reported (apodized and relief phase contrast, aperture reduction phase contrast and dark-field, digital dark-field and phase contrast, luminance contrast based on mirror lenses or modified glass lenses, variable bright-dark-field contrast [VBDC], variable and axial phase-dark-field contrast [VPDC and APDC], variable phase-bright-field contrast [VPBC], variable interference-phase- and dark-field contrast [VIPC, VIDC]). The optical effects achievable have been demonstrated for each technique described. By sophisticated selection of appropriate illumination modes and multimodal techniques, image quality and visual information can be significantly enhanced and optimally adjusted to the properties of specimens examined.

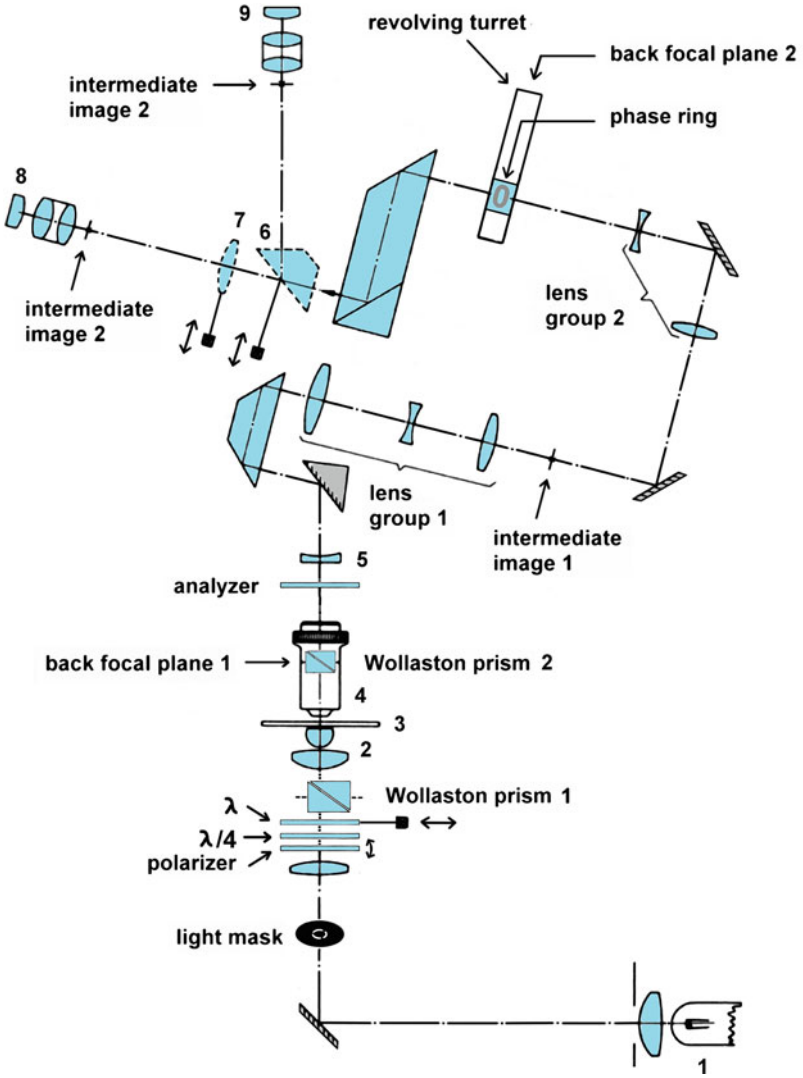

Fig. 5.70 Assembly for variable interference phase contrast (VIPC) based on Smith achieved with a special contrast tube designed for one light corridor, light source (1), condenser (2), specimen (3), objective (4), tube lens (5), tube prism (6), Bertrand lens (7), eyepieces (8, 9)

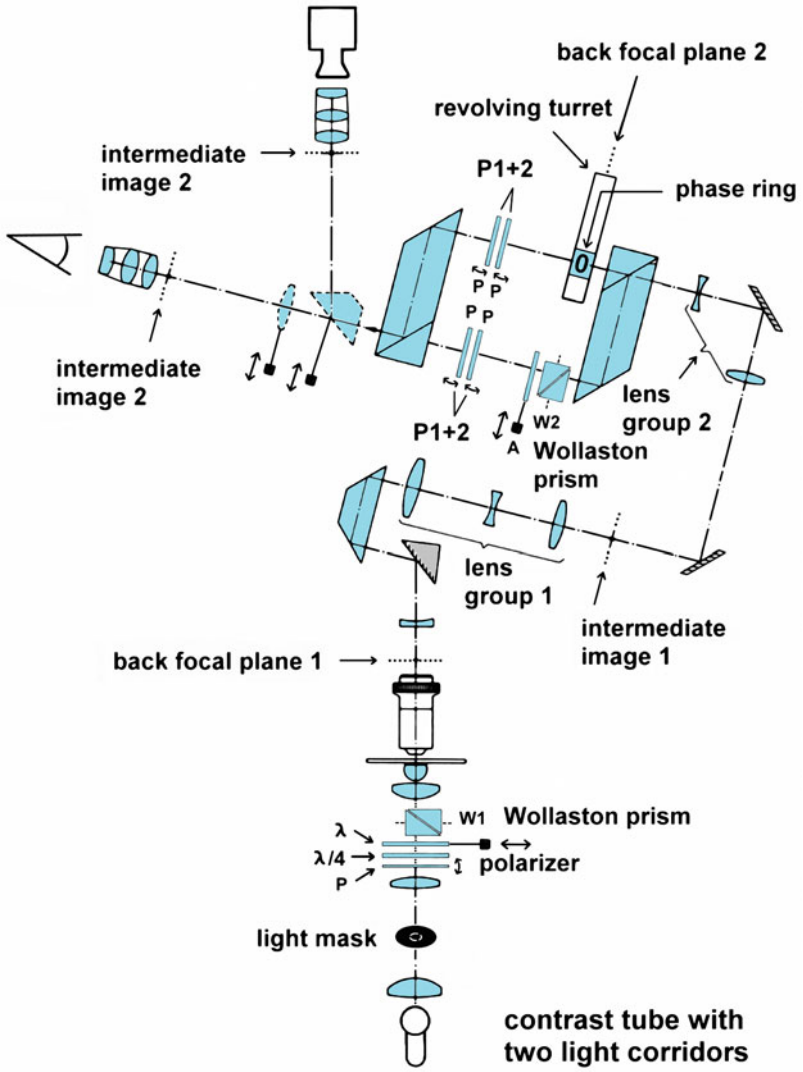

Fig. 5.71 Assembly for variable interference phase contrast (VIPC) achieved with a special contrast tube designed for two light corridors, further explanations in the text

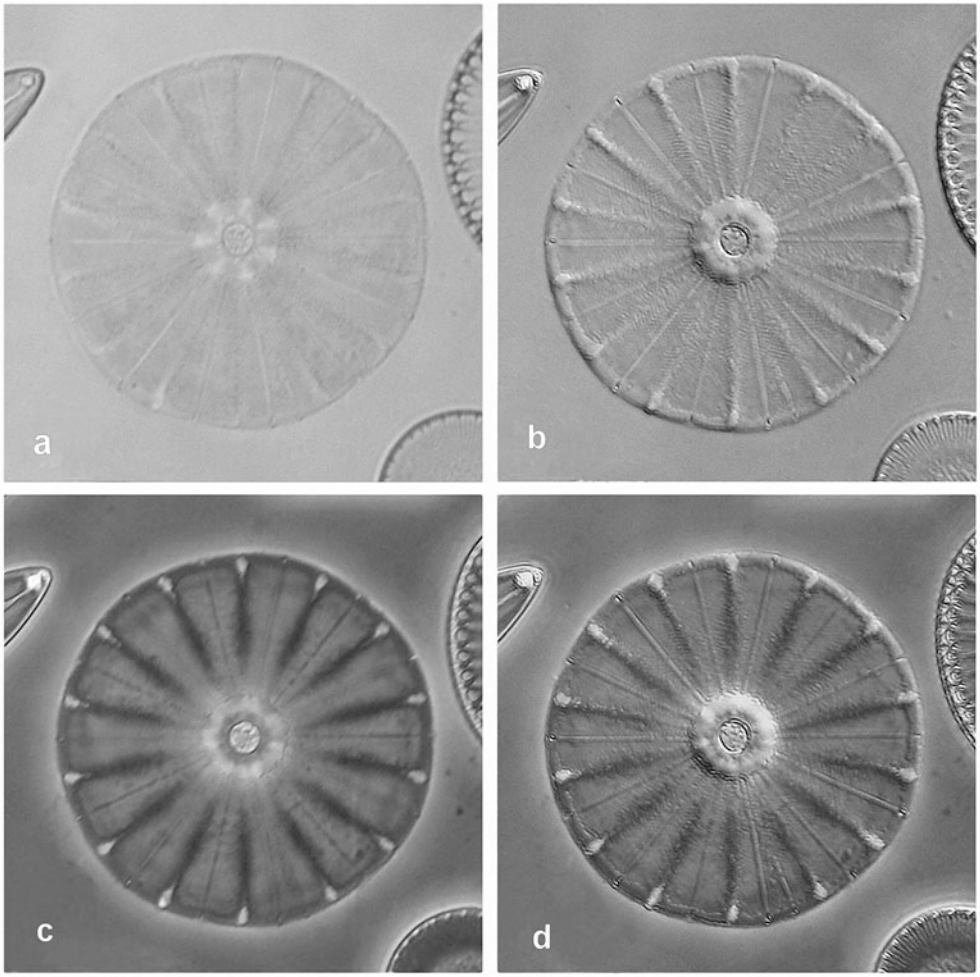

Fig. 5.72 Low-density diatom from Fig. 5.26, diameter: 0.07 mm, bright-field (**a**), interference contrast (DIC) (**b**), phase contrast (**c**), VIPC (**d**)

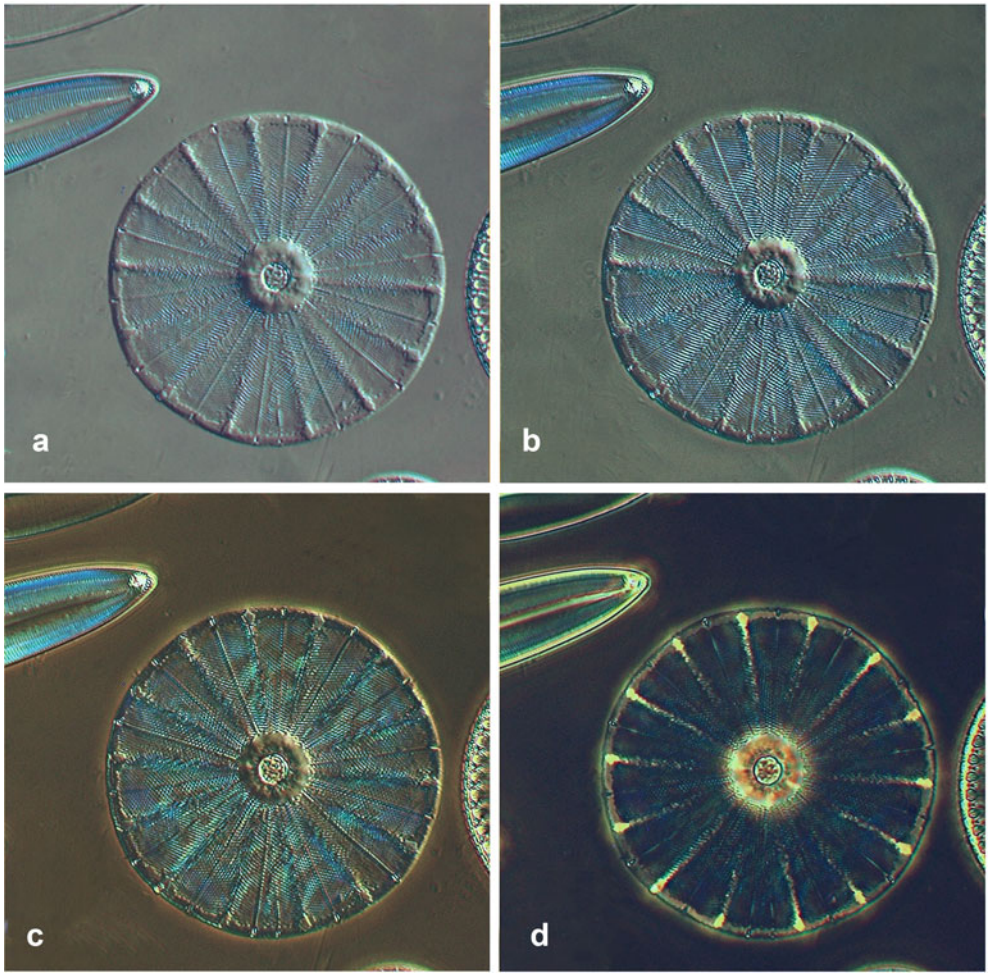

Fig. 5.73 Specimen from Fig. 5.72, VIDC, dominance of interference contrast/DIC (**a**), equalized proportions of DIC and axial dark-field/DF (**b**), dominance of DF (**c**), pure DF (**d**)

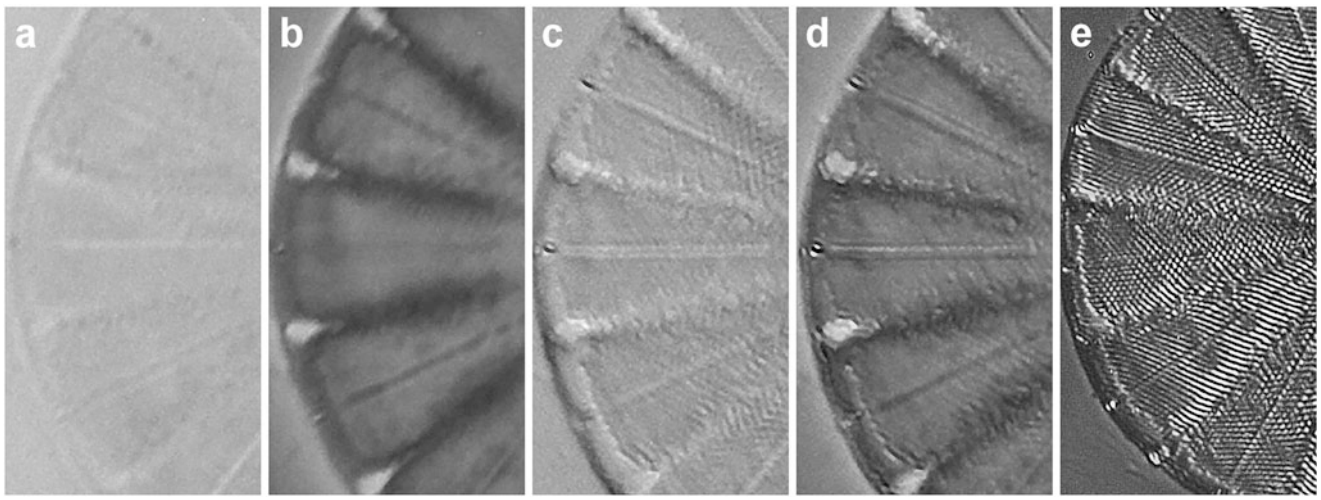

Fig. 5.74 Small sections cropped from Figs. 5.72 and 5.73, object field: 21.5 × 40.4 µm, bright-field (a), phase contrast (**b**), interference contrast (**c**), VIPC (**d**), VIDC (**e**)

Acknowledgments The authors thank Dipl. Ing. Frank Fox, Trier, Germany, for the photomicrographs shown in the Figs. 5.23 and 5.32.

References

1. Dobell, C.: Antony Van Leeuwenhoek and his "Little Animals". Harcourt, Brace and Company, New York. http://bit.ly/2KEI50G (1932)
2. Volgger, M., Lichtscheidl, I.K.: Light Microscopy, Theory and Use (Online Tutorial). http://bit.ly/2X43cQM (2008)
3. Determann, H., Lepusch, F.: The Microscope and Its Application. Ernst Leitz Wetzlar, List 512-69c/Engl. (1977)
4. Nobel Lectures: Physics 1942–1962. Elsevier, Amsterdam (1964)
5. Mulisch, M., Welsch, U. (Hrgs): Romeis – Mikroskopische Technik. 19. Auflage. Springer Spektrum, Berlin (2015)
6. Pappenheim, A.: Grundriss der Farbchemie. Zum Gebrauch bei mikroskopischen Arbeiten. Hirschwald, Berlin (1901)
7. Otaki, T.: Artifact halo reduction in phase contrast microscopy using apodization. Opt. Rev. **7**, 119–122 (2000)
8. Piper, J.: Relief-phase-contrast—a new technique for phase-contrast light microscopy. Microsc. Anal. **21**, 9–12 (2007)
9. Piper, J.: Condenser aperture reduction phase contrast—a new technique for improved imaging in light microscopy. J. Adv. Microsc. Res. **5**, 1–10 (2010)
10. Piper, J.: Artemia—a model specimen for educational microscopy—projects in biological and ecological fields. Microsc. Today. **26**, 12–17 (2018)
11. Piper, J.: Ultra-high contrast amplifying in bright-field images. Microsc. Today. **18**, 10–16 (2010)
12. Piper, J.: Mirror lenses in light microscopy—theoretical considerations and practical implications. Microsc. Res. Tech. **73**, 681–693 (2010)
13. Piper, J.: Luminance-contrast—a new visible light technique for examining transparent specimens. Microsc. Today. **15**, 26–34 (2007)
14. Piper, J.: Luminance contrast, a new illumination technique in light microscopy: optical basics, practical evaluations, further developments. Optik. **120**, 963–975 (2009)
15. Piper, T., Piper, J.: Variable bright-darkfield-contrast (VBDC)—a new illumination technique for improved visualizations of complex structured transparent specimens. Microsc. Res. Tech. **75**, 537–554 (2012). Article first published online: 14 OCT 2011). https://doi.org/10.1002/jemt.21089
16. Piper, T., Piper, J.: Universal variable bright-darkfield contrast—a variant technique for improved imaging of problematic specimens in light microscopy. Microsc. Microanal. **19**, 1092–1105 (2013)
17. Piper, T., Piper, J.: Phase contrast without phase plates and phase rings—optical solutions for improved imaging of phase structures. Microsc. Res. Tech. **76**, 1050–1056 (2013)
18. Piper, T., Piper, J.: Variable phase-darkfield contrast (VPDC)—a variant illumination technique for improved visualizations of transparent specimens. Microsc. Microanal. **18**, 343–352 (2012)
19. Piper, T., Piper, J.: Axial phase-darkfield-contrast (APDC), a new technique for variable optical contrasting in light microscopy. J. Microsc. **247**, 259–268 (2012)
20. Piper, T., Piper, J.: Variable phase bright-field contrast (VPBC)—an attractive illumination technique for improved imaging in transparent specimens. Microsc. Microanal. **19**, 11–21 (2013)
21. Piper, T., Piper, J.: Variable multimodal light microscopy with interference contrast and phase contrast; dark or bright field. J. Microsc. **255**, 30–41 (2014)

Light Filtering in Microscopy

6

J. Piper

Abstract

In digital photography and photomicrography, colorization and other quality determining parameters can be influenced by post-processing. Thus, in general, the current "importance" of light filtering seems to be somewhat lower than in the past. Nevertheless, light filters are relevant for optimization of image quality up-till now, especially in microscopy—in visual observations as well as in photomicrography. This chapter gives an introduction to the use of colorless (neutral) and color modulating filters. Results achievable are demonstrated by photomicrographs taken with a standard laboratory microscope. The filters presented are capable of optimizing the intermediate image so that they can be regarded as complementary tools promising substantial improvements of visual observations and photomicrographs—regardless of whether post-processing is additionally carried out or not.

6.1 Introduction

In the "pre-digital" era, light filtering was essential in photography and photomicrography, because the colorization and quality of photographs were only influenced by the circumstances and conditions of the respective scene, the optical equipment and the sort of analog film and/or photo paper used. In digital photography and photomicrography, however, colorization and other quality determining parameters can be influenced by post-processing. Thus, in general, the current "importance" of light filtering seems to be somewhat lower than in the past. Nevertheless, light filters are relevant for optimization of image quality up till now, especially in microscopy—in visual observations as well as in photomicrography.

This chapter gives an introduction to the use of colorless (neutral) and color modulating filters. Results achievable are demonstrated by photomicrographs taken with a standard laboratory microscope. The filters presented are capable of optimizing the intermediate image so that they can be regarded as complementary tools promising substantial improvements of visual observations and photomicrographs—regardless of whether post-processing is additionally carried out or not.

On detail UV- and IR-cut filters, diffusers, neutral gray, and double polarizing filters are described as typical representatives of colorless and "neutral" filters. Moreover, several sorts of color modulating filters are presented: Colorized glass filters, interference filters, and colorizing polarizers. Blue "daylight" filters are widely used as "compensating filters" for mitigation of red, orange, or yellowish hue in bulb and halogen light, and red or orange warming filters can be used for elimination of bluish taint in LED light. Especially in colorless specimens which are visualized based on gray values, contrast and distinctness can be improved by green light filtering. Monochromatic narrowband and monochrome band-pass interference filters can lead to substantial improvements in resolution, distinctness, and contrast. Images taken in monochromatic light are free from any chromatic aberration. Other sorts of interference filters act as RGB intensifiers leading to a high grade of color purification in images based on the RGB color space. These positive effects can also be used for multi-shot—or three-shot color imaging—a special technique which can be used in photomicrography as long as specimens do not move. "Vario-color" and "Pol-color" filters are special sorts of polarizing filters which are interesting tools in various microscopic tasks. They can be used for neutralization of color taint in any sort of light sources, and furthermore, they can lead to splendid multicolor contrast effects in polarized light microscopy and interference contrast so that fine details can be accentuated with higher precision and clarity.

J. Piper (✉)
Laboratory for Applied Microscopy Research, Bullay, Germany
e-mail: lab-appl-microscopy-research@t-online.de

G. Cristóbal et al. (eds.), *Modern Trends in Diatom Identification*, Developments in Applied Phycology 10,
https://doi.org/10.1007/978-3-030-39212-3_6

In the following sections, these capacities of light filtering are described in detail, and they are demonstrated with several photomicrographs. Lastly, the advantages and disadvantages of halogen and LED light are discussed because the character of colorization is not only influenced by light filters but also by the light source available.

6.2 Neutral Colorless Filters

6.2.1 UV–IR Cutters

Daylight, flashlight, and traditional bulb light have continuous spectra representing the visible light (circa 380–750 nm) and invisible components, i.e., infrared (IR) and ultraviolet (UV) light (Fig. 6.1, modified from [1]). An overview of visible spectral colors and corresponding wavelengths is given in Table 6.1 [1, 2]. Modern halogen bulbs are fitted with a UV absorbing layer, but older ones are uncoated so that they can emit a relevant proportion of ultraviolet light. Thus, even UV fluorescence can be achieved without using an emission filter, when a fluorescent specimen is illuminated with a 50 W halogen bulb in bright-field at maximum intensity filtered with a UV excitation filter (Fig. 6.2). IR can be emitted by each sort of bulb. Especially at high intensity of light, the human eye can be damaged by UV and IR light. Thus, UV–IR absorbing filters can be used for eye protection. Figure 6.3 shows the transmission band of an ideal UV–IR blocker. LEDs, however, can be designed for selective emission of

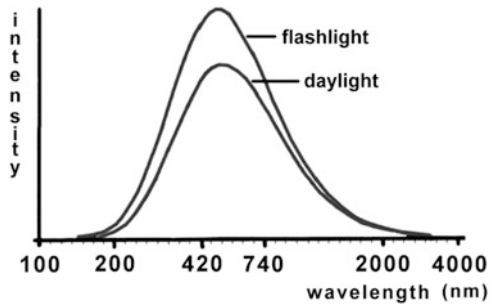

Fig. 6.1 Typical spectra of daylight and flash light (modified from [1])

Table 6.1 Ranges of wavelengths and typical nominal wavelengths of the spectral colors [1, 2]

Color	Range of wavelengths (nm)	Nominal wavelength (nm)
Ultraviolet (UV)	<380	
Violet	380–420	400
Blue	420–490	440
Magenta	450–480	465
Cyano	490–520	510
Green	490–575	540,546
Yellow	575–585	580
Orange	585–650	590
Red	650–750 (780)	700
Infrared (IR)	>750 (780)	

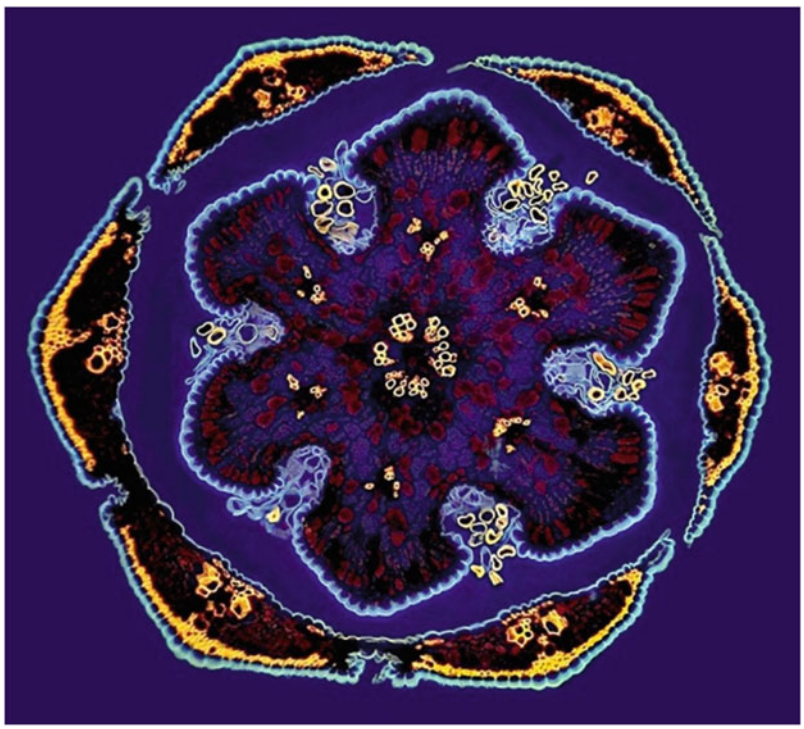

Fig. 6.2 Fluorescence image of a plant section (*Casuarina equisetifolia*, Wacker staining) carried out with transmitted UV light, halogen source (50 W), bright-field condenser, UV-filter (Baader U-filter, transmission: 310–390 nm, peak: 360 nm), objective 10/0.30, specimen diameter: 0.4 mm

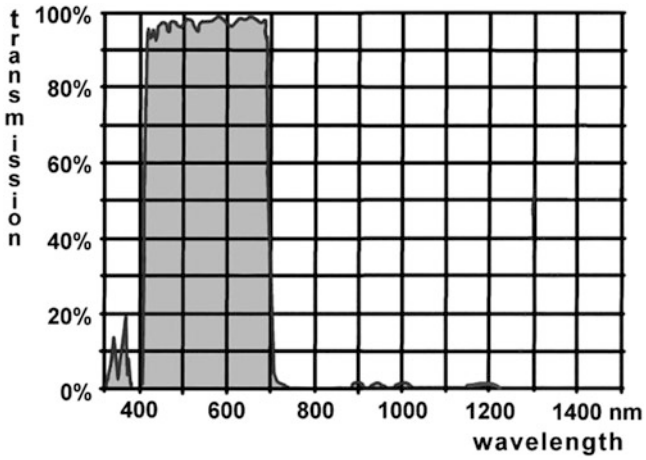

Fig. 6.3 Ideal transmission band of an UV–IR cut filter (modified from Baader)

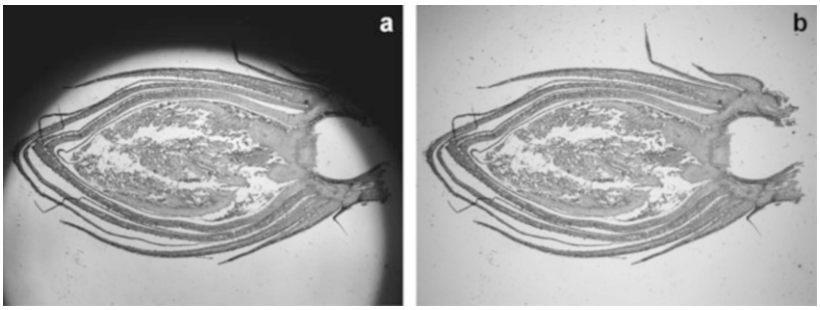

Fig. 6.4 Plant section (*Aesculus hippocastanum*), total length: 1.6 cm, objective 1/0.04, ocular 5×, bright-field, insufficient illumination (**a**), improved homogeneity of field resulting from a piece of paper used as "diffuser" (**b**)

visible light spectra so that protection filters of this sort are no longer necessary.

6.2.2 Diffusers

Such filters constructed as milk glass or frosted glass can be used for improving the homogeneity of field. Instead of a commercial filter, a piece of white paper can successfully be used for this task in many cases, too. An extreme example is given in Fig. 6.4. A plant section, specimen length, 1.6 cm, has been photographed with a standard laboratory microscope by use of a special objective of 1.0× magnification combined with a photo-ocular 5.0×, total magnification: 5×. This great field could not adequately be illuminated in bright-field with the condenser available. Moreover, the optical axis of the condenser deviates from that of the objective and the phototube used. Thus, the field of illumination is not centered so that the specimen can neither be observed nor photographed in a sufficient manner (Fig. 6.4a). Without changing any components a small piece of paper can be put on the light outlet of the microscope stand so that the homogeneity of field is significantly improved (Fig. 6.4b). Persisting slight vignetting at the periphery can be eliminated further with appropriate software for post-processing—as well as "disturbing" dust particles can be removed (Fig. 6.5). Thus, an optimized final image can be prepared "ready for presentation."

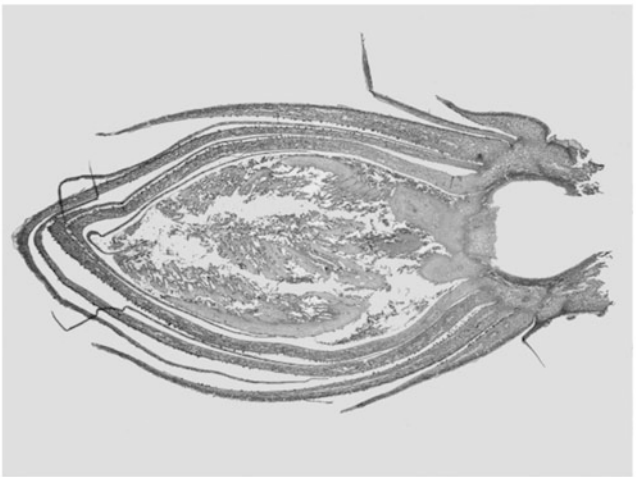

Fig. 6.5 Optimization of Fig. 6.4b by post-processing

The background homogeneity may also be disturbed by the light source used. An example of this problem is shown in Fig. 6.6. The LED presented in Fig. 6.6a consists of nine single LED's (so-called LEDs on board). This LED pattern can be projected near to the specimen plane so that the pattern from Fig. 6.6a appears in the visible field (Fig. 6.6b). Such patterns can be reduced, too, with the help of a diffuser (Fig. 6.6c), especially when the positions of LED and/or collector lens cannot be changed.

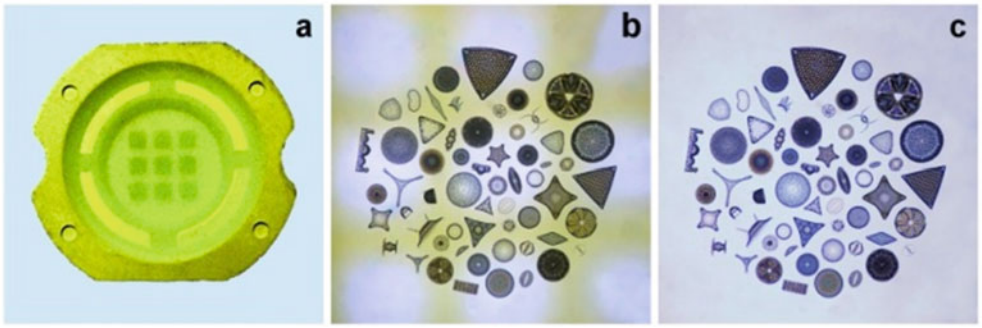

Fig. 6.6 LED (EPISTAR), consisting of nine single LEDs arranged to a 4 × 4 mm square (**a**), disturbing patterns in the visual field (**b**), purification of the background by use of a diffuser (**c**)

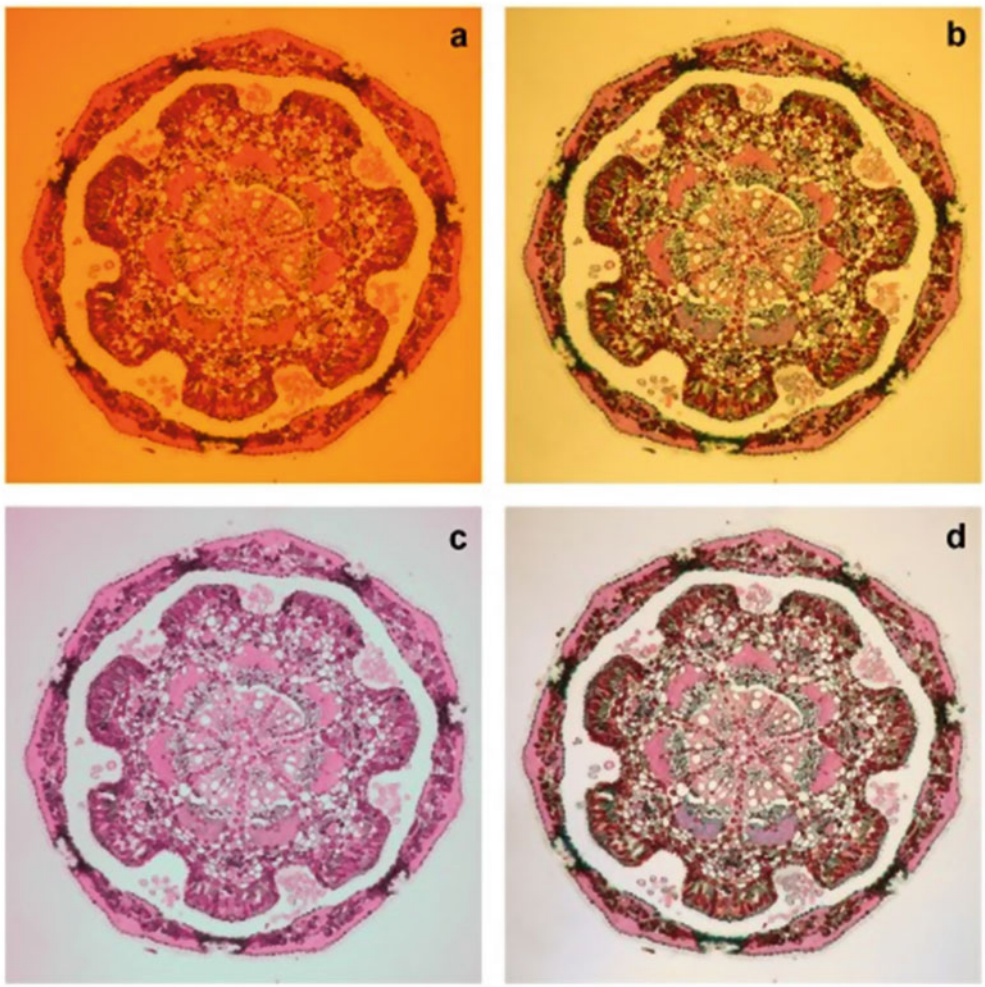

Fig. 6.7 Plant section (*Casuarina equisetifolia*), diameter: 0.5 mm, Wacker staining, bright-field, objective 10/0.30, 50 W halogen light. No filter, voltage: 2 V, exposure: 1/500 s (**a**), double polarizer used as light absorber, voltage: 12 V, exposure: 1/500 s (**b**), restoration of white balance (post-processing) in figure **a** (**c**) and **b** (**d**)

6.2.3 Neutral Gray and Double Polarizing Filters

Neutral light absorbing filters are suitable for reducing the intensity (amplitude) of illuminating light without changing the brightness of the light source used or influencing the colorization. When a (halogen) bulb is used for illumination, the color temperature is low so that the illuminating light will be affected with a red, orange, or yellow taint (Fig. 6.7a). This hue cannot be compensated by post-processing

in a satisfying manner (Fig. 6.7c). On the other hand, such color hue can be mitigated by increasing color temperature when the light source is combined with a gray or double polarizing filter and turned to a higher brightness (Fig. 6.7b). The colorization can be improved further when the white balance is optimized by use of image processing software (Fig. 6.7d). Photomicrographs as shown in Fig. 6.7b–d can only be created, when the effective intensity of light is reduced by the use of neutral light absorbing filters instead of turning the light source to a low intensity. While gray filters absorb light in well-defined proportions, rotatable polarizing filters reduce the effective brightness continuously so that the remaining intensity of light can be regulated in tiniest steps. In microscopes fitted with an LED, however, the color temperature remains constant over the full range of intensity. On the other hand, the lowest intensity of light can still be too high in some circumstances. In this case, the brightness of illuminating light can be reduced further with the help of the neutral filters mentioned.

6.3 Color Modulating Filters

Color modulating filters can be manufactured based on transparent colorized (pigmented) material (glass, acryl, and film), or they can be designed as an interference filter (multilayer systems). In filters of the first sort, wavelengths and colors transmitted remain constant regardless of whether the filter is inclined or the angle of incident light is varied. Interference filters, however, are designed for incoming perpendicular light. Otherwise, the wavelengths transmitted are shortened when the filter is inclined or hit by oblique incoming light, and the breadth of the transmission band (half-intensity width) is reduced, too. Thus, a monochromatic green filter, for instance, can be used as a monochromatic blue filter, when it is turned to an inclined position [3].

With regard to the transmission band, three types of filters can be distinguished: band-pass filters, narrow-band filters, and long-pass filters (Fig. 6.8). Band-pass filters are used for color filtering. They have a wide range of wavelengths representing a defined color. Narrow-band filters are typically used as monochromatic filters transmitting a well-defined wavelength (540 nm, for instance); they are characterized by a very small half-intensity width (circa 8–12 nm in most cases). Long-pass filters are mostly used as emission filters in fluorescence microscopy. They block wavelengths up to a defined limit and transmit all wavelengths beyond this limit; their color is determined by the wavelengths transmitted and the range of wavelengths being blocked.

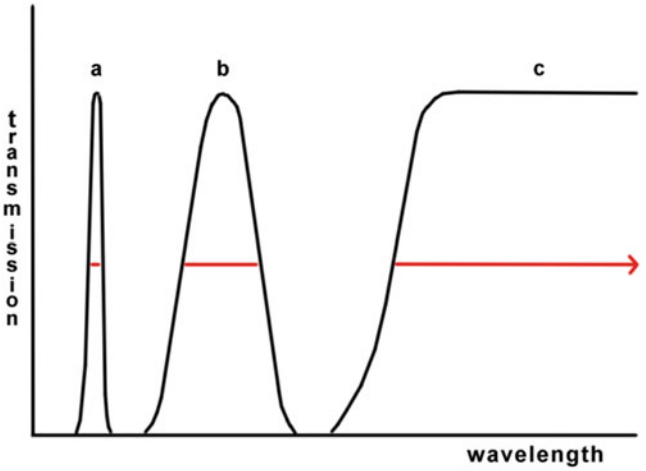

Fig. 6.8 Transmission bands of narrow-band (**a**), band-pass (**b**) and long-pass (**c**) filters

6.3.1 Blue "Daylight" Filters

Blue filters are traditionally used for compensation of red, orange, or yellow hue in halogen or bulb light. Especially in color photomicrography, such filters can contribute to neutral colorization and high differentiation of color tones. CB 12 or CB 16.5 filters are recommended for this task. The color modulating effect achievable can be compared with that of double polarizing filters combined with high energy halogen light (see Fig. 6.7b–d).

6.3.2 Green Filters

Green filters are traditionally used for the optimization of gray tones in black and white photomicrographs. It can be taken into account that the human eye has the highest sensitivity for green light; 50% of the retinal color receptors are detectors for green, and only 25% detect red and blue. Moreover, microscope objectives are traditionally optimized and corrected for green light (reference wavelengths: 546 nm), so that potential aberrations will be minimal when the specimen is illuminated in green. VG 9 is a commonly used glass filter of this sort. Alternatively, monochromatic interference filters can be used for still higher amplification of resolution, sharpness, and contrast, when the brightness of the light is appropriate. Figures 6.9 and 6.10 give examples of black and white imaging based on unfiltered white light versus monochromatic light.

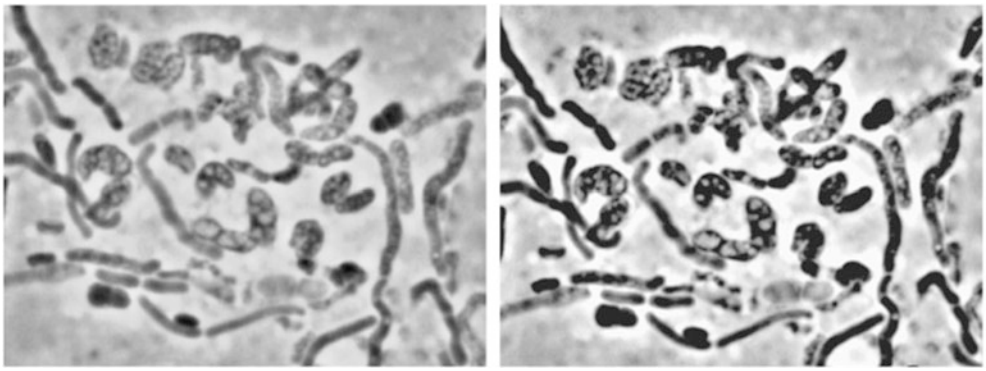

Fig. 6.9 *Bacillus megatherium*, fixation: osmium tetroxide, phase contrast, HFW: 20 µm, objective Oil 100/1.32, ocular: 12.5×, phase contrast, halogen light, no filter (left), monochromatic green light, 540 nm (right)

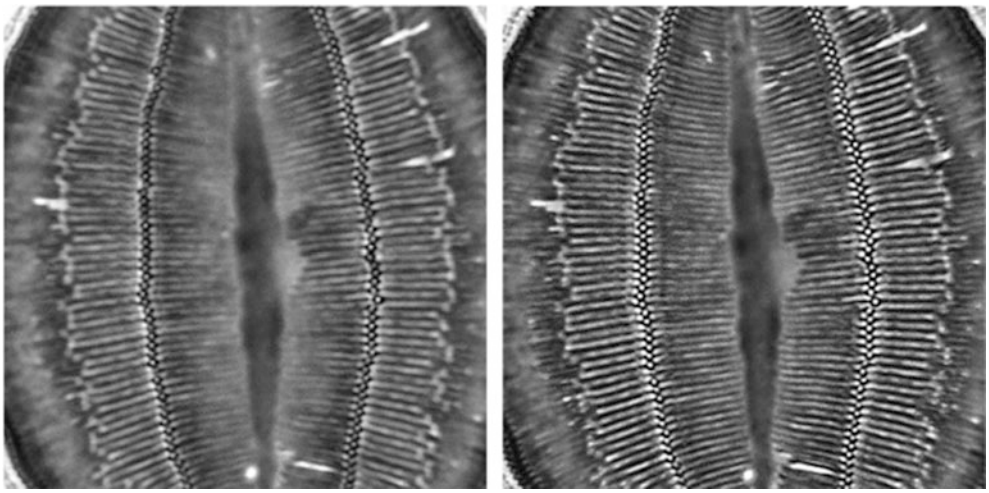

Fig. 6.10 Low density diatom (*Cocconeis* sp.), phase contrast, HFW: 35 µm, objective 40/0.65, ocular 12.5×, extreme post-magnification, halogen light, no filter (left), monochromatic green-blue filter, 500 nm (right)

6.3.3 Warming Filters for Blue LEDs

In most microscopes fitted with an LED, the illuminating light tends to a slight bluish taint caused by a high color temperature so that red tones may be converted to violet. This dominance of blue can be compensated with so-called warming filters which mostly are colorized in orange tones. B1A, 81D, 81 EF, and 85B filters, for instance, can be used as a set leading to successive reductions of the effective color temperature. When a filter set for polarized light microscopy is available consisting of polarizer, analyzer, and lambda compensator, the blue component in LED light can also be mitigated by turning the compensator to red. Examples of practical use are demonstrated in Fig. 6.11. A normal white piece of paper can also be used as the simplest and cheapest solution for the reduction of blue hue in LED light when inserted into the light path (Fig. 6.12).

6.3.4 "Vario-Color" and "Pol-Color" Polarizing Filters

For color photography in general, sophisticated polarizing filters have been developed called "vario-color" or "pol-color" filters. These filters are based on "pleochroism" or "dichroism;" they consist of two separate filters joined to a couple. The terms "pleochroism" and "dichroism" denote variations of color visible in some transparent colored anisotropic material when polarized white light is transmitted. In such material, the incoming polarized white light is divided into two light beams of different wavelengths, the primary and secondary beam, each polarized in different directions or planes. Both polarization planes differ by 90°. In some cases one of these light beams may be white, the other colorized in red, green, blue, yellow, or orange (white-color pleochroism). In other materials, both secondary light beams are colorized in different colors, such as red and blue,

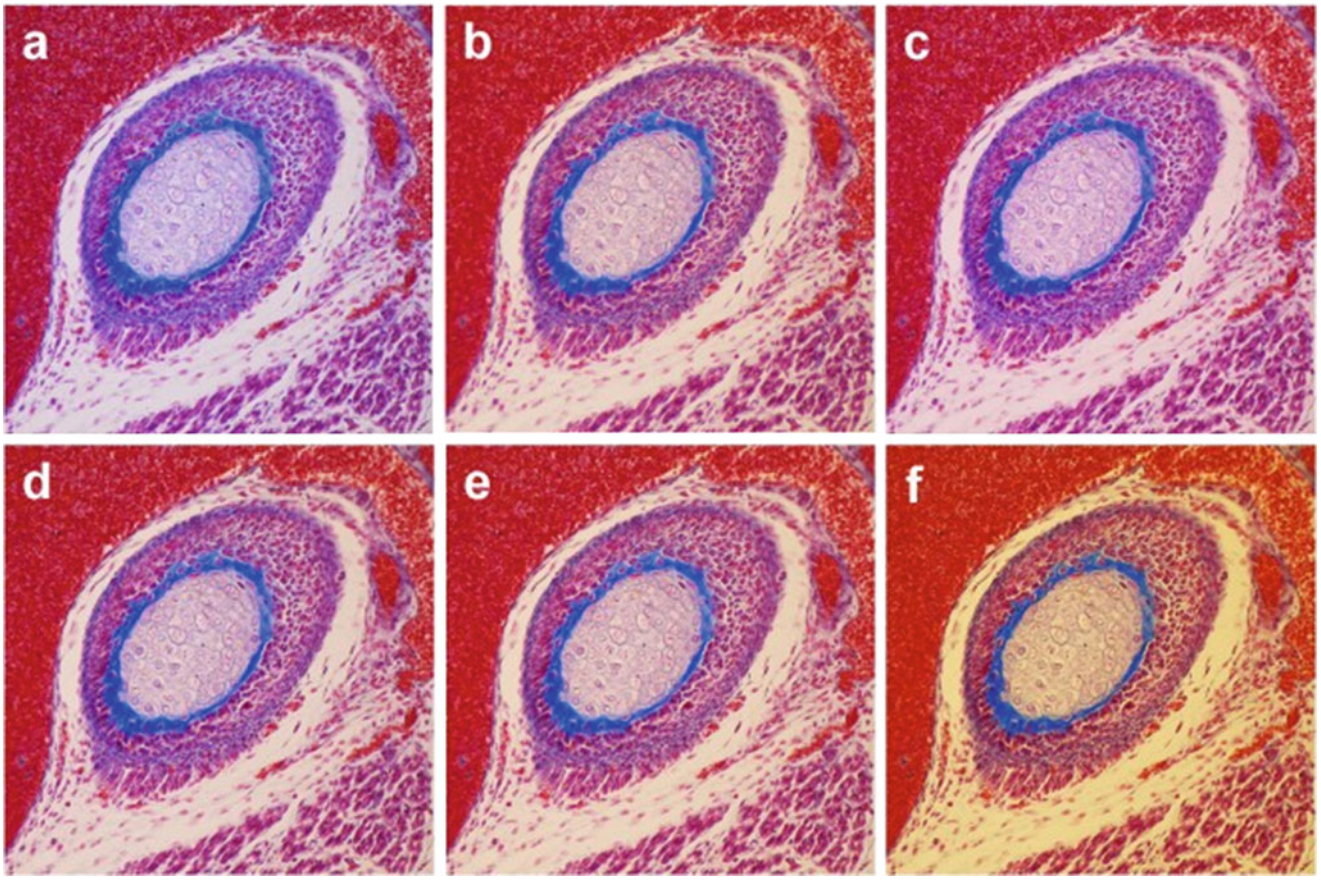

Fig. 6.11 Embryonic tissues, HFW: 0.45 mm, objective 16/0.40, bright-field, LED 6000 K, no filter (**a**), polarized light, lambda compensator (**b**), warming filters 81A (**c**), 81D (**d**), 81EF (**e**), 85B (**f**)

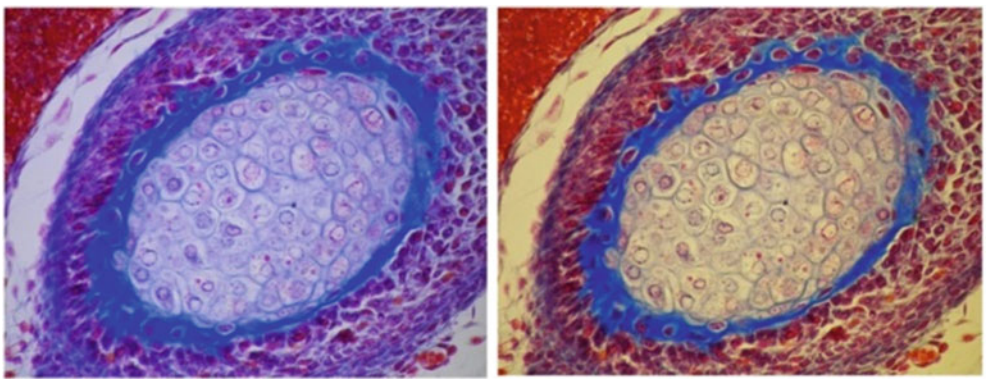

Fig. 6.12 Preparation from Fig. 6.11, HFW: 0.20 mm, objective 25/0.50, bright-field, LED 6000 K, no filter (left), insertion of a white piece of paper (right)

red and green, yellow and blue, yellow and green, or yellow and red (dichroism).

So-called pol-color filters are based on white-color pleochroism, "vario-color" filters on dichroism. A polarizer is mounted at the bottom and covered by a separate filter consisting of anisotropic material showing pleo- or dichroism. In this way, the illuminating light beams coming from the respective filter consist of two components of different color each polarized in different planes. In the case of white-color pleochroism, one of these beams is white, the other colorized in a well-defined color and in the case of dichroism both light components are differently colorized (red and blue, for instance, Fig. 6.13). A second rotatable polarizer has to be mounted above the "pol-color" or "vario-color" filter used. By turning this rotatable polarizer variable transitions and intensities of colors can be achieved. In "pol-

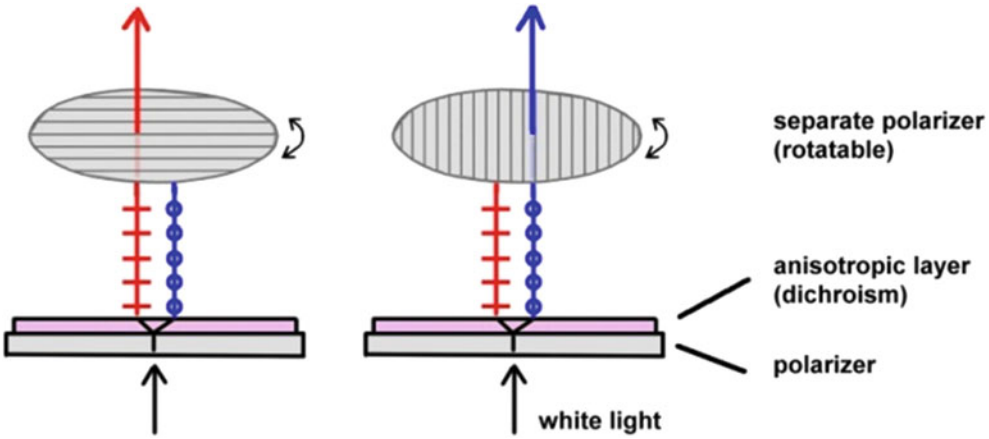

Fig. 6.13 Principle of a "vario-color" red–blue filter used for light filtering in microscopy

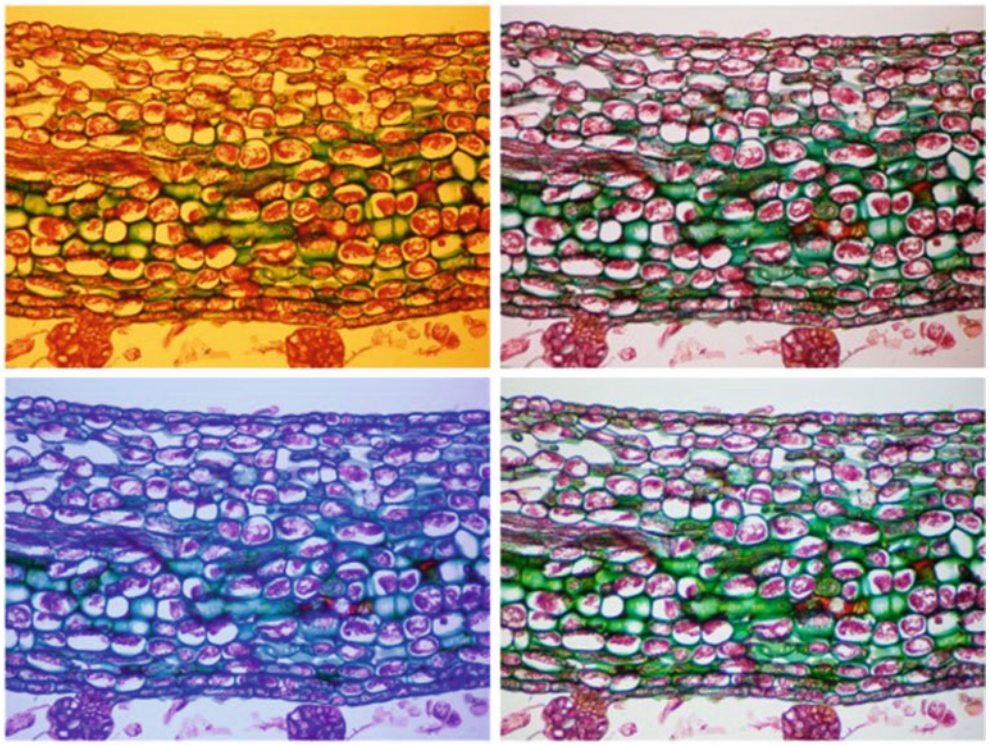

Fig. 6.14 Plant section (*Aesculus hippocastanum*), HFW: 0.45 mm, objective 16/0.40, bright-field, use of a "vario-color" red–blue filter for mitigation of color hue in halogen light (top) and LED light (bottom)

color" filters, the illuminating light can be filtered in white, or a defined color is added in variable intensity. When a dichroic "vario-color" filter is used, the color of the illuminating light can be switched from one color to the other, and well-balanced neutral or white light filtering can be achieved when the rotatable polarizer is turned into an intermediate position (ca. 45°) so that both light beams, the primary and the secondary beam, contribute to the illuminating light at nearly equal proportions. With the help of such filters, any hue of illuminating light can be eliminated—in bulb and halogen light as well as in LED light. Vario-color red-blue filters are predestined for color neutralization in each sort of light source. Blue pol-color filters are well suited for halogen and bulb light, and red or orange pol-color filters can be successfully used for elimination of blue hue in LED light. In polarized light microscopy and interference contrast, additional color effects can be achieved when such filters are inserted into the illuminating light path. Figure 6.14 demonstrates some color modulations carried out with a red–blue "vario-color" filter in order to mitigate color taint

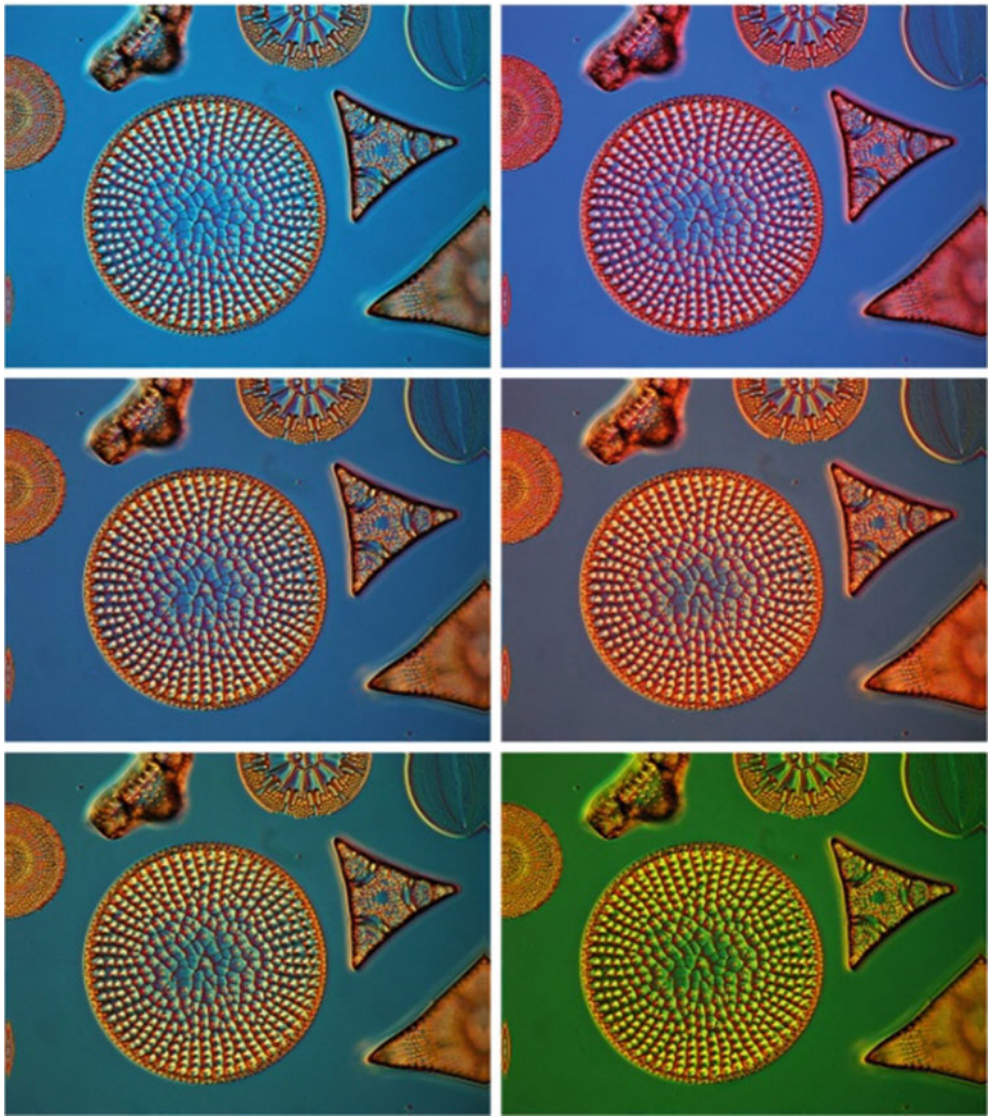

Fig. 6.15 Diatoms, arranged slide (*Coscinodiscus* sp., *Triceratium* sp.), differential interference contrast (DIC), HFW: 0.24 mm, examples of multicolor light filtering carried out with several "vario-color" and "pol-color" filters

in a bulb and LED light. Figure 6.15 gives some examples of multicolor light filtering in interference contrast. Variable color contrast effects achievable with polarized light are demonstrated in Fig. 6.16. In Fig. 6.16b–d, the standard polarizer was replaced by the respective "vario-color" or "pol-color" filter.

Moreover, "vario-color" filters can be used for alternating colorization in multimodal illumination techniques which are based on two or more different components of light. The principles of such variable color filtering are demonstrated for variable phase-bright-field contrast (see Sect. 5.4.12). When both condenser light outlets needed for phase contrast and (axial) bright-field are fitted with crossed polarizers, variable colorizations of both partial images can be achieved with the help, e.g., of a "vario-color" red-blue-filter (Fig. 6.17). When the "vario-color" filter is turned to 0°, the phase contrast image is colorized in blue, and the bright-field image filtered in red. These colorizations can be inverted by turning the filter to the 90° position. Alternatively, only one of the light outlets can be fitted with a polarizer, whereas the other outlet remains free. In this case, one of the contributing partial images is permanently filtered in the genuine color of the vario-color filter, and the other partial image can be variably colorized. In the example shown in Fig. 6.18, only the annular light outlet needed for phase contrast is fitted with a polarizer so that the phase contrast image can be colorized in blue, red, or intermediate tones. The bright-field light, however, is constantly colorized in magenta, i.e., the

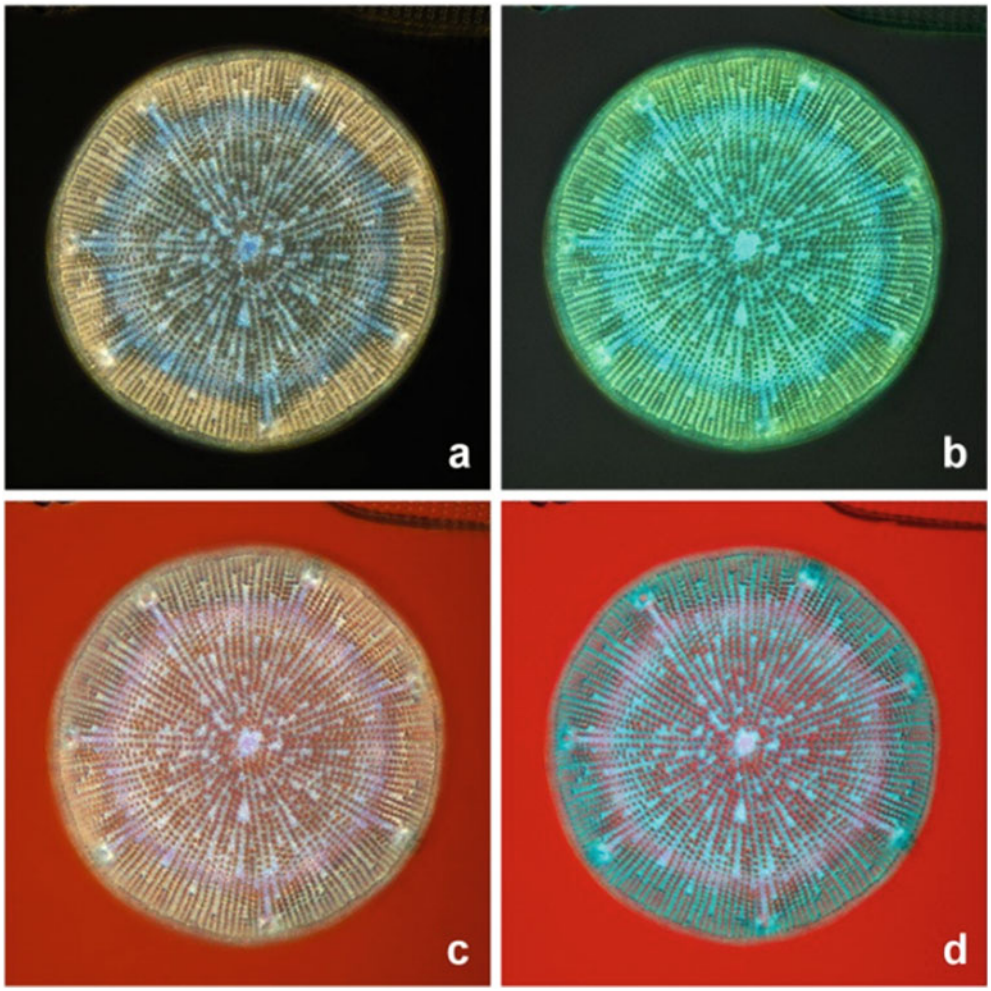

Fig. 6.16 Birefringent diatom shell (*Aulacodiscus* sp.), diameter: 0.11 mm, polarized light, standard polarizer and analyzer in crossed position (**a**), "vario-color" green-blue filter plus quarter lambda compensator (**b**), red "pol-color" filter plus quarter lambda compensator (**c**), "Cromo-Blend" red-blue filter plus lambda and quarter lambda compensators (**d**)

genuine color of the red-blue "vario-color" filter used (red + blue = magenta).

"Vario-color" and "pol-color" filters have been manufactured by Hoya and Cokin, Vivitar (named "Cromo-Blend" filters), Pentax (named "Fantastic filters"), Marumi, and Optex. At the present, three variant filters of this sort are still produced by Singh-Ray (LB Gold-N-Blue Polarizer [similar to "vario-color red-blue"], LB Color Combo filter [similar to "vario-color red-green"], LB Warming Polarizer [similar to "pol-color red" or "pol-color orange"]). The other filters previously produced may be obtained from second-hand dealers.

6.3.5 Monochromatic Interference Filters

Monochromatic light can be used for optimization of lateral resolution and distinctness, especially when medium or short wavelengths are transmitted corresponding with green or blue. Chromatic aberration is absolutely eliminated in monochromatic illumination, the coherency of light is enhanced and the resolution is maximized, especially by short wavelength light. Moreover, monochrome structures can be revealed in the highest contrast and clarity when the illuminating monochromatic light is filtered in an aberrant (complementary) color. Beside special monochromatic filters designed for light microscopy, astronomy interference filters can be used as well [4]. These narrow-band filters are associated with well-defined wavelengths: H-beta (blue, $\lambda = 480$ nm), O-III (blue-green, $\lambda = 500$ nm), Solar continuum (green, $\lambda = 540$ nm), H-alpha (red, $\lambda = 656$ nm), and S-II (red, $\lambda = 670$ nm). Figure 6.19 shows a typical transmission band of a monochromatic green filter ($\lambda = 540$ nm). Positive effects of monochromatic light filtering concerning improvements of lateral resolution, contrast, and distinctness are demonstrated in Fig. 6.20. When a nonmotile speci-

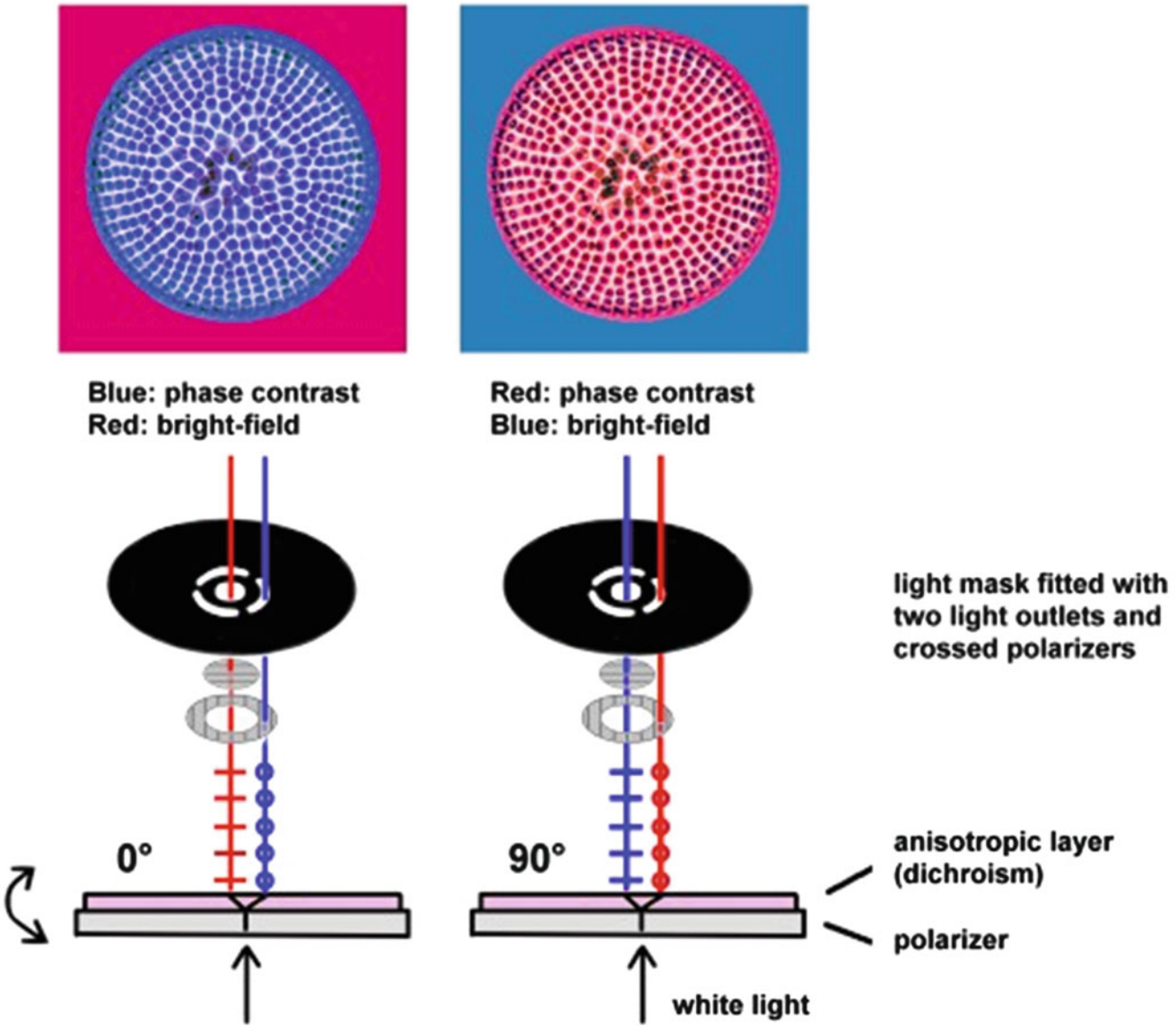

Fig. 6.17 Alternating colorization of phase contrast and bright-field in variable phase-bright-field contrast (VPBC) by use of a "vario-color" red-blue filter interacting with crossed polarizers situated at the condenser's light outlets for phase contrast and axial bright-field

men is successively photographed and filtered at different monochrome colors, additional multicolor contrast can be achieved when the images are superimposed to a composite image [5]. In this way, "colorized phase contrast" can be generated showing fine details in superior clarity as any chromatic aberration is eliminated (Fig. 6.21). Even in bright-field images some details can be accentuated further, when bi- or multicolor sandwiches are created (Fig. 6.22). Monochrome or monochromatic filters can also be used for selective contrast enhancement of definite colors. Some colors appear in higher contrast when illuminated with appropriate monochrome light, whereas other colors may be lost or barely visible (Fig. 6.23). Thus, for instance, green and blue structures can be selectively highlighted (together with black, gray, and brown) when illuminated in red, whereas other structures colored in red, orange, yellow, or violet will be invisible in the same illuminating light.

6.3.6 RGB Filter Sets (Three-Shot Techniques)

RGB filter sets consist of three single band-pass or narrow-band filters colored in red, green, and blue (Fig. 6.24). Alternatively, also narrow-band filters can be used. When digital photographs are taken based on the RGB color gamut, three single shots can be made filtered in red, green, and blue. Each photograph can be separately focused so that a defined detail can appear in maximized distinctness regardless of

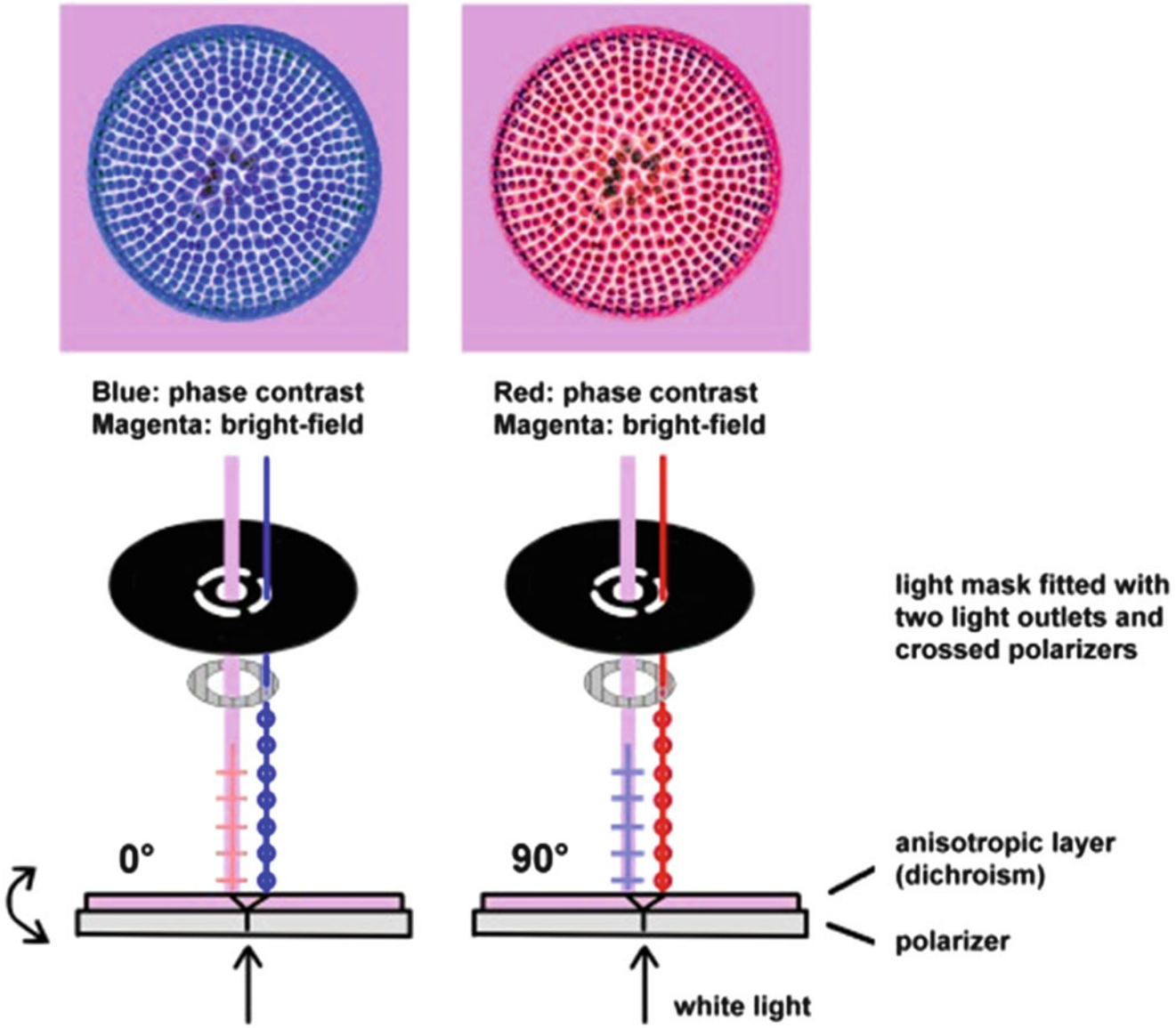

Fig. 6.18 Alternating colorization of phase contrast in variable phase-bright-field contrast (VPBC) by use of a "vario-color" red-blue filter interacting with a single annular polarizer situated at the condenser's light outlet for phase contrast. The bright-field image is colorized in magenta

whether it is colored in red, green, or blue. These three monochrome single images are superimposed to a true color sandwich. In this way, any artifacts caused by chromatic aberration can be avoided [6]. Photomicrographs based on this so-called three-shot technique will show apochromatic quality even when they are taken with a simple achromatic lens. Of course, this technique can only be carried out with nonmotile specimens.

The photomicrographs are shown for example in Fig. 6.25 are taken with an achromatic 20-fold lens calculated for a long working distance and fitted with an iris diaphragm. Such constructions are optical "compromises" so that the optical correction and thus the image quality is somewhat lower than in standard lenses of the same magnification. When the specimen is illuminated in red or blue, the focus plane at the camera sensor differs by 8 μm in the arrangement described (chromatic aberration). Three single images, each separately focused, taken in monochromatic red, green, and blue light are presented in Fig. 6.25a–c. By digital superimposition of these three monochromatic images a high-resolution true color image can be achieved (Fig. 6.25d). The quality of a corresponding image taken with unfiltered halogen light (Fig. 6.25e) is of significantly lower quality as well as a white balanced image derived (Fig. 6.25f).

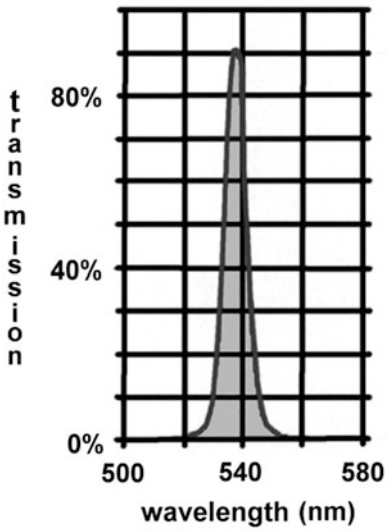

Fig. 6.19 Typical transmission of a monochromatic green filter, $\lambda = 540$ nm (modified from Baader)

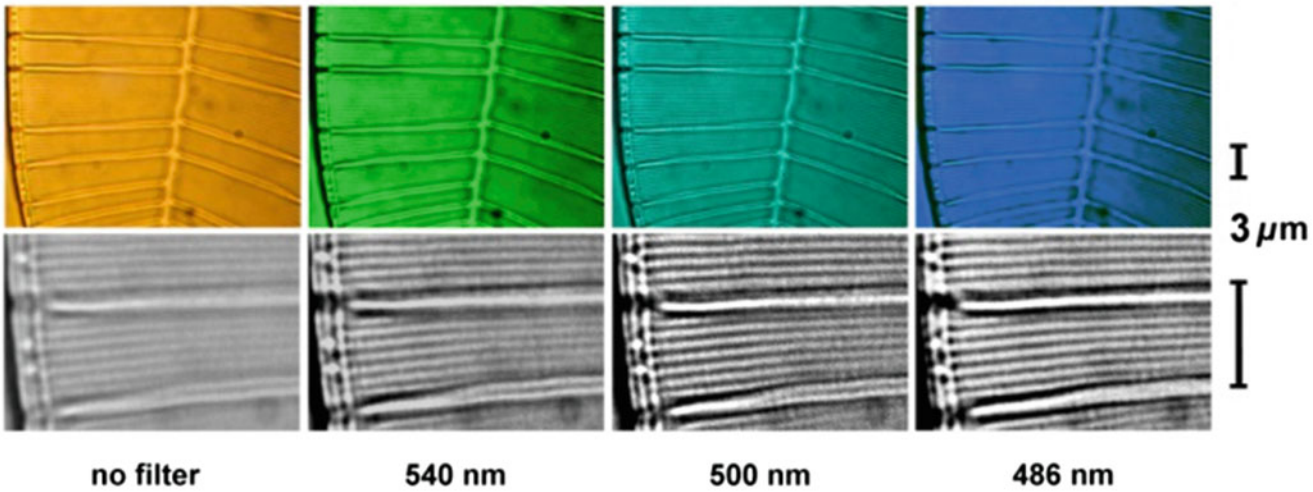

Fig. 6.20 *Surirella gemma*, objective Oil 160/1.4, bright-field, line spacing: 0.33 µm, comparison of unfiltered halogen light and monochromatic light filtering at different wave lengths

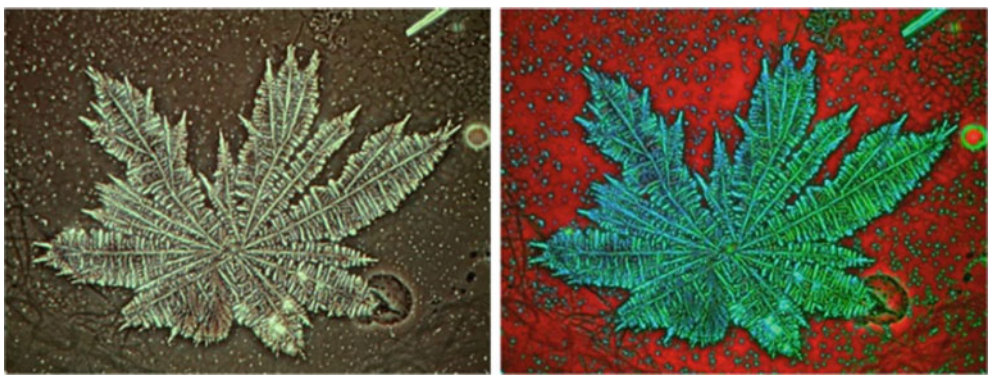

Fig. 6.21 Thin layer crystallization, objective 40/0.65, phase contrast, HFW: 0.25 mm, standard view (left), multicolor sandwich (right) based digital superimposition of three single images taken with monochromatic red, green, and blue light

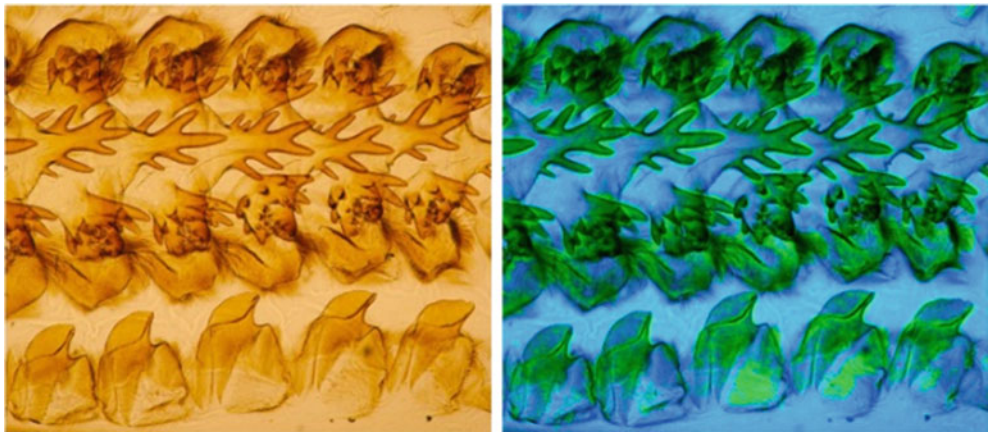

Fig. 6.22 Stomach of a cricket, bright-field, HFW: 1 mm, objective 10/0.30, standard view in unfiltered halogen light (left), bicolor sandwich based on two single images superimposed, taken with monochromatic blue and green light

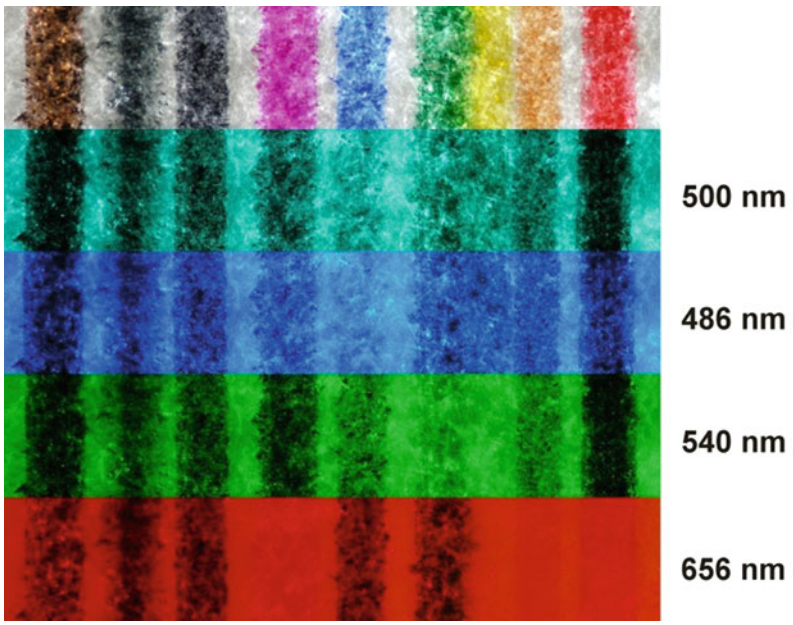

Fig. 6.23 Multicolor stripes taken in white and monochromatic light (blue-green, blue, green, and red), bright-field, objective 2.5/0.08, HFW: 6 mm

6.3.7 RGB-Intensifying Filters

RGB intensifiers are special interference filters which can be passed by red, green, and blue light, whereas the amplitudes of other colors or wavelengths are strongly reduced or blocked. Thus, RGB colors appear "purified," and images show a high grade of differentiation and clarity—in visual observations as well as in color photomicrographs. Artifacts caused by chromatic aberration are mitigated or eliminated. Flashlight filtered with RGB intensifiers is purified from any bluish hue, and achromatic lenses can be "tuned" to an apochromatic appearance [4]. Figures 6.26 and 6.27 show the transmission bands of two RGB intensifiers well suited for microscopic observations and color photomicrography. Figure 6.28 gives an example of practical use.

6.4 LED Versus Halogen (Bulb) Light

Various LED kits for light microscopy are offered by several manufacturers characterized by different designs, emission spectra, and color temperatures. For standard applications such as bright- and dark-field, phase and interference contrast LEDs are mostly offered and preferably used with a color temperature of 6000 K. Such color temperature is commonly regarded as equivalent with daylight and associated with "neutral" colors.

Nevertheless, LEDs of this sort are often affected with a typical bluish taint as described above. This problem is apparent even today, although a high variety of differently designed 6000 K LEDs are available. Thus, colors may not only appear somewhat "cool" but also somewhat faint.

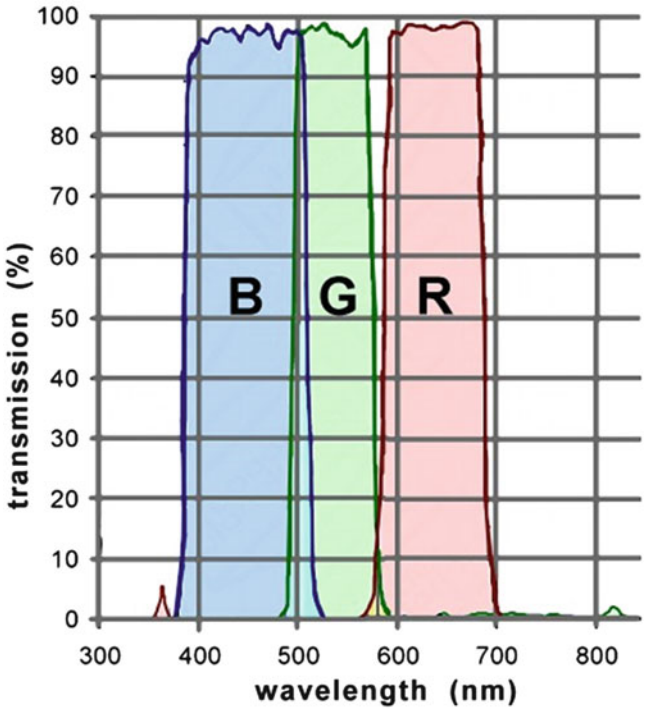

Fig. 6.24 Transmission band of a RGB filter set consisting of three band-pass filters in red, green, and blue (modified from Baader)

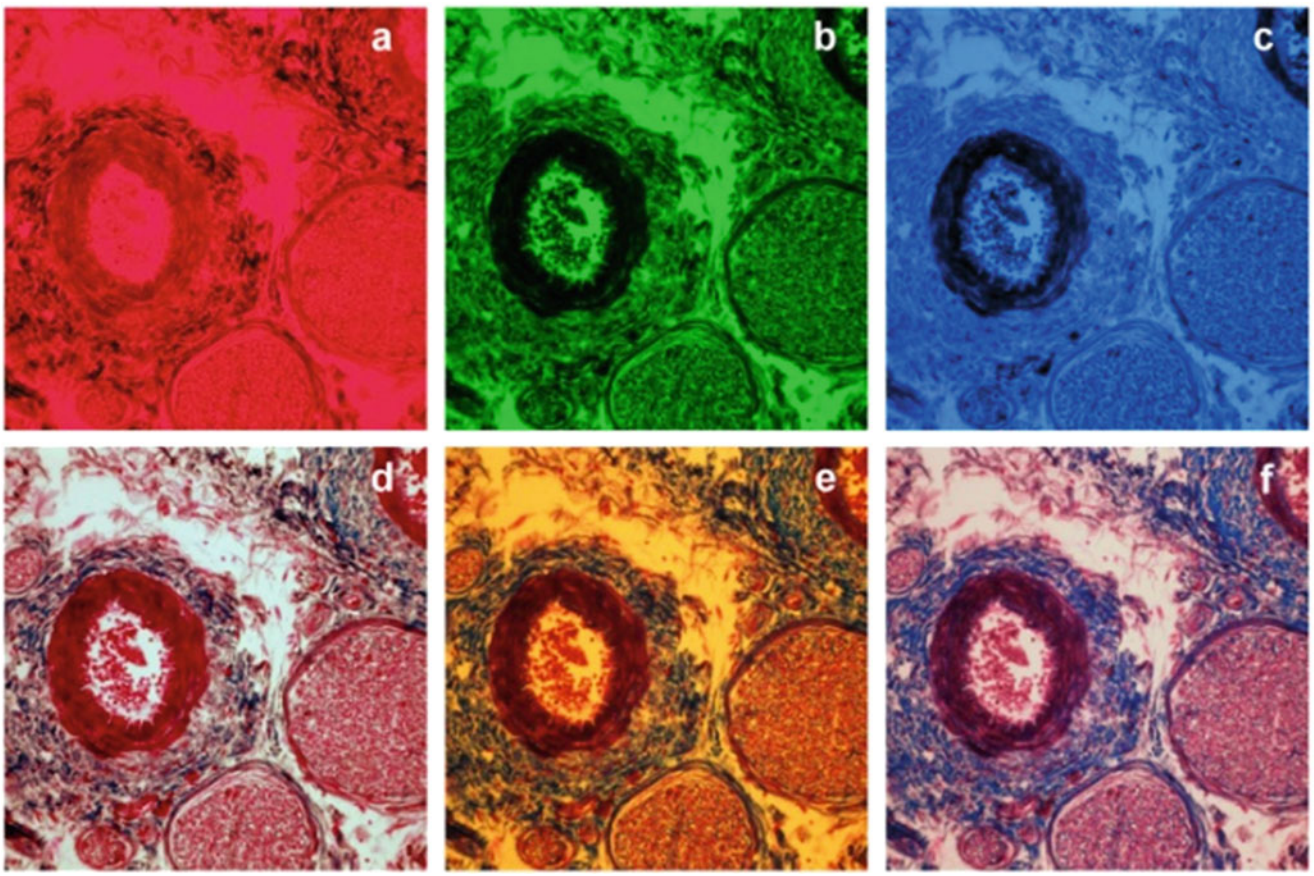

Fig. 6.25 Embryonic tissue, HFW: 0.35 mm, bright-field, objective L 20/0.32, monochromatic images taken in red, green, and blue (**a**–**c**), true color "three-shot" image based on superimposition of images **a**–**c** (**d**), unfiltered version taken in halogen light (**e**), digital restoration of white balance in image **e** (**f**)

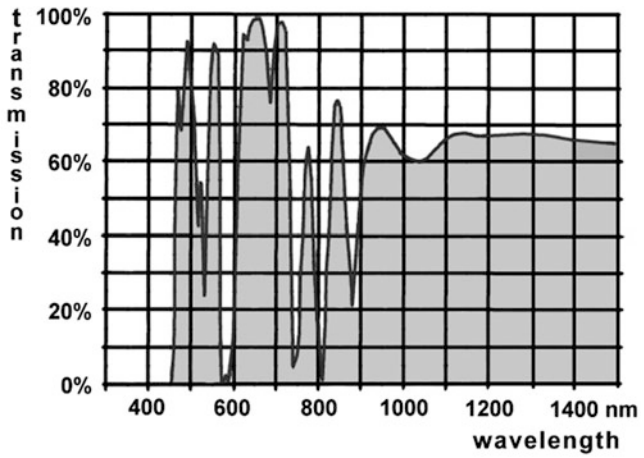

Fig. 6.26 Transmission band of the Baader contrast booster filter (RGB intensifier used for neutralization of flash light, modified from Baader)

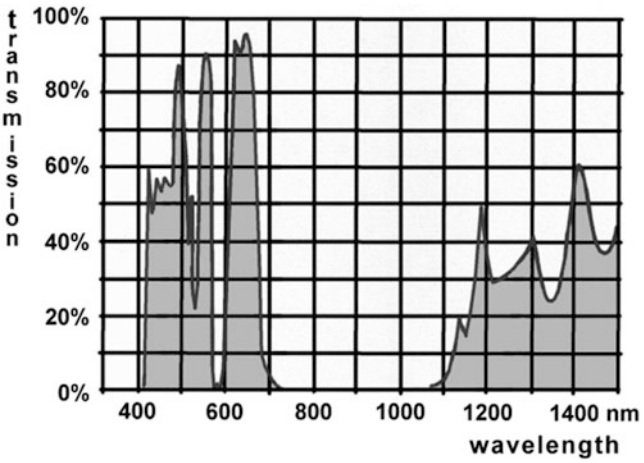

Fig. 6.27 Transmission band of the Baader semi APO filter (RGB intensifier used for "tuning" of achromatic lenses, modified from Baader)

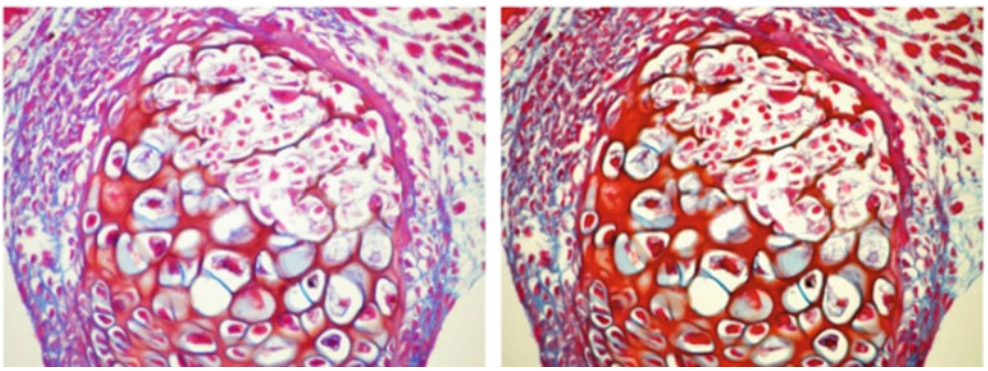

Fig. 6.28 Embryonic cartilage, HFW: 0.15 mm, bright-field, objective 40/0.65, flash light, unfiltered (left), filtered with the Baader contrast booster filter from Fig. 6.26 (right)

Details colored in blue can appear somewhat "overmodulated" and red structures may be converted to blue–violet tones. Other LED designed for a lower color temperature, 5000 or 4500 K, for instance, is often affected with a slight green taint. All in all, the character of colors will be strongly different in the same preparation when an LED is used as a light source instead of a "traditional" halogen bulb. Thus, color filtering can be strongly recommended for many tasks, not only for halogen but also for LED light.

Additional problems can occur in photomicrography, especially when standard cameras are used, because, until now, there are none of the LEDs that have a continuous light spectrum comparable with daylight or bulb light. In standard digital cameras, however, displays and sensors are designed for continuous light spectra; their white balance

can normally be adjusted to daylight or bulb light, but appropriate algorithms are often missing which could be used for adapting the white balance to LED light. Thus, the hue of colors can strongly deviate from the visual perception, when LEDs are used in photomicrography so that colors seen through the eyepieces are different from their corresponding pendants seen on a display and screen or detected by the camera sensor. Also for this reason, adequate consideration must be given to appropriate light filtering. Moreover, the typical color aspect of halogen illumination, many examiners are familiar with, is lost. Thus, in histopathology and histochemistry, for instance, users must "learn" the interpretation of staining, when halogen light is replaced by LED light. For this reason, most anatomists and histopathologists prefer halogen light even today. And in the case that only LED light is available, it may be interesting and useful to adapt the respective LED light to the "traditional" character of halogen light.

On the other hand, LEDs are associated with some advantages: very long lifetime, constant color temperature over the full range of intensity, low heat (when compared with a bulb of the same intensity), highest grade of intensity and loss of UV and/or IR on demand. Moreover, discontinuous light spectra of LEDs can be adapted to the RGB color space so that any chromatic aberration may be lower than using a halogen or bulb lamp. This "light purifying" effect can be compared with that of an RGB-intensifying interference filter used for halogen illumination. In fluorescence microscopy, special monochrome or monochromatic LEDs can be used for excitation so that excitation filters will no longer be needed. This aspect can be regarded as a specific additional advantage of LED techniques, too.

All in all, at present it may be determined by the individual preferences of the user and the particular task whether halogen or LED light is preferred. With regard to further developments, it may be expected that new generations of LEDs will be designed leading to continuous light spectra emitted in a manner comparable with traditional bulb, halogen, or flashlight. The first prototypes of such LEDs have recently been presented by Olympus.

Despite the problems discussed, LED light may be regarded as adequate in most applications of routine, when diatom frustules or native unstained cells have to be examined. Specimens of this sort are free from natural colorization so that color trueness may be of lower importance, and some potential hue will not degrade the visual information in structural images taken from such specimens.

6.5 Conclusions

Various sorts of light filters are described which can be used in light microscopy and photomicrography. Neutral (colorless) filters can be used for modulation of brightness (gray filters or double polarizing filters), improvement of homogeneity (diffusers) and eye protection (UV–IR cutters). Color modulating filters are well suited for elimination of color taint, improvement of contrast, resolution, distinctness, and differentiation of colors, and for mitigation of chromatic aberration. Moreover, multicolor contrast can be achieved with appropriate filters, especially in interference contrast and polarized light microscopy. The filters described are useful for modulating bulb (halogen) and LED light. Advantages and disadvantages of these different light sources are finally discussed. In the field of diatom research LED light might be the preferable solution. In white or bluish LED light, fine details in diatom frustules may be perceived with a higher resolution and clarity, because red tones (i.e., long wavelength light components) are reduced or missing. Ultraviolet and infrared components which may lead to degradations of image quality, too, are absent in LED light. Moreover, LED light will be the more economical source, because a lower wattage is needed for achievement of sufficient brightness and the "life span" of this light source will be longer than in bulb light.

Acknowledgments The author thanks Mr. Thomas Baader, Mammendorf, Germany, for the astronomy filters and transmission graphs mentioned and Mr. Timm Piper for critical revision of the manuscript.

References

1. Puchner, R.: Light and Colors (in German), Online Tutorial. http://bit.ly/2X6l5OS (2012)
2. Sommers, H.J., Motzko, M., Oberhage, R.: Light and Colors, Online Tutorial. http://bit.ly/2wNpGXF (2007)
3. Piper, J.: Transmission shift in fluorescence microscopy—adjustable interference filters, theoretical considerations and practical implications. J. Adv. Microsc. Res. **6**, 241–254 (2011)
4. Piper, J.: Use of astronomy filters in light microscopy and photomicrography. Microsc. Today. **15**, 30–35 (2007)
5. Piper, J.: Multicolor contrast effects by monochromatic astro filters—utilization in light microscopy and photomicrography. Microsc. Today. **16**, 20–26 (2008)
6. Piper, J.: RGB-splitting and multi-shot techniques in digital photomicrography—utilization of astronomic RGB-filters in true color imaging. Microsc. Today. **17**, 48–51 (2009)

Automatization Techniques. Slide Scanning

7

Carlos Sánchez, Jesús Ruiz-Santaquiteria Alegre, José Luis Espinosa Aranda, and Jesús Salido

Abstract

This chapter is focused on automatic microscopy techniques. It covers a practical approach to different possible automation in microscopes. All the techniques presented in this chapter aim at capturing images with the best quality as well as do it automatically. The main section (Sect. 7.5) of the chapter focuses on slide scanning and it covers all the techniques necessary to do it such as stage motorization, automatic slide scanning approaches, and autofocus of the samples. The rest of the chapter is devoted to illumination control, and its implementation (Sect. 7.3); image calibration using basic tools (Sect. 7.4) and finally preprocessing techniques to improve image quality reducing the noise introduced by the camera or the illumination defects (Sect. 7.6). In addition to the theoretical explanation, the sections include implementation examples for clarification purposes.

7.1 Introduction

The conventional approach in the taxonomic identification of diatoms has usually consisted in its analysis and quantification by optical microscopy. Nevertheless, there is a need to apply automated recognition techniques to obtain diagnostic tools (environmental monitoring networks, early warning systems) suitable to facilitate the management of water resources and decision-making processes. However, manual image analysis of such systems is impractical due to the enormous diversity of this group of microalgae and its great morphological plasticity. These algae are very useful in monitoring quality of water, hence the importance that automation of the analysis processes entails. New image analysis systems offer a potentially advantageous solution compared to manual counting and identification methods. In addition, there is a need to implement robust and flexible software tools for the classification of diatomaceous images, which allow post-processing of data for environmental assessment and other applications.

C. Sánchez (✉)
Instituto de Óptica Daza de Valdés - CSIC, Madrid, Spain
e-mail: c.sanchez@csic.es

J. Ruiz-Santaquiteria Alegre · J. L. Espinosa Aranda · J. Salido
VISILAB - UCLM, Ciudad Real, Spain
e-mail: Jesus.Ralegre@uclm.es; JoseL.Espinosa@uclm.es; Jesus.Salido@uclm.es

7.2 Materials and Methods

For automatic identification and diatom counting, it is necessary to obtain suspensions of frustules (the silica cover) free of organic matter. The shape and ornamentation of frustules constitutes the basis of the taxonomy of these algae. To capture the images the following materials have been used:

- Brunel SP30 monocular transmission microscope, used to provide a white LED illumination ($\lambda = 443$ nm).
- Brunel DIN standard lens parfocal 60× (0.85 NA) as part of the microscope optical system to visualize the specimens.
- Arduino MEGA 2560 board with RAMPS 1.4 shield to control the motors.
- Three NEMA 14HR08-0645 stepper motors to motorize the XYZ axes. The adaptation of the XY motors to the stage was made by means of a set of pulleys and belts attached to the microscope using a 3D printed support structure. The Z axis was joined to the motor using a 4–5 mm flexible coupler.
- NEMA 17H19-2004S1 stepper motor coupled to the turret of the objectives through a 3D printed adapter to motorize the change of objectives.
- For the support of the XY motors, a rectangular piece of PLA (polylactic acid biodegradable filament), a

G. Cristóbal et al. (eds.), *Modern Trends in Diatom Identification*, Developments in Applied Phycology 10,
https://doi.org/10.1007/978-3-030-39212-3_7

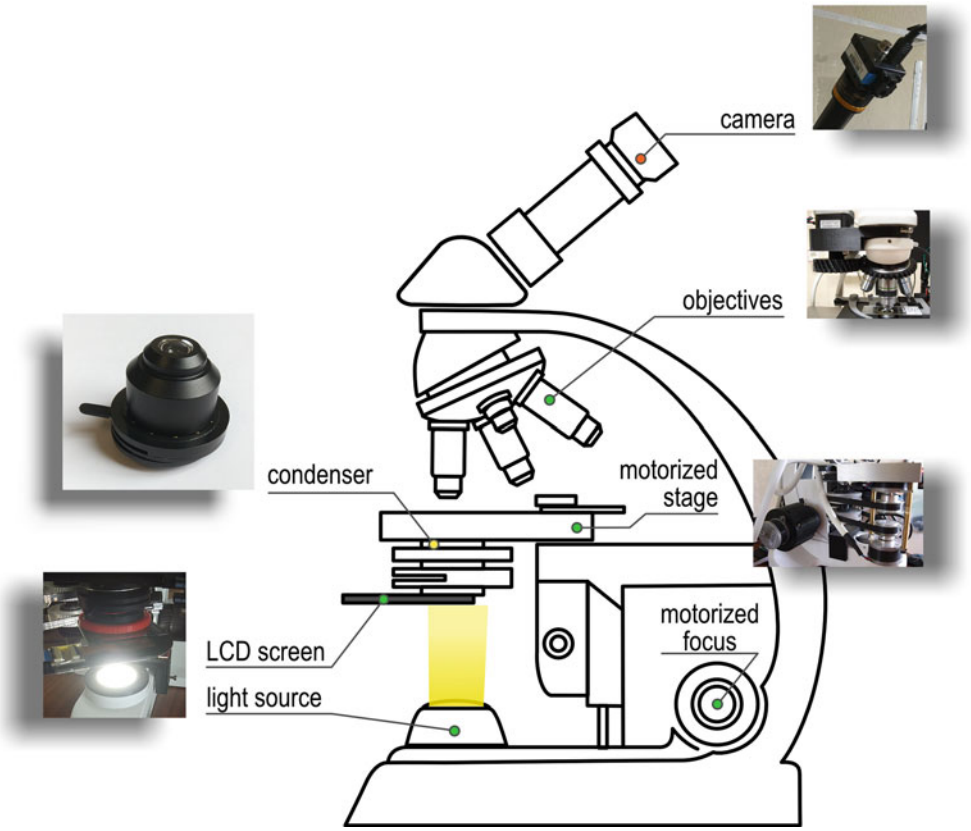

Fig. 7.1 Scheme of the low-cost microscope motorized system

biodegradable thermoplastic polymer, was 3D printed and fixed to the stage.
- LCD screen obtained from a LED projector (Generic Model UB28+) to control the illumination. It has a resolution of 320 × 240 pixels and it is placed in the back focal plane of the condenser. The LCD screen can be easily controlled with the HDMI board of the video projector.
- Raspberry Pi Zero single-board computer to control the LCD.
- Imaging Source (5 MP) DMK72 camera to capture images.

As an alternative to the LCD system, a 3D printed opaque filter with different shapes (e.g., notch, circular ring, etc.) wheel can be used. It can be moved with a servo-motor allowing to change between brightfield, darkfield, and other illumination modes. Figure 7.1 shows a scheme of the low-cost microscope motorized system.

7.2.1 Optical and Mechanical Performance

The point spread function (PSF) is a powerful tool to determine the spatial resolution of an imaging system. The PSF can be defined as the impulse response of an optical system to a point source and it can be measured using fluorescent microbeads in fluorescence microscopy. However, in brightfield microscopy due to the low contrast of the microbeads and the low signal-to-noise ratio due to working conditions close to the resolution limit, they make it difficult its measurement. For such reasons, Smith et al. [28] proposed an alternative procedure to determine the PSF. This method uses the edge response or its derivative, the line spread function (LSF), for the extraction of a parameter related to spatial resolution. It is common to consider the LSF as a good substitute of the PSF in many imaging system since it can be a good approximation of it [28]. Applying the one-dimensional fast Fourier transform (FFT) to the LSF will give the modulation transfer function (MTF) of the system, unlike the PSF to MTF conversion that requires the use of a 2D FFT. Figure 7.2 shows a measured edge spread function and its corresponding LSF and MTF. One of the main advantages of the LSF-based method is the fact that the measurement of the response to the edge is simpler through any of the commercially available resolution tests such as the USAF target (Fig. 7.3).

7.3 Programmable Illumination

In microscopy, the illumination control can be used to improve the final quality of images. In this way, many operations can be performed: light intensity control, wavelength of the light, correct alignment of the condenser, use of dif-

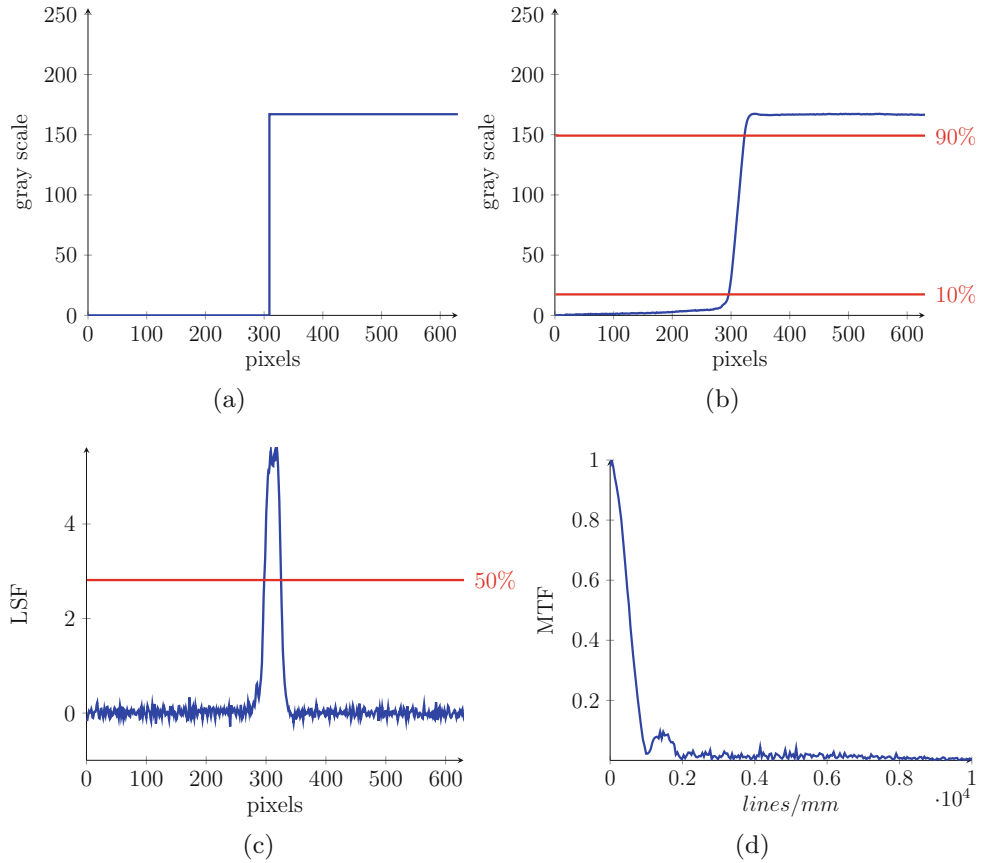

Fig. 7.2 Theoretical edge spread function (ESF) (**a**) and measured ESF (**b**). Resolution can be measured in (**b**) as the width of the slope in which it raises from 10% to 90% edge rise distance (ERD). (**c**) is the linear spread function (LSF) corresponding to the derivative of ESF. Using the LSF, the resolution can be measured as the width of the graph at the 50% of its height (an alternative measure to the ERD). The Fourier transform of the LSF (**d**) is the modulation transfer function (MTF). These measures were used by the authors in [26] to compare the resolution between brightfield and oblique illumination

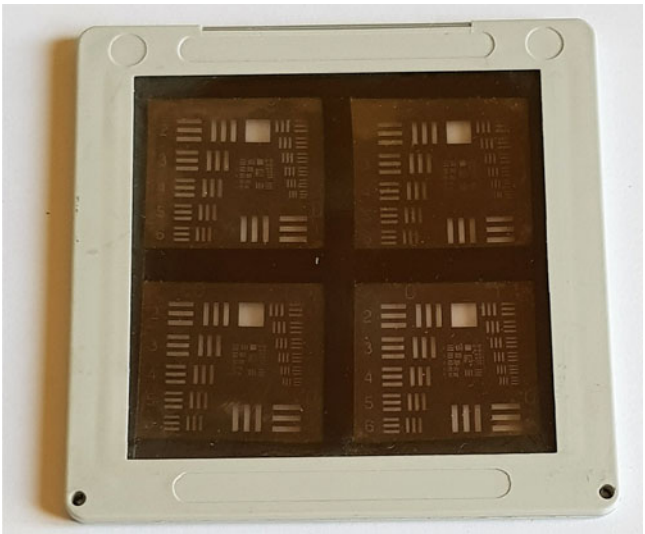

Fig. 7.3 Resolution target for testing optical performance (USAF 1951 test target). The edges of the bigger elements can be used as an edge step to calculate overall response of the system and then the LSF

ferent illumination modalities, etc. This section covers how to control automatically the most influential properties of illumination, i.e., modality and intensity. Other illumination properties are covered in depth in Chap. 5 of this book.

7.3.1 Light Intensity Control

There are different lighting sources used in microscopy. The intensity control of the light will depend on the type of the source. Traditionally, incandescent light bulbs have been used as main light source in microscopes. However, nowadays it is getting more common the use of LEDs for microscope illumination. Lasers are other type of lighting typically used in confocal microscopy.

Controlling the amount of light used in a microscope can help to obtain a better quality image. On the one hand, if there is not enough light, the image will be very dark and most probably details of the objects under study will be missing. On the other hand, if there is a brightness excess object will appear saturated and therefore indistinguishable. In digital imaging, this effect of the light will also happen with the particularity that the camera exposure time needs to be set according to the light source. Figure 7.4 shows how different can look an image depending on the correct combination of illumination and exposure time.

The LED light intensity can be modified in a controlled manner. The standard way of carrying it out is using a pulse width modulation (PWM) digital signal [15]. A PWM signal reduces the output power an output delivered to the LED by switching the input voltage between `ON`/`OFF` states with an specific frequency over a threshold (see Fig. 7.5). The amount of power is determined by the duty cycle, i.e., the fraction of the pulse that is `ON`.

$$D = \frac{t_{\mathrm{ON}}}{T} \times 100\%$$

PWM signals can be created using the analog outputs of an Arduino board. The Arduino library includes the function `analogWrite(pin,value)` that implements the PWM protocol. Where `pin` is the output pin and `value` is the duty cycle (it ranges from 0, always `OFF`, to 255, always `ON`). Arduino Mega has 16 PWM capable pins (2–13 and 44–46). The base frequency of Arduino PWM is 490 Hz.

Usually an Arduino board will not be able to deliver enough current to the LED or it uses a different voltage. In such case a MOSFET (metal-oxide-semiconductor field-effect transistor) can be used to drive the LED current. It is also possible to use a driver to control the LED illumination when more current is needed.

7.3.2 Programmable Illumination Modes

Controlling illumination modes by means of software is another powerful tool. Being able to change between bright-field, darkfield, or oblique illumination can help to improve the overall captured image quality. This can be achieved

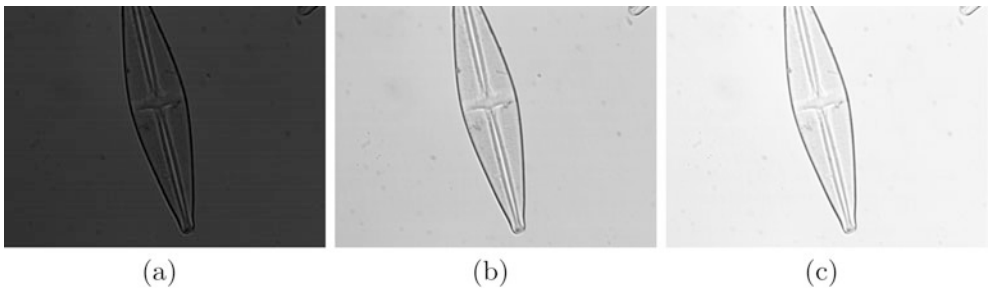

Fig. 7.4 Exposure time effect on image: (**a**) under exposition, (**b**) correct exposition, (**c**) over exposition

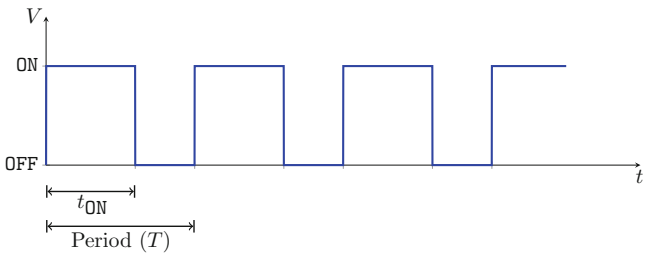

Fig. 7.5 Pulse width modulation (PWM) signal. The signal takes a `ON` value during the duty cycle and `OFF` during the rest of the period. Changing the duration of the duty cycle allows to control the power delivered by the signal

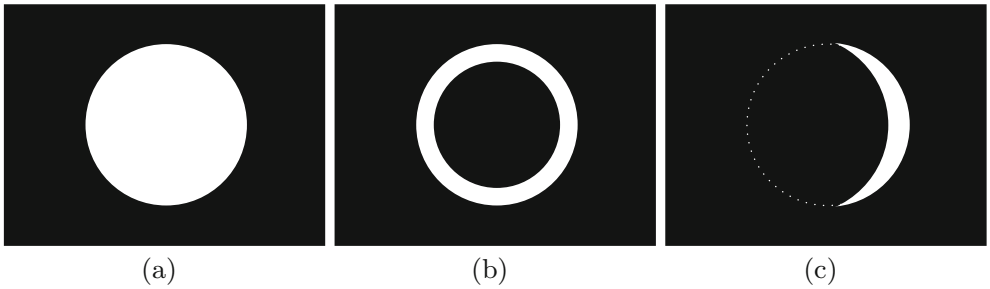

Fig. 7.6 Different examples of images depending on the desirable illumination. (**a**) Brightfield. (**b**) Darkfield. (**c**) Oblique illumination

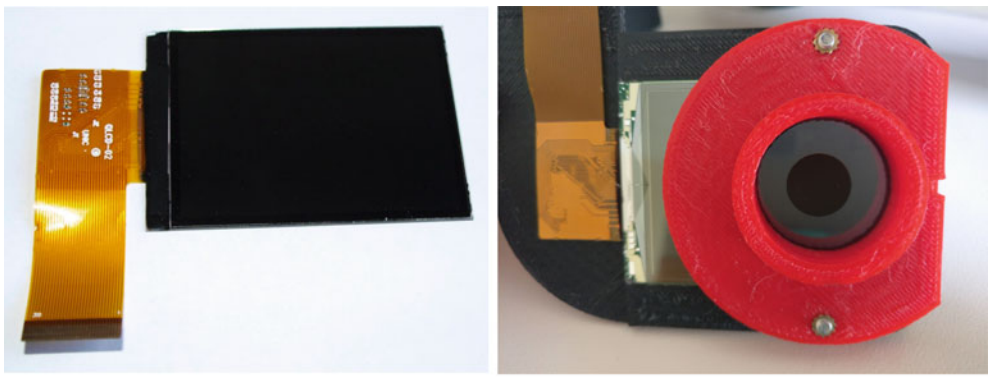

Fig. 7.7 (**a**) Example of LCD obtained from a video projector used for programmable illumination. (**b**) LCD in its 3D printed adapted mount showing a black disk at the center of the LCD for darkfield microscopy

using an LCD. The idea behind this is the same as in image projection, i.e., use an LCD to block the light from the source. Figure 7.1 shows the configuration required to implement it. The LCD is between the light source and the condenser as showed in Fig. 7.1.

There are numerous LCD available at the market to buy, but they can be hard to control depending on the protocol used. A smarter choice would be to use the LCD present in most digital projectors, like Fig. 7.7a. This option has the advantage that the controller board is included in the projector and it only needs an input image via HDMI, VGA, etc. To provide the image a small single-board computer like Raspberry Pi Zero can be used. Another advantage is that the projectors usually come with a powerful LED that can be used as light source for the microscope.

Figure 7.6 shows examples of images that can be displayed with the LCD for different illumination modes. The LCD can also produce colored illumination (Rheinberg filters) as well as different light intensity using darker or brighter images. Figure 7.7b shows one of these images on the LCD.

7.4 Image Calibration

Without a proper calibration it is difficult to measure actual distances on captured images by means of a microscope. In general image calibration is establishing a relation between pixels and the real size of what is under observation. It mainly depends on the microscope optics (magnification) and the camera sensor. In commercial systems that include the image capture device usually the manufacturer provides the calibration information. The problem arises when camera and microscope are bought separately.

In order to calibrate the system it a calibration slide is required or any other calibrated object. There is a wide range of calibration slides available depending on the manufacturer. In these slides a ruler is engraved in which the distance between divisions is indicated. Figure 7.8a shows an example of a calibration slide and how it is displayed on the oculars or camera (b).

The process of calibration can be described as taking a picture and counting the number of pixels between two

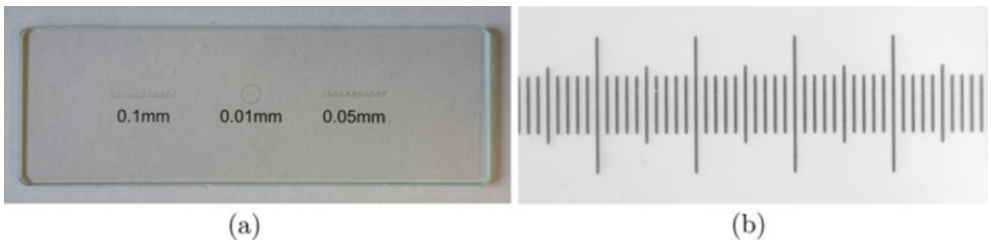

Fig. 7.8 (**a**) Calibration slide with three different rulers (0.1, 0.01 and 0.05 mm between divisions). (**b**) View of one of the rulers on the microscope using a 60x objective. The spacing between lines is 100 microns

known divisions. Then the calibration value is the relationship between number of pixels and the known distance. It is measured in pixels per distance unit (calibration factor). It is important to note that this process needs to be repeated for all the different objectives and cameras available for the microscope since the calibration will be different from each other.

7.4.1 Usage with ImageJ

ImageJ[1] is an open source image processing package. It is multiplatform and available for Windows, macOS, and Linux. It provides thousands of plugins that allow to perform many common image processing tasks and it is highly extensible with a large user community behind it.

Calibrating a microscope is an easy task with ImageJ, and it can be accomplished in several stages. The first step is open the image taken from the calibration slide. It can be done via the menu `File` → `Open...` or drag and dropping the image into the ImageJ window. A line is drawn using the `straight` option between two marks of the ruler. Now in the menu `Analyze` → `Set scale...` the program will automatically count the length in pixels of the drawn line and will ask for the known distance that is equivalent to it. If the checkbox `Global` is selected in the menu, then the calibration will affect all the images opened with ImageJ; otherwise the calibration will be used only for the selected image. Once the calibration is finished, the size in distance units of the image will appear in the top-left corner of the ImageJ window. With ImageJ it is also possible to overlay a scale bar in images via the menu `Analyze` → `Tools` → `Scale bar...`. This menu will ask for the bar properties: size, color, location, and font.

ImageJ also has capabilities to save different microscope calibration profiles with the `Scale Bar Tools for Microscopes` tool set. This tool set is located under the menu `More Tools`→ `Scale Bar Tools for Microscopes`. When the tools are loaded, several items appear on the tool bar that will allow us to calibrate images as well as establish different microscope profiles. First of all it is needed to create a new microscope profile. It can be done in `Microscope Profile Manager Menu`→`Create a New Microscope Profile`. A new window will be opened where all the information about the microscope calibration will be set. Up to five different objectives can be defined setting the distance in pixels, the corresponding known distance and the default scale bar size. Once the information is completed, the profile will be available in `Available Microscope Profile Menu`. With the profile selected and the image opened, the `Scale Bar Tool` will calibrate the image as well as draw a scale bar on the image. The configuration window that will be opened with the menu allows choosing among the different objectives available on the microscope and the information that will appear on the image (scale bar, calibration info, etc.).

7.5 Slide Scanning

Usually in microscopy there is not only a region of interest inside a sample, instead it is needed to analyze the whole slide or even more than one slide per session. For example, when using diatoms as biological index to study water quality, according to an European Normative a total of 400 valves has to be counted inside a sample to take the study as valid [4]. This task can be tedious and repetitive for experts. At this point, automatic slide scanning techniques provide a great help. Ideally they are a process that allows to extract all the information available on the sample without the user interaction. To perform an automatic slide scanning it is necessary to use a motorized microscope as well as the definition of strategies used to cover the area of the sample.

7.5.1 Platform Motorization

In general, a motorized microscope platform can move along three axes. X and Y axes for horizontal positioning the slide under the objective and vertically along Z to focus the specimens under study. In order to perform an automatic slide scanning it is needed to control the motion along

[1] https://imagej.nih.gov/ij/index.html.

the three axes. The easiest way is to motorize both the microscope platform and its focus. This motors can be preinstalled by the manufacturer or installed afterwards with a compatible platform or a do-it-yourself (DIY) approach. Preinstalled or already existent stages are the easiest and less effort ways of motorize the platform. However, this option is not always available and it is usually costly. If the only option is a DIY strategy, then a possible configuration would be using Arduino platform and stepper motors with their correspondent motor drivers. This option requires more work but offers the highest flexibility and usually will be cheaper. On the downside, it does not only need to assemble the hardware but to code the firmware to control it.

Commercial automated platforms usually will have their own software to control them from a computer. However, DIY motorizations will require its own software implementation. It is also possible to use already existing tools like the open source $\mu Manager$[2] and code the firmware to maximize compatibility with it. $\mu Manager$ can not only be used to control the motors but also to control the camera and process the obtained images as it is bundled with ImageJ.

In a microscope with motorized stage it is needed to know the relation between the motors steps and the final position for the stage. This relation is accomplished by motors calibration. When the motors are preinstalled or the motorized stage is bought afterwards, the calibration will be provided by the manufacturer. In DIY solutions the calibration has to be done by the user. Calibration can be split into two different parts. On the one hand, X–Y axes calibration (the slide plane). On the other hand, the Z axis calibration.

To calibrate motors in the X–Y axes it is possible to use a ruler like the one used to calibrate the image (Sect. 7.4). A reference image is taken. Then one of the axis is moved a certain number of steps. A new image is taken. Comparing both images the relation between the motor movement and the stage movement can be calculated. The other axis can be calibrated analogously. In case that the calibration slide only has a ruler in one direction, it is needed to rotate the slide 90°.

Calibration along the Z axis can be done using the method described in [2] by Boddeke et al. This method uses a slide with a flat bar pattern that is tilted rising one of the laterals. The main idea behind this method is that in the tilted slide only a line perpendicular to the slope is focused at a time. A first reference image is taken. Then the focus is moved and a new image is taken. In this new image the in focus line will be moved a certain distance. Measuring this displacement and the tilt angle of the slide it is possible to determine the relation between the motor and the Z axis movement using trigonometry.

[2] https://micro-manager.org/.

7.5.2 Automatic Slide Scanning

There are several ways to scan a slide containing diatoms. The most used for this particular scenario are the sequential, the random, and those based on regions of interest scanning. All of them try to mitigate the backslash effect produced by the clearance between the different mechanical components of the system, and can be used afterwards to do the stitching of the images.

7.5.2.1 Sequential Scanning

The sequential scanning represents different organized ways to scan the slide. Most of them are based on patterns that the objective will depict through the slide. Some examples are the rectangular, circular, and cross (+ and ×) patterns.

To represent these patterns, it is necessary to define also a starting point and a trajectory for the objective, that is, the behavior of the objective when it detects it has finished to capture pictures of the slide on a particular axis.

For example, a typical way of scanning a diatom slide is depicting a rectangle that covers all the region the user decides to scan. Afterwards, the scan can be done starting from the upper-left point of the slide, left to right (and vice versa), and from top to bottom as shown in Fig. 7.9. It is worth noting that, although it is possible to change the direction of the slide at any moment, it is better to limit them to the minimum to reduce the backslash effect produced. Because of that, in this particular example the FOV is changed on the X axis until it reached the end, coming back to the initial point and moving one FOV on the Y axis.

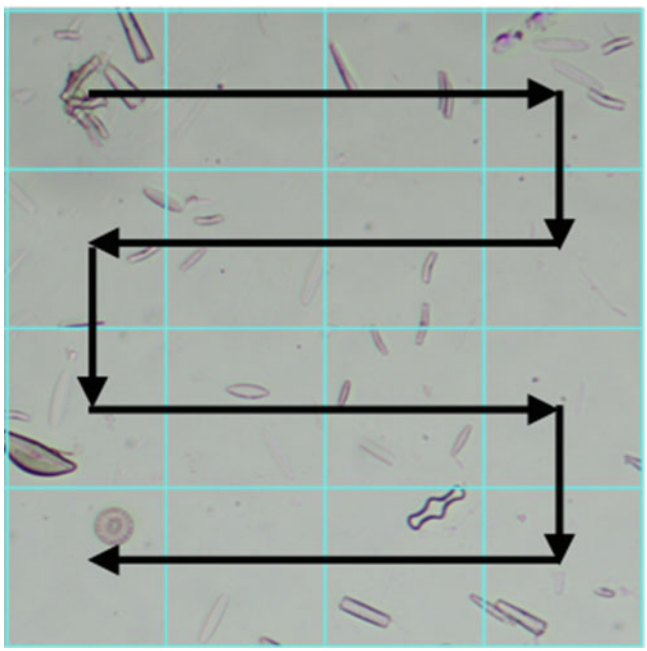

Fig. 7.9 Sequential scanning pattern [21]

Normally, between every FOV, and just after doing the movement to acquire another FOV, it is necessary to wait a slight period of time (which will depend on the quality of the microscope) to stabilize the stage, and therefore reducing the noise of the image captured. A sequential scanning also allows to create a mosaic from all the images obtained. Mosaics are useful when the specimen under observation is too big to fit on a single field at the magnification used for the observation.

For this purpose, there are two main procedures, *mosaicking* and *stitching*. Both techniques try to join the individual acquired images to generate a single panoramic image. *Mosaicking*, which is a special case of *stitching*, is just a simple image paste, without any overlapping between them. However, to correctly perform a *stitching* algorithm is necessary to capture the adjacent images with a certain overlap, generally 5% or 10% in both X and Y axes.

A standard *stitching* algorithm can be divided into several steps:

1. *Feature extraction:* In this step, a keypoint detection is carried out to find correspondences between images. Then, these features or patches are used to estimate the necessary transformations to be applied for aligning an image with the reference one. Two famous and commonly used keypoint detector are *SIFT* (Scale-Invariant Feature Transform) [11] and *SURF* (Speeded Up Robust Features) [1].
2. *Image registration:* The second step is the process of geometrically aligning two images, one of them taken as reference. This technique, also known as image registration, tries to align the images searching those transformations that minimize the sum of absolute differences between the key points extracted in the previous step.
3. *Blending:* The last part of a *stitching* algorithm is the image blending. In this step, the transformations calculated in the registration step are applied. Also, to minimize the visibility of differences between the merged images, colors and intensities are adjusted to compensate different exposure times during acquisition. For microscopic images, like diatoms or pathology images, a background correction is needed too in order to remove illumination defects caused by a bad quality light source or a misaligned light condenser, such as shadows or dark areas.

In ImageJ/Fiji there are different plugins to perform the *stitching* of a set of images, e.g., the *pairwise stitching* and *grid/collection stitching* [21]. Both are preinstalled in Fiji and can be downloaded for ImageJ. Both plugins are located in `Plugins` → `Stitching`.

The *pairwise stitching* plugin allows the user to carry out the stitching of two previously loaded images. In the menu, several options can be configured, such us the fusion method (linear blending, average, median, maximum or minimum intensity, overlay into composite, etc.), the number of peaks to be examined, the image channels desired to compute the overlap or the registration method. Figure 7.10 shows an

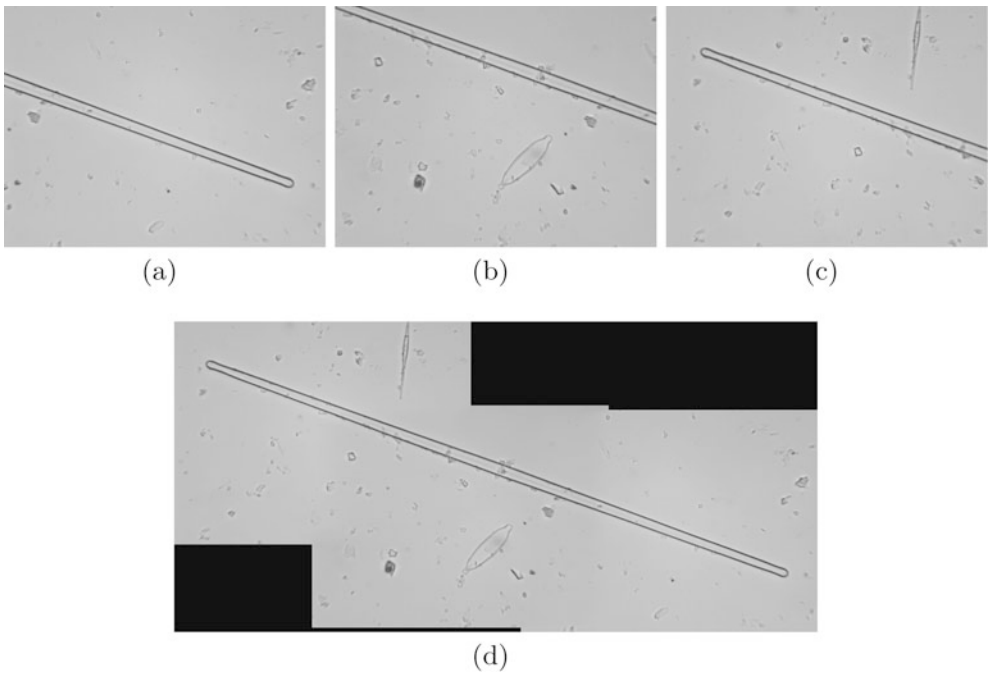

Fig. 7.10 Example of stitching. (**a**)–(**c**) Input images. (**d**) Pairwise stitching result [21]

example of image stitching of three adjacent microscopic fields covering a large diatom specimen using the pairwise stitching plugin.

On the other hand, with the *grid/collection stitching* plugin the procedure can be applied to a set of images, as opposite as in the previous method, which only allow to perform the stitching of two images. In the first window, the user is asked for the way the images are ordered, which is related to the scanning algorithm. In this way, the possible options to choose are row by row, column by column, snake by rows, snake by columns, or unknown positions (the algorithm will try to determine it). Then, other configuration parameters have to be completed, such as the grid size (rows and columns), the overlapping area between tiles, the source images folder, and filenames pattern. Finally, the rest of configuration settings are the same as in the pairwise method.

7.5.2.2 Random Scanning

In classical microscopy, random-access scanning refers to a form of laser beam scanning in which the beam focus is selectively positioned at individual sites, typically user-selected, in either a two-dimensional (2D) plane or a three-dimensional (3D) space [22]. The positioning is considered random since there is no direct relationship in the order the sites will be scanned (Fig. 7.11). This approach contrasts with the widely used sequential scanning which normally follows a regular pattern.

The same concept is being currently used with optical microscopes to scan diatom slides. To do that, the user requires to define the zones that should be scanned. This procedure will require, in the case of the diatoms, a previous study of the slide preparation. Afterwards, the stage is moved iteratively from a FOV to other not scanned regions. Thus, this process requires keeping a record of previously visited areas. The main drawback of this approach is that, due to the irregularities of the preparation, large variations may appear to find the best focus in the next FOV. This situation makes the autofocus algorithm implemented a key factor to be able to obtain an acquisition with good quality.

7.5.2.3 Scanning Based on Regions of Interest

A complete workflow to locate and scan valves of interest containing diatoms is proposed in [9]. This approach scans initially the slide at low magnification and locates the regions of interest in it. In the next step, only such regions are scanned at high magnification, reducing the time and data storage requirements. It is necessary that the preparation has been carried out in such a way that the objects have good contrast. It is also required that the sample has been diluted so that the objects have a sufficient separation between them to be able to effect the focus.

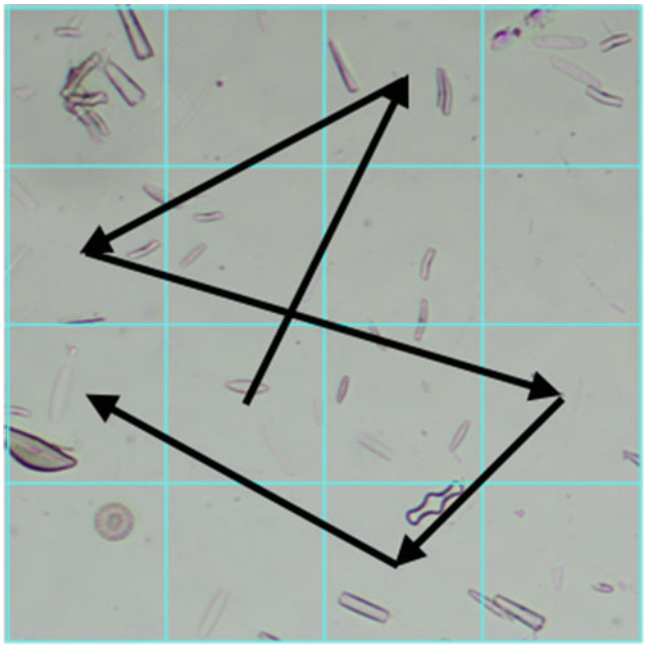

Fig. 7.11 Random scanning pattern

Once the slide preparation is finished, the image analysis procedure starts scanning at a low-resolution area, usually using a 20× magnification objective and creating an initial focus map that will be subsequently improved by fine focusing, which will generate a slide overview. This overview is composed of images at ten different focus positions in Z-distances for each FOV captured. These stacked images represent the required input for the stitching procedure to generate the final overview slide and locating diatom valves. Finally, to select the objects/regions of interest to be scanned at high resolution the low-resolution images are processed comparing the object outlines with a set of shape templates defined by the user, which define the taxonomic scope of a certain analysis. Then the system allows to scan the valves selected automatically or to be reviewed by the user before starting the higher magnification scan.

7.5.3 Autofocusing

Normally, when using any type of scanning method, it will be necessary to change the focusing dynamically as every FOV does not have the same focusing point due to the irregularity inherent to the sample. In this section the criteria to measure the focusing level on a particular FOV and the autofocusing methods used in the case of diatoms images will be explained.

7.5.3.1 Criteria to Measure the Focus Level

The first step prior to design an autofocus algorithm is to determine the degree of defocusing of each FOV contained on the sample [19]. This degree is normally represented as a numerical value which can be calculated using several functions based on the differences between focused and defocused images [27], like the high frequency contents of the images [6] or the edge contents on the FOV [34]. This section will provide an insight into several state-of-the-art methods to measure the level of focusing.

Brenner Function

Another way to determine the level of focusing is through the use of derivative operators [27]. In this case, the use of such techniques is based on the fact that in an unfocused image the edges are averaged generating different levels of gray, while a focused image has less gray levels variability.

In the diatom field, and based on that concept, the modification of the Brenner function that considers both the horizontal and the vertical gradients is used [3]. This function calculates the first difference between a pixel and its neighbor two points away, as shown in Eq. (7.1), being $g(m,n)$ the gray level intensity of pixel (m,n) and v the gradient threshold.

$$F_{\text{Brenner}} = \sum_{m}^{M}\sum_{n}^{N} |g(m,n+2) - g(m,n)|^2 \quad \text{while } |g(m,n+1) - g(m,n)| \geq v \tag{7.1}$$

Laplacian Variance

One technique to determine the high spatial frequency contents, which are commonly associated with the sharpness of the edges of an image, is the use of second derivative operators such as the Laplacian variance, which has been proved to be appropriated for the focusing on diatoms FOV [17]. The Laplacian operator applies a kernel through a convolution operation to the gray scale image g through the following kernel:

$$L = g * \begin{bmatrix} 0 & 1 & 0 \\ 1 & -4 & 1 \\ 0 & 1 & 0 \end{bmatrix} \tag{7.2}$$

Afterwards, the variance of the absolute values obtained on the previous step is calculated to provide a dispersion measurement, as shown in Eq. (7.3). $\overline{L}$ is the mean of the absolute values given in Eq. 7.4 and $L(m,n)$ is the convolution of the input image $g(m,n)$ with the Laplacian kernel. On the one hand, as this operator is also used to detect contours, the obtained numerical value will be directly proportional to the focusing level of the FOV, indicating that the image contains a great quantity of well-defined contours, being focused. On the other hand, if the value is low it will mean that the image is blurry.

$$\text{LAP\_VAR}(g) = \sum_{m}^{M}\sum_{n}^{N}[|L(m,n)| - \overline{L}]^2 \tag{7.3}$$

$$\overline{L} = \frac{1}{\text{NM}}\sum_{m}^{M}\sum_{n}^{N}|L(m,n)| \tag{7.4}$$

Deep Learning Techniques

Deep learning techniques have been able to achieve similar accuracy to a human on several image classification problems. This approach has been recently applied to create neural networks capable to predict a measure of image focus. It operates at image-patch level providing also a measure of prediction certainty [32]. An ImageJ/Fiji plugin is available from the ImageJ repository.[3]

The main drawback of this approach compared to the previous ones is that it requires an initial training dataset, normally labelled manually, to generate a model accurate enough to be used. Moreover, not only the labelling quality of the dataset, but also the quantity of scenarios represented and, therefore, images contained, will be key for the model to be robust at any particular situation that may be presented to the classifier. To remove the bias, the model may suffer from the original dataset, normally requiring several data augmentation techniques to be used [18].

7.5.3.2 Autofocus Strategies

Once a function is defined to represent the focusing level of an image, it is necessary to select a methodology to find the limit in which the image can be considered as focused for a given FOV. Although normally the focusing level between consecutive FOV may be similar, there might be cases in which it differs greatly. Furthermore, it will also depend on several external factors as the microscope, the slide preparation, etc.

Moreover, in the particular case of slides containing diatoms, the number of individuals on each FOV is an important factor when calculating the focusing level as having very few elements in the image will increase the uncertainty of the focusing criteria used. In this section, two autofocusing methodologies will be discussed.

Two-Stage Autofocus

This technique is based in two main steps: (1) an initial step in which the best focusing level is detected using a wide margin and (2) a more precise focus obtained starting from the best focused level given by the previous step [10].

For the first step, the so-called hill-climbing methodology is used. This algorithm selects a direction, the one which

[3] https://imagej.net/Microscope_Focus_Quality.

initially improves the focusing measure, and modifies the lens position continuously on that direction until a stopping criterion is met, which usually is related to the focusing level decreasing instead of increasing. After the stopping criterion is met, the lens will be moved to the position in which the best focus level has been attained. From this point, a more precise lens movement will be performed in the direction the focusing level increases until the focus measurement starts to decrease again, selecting the prior position as the final best focused position.

Autofocus Based on Lorentzian Function

This approach stands out for its simplicity and speed. It combines the focusing level calculation techniques with a curve fitting algorithm, requiring no more than three images to calculate the best focal position [33]. Its main drawback is that, although it is able normally to provide a good lens position, in the situation in which there is a big difference between two consecutive FOV focus levels, for example, when using random scanning, its convergence drops. Its main drawback is that although in general it provides a good estimator of the best focus, its degree of convergence decreases when there is a large difference between two consecutive measures of focus as in the case of random sampling.

In detail, the autofocus procedure is divided into three main steps. In the first one, several images along the Z axis are taken to calculate their focusing value. The number of images required will depend on the desired relation between speed and accuracy. Then, an autofocus function will be approximated by interpolation using the previously acquired images and, finally, the focal position will be selected as the peak of the fitted function without requiring to acquire more images from that particular FOV. Afterwards, the servo-controlled microscope will configure the objective lens in the focal plane where the estimated focus peak is calculated.

Although it is possible to use several criteria to measure the focus level following this approach, the Brenner gradient can be well approximated by a Lorentzian function (Eq. (7.5)), where z is the position of the Z axis.

$$f(z) = \frac{\alpha}{\beta + (z - z_0)^2} \tag{7.5}$$

Note that the inverse of Eq. (7.5) represents a quadratic function that can be easily fitted from the Brenner gradient of only three images. Figure 7.12 shows an example of this technique is presented. A stack of 29 images was taken, measuring for each of them the reciprocal of the Brenner gradient and the Z position. The red line represents these measurements, so the best focal position is located at the minimum point ($-0.90\,\mu$m). Then, as explained before, taking only three images a parabola can be fitted to obtain an approximated focusing position. The blue line represents this approach, whose minimum point will provide the best focal position ($-0.99\,\mu$m).

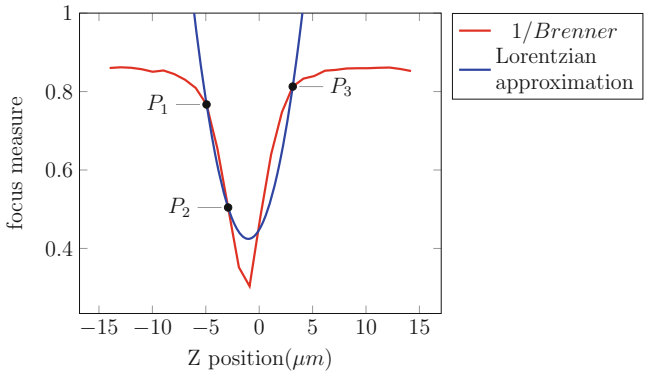

Fig. 7.12 Autofocus example using the Brenner gradient as focus measure and Lorentzian function approximation. The red line represents the inverse of the measured Brenner gradients from a stack of 29 images. The red curve has a Lorentzian function shape. It can be approximated as a parabola (blue line) using only the measures of three images (P_1, P_2, and P_3)

7.6 Preprocessing

The acquisition of images in microscopy can lead to different types of problems that can alter their final quality. The presence of artifacts in the images may be due to, e.g., conditions of low lighting, background inhomogeneities, or the presence of dirt in the optical pathway.

7.6.1 Noise Reduction

Camera's sensor is an electronic device, therefore it is susceptible to electronic noise due to different sources: thermal noise, shot noise, etc.

There is an extensive literature in noise modeling and image denoising and more specifically applied to images in microscopy. The noise present in microscopic images can be usually modeled as additive white Gaussian noise (AWGN) [14]. That means that to every pixel on the image a random component n is added following a Gaussian distribution with zero mean and constant variance $n \sim \mathcal{N}(0, \sigma^2)$.

One of the simplest methods to reduce noise in a microscopy image consists of the averaging of a few images of the same field [16]. In this way, the noise can be modeled as a zero mean normal distribution. Figure 7.13 shows an example of noise reduction using this procedure. ImageJ of Fiji has the necessary tools to do it. After loading a video clip all the frames will form an ImageJ stack. To average them the tool is `Image→Stacks→Z Project...`. In the opened window select `Average intensity` as projection type

Fig. 7.13 Detail of an image where noise has been reduced by averaging 50 frames of a static video. (**a**) One of the frames of the video with visible noise. (**b**) Average result. (**c**) The image difference represents the amount of noise that has been reduced averaging the video. The image's pixel range has been re-scaled for visualization purposes

and press `OK` button. The resulting image is the average of all the frames of the video.

7.6.2 Background Correction

Illumination defects can be originated for different reasons. For example, when using a bad quality light source or a misaligned light condenser different shadows or dark areas can appear in the image. Moreover, if the optics of the microscope or the camera sensor are dirty (dust, immersion oil rests, etc.), obtained images will be defective. Figure 7.14 shows an example image with inhomogeneous illumination.

In the next section different methods that help to minimize these errors are described. These methods are based on a similar idea, obtain a background image and then dividing the sample image by this background image to obtain the corrected image [13]. The main difference between them is how this background image is obtained.

7.6.2.1 Division by Blank Image

In this method the background image is a blank image. To capture this image it is necessary to place the sample into an empty field and capture an empty image. This image can be used as long as the illumination does not change or the optics are kept in the same cleanness state. Once the blank image has been captured, it is time to take pictures of the subjects of study. For removing the artifacts that are present in the image due to bad illumination or dirtiness, the sample image is divided by the blank image. After the division, the resulting image needs to be scaled to preserve the range of the original image, i.e., the original image and white image pixels values are in the range 0-255; after the division this range will be reduced to 0–1 therefore it is needed to multiply all the image by 255 to recover the original range. Figure 7.14 shows an example of the background correction operation.

7.6.2.2 Division by Unfocused Image

In this technique, the background image is obtained by defocusing the image moving the Z axis of the microscope until the specimen disappears completely from the focal plane. In that way, a background image is obtained similar to the blank image previously described. Now, the sample is re-focused and acquired as always. From now on the process continues as previously described, the image is divided by the background image and then scaled.

7.6.2.3 Division by Polynomial Approximated Image

Capturing the background image is not always possible for different reasons. In these cases, there are algorithms that allow us to estimate the background image from an acquired image. The background image is approximated using a polynomial fit, in which the coefficients of the polynomials are calculated to match the original image. Once this image generated, the rest of the operations are similar as before. First, the acquired image is divided by the background image and then re-scaled. There is a plugin for ImageJ that compute this polynomial approximation of the image: `Polynomial Fit` available to download from the developer website.[4] This plugin allows to select the order of the polynomial in the X and Y axes. Higher orders will produce better approximations but it will take longer to generate them.

7.6.2.4 Division by Rolling Ball Background Image

The rolling ball algorithm is an example of an algorithm that can generate a background approximation of an image. It was first described by [29]. The rolling ball algorithm consists of a gray scale opening of the image, i.e., a gray scale erosion followed by a gray scale dilation using a gray scale structuring element. With this opening the background of the image is estimated so that it can be subtracted from the original image. The gray scale structuring element can be understood as a 3D sphere that rolls along all the surface formed by the image (the third dimension is defined by the intensity value at every pixel). The non-background elements will be represented as peaks in this surface. Smooth areas

[4] http://www.optinav.info/Polynomial_Fit.htm.

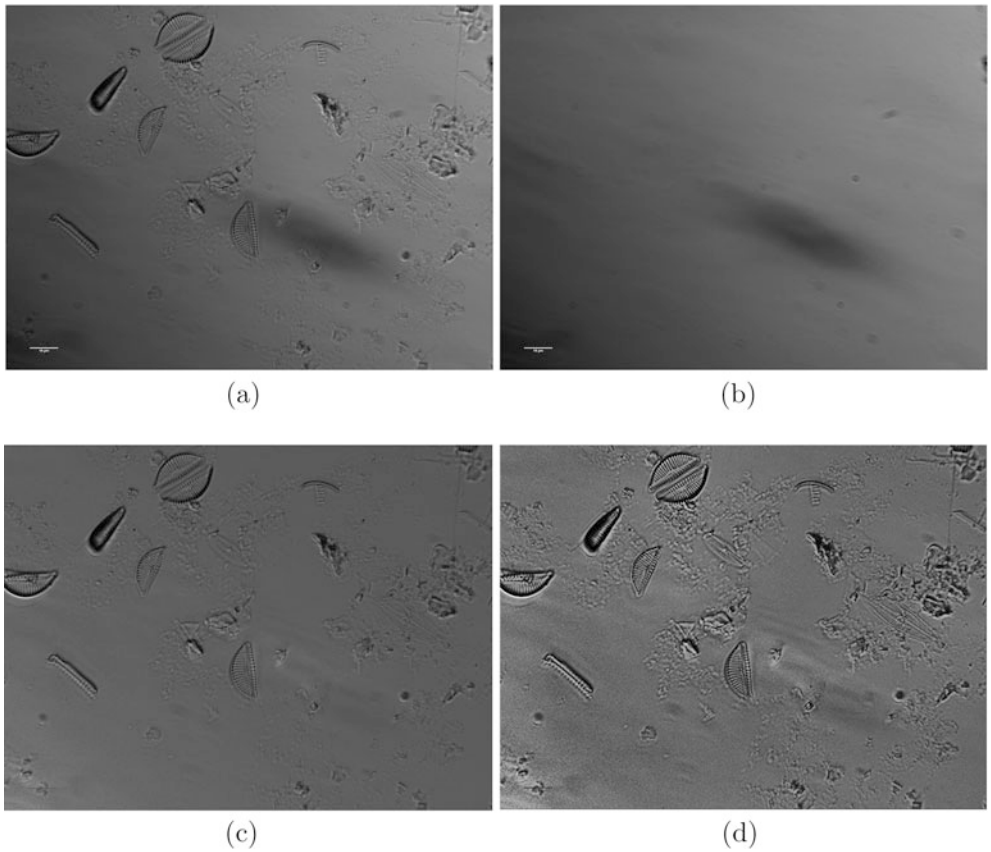

Fig. 7.14 Example of image background suppression. (**a**) Brightfield image captured showing a dark shadow at the near center due to inhomogeneous illumination; (**b**) flat field image showing better the dark artifact; (**c**) resulting image after dividing by the flat field image; (**d**) same result after histogram correction using the CLAHE algorithm [34]. Scale bars represent 10 μm

will be flattened by the pass of the rolling ball. It is important to choose a correct structuring element size. It has to be bigger than the biggest element in the image. Otherwise the algorithm will treat this element as background and as a result it will flatten that peak. Once the background is generated, the rest of the correction procedure proceeds before applying the division of the original image by the generated one and by re-scaling. Figure 7.15 shows an example of the background correction using the rolling ball algorithm.

The Rolling ball algorithm is available on ImageJ under the menu `Process` → `Background Subtraction...`. The preinstalled plugin allows to choose the value of the radius of the ball as well as other options of the algorithm. It is important to select the `Generate Background Image` option in order to generate the background image instead of subtracting directly from the original image.

7.6.2.5 Usage with ImageJ

All these background illumination correction methods can be carried out using ImageJ. First of all it is needed to open the image of the sample that needs corrections. If the blank or unfocused image is not available, the next step is to generate an artificial background image using one of the algorithms described before. Otherwise, the next step is loading the background image. Once both images are available, the division is performed using the Image Calculator option under the menu `Process` → `Image Calculator...` It will open a new window to select the options and the images to process. Image 1 is the original image, Image 2 is the background image. Between all the available operations choose Division. Finally, it is important to check the `32-bit (float) result` since a pixel-wise division will be done between both images and most of the results will carry decimals.

7.6.2.6 Batch Processing

Correcting the background of an image is not a difficult task using the methods described in the previous sections. However, when the number of images increases it can become a tedious work. As any other repetitive task it can be automated. There are different programming languages and libraries that can be used for it. ImageJ offers the possibility

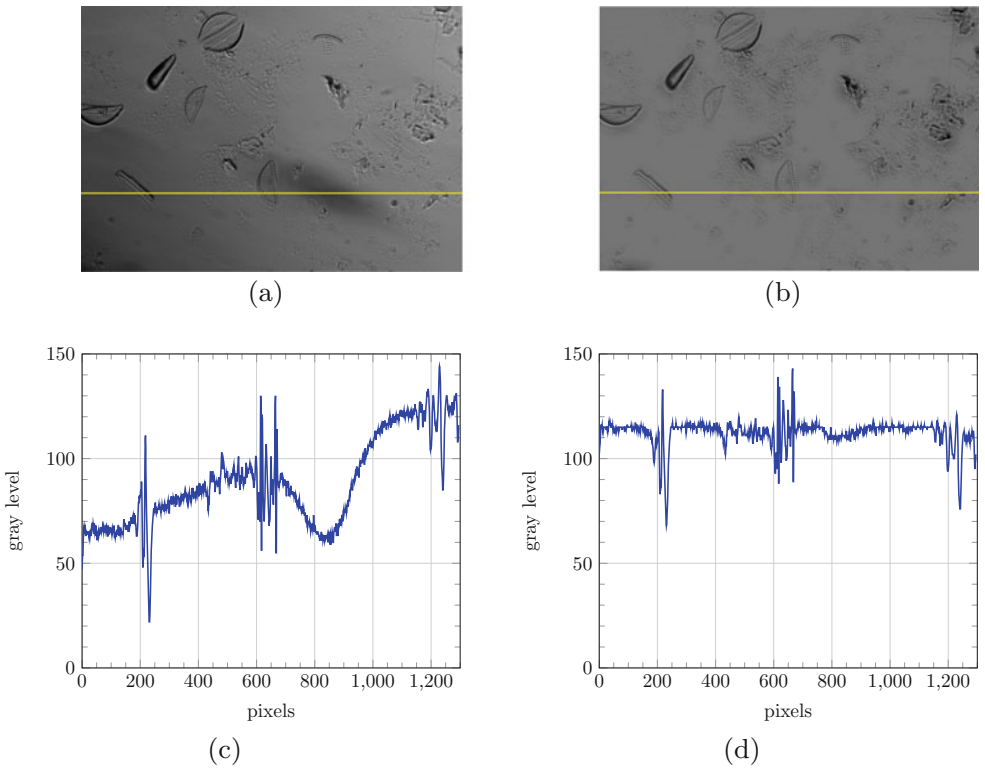

Fig. 7.15 Example of background illumination defects correction using Rolling ball algorithm. (**a**) Is the image as captured on the microscope, it has a dark shadow in the middle and the illumination is not uniform. (**b**) Corrected image applying a division between the original and a background image generated with Rolling ball algorithm. (**c**) Gray level profile of the line marked on (**a**). (**d**) Gray level profile of the line marked on (**d**) showing a more uniform gray level

of easy processing all those images that are in a folder. It can be found on the menu `Process` → `Batch` → `Macro`. It will open a new window to select the input folder where images are, the output folder where all the resulting images will be saved as well as their format and the macro operations applied to the image. Figure 7.16 shows an example of a macro for the background correction of a set of images using the rolling ball algorithm.

7.6.3 Contrast Enhancement

Image enhancement is the process of improving the quality and the information content with the aim to obtain better contrast or visualization. Contrast can be defined as the difference of luminance between different areas of an image. There is a direct relationship between the histogram of an image and its contrast. Low contrast images present a compact histogram (Fig. 7.17b). High contrast images present a wide histogram that fills the full dynamic range of the image (Fig. 7.17d). Comparing both histograms, the former has all the pixels concentrated in a small range of the possible values. In low contrast images it is harder to appreciate details.

It is possible to enhance the images contrast using different techniques [31]. One of the most common techniques to enhance contrast is histogram equalization (HE) [8, 30]. HE applies a histogram transformation to all the pixels trying to increase image contrast. It has the problem that the same transformation is applied to all the regions of the image. To solve this problem, adaptive histogram equalization (AHE) [20] calculates the histogram transformation for different regions of the image. The drawback is that this algorithm can amplify noise in homogeneous regions. The contrast limit adaptive histogram equalization (CLAHE) [35] is an AHE variation that limits the contrast amplification not allowing to amplify the noise as in AHE. Figure 7.17c shows an example of histogram equalization using CLAHE.

CLAHE is available for ImageJ as a plugin.[5] Moreover, it is already preinstalled on Fiji (https://fiji.sc/) under the menu `Process → Enhance Local Contrast`. Fiji is a fork of ImageJ with more preinstalled plugins. It is also open source and free to use.

[5] https://imagej.net/Enhance_Local_Contrast_(CLAHE).

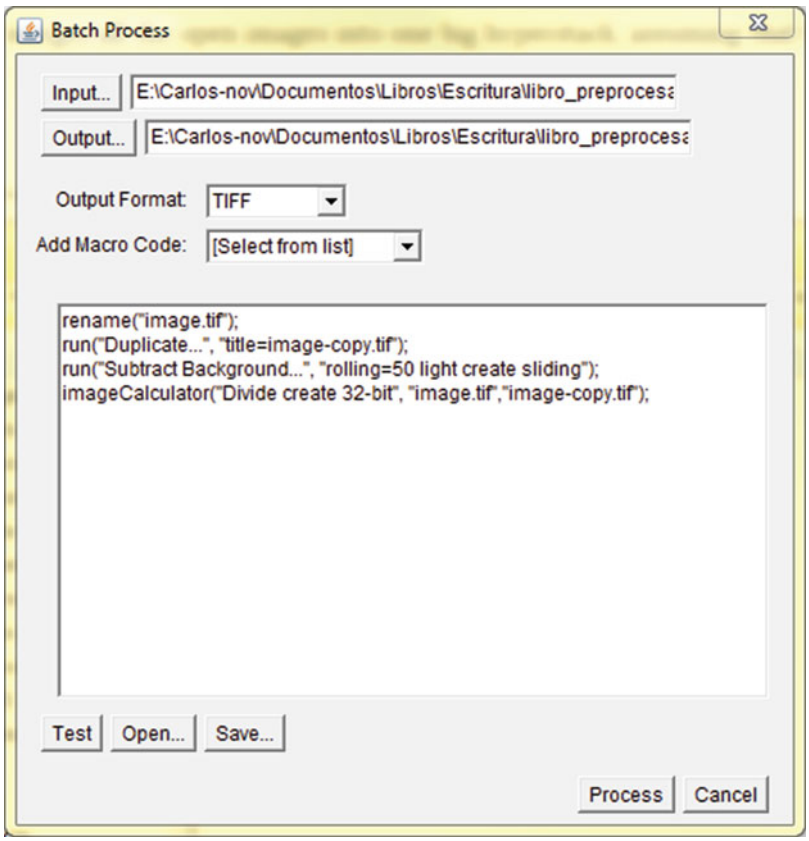

Fig. 7.16 ImageJ example macro for batch processing background illumination correction using rolling ball algorithm to generate the background image

7.7 Conclusions

In this chapter, different techniques for microscope automation have been reviewed. The microscope motorization, its calibration, and the techniques used for slide scanning have been described. It has been also showed how to control the microscope lighting and different image preprocessing algorithms for enhancement of the acquired images.

The software and hardware proposed in this chapter are both open source and free. This is important because it helps to reduce the budget necessary to modify a microscope into a more powerful equipment with automatic capabilities. Using a 3D printer to make prototypes of the modifications can reduce even more the cost of the equipment required. It allows easily the design of pieces until they fit perfectly into the microscope at a very low price.

Self-modifying the microscope comes with the advantages that new modules can be easily included in the future. An example of future add-on is a fluorescence module. Using only a filter cube and epifluorescent illumination attached to a 3D printed module it is possible to turn a brightfield microscope into a fluorescence one.

Another possible future improvement is adding a focus tunable lens between the camera and the objectives, replacing the motorized Z axis. This would be a faster and more stable solution to change the focal plane of the captured image allowing a more accurate and faster Z-stack capture and autofocus.

Appendix

Microscope Control Application

An application with a graphical user interface (GUI) has been developed to control the prototype described in this chapter. Most of the application has been developed using *Python* programming language, although some algorithms have been developed in *C* to improve the performance. *OpenCV* library has been used to manage image processing operations and *PyQt* for the GUI design. In this section, the most important implemented functionalities are reviewed.

First, in Fig. 7.18 the main window of the designed GUI is presented. Basically, it is divided into two different sections, the camera viewer and the control panel. In the first one, the user is capable to visualize in real time the images captured by the camera, according to the established camera settings. In the control panel section, through GUI elements such as buttons, text fields, or check boxes, the user can manage and configure some options related to the camera or the motorized stage, as well as to run the implemented algorithms and procedures. Also, under the camera viewer,

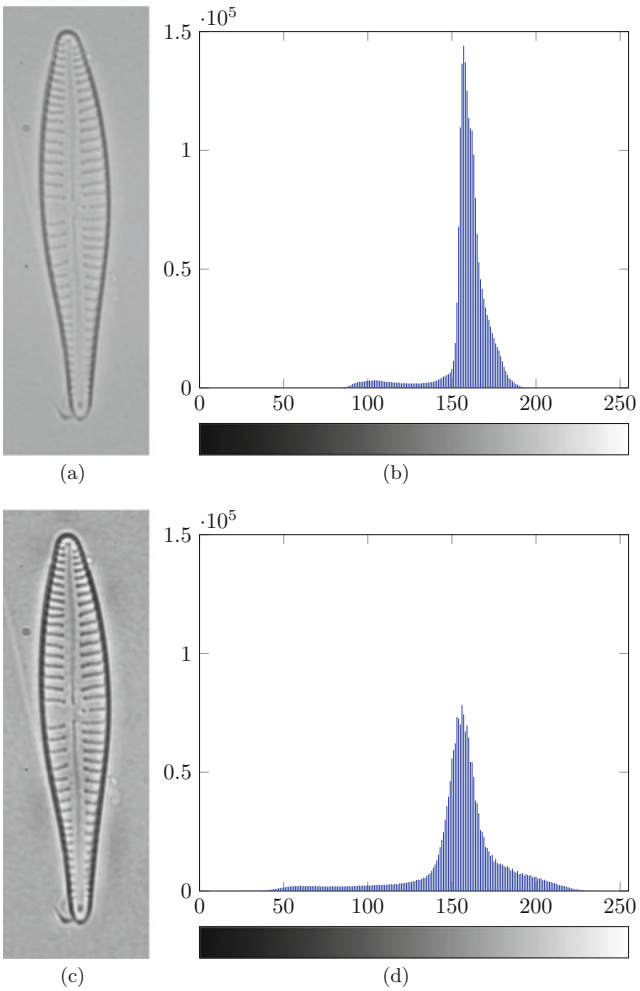

Fig. 7.17 Example of image with low contrast (**a**) and the same image after applying contrast limited adaptive histogram equalization (**c**). (**b**) and (**d**) are its corresponding histogram. The colors bar represents the corresponding gray value of the above histogram values

some information about the stage position and the camera focusing value is presented.

In the next sections, the different GUI elements are briefly described, along with its functionality.

General Configuration

In Fig. 7.19, a detail view of the general configuration section is shown. In this panel, the user can manage the next functions:

- *Enabling and disabling the camera view:* Using the *Show* and *Not show* buttons, the user can enable and disable the camera view. When the *Not show* button is enabled, the camera panel change into a black window.
- *Color mode:* The *RGB* check box allows swapping between the gray scale and RGB color mode, for cameras that support this feature.
- *Illumination mode:* As explained in Sect. 7.3.2, using an LCD several illumination modes can be achieved. The *Dark-field* check box allows the user to switch between brightfield and darkfield illumination modes.
- *Background correction:* In Sect. 7.6.2, different methods to correct illumination defects are described. In this application, this correction is done dividing the original image by an unfocused image. The background image can be obtained automatically through *Take background image* button. After doing that, the live background correction can be activated enabling the *Background correction* check box. Then, the camera view panel shows the corrected image instead of the original captured image.
- *Save images:* The application allows the user to capture an individual image at any time, through the *Save* button. The file name, image format, and location can be selected in a folder browser window.
- *Autofocus:* An implementation of the autofocus algorithm based on Lorentzian function described in Sect. 7.5.3.2 is included, which required no more than three images. The *Autofocus* button allows the user to use this approach at any time.
- *Live diatoms detection:* A trained diatom detector has been included. It is based on YOLO framework [23, 24],

Fig. 7.18 Main window of the GUI

whose speed and accuracy allows making inference in real time, even in modest devices. The user can enable this feature through the *Live detection* check box. Then, in the camera panel, for each detected diatom a bounding box will be overlaid. Additionally, another algorithm has been included to merge possible overlapping bounding boxes. This feature can be activated enabling the *Merge Box* check box.

- *Setup and Home:* Using the *Setup* button, the user can define the "Home" position. Then, the *Home* button automatically moves the stage to this position.
- *Scale bar:* A useful tool commonly required by diatomists and other experts is the possibility to add a scale bar to the images. Enabling the *Scale bar* check box, a calibrated scale bar will be added to an image corner.

Stage Control

The motorized stage control panel is presented in Fig. 7.20. In this section, the user can configure the motion parameters and carry out the manual displacements through the sample.

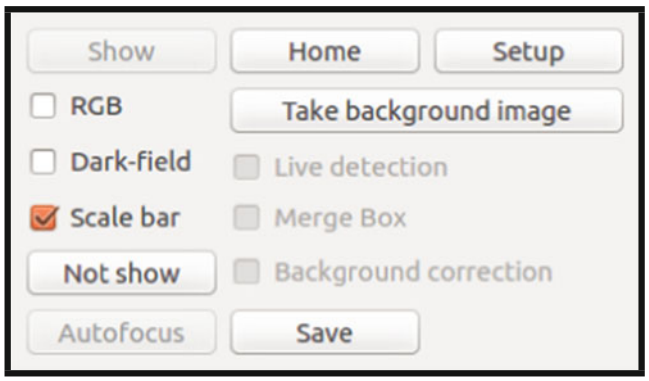

Fig. 7.19 General configuration panel

First, the distance measurement unit can be switched between mm and µm. Then, the user can move the stage using the arrow buttons for X and Y axes and $Z-$ or $Z+$ buttons for Z axis. For this case, the movement step can be configured between 5, 20, or 100 (mm or µm depending on the unit selected). Furthermore, if the user needs more accuracy, the desired step size can be set into the

text fields for each axis. The *Move* button performs then a relative displacement taking into account the introduced values.

Scanning and Processing Functions

A set of automated functionalities can be found in the last panel (Fig. 7.21), which are briefly described:

- *Objective selection:* In addition to the stage, the objective nosepiece is motorized too, so the automatic change between objectives has been included. To perform this action, the user only has to select the desired objective from the list and the procedure will automatically start.
- *Sequential scanning:* A sequential scanning algorithm has been implemented, following the pattern described in Sect. 7.5.2.1. The user only has to set the number of FOVs for *X* and *Y* axes and then click the *Scan* button. During the scanning, the autofocus algorithm is executed for each FOV, as well as a background correction. Also, for color images, a color normalization through Reinhard algorithm [12,25] can be applied enabling *Reinhard* check box.
- *Random scanning:* For certain applications, it is desirable not to acquire the FOVs according to a predefined pattern, as discussed in Sect. 7.5.2.2. For this reason, a random scanning procedure has been included to complement the sequential one. Clicking on the *Random fields* button, the algorithm will take as many FOVs as defined in the configuration file. In this case, due to the possible large differences in the focusing point between two consecutive FOVs, the two-phase autofocus algorithm described in Sect. 7.5.3.2 is applied for each step.
- *Stitching:* The images in the sequential scanning procedure are captured with a certain overlap between them. This fact allows to perform a stitching algorithm to combine all individual FOVs into a high resolution image. Once the sequential scanning is finished, the user can carry out the stitching through the *Stitching* button.
- *Stack acquisition and multifocus fusion:* In addition to capture images along *X* and *Y* axes, it is possible to acquire them at *Z* axis, that is, a stack of images at different focusing points. The user has to select the number of images to capture (*# Images*) and the distance between them (*Step*) and then click on the *Take stack* button to start the procedure at the current *Z* position. Also, once the stack is already captured, a multifocus fusion algorithm can be applied, clicking on *EDF* button

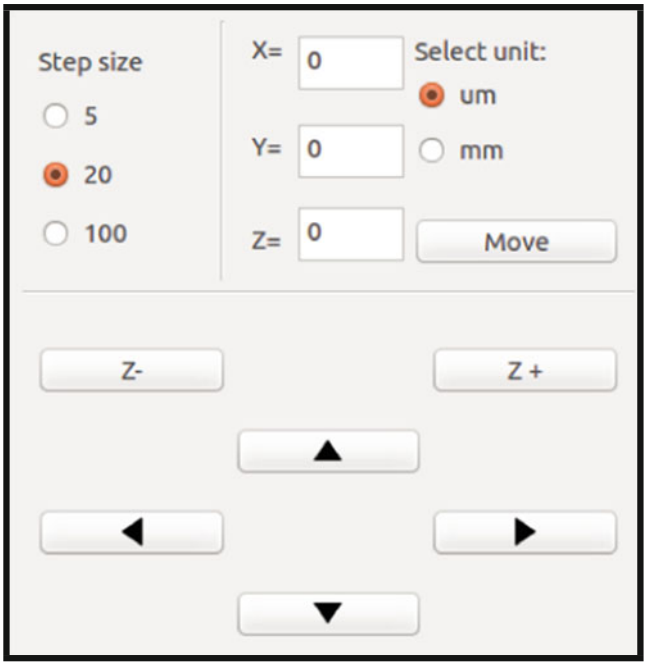

Fig. 7.20 Motorized stage control

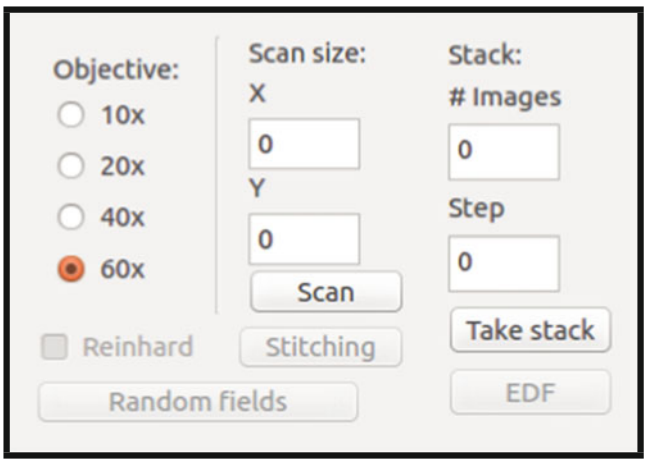

Fig. 7.21 Scanning and processing settings

that is an implementation of the *Extended Depth of Field* technique [5, 7].

References

1. Bay, H., Ess, A., Tuytelaars, T., Van Gool, L.: Speeded-up robust features (SURF). Comput. Vis. Image Underst. **110**(3), 346–359 (2008)
2. Boddeke, F., Van Vliet, L., Young, I.: Calibration of the automated z-axis of a microscope using focus functions. J. Microsc. **186**(3), 270–274 (1997)
3. Brenner, J.F., Dew, B.S., Horton, J.B., King, T., Neurath, P.W., Selles, W.D.: An automated microscope for cytologic research a preliminary evaluation. J. Histochem. Cytochem. **24**(1), 100–111 (1976)
4. European Committee for Standardization: Water quality—Guidance standard for the identification, enumeration and interpretation of benthic diatom samples from running waters. Technical report (2004)
5. Forster, B., Van De Ville, D., Berent, J., Sage, D., Unser, M.: Complex wavelets for extended depth-of-field: a new method for the fusion of multichannel microscopy images. Microsc. Res. Tech. **65**(1–2), 33–42 (2004)
6. Groen, F.C., Young, I.T., Ligthart, G.: A comparison of different focus functions for use in autofocus algorithms. Cytometry: J. Int. Soc. Anal. Cytol. **6**(2), 81–91 (1985)
7. ImageJ plugins website. https://imagej.net/Extended_Depth_of_Field (2010). Accessed 25 Apr 2019
8. Jain, A.K.: Fundamentals of Digital Image Processing. Prentice Hall, Englewood Cliffs, NJ (1989)
9. Kloster, M., Esper, O., Kauer, G., Beszteri, B.: Large-scale permanent slide imaging and image analysis for diatom morphometrics. Appl. Sci. **7**(4), 330 (2017)
10. Li, J.: Autofocus searching algorithm considering human visual system limitations. Opt. Eng. **44**(11), 113201 (2005)
11. Lowe, D.G.: Distinctive image features from scale-invariant keypoints. Int. J. Comput. Vis. **60**(2), 91–110 (2004)
12. Magee, D., Treanor, D., Crellin, D., Shires, M., Smith, K., Mohee, K., Quirke, P.: Colour normalisation in digital histopathology images. In: Proceedings of the Optical Tissue Image analysis in Microscopy, Histopathology and Endoscopy (MICCAI Workshop), vol. 100. Daniel Elson, London (2009)
13. Marty, G.D.: Blank-field correction for achieving a uniform white background in brightfield digital photomicrographs. BioTechniques **42**(6), 716–720 (2007)
14. Meiniel, W., Olivo-Marin, J.C., Angelini, E.D.: Denoising of microscopy images: a review of the state-of-the-art, and a new sparsity-based method. IEEE Trans. Image Process. **27**(8), 3842–3856 (2018)
15. Narra, P., Zinger, D.S.: An effective led dimming approach. In: Conference Record of the 2004 IEEE Industry Applications Conference, 2004. 39th IAS Annual Meeting, vol. 3, pp. 1671–1676. IEEE, New York (2004)
16. Papini, A.: A new algorithm to reduce noise in microscopy images implemented with a simple program in Python. Microsc. Res. Tech. **75**(3), 334–342 (2012)
17. Pech-Pacheco, J.L., Cristóbal, G., Chamorro-Martinez, J., Fernández-Valdivia, J.: Diatom autofocusing in brightfield microscopy: a comparative study. In: Proceedings 15th International Conference on Pattern Recognition. ICPR-2000, vol. 3, pp. 314–317. IEEE, New York (2000)
18. Perez, L., Wang, J.: The effectiveness of data augmentation in image classification using deep learning (2017). Preprint. arXiv:1712.04621
19. Pertuz, S., Puig, D., Garcia, M.A.: Analysis of focus measure operators for shape-from-focus. Pattern Recognit. **46**(5), 1415–1432 (2013)
20. Pizer, S.M., Amburn, E.P., Austin, J.D., Cromartie, R., Geselowitz, A., Greer, T., ter Haar Romeny, B., Zimmerman, J.B., Zuiderveld, K.: Adaptive histogram equalization and its variations. Comput. Vis. Graph. Image Process. **39**(3), 355–368 (1987)
21. Preibisch, S., Saalfeld, S., Tomancak, P.: Globally optimal stitching of tiled 3D microscopic image acquisitions. Bioinformatics **25**(11), 1463–1465 (2009)
22. Reddy, G.D., Cotton, R.J., Tolias, A.S., Saggau, P.: Random-access multiphoton microscopy for fast three-dimensional imaging. In: Membrane Potential Imaging in the Nervous System and Heart, pp. 455–472. Springer, New York (2015)
23. Redmon, J.: Darknet: Open source neural networks in C (2013–2016). http://pjreddie.com/darknet/
24. Redmon, J., Farhadi, A.: YOLO9000: better, faster, stronger (2016). Preprint. arXiv:1612.08242
25. Reinhard, E., Adhikhmin, M., Gooch, B., Shirley, P.: Color transfer between images. IEEE Comput. Graph. Appl. **21**(5), 34–41 (2001)
26. Sanchez, C., Cristóbal, G., Bueno, G., Blanco, S., Borrego-Ramos, M., Olenici, A., Pedraza, A., Ruiz-Santaquiteria, J.: Oblique illumination in microscopy: a quantitative evaluation. Micron **105**, 47–54 (2018)
27. Santos, A., Ortiz de Solórzano, C., Vaquero, J.J., Pena, J., Malpica, N., Del Pozo, F.: Evaluation of autofocus functions in molecular cytogenetic analysis. J. Microsc. **188**(3), 264–272 (1997)
28. Smith, S.W., et al.: The Scientist and Engineer's Guide to Digital Signal Processing. California Technical Publishing, San Diego, CA (1997)
29. Sternberg, S.: Biomedical image processing. Computer **16**(1), 22–34 (1983). https://doi.org/10.1109/MC.1983.1654163
30. Wu, Q., Merchant, F., Castleman, K.: Microscope Image Processing, 548 pp. Academic (2008). https://www.ebook.de/de/product/7100910/microscope_image_processing.html
31. Wu, Q., Merchant, F., Castleman, K.: Microscope Image Processing. Elsevier, Amsterdam (2010)
32. Yang, S.J., Berndl, M., Ando, D.M., Barch, M., Narayanaswamy, A., Christiansen, E., Hoyer, S., Roat, C., Hung, J., Rueden, C.T., et al.: Assessing microscope image focus quality with deep learning. BMC Bioinf. **19**(1), 77 (2018)
33. Yazdanfar, S., Kenny, K.B., Tasimi, K., Corwin, A.D., Dixon, E.L., Filkins, R.J.: Simple and robust image-based autofocusing for digital microscopy. Opt. Express **16**(12), 8670–8677 (2008)
34. Yeo, T., Ong, S., Sinniah, R., et al.: Autofocusing for tissue microscopy. Image Vis. Comput. **11**(10), 629–639 (1993)
35. Zuiderveld, K.: Graphics gems IV. In: Contrast Limited Adaptive Histogram Equalization, pp. 474–485. Academic Press Professional, Inc., San Diego, CA (1994)

Part III

Analysis

Segmentation Techniques

8

Gloria Bueno, Manuel G. Forero, Carlos A. Jacanamejoy,
J. Alejandro Libreros, M. Milagro Fernandez-Carrobles, and Oscar Deniz

Abstract

This chapter presents different image segmentation methods that have been proven to be suitable for diatom detection. Methods are divided into classical and deep learning techniques. Moreover, within these methods, a distinction can be made according to the segmentation of images containing several taxon shells or single taxa. For this purpose, an overview of the most important contributions to diatom segmentation is performed. This survey covers a wide range of techniques from region and contour based on those using textural and frequency-based features and the state-of-the-art methods based on deep learning, such as semantic and instance segmentation.

8.1 Introduction

Image segmentation is the process of partitioning a digital image into several regions of interest (ROIs). These ROIs can be structures or objects present in the images, like diatoms, composed of a set of connected pixels that define certain features of the ROI. Typically, segmentation techniques follow two detection approaches, that is, region-based and a contour-based method. Contour detection is given by local discontinuities of the ROIs. On the contrary, the extraction of the regions is determined by the search of homogeneous areas in terms of different properties such as intensity levels, texture, and periodicities.

Identification of diatoms is essential to estimate water quality. Currently, this task is done manually through the observation of water sample preparations through optical microscopes. According to an EU directive, a minimum of 400 valves through different fields of views (FoVs) need to be identified for determining a water quality index. This task is very tedious, and therefore, techniques that allow automatic diatom segmentation and classification are required.

Usually automatic diatom classification is done to foretell the correct name of the taxon from image samples containing a single diatom (see next chapter). However, it is common for multiple diatoms of different taxa, sizes, and shapes to appear in a single FoV along with other elements such as fragments or debris. In these cases, object detection or segmentation techniques are required to locate all the ROIs present in the image, i.e., diatom shells.

Methods of segmentation applied to diatom detection in microscopic pictures are based primarily on traditional techniques such as regional segmentation [1, 2], filtering [3, 4], and deformable models [5–7]. There are currently only three works released using deep neural networks for diatom segmentation [8–10].

Moreover, most of these methods have been demonstrated on images containing a single diatom or a single taxon. An overview of the abovementioned methods is presented in the following sections.

8.2 Classical Methods

Standard techniques like thresholding and edge detection are employed in the segmentation of diatoms. The most popular edge detection techniques used for diatom detection

G. Bueno (✉)
VISILAB, Universidad de Castilla-La Mancha, Ciudad Real, Spain
e-mail: Gloria.Bueno@uclm.es

M. G. Forero
Semillero Lún, Facultad de Ingeniería, Universidad de Ibagué, Ibagué, Colombia

C. A. Jacanamejoy
Semillero Lún, Facultad de Ciencias Naturales y Matemáticas, Universidad de Ibagué, Ibagué, Colombia

J. A. Libreros
Multimedia and Computer Vision Group, Universidad del Valle, Cali, Colombia

M. M. Fernandez-Carrobles · O. Deniz
UCLM, E.T.S.I. Industriales, Ciudad Real, Spain

G. Cristóbal et al. (eds.), *Modern Trends in Diatom Identification*, Developments in Applied Phycology 10,
https://doi.org/10.1007/978-3-030-39212-3_8

are Canny, active contours, and level set models. Another set of classical methods use filtering previous to thresholding segmentation. These methods are described as follows.

8.2.1 Region- and Contour-Based Methods

Diatoms can be obtained by identifying the homogeneous regions in the image, i.e., those areas where pixels share similar properties, or identifying pixels where a change and dissimilarity happen, these are, respectively, region-based and contour-based methods. There are several techniques for region extraction, such as clustering, region growing, splitting, and merging, being the most common techniques for diatoms detection those based on thresholding. In the case of contour detection, the most common techniques are based on gradient methods such as Canny and Deriche. Other methods based on contour detection used for diatom segmentation are deformable models such as active contour models and level sets.

8.2.1.1 Thresholding

Thresholding techniques applied to diatom segmentation allow to separate the pixels of an image between two classes: object (diatom) and background, that is, a bi-level technique also called binarization methods, which allow separating an image in regions according to a selected optimal gray value t^* based on a given criterion. Thus, pixels below the threshold value t^* take a gray value, usually zero and those above the threshold the value one.

To carry out the binarization process of an image $f(x, y)$, it is necessary to look for a threshold value $0 < t < L - 1$, where L is the maximum number of gray levels in the image (usually $L = 255$), which allows applying a transformation function defined as:

$$r(x, y) = \begin{cases} 0 \text{ if } f(x, y) > t \\ 1 \text{ if } f(x, y) \leq t \end{cases} \tag{8.1}$$

The thresholding methods may be divided into two groups according to the number of thresholds used, that is, global and local thresholding methods.

Global Thresholding Methods

In global techniques, a single threshold value is calculated for the entire image, while local methods partition the image into sub-images and a threshold value is determined for each of them. In general, global techniques are used when there is a clear definition between the background and the objects of interest in the image, and the gray levels of each region are relatively uniform. Local techniques are more adequate to binarize an image whose background varies locally or when there are variations in the gray level of the objects.

There are several criteria for the calculation of t^*. Two relevant studies of thresholding techniques have been carried out by Sahoo et al. [11] and Sezgin and Sankur [12]. Two of the most popular methods were developed by Otsu [13] and Kapur et al. [14]. Otsu considers that the histogram of the image consists of two Gaussian populations, corresponding to the background and the object. An optimal threshold value of t^* can be found by maximizing the relationship between the covariances of the object and the background, i.e., the threshold value that separates the means of the two classes as much as possible and where each gray level is closer to its class mean, that is, when the variances take the minimum possible value, which is similar to the Fisher criterion employed in probability and pattern recognition. The entropy methods are based on Information Theory developed by Claude Shannon. In the Kapur et al. method, the optimum threshold is obtained by maximizing the a priori entropy of the classes corresponding to the background and the object. Figure 8.1b and c shows the results obtained with the Otsu and maximum entropy methods, respectively.

Local Thresholding

In the local or adaptive binarization methods, the threshold changes dynamically through the image according to the local information. Local binarization can be done by moving a window over the image and calculating the threshold over each window, applying any binarization technique, like Otsu or maximum entropy. When performing local binarization, false regions can be generated, especially when the window is placed over regions that present a very slight variation in gray levels and where the gray level of the central pixel on which the window is located above the gray level. In addition, this technique is time consuming because the threshold must be calculated for each pixel of the image. To avoid this problem, Phansalkar et al. use the Otsu method to obtain a global threshold and calculates a local threshold only on regions below this threshold [15]. They propose a threshold based on the average and standard deviation of the pixels within each window. This method is an extension of the one proposed by Sauvola [16], used for the binarization of texts. Figure 8.1c shows the result obtained with the Phansalkar method. As it can be observed, a better contour can be achieved given the local nature of the threshold.

8.2.1.2 Gradient-Based Methods

Another way to detect diatoms is based on edge detection, which can be achieved through the use of gradient operators, which highlight the points where there are intensity changes in the image. For this, convolution masks to calculate approximations of the image derivatives one for horizontal changes $\mathbf{G}_x$, and one for vertical, $\mathbf{G}_y$, are applied. The convolution

Fig. 8.1 Diatom binarization by gray level thresholding: (**a**) original image, (**b**) Otsu, (**c**) maximum entropy, and (**d**) Phansalkar

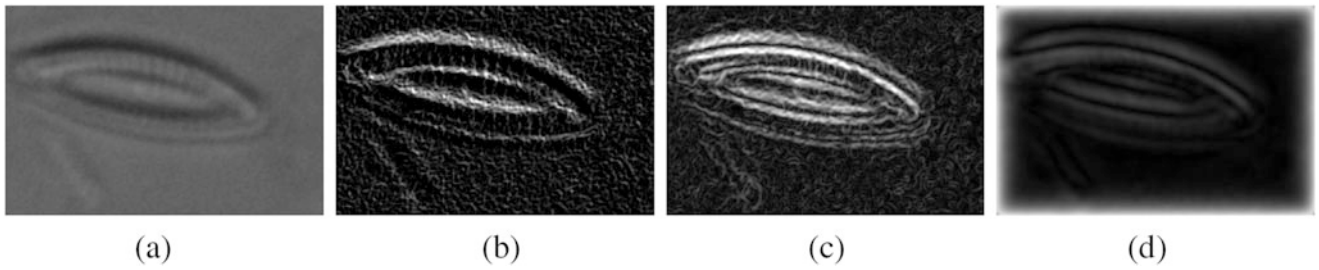

Fig. 8.2 Edge detection with gradient methods: (**a**) original image, (**b**) Sobel, (**c**) Canny, and (**d**) Deriche

masks for the Sobel operator are

$$\mathbf{G}_x = \begin{bmatrix} -1 & 0 & +1 \\ -2 & 0 & +2 \\ -1 & 0 & +1 \end{bmatrix} \quad \text{and} \quad \mathbf{G}_y = \begin{bmatrix} -1 & -2 & -1 \\ 0 & 0 & 0 \\ +1 & +2 & +1 \end{bmatrix} \tag{8.2}$$

The first to propose analytical expressions to define some optimization criteria for contour detection was John Canny in 1986. He suggested the following detection criteria:

- Good detection: The edge detector should respond only to borders and must detect them all, i.e., it is essential to detect all edges in the image without getting false edges.
- Good localization: The distance between the edge pixels found by the detector and the actual edge should be as small as possible.
- The detector should not identify multiple pixels as belonging to an edge when there is only one edge.

Canny found the optimal filter was closely given by the first derivative of a Gaussian function, which is a simple function to calculate and extend to two dimensions. Figure 8.2c shows the result obtained with this operator.

Rachid Deriche presented an extension of Canny's edge detection. Thus, he uses the same Canny criteria, seeking the realization of an infinite impulse response (IIR) filter [17].

To avoid truncation of the filter, Deriche employs a second-order recursive implementation. The application of a recursive formulation allows to accelerate the filtering and achieve a better approximation to the shape of the filter compared with the filtering technique using convolution masks, which approximates its shape through truncated sampling. Results obtained with the Deriche filter show improvement with respect to those of Canny, particularly in terms of the reduction of multiple responses [18].

When a gradient operator, as Canny or Deriche, is employed for edge detection, the gradient is available in each pixel of the image. The magnitude or norm of the gradient must be greater at the edges than on each side of the edge. In this way, the magnitude of the gradient in a pixel is large if it belongs to an edge, and it is small if it is not. Figure 8.2 shows the results of the gradient operators applied to diatom edge detection.

Once the gradient images are obtained, it is necessary to separate diatom edges from the background. The most straightforward technique consists of selecting a threshold value of the gradient magnitude and takes as edge pixels those that are higher to this threshold. However, even when an adequate selection of the threshold is made, the obtained contours may be choppy. This is due to fluctuations of the maximum gradient above and below the chosen threshold along the contour since there will always be some fluctuation in the edges of the original image due to noise. It is to be expected that only about half of the edge pixels are above the threshold, so obtained edges will not be continuous. Unfortunately, this problem occurs in most cases and it is complicated to find a low threshold value, i.e., with a high sensitivity to produce continuous edges and, at the same time, not sensitive to false edges produced by noise. Besides, this technique delivers results quite incorrect when the gradient magnitude changes strongly along contours, which may be higher than the threshold in some zones and inferior in

others, mistakenly selecting as contour pixels others whose gradient magnitude is also high. No threshold value allows obtaining the exact pixels of the edge correctly without wrongly selecting others due to noise.

8.2.1.3 Deformable Models

Deformable models allow segmenting the ROIs by closed contours. The mathematical foundations of deformable models represent the confluence of geometry, physics, and optimization. Geometry serves to represent object shape, physics impose constraints on how the shape may vary over space and time, and optimal approximation theory provides the formal mechanism for fitting the model to measure data [19]. Two deformable models have been used for diatom segmentation, that is, active contour (AC) and level set (LS) models [5–7].

Active Contour Models

Active contour modes are parametric contours embedded in the image plane, represented as closed curves $\upsilon(s) = (x(s), y(s))$. This curve may be generated automatically alongside the image boundary or manually with a closed contour next to the ROI. The curve evolves up to the boundary of the ROI, aiming to minimize an energy functional defined as:

$$E_{\upsilon}(s) = \int_0^1 (E_{internal}(\upsilon(s)) + E_{ext.potential}(\upsilon(s)))ds \tag{8.3}$$

The first term $E_{internal}$ represents the internal energy of the spline curve due to the mechanical properties of the contour, stretching, and bending [20]. Thus, the $E_{internal}$ is the sum of two components: the elasticity and rigidity energy. The second term $E_{ext.potencial}$ is a potential function that couples the curve to the image. This can be, for example, a gradient and it is responsible for attracting the contour toward the ROI in the image.

The main limitation of AC models is their sensitivity to the initial contour and not handling changes in the topology of the shape. That is, when considering more than one ROI in the image, for an initial prediction of $\upsilon(s)$ that surrounds all ROIs, the AC model is not able to detect and segment all of them, Fig. 8.3 illustrates this problem. The examples shown here use the boundaries of the entire image as the initial curve. Special topology-handling procedures must be added to solve these drawbacks. These procedures were introduced by geodesic active contour or level set (LS) models.

Level Set Models

Level set, introduced in [21], involves solving the AC minimization by the computation of minimal distance curves. Thereby, the AC evolves following the geometric heat flow equation. LS considers that there is no rigidity energy and in this way, the total curvature is reduced and smooth curves are obtained. LS can cope with changes in the topology of the shape as the surface evolves in time and it is less sensitive to the initialization. However, there are also some drawbacks in terms of convergence. The curve not always finds minimum energy and does not find the proper contour. Figure 8.4 illustrates the results of the LS applied to diatoms.

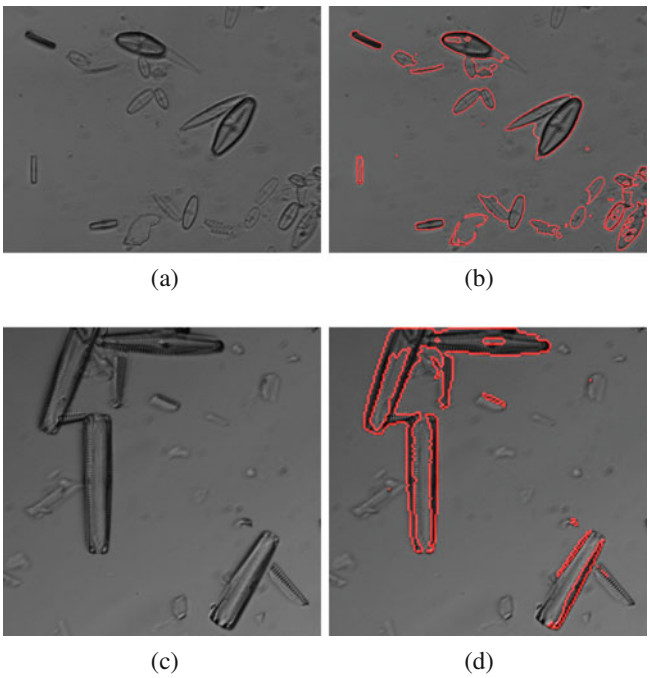

Fig. 8.3 Active contours applied to segment diatoms in a FoV image. (**a**, **c**) Original. (**b**, **d**) AC model

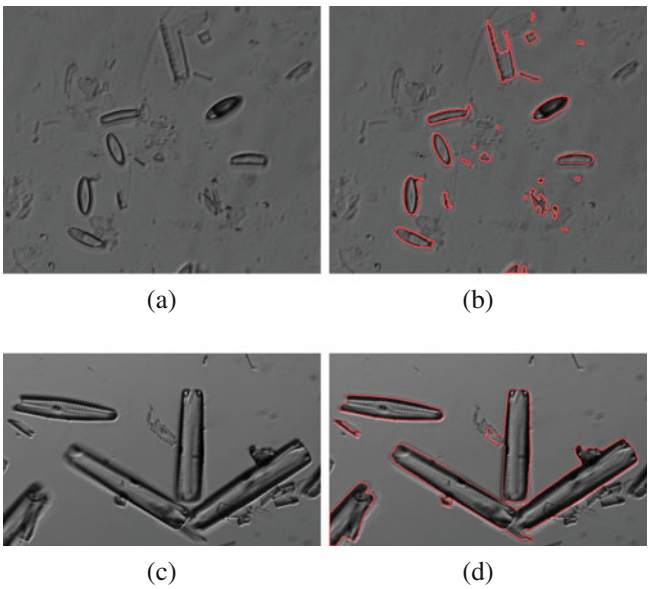

Fig. 8.4 Deformable models applied to segment diatoms in a FoV image: (1st column) original image, (2nd column) LS model. (**a**, **c**) Original. (**b**, **d**) LS model

Diatom segmentation employing deformable models works properly when only there is present a single diatom, but it is not the case when multiple diatom shells are present in the image.

8.2.2 Featured Based on Methods

8.2.2.1 Phase Congruency

The phase congruency approach (PC) analyzes local frequency information and is based on the idea that all frequency components, that is, Fourier components, are in phase in areas such as corners, edges, and texture of the objects, i.e., where signal changes occur [22].

Since the method deals with the phases of the Fourier components instead of their frequency, it is very robust to changes in contrast and lighting.

Previously, phase congruence was used as a preprocessing stage to detect contours and image enhancement [3]. Sosik and Olso have found that a threshold-based edge detection applied to phase congruency gives good results in phytoplankton images [23].

There have been different implementations since its inception, but only after Kovesi's proposal, it could be used for image processing.[1] To see further details of the implementation, the reader is referred to the journal by Verikas et al. [3].

Edges, ridges, and valleys are the main image features that are highlighted in the phase congruence analysis, as it is shown in Fig. 8.5. $PC(x)$, like the gradient operator, is sensitive to noise. However, $PC(x)$ can extract more detailed information than the Canny edge detector [24]. Once the $PC(x)$ is performed, a threshold is applied together with mathematical morphology operations such as dilation, erosion, and filling [25] that are needed to obtain a mask of each diatom and segment them (see Fig. 8.5). Though the results are better than previous segmentation methods, some diatoms are missed due to the thresholding.

8.2.2.2 Scale and Curvature Invariant

Scale and curvature invariant ridge detector (SCIRD) was presented for segmenting corneal nerve fibers [26]. It has been improved in SCIRD-TS by the modification of the derivation of the curved-support ridge detector. That means to eliminate the 0/0 indeterminate by applying SCIRD on thin structures [27]. SCIRD-TS has also been used for detecting diatoms [28].

SCIRD-TS is obtained from a Gaussian non-linear transformation, as follows:

$$F(x;\sigma;k) = \frac{1}{\sigma_2^2}\left[\frac{\left(x_2 + kx_1^2\right)^2}{\sigma_2^2} - 1\right] \times \exp\left[-\frac{x_1^2}{2\sigma_1^2} - \frac{\left(x_2 + kx_1^2\right)^2}{2\sigma_2^2}\right] \tag{8.4}$$

where (x_1, x_2) represents a point in an image coordinate system, k is a shape parameter, and $\sigma = (\sigma_1, \sigma_2)$ corresponds to standard deviations in the Gaussian distribution, at each coordinate direction. k, σ_1, and σ_2 are parameters provided by a user. From Eq. 8.4, it is possible to obtain a set of predefined filter banks by spanning a set of values as parameters of mentioned variables.

Using the set of filters, a convolution operation is performed after generating the filters bank through the non-linear function transformation. The final result is obtained as the maximum value for each pixel position between the convolution results. Each filter represents different shapes depending on the values of the $\sigma = (\sigma_1, \sigma_2)$. The method is very sensitive to noise and contrast image, so different parameter setting for sigma is needed.

Figure 8.6 shows the general scheme of the segmentation method and the different parameter setting required according to the image noise and contrast.

In this context, SCIRD-TS filters bank is applied to diatom images, following by a post-processing method in order to segment diatoms, which is similar to previous methods based on the image gradient. Besides the parameter setting, the main drawback of these methods is their limitation to properly separate diatoms when they are grouped.

8.2.2.3 Viola–Jones

Viola–Jones is an object detection method in which the main learned features are based on histogram of oriented gradients (HOG) [29]. This technique is intended to calculate and group in histograms the gradient (direction and magnitude) of the pixels in a region. This descriptor is helpful for detecting forms and contours, one of the diatom characterization's most reliable features. However, object orientation is not invariant for this method, so augmentation methods such as rotation and flips should be performed to make it more robust.

A cascade of weak classifiers are taught to use a sliding-window strategy to detect objects at various scales and positions in the picture. A scheme of how this method structured is shown in Fig. 8.7.

[1] Available on: https://www.peterkovesi.com/matlabfns/PhaseCongruency/phasecongmono.m.

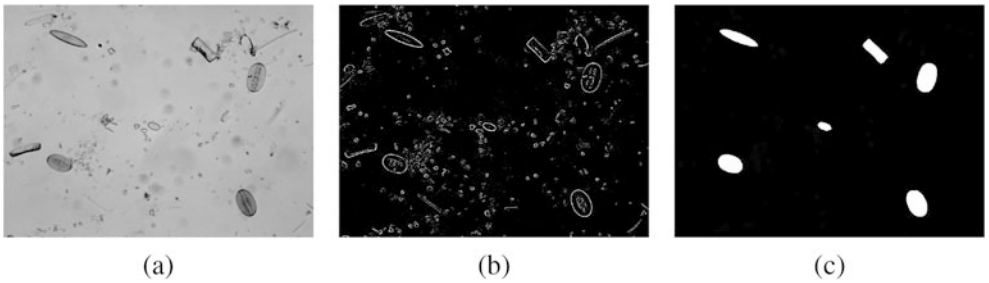

Fig. 8.5 Phase congruency in diatom images. (**a**) Original image, (**b**) result of $PC(x)$, and (**c**) result of segmentation

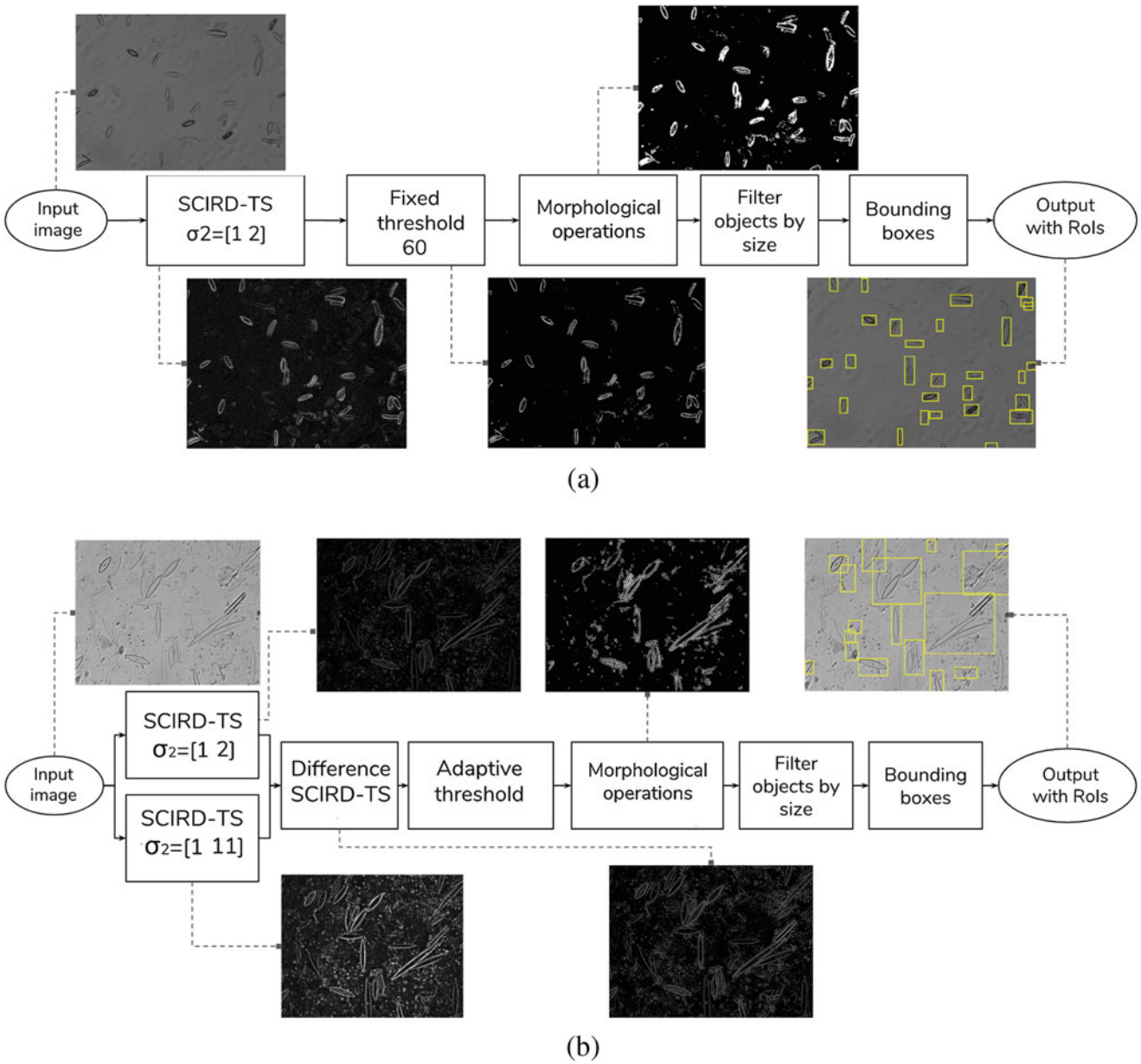

Fig. 8.6 Flowchart of the SCIRD-TS-based method. (**a**) Original. (**b**) Phase congruency

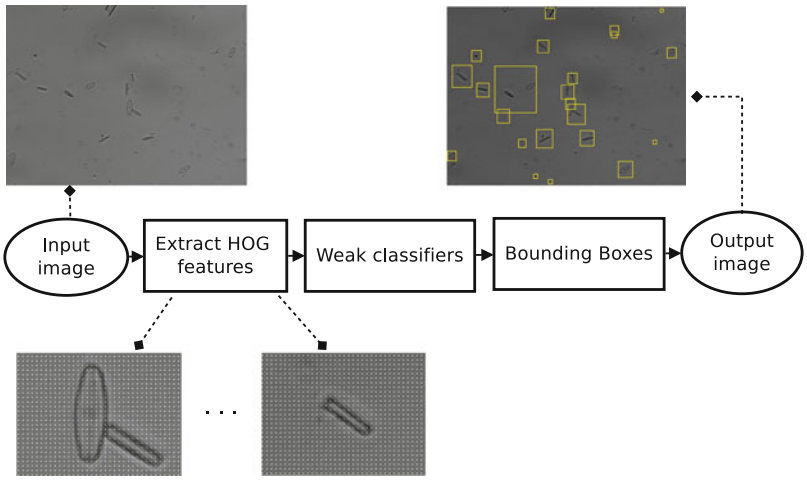

Fig. 8.7 Diagram of the Viola–Jones method

In order to train a model based on this technique, the process is carried out following these steps:

1. *Negative generation.* To improve the detector effectiveness, an appropriate set of negative pictures is developed. Usually this set is acquired from the background of regular images. In the case of diatoms, the background usually has a small range of gray values, without any kind of border. In view of this, an algorithm can be developed to generate random samples automatically according to this rule.
2. *Training process.* In order to modify the learning process, some parameters have to be set up: object training size, number of stages, true positive rate, false alarm rate, and negative samples factor.
3. *Model testing.* The parameters for detection are customized to prevent the over detection of artifacts, which is the main drawback of this technique. They are explained as follows:
   - *Minimum and maximum bounding box size.* This parameter defines the pixel size range that is considered to detect in the image.
   - *Scale factor.* After each step, the scale of the window is modified by this factor, to look for objects of different sizes.
   - *Merge threshold.* Due to the sliding-window process, multiple detection may be performed around the same object instance. With this parameter, they can be merged in a single bounding box. In this way, it proves to be useful to control the trade-off between false alarm rate and the missing detection ratio.

8.3 Deep Learning Techniques

Deep learning is currently a very active area, thanks to the increase in the computational power of the graphics processing units (GPUs) as well as the efficiency performing image convolutions. The main difference between handcrafted methods and deep learning is that the latest can automatically learn which features should be extracted from each image.

8.3.1 Neural Networks

The main idea is to construct a mathematical representation inspired by the biological neural networks of the brain, with the key component called *neuron*. This is done in accordance with two guidelines:

1. The base of knowledge is the learning process.
2. This knowledge remains accessible because of the connections that are established among the neurons, which they call synaptic weights.

So, it is feasible to state that tuning its synaptic weights is the process that enables a neural network to learn the knowledge. This is the key idea of artificial neurons. An artificial neuron (Fig. 8.8), originally called *perceptron* [30], is the basic unit with processing capabilities to build an artificial neural network. In the original definition, the components of this unit were:

- Synaptic links and a value (weight) associated with each one.
- An adding operation to sum up all the weights connected to an input.
- An activation function that conducts some non-linear conversion to the inputs.

The first implementation of a neural network was the so-called multi-layer perceptron (MLP) and was developed to separate classes linearly [31]. Generally speaking, if the n features that define a class are linearly separable, an n-

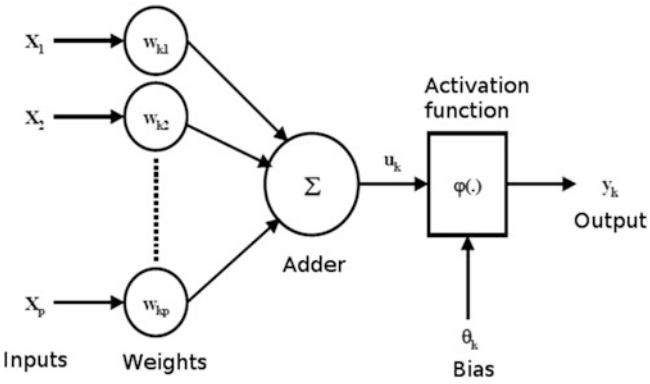

Fig. 8.8 Mathematical model of a single neuron

dimensional hyperplane can be constructed to separate them. The two most popular activation functions are the *sigmoid* and the *hyperbolic tangent*.

8.3.2 Convolutional Neural Networks

Regular neural networks are suitable for solving linear problems (e.g., representation of logical functions, numerical problems, etc.), but some problems (in image analysis processing field too) are not linearly dependent on input. As a result, these techniques cannot be used to solve them. This implies that to cope with this issue, more complicated structures need to be added to the model. For this reason, convolutional neural networks (CNNs) were developed. CNNs are a step over regular neural networks, with additional features and operations that enhance their capabilities. The "convolutional" term of their name refers to the convolutional layers that are added to emulate the response of individual neurons to a visual stimulus. These are primarily new methods to organize and apply the neurons to the information in order to extract features automatically. The learning method is guided by numerical parameters and their tuning can be essential for achieving accurate outcomes.

8.3.2.1 CNN Components

It is essential to change the dimensionality of the problem by adding image features and then compressing the information in order to enhance traditional neural networks. This is accomplished with the use of certain mathematical tools. The *convolutions* and *pooling* are the most significant ones. There are also some sophisticated methods that are helpful but not so prevalent as *L2-regularization*, *inception modules*, and *dropout*.

About activation functions, rectified linear units (ReLUs) are more prevalent rather than the traditional sigmoid or hyperbolic tangent. These functions do not depend on the input linearly. They either pass or cancel the input entirely. They have some benefits and some disadvantages, although they are appropriate in most of the cases [32]. The two main advantages are a rising in sparsity and the decrease in the probability of the vanishing gradient phenomenon. One of the primary drawbacks of ReLU functions, however, is that there is no possibility to change the amplitude of the output, as it is canceled or transferred entirely, so this can cause some issues with very large values.

The most significant parts of CNNs are the *convolution modules*, from which they take their name. The goal is to change and decrease the input dimensionality [33]. They are made of k kernels of $X \times Y$ size, so each component of the model is a neuron with its respective links.

They are defined by two parameters, apart from the size of the filter:

- *Striding*. The number of positions to move at each step. As it gets bigger, the decrease in dimensionality rises.
- *Padding*. Since the kernel may need to be computed where certain values are not present in the input (e.g., boundaries outside because of striding move), some policy needs to be set to fill these values. The primary ones are: *same padding*, filling with 0s or a fixed value the positions which are not defined, or *valid padding*, in which the kernel filter is prevented to operate before reaching the border.

Although each convolution reduces the size of the input, the use of a large amount of them in each layer leads to an increase in the problem size. To deal with that, *pooling* layers are introduced for dimensionality reduction. Using low cost operations like taking the *mean* or the *maximum* , they group and summarize the values from a previous layer. As a trade-off of this loss of information, the model becomes more general, which is one of the main objectives of these modules.

8.3.3 R-CNN

Region-based convolutional neural network [34] is a technique for deep learning applied to object detection that has been extensively used in recent years (a general scheme is presented in Fig. 8.9), along with some variants that improve the performance of certain details to enhance its speed and accuracy. This method is based on three fundamental steps:

1. Edge boxes for region proposal
   Using the algorithm described in [35], several candidate regions are obtained. These are proposed according to the concentration of edges over different areas of the input image. Moreover, a score is provided so that the likeliness of a specific region to contain an object can be measured, being possible to use it as a threshold too.
2. Region proposals rejection
   Since the previous algorithm provides several candidate regions, and most of them are overlapped, it is necessary to process them. For this reason, this step takes as input the raw regions that are highlighted previously and merges them using these criteria and a threshold:
   - Union area: given two bounding boxes, the overlap index is calculated using the intersection of both areas and also its union, as stated in Eq. 8.5.

$$\text{Union} = \frac{\text{area}(A \cap B)}{\text{area}(A \cup B)} \tag{8.5}$$

   - Minimum area: criterion is similar to the previous one, but taking into account the area of the minimum box, as stated in Eq. 8.6.

$$\text{Min} = \frac{\text{area}(A \cap B)}{\min(\text{area}(A), \text{area}(B))} \tag{8.6}$$

   Using these criteria, the obtained overlap intersection metric states how much both boxes overlap, so depending on the threshold it is decided whether it is enough or not to merge them. To perform this operation, the minimum area that includes both boxes is calculated.
3. Classification of regions
   Once the region proposals are processed, they are classified using the neural network that R-CNN has trained.

8.3.3.1 Post-processing

One of the facts that have to be considered when using this detector is that the overall performance highly relies on how well proposed these regions are. Whether artifacts or inaccurate boxes are provided to the network or, on the other hand, are discarded, they may have a significant impact over final results. For this reason, the parameters that rule this candidate box proposal have to be wisely chosen, depending on the intrinsic features of the input images and the kind of objects that ought to be detected. By tuning these parameters, every raw box can be obtained, or some of them may be thresholded, depending on their distance and similarity to other boxes.

In order to overcome this problem, a custom algorithm was developed that, given a list of candidate bounding boxes, merges them taking into account the classes they predict and their overlap ratio. The main steps of this algorithm are:

1. Check the overlap of each pair of boxes, using the criteria exposed in Eqs. 8.5 and 8.6.
2. When a positive merge is detected, a new box is built that includes both of them, and they are appended to the list for the next iteration. If not, they are appended as is (if they were not included before).
3. Go back to step 1 until the list does not change in two consecutive iterations.

8.3.4 You Only Look Once

The so-called YOLO framework (you only look once) is based on fully convolutional networks (FCNs), an evolution of the R-CNN approach and their derivatives (Fast/Faster-R-CNN), which speeds up their runtime performance by far [36]. The former methods were based on taking a model and apply it to an input image at different positions, varying also the scale, so that all the objects could be detected. However, the latter employs a single neural network to the whole input image, once. It is designed to divide the image into candidate cells (while the former carried out this process relying on extra processing algorithms, which supposed additional performance cost). Moreover, as the entire picture is supplied to the network (instead of small and isolated patches), the model is able to learn from the whole context of the objects present in the data, so its predictions are potentially more accurate.

The YOLO network splits the pictures into a cell matrix, so that each cell is accountable for voting a suggestion of candidate object. Then each box is shifted in accordance with an expected offset, so that it fits into what is expected its class in size and place. In addition, the model also outputs a confidence value to both the class of the object and the

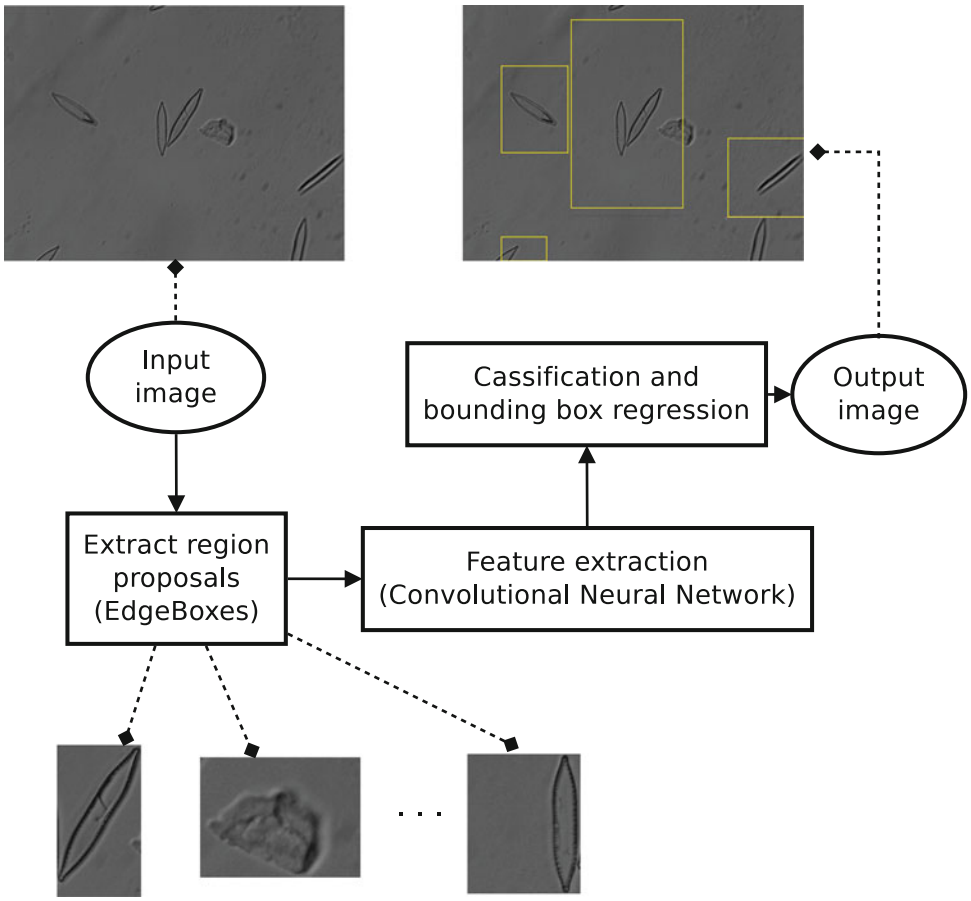

Fig. 8.9 R-CNN flowchart

bounding box. The outcome is that lots boxes are suggested, but most of them have shallow trust, so they are dismissed using a threshold. In Fig. 8.10, the structure of the method components is provided.

8.3.5 Semantic Segmentation

Semantic segmentation is referred as the task of associating each pixel of an image with a class label. The first deep learning semantic segmentation models attempted to use the deep neural networks architectures previously designed for image classification problems in pixel-wise classification. However, some key operations performed by CNNs such as convolution, pooling, and sub-sampling may cause a feature map resolution to decrease, resulting in the loss of spatial data, which is crucial for boundary delimitation. New methods have appeared to fix this, such as fully convolutional networks (FCNs) [37], DeconvNet [38], U-Net [39], or SegNet [40]. With slight variations, these models share a comparable architecture. Due to the accuracy, memory efficiency, and execution time, SegNet is chosen for this study.

SegNet's architecture consists of an encoder network, a matching decoder network, and a final pixel-wise classification step. The encoder network is composed of VGG16 network's first 13 layers, pretrained on big image classification datasets, such as COCO or ImageNet. These layers generate the feature maps through a set of convolution, batch normalization, ReLU, and max-pooling operations. Convolution and pooling operations, as mentioned above, cause a reduction in the resolution of the feature map, modifying the accuracy of the final segmentation. In SegNet, a decoder network is responsible for upsampling the input feature maps to a higher resolution and replaces the fully connected layers of VGG16. This is achieved storing the position of the

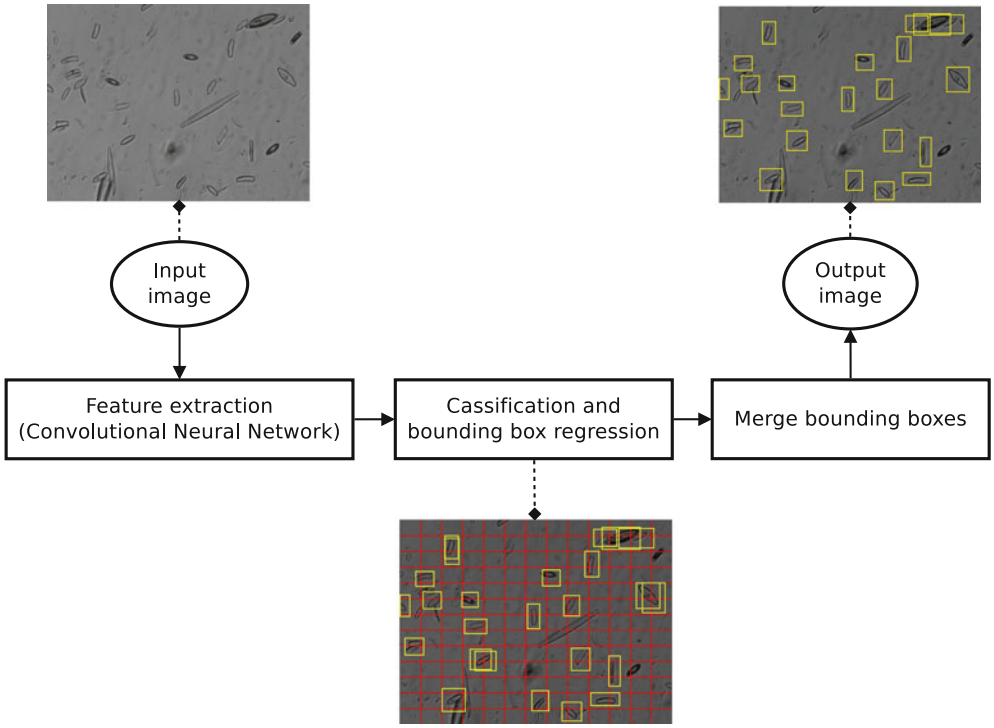

Fig. 8.10 Scheme of YOLO architecture

maximum feature value of each max-pooling layer. In this way, these indices are used for upsampling at decoding stage and the spatial information is maintained. Finally, a softmax layer performs a pixel-wise classification taking as input the high resolution feature maps of the decoding phase. A general method scheme is presented in Fig. 8.11.

Comparison of R-CNN and YOLO was presented in [9] obtaining a better result for YOLO. Another comparison between classic and deep learning methods has been made in [41] and [10]. Figure 8.12 shows results for this comparison. YOLO and semantic segmentation are the best methods. However, there is still false negative, missing some diatoms, and false positive, segmenting debris instead of diatoms. The sensitivity is improved with semantic segmentation as compared to the other methods, but there is still room to improve the precision. The main problem with these methods is that they do not separate the ROIs properly when overlapping occurs. Therefore, the quantification of diatoms is limited. To solve this, a procedure called instance segmentation can be applied. Next section describes this method also based on deep learning.

8.3.6 Instance Segmentation

Another important group of image segmentation frameworks is known as instance segmentation. These models can be defined as a combination of object detection and semantic segmentation methods. Instance segmentation relies on object detection algorithms to obtain the individual instances of all classes present in an image. Then, each ROI is classified at the pixel level to generate the output mask. These approaches have several advantages, like segmentation accuracy and overlapping object differentiation. In the first case, as only individual ROIs are taken into account (instead of the whole image), the segmentation accuracy improves. Also, overlapping objects of the same class are easily separated, unlike in semantic segmentation techniques (which only have pixel-level classification). This is important in applications like diatom identification, in which it is essential to count the number of specimens of each class. However, instance segmentation has an important drawback. As they trust in object detection methods to find the individual instances, only the

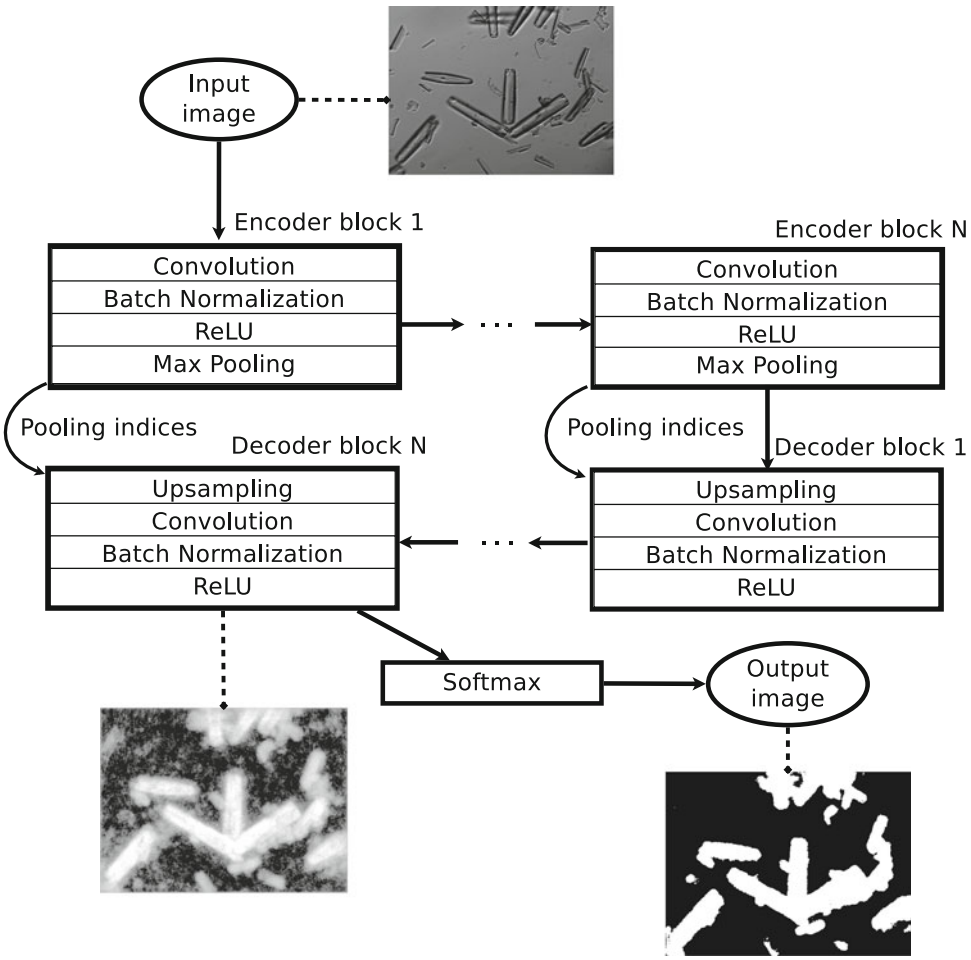

Fig. 8.11 SegNet architecture scheme

detected ones will be segmented, so its performance depends on the performance of the object detection technique used.

Mask-R-CNN provides a simple and flexible framework for instance segmentation [42]. It is a modified version of the Faster-R-CNN object detection framework with an additional branch to perform the segmentation of the detected ROIs. The first step of the framework is to create a feature map from a given image, using a CNN. Then, a region proposal network (RPN) proposes candidate object bounding boxes. The RPN takes the input feature map and, using a sliding window, several anchor boxes (of multiples scales and aspect ratios) are tested. As an output, RPN gives both the box coordinates and an object probability.

Until this point, the architecture is the same as that of the Faster-R-CNN framework, although next, we describe some important differences. *RoiPool* is the Faster-R-CNN layer that obtains the individual ROI feature maps using the bounding box proposals of the RPN. The way this operation is done introduces misalignments between the ROI and the feature maps. In segmentation tasks, an exact spatial location is crucial to predict accurate pixel masks, so in Mask-R-CNN this layer has been changed to a *RoiAlign* layer, which properly aligns the feature maps with the bounding boxes. *RoiAlign*, instead of using quantized bins in *RoiPool*, uses continuous bins and bilinear interpolation to preserve the spatial correspondence better. A fully connected branch

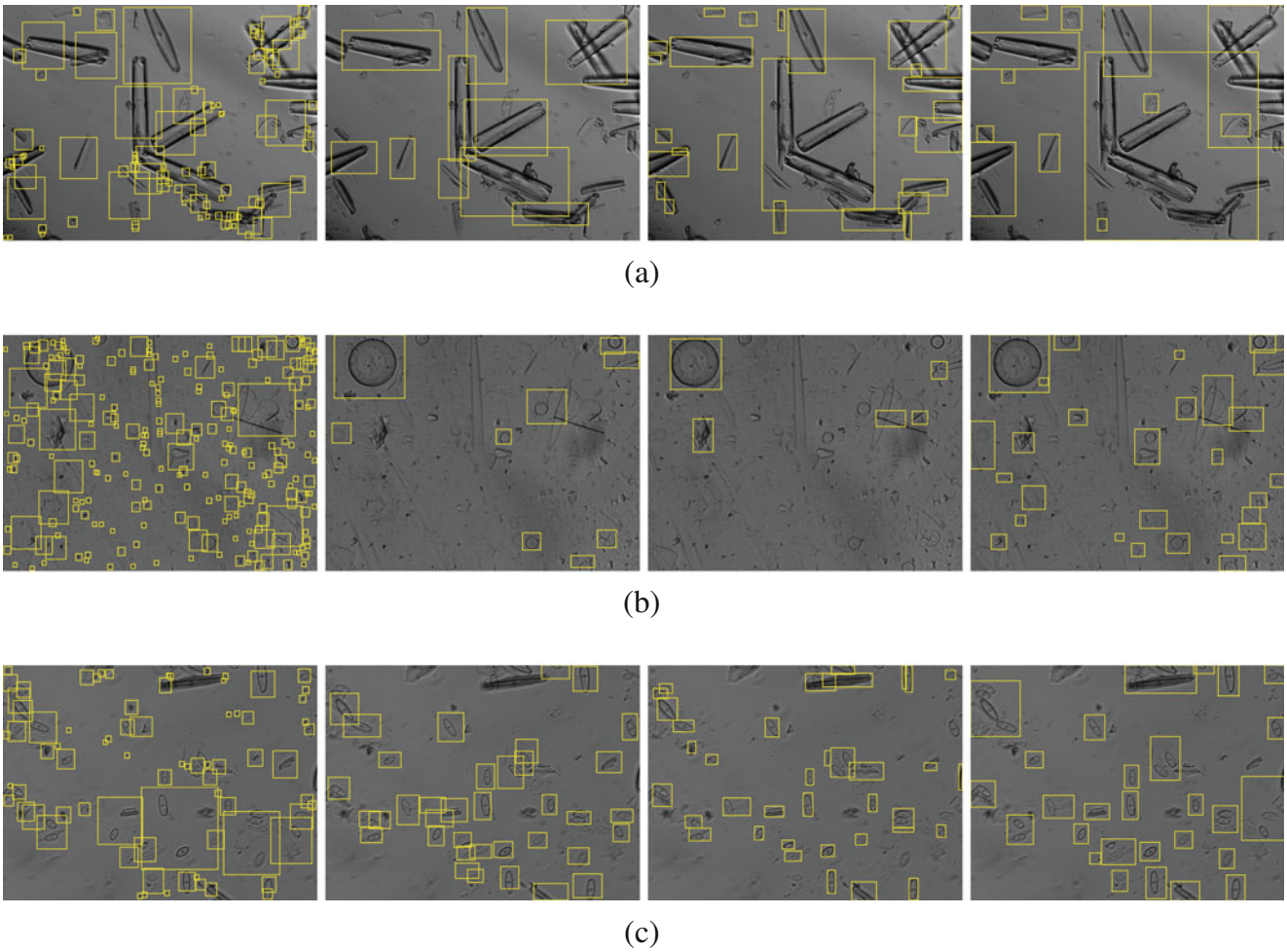

Fig. 8.12 Example of diatoms detection methods. Each column shows the output of each method: (1st) Viola–Jones; (2nd) YOLO; (3rd) SCIRD; and (4th) SegNet. (**a**) Segmentation of *Gomphonema rhombicum* taxon samples. (**b**) Segmentation of *Skeletonema potamos* taxon samples. (**c**) Segmentation of *Eolimna minima* taxon samples

predicts at the same time both the class (using a softmax layer) and the object bounds (bounding box regression). Also, Mask-R-CNN adds a parallel mask prediction branch to perform ROI segmentation. In this stage, a FCN performs a pixel-level classification for each ROI and each class, that is, a mask is generated for each class, so there is no competition between classes. A general scheme of the method is presented in Fig. 8.13.

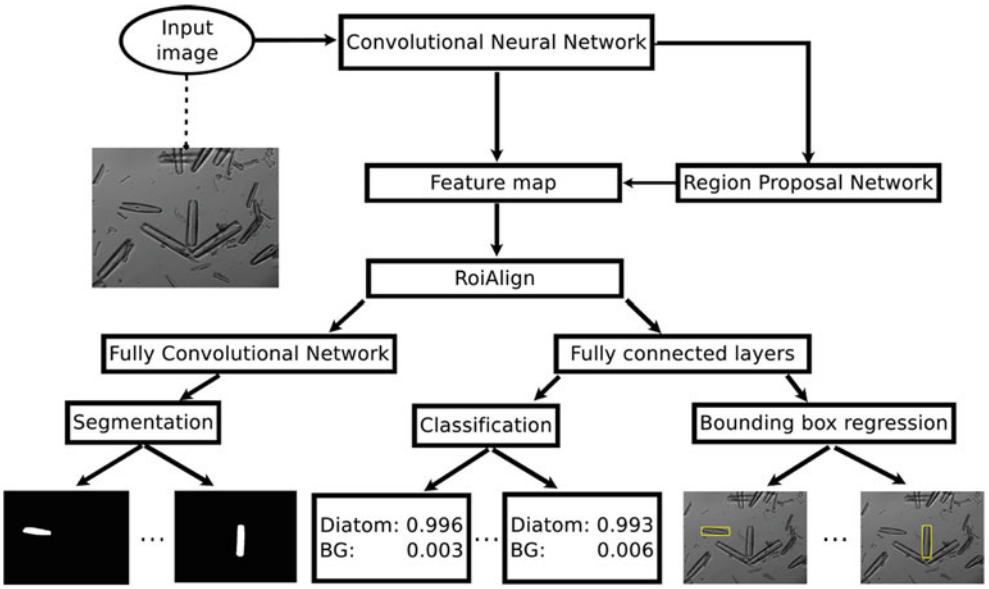

Fig. 8.13 Mask-R-CNN architecture flowchart

8.4 Conclusions

In this chapter, different segmentation methods applied to diatom detection have been described. Due to the large variety of species and the small differences between them, this is a complex challenge. The methods mentioned were both based on classical techniques such as thresholding, filtering and Viola–Jones, and deep learning. It has been shown that the best segmentation techniques are those based on deep learning due to their capability to segment diatoms on FoV composed of different shells and taxa. The best methods are YOLO, semantic segmentation, and instance segmentation. Semantic segmentation by means of pixel-wise binary classification with SegNet and instance segmentation by means of object detection by means of Mask-R-CNN. This may be due to the fact that the model has information on the global context since the network is fed with the full image. The best sensitivity is achieved by SegNet with an average of 0.95 versus 0.86 obtained with the Mask-R-CNN for instance segmentation. However, the precision with the SegNet goes down to 0.57 and is higher, about 0.85, with the Mask-R-CNN. The promising results of the instance segmentation encourage us to continue working on this complex problem to explore and improve the architecture in order to properly separate the diatoms.

References

1. Zheng, H., Zhao, H., Sun, X., Gao, H., Ji, G.: Automatic setae segmentation from Chaetoceros microscopic images. Microsc. Res. Tech. **77**(9), 684–690 (2014)
2. Rojas Camacho, O., Forero, M., Menéndez, J.: A tuning method for diatom segmentation techniques. Appl. Sci. **7**(17), 762 (2017)
3. Verikas, A., Gelzinis, A., Bacauskiene, M., Olenina, I., Olenin, S., Vaiciukynas, E.: Phase congruency-based detection of circular objects applied to analysis of phytoplankton images. Pattern Recogn. **45**(4), 1659–1670 (2012)
4. Libreros, J.A., Bueno, G., Trujillo, M., Ospina, M.: Automated identification and classification of diatoms from water resources. In: Lecture Notes in Computer Science. Progress in Pattern Recognition, Image Analysis, Computer Vision, and Applications. CIARP 2018. Lecture Notes in Computer Science, pp. 496–503. Springer, Berlin (2019).
5. Jalba, A.C., Wilkinson, M.H., Roerdink, J.B., Bayer, M.M., Stephen, J.: Automatic diatom identification using contour analysis by morphological curvature scale spaces. Mach. Vis. Appl. **16**(4), 217–228 (2005)
6. Gelzinis, A., Verikas, A., Vaiciukynas, E., Bacauskiene, M.: A novel technique to extract accurate cell contours applied for segmentation of phytoplankton images. Mach. Vis. Appl. **26**(2–3), 305–315 (2015)
7. Pereira-Borges, V.R., Hamann, B., Silva, T.G., Vieira, A.A.H., Oliveira, M.C.F.: A highly accurate level set approach for segmenting green microalgae images. In: 28th SIBGRAPI Conference on Graphics, Patterns and Images, pp. 87–94. IEEE, Piscataway (2015)
8. Tang, N., Zhou, F., Gu, Z., Zheng, H., Yu, Z., Zheng, B.: Unsupervised pixel-wise classification for Chaetoceros image segmentation. Neurocomputing **318**, 261–270 (2018).
9. Pedraza, A., Bueno, G., Deniz, O., Ruiz-Santaquiteria, J., Sanchez, C., Blanco, S., Borrego-Ramos, M., Olenici, A. and Cristobal, G.: Lights and pitfalls of convolutional neural networks for diatom identification. In: Optics, Photonics, and Digital Technologies for Imaging Applications, vol. 10679, p. 106790G (2018)
10. Ruiz-Santaquiteria, J., Bueno, G., Deniz, O., Noelia, V., Cristobal, G.: Automated diatom classification (part A): handcrafted feature approaches. Eng. Appl. Artif. Intell. **87**, 103271 (2020)
11. Sahoo, P.K., Soltani, S., Wong, A.K.: A survey of thresholding techniques. Comput. Vis. Graph. Image Process. **41**(2), 233–260 (1988)
12. Sezgin, M., Sankur, B.: Survey over image thresholding techniques and quantitative performance evaluation. J. Electron. Imaging **13**(1), 146–166 (2004)

13. Otsu, N.: A threshold selection method from gray-level histograms. IEEE Trans. Syst. Man Cybern. **9**(1), 62–66 (1979)
14. Kapur, J.N., Sahoo, P.K., Wong, A.K.: A new method for gray-level picture thresholding using the entropy of the histogram. Comput. Vis. Graph. Image Process. **29**(3), 273–285 (1985)
15. Phansalkar, N., More, S., Sabale, A., Joshi, M.: Adaptive local thresholding for detection of nuclei in diversity stained cytology images. In: 2011 International Conference on Communications and Signal Processing, pp. 218–220 (2011)
16. Sauvola, J., Pietikäinen, M.: Adaptive document image binarization. Pattern Recogn. **33**(2), 225–236 (2000)
17. Deriche, R.: Using Canny's criteria to derive a recursively implemented optimal edge detector. Int. J. Comput. Vis. **1**(2), 167–187 (1987)
18. Bourennane, E., Paindavoine, M., Truchetet, F.: Amélioration du filtre de canny deriche pour la détection des contours sous forme de rampe. Traitement du signal **10**(4), 297–310 (1993)
19. Bueno, G.: Fuzzy Systems and Deformable Models, Ch. 10, pp. 305–329. Taylor and Francis, Milton Park (2008)
20. Chan, T.F., Vese, L.A.: Active contours without edges. IEEE Trans. Image Process. **10**(2), 266–277 (2001). https://doi.org/10.1109/83.902291
21. Li, C., Xu, C., Gui, C., Fox, M.D.: Distance regularized level set evolution and its application to image segmentation. IEEE Trans. Image Process. **19**(12), 3243–3254 (2010). https://doi.org/10.1109/TIP.2010.2069690
22. Morrone, M.C., Ross, J., Burr, D.C., Owens, R.: Mach bands are phase dependent. Nature **324**(6094), 250 (1986)
23. Sosik, H.M., Olson, R.J.: Automated taxonomic classification of phytoplankton sampled with imaging-in-flow cytometry. Limnol. Oceanogr. Methods **5**(6), 204–216 (2007)
24. Li, Y., Belkasim, S., Chen, X., Fu, X.: Contour-based object segmentation using phase congruency. Int Congress Imaging Sci. **6**, 661–664 (2006)
25. Gonzalez, R.C., Woods, R.E.: Digital Image Processing, 2nd edn. Addison-Wesley Longman Publishing Co., Inc., Boston (2001)
26. Annunziata, R., Kheirkhah, A., Hamrah, P., Trucco, E.: Scale and curvature invariant ridge detector for tortuous and fragmented structures. In: International Conference on Medical Image Computing and Computer-Assisted Intervention, pp. 588–595 (2015)
27. Annunziata, R., Trucco, E.: Accelerating convolutional sparse coding for curvilinear structures segmentation by refining SCIRD-TS filter banks. IEEE Trans. Med. Imaging **35**(11), 2381–2392 (2016)
28. Libreros, J., Bueno, G., Trujillo, M., Ospina, M.: Diatom segmentation in water resources. In: Advances in Computing, pp. 83–97. Springer International Publishing, New York (2018)
29. Dalal, N., Triggs, B.: Histograms of oriented gradients for human detection. In: International Conference on Computer Vision & Pattern Recognition (CVPR'05), vol. 1, pp. 886–893 (2005)
30. Rosenblatt, F.: The perceptron: a probabilistic model for information storage and organization in the brain. Psychol. Rev., 65–386 (1958)
31. Bishop, C.: Neural Networks for Pattern Recognition. Oxford University Press, Inc., Oxford (1996)
32. Belisle, F., Bengio, Y., Dugas, C., Garcia, R., Nadeau, C., et al.: Incorporating second-order functional knowledge for better option pricing. Technical Report, CIRANO (2002)
33. Dumoulin, V., Visin, F., A guide to convolution arithmetic for deep learning, arXiv preprint arXiv:1603.07285
34. Girshick, R., Donahue, J., Darrell, T., Malik, J.: Region-based convolutional networks for accurate object detection and segmentation. IEEE Trans. Pattern Anal. Mach. Intell. **38**(1), 142–158 (2016)
35. Zitnick, C.L., Dollár, P.: Edge boxes: locating object proposals from edges. European Conference on Computer Vision, pp. 391–405 (2014)
36. Redmon, J., Farhadi, A.: Yolo9000: better, faster, stronger, arXiv preprint arXiv:1612.08242
37. Long, J., Shelhamer, E., Darrell, T.: Fully convolutional networks for semantic segmentation. Proceedings of the IEEE Conference on Computer Vision and Pattern Recognition, pp. 3431–3440 (2015)
38. Noh, H., Hong, S., Han, B.: Learning deconvolution network for semantic segmentation. In: Proceedings of the IEEE International Conference on Computer Vision, pp. 1520–1528 (2015)
39. Ronneberger, O., Fischer, P., Brox, T.: U-net: convolutional networks for biomedical image segmentation. In: International Conference on Medical Image Computing and Computer-assisted Intervention, pp. 234–241 (2015)
40. Badrinarayanan, V., Kendall, A., Cipolla, R.: Segnet: a deep convolutional encoder-decoder architecture for image segmentation, arXiv preprint arXiv:1511.00561
41. Pereira-Borges, V.R., Hamann, B., Silva, T.G., Vieira, A.A.H., Oliveira, M.C.F.: A highly accurate level set approach for segmenting green microalgae images. In: 28th SIBGRAPI Conference on Graphics, Patterns and Images, pp. 87–94. IEEE, Piscataway (2015)
42. He, K., Gkioxari, G., Dollár, P., Girshick, R.: Mask R-CNN. In: 2017 IEEE International Conference Computer Vision (ICCV), pp. 2980–2988 (2017)

Diatom Feature Extraction and Classification

9

Noelia Vallez, Anibal Pedraza, Carlos Sánchez, Jesus Salido, Oscar Deniz, and Gloria Bueno

Abstract

This chapter presents the most relevant image processing techniques and algorithms related to computing features that are able to characterize diatoms as objects in the computer vision field for further analysis and classification. For this purpose, a wide revision of the most important contributions to diatom classification is performed. Moreover, features that have been found to be suitable for this task are covered. Later on, the reader will find the main techniques for diatom classification for the two paradigms that are used nowadays: machine learning with classical methods that rely on previously selected features, or deep learning, which learns the features from the images automatically.

9.1 Introduction

Automatically classifying diatoms remains a challenge. This task requires experts with specific abilities, i.e., trained diatomists educated to identify their taxon. The number of diatom species is estimated to be over 200,000, although the number of species already studied is around 10,000 [1]. Acquiring a sufficiently large dataset of tagged data for all the species is one of the problems in automatic characterization. Another one is the fact that diatom classification is a complex task ever for experienced diatomists. Diatom characteristics are obtained on the basis of the relative abundance of distinct taxa in an assembly and the autoecological parameters of each species, which is a time-consuming task. Currently, there is no automatic system able to use differences in both texture and contour or a comparatively big amount of species to classify them [2]. Moreover, the scores of the diatom-based biological indicators are extremely susceptible to the accuracy results of the taxonomic classification as demonstrated in several studies [3].

Taxonomic identification is normally conducted using the main characteristics of the sample or visually comparing it with reference images of the taxa (see Chap. 3) [4]. In most cases, samples are examined under a microscope. Bright-field (BF), phase contrast (PC), differential interference contrast (DIC), and reflection interference contrast (RIC) are examples of the microscopes used to evaluate such microalgae. PC microscope could be appropriate for the visualization of these specimens since they are transparent. Nevertheless, the halos and shading-off that is produced is a drawback to have into account. While Halos appear altering the intensity of the boundary of the specimen, shading-off reduces the contrast towards the center part of it [5]. On the other hand, DIC microscopy is usually used to improve the contrast of diatoms. On the contrary, DIC does not have the halo problems presented in PC microscopy obtaining similar images. Regarding darkfield microscopes, using them the specimen is highlighted by a hollow cone of light that is too broad to go inside the lens of the objective. In many situations, darkfield is an appropriate way of visualizing diatoms and can replace PC or DIC.

In order to proceed further, the distinction between classification and identification in the pattern recognition (PR) terminology is worth highlighting. While the word identification answers the question: "What is the name of the taxon in front of me?" Classification, however, responds to questions like "How is this taxon related to other taxa?" A class is a collection of entities, which is identified as being similar within a specific context, according to the terminology of pattern recognition. Each class generally has a name that identifies it with each object in a class having a label that

N. Vallez (✉) · A. Pedraza · J. Salido · O. Deniz
UCLM - ETSI Industriales, Ciudad Real, Spain
e-mail: Noelia.Vallez@uclm.es

C. Sánchez
CSIC - Instituto de Óptica Daza de Valdés, Madrid, Spain

G. Bueno
VISILAB, Universidad de Castilla-La Mancha, Ciudad Real, Spain

G. Cristóbal et al. (eds.), *Modern Trends in Diatom Identification*, Developments in Applied Phycology 10,
https://doi.org/10.1007/978-3-030-39212-3_9

refers to it. In addition, classification involves assigning a class name to an entity through the evaluation of a classifier trained to automatically recognize it. In this case, we will refer to diatoms as objects or classes and classify them to obtain their corresponding taxon-name label. Therefore, each diatom taxa will be assigned to a class (using PR terminology).

Automatic diatom identification has been deeply studied in the literature from 1979. In [6], the authors proposed the identification of diatoms using coherent optics and holography-based methods. Unfortunately, this research did not affect diatomic studies, particularly as the identification scheme was too specialized and presumably too costly to be utilized by the diatomist society [7]. The work in [8] contributes to methods for phytoplankton identification using neural networks. However, the method provided is not completely automatic. Other authors suggested a hybrid optical-digital technique to identify five phytoplankton species using translation, rotation, and scale invariant operators [9]. In [10], the authors use principal component analysis (PCA) and features based on the Legendre polynomials to identify different *Cymbella cistula* species.

In addition to the above studies, the automatic diatom identification and classification (ADIAC[1]) project arose as a major effort to automatically classify diatoms [7, 11]. The studies reported 97% of the samples correctly classified using a dataset composed of 37–55 classes. To represent the diatoms, 171 features were employed. Those features used the following descriptors between others:

- Rectangularity
- Circularity
- Length–width ratio
- Size
- Stria density orientation
- Gray-level co-occurrence matrix (GLCM)
- Moment invariants
- Gabor wavelets
- Fourier or scale-invariant feature transform (SIFT).

After features were obtained, classifiers were trained to perform the desired classification.

Other works reported in the literature using shape descriptors can be found in [10] and [12]. The authors in [10] used Legendre polynomials for shape descriptors with multiple discriminant analysis for the classification of one class (*Cymbella cistula*). Falasco et al. used PCA with five classes. They obtained similar results with about 80.5% accuracy. The probability of Kohonen's self-organizing maps (SOMs) has also been used [13] to give a probability of the presence of diatoms as a biological indicator.

[1] http://rbg-web2.rbge.org.uk/ADIAC/.

Nowadays, most attempts continue to be made using hand-crafted methods or "hand-designed" techniques in which fixed characteristics are used. In other words, the techniques use specialist expertise to obtain the most important features. This approach remains useful when the available dataset is not big enough to train a convolutional neural network (CNN) [14]. CNNs are replacing hand-crafted methods obtaining higher accuracies and learning the features automatically from data. CNNs have proved to have great results in diatom classification [15].

The following sections will expose the main techniques that are employed in both paradigms.

9.2 Classification Using Machine Learning Hand-Crafted Techniques

This section is focused on presenting the main techniques and descriptors that are used to extract meaningful features from objects in images for further classification. Firstly, a revision of the main kinds of features and its analysis is stated. Later on, a review of the main algorithms for classification with this kind of features is presented.

9.2.1 Feature Extraction

Efforts are needed to translate diatomists know-how in order to identify the most appropriate characteristics to differentiate diatom species using pattern classification. The objective is to imitate human capabilities of recognizing a 3D object, i.e., diatoms, from a 2D picture. Whether specialists can differentiate diatom species with great similarities is not always fully clear. However, some diatom characteristics can be suggested regarding pattern classification.

In the following sections, hand-crafted features are defined and grouped according to their domain definition (Table 9.1). Features can be classified as spatial-domain descriptors if they are computed directly from the image or transform-domain descriptors if they are obtained from a transform of the image. Morphological, statistical, local binary patterns (LBP), and Hu moments features are examples from the former category. On the other hand, Gabor, elliptical Fourier, and phase congruency-based features are categorized as transform-domain descriptors.

As a primary step to extract useful features, segmentation of the diatoms is usually required. The segmentation process is covered in Chap. 8.

9.2.1.1 Morphological Descriptors

Morphological descriptors are usually computed from the binary masks obtained during diatom segmentation. They have mainly related to the frustule's contour and the area.

Table 9.1 List of hand-crafted feature descriptors divided into categories

Domain	Type	Description
Spatial	Morphological	Extract some properties from the segmented area such as size, shape, or roundness
	Statistical	Measure the statistical properties of a texture based on the image histogram and the co-occurrence matrices
	LBP	Used for texture characterization. Extract a vector from the entire image with a predefined neighborhood
	Hu moments	Describe both morphologically and statistically the texture
Transform	Log Gabor	Compute texture features though the Log Gabor transform
	Elliptical Fourier	Describe the contour of the segmented area
	Phase congruency	Characterize the texture

The most common measures employed are the following:

- *Area*. Measures the diatom size by calculating the amount of pixels in the binary mask.
- *Eccentricity*. It reflects how the form of the object is similar to a circle. It is possible to define three eccentricity measures. The first one defines the ratio between the larger and the lower radius of the diatom measured from the center of mass or centroid. These distances are also known as the outer and the inner circumference radius. Similarly, another one fit an ellipse to the mask and calculated the semi-axis ratio from it. The last measure uses the above ellipse semi-axis but obtaining the ratio of their inertia moments (see Sect. 9.2.1.4 for more information about the moments).
- *Perimeter*. It is defined as the number of pixels contained in the diatom's contour. The pixels that belong to the diatom boundary are the ones that have in the mask non-zero values but have at least one neighbor equals to 0.
- *Shape*. This is a metric of the object's elongation.
- *Fullness*: It measures the relation between the area of the mask and the area of the bounding-box. The bounding-box area is the area of the rectangle that encapsulates the diatom mask.

9.2.1.2 Statistical Descriptors

While examining some materials, certain homogeneity in their appearances can be observed as if they followed some pattern. These visual patterns are known as textures (see Fig. 9.1 that contain diatoms with different striae textures). Textures may vary depending on each object and its resolution. Moreover, the appreciation of a pattern at a given resolution could be different from the appreciation of the same pattern at higher or lower resolutions. In texture analysis, the study of the image through statistics with order one or higher is usually applied [16].

Statistical texture analysis studies the properties of the image using a set of features that characterize it. These features can be classified into first, second, or higher order features based on how they are calculated. In this case, all statistical features have been drawn from 1st and 2nd order analysis.

- *First order statistical descriptors*. They compute common statistics measures from the histogram of an image, $h(i)$, using the same number of bins as intensity levels (255 bins for a grayscale image with 8 bits) [17]. The values of the descriptors that belong to this group vary when intensity levels vary but they ignore any permutation of those values. Some common statistics used are mean, variance, quartiles, asymmetry, etc.
- *Second order statistical descriptors*. They were proposed due to the inability of 1st-order statistics to classify different textures with equal histogram distributions. They are computed from gray level co-occurrence matrices (GLCMs). A GLCM, $c(m, n)$, describes the distribution of the pixel values co-occurring at a specified distance (d) and angle (θ). In addition, they can be employed to characterize image texture patterns calculating the so-called Haralick coefficients defined in [16] such as energy, contrast, correlation, and homogeneity.

9.2.1.3 Local Binary Patterns

Local binary pattern (LBP) operators are based on the concept that texture characteristics can be seen as patterns within homogeneous areas [18–21]. They represent micro-characteristics of the object and provide a "texture spectrum." LBPs usually use a 3×3 window and compare the value of the central pixel with those of the rest of the windows. Pixels with greater values than the central pixel value are marked with "1" and the rest are marked with "0". After that, the marked pixels are linearly combined using a defined weighting function to be assigned with a label. Although the 3×3 window is the most used structure, other shapes like circles can also be applied to select the neighborhood [22].

Once the labeled image is computed, its information is represented through a histogram. This histogram is then used as a "fingerprint" of the analyzed area, i.e., the part of the diatom under examination [14].

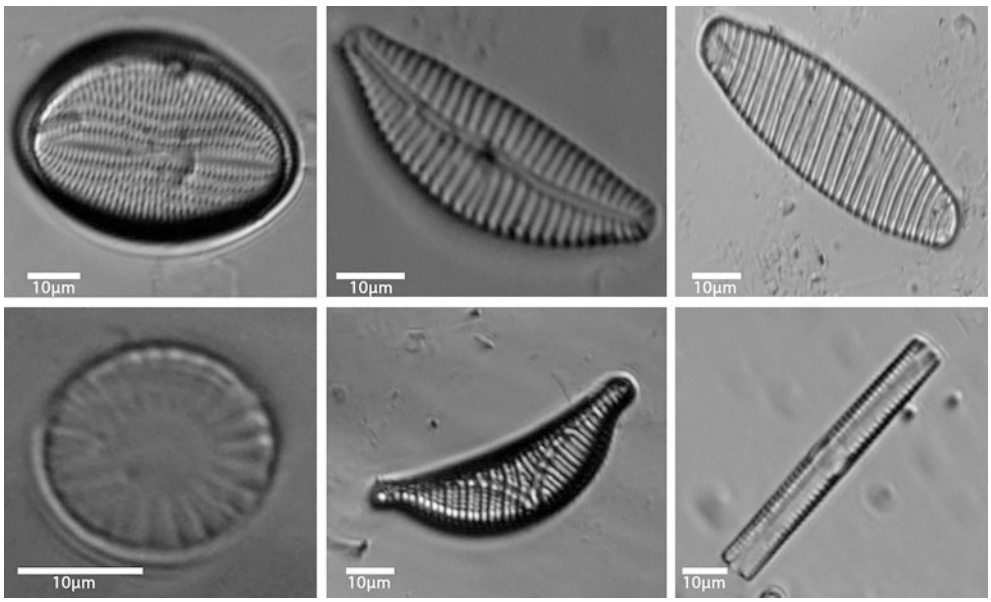

Fig. 9.1 Diatoms with different striae texture

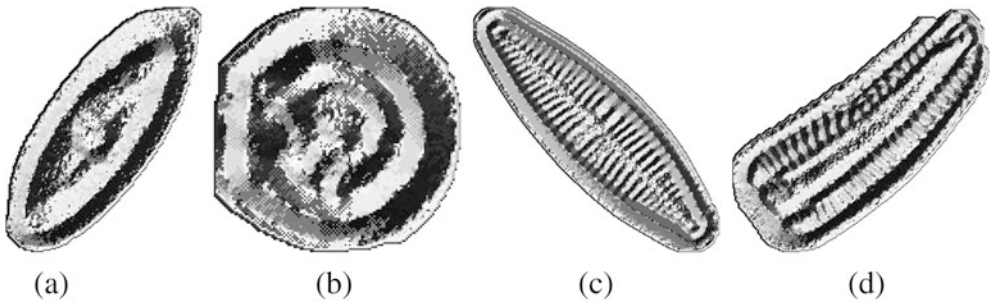

Fig. 9.2 Images obtained from the application of the LBP. (**a**) *Achnanthes subhudsonis* var *angusta*; (**b**) *Discostella pseudostelligera*; (**c**) *Gomphonema micropus*; (**d**) *Rhoicosphenia abbreviata* [23]

Figure 9.2 shows some examples of LBP corresponding to some diatom species.

9.2.1.4 Hu Moments

The moments from an image offer good morphological and statistical shape descriptions. They were evaluated in order to describe image patterns in a multitude of applications. Commonly used moments are "geometric (or Hu's) moments" [24], "Zernike moments" [25], "rotational moments" [26], "complex moments' [27], etc. Since Hu moments are translation, rotation, and scale invariant, they have been widely employed in the literature [28]. From the Hu moments, seven features are usually calculated [15].

9.2.1.5 Log Gabor Transform

Features which are concealed in some way are expected to be more visible in the frequency domain. Some transformations can therefore be applied in this domain to the image in order to evaluate its characteristics. As a result, the diatom texture can also be analyzed with Log Gabor filters. In the frequency domain, they are defined as shifted from the origin Gaussian functions avoiding the singularity of the logarithmic function. This Gaussian envelope is then modulated by a complex exponential with even and odd phases to characterize diatom edges. Finally, the Log Gabor descriptors are obtained from the energy of each scaled level and first and second order statistics features are commonly measured for each subband.

Figure 9.3 depicts the results of applying the log Gabor filters to a diatom image using four bands.

9.2.1.6 Elliptical Fourier Descriptors

Elliptical Fourier descriptors (EFD) obtain the Fourier coefficients of a closed contour [29]. First, a point in the image contour is selected as the initial point. From that point, the Freeman chain code is obtained. With the chain code, it is possible to define the complete contour as a set of segments between two consecutive points. Finally, the Fourier coefficients corresponding to the first n harmonics of the x and y projections are calculated from the Freeman

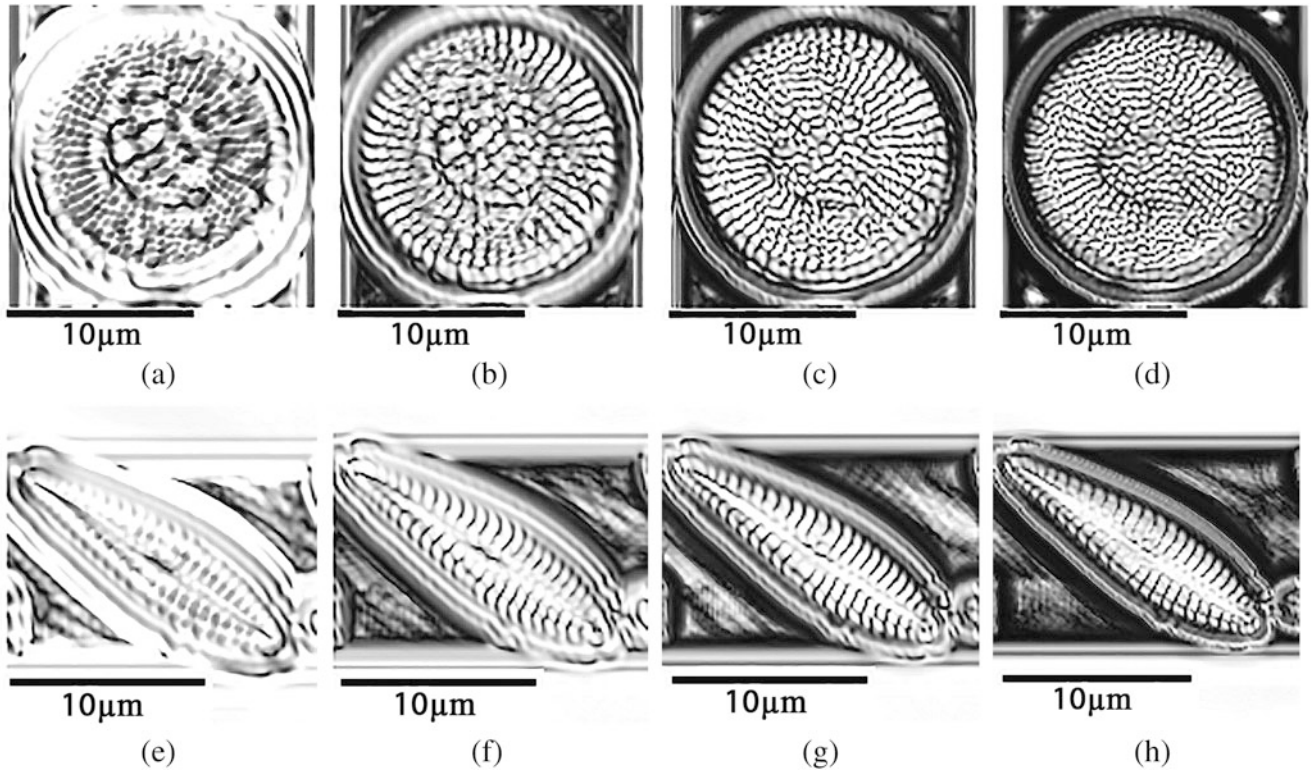

Fig. 9.3 Results from the application of the Log Gabor filters to a diatom image: (**a–d**) *Cyclostephanos dubius*; (**e–h**) *Gomphonema insigniforme* [23]. Four bands were applied (G1, G2, G3 and G4): (**a**) and (**e**) are from G1, (**b**) and (**f**) are from G2, (**c**) and (**g**) are from G3, and (**d**) and (**h**) are from G4

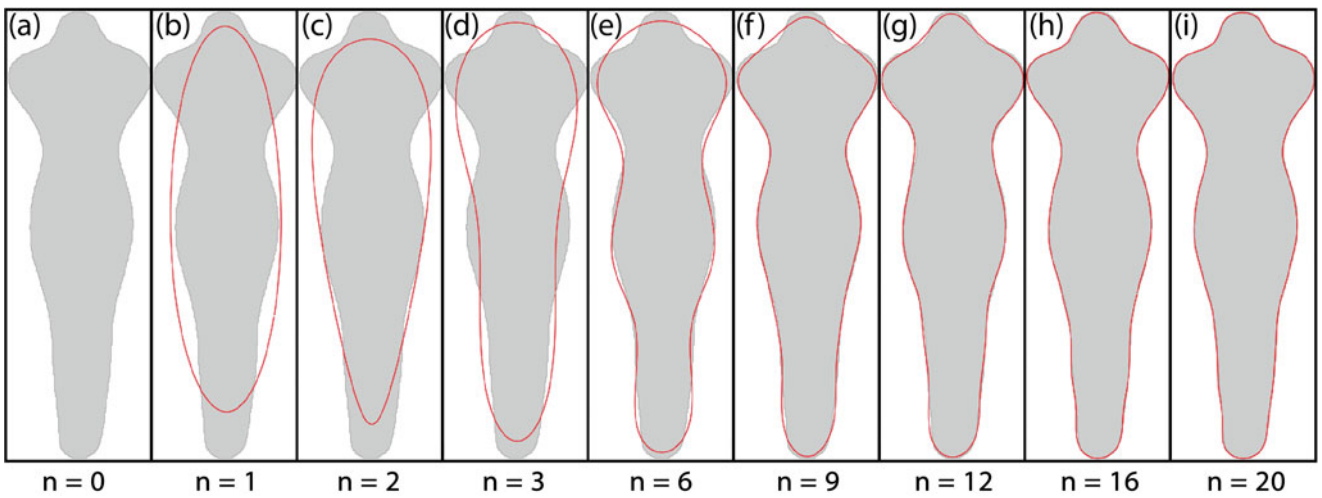

Fig. 9.4 Reconstruction of the diatom contour using EFD with different order descriptors (**a**)–(**i**) using n harmonics [23]. Generated using the code available in [30]

chain code. The more coefficients are used to provide the approximation of the contour, the more accurate it will be (Fig. 9.4).

9.2.1.7 Phase Congruency Descriptors

Phase congruency (PC) has been described in Chap. 8 for contour improvement and segmentation. Here, PC is applied for extracting discriminant descriptors. Mean and standard deviation are obtained from two PC momentum images. One represents the PC maximum (M) momentum, whereas the other represents the PC minimum (m) [31, 32]. In the end, four phase congruency descriptors can be obtained. Figure 9.5 depicts m and M images obtained from one diatom sample.

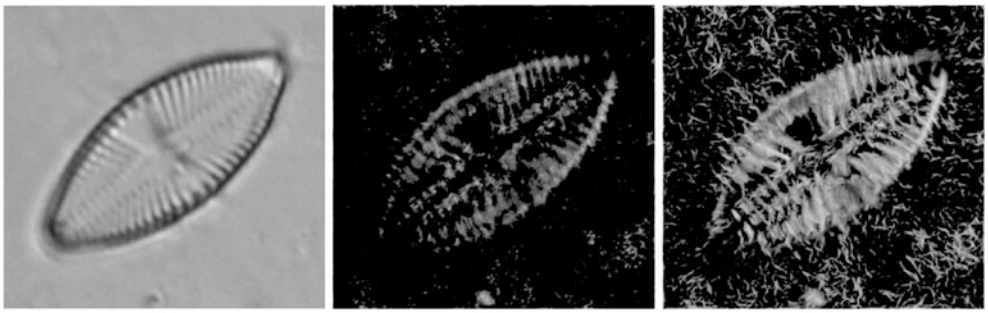

Fig. 9.5 (**a**) Sample (*L. goeppertiana*). (**b**) PC minimum momentum image (m). (**c**) PC maximum momentum image (M) [23]

9.2.2 Feature Discriminant Analysis and Dimensionality Reduction

Not all the features that can be extracted are discriminating for the problem we are facing because they define characteristics that are shared between groups or are correlated with other characteristics (redundant). In this situation, these features will provide unnecessary data that is likely to affect classification performance not only in terms of accuracy, but also in terms of training and classification required times [33, 34]. Thus, feature selection methods should be used to remove the redundant features. As a necessary procedure, the correlation coefficient can be used as a way of measuring the differences between features to discard unnecessary descriptors. Other techniques such as sequential forward feature selection (SFFS), linear discriminant analysis (LDA), and principal component analysis (PCA) are commonly applied to reduce the number of descriptors.

9.2.2.1 Correlation-Based Feature Selection

With the correlation-based feature selection method, the "maximal information compression index" is used to measure feature similarities for the entire bank of the calculated descriptors [35]. This index is the smallest eigenvalue, λ, of the covariance matrix obtained from the examined set of features. For those features that are not linearly independent, the value of λ is equals to 0. Otherwise, its value is proportional to the dependency degree between the features. Finally, to remove the redundant features, a threshold is established (usually 95%).

9.2.2.2 Sequential Forward Feature Selection

Sequential forward feature selection (SFFS), also called "floating search method," can also be applied to discriminate which descriptors are redundant [36]. The SFFS algorithm finds the group of features from the original set which provides the higher classification performance. The selected set starts empty and then features are added until there are not features that increases the classification accuracy of the subset. Therefore, the SFFS algorithm relies on a classifier. There is a similar method called sequential backward selection (SBS). In this case, features are removed from the full set until removing any feature increases the classification error. In both cases, the set of features is an ordered list that is sort according to their discriminant capability.

9.2.2.3 Principal Component Analysis (PCA)

Principal component analysis (PCA) is a feature extraction method that transforms several features into a smaller set of uncorrelated features that are the so-called principal components. It also finds a new feature space where the basis vectors represent the directions in which data has the maximum-variance in the original space [37].

To perform PCA and obtain the new features, the covariance matrix of the standardized[2] original features is diagonalized obtaining the eigenvectors and the eigenvalues. Since eigenvectors are in the descending order, the first new features can explain the largest amount of variability of all the original ones.

9.2.2.4 Linear Discriminant Analysis (LDA)

Another common technique applied for reducing the problem dimensionality is the linear discriminant analysis (LDA) [38]. This method projects the features onto a new space with lower dimensionality. Moreover, this new space enhances the separability of the classes and helps to minimize the overfitting effect and the computational cost.

9.2.3 Classifiers

Once the best feature subset is obtained, the purpose is to find a classifier that achieves the highest possible accuracy when it is applied to predict the taxon. There are two main classifier types according to the learning task they resolve:

[2] A standardized feature is a feature rescaled to have mean = 0 and std = 1.

supervised and unsupervised. Whereas supervised classifiers use the known ground truth of the data (data needs to be labeled according to the taxa), unsupervised classifiers do not have prior knowledge of the correct output values. The most representative classifiers for each type are explained below.

9.2.3.1 Supervised Classifiers

Supervised classifiers are functions that map the extracted features to an output probability of belonging to a given class. There is an extensive range of classifiers in the literature such as *k-nearest neighbors* (kNN), *support vector machines* (SVM), and *decision trees*.

k-Nearest Neighbors (kNN)

The *k-nearest neighbors* (kNN) classification method labeled each sample with the name of one of the available classes. To achieve that, it takes into account the classes from the k nearest neighbors selecting the one shared between most of them. As other methods, it gives a value indicating the degree of confidence of the class assignation [39]. In general, the distance between two samples is calculated using the Euclidean distance between their feature vectors. Although kNN is probably the simplest classification techniques, it depends heavily on the k value selected and, since there is no rule to select its value automatically, a process of trial and error should be accomplished.

Support Vector Machines (SVM)

Support vector machines (SVM) classifier is one of the best available classifiers that has been employed to solve many classification problems. SVM obtains a function to discriminate samples from different classes maximizing the margin existing between them. To achieve this goal, the feature space is transformed into another one where classes can be separated by the wider possible hyperplane. SVM may act as both linear and non-linear classifiers according to the *kernel* function selected. The *kernel* is the function able to map the set of features onto the new space where they can be separated linearly. Associated with SVM, the concept of "functional margin" is defined as the distance between the obtained hyperplane and the nearest training data. This margin is used as an confidence interval of the classifier results [40]. Thus, the objective of the SVM classifier is to maximize not only the training accuracy but also this margin [40]. The resulting margin is also related to the classifier generalization capability.

Bagging Trees

Both a *decision tree* (DT) and a random forest are methods that use a tree data structure to perform the classification. In these trees, the leaves are the class labels, whereas a branch accounts for the specific feature combination and values that conduct to a leaf [41]. The root of the tree and each intermediate node represent the initial state of the tree and the middle states in which features are evaluated for selecting a specific branch.

DTs learn how to classify new instances by splitting the input dataset into different subsets depending on a feature value in each node. This step is then repeated until a leaf is reached. When this occurs, the sample is assigned to the class specified by the leaf.

Once the decision tree has been constructed, classification of new samples starts from the root applying the feature test condition of the node to the sample and then following the corresponding branch, depending on the feature value, to reach a leaf or a new node. This process is repeated until the sample reaches a leaf. When the sample reaches a leaf, the class label of that leaf is assigned to it.

The *bagging tree* classifier improves the robustness of the solutions and the tree-based classifier accuracy by selecting between the outputs of several trees trained with subsets of the original training set. The method uses the bootstrap procedure with replacement to obtain those subsets. Every tree is a grown and unpruned binary tree, with each intermediate node of the tree dividing the data according to the value of a certain feature [42].

9.2.3.2 Unsupervised Classifiers

Contrary to supervised classifiers, the unsupervised ones are used to cluster the data without using the ground truth labels. They are capable of learning the inherent groups of our data. When the number of classes is known, these methods are categorized as "semi-unsupervised" methods because the number of clusters can be fixed.

Some common algorithms include *k-means clustering*, *hierarchical agglomerative clustering*, and *balanced iterative reduced clustering using hierarchies* (BIRCH).

k-Means

The *k-means* procedure divides all the samples in the dataset into k clusters, minimizing the difference between the mean of all the data (cluster centroid) and their particular value [43]. The initial centroids are calculated randomly and are updated when the assignation of a feature to a cluster is performed. The result of the algorithm is a space partitioned in k regions known as Voronoi cells. A different but related approach is the *k-medoids* [44], which uses instead the squared Euclidean distance to certain datapoints initially selected (medoids).

Hierarchical Agglomerative Clustering

Hierarchical agglomerative clustering [45] is another clustering method that builds a hierarchy of clusters following either a "bottom-up" or a "top-down" procedure.

- *Bottom-up* or *Agglomerative*. The process starts assigning each sample to a different cluster. Then, all the clusters start to be merged in order to minimize the distance between the elements inside each cluster (typically the Euclidean distance). This process is repeated until the provided number of clusters is reached.
- *Top-down* or *Divisive*. All observations are assigned to a unique cluster at the start. Then, each cluster is split recursively until the number of clusters is one established.

Balanced Iterative Reduced Clustering Using Hierarchies (BIRCH)
Balanced iterative reduced clustering using hierarchies (BIRCH) is a clustering algorithm that consists of four defined steps to construct a *clustering feature* (CF) tree used for multiple clustering [46].

- *Phase 1*. The available date is used to build an initial CF tree.
- *Phase 2*. Outliers are removed from the CF tree and crowded subclusters are grouped to form a smaller CF tree (clustering the leaves).
- *Phase 3*. It performs a tree size reduction through a global clustering method.
- *Phase 4*. This phase is not mandatory. It is used to refine the results from the previous clustering and obtain new clusters using the phase 3 centroids to feed the clustering algorithm.

9.2.4 Classification Performance

Classifier performance is commonly represented by the ability to recognize new instances, known as accuracy. If it were possible to use all the possible observations from the feature space, it would be possible to calculate the exact accuracy of a classifier. Since this is impossible, there are some methods to estimate its performance.

- *Re-substitution*. The classifier is trained with all the available observations and tested it with all of them too. In this case, the classifier is trained and tested using the same dataset and overfitting may arise being the accuracy estimation could be too optimistic.
- *Hold-out*. The dataset is divided into a set used for training and a set used for testing. With this method, the accuracy is underestimated. This fact is aggravated where it is applied to a small dataset.
- *Cross-validation*, also called k-fold cross-validation (*k-fcv*). It starts dividing the dataset into k with the same number of samples if possible. After the division, one part is selected to test the classifier and the remaining $k-1$ parts are joined to get the training set. The process is repeated k times (one for each subset). Finally, the accuracy is computed as the average of the accuracies of the k tests. This estimation is considered the best among all the methods.

For unsupervised techniques, other metrics have been proposed in the literature [47, 48]. They are based on the clusters obtained and the ground truth of the test dataset in some cases.

- *Adjusted Rand Index (ARI)*: This index varies in range $[-1, 1]$, being 1 a perfect score. It is used to measure the similarity between the ground truth and the assigned clustering labels.
- *Silhouette*: This index varies in range $[-1, 1]$. It measures the similarity existent between a certain element of a cluster and the other members of the same group compared to the members of other clusters. Values close to 1 represent well-defined clusters.
- *Adjusted Mutual Information (AMI)*: This metric varies in range $[-1, 1]$. It is used to compare the level of agreement existing between the ground truth and the clustering class assigned, indicating a significant agreement if its value is close to 1.
- *Homogeneity*: This metric indicates if a cluster is composed only of elements of one same class or different ones.
- *Completeness*: This metric indicates if all the elements of a particular class have been assigned to the same cluster.

9.3 Classification Using Deep Learning Techniques

Deep learning and convolutional neural networks has been presented in Chap. 8. Here we describe the learning process and parameters of the CNN for classification purposes. The insights visualization of the learned features of one CNN used for diatoms classification is also described. Finally, the diatom classification results obtained with CNN compared to other techniques are presented.

9.3.1 Learning Process

In traditional classifiers, features are manually selected (contrast, contours, eccentricity, shape, or intensity, for example). Nevertheless, deep learning learns how to classify not only the images in classes, but also the most appropriate features to represent them. This is achieved by reducing the dimensionality of the first layers and the weights learned, which store this information within them. Considering this,

it is worth noting that these models' normal architecture organization is usually as follows:

1. First, the input layer, which is provided with a picture (a collection of organized pixels).
2. Then, a concatenation of convolutions, poolings, or rectifiers. In earlier layers, the basic shape characteristics are learned. As the layers go deeper, the learned features are more complex and linked to the particular objects present in the classes.
3. Later, fully connected are employed. They do not reduce the dimensionality, so no information is lost, and take advantage of every learned feature to establish relationships between features and layers.
4. Finally, a classifier as *softmax* is used so, from the probability distributions of the fully connected layers, the class to which the input sample belongs is determined.

CNNs learn because they iteratively modify the weights of the neural connections to adjust them towards the solution. This is mainly achieved by the stochastic gradient descend (*SGD*) algorithm based on a *loss function* that measures the quality of the weights depending on how well the model scores on the validation data. Thus, the objective is to minimize the value of the loss function.

9.3.2 Parameters

The use of all these parts in the learning process, as it can be assumed, presents enormous opportunities for creating models based on the distinct transformations that fit a particular problem. In addition, how the training is regulated also implies the presence of many parameters to be adjusted to ensure the model converges to a solution. The main techniques to achieve this purpose are going to be explained here: *weight decay*, *learning rate*, *momentum*, and *learning policy*.

Weight decay determines how the loss function will be affected by the weights. This parameter is quite helpful in preventing overfitting (the model will learn the training samples quite well, but the efficiency will drop when unseen samples are tested). An standard value is ≤ 0.0005.

Another significant element is how much weights are adjusted in each step (each moment a batch of samples is supplied to the net during the learning phase) with regard to the gradient of loss. The *learning rate* controls this. As an advise, maintaining a small value, around 0.01, is appropriate, as any bigger one could unstable the learning process, making it difficult to converge. Small values, however, could remain the training stuck to a minimum local level.

The *momentum* is a parameter linked to the prior one. Its objective is to complement the learning rate, so it is important not only the weight variation, but also the values before. This parameter works as a way to remember when the weight is changed and consider the past values. For example, a value of 0.9 implies that, when calculating the weights in the present step, prior weights will still influence a 90% in the final value.

In addition, decreasing the value of the *learning rate* may be logical when the model approaches the solution to avoid divergence. The *learning policy* does this. It indicates how to reduce the rate of *learning* as the training advances. For instance, a *step* policy that lowers the learning rate with a factor of 10^{-1} every n iteration is usual. Other options such as *sigmoid*, *exponential*, *inverse*, or *polynomial* are also common [49].

9.3.3 Insights Visualization

When applying convolutional neural networks, it is appropriate to visualize the filters containing the learned features as well as the activations produced with a given example. A CNN model's learned knowledge is stored in the weights of its layers, mostly in the convolutions. The illustration will be limited to the layers of convolution 1 and convolution 2 as they are the most important and visually expressive layers.

Since AlexNet is the only CNN used for the classification of diatoms, we are going to use it to illustrate the learned features [15]. AlexNet contains five convolutional layers with max-pooling layers after them. Finally, three fully connected layers are placed at the end (Fig. 9.6). Figure 9.7 illustrates the filters in the first convolution layer in AlexNet. As an interpretation of the layer size ($96 \times 11 \times 11$), there are 96 filters with 11×11 pixels size each, as it is also observed in the shape of the patches matrix. In an inference step, an image is fed throughout this and the rest of layers, applying these filters over it, producing the results observed in the second row of Fig. 9.8.

Figure 9.9 shows the weights learned in convolution layer 2. This layer has a more complex structure (as usual when layers are deeper in the architecture). Its filters are structured in 48×48 channels with 5×5 pixels size each. The figure represents each of these channels in a single patch. In total, this layer has 256 filters, so the output activation when these filters are applied has the same shape, as shown in the last row of Fig. 9.8.

Following, Fig. 9.8 shows two diatoms of *Diatoma mesodon* and *Cyclostephanos dubius* species respectively, with and their corresponding activations for the first two convolutions. Notice that the image aspect ratio has been altered to be adjusted to the input size of the network. The image input size of the CNN network is fixed at designing time and then, all training images are resized to fit it. Once the model is obtained, test samples must be resized to fit the input size too.

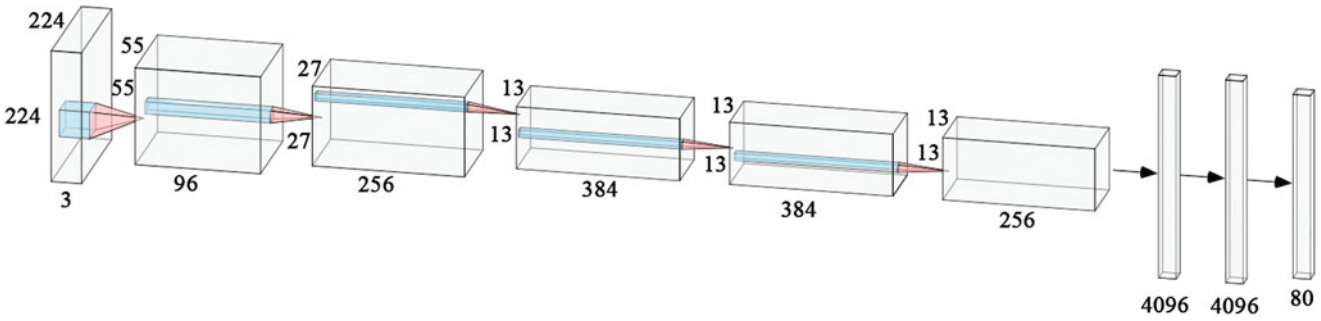

Fig. 9.6 Scheme of the AlexNet network tested. Source: http://alexlenail.me/NN-SVG/AlexNet.html

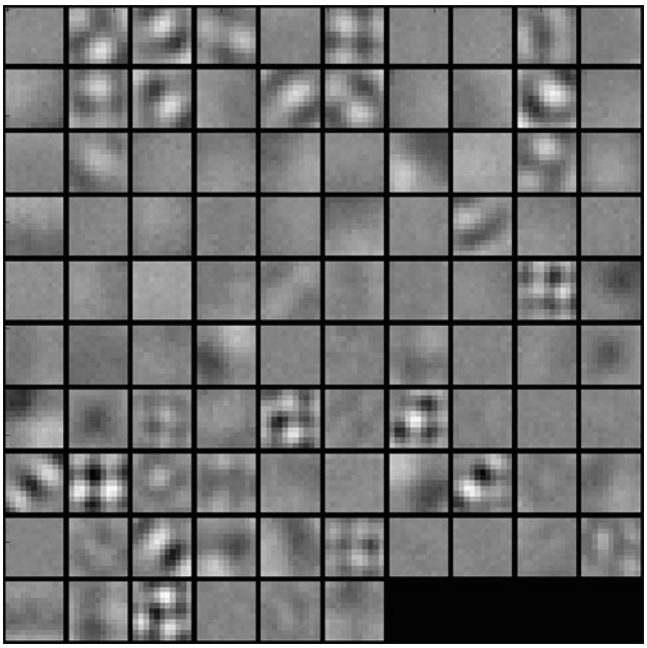

Fig. 9.7 Filter visualization for the first convolution layer in AlexNet

9.4 Diatom Classification Results

The most common classification techniques based on selected features have been used in the state of the art to classify diatoms. The number of classes used ranges between 14 and 80 species, with 30,000 samples for the largest database. The best accuracy is 99.51% for a CNN-based method and a dataset of 80 species and 24,000 samples [15]. For the hand-crafted approach, the best results show a 98.1% of accuracy using morphological, statistical, space-frequency, and other textural features and a Bagging tree classifier [14]. Table 9.2 presents a summary of the above, in comparison with the CNN method proposed by the authors. Table 9.2 summarizes the classifiers, databases, and features adopted and the accuracies they obtained.

9.5 Conclusions

In this chapter, different classification techniques applied to the problem of the identification of diatoms, from the classical methods to the new deep learning paradigm, have been presented. Since machine learning with classical methods relies on previously selected features, different ways of obtaining the characteristics and some methods of reducing their number have also been shown. Finally, a wide revision of the most important contributions to diatom identification has been performed showing the potential of learning the features from the images automatically. With datasets containing between 14 and 80 species, whereas the hand-crafted approach shows a 98.1% of accuracy using a set of extracted textural features in combination with a Bagging

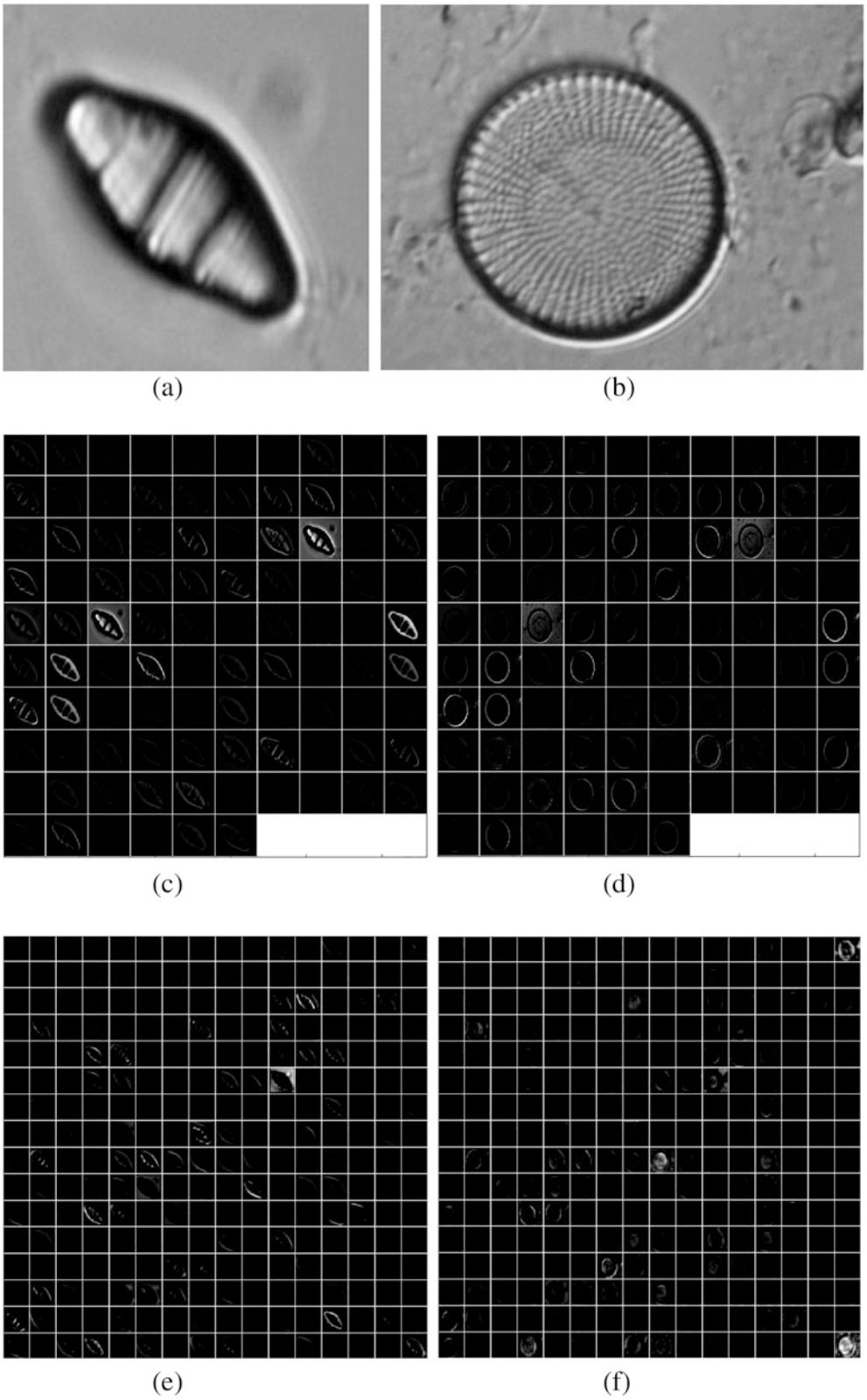

Fig. 9.8 Activation visualization in the convolution layers 1 and 2 for two different diatoms. (**a–b**) Original images, (**c–d**) convolution 1 layer activations (filters of 11×11), and (**e–f**) convolution 2 layer activations (filters of 48×48)

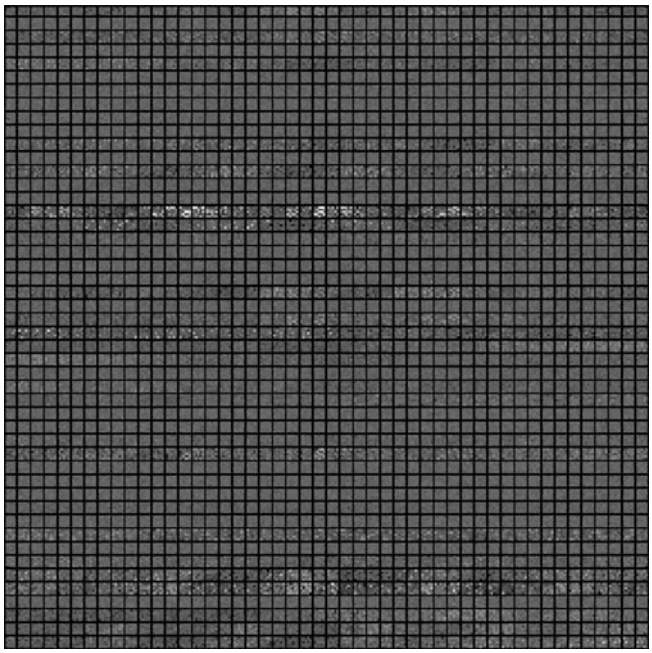

Fig. 9.9 Filter visualization for the second convolution layer in AlexNet

Table 9.2 Diatom classification results

Year [Ref.]	No. of species	No. of samples	No. of features and type	Classifier	Accuracy
2002 [7]	37	781	321 from geometrical, textural, morphological, and frequency	Bagging tree	96.9%
2003 [10]	1	66	10 morphological	Multiple discriminant analysis	80.3%
2012 [50]	38	837	30 morphological and 200 texture	Random forest	97.97%
	48	1019	30 morphological and 200 texture	Random forest	97.15%
	55	1098	30 morphological and 200 texture	Random forest	96.17%
2016 [51]	14	10, 000	4 geometrical, 7 moments, and 33 morphological	SVM	94.7%
2017 [14]	80	24, 000	273 morphological, statistical, textural, and space-frequency	Bagging tree	98.1%
2017 [15]	80	24, 000	–	CNN-AlexNet	95.62%
	80	160, 000	–	CNN-AlexNet	99.51%
2019 [23]	8	703	211 elliptical Fourier, Gabor, and phase congruency	Unsupervised classifiers	98.9%
	8	703	211 elliptical Fourier, Gabor, and phase congruency	Supervised classifiers	99.9%

tree classifier, state-of-the-art CNNs achieve an overall accuracy of 99.51%. However, although deep learning results surpass the ones obtained with the classical methods, it is worth noting that deep learning methods usually require a large number of images to train a classifier. If the dataset does not contain enough samples per taxa, the use of hand-crafted classifiers will be a better choice.

Appendix

In this section, the reader can find the links of some of the methods explained in this chapter.

- Log Gabor Matlab toolbox. https://figshare.com/articles/LogGabor_Matlab_toolbox/2067504
- MATLAB and Octave Functions for Computer Vision and Image Processing. http://www.peterkovesi.com/matlabfns
- PRTools, a Matlab toolbox for pattern recognition. http://www.37steps.com
- Caffe Deep Learning Toolbox. http://caffe.berkeleyvision.org/

References

1. Mann, D.: The species concept in diatoms. Phycologia **38**(6), 437–495 (1999)
2. Hicks, Y.A., Marshall, D., Rosin, P., Martin, R.R., Mann, D., Droop, S.: A model of diatom shape and texture for analysis, synthesis and identification. Mach. Vis. Appl. **17**(5), pp. 297–307 (2006)
3. John, D.: Use of algae for monitoring rivers III. J. Appl. Physiol. **11**(6), 596–597 (1999). http://dx.doi.org/10.1023/A:1008182326039
4. Smol, J., Stoermer, E.: The Diatoms: Applications for the Environmental and Earth Sciences. Cambridge University Press, Cambridge (2010)
5. Wayne, R.: Light and Video Microscopy, 2nd edn., Elsevier, Amsterdam (2014)
6. Cairns, J., Dickson, K., Pryfogle, P., Almeida, S., Case, S., Fournier, J., Fuji, H.: Determining the accuracy of coherent optical identification of diatoms. J. Am. Water Resour. Assoc. **15**, 1770–1775 (1979)
7. du Buf, H., Bayer, M.: Automatic Diatom Identification. In: Series in Machine Perception and Artificial Intelligence. World Scientific Publishing Co., Singapore (2002)
8. Culverhouse, P., Simpson, R., Ellis, R.G., Lindley, J., Williams, R., Parisini, T., Reguera, B., Bravo, I., Zoppoli, R., Earnshaw, G., MacCall, H., Smith, G.: Automatic classification of field-collected dinoflagellates by artificial neural network. Mar. Ecol. Prog. Ser. **139**, 281–287 (1996)
9. Pech-Pacheco, J., Alvarez-Borrego, J.: Optical-digital system applied to the identification of five phytoplankton species. Mar. Biol. 132, 357–365 (1998)
10. Pappas, J., Stoermer, E.: Legendre shape descriptors and shape group determination of specimens in the Cymbella cistula species complex. Phycologia **42**(1), 90–97 (2003)
11. Du Buf, H., Bayer, M., Droop, S., Head, R., Juggins, S., Fischer, S., Bunke, H., Wilkinson, M., Roerdink, J., Pech-Pacheco, J., et al.: Diatom identification: a double challenge called ADIAC. In: Proceedings of International Conference on Image Analysis and Processing, pp. 734–739. IEEE, Piscataway (1999)
12. Falasco, E., Blanco, S., Bona, F., Goma, J., Hlubikova, D., Novais, M., Hoffmann, L., Ector, L.: Taxonomy, morphology and distribution of the Sellaphora stroemii complex (bacillariophyceae). Fottea **9**(2), 243–256 (2009)
13. Bottin, M., Giraudel, J.-L., Lek, S., Tison-Rosebery, J.: diatSOM: a R-package for diatom biotypology using self-organizing maps. Diatom Res. **29**(1), 5–9 (2014)
14. Bueno, G., Deniz, O., Pedraza, A., Salido, J., Cristobal, G., Saul, B.: Automated diatom classification (part A): handcrafted feature approaches, Appl. Sci. **7**(8), 753 (2017)
15. Pedraza, A., Bueno, G., Deniz, O., Cristóbal, G., Blanco, S., Borrego-Ramos, M.: Automated diatom classification (part B): a deep learning approach. Appl. Sci. **7**(5), 460 (2017)
16. Haralick, R., Shanmugam, K., et al.: Textural features for image classification. IEEE Trans. Syst. Man Cybern. **3**(6), 610–621 (1973)
17. Vállez, N., Bueno, G., Déniz, O., Dorado, J., Seoane, J.A., Pazos, A., Pastor, C.: Breast density classification to reduce false positives in CADe systems. Comput. Methods Prog. Biomed. **113**(2), 569–584 (2014)
18. Wang, L., He, D.: Texture classification using texture spectrum. Pattern Recogn. **23**, 905–910 (1990)
19. Ojala, T., Pietikainen, M., Harwood, D.: Performance evaluation of texture measures with classification based on Kullback discrimination of distributions. In: Proceedings of the 12th International Conference on Pattern Recognition – Conference A: Computer Vision Image Processing (IAPR), vol. 1, pp. 582–585 (1994). https://doi.org/10.1109/ICPR.1994.576366
20. Nava, R., Cristobal, G., Escalante-Ramirez, B.: A comprehensive study of texture analysis based on local binary patterns. In: Optics, Photonics, and Digital Technologies for Multimedia Applications II, vol. 8436, pp. 84360E–84372. International Society for Optics and Photonics. SPIE, Bellingham (2012)
21. Sahu, H.: An analysis of texture classification: local binary patterns. J. Glob. Res. Comput. Sci. **4**, 17–20 (2013)
22. Ojala, T., Pietikäinen, M., Maenpaa, T.: Multiresolution gray-scale and rotation invariant texture classification with local binary patterns. IEEE Trans. Pattern Anal. Mach. Intell. **24**(7), 971–987 (2002)
23. Sánchez, C., Cristóbal, G., Bueno, G.: Diatom identification including life cycle stages through morphological and texture descriptors. PeerJ **7**, e6770 (2019). https://doi.org/10.7717/peerj.6770
24. Hu, M.K.: Visual pattern recognition by moment invariants. IRE Trans. Inf. Theory **8**, 179–187 (1962)
25. Teague, M.R.: Image analysis via the general theory of moments. J. Opt. Soc. Am. **70**(8), 920–930 (1980)
26. Boyce, J.F., Hossack, W.: Moment invariants for pattern recognition. Pattern Recogn. Lett. **1**(5–6), 451–456 (1983)
27. Abu-Mostafa, Y.S., Psaltis, D.: Recognitive aspects of moment invariants. IEEE Trans. Pattern Anal. Mach. Intell. **6**, 698–706 (1984)
28. Chen, Q., Petriu, E., Yang, X.: A comparative study of Fourier descriptors and Hu's seven moment invariants for image recognition. In: Canadian Conference on Electrical and Computer Engineering 2004 (IEEE Cat. No. 04CH37513), vol. 1, pp. 103–106. IEEE, Piscataway (2004)
29. Kuhl, F.P., Giardina, C.R.: Elliptic Fourier features of a closed contour. Comput. Graphics Image Process. **18**(3), 236–258 (1982)
30. BielStela, Elliptic-Fourier-Python, https://github.com/BielStela/Elliptic-Fourier-Python (Jul. 2017)
31. Verikas, A., Gelzinis, A., Bacauskiene, M., Olenina, I., Olenin, S., Vaiciukynas, E.: Phase congruency-based detection of circular objects applied to analysis of phytoplankton images. Pattern Recogn. **45**(4), 1659–1670 (2012)
32. Kovesi, P.: Phase congruency detects corners and edges. In: The Australian Pattern Recognition Society Conference: DICTA, vol. 10–12, pp. 309–318 (2003)
33. Guyon, I., Elisseeff, A.: An introduction to variable and feature selection. J. Mach. Learn. Res. **3**, 1157–1182 (2003)
34. Duda, R.O., Hart, P.E., Stork, D.G.: Pattern Classification, 2nd edn. Wiley, New York (2001)
35. Mitra, P., Murthy, C., Pal, S.K.: Unsupervised feature selection using feature similarity. IEEE Trans. Pattern Anal. Mach. Intell. **24**(3), 301–312 (2002)
36. Pudil, P., Novovicova, J., Kittler, J.: Floating search methods in feature selection. Pattern Recogn. Lett. **15**(11), 1119–1125 (1994)
37. Martínez, A.M., Kak, A.C.: PCA versus LDA. IEEE Trans. Pattern Anal. Mach. Intell. **23**(2), 228–233 (2001)
38. Fisher, R.A.: The use of multiple measurements in taxonomic problems. Ann. Eugenics **7**(2), 179–188 (1936)
39. Friedman, J.H., Bentley, J.L., Finkel, R.A.: An algorithm for finding best matches in logarithmic expected time. ACM Trans. Math. Softw. **3**(3), 209–226 (1977)
40. Wang, F., Zhen, Z., Wang, B., Mi, Z.: Comparative study on KNN and SVM based weather classification models for day ahead short term solar PV power forecasting. Appl. Sci. **8**(1), 28 (2017)
41. Kuncheva, L.I.: Combining Pattern Classifiers Methods and Algorithms. John Wiley & Sons, Inc., Hoboken (2004)
42. Breiman, L.: Bagging predictors. Mach. Learn. **24**(2), 123–140 (1996)
43. Lloyd, S.: Least squares quantization in PCM. IEEE Trans. Inf. Theory **28**(2), 129–137 (1982)

44. Park, H.-S., Jun, C.-H.: A simple and fast algorithm for K-medoids clustering. Expert Syst. Appl. **36**(2), 3336–3341 (2009)
45. Schütze, H., Manning, C.D., Raghavan, P.: Introduction to Information Retrieval, vol. 39. Cambridge University Press, Cambridge (2008)
46. Zhang, T., Ramakrishnan, R., Livny, M.: BIRCH: an efficient data clustering method for very large databases. In: ACM SIGMOD Record, vol. 25, pp. 103–114. ACM, New York (1996)
47. Vinh, N.X., Epps, J., Bailey, J.: Information theoretic measures for clusterings comparison: variants, properties, normalization and correction for chance. J. Mach. Learn. Res. **11**(Oct), 2837–2854 (2010)
48. Kassambara, A.: Practical Guide to Cluster Analysis in R: Unsupervised Machine Learning, vol. 1. STHDA (2017)
49. Loshchilov, I., Hutter, F.: SGDR: stochastic gradient descent with restarts. CoRR abs/1608.03983. arXiv:1608.03983. http://arxiv.org/abs/1608.03983
50. Dimitrovski, I., Kocev, D., Loskovska, S., Dzeroski, S.: Hierarchical classification of diatom images using ensembles of predictive clustering trees. Eco. Inform. **7**(1), 19–29 (2012)
51. Lai, Q.T., Lee, K.C., Tang, A.H., Wong, K.K., So, H.K., Tsia, K.K.: High-throughput time-stretch imaging flow cytometry for multi-class classification of phytoplankton. Opt. Express **24**(25), 28170–28184 (2016)

Multifocus and Multiexposure Techniques

10

Harbinder Singh, Gabriel Cristóbal, and Vinay Kumar

Abstract

In diatom identification process, image fusion is performed as a preprocessing step that can enhance the contours and ornamentation features (e.g., the striation pattern) characteristic of diatom frustules. These enhanced features help to improve the performance of diatom identification process. In doing so, defining activity level based on local sharpness measure is the main challenge. In this chapter, the pixel-wise weighted average multifocus image fusion technique is described that can extend the depth of field (DOF) by selecting the most focused region from source images. First, each source image is decomposed into base layer (BL) and detail layer (DL) to extract sharp and fine details, respectively. Sharp edge details of source images are important determinants of local sharpness measure that yields initial weight maps, which are further refined using weighted least squares (WLS) optimization. For detail enhancement, sharp details and fine details are fused with the refined weight maps, separately. Finally, the fused BL is combined with fused DL to obtain an all-in-focus fused image. In addition to the use of fixed time exposure light microscopy (LM), we propose that multiexposure image fusion can be of great importance for improving the final identification process.

H. Singh (✉)
ECE, Chandigarh Engineering College, Landran, Mohali, India
e-mail: harbinder.ece@cgc.edu.in

G. Cristóbal
Instituto de Optica (CSIC), Madrid, Spain
e-mail: gabriel@optica.csic.es

V. Kumar
ECE Department, Thapar Institute of Engineering & Technology, Patiala, India
e-mail: vinay.kumar@thapar.edu

10.1 Introduction

Nowadays, groups of researchers around the globe are working to develop systems for monitoring the health of aquatic systems. World ecosystems, including aquatic (marine and freshwater) environments, integrate both abiotic and biotic components. Aquatic ecosystems are mainly divided into two categories: freshwater ecosystems and marine ecosystems. Three-fourths of the Earth's surface is covered by the marine ecosystems and only 0.78% of the Earth's surface is covered by the freshwaters. To monitor the health of any aquatic ecosystem, diatoms are important organisms provided their biological features (see Chap. 2). Diatoms are single-celled organisms containing light-absorbing molecules, which are responsible for photosynthesis. It has been stated that 20% of the oxygen is produced by marine microalgae (mainly diatoms) that remove a huge amount of carbon dioxide (CO_2) from the planet. The structural layers outside the cell membrane made of silica are called frustules. The nano-scale patterns in the frustules yield unique features that are used for the identification and classification of diatoms.

Almost every diatom is microscopic and the cell size of the diatom is between 2 μm to 2 mm. To visualize the features in cell structure, microscopy imaging techniques have been developed. In light microscopy (LM), visible light and magnifying lenses are used to visualize the cell structure. When diatoms are seen with a LM, the nano-scale patterns in the frustules appear transparent. Since most diatom walls have a 3D structure, therefore the majority cannot be adequately represented in a single focal plane. Many recent computational photography techniques play a significant role to overcome the limitation of LM to handle 3D structure of diatom walls ornamented by intricate and striking patterns of silica. In many of these techniques, it is often desirable to fuse details from images captured at different focal planes so that both contour and striation are

G. Cristóbal et al. (eds.), *Modern Trends in Diatom Identification*, Developments in Applied Phycology 10,
https://doi.org/10.1007/978-3-030-39212-3_10

well defined for feature extraction. These cell wall features are vital for distinguishing diatom species.

In recent years, several fusion algorithms have been developed to combine substantial information from multiple input images into a single composite image. For instance, most of the image fusion techniques are based on multi-resolution decomposition [1, 2]. The principal motivation for image fusion is to extend the depth of field (DOF) [3], to improve spatial and temporal resolution [4, 5], and finally to extend the dynamic range of the fused image in the case of the multiexposure techniques [6]. Image fusion has a fundamental difficulty in preventing artifacts and preserving local contrast when fusing the characteristics recorded from the source data, such as exposure value, focusing, modality, and environmental conditions. In particular, the choice of parameter settings during input stacks acquisition will have a large impact on the outcome of the image fusion framework. Two examples of multifocus and multiexposure stacks, and corresponding fusion results are shown in Fig. 10.1. The automated procedure of extracting all the meaningful details from the input images to a final fused image is the main motivation of image fusion.

In this chapter, we present a two-scale decomposition-based weighted average multifocus image fusion (TSD-MF) method. The aim of two-scale decomposition (TSD) is to produce a detail-enhanced image from a set of images that have been taken at different focal lengths of a camera sensor. Since the goal of mutifocus image fusion is to create a new image that is focused throughout, it is always a challenging task to decide a local measure of information content of source images. In the case that optical defocus is the major source of quality degradation, it is natural to assume that the image region that has sharper edges is more active and thus more informative [7]. In existing multifocus image fusion techniques, a common implicit assumption is that finding the sharper edges regions is associated with finding the focused region.

This chapter is organized as follows. In Sect. 10.2, we explore in detail one multifocus image fusion algorithm to extend the DOF by combining in-focus details from several images of diatom species captured by LM. In order to obtain a sharp valve contour and striation pattern, images captured at different exposure settings can be fused. This example of multiexposure image fusion is described in Sect. 10.3. The fusion quality metrics are presented in Sect. 10.4. To perform a rapid mathematical calculation using graphics processing unit (GPU), the efficient implementation of the proposed fusion method is discussed in Sect. 10.5. Finally, Sect. 10.6 contains concluding remarks.

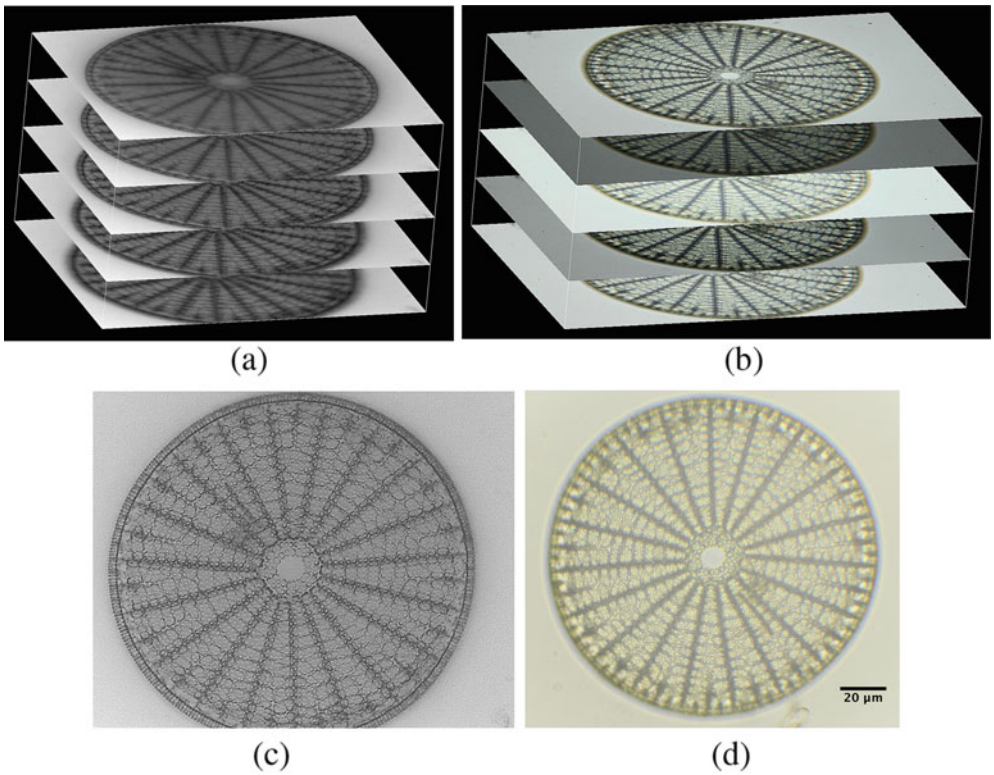

Fig. 10.1 Top row: (**a**) example of a multifocus stack and (**b**) example of a multiexposure stack. Bottom row: (**c**) fused image obtained from image stack shown in (**a**) and (**d**) fused image obtained from image stack shown in (**b**)

10.2 Multifocus Fusion Methods

10.2.1 Two-Scale Decomposition (TSD)

The first TSD-based image fusion was introduced in 2013 by Li et al. [8]. They aimed to propose fast two-scale image fusion techniques that do not rely heavily on a specific multi-resolution method. A simple average filter was used to decompose source images into base layers (BLs) and detail Layers (DLs). To perform weighted average fusion, the guided filtering (GF) [9] based spatial consistency principal was introduced. In this study, we selected an edge-preserving filter (EPF) based two-scale fusion approach [10]. The aim of EPF-based decomposition is to better approximate the DL for detail enhancement. Applying this fusion technique requires additional computation but performs better for both multifocus and multiexposure microscopy data sets.

Let I_n be the n_{th} source image which needs to be operated by an EPF. In order to compute BL and DL, we first decompose source images into two-scale representations by using anisotropic diffusion [11]. The BL B_n of each source image is obtained as follows:

$$B_{s,n}^{t+1} = I_{s,n}^{t} + \frac{\gamma}{|\eta_s|}\left[g_N \cdot \nabla_{N_s} I_n + g_S \cdot \nabla_S I_n + g_E \cdot \nabla_E I_n + g_W \cdot \nabla_W I_n\right]_s^t \tag{10.1}$$

where ∇_N, ∇_S, ∇_E, and ∇_W indicate the difference of North, South, East, and West neighbor for pixel position s, respectively. The corresponding diffusion coefficients [11] g_N, g_S, g_E, and g_W are computed from local window of size (3×3).The pictorial view of gradient computation from 1-D grid structure and 2-D grid structure is illustrated in Fig. 10.2. The diffusion functions $g(\cdot)$ used in our TSD approach can be defined as follows:

$$g(\nabla I) = \mathrm{e}^{\left(-\left(\frac{\|\nabla I\|}{K}\right)^2\right)} \tag{10.2}$$

and in Eq. 10.1, the variable t determines iterations, the constant γ is a scalar that determines the rate of diffusion, η_s represents the spatial neighborhoods of current sample position s, and $|\eta_s|$ is the number of neighbors. In this chapter, these parameters are empirically determined. In practice, a set of $t = 5$, $\gamma = 1/7$ yield plausible results.

Once the BL is computed for each n_{th} input image, the DL D_n can be directly calculated by subtracting the B_n from the corresponding source image I_n as follows:

$$D_n = I_n - B_n \tag{10.3}$$

To see the behavior of Perona et al. [11] filter at edges, we first analyze 1-D signal into BL and DL. As can be seen in Fig. 10.3, in BL (i.e., the coarser level after diffusion), high-frequency textures disappear. The weak texture details filtered out from the BL are exactly reconstructed in the DL.

The BL and DL decomposition of *Actinocyclus ralfsii* image data set is illustrated in Fig. 10.4. From Fig. 10.4, it can be visually seen that the BL provides coarse details and the textures are almost eliminated. The texture details compressed in the BL are exactly reconstructed in DL.

10.2.2 Detection of a Focused Region and Weight Map Computation

Sharp edge details are important determinants in weight map computation. A traditional view is that an in-focus region yields sharper edge details than out-of-focus region. A wide variety of criteria functions have been proposed in the literature for selecting the in-focus region from source images to construct an all-in-focus fused image. Examples of these criteria functions include variance (VAR), Tenengrad (TNG), spatial frequency (SF), energy of image gradients (EOG), energy of Laplacian (EOL), sum modified Laplacian (SML), Laplacian of Gaussian (LOG) [12], and frequency selective weighted median filter (FSWM) [13]. The authors in [13] have provided comparative studies of different criteria functions. In literature [14, 15], EOL-based criteria function

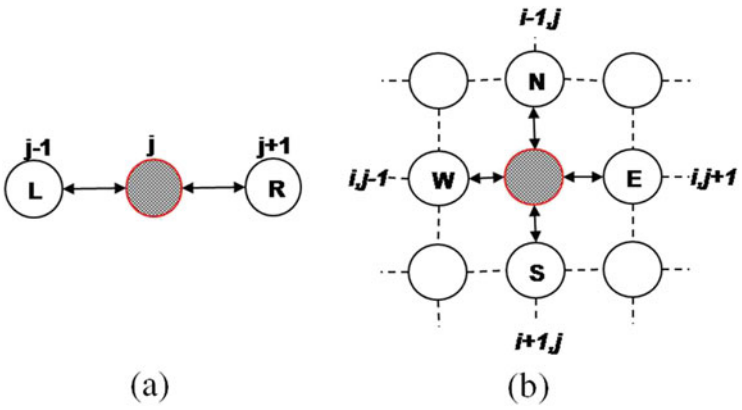

Fig. 10.2 Gradient computation: (**a**) from 1-D grid structure by considering left (L) and right (R) neighbors and (**b**) from 2-D grid structure by considering North (N), South (S), East (E), and West (W) neighbors

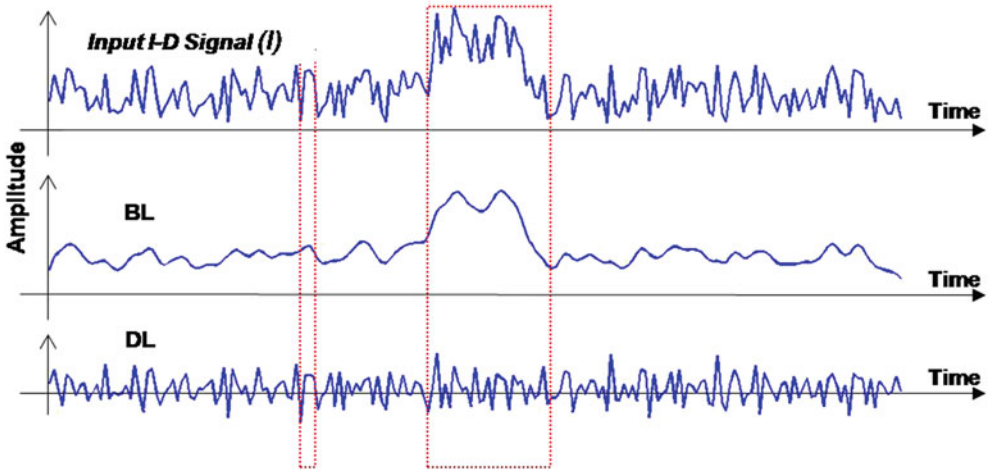

Fig. 10.3 The TSD of 1-D signal based on EPF after 5 iterations with $K = 30$, $\gamma = 1/3$, and $|\eta_s| = 2$ (left and right neighbors). The 1-D input signal (I) is decomposed into two main components: a low-frequency BL and a high-frequency DL. Notice that the edges are preserved in the diffused image (i.e., BL) and the DL yields fine details only

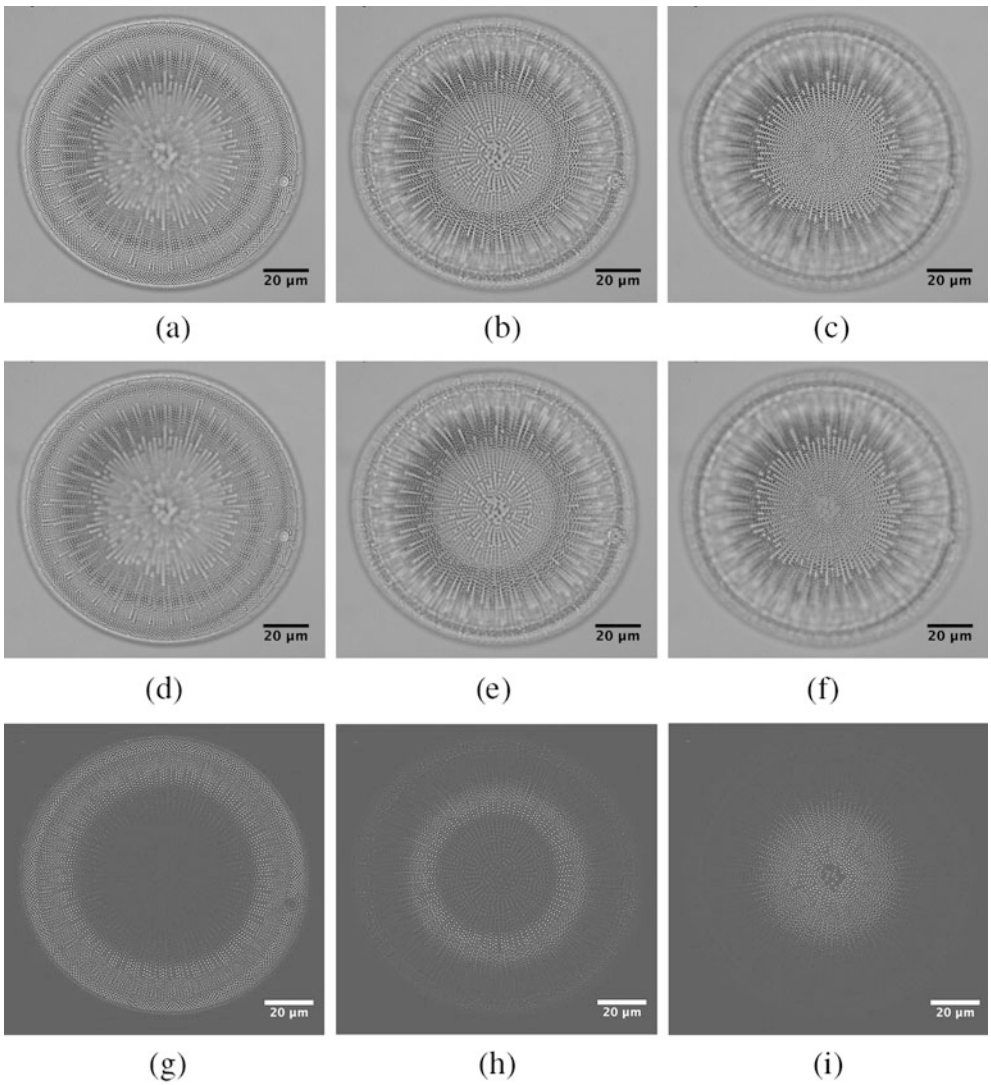

Fig. 10.4 (**a–c**) Multifocus images of *Actinocyclus ralfsii* diatom species. (**d–f**) Example of BL decomposition. (**g–i**) Example of DL decomposition. In order to better visualize the DLs, a constant value is added to each pixel, e.g., 100

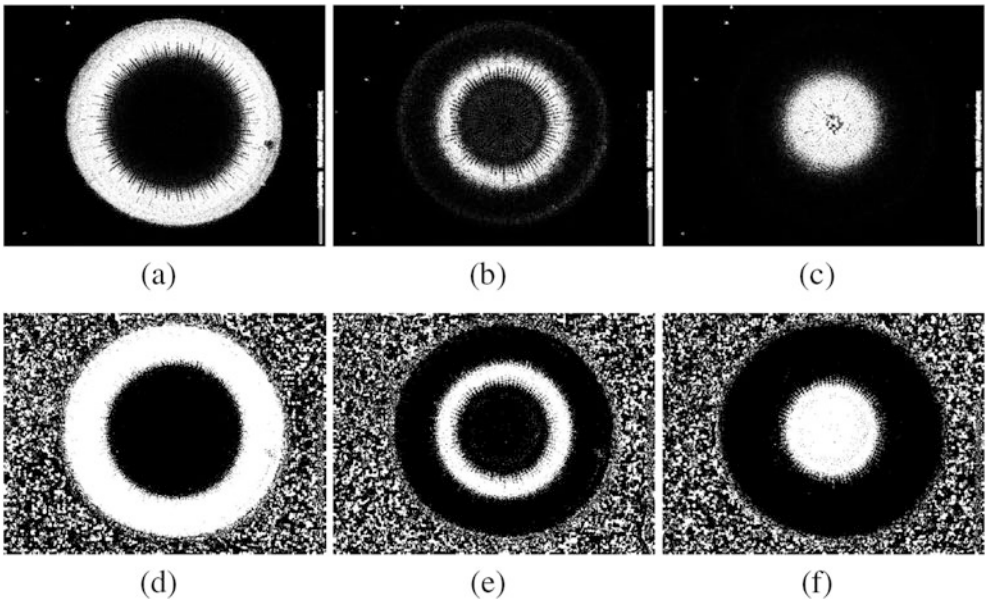

Fig. 10.5 (**a–c**) Saliency maps of *Actinocyclus ralfsii* diatom species, computed using Eq. 10.5 and (**d–f**) noisy weight maps computed using Eq. 10.6

provided better performance for multifocus image fusion than SF and EOG.

In this chapter, to identify the block having high frequencies, the EOL is computed in each $M \times N$ block of input images. The higher value of EOL indicates that an image block is in-focus and the lower value of EOL indicates that an image block is faint/out-of-focus. The EOL of the n_{th} input image is computed as follows:

$$\mathrm{EOL}_n = \sum_i \sum_j (\nabla^2 I_n(i, j))^2 \tag{10.4}$$

The 3×3 Laplacian kernel: $[0, -1, 0; -1, 4, -1; 0, -1, 0]$ is used for gradient computation. The result of computing an EOL with this Laplacian kernel is a filtered image that contains strong edges in areas where rich details are present. In order to compute initial saliency maps SM_n, we apply the Gaussian low pass filter G having 5×5 symmetric kernel size r with standard deviation $\sigma = 5$, which is formulated as follows:

$$SM_n = |\mathrm{EOL}_n| \otimes G_{r,\sigma} \tag{10.5}$$

where $\otimes$ denotes the convolution operator. Next, the saliency maps are compared to determine the weight maps as follows:

$$WM_n^k = \begin{cases} 1 & \text{if } SM_n^k = \max\left(SM_1^k, SM_2^k, \ldots, SM_N^k\right), \\ 0 & \text{otherwise} \end{cases} \tag{10.6}$$

where WM_n^k and SM_n^k are, respectively, the weight map and saliency value of the pixel k in the n_{th} image.

Figure 10.5a–c shows the saliency maps computed by using Eq. 10.5, and the initial weight maps (computed by using Eq. 10.6) are shown in Fig. 10.5d–f. From Fig. 10.5d–f, we can easily notice that the initial weight maps computing by using Eq. 10.6 yield noisy outputs that are not suitable for the fusion process. To refine these noisy weight maps, weighted least squares (WLS) [16] based weight map refinement process is introduced in our fusion algorithm, which is discussed in the forthcoming section.

10.2.3 Weight Map Refinement

The weight maps computed in Eq. 10.6 are hard, noisy, and not aligned with the object boundaries. In our implementation, the WLS framework [16] is used for weight map refinement. WLS-based edge-preserving operator may be viewed as a compromise between two possible contradictory goals. Given an input image v, we seek a new image w, which, on the one hand, is as close as possible to v, and at the same time, is as smooth as possible everywhere, except across significant gradients in v. To achieve these objectives, we seek to minimize the following quadratic functional:

$$\sum_p \left((w_p - v_p)^2 + \gamma \left(q_{x,p}(v) \left(\frac{\partial w}{\partial x} \right)_p^2 + q_{y,p}(v) \left(\frac{\partial w}{\partial y} \right)_p^2 \right) \right) \tag{10.7}$$

where the subscript p denotes the spatial location of a pixel. The goal of the expression term $(w_p - v_p)^2$ is to minimize the

distance between w and v, while the second (regularization) term strives to achieve smoothness by minimizing the partial derivatives of w. The smoothness requirement is enforced in a spatially varying manner via the smoothness weights q_x and q_y, which depend on v:

$$q_{x,p}(v) = \left(\left| \frac{\partial l}{\partial x}(p) \right|^{\alpha} + \epsilon \right)^{-1},$$
$$q_{y,p}(v) = \left(\left| \frac{\partial l}{\partial y}(p) \right|^{\alpha} + \epsilon \right)^{-1} \tag{10.8}$$

where l is the log-luminance channel of the input image v, the exponent α (typically between 1.2 and 2.0) determines the sensitivity to the gradients of v, while ϵ is a small constant (typically 0.0001) that prevents division by zero in areas where v is constant.

Let $w = WLS_{\gamma,\alpha,\epsilon}(v)$ represent the WLS filtering operation. In our case, WM_n^k computed in Eq. 10.6 serves as the input image to WLS filter (i.e., $v = WM_n^k$), and W_n^B or W_n^D is the output of WLS filter ($w = W_n^B$ for BL and $w = W_n^D$ for DL). More specifically, the coarser version of weight map WM_n^k will serve as refined weight map for n_{th} base layer and detail layer:

$$W_n^B = WLS_{\gamma_1,\alpha_1,\epsilon}(v) \tag{10.9}$$

$$W_n^D = WLS_{\gamma_2,\alpha_2,\epsilon}(v) \tag{10.10}$$

where W_n^B and W_n^D are refined weight maps for corresponding B_n and D_n, respectively. We have found that the weight refinement for most of the data sets with the parameters $\gamma_1 = 1.2$ and $\alpha_1 = 0.9$ is suitable for the fusion of BLs. In Eq. 10.10, $\gamma_2 = 0.2$ and $\alpha_2 = 0.1$ will work for preserving details in the fused image.

The refined weight maps computed from Eq. 10.9 are shown in Fig. 10.6a–c. To demonstrate in-focus region selection efficiently, different selected regions are visualized in false color, as shown in Fig. 10.6d. The false color image visualizes that the sharp regions across source images (shown in Fig. 10.4a–c) are detected perfectly. The red shows where the first input image contributes, green the second image, and blue shows the contribution of the third image.

10.2.4 Weighted Average Fusion of BL and DL

The final step of weight map refinement consists of weight map normalization so that they sum to one at each pixel k. These normalized weight maps are used to compute fused base layer B_F and fused detail layer D_F as follows:

$$B_F = \sum_{n=1}^{N} W_n^B B_n \tag{10.11}$$

$$D_F = \sum_{n=1}^{N} W_n^D D_n \tag{10.12}$$

and the resulting fused image I_F can be directly calculated as follows:

$$I_F = B_F + D_F \tag{10.13}$$

To enhance details, we found that a simple interactive tool is very effective for DL manipulation. The enhanced detail fused image can be computed by:

$$I_F^e = B_F + \sum_{n=1}^{N} W_n^D S(a, D_n) \tag{10.14}$$

where S is a sigmoid function $S = 1/(1 + \exp(-ax))$, applied on n_{th} DL for detail manipulation. The parameter a is the user-defined boosting factor, which can be selected empirically. We have found that the free parameter $a = 4$ is very effective for boosting fine details in the fused image with fewer visible artifacts near strong edges. The effective manipulation range is very wide and will vary in accordance with the texture details present in the source images.

Figure 10.7a shows a fused base layer B_F that is produced from a sequence of three base layers of *Actinocyclus ralfsii* diatom species, shown in Fig. 10.4d–f. An example result of detail layer fusion using Eq. 10.12 is shown in Fig. 10.7b, along with the final fused image shown in Fig. 10.7c. From the image shown in Fig. 10.7c, We can see that single all-in-focus image is produced from three partially focused images. Most notable, the fine details appear without introducing visible artifacts.

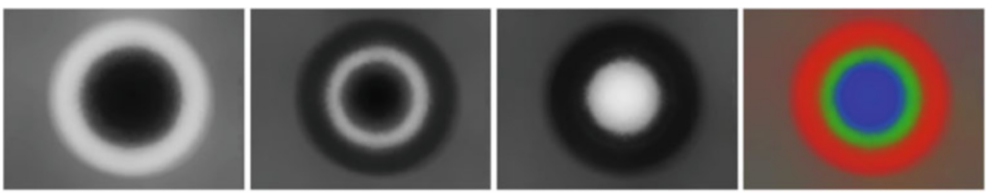

Fig. 10.6 (**a–c**) Refined weight maps computed from Eq. 10.9 and (**d**) false color visualization of in-focus regions detected across source images

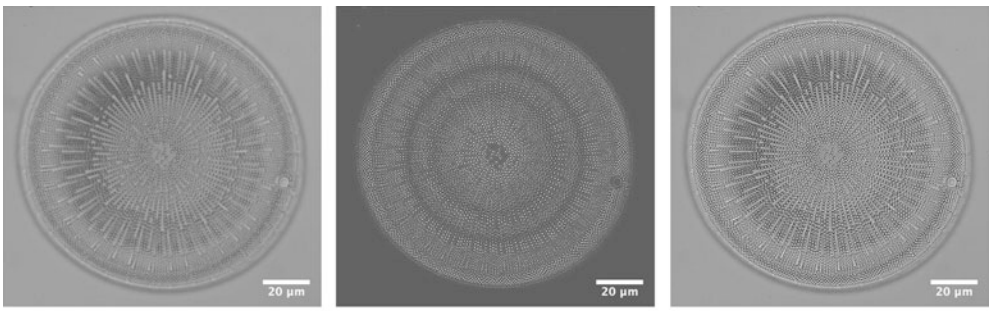

Fig. 10.7 (**a**) Fused base layer B_F was computed using Eq. 10.11, (**b**) fused detail layer D_F was computed using Eq. 10.12, and (**c**) fused image I_F was computed using Eq. 10.13

10.3 Exposure Fusion (EF) vs High Dynamic Range (HDR)

Nowadays, much research is going on for developing exposure fusion techniques for real-world scenes. Yet, multiexposure image fusion which enhances the contrast of fused image has not been applied to diatoms. Actually, study and characterization of intricate micrometer-sized silica pattern of diatom becomes more desirable for classification of species in different aquatic systems. Recently, Ferrara et al. have found that the period of exposure of the sensor plays an important role to exploit the optical properties of micro- and nano-structures of diatoms [17]. Beyond visualization and localization of intricate micrometer-sized silica pattern, on the other hand, the full dynamic range of the sensor can be utilized by variable exposure time to produce more details. In this section, we hypothesize that multiexposure image fusion techniques are expected to provide better performance in diatom identification and classification.

In recent years, several techniques have been developed that are capable of providing precise representation of complete information of shadows and highlights present in the real-world natural scenes [6]. The direct 8-bit gray and 24-bit RGB representation of visual data, with the standard digital cameras at single exposure settings, often causes loss of information. This is because the dynamic range of most scenes is beyond what can be captured by the standard digital cameras. Such representation is referred to as low dynamic range (LDR) image. To handle such typical cases, digital cameras have the aperture setting, exposure time, and ISO value that regulate the amount of light to be captured by the sensors. Therefore, it is important to somehow determine exposure setting for controlling the response of charge coupled device (CCD). For single exposure setting, either detail in the poorly illuminated area (i.e., shadows) is visible with long exposure or brightly illuminated area (i.e., highlights) with short exposure. Thus, the image captured by the standard digital camera for single exposure setting is partially over- or underexposed. As a result, there will always be a need to capture the detail of the entire scene with a sufficient number and value of exposures.

The idealized response of digital camera sensor from highlights, mid-tones, and shadows present in the scene is shown in Fig. 10.8. In Fig. 10.8, the graph represents collected charges versus exposure times for three illuminations. We assume that both the aperture and ISO setting are kept fixed over integration times (t_{int1}, t_{int2}, and t_{int3}). There is one setting (i.e., exposure time), which determines how long the sensor is exposed to light. The charge (Q) produced at the end of integration is a functional $f[.]$ of the current $I(t)$ over the integration time $0 \leq t \leq t_{int}$. When the sensor is operating in integration mode, functional $f[.]$ is given by:

$$f[x] = \int_0^{t_{int}} I(t)\, dt \tag{10.15}$$

As depicted in the graph shown in Fig. 10.8, in difficult lighting situations, where highlights, shadows, and mid-tones appear simultaneously, the camera sensors under the influence of highlights are saturated at integration time (t_{int1}). As the exposure time increases further, the camera sensors under the influence of mid-tones are saturated at integration time (t_{int2}). Similarly, as we have seen for integration time (t_{int3}), the camera sensors under the influence of shadows are producing non-saturating signal, while the sensors under the influence of highlights and shadows have been saturated. Therefore, after a short integration time, highlights are captured before the sensor saturates, and adequate integration time is required for capturing the shadows present in the scene.

10.3.1 HDR and Tone-Mapping

In principle, there are two major approaches to handle the limitations of the existing image capturing devices. The first approach is to develop HDR reconstruction from multiple exposures. Debevec and Malik [19] has estimated camera

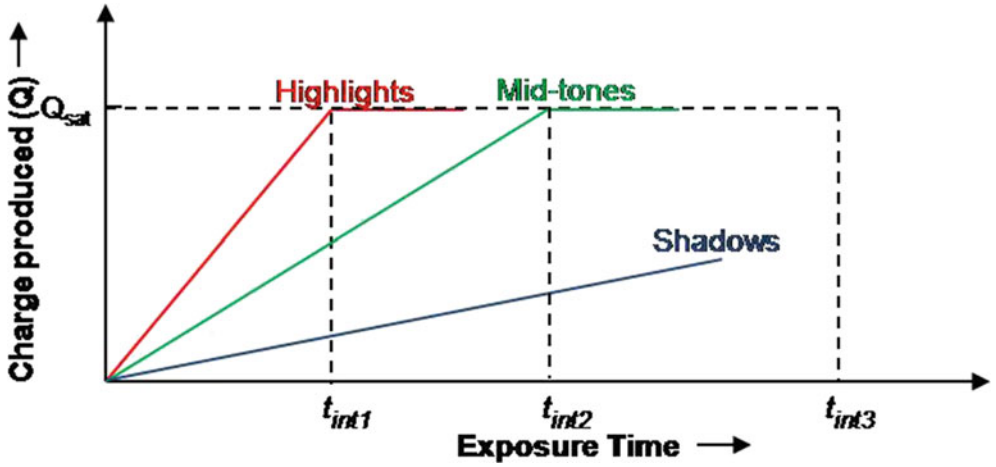

Fig. 10.8 Idealized repose of CCD sensor from highlights, mid-tones, and shadows present the scene. Image courtesy of [18]

response function (CRF) from images acquired at different exposure settings. The CRF recovered from differently exposed images is used to create HDR image whose pixel values are equivalent to the true radiance value of a scene. Let multiple exposures of a scene are captured with different exposure times $\triangle t_j$, where j is an index over exposure times $j = 1, 2.....N$ that determines the number of images to be captured from the scene. The pixel values Z_{ij} at each jth spatial location can be computed as:

$$Z_{ij} = f(E_i \triangle t_j) \tag{10.16}$$

where E_i is irradiance values of ith pixel, and $f(.)$ is the CRF. If CRF is assumed to be monotonic and invertible, we then can rewrite Eq. 10.16 as:

$$f^{-1}(Z_{ij}) = E_i \triangle t_j \tag{10.17}$$

This equation can be solved by taking the natural logarithm of both sides:

$$g(Z_{ij}) = InE_i + In\triangle t_j \tag{10.18}$$

where g is the monotonic and invertible function [19]. In this equation, E_i and g are unknowns. A quadratic objective function based on linear least squares optimization was proposed by Debevec and Malik to derive response function, which is defined as:

$$O = \sum_{i=1}^{N}\sum_{j=1}^{P}\left\{w(Z_{ij})\left[g(Z_{ij}) - InE_i - In\triangle t_j\right]\right\}^2 + \gamma_1 \sum_{z=Z_{\min}+1}^{Z_{\max}-1}\left[w(z)g''(z)\right]^2 \tag{10.19}$$

Therefore, the second term $g''(z) = g(z-1) - 2g(z) + g(z+1)$ is a smoothness term on the sum of squared values, and γ_1 is a scalar that helps to control noise level in Z_{ij}. The weighting function $w(z)$ chosen in [19] is a simple hat function:

$$w(z) = \begin{cases} z - Z_{\min} & \text{for } z \le \frac{1}{2}(Z_{\min} + Z_{\max}), \\ Z_{\max} - z & \text{for } z > \frac{1}{2}(Z_{\min} + Z_{\max}) \end{cases} \tag{10.20}$$

Once the response function g is recovered, the desired HDR radiance values are computed using weighting function as:

$$InE_i = \frac{\sum_{j=1}^{P} w(Z_{ij})\left(g\left(Z_{ij}\right) - In\triangle t_j\right)}{\sum_{j=1}^{P} w(Z_{ij})} \tag{10.21}$$

It reconstructs the full dynamic range up to 8 orders of magnitude. HDR imaging is called scene-referred representation which represents the original captured scene values as close as possible [19]. Such representation is sometimes also referred to as extrasensory data representation. After acquiring HDR data, an efficient encoding technique is needed to avoid taking an excess of disk space. Various possible formats to store radiance maps have been developed that are described by Reinhard et al. [6].

HDR reconstruction recovers a much wider range of brightness from input exposures, but it is impractical to display such images on standard display devices and printing media, as shown in Fig. 10.9b. Although HDR display devices will be developed in the near future, conventional printers may lead to inconsistencies which will be responsible for the loss of details in the output. Recently, Sunnybrook technologies, BrightSide, and Dolby prototypes of HDR display devices have been proposed [20] that can display HDR data directly. As a result, to avoid these inconsistencies, we must use tone-mapping operators [21] to prepare HDR imagery for depiction on LDR devices.

The problem of recovering HDR image by combining multiple frames captured at variable exposure settings is well described in the literature, and up to now, different software to build HDR photograph have been proposed, e.g., HDR-

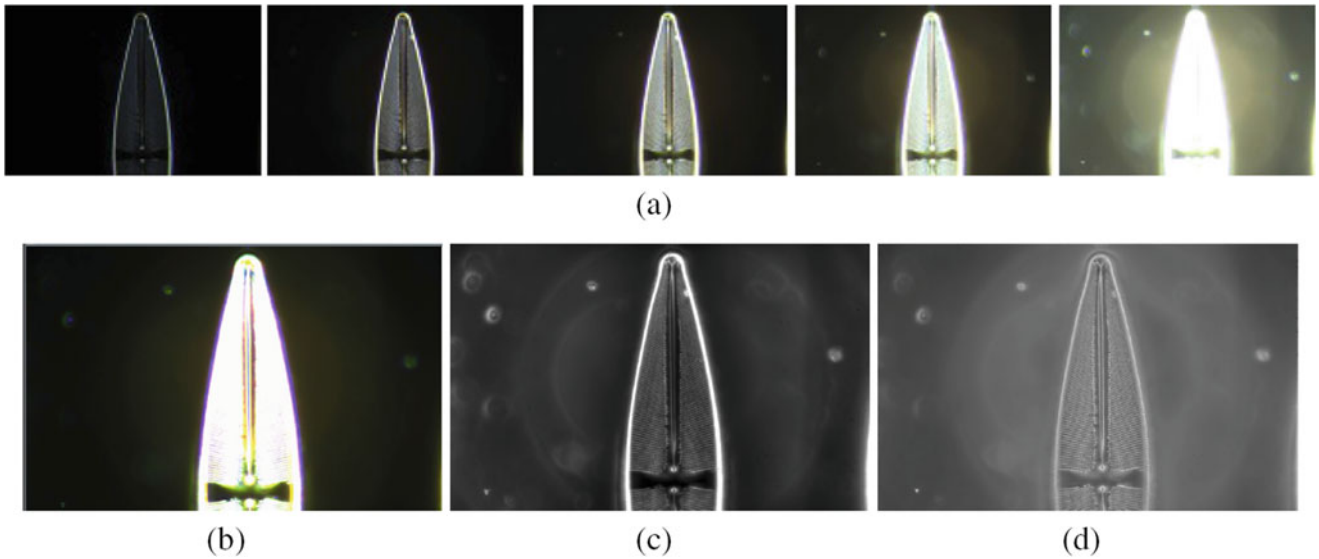

Fig. 10.9 (**a**) Images acquired at different exposure settings, (**b**) depiction of unprocessed HDR image constructed by Photomatix Pro [23] on a standard monitor, (**c**) the tone-mapped image, and (**d**) exposure fusion results

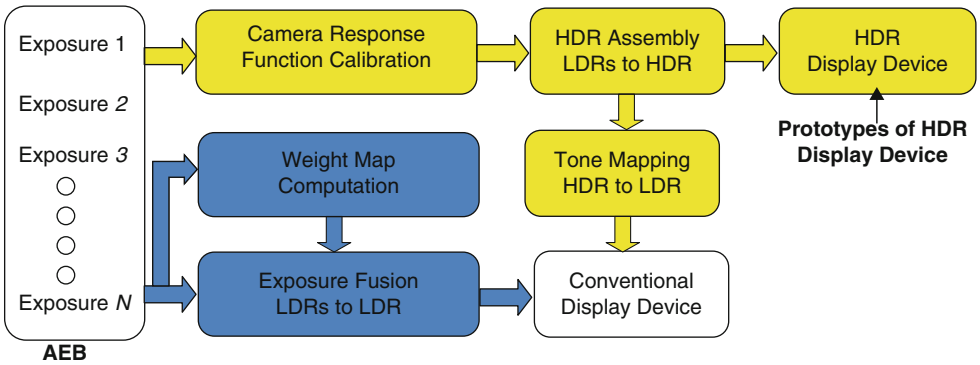

Fig. 10.10 Comparison of high resolution imaging pipeline (i.e., HDR imaging followed by tone-mapping process, and exposure fusion process). The yellow color depicts HDR and tone-mapping pipeline, and blue color depicts exposure fusion pipeline

shop [22] and Photomatix [23]. Photomatix is developed by HDRsoft to fuse a series of differently exposed images. Photomatix Pro and Photomatix Essentials are two standalone versions of Photomatix that can be run on Windows and Mac OS X. Photomatix Essentials is an excellent simple tool for constructing HDR images and is user-friendly. Photomatix Pro offers more options and includes advanced features such as batch processing and selective deghosting. An example of constructing HDR photograph and tone-mapping is shown in Fig. 10.9.

Here, to visualize all important details of the diatom, we have captured five different multiexposure images (shown in Fig. 10.9a). We can observe that appearance of details in multiexposure images depends upon the exposure settings. These five frames are merged to construct 32-bit HDR image. The HDR image has significantly larger dynamic range and does not fit into the display limits of a standard monitor. For demonstration purpose, we depict the HDR image on a standard monitor, which is shown in Fig. 10.9b. Therefore, dynamic-range reduction based on tone-mapping operator would need to be applied on HDR image. The resultant tone-mapped image is shown on the left in Fig. 10.9c. Alternatively, we may directly generate 8-bit LDR image that looks like a tone-mapped image (as shown in Fig. 10.9d), which is described in the following section.

10.3.2 Exposure Fusion

The second alternative approach for the purpose is combining multiexposure images directly into 8-bit single LDR images that do not contain underexposed and overexposed regions [10]. It provides a convenient and consistent way for preserving details in both brightly and poorly illuminated areas by skipping the construction of HDR image, and the use of tone-mapping operators. The incorporation of

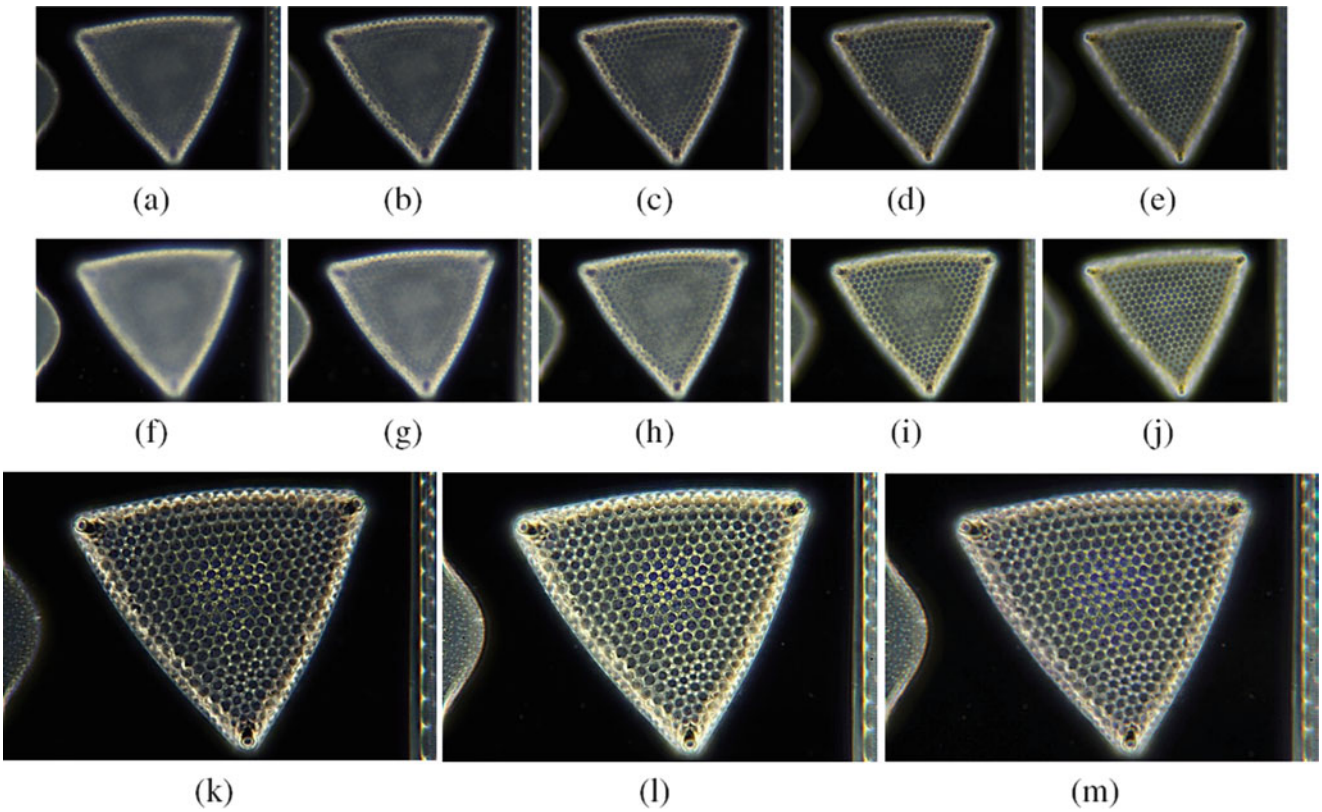

Fig. 10.11 (**a–e**) Multifocus image series of *Triceratium favus* diatom species, acquired at low exposure settings (i.e., shutter speed of 1/160 s and ISO 400), (**f–j**) multifocus image series acquired at high exposure settings (i.e., shutter speed of 1/100 s and ISO 400), (**k**) multifocus fusion result obtained from total five images shown in top row, (**l**) multifocus fusion result obtained from total five images shown in middle row, and (**m**) exposure fusion result obtained from total two images shown in (**k**) and (**l**)

the notion of combining multiple exposures without typical HDR and tone-mapping steps is known as exposure fusion (EF), as shown in Fig. 10.10. The underlying idea of various exposure fusion approaches [24] is based on the utilization of different local measures for generating a weight map to preserve details present in the several exposures. In [24], the pyramid-based multi-resolution decomposition (MRD) [25] was utilized as an analysis and synthesis tool for image fusion. The Laplacian pyramid of source images and the Gaussian pyramid of weight maps were computed to produce a seamless fused image.

In our exposure image fusion approach, we additionally incorporate the exposure measure into our weighting function. To compute exposure value, we normalize the intensity values of input image so that they lie between 0 and 1. A correctly exposed picture is one that has intensities, not near zero (underexposed), or one (overexposed). Therefore, a pixel is said to be well-exposed if the intensity value is close to 0.5. The weight intensity value (I) of each pixel k based on how close it is to 0.5 using a Gauss curve can be computed as:

$$EX_n = \mathrm{e}^{\left(-\frac{(I-0.5)^2}{2\sigma_2}\right)} \tag{10.22}$$

Therefore, the saliency map computation in Eq. 10.5 can be redefined as follows:

$$\hat{SM}_n = |EX_n| \otimes G_{r,\sigma} \tag{10.23}$$

The effect of exposure settings on multifocus images of *Triceratium favus* diatom species acquired by dark-field microscopy is shown in Fig. 10.11a–e. The image series shown in top row (a–e) were acquired with a shutter speed of 1/160 s. To acquire sufficient details, a second series was acquired with a shutter speed of 1/100 s (shown in middle row (f–j)). For demonstration purposes, Fig. 10.11k,l shows the resulting multifocus fusion results for image series captured at low exposure settings and high exposure settings, respectively. These figures show the images fused by considering the saliency maps computed from Eq. 10.5. Thus, a single fused image with improved DOF is obtained from two or more images of the same scene acquired at different focal lengths of a camera sensor.

The fused result shown in Fig. 10.11m is generated by considering the multifocus fusion results shown in Fig. 10.11k,l. This figure shows the image constructed by considering the saliency maps computed from Eq. 10.23.

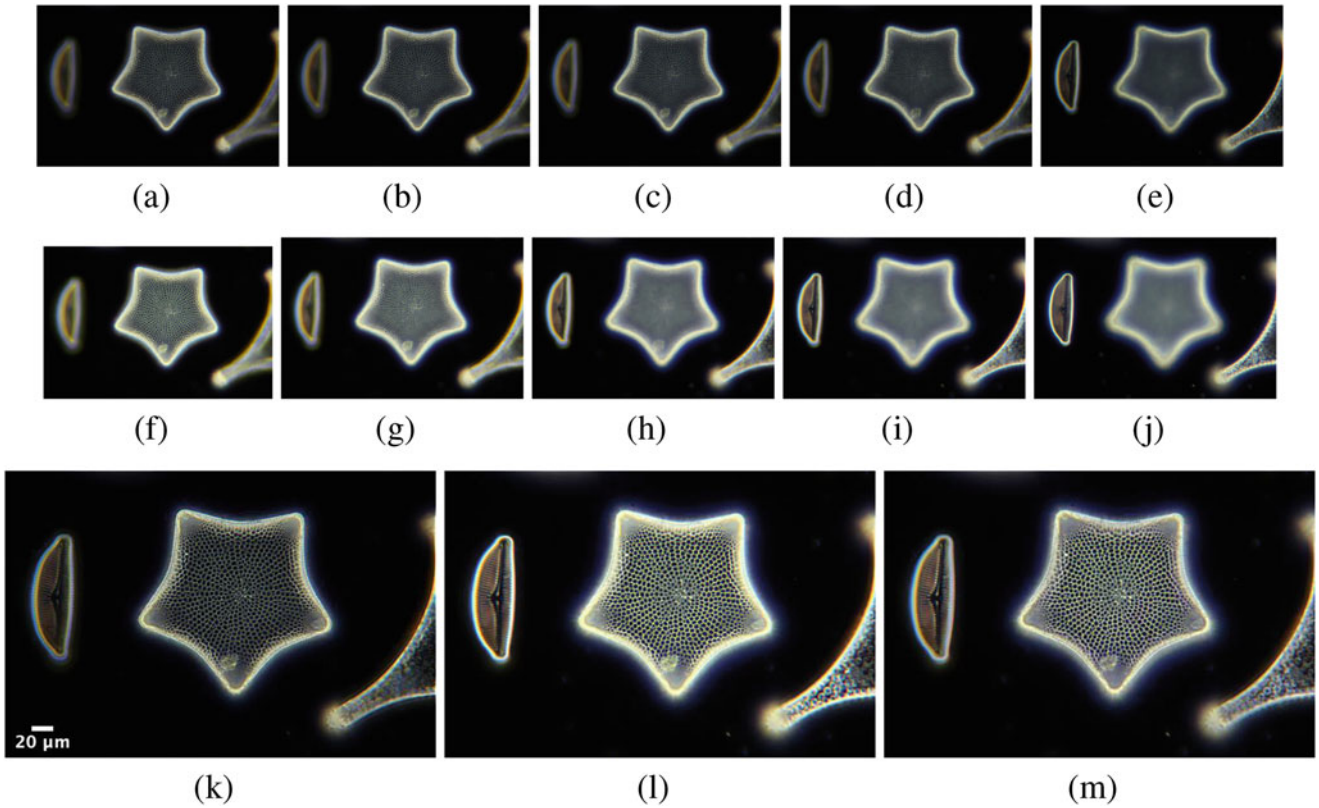

Fig. 10.12 (**a–e**) Multifocus image series of *Triceratium pentacrinus* diatom species, acquired at low exposure settings (i.e., shutter speed of 1/160 s and ISO 400), (**f–j**) multifocus image series acquired at high exposure settings (i.e., shutter speed of 1/100 s and ISO 400), (**k**) multifocus fusion result obtained from total five images shown in top row, (**l**) multifocus fusion result obtained from total five images shown in middle row, and (**m**) exposure fusion result obtained from total two images shown in (**k**) and (**l**)

For detail enhancement, multifocus results are generated using Eq. 10.14. It should be noted that the details produced in Fig. 10.11m are therefore more pronounced than for multifocus fusion results shown in Fig. 10.11k,l. The fusion results of multifocus images of *Triceratium pentacrinus* diatom species shown in Fig. 10.12 are also generated in a similar manner. In our opinion, the precise selection of exposure settings of image acquisition device leads to produce plausible results; it seems to handle very bright and too dark areas in all exposures. Finally, the fusion results show that a sharp and enhanced image can be generated by combining multifocus image fusion with a multiexposure image fusion. This would, of course, be desirable for capturing features of micro- and nano-structures found in diatom species that is helpful for distinguishing the living organism.

10.4 Depth Map and 3-D Surface Visualization of Fusion Results

In this section, the depth map and 3-D visualization have been obtained from the fusion results of *Triceratium favus* diatom species. To indicate the regions where sharp structures are detected in the fusion results, depth map was generated using PICOLAY [26]. PICOLAY, developed by Heribert Cypionka, is a scientific software that allows to perform focus stacking and generate three-dimensional views from image series acquired at sequential focus levels. The depth map of fusion results is shown in Fig. 10.13a–c. The depth map shows colors from yellow (top) over green (middle) to blue (bottom). Gray indicates regions without detected structures and no depth localization.

Another extremely useful way to analyze the diatom shape and its structural variation is to consider that the fused image can be modeled as a 3-D surface. The depth map can also be used to generate a 3-D view of depth levels. The use of a depth map for 3D surface reconstruction was used by the authors in [27], The constructed depth map in Fig. 10.13a–c and the corresponding 3-D surface visualizations are shown in Fig. 10.13d–f. The additional dimension helps to identify each pixel from different angles that have better physical relevance. The 3-D surface visualizations shown in Fig. 10.13d–f are constructed by using Fiji [28]. Fiji was developed at the Laboratory for Optical and Computational Instrumentation (LOCI) at the University of Wisconsin-Madison and is maintained by Curtis Rueden. It allows to explore scientific data and includes features in the form of plugins and scripts.

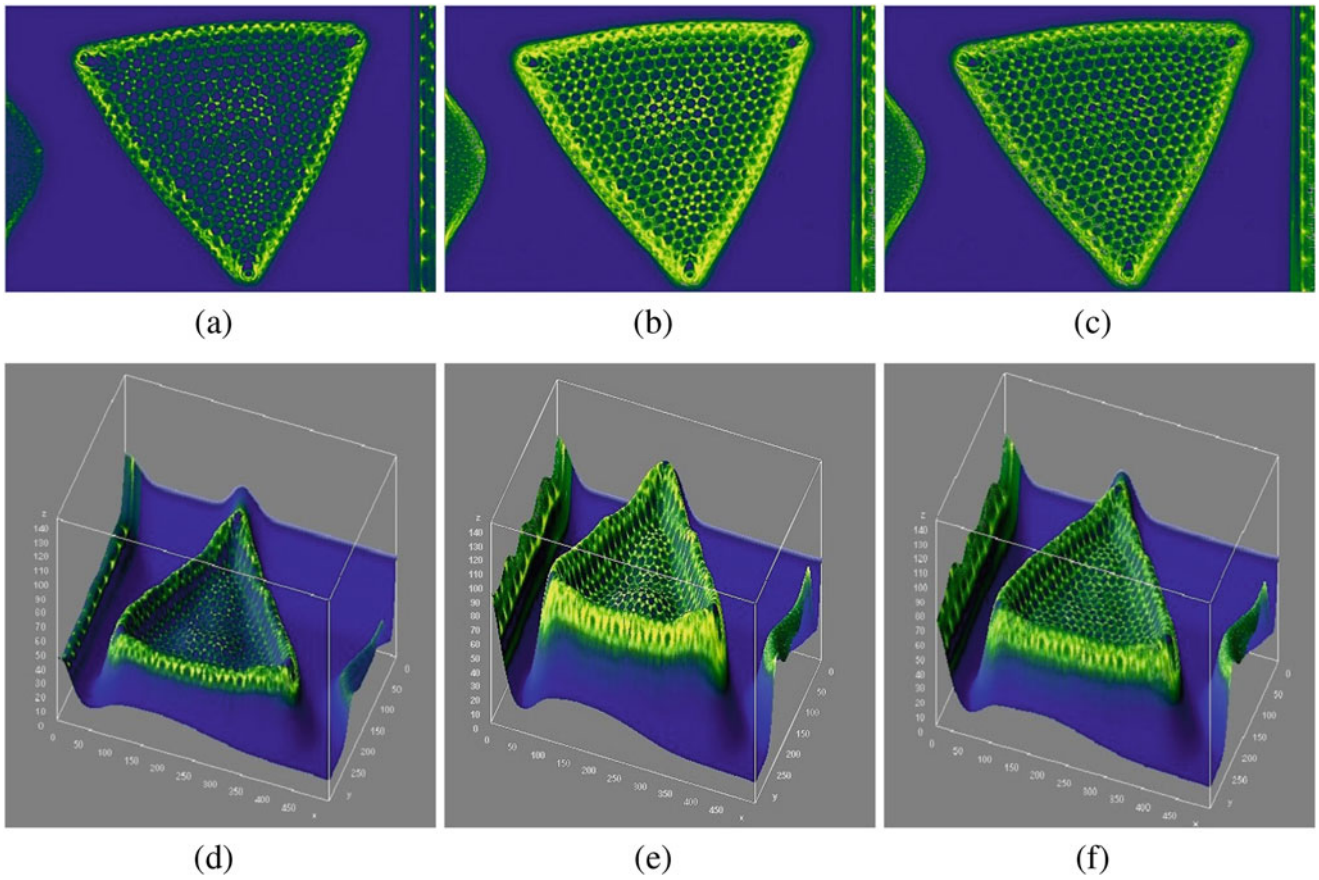

Fig. 10.13 2-D and 3-D visualization of depth map of *Triceratium favus* diatom: (**a**) depth map of fusion result shown in 10.11k, (**b**) depth map of fusion result shown in 10.11l, (**c**) depth map of fusion result shown in 10.11m, and (**d–f**) their 3-D surface visualization

A 3-D projection of fusion results can give a better visualization of structures that belong to different layers. Eventually, different structures can be visualized by changing the viewing angle. For demonstration purpose, Fig. 10.14 shows 3-D reconstruction of the fusion results of *Triceratium favus* diatom. In this way, 3-D surface visualization of a fused image having sharp contour and striation pattern can be used by the diatomists to attempt diatom identification and classification.

10.5 Fusion Quality Metrics

The quality assessment of fused images is necessary before using them for different applications such as machine vision, surveillance applications, scientific, and medical imagery, in which data is analyzed and visualized to record more details. The subjective evaluation of fusion results is time-consuming process, and expert viewers are need to be involved for assessing the performance. In addition, as per ITU recommendation [29], equal viewing conditions are also needed for all viewers for accuracy and fair comparison. On the other hand, the fusion quality metrics quantify the performance of a fusion process without involving the expert viewers. The goal is to measure the amount of complementary information transferred from the source images to the fused image. Therefore, it is essential to use objective image quality metric, which has relevance with the subjective quality measures for validation purpose [30].

In order to quantify the performance of image fusion framework, two assessment strategies are preferred, either referenced or non-referenced assessment. In full referenced assessment, the fused image is compared with a reference image (or ground truth). However, ground truth is not always obtainable in practical applications. The input source images are used as a reference for quality assessment. The second strategy, the quality assessment, is obtained from the fused image without considering any reference or ground truth and is called blind assessment. Numerous non-referenced conventional objective performance measures including spatial frequency (Q^{SF}), average gradient (Q^{AG}), and entropy (Q^{H}) have been proposed [31,32]. The newly developed referenced assessment-based fusion performance measure has been demonstrated by Xydeas and Petrovic [33] in which the amount of edge information transferred from input images to the fused image is evaluated. The detailed description of

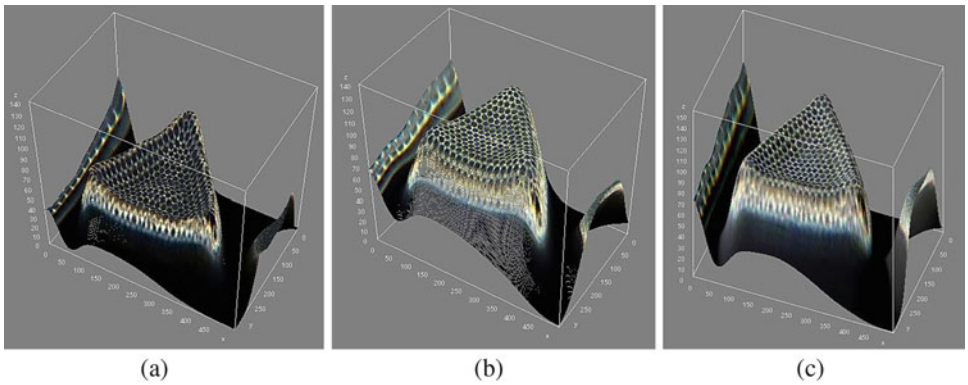

Fig. 10.14 3-D surface visualization of fusion results of *Triceratium favus* diatom: (**a**) 3-D surface visualization of fusion result shown in 10.11k, (**b**) 3-D surface visualization of fusion result shown in 10.11l, and (**c**) 3-D surface visualization of fusion result shown in 10.11m

fusion performance measures is introduced in the following sections.

10.5.1 Gradient-Based Fusion Performance ($Q^{AB/F}$)

Xydeas and Petrovic [33] proposed a feature-based fusion quality metric that evaluates the amount of edge information transferred from input images to the fused image. A Sobel operator is applied to yield the edge strength and orientation information for each pixel. For two input images A and B, and a resulting fused image F, the Sobel edge operator is applied to compute edge strength $e(m,n)$ and orientation $\beta(m,n)$ information of input image A for each pixel, which can be defined as follows:

$$e_A(m,n) = \sqrt{s_A^x(m,n)^2 + s_A^y(m,n)^2} \tag{10.24}$$

$$\beta_A(m,n) = tan^{-1}\left[\frac{s_A^x(m,n)}{s_A^y(m,n)}\right] \tag{10.25}$$

where $s_A^x(m,n)^2$ and $s_A^y(m,n)$ are horizontal and vertical Sobel template cantered on pixel (m,n) and convolved with the corresponding pixels of image A. The relative strength and orientation values of an input image A with respect to F are formed as:

$$\begin{aligned}&\left(G^{AF}(m,n), A^{AF}(m,n)\right)\\ &= \left(\left(\frac{e^F(m,n)}{e^A(m,n)}\right)^{\psi}, 1 - \frac{|\beta_A(m,n) - \beta_F(m,n)|}{\pi/2}\right)\end{aligned} \tag{10.26}$$

where ψ is

$$\psi = \begin{cases} 1 & \text{if } e_A(m,n) > e_F(m,n), \\ -1 & \text{otherwise} \end{cases} \tag{10.27}$$

The edge strength and orientation preservation values can be derived:

$$Q_e^{AF}(m,n) = \frac{\Gamma_e}{1 + e^{\kappa_e(G^{AF}(m,n) - \sigma_e)}} \tag{10.28}$$

$$Q_\beta^{AF}(m,n) = \frac{\Gamma_\beta}{1 + e^{\kappa_\beta(A^{AF}(m,n) - \sigma_\beta)}} \tag{10.29}$$

where Γ_e,κ_e,σ_e and Γ_β,κ_β,σ_β determine the shape of sigmoid functions used to form the edge strength and orientation preservation. Edge information preservation value is then defined as follows:

$$Q^{AF}(m,n) = Q_e^{AF}(m,n) Q_\beta^{AF}(m,n) \tag{10.30}$$

Finally, the metric value $Q^{AB/F}$ is defined as:

$$\begin{aligned}&Q^{AB/F}\\ &= \frac{\sum_{n=1}^{N}\sum_{m=1}^{M}\left(Q^{AF}(m,n)\omega^A(m,n) + Q^{BF}(m,n)\omega^B(m,n)\right)}{\sum_{n=1}^{N}\sum_{m=1}^{M}\left(\omega^A(m,n) + \omega^B(m,n)\right)}\end{aligned} \tag{10.31}$$

which evaluates the sum of edge information preservation values for both inputs Q^{AF} and Q^{BF} weighted by local importance perceptual factors ω^A and ω^A. We defined $\omega^A(m,n) = [e^A(m,n)]^L$ and $\omega^B(m,n) = [e^B(m,n)]^L$, where L is a constant.

For the "ideal fusion," the sum of $Q^{AB/F}$, total loss of information $L^{AB/F}$, and noise added in the fused image due to fusion process $N^{AB/F}$ should be equal to unity [32], as shown in 10.32.

$$Q^{AB/F} + L^{AB/F} + N^{AB/F} = 1 \tag{10.32}$$

In most of the cases, fusion artifact measure introduced in [33] could not lead to unity. In order to overcome this problem, the revised fusion artifact measure was proposed by B.K.S. Kumar [32], which is defined as follows:

$$N^{AB/F} = \frac{\sum_{n=1}^{N}\sum_{m=1}^{M} AM(m,n)\left[\left(1-Q^{AF}(m,n)\right)\omega^{A}(m,n)+\left(1-Q^{BF}(m,n)\right)\omega^{B}(m,n)\right]}{\sum_{n=1}^{N}\sum_{m=1}^{M}\left(\omega^{A}(m,n)+\omega^{B}(m,n)\right)} \tag{10.33}$$

where $AM(m,n)$ indicates the location of fusion artifacts in the fused image and is defined as follows:

$$AM(m,n) = \begin{cases} 1 & \text{if } e_F(m,n) > e_A(m,n) \text{ and } e_F(m,n) > e_B(m,n), \\ 0 & \text{otherwise} \end{cases} \tag{10.34}$$

The outcomes of objective performance measures are tabulated in Table 10.1.

10.5.2 Image Fusion Metric Based on Spatial Frequency (Q^{SF})

The spatial frequency, which is originated from the human visual system (HVS), indicates the overall activity level in an image and has led to an effective objective quality index for image fusion [34]. The total spatial frequency of the fused image is computed from row (RF) and column (CF) frequencies of the image block and Q^{SF} is defined as:

$$Q^{SF} = \sqrt{RF^2 + CF^2} \tag{10.35}$$

$$RF = \sqrt{\frac{1}{MN}\sum_{m=1}^{M}\sum_{n=1}^{N}\left(I_F(m,n) - I_F(m,n-1)\right)^2} \tag{10.36}$$

$$CF = \sqrt{\frac{1}{MN}\sum_{m=1}^{M}\sum_{n=1}^{N}\left(I_F(m,n) - I_F(m-1,n)\right)^2} \tag{10.37}$$

where $I_F(m,n)$ is the gray value of pixel at position (m,n) of image I_F.

Table 10.1 Quantitative assessments of multifocus image fusion results

Measure	$Q^{AB/F}$	$L^{AB/F}$	$N^{AB/F}$	Sum Eq. 10.32	Q^{SF}	Q^{AG}	Q^{H}
Actinocyclus ralfsii							
MRD [24]	0.6658	0.3189	**0.0153**	1	8.774	7.363	5.781
TSD-MF	**0.8891**	**0.0826**	0.0283	1	**9.289**	**10.403**	**6.024**
Actinoptychus senarius							
MRD [24]	0.2573	0.7331	**0.0096**	1	2.608	1.456	4.999
TSD-MF	**0.5419**	**0.3849**	0.0732	1	**5.795**	**3.303**	**5.365**
Triceratium favus (1/160 s)							
MRD [24]	0.7157	0.2378	**0.0465**	1	3.971	2.219	5.892
TSD-MF	**0.7587**	**0.1902**	0.0511	1	**4.040**	**2.255**	**5.780**
Triceratium favus (1/100 s)							
MRD [24]	0.7119	0.2292	**0.0589**	1	4.323	2.552	6.462
TSD-MF	**0.7688**	**0.1507**	0.0805	1	**4.799**	**2.922**	**6.565**
Triceratium pentacrinus (1/160 s)							
MRD [24]	**0.9361**	**0.0515**	**0.0124**	1	3.895	1.936	4.762
TSD-MF	0.9265	0.0535	0.0200	1	**4.330**	**2.200**	**4.671**
Triceratium pentacrinus (1/100 s)							
MRD [24]	0.8490	0.1365	**0.0145**	1	4.559	2.458	5.575
TSD-MF	**0.8765**	**0.0953**	0.0282	1	**5.228**	**3.073**	**5.605**

10.5.3 Average Gradient-Based Fusion Metric (Q^{AG})

It estimates a degree of clarity and sharpness in the fused image and is computed as

$$Q^{AG} = \frac{\sum_i \sum_j \left(((I_F(i,j) - I_F(i+1,j))^2 + I_F(i,j) - I_F(i,j+1))^2\right)^{1/2}}{mn} \tag{10.38}$$

In general, we desire that a good image fusion method should yield a higher score in terms of Q^{AG}.

10.5.4 Entropy-Based Fusion Metric (Q^H)

This metric is based on information theory. It quantifies the amount of information present in the fused image, and is defined as follows:

$$Q_H = -\sum_{k=0}^{255} p_k \log_2 p_k \tag{10.39}$$

where p_k is the probability of intensity value k in an 8-bit fused image.

To better analyze the performance of fusion approaches with the help of assessment metrics, the outcomes of two-scale decomposition-based weighted average multifocus image fusion (TSD-MF) and the results proposed by multi-resolution decomposition (MRD) [24] are given in Table 10.1, better values are depicted in bold. The higher the value of $Q^{AB/F}$ is, better is the quality of the composite image. On the other hand, the lower the values of $L^{AB/F}$ and $N^{AB/F}$ are, the better the quality of composite image. In relation to non-referenced quality metrics Q^{SF}, Q^{AG}, and Q^H, higher values are expected from the ideal fusion process. The analysis presented in Table 10.1 shows that on six microscopy data sets the TSD-MF outperformed MSD. It can be observed that TSD-MF has scored higher value in terms of $Q^{AB/F}$ and lower value in terms of $L^{AB/F}$, for all data sets except *Triceratium Pentacrinus* (acquired at exposure time of 1/160 s). It can be noticed that MSD has better performance in terms of $N^{AB/F}$ that gives the lower metric outcome. On the other hand, MSD did not perform well in terms of $Q^{AB/F}$ and $L^{AB/F}$. In terms of Q^{SF}, Q^{AG}, and Q^H, TSD-MF has scored a higher value for all six data sets. Thus, the performance of TSD-MF is excellent for improving DOF, while avoiding visual artifacts.

10.6 Efficient Implementations

The average execution time of the TSD-MF algorithm on microscopy data is presented in Table 10.2. The algorithm is implemented in MATLAB 2014a and executed on the machine with 3.70 GHz Intel Core i3 processor and 8 GB RAM. The total execution time includes the n number of source images read time, the BL computation time, the DL computation time, the computation time of n number of weight maps for BL, the computation time of n number of weight maps for DL, and the computation time of the resultant fused image generation, while the write time of the resultant fused image is not included.

As shown in Table 10.2, the weight map refinement based on WLS operator in Eq. 10.9 and Eq. 10.10 is the most time-consuming. In our fusion approach, the WLS operator uses the preconditioned conjugate gradients (PCG) [35]. It was reported in [16] that the average time of PCG-based sparse matrix solver is 3.5 s per megapixel on a 2.2 GHz Intel Core 2 Duo. We believe that the overall execution time of weight map optimization can be reduced through an efficient GPU implementation of the solver proposed by Weber et al. [36].

Table 10.2 Comparison of execution time in seconds (s). The number of input images is shown in brackets

Algorithm/operation	Input read	BL	DL	W^B	W^D	I_F	Total
Actinocyclus ralfsii 925 × 694 (3)							
TSD-MF	0.05	0.41	0.02	7.06	7.06	0.08	14.64
Actinoptychus senarius 454 × 439 (5)							
TSD-MF	0.08	0.21	0.01	3.30	3.30	0.04	6.86
Triceratium favus 2592 × 1728 × 3 (5)							
TSD-MF	0.76	61.92	0.71	540.8	540.8	49.05	1194.1

10.7 Discussion and Conclusions

In this chapter, we have presented TSD-MF scheme that can extend DOF of the fused image by selecting the in-focus region from source images of diatom species. The EOL is utilized as a criteria function that identifies the in-focus region to compute the initial saliency maps. The weight maps are determined by comparing the edge strength that explicitly defined which region should be selected from source images to obtain a single composite image. The weight maps are hard, noisy, and not aligned with the object boundaries, which are not suitable for pixel-level weighted overage fusion. In this chapter, we have introduced a weight map refinement approach based on WLS edge-preserving operator. The results show that significant improvements have been obtained by fusing BLs and DLs separately, with different weight maps for BLs and DLs fusion rather than same weight map.

We have observed that the appearance of details in the multiexposure images of diatom species depends upon exposure settings. By using exposure measure as a criteria function, multiexposure images can be used to enhance intricate micrometer-sized silica patterns of diatom. This study has opened up a potent way to provide a clue to their role in diatom identification and classification. The fusion results from two very different data sets acquired at a shutter speed of 1/160 s and a shutter speed of 1/100 s revealed that further developments would undoubtedly perform better for identification and classification of diatom species.

The quantitative analysis of fusion results using four quality metrics clearly demonstrates that TSD-MF method preserves more details to improve the clarity and sharpness in the fused image. It should be noted that the fixed parameter setting was used to obtain fusion results for all data sets. In future work, we would like to experiment with more precise parameter selection for improving the DOF of fused image. Another direction for future work is to explore which GPU implementation of sparse matrix solver might reduce the execution time of our fusion method. In particular, we would like to develop a more computationally efficient scheme for generating the fused image with improved DOF and robustness.

References

1. Liu, Y., Jin, J., Wang, Q., Shen, Y., Dong, X.: Region level based multi-focus image fusion using quaternion wavelet and normalized cut. Signal Process. **97**, 9–30 (2014)
2. Tian, J., Chen, L.: Adaptive multi-focus image fusion using a wavelet-based statistical sharpness measure. Signal Process. **92**(9), 2137–2146 (2012)
3. Redondo, R., Šroubek, F., Fischer, S., Cristóbal, G.: Multifocus image fusion using the log-Gabor transform and a Multisize Windows technique. Inf. Fusion **10**, 163–171 (2009)
4. Zhai, Y., Shah, M.: Visual attention detection in video sequences using spatiotemporal cues. In: Proceedings of the 14th ACM International Conference on Multimedia, pp. 815–824. ACM, New York (2006)
5. Zhou, Z., Wang, B., Li, S., Dong, M.: Perceptual fusion of infrared and visible images through a hybrid multi-scale decomposition with Gaussian and bilateral filters. Inf. Fusion **30**, 15–26 (2016)
6. Reinhard, E., Ward, G., Pattanaik, S., Debvec, P.: High Dynamic Range Imaging Acquisition, Manipulation, and Display. Morgan Kaufmann, Burlington (2005)
7. Aslantas, V., Kurban, R.: A comparison of criterion functions for fusion of multi-focus noisy images. Opt. Commun. **282**(16), 3231–3242 (2009)
8. Li, S., Kang, X., Hu, J.: Image fusion with guided filtering. IEEE Trans. Image Process. **22**(7), 2864–2875 (2013)
9. He, K., Sun, J., Tang, X.: Guided image filtering. IEEE Trans. Pattern Anal. Mach. Intell. **35**(6), 1397–1409 (2013)
10. Singh, H., Kumar, V., Bhooshan, S.: Weighted least squares based detail enhanced exposure fusion. ISRN Signal Process. **2014**, 1–18. Article ID 498762 (2014). https://doi.org/10.1155/2014/498762
11. Perona, P., Malik, J.: Scale-space and edge detection using anisotropic diffusion. IEEE Trans. Pattern Anal. Mach. Intell. **12**(7), 629–639 (1990)
12. Hariharan, R., Rajagopalan, A.N.: Shape-from-focus by tensor voting. IEEE Trans. Image Process. **21**(7), 3323–3328 (2012)
13. Aslantas, V., Kurban, R.: A comparison of criterion functions for fusion of multi-focus noisy images. Opt. Commun. **282**(16), 3231–3242 (2009)
14. Huang, W., Jing, Z: Multi-focus image fusion using pulse coupled neural network. Pattern Recogn. Lett. **28**(9), 1123–1132 (2007)
15. Subbarao, M., Choi, T., Nikzad, A.: Focusing techniques. In: Machine Vision Applications, Architectures, and Systems Integration. International Society for Optics and Photonics, pp. 163–174 (1992)
16. Farbman, Z., Fattal, R., Lischinski, D., Szeliski, R.: Edge-preserving decompositions for multi-scale tone and detail manipulation. ACM Trans. Graph. **27**(3) (2008)
17. Ferrara, M.A., Dardano, P., De Stefano, L., Rea, I., Coppola, G., Rendina, I., Congestri, R., Antonucci, A., De Stefano, M., De Tommasi, E.: Optical properties of diatom nanostructured biosilica in *Arachnoidiscus* sp: micro-optics from mother nature. PLOS ONE **9**(7), e103750 (2014)
18. Singh, H., Bhooshan, S.V.: Detail enhanced multi-exposure image fusion based on edge preserving filters. Electron. Lett. Comput. Vis. Image Anal. **16**(2), 13–16 (2018)
19. Debevec, P.E., Malik, J.: Recovering high dynamic range radiance maps from photographs. In: Proceedings of the Conference on Computer Graphics (SIGGRAPH '97), pp. 369–378 (1997)
20. Seetzen, H., Heidrich, W., Stuerzlinger, W., et al.: High dynamic range display system. ACM Trans. Graph. **23**(3), 760–768 (2004)
21. Reinhard, E., Stark, M., Shirley, P., Ferwerda, J.: Photographic tone reproduction for digital images. ACM Trans. Graph. **21**(3), 267–276 (2002)
22. HDR image formation software: http://www.hdrshop.com/
23. McCollough, F.: Complete Guide to High Dynamic Range Digital Photography. Lark Books, New York (2008)
24. Mertens, T., Kautz, J., Van Reeth, F.: Exposure fusion: a simple and practical alternative to high dynamic range photography. Comput. Graphics Forum **28**(1), 161–171 (2009)
25. Burt, P.J., Adelson, E.H.: The Laplacian pyramid as a compact image code. IEEE Trans. Commun. **31**(4), 532–540 (1983)
26. Picolay. https://bit.ly/2KGOQNx. Accessed 29 Nov 2018
27. Sroubek, F., Gabarda, S., Redondo, R., Fischer, S., Cristobal, G.: Multifocus fusion with oriented windows. Proceedings of SPIE, vol. 5839, Bioengineered and Bioinspired Systems II. https://doi.org/10.1117/12.608399 (2005)
28. Fiji. http://fiji.sc/. Accessed 29 Nov 2018

29. ITU, Methodology for the Subjective Assessment of the Quality of Television Pictures, ITU-R Rec. BT. 500-9 (1998)
30. Petrovic, V.: Subjective tests for image fusion evaluation and objective metric validation. Inf. Fusion **8**(2), 208–216 (2007)
31. Shah, P., Srikanth, T.V., Merchant, S.N., Desai, U.B.: A novel multifocus image fusion scheme based on pixel significance using wavelet transform. In: Proceedings of Image, Video, and Multidimensional Signal Process (IVMSP), pp. 54–59 (2011)
32. Shreyamsha Kumar, B.K.: Multifocus and multispectral image fusion based on pixel significance using discrete cosine harmonic wavelet transform. SIViP **7**(6), 1125–1143 (2013)
33. Xydeas, C.S., Petrovic, V.: Objective image fusion performance measure. Electron. Lett. **36**(4), 308–309 (2000)
34. Zheng, Y., Essock, E.A., Hansen, B.C., Haun, A.M.: A new metric based on extended spatial frequency and its application to DWT based fusion algorithms. Inf. Fusion **8**(2), 177–192 (2007)
35. Saad, Y.: Iterative Methods for Sparse Linear Systems, 2nd edn. SIAM, Philadelphia (2003)
36. Weber, D., Bender, J., Schnoes, M., Stork, A., Fellner, D.: Efficient GPU data structures and methods to solve sparse linear systems. Comput. Graphics Forum **32**(1), 16–26 (2003)

Stereoscopic Imaging of Diatoms in Light and Electron Microscopy

11

Robert Sturm

Abstract

During the past decade stereoscopic photography, which had already been developed in the 1850s, experienced a noticeable renaissance in natural sciences. In diverse biological disciplines such as cell biology, morphology and histology, stereoscopic imaging became a supporting technique in both light- and electron-microscopy. Meanwhile, generation of stereo pairs can be attained in different ways. Besides the classical method, according to which an object is photographed from two slightly different perspectives, also new computer-aided processes of 3D imaging have been established. In transmitted light microscopy software-based generation of stereoscopic images is commonly realized by using an image stack, where the transparent object has been *repeatedly* photographed with different positions of the focus plane. With the help of this image stack, an object depth map is computed, which includes spatial information of the photographed item. Based on this information a slight stereoscopic rotation of the object can be modeled by application of surface rendering processes. In light-microscopy of opaque objects and scanning electron microscopy, computer-aided object depth mapping is mainly founded upon light-dark gradients recorded on single photographs. If the degree of brightness continuously declines from foreground to background, highest stereoscopic modeling accuracy can be obtained. Three-dimensional imaging of diatom frustules is mainly carried out with the help of software-based techniques and should be of major interest in future research due to several reasons: First, stereoscopic images offer a valuable support for detailed investigations of surface structures occurring on the valves; second, stereo photography can be used for the effective description of distinctive marks of a given species; third, stereo pairs can represent useful fundamentals for morphometric investigations.

11.1 Introduction

11.1.1 Stereoscopy: Basic Concepts and Brief History

Stereoscopy (Greek: stereos = firm, solid; skopein = to look, to see) represents an advanced optical technique that allows the three-dimensional visualization of arbitrary objects. Concretely speaking, the method produces or amplifies the illusion of depth in an image by means of the human ability of stereopsis (Greek: opsis = sight), where the perception of depth is associated with the visual information generated in two eyes [1–3]. The stereoscopic effect is commonly achieved by photographing the study object from two slightly different perspectives. The resulting pics, better known as stereoscopic semi-images, are subsequently combined to a stereo pair or stereogram, which can be presented to the viewer in various ways. In classical stereoscopy, the semi-images are simply arranged side by side, whereby the overall width of the stereogram should not exceed 130 mm [1]. In the next step, the semi-images are separately shown to the left and right eye of the spectator, so that an image fusion process can be initiated in the primary visual cortex of the brain. This physiological mechanism, however, is accountable for the perception of three-dimensional depth [2, 3]. In modern stereoscopy, the semi-images are encoded with different colors (commonly red and cyan/green) or oscillation directions of polarized light and afterward subjected to systematic superposition [1–3]. The resulting anaglyphs (Greek: ana = on each other, glyphein = to carve) can be only inspected with the help of optical devices such as red-cyan glasses or glasses with specifically oriented polarizing filters [4–6].

R. Sturm (✉)
Department of Material Sciences and Physics, University of Salzburg, Salzburg, Austria
e-mail: sturm_rob@hotmail.com

G. Cristóbal et al. (eds.), *Modern Trends in Diatom Identification*, Developments in Applied Phycology 10,
https://doi.org/10.1007/978-3-030-39212-3_11

Some fundamental ideas of stereoscopy already date back in the fifteenth century, when the universal genius and inventor Leonardo da Vinci performed several experiments figuring out the relationship between the course of light beams and the visibility of object structure and depth. At the end of the sixteenth century, the Italian painter Jacopo Chimenti da Empoli published the first stereoscopic picture in terms of two ink drawings depicting a young artist at his work [1–3]. In the middle of the nineteenth century, stereoscopy flourished for the first time with the invention of daguerreotypy, the most initial form of photography. First stereo photographs were produced in the 1840s and 1850s, so that the optical technique became acquainted to a broader public. At this time, also first optical devices, known as stereoscopes, were developed, which allowed a specific inspection of the stereograms [7, 8]. Toward the end of the nineteenth century, production of stereoscopic photographs was remarkably facilitated by the development and commercial distribution of rather handy stereo cameras including two separate lenses for the shot of the left and right semi-image [1–6]. The subsequent hype of stereo photography, however, persisted till the 1930s. A renaissance of the optical technique started in the 1980s, when both cinematic art and science showed increased interest in the three-dimensional imaging of diverse objects [2, 9, 10].

Primary scientific applications of stereo photography date back to the early twentieth century, when particularly archeologists, meteorologists, and topographers benefited from the potential of 3D imaging. Besides numerous excavation sites also various landscapes and even different types of clouds were captured on the stereo camera [10, 11]. In the following decades, scientific interest in stereoscopy became continuously increased, because the optical technique among others enabled the targeted presentation of complex superficial structures and the associated answering of numerous open questions. Since the 1980s stereo photography has found its increased way into light- and electron microscopy [12–15]. With modern digital recording systems, 3D imaging of microscopic study objects more and more turns out as rather easy task that can be also managed by inexperienced snapshooters [14, 15]. In the meantime, microscopic stereo photography has found its eligible place in a great number of natural sciences, among which biology, physics, chemistry, and crystallography have to be specifically highlighted [1–3].

Since about two decades scientific disciplines relying on enhanced use of the microscope commonly declare noticeable demand of 3D imaging, because smallest objects can be more effectively studied with the help of additional depth information provided by stereoscopic photographs. This essential development within the microscopic methodology has also reached botanical and zoological cell biology in the meantime.

11.1.2 Physical Principles of Stereoscopy

The main physical principles standing behind the creation of depth illusion by the stereoscopic method were formulated by Hermann von Helmholtz at the beginning of the twentieth century [16]. The geometric fundamentals of 3D imaging are summarized in the sketches of Fig. 11.1. Like you can see there, the left and right eye are focused on the central point (F) of a bar-shaped object. Any light beams emerging from this point (red, dashed lines) impinge upon the same areas of the left and right retina. Another point (P) marking the back end of the object is positioned behind the central point. Its light beams impinge upon different retinal areas of the left and right eye, but within Panum's or fusional space [2, 17]. The retinal distances between the intersection points of the left and right light beams are labeled with q_l and q_r, respectively. The images of the object projected on the left and right retina are subjected to a fusion process in the primary visual cortex, resulting in the generation of appropriate spatial information. From a physical point of view, the extent of this depth perception can be estimated by the deviation (d), which is defined according to the simple formula

$$d = q_\mathrm{l} – q_\mathrm{r}, \tag{11.1}$$

whereby negative values of this parameter denote a reverse expansion of the object, while positive values indicate a forward expansion. The factors q_l and q_r can adopt a plus sign if the retinal intersection of the light beam of P is relocated against the intersection of the light beam of F in nasal direction. On the other hand, the factors adopt a minus sign, if a respective relocation in temporal direction can be noticed [1–5].

If the object is photographed, it has to be recorded on an image plane (IP) that is positioned between the viewer and the studied item. Light beams cause a projection of the points F and P on the image plane, resulting in the newly generated points F' and P' (left lens) and, alternatively, F'' and P'' (right lens). On the image plane, the deviation or "horizontal parallax" in terms of Helmholtz can be derived from the mathematical equation

$$d = \left(F' - F''\right) - \left(P' - P''\right), \tag{11.2}$$

where $F' - F''$ and $P' - P''$ mark the horizontal distances between the projected points F' and F'' as well as P' and P''. As illustrated in the sketch of Fig. 11.1a, the position of the projected points on the image plane chiefly depends on the distance between the eyes or camera lenses and the image plane (a) and the distance between image plane and object (e). Since length values of the deviation exhibit a strict mathematical dependency on these factors, they are often substituted by constant angular values [16].

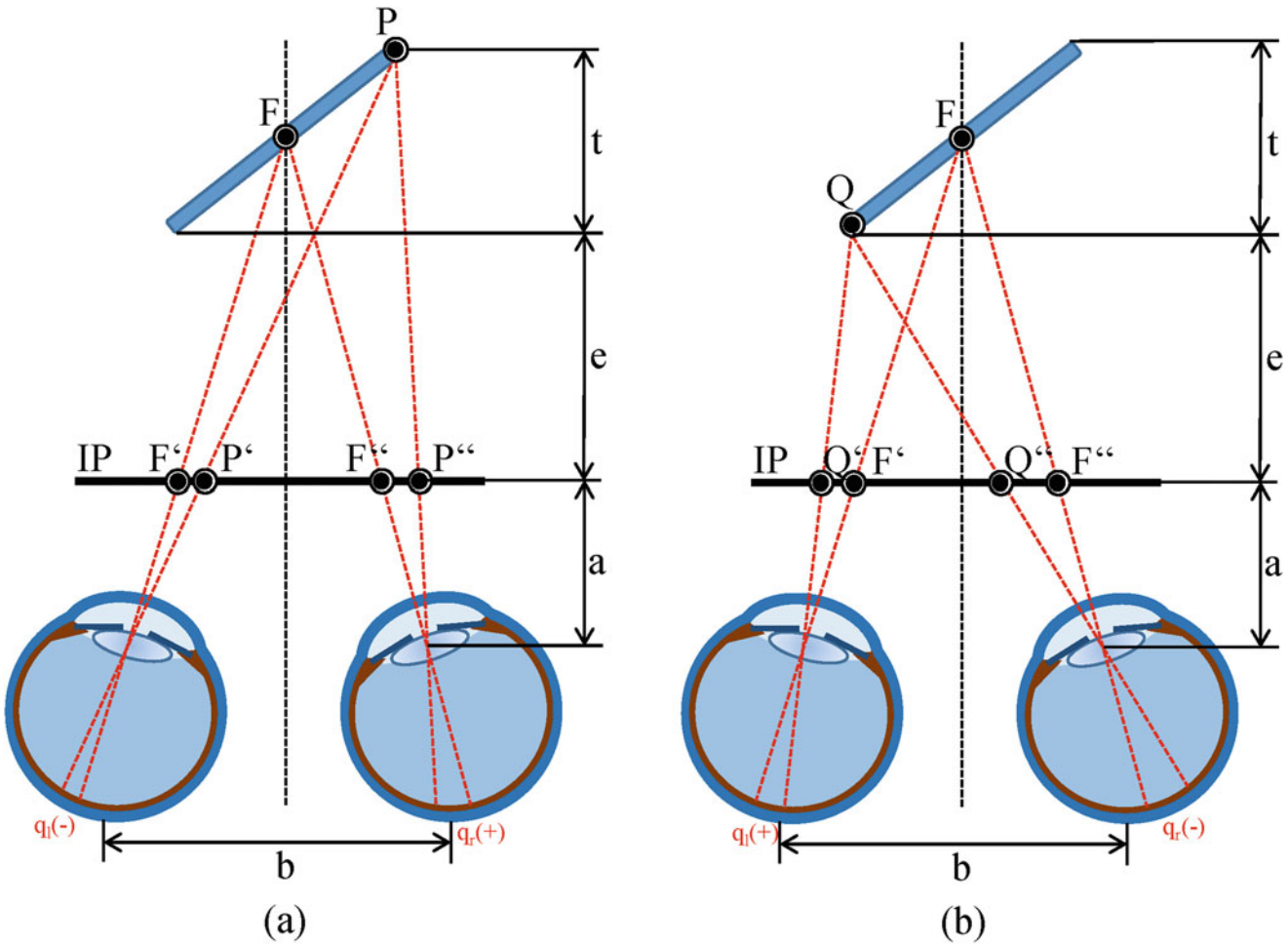

Fig. 11.1 Physical and geometric approach to the stereoscopic effect: (**a**) generation of a negative deviation; (**b**) production of a positive deviation (a = distance between eyes and image plane [IP], b = interocular distance, e = distance between image plane and object, F = focus point, P/Q = object points, q_l = deviation in the left eye, q_r = deviation in the right eye, t = object depth)

In Fig. 11.1b, the point Q marking the anterior end of the object is considered instead of the point P. In contrast to the first situation, both retinal deviation as well as horizontal parallax are distinguished by positive values. This implicates a visual perception of the point Q in front of the point F. The main physical principle standing behind stereoscopy is reflected by the essential circumstance that inspection of the semi-images included in the image plane produces the same optical signals on the left and right retina as viewing of the object itself. Hence, the stereo pair pretends to the eyes the sight on a non-existing item and, thus, has to be classified as an optical illusion [1–3, 16].

As illustrated in Fig. 11.2, the deviation can be also measured on the stereo pair itself, if only one pair of corresponding points (P_l and P_r) is known and the position of the focus points is not obvious. In this specific case, the mathematical equation

$$d = x_l - x_r \tag{11.3}$$

has to be applied, where x_l and x_r, respectively, denote the distances of P_l and P_r from the right vertical edge of the left and right semi-image, respectively. Negative values of this parameter mark a displacement of the object behind the image plane, whereas positive values cause the (partial) protrusion of the object out of the image plane. For the attainment of optimal stereoscopic results, the width of a semi-image (L) should be on the order of 65 mm and the width of the complete stereo pair should amount to 130 mm. Deviation values should always remain below 3 mm, corresponding to about 4% of the horizontal image length.

11.1.3 Types of Stereo Images and Viewing Techniques

In traditional stereoscopic photography, the 3D effect is produced by means of two 2D images that are arranged to a stereo pair. Both images should be characterized by identical

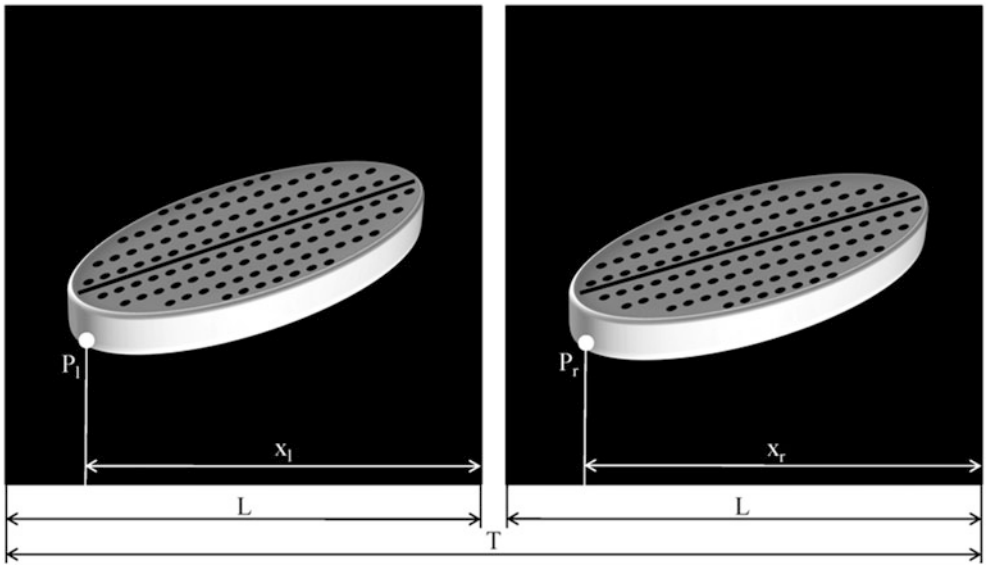

Fig. 11.2 Measurement of the deviation on a classical stereo pair with left and right semi-image. Mathematically, this factor is expressed by the formula $d = x_l - x_r$, with x_l/x_r denoting the distance between P_l/P_r and right edge of the left/right image (L = width of the semi-image, T = total width of the stereo pair)

contrast, brightness, and depth of field. In addition, any vertical parallax, denoting a vertical misalignment between the object depicted on the left image and the object depicted on the right image should be avoided [1–3]. Stereo pairs positioned side by side can be inspected by free viewing, also known as autostereoscopic viewing, or with the help of specific optical devices [2, 4, 5].

Autostereoscopic inspection of stereo pairs includes parallel and cross-eyed viewing (Fig. 11.3). In the first case, the left-eye image is positioned on the left and the right-eye image on the right. The viewer is encouraged to produce a preferably parallel alignment of the optical axes so that he looks "through" the images. This intention can prove difficult with normal vision because eye focus and binocular convergence are subject to close coordination. In order to uncouple these two functions, the viewer can use his flat hand as a partition between the two optical axes, which eventually diminishes the convergence effect and facilitates the viewing of the 2D images with completely relaxed eyes [1–3, 17]. Parallel viewing entails the remarkable disadvantage that corresponding points of distant objects should be separated by identical distances as the viewer's eyes (65 mm). Larger images can be only inspected by a systematic enhancement of the distance between the image plane and eye lens. In the case of cross-eyed viewing, the left eye stares on the right image and the right eye on the left image, so that arrangement of the semi-images has to be interchanged at first. Although the eyes are forced to adopt a convergent position, this viewing method can be rather easily effectuated by placing a fingertip below the division between the two images. In the next step, the fingertip is slowly relocated toward the viewer's eyes, whereby the view of both eyes remains focused on this part of the finger. At a certain distance, the convergence of the optical axes initiates the image fusion process in the primary visual cortex [1–3]. With the use of the cross-eyed viewing technique, any limitations of image size are commonly omitted. On the other side, permanent convergence of the optical axes results in rapid visual fatigue.

Optical devices used for an appropriate inspection of stereo pairs are commonly termed stereoscopes or stereo glasses and operate according to two different physical principles (Fig. 11.4a, b). The more original mirror stereoscopes are based on the principle of light reflection and follow the intention to compensate for the slightly convergent position of the optical axes. This implicates a perfect parallel viewing of the semi-images. Prism stereoscopes deploy the physical principle of light refraction in order to generate either a parallel or a crossed-eyed viewing of the 2D images [4–9].

In modern stereoscopic photography, the 2D images exhibiting the object from two different perspectives are encoded with complementary colors (e.g., red and cyan) and superimposed to a so-called anaglyph. This type of stereoscopic image, however, is not hallmarked by any size limitations and, therefore, can be also used for large-format presentations. Red-cyan anaglyphs are ordinarily viewed with the help of red-cyan glasses operating according to the physical principle of light filtering (Fig. 11.4c). The red filter blocks the light reflected by the cyan semi-image, whereas the cyan filter blocks the light reflected by the red semi-image. This phenomenon implicates a separate perception of the 2D images by the left and right eye and the initiation of the image fusion process in the brain [1, 2, 17, 18].

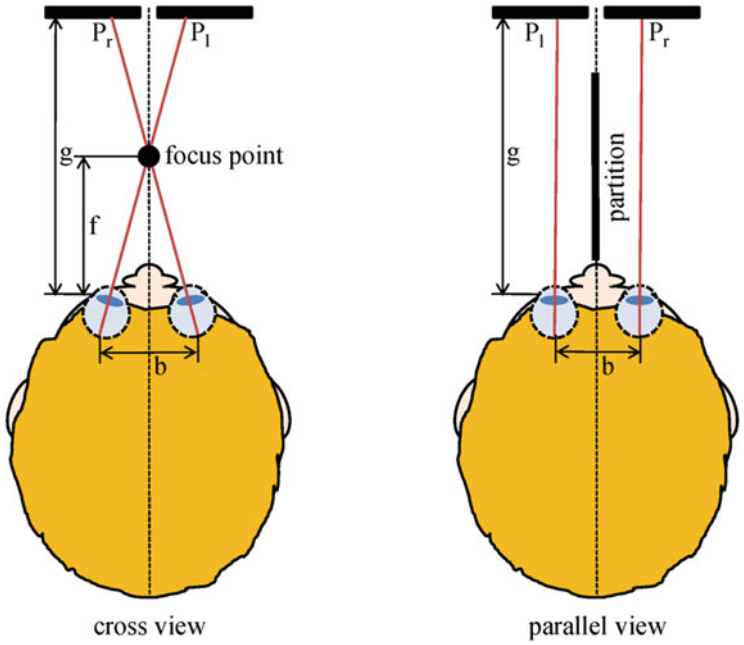

Fig. 11.3 Free-viewing or autostereoscopic techniques for an appropriate inspection of stereo pairs with semi-images placed side by side. With the help of these methods any use of optical devices can be relinquished (b = interocular distance, f = distance of the focus point, g = image distance, P_l/P_r = corresponding points on the left and right semi-image)

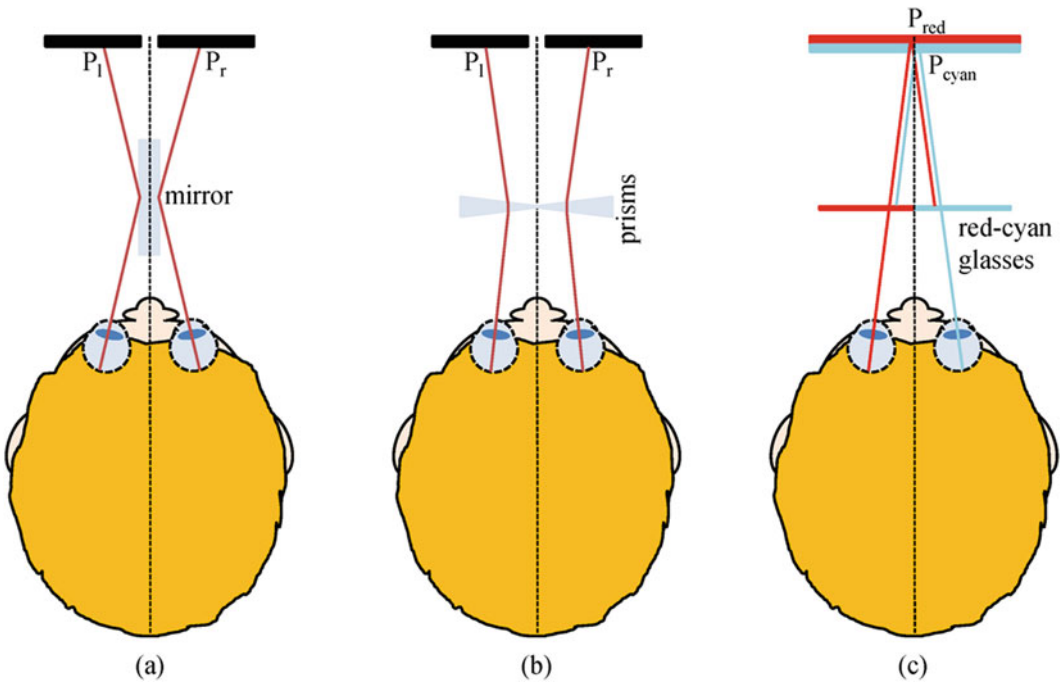

Fig. 11.4 Viewing of classical stereo pairs and red-cyan anaglyphs with respective optical devices: (**a**) mirror stereoscope, (**b**) prism stereoscope, (**c**) red-cyan glasses

11.2 Three-Dimensional Imaging in LM

11.2.1 Basic Visualization Techniques

In light microscopy, the scientist can select between several methodical accesses to 3D imaging. According to the classical technique illustrated in Fig. 11.5a, the study object is first photographed in its basic position. Afterward, the sample is submitted to a slight rotation ranging from 2° to 10°, and a second shot of the item is produced [19]. Both images have to be made by using the same photographic setup (exposure, magnification, contrast, and depth of field) and under avoidance of a vertical parallax, which denotes a vertical offset of the object between the two photographs [1–3]. In a final step, the two images are arranged to a stereo pair, whereby selection of the left and right semi-image decides on the generation of positive or negative deviation values. In the first case, structural features of the object are partly lifted out of the image plane, whereas in the second case the whole item is relocated behind the image plane.

In transmitted light microscopy usually operating with 40-fold to 1000-fold magnification, the sample rotation technique is frequently stretched to its limits. This observation can be traced back to the circumstance that viewing of embedded objects from two different perspectives is only possible in a very constrained form. Here the principle holds that larger objects (>100 µm) are much easier to handle than small objects (<100 µm), because the depth of a structure generally correlates with its size so that large study items include more spatial information than small ones [19]. Typical objects examined in stereo by transmitted light comprise microfossils such as radiolarians, foraminifera, or diatoms as well as microorganisms such as bacteria or different types of eukaryotic cells [19, 20]. However, all these items have to be characterized by a certain pellucidity in order to uncover their internal structures. The study objects are usually embedded in a highly viscous substance with rather high refraction index (e.g., Canada Balsam, $n = 1.53$; Naphrax, $n = 1.65$). This step mainly serves for an accentuation of the object contours.

In the case of small transparent objects embedded in a highly viscous medium, classical sample rotation is frequently replaced by the so-called image stack method illustrated in Fig. 11.5b. Here the selected item is photographed

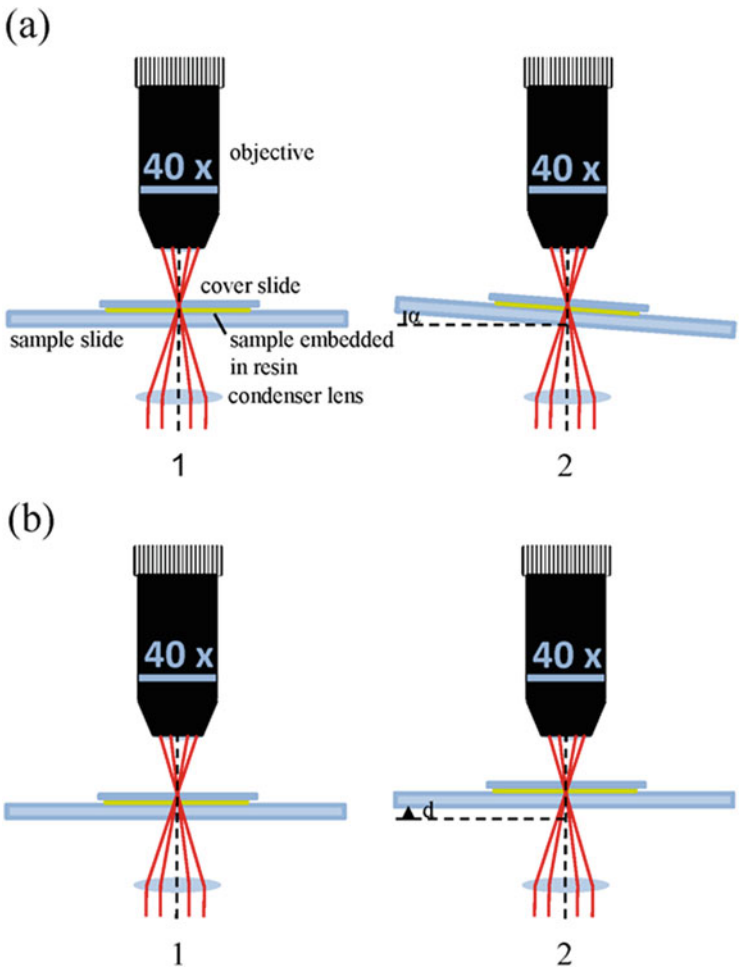

Fig. 11.5 Techniques of 3D imaging in transmitted light microscopy: (**a**) sample-rotation method with direct production of stereoscopic semi-images; (**b**) generation of image stacks and their subsequent digital processing using appropriate computer software [19, 20]

in the same position, but the focus plane is displaced stepwise through the structure. This procedure, however, results in the creation of an image stack [19–21]. Photographs with a certain number of different focus planes cutting the small transparent object presume the application of rather high objective magnifications (e.g., 40-fold, numerical aperture ~0.65) in order to limit the depth of field captured at each focus plane [19]. Basically, the distances between single focus planes depend on the size of the investigated structure, but they are commonly on the order of several micrometers. For effective 3D imaging, each stack should contain 10–20 photographs [21].

For the generation of stereo pairs or red-cyan anaglyphs on the basis of the image stacks described above, the respective photographs have to be processed digitally using appropriate computer software. This essential step can be realized by the application of the freely available computer code PICOLAY [21, 22]. This program commonly enables the processing of high numbers of raw pictures. In addition, it offers numerous opportunities for digital image manipulation. As exhibited in Fig. 11.6, the first working step consists in the import of the image stack into the processing form of the software. In the next step, single photographs are submitted to a fusion process, resulting in an object depth map (ODM) of the depicted object. With the help of the ODM three-dimensional information of the photographed structure can be generated and spatial extrapolation of partly visible surfaces can be modeled. This last procedure is necessary for providing the study object with the ability of slight rotation so that it can be viewed from different perspectives [14, 19–22]. In the last step, the possibility of multi-perspective viewing of the structure is used for the digital generation of stereo pairs or red-cyan anaglyphs. Here, PICOLAY among other things allows the modification of the viewing distance, the rotational axes and the coordinate system [21, 22].

11.2.2 Stereoscopic LM Images of Diatoms

The following examples show stereoscopic LM images of diatom frustules that have been obtained by the application of sample rotation or image stacking method [19–22]. All frustules are presented in terms of classical stereo pairs and red-cyan anaglyphs for the purpose of a direct comparison. Stereo pairs are arranged for cross-eyed viewing, and corresponding points are commonly characterized by positive deviation values. This results in a protrusion of three-dimensional structures out of the image plane.

In Fig. 11.7 upper valves (epithecas) of the frustules of two diatom species (*Triceratium reticulum* and *Aulacodiscus recedens*) are exhibited. The size of these structures varies between 30 and 50 μm. The objects are marked by a multitude of pores that are evenly distributed over the sculptured surface. In the stereoscopic images single structural components at the edges and corners are clearly recognizable and, therefore, can be better utilized for any purposes of species identification. Structural elements such as lines, ridges, and pores undergo a significant enhancement of contrast by 3D imaging so that they become better discernable from the surrounding areas.

The direct comparison between stereo pairs on the one side and red-green anaglyphs on the other leads to several interesting results: (1) Stereo pairs bear the great advantage that single structural components of the frustules are depicted with maximal sharpness, which remarkably facilitates the visual description of the objects. (2) By application of the cross-eyed viewing technique, the central 3D image emerging from the fusion of the lateral 2D images in the primary visual cortex becomes slightly reduced in size. This side effect can be mostly compensated by decreasing the distance between eyes and image plane. (3) The use of the cross-eyed viewing method causes a rather fast visual fatigue, whereas respective study of the red-cyan anaglyph can be carried out for a much longer period of time. (4) Anaglyphic images can

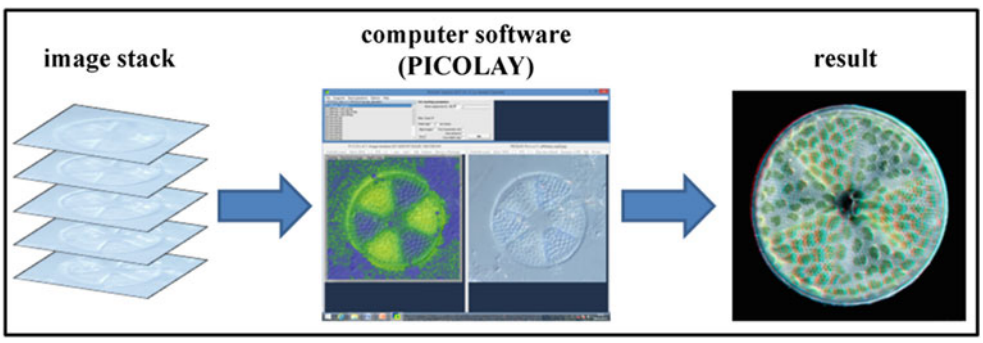

Fig. 11.6 Single work steps for the computer-aided generation of stereoscopic images from respective image stacks. With the help of the computer code PICOLAY, single stacks of photographs shot under the light microscope are submitted to a fusion process, at the end of which stands the production of an object depth map (ODM). This map forms the basis for digital surface rendering and, thus, offers the possibility of viewing the study item from two slightly different perspectives. The resultant image shown above corresponds to an anaglyph [21, 22]

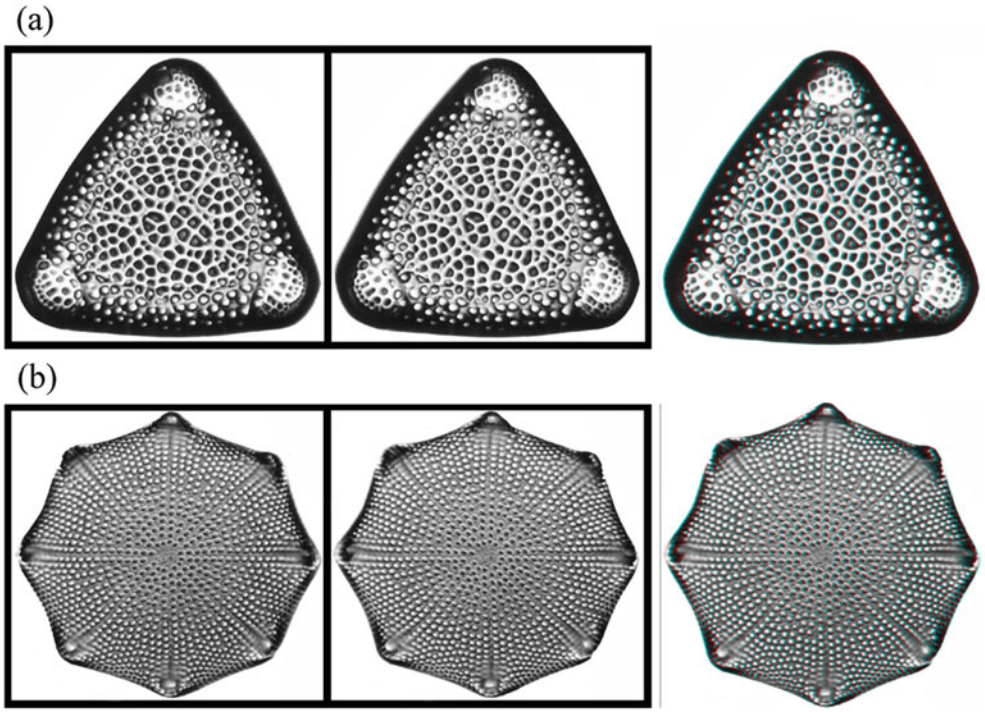

Fig. 11.7 Stereoscopic LM photographs of diatom frustules. Stereo pairs (left, middle) and anaglyphs (right) were generated by means of image stacking and computer-aided processing of the stacks, thereby using the program PICOLAY [21, 22]. Stereo pairs are conceived for a cross-eyed view ($d > 0$). (**a**) *Triceratium reticulum* (size: ~40 μm), (**b**) *Aulacodiscus recedens* (size: ca. 60 μm) [23]

be arbitrarily magnified so that even very small structural components of the diatom frustules become recognizable. For a more targeted inspection of anaglyphs, also additional optical devices such as magnifying glasses can be used.

The main question concerns the use of LM stereo pairs such as those depicted in Fig. 11.7 for exact morphometric measurements. Under specific circumstances, it might become necessary to determine the spatial dimensions of certain structures occurring on the frustules. This complex task can be mastered in two different ways. First, the stereo pair can be submitted to a comprehensive deviation mapping, whereby higher deviations indicate increased spatial expansion of the measured structures. The computed deviation map needs to be subjected to a respective standardization process, where a metric scaling of the deviation values takes place. Second, the pair of semi-images can be examined with a so-called Pulfrich stereoscope, which was already conceived at the beginning of the twentieth century and combines an ordinary prism stereoscope with a magnifying device. After the performance of a standardization procedure, this optical tool allows the direct measurement of spatial distances between two aimed points. Modern computer systems enabling the production of scaled deviation maps represent the preferred method because they can be also handled by less experienced users [2, 3].

In Fig. 11.8 further impressive examples of stereoscopic photographs of diatom frustules are shown. Concerning the perfectly spherical epitheca of the species *Actinoptychus adriaticus*, 3D imaging represents an appropriate support for the detailed description of the superficial shaping, which can only be imagined very coarsely from the 2D photographs themselves. In the concrete case, a regular sequence of protruded and receded areas adopting triangular shapes can be observed. Even the chloroplasts accommodating the photosynthetic reactions in the included cell are characterized by a certain extent of plasticity (Fig. 11.8a). The second example exhibits the x- or cross-shaped epitheca of the diatom species *Stictodiscus californicus*, where 3D imaging can also contribute to a much clearer description of the surface relief. Besides a multitude of pores being scattered all over the silica valve, also a central crater-like structure can be recognized, which is considerably deepened into the upper part of the frustule. The amount of this deepening can be rather easily determined by means of respective deviation measurements (stereoscopic morphometry; Fig. 11.8b). Both examples express very clearly that stereoscopic techniques prove to be indispensable in all those situations, where detailed investigations of surface structures constitute a primary and elementary contribution to the total understanding of a study object.

Finally, it can be stated that 3D imaging disposes of a certain value in LM. It becomes highly important in all those cases, where the studied items and structures are characterized by any three-dimensional attributes that cannot

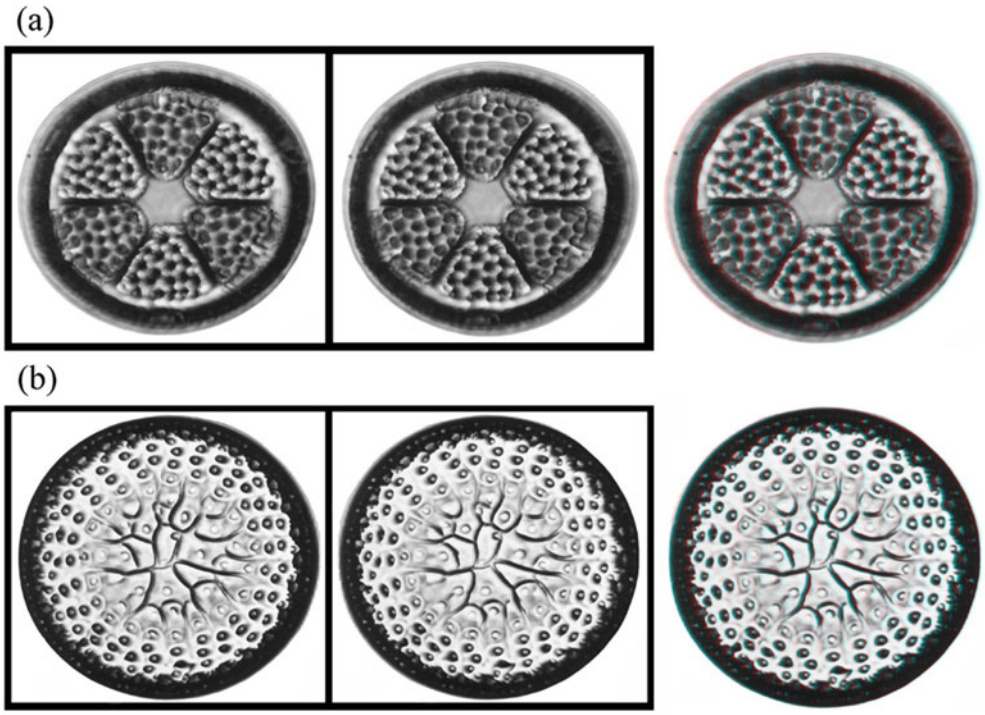

Fig. 11.8 Stereoscopic LM photographs of other diatom frustules. Stereo pairs (left, middle) and anaglyphs (right) were generated by means of image stacking and computer-aided processing of the stacks, thereby using the program PICOLAY [11, 12]. Stereo pairs are conceived for cross-eyed view ($d > 0$). (**a**) *Actinoptychus adriaticus* (size: ~30 μm), (**b**) *Stictodiscus californicus* (size: ca. 40 μm) [23]

be resolved by ordinary 2D photography. This phenomenon, however, often occurs with regard to the microscopic documentation of diatom frustules, which are distinguished by high morphological diversity. In this context, it has to be mentioned that generation of usable 3D effects requires highly professional optical equipment going far beyond the standard of hobby or school microscopists. For the solution of scientific questions, the sample rotation technique and image stacking method seem to bear a rather high potential, which has to be further explored in numerous future studies.

11.3 Three-Dimensional Imaging in EM

11.3.1 Basic Visualization Techniques

In scanning electron microscopy (SEM), 3D imaging of small study objects has been developed to a standard procedure during the past decades, which has found entrance into numerous scientific disciplines. Since SEM represents an appropriate method for the investigation of superficial structures belonging to the micro- or even nanoscale, generation of images with spatial information holds several advantages: (1) surface structures of small study items can be subjected to a more comprehensive evaluation, (2) spatial arrangement of determinative components can be elucidated with higher accuracy, and (3) structural elements can be measured precisely by application of certain morphometric methods [13–15].

Basically, SEM has the ability to produce a large depth of field along the optical axis, which is typically 100 times larger than that provided by light microscopy [13, 24]. This specific quality has resulted in a continuous increase of significance of electron microscopy since its inception in the 1950s. By using the enhanced depth of field in the SEM, a sub-millimeter object can be processed stereoscopically by taking a pair of images, where the specimen was tilted by 2–10° between them (Fig. 11.9a). This classical technique is very easily applicable in modern electron microscopes and commonly leads up to stunning results [13, 24–26]. Since photography of the study objects takes place by using a digital recording system, results of 3D imaging can be immediately evaluated on the computer system coupled with the electron microscope.

The classical stereoscopic recording method used in the SEM holds several serious disadvantages. For the generation of stereo images, the researcher has to work at the microscope, which commonly represents a rather costly and time-consuming procedure. Furthermore, all samples used for 3D imaging have to be preserved for any additional stereoscopic investigations carried out in the future. In the past years, scientists announced an increased demand for a stereoscopic

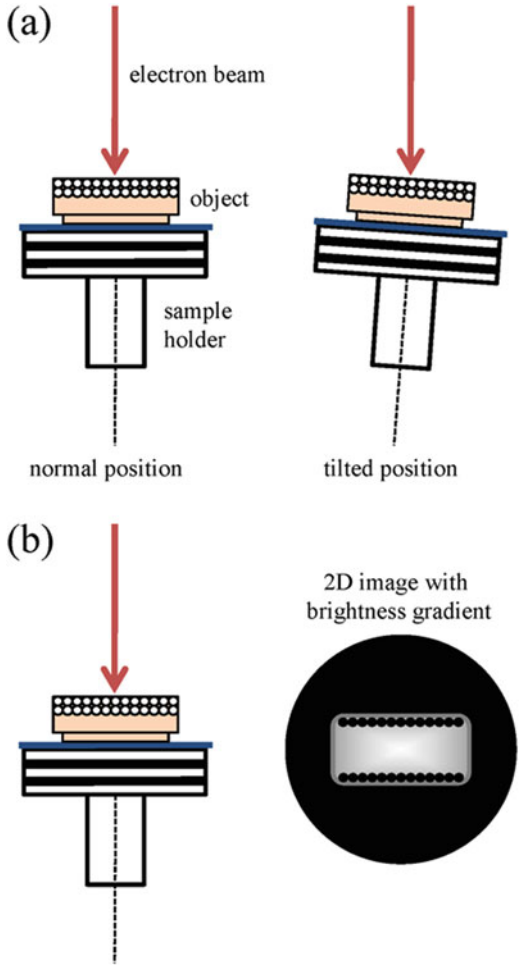

Fig. 11.9 Techniques of 3D imaging in scanning electron microscopy: (**a**) sample-tilting method with tilting angles ranging from 2 to 10°; (**b**) production of 2D images with well recognizable brightness gradients parallel to the optical axis of the microscope. The highly contrasted photographs are submitted to a computer-aided modeling process with the generation of object depth maps and stereoscopic images [22, 24]

revision of old two-dimensional SEM photographs. Recently, computer algorithms have been developed that allow the production of stereo images on the basis of single SEM micrographs [1–3, 14, 22, 26]. This software works on the principle of object depth mapping (ODM) based on a gradient of brightness parallel to the optical axis.

The fundamental idea standing behind brightness-gradient-associated ODM is that parts of an object nearer to the viewer (electron source) are brighter in appearance, whereas parts of the object at a greater distance from the viewer (electron source) appear darker [22, 24]. At this point, it has to be critically mentioned that small study items disposing of very complex surface structures may produce rather disturbing shadow effects, which may significantly affect the accuracy of ODM. As a consequence of that, image errors such as pseudo-stereoscopic effects may be produced [1–3]. In ODM, different levels of brightness and darkness are attributed to respective color codes, finally resulting in a color map of the object (Fig. 11.9b). As already described in Sect. 11.2.1, modeling of object depth opens the possibility for obtaining additional three-dimensional information of the structure, which can be used for various stereoscopic purposes [22, 24].

Three-dimensional imaging of single SEM micrographs can be conducted by using the freely available computer code PICOLAY [21, 22]. Most suitable for 3D modeling are such photographs, where all heights of the recorded object are in focus. In SEM the desired large depth of field is rather easily obtained by switching to a small objective aperture and creating a long working distance between specimen and final lens. This last step can be realized by lowering the specimen on the stage [22, 24]. SEM images evaluated as appropriate for computer-aided 3D imaging are imported into the working space of PICOLAY and subjected to a two-stage process: (1) import of the micrograph to the results window, and (2) generation of the ODM. Both steps are carried out by using the EDIT context menu in the menu bar of PICOLAY (Fig. 11.10). After the creation of the ODM, the user is enabled to activate the respective 3D context menu, where different setups and types of stereo images can be selected. In this section of the program, the user can select between classical stereo pairs, red-cyan anaglyphs, and animated GIFs ("rocking GIFs"), which are mainly thought for the purpose of presentation, because they make special stereo viewing devices unnecessary [26]. The intensity of the three-dimensional effect can be varied by changing the computed rotation angle of the item or the extent of the spatial dimension of the *z*-direction [22, 24].

11.3.2 Stereoscopic SEM Images of Diatoms

Scanning electron microscopy bears the essential advantage of a large depth of field, with the help of which the whole surface structure of a study object can be analyzed at once. As exhibited in Fig. 11.11, the frustules of diatoms can adopt shapes of very different complexity that are well suitable for detailed stereoscopic documentation in most cases. An excellent example for 3D imaging is represented by the valve of the diatom species *Surirella spiralis*, which measures about 100 µm in length and about 50 µm in width. Besides its spiral shape approximately adopting the form of an eight in side view, the surface of the object is characterized by several structural elements, whose plasticity can be well explored in the three-dimensional image. Most noticeable are the upper and lower edge lines that are connected by pillar-like components (Fig. 11.11a).

With much less spectacularity presents the frustule of the marine diatom species *Psammodiscus* sp., which is distinguished by simple spherical geometry. The upper and lower

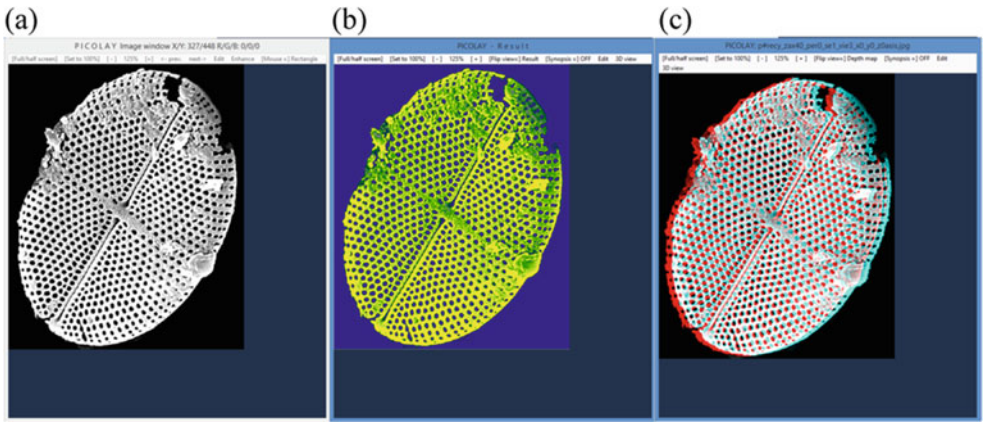

Fig. 11.10 Procession of two-dimensional SEM photographs with the computer program PICOLAY [22, 24]: (**a**) working space of the program with several possibilities for image editing; (**b**) results window with the modeled depth map of the object, which is required for further stereoscopic computations; (**c**) red-cyan anaglyph of the study item that can be saved as JPG or BMP file or can be directly exported to other programs (original photograph from UCL-MIRACLE)

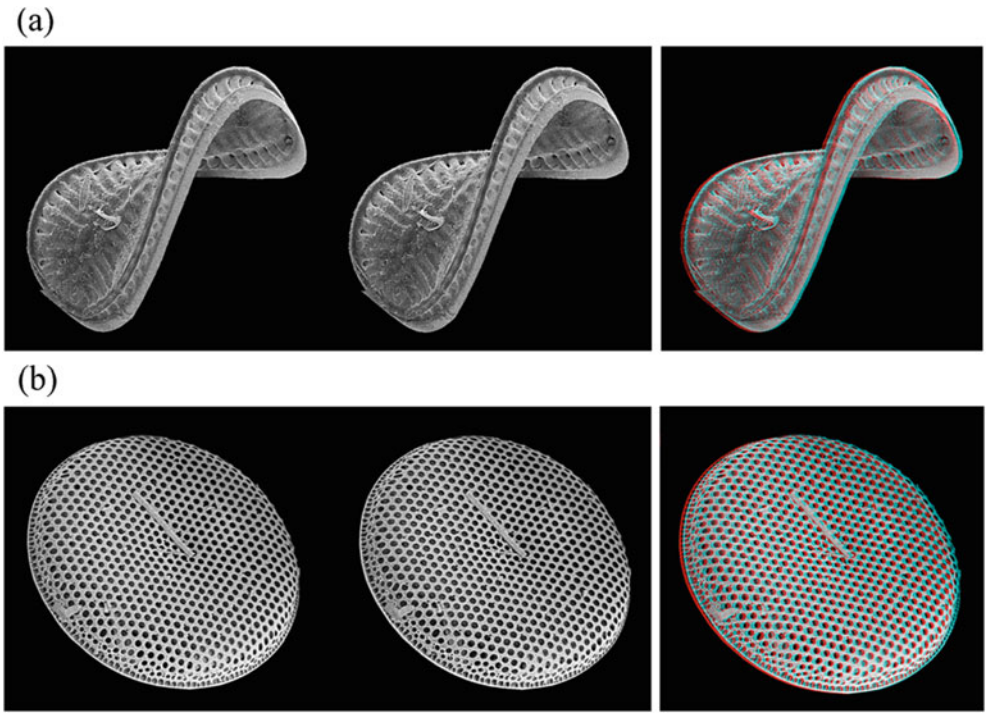

Fig. 11.11 Stereoscopic SEM photographs of selected diatom frustules. Stereo pairs (left, middle) and anaglyphs (right) were generated by means of sample tilting and computer-aided processing of brightness gradients, thereby using the program PICOLAY [22, 24]. Stereo pairs are conceived for cross-eyed view ($d > 0$). (**a**) *Surirella spiralis* (size: ~100 μm; original: Nicola Angeli/MUSE CC3.0), (**b**) *Psammodiscus* sp. (size: ca. 30 μm; original: Mogana Das Murtey and Patchamuthu Ramasamy CC3.0)

valve of the unicellular organism is marked by very regular patterns of isometric pores allowing the establishment of contact of the plant cell with the environment. At the rim of the valve measuring about 30 μm in diameter, the pores become significantly smaller and are arranged in a more random fashion. In the concrete case, 3D imaging remarkably helps to explore the convexity of the whole structure as well as possible unevennesses of the given surface (Fig. 11.11b). In the two examples introduced above, the application of stereoscopic visualization techniques pursues the primary aim of a more detailed description of morphological specificities and their spatial arrangement. Thereby, anaglyphic photographs can be again inspected with specific optical devices in order to obtain more comprehensive results.

Even more spectacular examples of diatom frustules photographed with the SEM are summarized in Fig. 11.12.

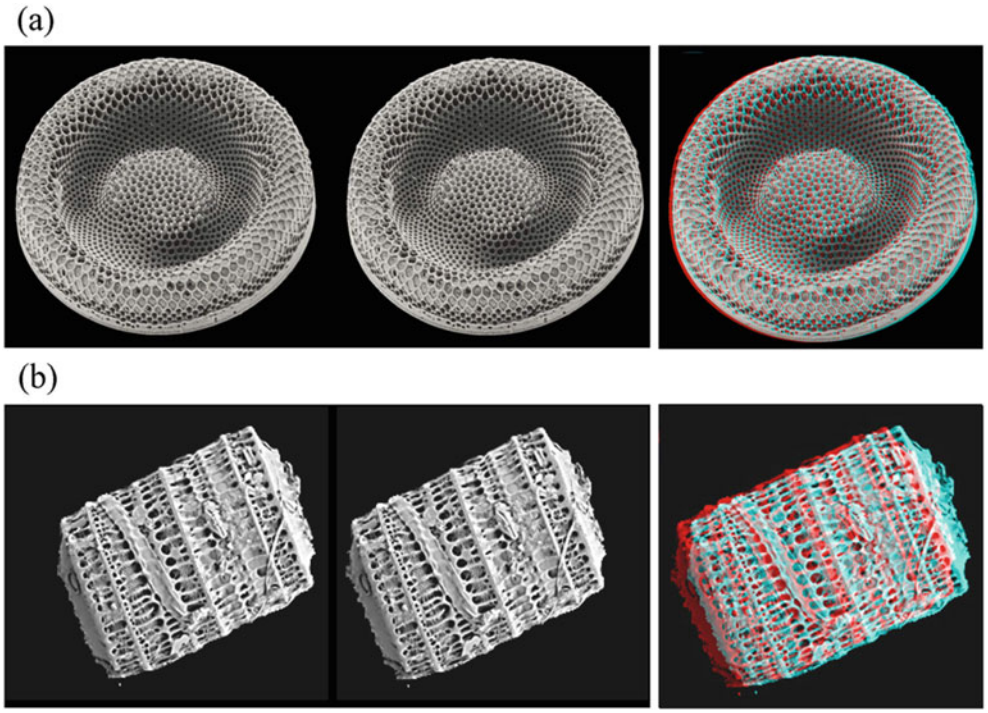

Fig. 11.12 Stereoscopic SEM photographs of other diatom frustules. Stereo pairs (left, middle) and anaglyphs (right) were generated by means of sample tilting and computer-aided processing of brightness gradients, thereby using the program PICOLAY [22, 24]. Stereo pairs are conceived for cross-eyed view ($d > 0$). (**a**) *Actinocyclus* sp. (size: ~50 μm; original: Jovita Yesilyurt CC3.0), (**b**) *Paralia sulcata* (size: ca. 40 μm; original: Impost CC3.0)

Respective structures developed by the species *Actinocyclus* sp. are distinguished by highly enhanced plasticity, which is accomplished by a torus-shaped element at the margin and a hemispherical element at the center of the structure. The marginal surface of the valve measuring about 50 μm in diameter is covered by a honeycomb-shaped pattern of pores, whereas the small passages adopt approximately spherical geometries in the center. In the given case, 3D photography significantly supports the precise description of the variable shaped superficial elements. Besides the basic sharpening of the frustule also small irregularities in growth can be made visible by the application of the method (Fig. 11.12a). As already mentioned before, exact documentation of structural components is of immense value for both the morphological and systematic classification of diatoms.

In the last example, the frustule of the diatom species *Paralia sulcata* was subjected 3D imaging resulting in the generation of both a stereo pair and a red-cyan anaglyph. The structure measures about 50 μm in length and 35 μm in width and is generally characterized by a complex sequence of ridges and porous elements. The object reminding on a cylindrical basket with lid represents nothing short of a show example for stereoscopic photography because the structural complexity mentioned above is accompanied by rather high plasticity of the surface, which can be only resolved in the three-dimensional image. Here, the ridges and hollow components become much more accentuated than on a normal 2D photograph (Fig. 11.12b).

From the examples presented in this section, it can be summarized that 3D imaging plays a superior role in SEM, if morphological and morphometric aspects are placed into the foreground of scientific investigations. Especially distinctive marks of different diatom species can be effectively pointed out with the help of this optical technique. Thereby, qualitative differences between the classical and computerized approach to stereoscopy are scarcely recognizable because of advanced surface extrapolation and rendering models used by the software.

11.4 Conclusion: Role of 3D Imaging in Diatom Research

As demonstrated in numerous scientific and amateur studies of the past years [18–22, 24–27], stereoscopic techniques are characterized by a constantly increasing relevance in microscopic sciences. Given the way things stand today, 3D imaging could also play a major role in diatom research in nearer future, because comprehensive structural analysis of the frustules cannot dispense with spatial information obtained from stereo photography. This development is largely supported by the circumstance that generation of publishable

stereoscopic images no longer represents a challenge, which can only be mastered by photographic specialists. Due to new computer-aided procedures of 3D imaging, the fascinating world of stereoscopy also becomes accessible for all those people, who have not come into contact with this optical method hitherto.

In modern science, 3D images are usually presented in terms of classical stereo pairs or more innovative red-cyan anaglyphs. Stereo pairs have the advantage that they can be viewed without the use of any optical devices. In addition, stereoscopic semi-images placed side by side can be published in monochrome printed works without losing their spatial information. Red-cyan anaglyphs admittedly require the use of respectively colored glasses, but these optical devices are available on the cheap in the world wide web. The great advantage of the anaglyph method consists in the convenient handling of single images, whereby any depicted objects can be studied for any length of time without taking the risk of visual fatigue. Additionally, anaglyphs can be inspected more in detail by using respective magnifying devices. Hence, both approaches of stereoscopic visualization dispose of a certain scientific appropriateness, which can crystallize out as essential for the solution of one or another research question.

As summarized in Table 11.1, stereoscopic visualization techniques dispose of a broad application area in the meantime. In scientific disciplines with an increased presence of morphological topics, both stereo pairs and anaglyphs can provide essential contributions to the comprehensive description of macro- and microscopic structures. The precise morphometric analysis of such structural elements requires the computer-aided construction of a deviation map by means of the stereoscopic semi-images. In anaglyphic photographs, stereoscopic deviation is commonly defined by the horizontal displacement between red and cyan semi-image. Thus far, this distance can be only measured manually and is not recorded appropriately by a computer system. Independent of the presentation technique, stereoscopy can also contribute to the safe determination and classification of organisms. Meanwhile, from many a side the interesting idea was expressed that future determining works could also include 3D photographs.

One of the main application fields of stereoscopy includes all kinds of scientific and popular scientific presentations. Anaglyphic images of macroscopic and microscopic structures can remarkably revaluate a presentation at a scientific congress, whereby for oral presentations the prior distribution of optical devices is indispensable. Three-dimensional effects can also be visualized by means of animated GIFs, where slight rotational movements of the study object produce remarkable spatial impressions in the viewers [21, 22, 27]. Classical stereo pairs prove to be inappropriate for purposes of public presentations because many people are not able to apply autostereoscopic viewing techniques without previous training. Stereoscopic imaging represents a predestined optical technique in the educational and university environment [1–3, 26–29]. Besides the use of innovative teaching materials including three-dimensional photographs, disciples and students can also be encouraged to produce their own stereoscopic images. In modern course books, however, three-dimensional visualization successively grows in importance.

How does the stereoscopic impact in science affect diatom research? So far, only marginal repercussions of this methodical development are perceptible in the cytological discipline, which can be ascribed to several reasons: First, the scientific value of the optical method is only gradually recognized, whereby additional publications may help to accelerate this process. Second, many researchers working with diatoms are still not aware of the fact that computer programs allowing a rapid generation of 3D images are freely available and accompanied by comprehensive documentations in most

Table 11.1 Simplified compilation of present and future application fields of stereoscopic techniques

Fields of application	Stereoscopic method	
	Stereo pair	Red-cyan anaglyph
Detailed morphological description of surface structures	✓	✓
Deviation-based measurement of spatial structures	✓	
Generation of additional spatial information for species determination and advanced systematic classification	✓	✓
Presentation of noticeable three-dimensional structures at congresses and workshops		✓
Use of 3D imaging for scholar and educational purposes		✓
Innovative conception of scientific and popularized printed matters using various stereoscopic techniques	✓	✓
Further development of improved computer programs enabling the production of stereo images on the basis of single LM or SEM photographs	✓	✓

While the majority of usages concerns both classical stereo pairs and modern red-cyan anaglyphs, some points are restricted to one specific type of 3D imaging

cases. Third, cytological science does often not max out the potential of digital systems associated with light and electron microscopes. These systems frequently offer the possibility of an automatic recording of stereoscopic semi-images.

Based on the remarks made in this chapter it can be concluded that 3D imaging has the chance to become a multiple-used examination method in diatom research because of its multifaceted scientific potential. As a result of this, the optical procedure would finally be well on the way to pass a similar methodological development as has already happened in other disciplines such as micropaleontology, entomology or crystallography [1–3, 14, 20, 23, 24, 26].

A.1 Appendix

Links to the SEM images cited in the text.

- *Suriella spiralis* by Nicola Angeli/MUSE. This file was derived from: *Surirella spiralis*—SEM MUSE.tif, CC BY-SA 3.0, https://bit.ly/2Y53zr6
- *Paralia sulcata* by Jmpost—University of Tasmania Scanning Electron Microscope, CC BY-SA 3.0, https://bit.ly/2vOF5qd
- *Psammodiscus* sp. by Mogana Das Murtey and Patchamuthu Ramasamy—[1], CC BY-SA 3.0, https://bit.ly/2H48YrF
- *Actinocyclus* sp. CC3.0 Jovita Yesilyurt, https://bit.ly/2DPIwkC

References

1. Sturm, R.: Die Stereofotografie und ihre Nutzung zur Klärung wissenschaftlicher Fragestellungen. Mikroskopie. **3**, 86–100 (2016)
2. Sturm, R.: Stereoskopie in Mathematik und Naturwissenschaften. Cuvillier, Göttingen (2016)
3. Sturm, R.: Stereoskopische Methoden in Mathematik und Naturwissenschaften. NR. **70**, 168–174 (2017)
4. Sturm, R.: 3D photography of fossils: ammonites from the Northern Limestone Alps in Austria. Dep. Mag. **18**, 10–13 (2009)
5. Sturm, R.: Die Stereofotografie biologischer Objekte. BIUZ. **45**, 52–55 (2015)
6. Tauer, H.: Stereo 3D. Schiele & Schön, Berlin (2010)
7. Wheatstone, C.: Contributions to the physiology of vision, part the first, on some remarkable, and hitherto unobserved, phenomena of binocular vision. Phil. Trans. R. Soc. London. **128**, 371–394 (1838)
8. Brewster, D.: The Stereoscope; Its History, Theory, and Construction, with Its Application to the Fine and Useful Arts and to Education. John Murray, London (1856)
9. Pietsch, W.: Stereophotographie – Die theoretischen Grundlagen der Stereoskopie. Photokino-Verlag, Halle an der Saale (1959)
10. Lorenz, D.: Das Stereobild in Wissenschaft und Technik - Ein dreidimensionales Bilderbuch. Rita Wittig Fachbuchverlag, Hückelhoven (1987)
11. Klette, R.: Concise Computer Vision. Springer, London (2014)
12. Helmcke, J.G.: Mikroorganismen stereoskopisch betrachtet. In: Kemner, G. (ed.) Stereoskopie, pp. 71–78. Museum für Verkehr und Technik, Berlin (1989)
13. Goldstein, J.I., Newbury, D.E., Joy, D.C., Lyman, C.E., Echlin, P., Litshin, E., Sawyer, L., Michael, J.R.: Scanning Electron Microscopy and X-Ray Microanalysis. Springer, New York (2003)
14. Sturm, R.: Stereofotografie in der Elektronenmikroskopie – Teil 1: Entomologie. Mikroskopie. **5**, 66–72 (2018)
15. Sturm, R.: Stereofotografie in der Elektronenmikroskopie – Teil 2: Mikropaläontologie. Mikroskopie. **5**, 129–136 (2018)
16. Helmholtz, H.: Handbuch der physiologischen Optik, Band 3. Leopold Voss-Verlag, Hamburg (1910)
17. Steinman, S.B., Steinman, B.A., Garzia, R.P.: Foundations of Binocular Vision: A Clinical Perspective. McGraw-Hill Medical, New York (2000)
18. Sturm, R.: 3D photographs of fossil gastropods from the ancient Paratethys ocean. Dep. Mag. **24**, 12–15 (2011)
19. Sturm, R.: Stereoscopic photography in transmitted light microscopy. Microsc. Today. **27**, 47–49 (2017)
20. Sturm, R.: Use of stereo photography in insect science—methods and applications. Linzer biol. Beitr. **49**, 1209–1218 (2017)
21. Raap, E., Cypionka, H.: Vom Bildstapel in die dritte Dimension: 3D-Mikroaufnahmen mit PICOLAY. Mikrokosmos. **100**, 140–144 (2011)
22. Cypionka, H., Völcker, E., Rohde, M.: Stacking-Programm PICOLAY – Erzeugung virtueller 3D-Bilder mit jedem Lichtmikroskop oder REM. BIOspektrum. **22**, 143–145 (2016)
23. Stidolph, S.R., Sterrenburg, F.A.S., Smith, K.E.L., and Kraberg, A. "Stuart R. Stidolph Diatom Atlas", U.S. Geological Survey, Washington (2012)
24. Sturm, R.: Stereoscopic effects from single SEM images. Microsc. Today. **28**, 34–39 (2018)
25. Sturm, R.: Stereofotografie in der Elektronenmikroskopie – Teil 3: Kristallografie. Mikroskopie. **5**, 188–199 (2018)
26. Sturm, R.: Stereofotografie in der Elektronenmikroskopie – Teil 4: Humanmedizin. Mikroskopie. **6**, 45–54 (2019)
27. Sturm, R.: Cricket embryos in 3D. Micscape Mag. **6**, 4 (2017)
28. Sturm, R.: Stereoscopic light-microscopy in biology—a review. Linzer biol. Beitr. **50**, 1697–1705 (2018)
29. Sturm, R.: Stereophotography of malacological objects. Linzer biol. Beitr. **50**, 723–731 (2018)

Geometric Morphometrics and the Shape of Microscopic Organisms

12

Ecaterina Fodor and Ovidiu Ioan Hâruţa

Abstract

Morphology of an organism is a complex descriptor and occupies a distinct region in the feature hyperspace. At a microscopic scale, the evaluation of shape and form depend on limiting factors introduced by visualization techniques provided by microscopy. Geometric morphometrics produced a major revolution in shape assessment, both at macroscopic and microscopic levels. In this context, the shape is considered as a whole but also taking into account the interdependence of its parts and applying efficient statistical tools for shape characterization, visualizations and, comparisons. Rooted in the mathematical theory of shape and in the early work on biological shapes of D'Arcy Thompson, geometric morphometrics contributed massively to the understanding of evolutionary and ecological processes during the last decades. The contributions of geometric morphometrics in elucidating evolutionary, functional roles, and processes characterizing the microscopic world of bacteria, fungi, and fungi-like organisms, or diatoms are briefly presented as well as an overview of methods and principles of geometric morphometrics.

12.1 Introduction

> What is the natural mathematical home for shape?...the idea is to filter out effects resulting from translations, changes of scale and rotations and declare that shape is "what is left"
>
> D.G. Kendall, 1989

E. Fodor (✉) · O. I. Hâruţa
Faculty of Environmental Protection, Department of Forestry and Forest Engineering, University of Oradea, Oradea, Romania
e-mail: efodor@uoradea.ro

The shape is one of the oldest and yet among most reliable descriptors for species or more generally, pattern recognition. Particularly, concerning living entities, the shape is a large-scale expression of many organizing, competing, and highly regulated biological processes. Shape mirrors environmental constraints and evolutionary directions. The aim of the quantitative description of the shape is to produce a number or a set of numbers to assess essential characteristics of the shape and these numbers are called shape descriptors [1]. Ecological and evolutionary processes modeled the shape of organisms and added a new dimension to biodiversity including the amount of variability, expressed in diversity of shapes [2]. The subfield of ecomorphology expands the concept of diversity to include morphological similarity, the relationship between morphological and correlated ecological differences within species and among species, also the extent to which greater morphological packing and expansion of morphological variance among species leads to the increase in numbers of species within communities [3–5]. Ultimately, paraphrasing Hutchinson [6] in his "Homage to Santa Rosalia", *why are there so many types of species* as we add *so many shapes?*, one understands that there are the two sides of the same coin—biodiversity. Microscopic world is no exception.

If the identification of organisms relies more and more on molecular features, the shape still conveys important information on processes and functions. The quantitative link between environmental conditions, variations in cell morphology and genetics is the next step in gaining a unified knowledge about how genes work at the corresponding phenotypes [7]. For instance, the evolutionary process responsible for the emergence of new structural plans takes place in two spaces: the genotype space that consists of all possible genotypes, and phenotype space where natural selection operates [8]. The properties of the produced phenotype influence its probability of survival. However, as David Houle [9] wrote: "the depth of our knowledge of genomes

G. Cristóbal et al. (eds.), *Modern Trends in Diatom Identification*, Developments in Applied Phycology 10,
https://doi.org/10.1007/978-3-030-39212-3_12

is approaching completeness, whereas our knowledge of phenotypes remains, by comparison, minimal."

Compared to multicellular structures differentiated in tissues, single cells, and aggregates of cells encountered among prokaryotes, fungi, bacteria, or protists show less shape complexity. Nevertheless, shape analysis has huge explanatory power concerning functions, variation induced by environment, ontogenetic differences, phylogeny, etc. As a common property, for most microscopic organisms, shape analysis starts with microscopy.

Among the fungal structures, spores are the beneficiaries of the largest attention in terms of shapes, in systematics and taxonomy due to their unique features used in species and also, higher taxa discrimination according to Hawksworth et al. [10]. Spores are common for large systematic groups such as bacteria. In pre-molecular era, among the assessed characteristics, shape always represented an important descriptor. Traditionally, shapes are qualitative multistate attributes standardized by some general convention, such being the case of the *Ainsworth and Bisby's Dictionary of Fungi*, in its' seventh edition [10] in which an illustration is attached to a list of 47 spore shapes (page 444). The illustrated list contains terms such as globose, prolate or ellipsoidal, broadly ellipsoidal or subprolate, oblate, filiform, acerose, bacilliform, lenticular or discoid, sigmoid, falcate, pyriform, lunate or crescentic, obpyriform, clavate, campanulate, bicampanulate, turbinate, cuneiform, peltate, acicular hamate, circinate. One can easily observe that some of the terms are of geometric origin and many others are metaphors based on similarities with natural or cultural objects. The subtle grading within each category relies greatly on the descriptive talents of the researcher and cannot be included as such in statistical analysis, or cannot be utilized as an algorithmic framework. Not considering the degree of within-sample or population variability of the spore shape that cannot be assessed based on shape descriptors of this category.

The shape is changing during the life cycle of an organism: (1) the organism progresses from immature stages to adult stage, (2) organism is pleomorphic as shapes characterize anamorphic and teleomorphic states of fungi, and (3) the organism adapts, as pathogens/mutualists are changing shape when a host is found [11].

The study of form and, the quantitative study of shape progressed from univariate or bivariate approach (largely used measurement data such as length and/or width) to multivariate statistics or multivariate biometry using covariance matrices and later, to methods permitting the visualization of changes in biological shape and/or form [12]. Other shape descriptors derived from dimensional analysis (linear or surface descriptors) such as circularity, compactness or fullness, roughness, and convexity [13].

Inception of the geometric morphometrics (GM hereafter) dates back to 1917 with the publication of D'Arcy Thompson's book *On Growth and Form* [12]. The author stated that biological form could be studied using mathematical transformations, pioneering quantitative shape description. However, as Bookstein [12] pointed out, the shape variability depicted by transformation grids was used much earlier in the book of Albrecht Dűrer (1528) *Vier Biicher von Menschlicher Proportion*, to explore the variation of human body shapes.

The emergence and development of GM were triggered by the progress achieved in the fields of differential geometry, computer science, image acquisition, and multivariate statistics. The main progress compared to traditional multivariate morphometrics consisted in the fact that the GM approach to shape retained all geometric information and used it in further analysis [14]. Traditional morphometrics deals with shape and forms analysis relying on multivariate statistic tools such as regression, canonical variate analysis, and factor analysis still not providing elements for shape interpretation [12].

Blackith and Reymert [15] first coined the term morphometrics. The first half of the twentieth century brought multivariate statistics that were integrated with morphological studies leading to the development of multivariate morphometrics. However, multivariate (traditional) morphometrics employing measurements of lengths, width, area, perimeters, or more complex shape descriptors as elongation, circularity, fractal dimension did not allow for shape reconstruction, one of the primary goals of GM.

Mosimann [16], in a paper on allometry, introduced for the first time the size vector and provided a definition for shape space based on geometric similarity, marking a starting point in the geometrical approach to morphometry. The major revolution in the quest for reliable quantitative shape description has happened in the 1980s, triggered by the invention of coordinate-based and outline-based methods, in the same time with the discovery of the statistical theory of shape and the beginning of the personal computers' era [17]. This new morphometric approach called *Geometric Morphometrics* resulted from a synthesis of multivariate statistics and biometrics with non-Euclidean geometry. First to be employed in the new subdomain of GM were the coordinate-based methods in the frame of the newly established statistical theory of shape. It is currently included as a subfield within statistics, focused on measuring differences between shapes and the amount of their variation using different methods, most widely employed being the Procrustes distances. Morphometric analyses respond to questions raised in the biological quest by going back and forth between abstract representations of variation as scatter of data points in shape space and the concrete morphological changes [18].

Two main approaches in extracting shape (in 2D and 3D) variables are currently in use: Procrustes coordinates obtained after superimposition of sets of landmarks and co-

efficients of shape functions fitted to outlines or surfaces (for example, Elliptic Fourier analysis and Eigenshape analysis).

At the moment GM is one of the leading methods in quantitative biology generating the data and analytical tools in the emerging field of phenomics, the large-scale study of high-dimensional phenotypes, one of the latest "-omics" [9, 19].

Other shape analysis approaches include *fractals* that are sets with fractional dimensions [20]. Rugged boundaries and branchiness are described by fractal dimension analysis [21], being useful in the study of mycelia. Non-fractal objects still can be studied using fractals if they present self-similarity [22] employing a different algorithm, Multi-Scale Fractal Dimension in which fractal dimension of the same object is calculated at different scales of observation obtaining a vector of fractal dimension exponents, currently employed in medicine, botany, marine sciences, and genetics. It appears to be a promising direction in microscopy [23, 24] in relation to magnification and scaling effects on the observed morphological details. The limitation imposed by the fact that the fractal dimension is a single real-valued number that cannot fully describe the complexity of the shape, is bypassed by new fractal descriptors using the aforementioned algorithm.

Multispectral analysis of images and *Discrete Wavelet Transform* use different distance methods to assess shapes (Mahalanobis or Euclidean). Wavelet decomposition consists of feature extraction based on a discrete wavelet transform (DWT).

Machine vision systems recognize size, shape, and texture of objects and provide numerical attributes to the objects. Automatic identification using machine vision was applied in the study of shapes of diatoms [25].

Machine learning (ML) techniques rely on developing models of image groups in order to address problems of group discrimination and characterization, placing of the unknown images into groups, and specimen identification from morphological data [26]. Placing images in such groups do not require abstraction of the image into subsidiary sets of landmarks or semi-landmarks. Application of these techniques removes the requirement of making a priori decisions concerning which morphological aspects of the image might be important for group characterization. As individual pixel brightness or/and color values are used as input variables of the digital images, the resolution can be controlled by adjusting the digital resolution of the images submitted for the analysis. ML algorithms use training sets of images in which a search for the pixel elements is performed, all training sets of images having in common the characterization of the group irrespective of the individual features of those images.

The following presentation is an incursion in Geometric Morphometrics (GM) domain, maintaining the technical background at minimum, emphasizing the progresses obtained in the quantitative study of shape mainly in microscopic organisms. Microscopy evolution during the last decades paralleled the preoccupation for shape objective and formal description as valuable type of information, complementary to molecular insights.

12.2 Theory of Shape and Morphospaces

The interest for phenetic characters and their variation has a long history as species identification and classification in Linnean times was entirely based on morphological data. As quantification of phenetic characters described by linear measurements progressed from the end of the nineteenth century to the first half of the twentieth century, this direction led to the emergence of multivariate morphometrics using ordination techniques and multivariate statistics to construct morphospaces. In this context, the size determines a distinct morphometric space, i.e., the size space.

The next logical step progressed in the direction of shape quantification per se. Size and shape are classic geometric concepts, but historically, the size was first chosen for sound quantitative approaches. Still, measurements of lengths, volumes, or widths did not convey much information on the actual shape of organisms and frequently did not share a common scale.

Metric size measurements dominated areas focused on the description, ordination, or classification of organisms being important descriptors, with high discriminant power. Combined with various multivariate techniques, these features continue to deliver important information for species separation but, as extended tests demonstrated, only metric measurements do not suffice. Shape and shape quantification are better predictors for species and population discrimination in combination with metric size descriptors [27].

Methods employed for shape comparisons are classified into two categories: those that derive features (called shape descriptors) for each shape separately using standard distance functions and those that map one shape onto another, providing local and nonlocal elements of comparison. Ideally, the techniques of the second category, aim to define directly a map between any two shapes that are closely isometric (a map that precisely aligns two shapes with no distortion of distances) [28].

Now, the shape is approached from two main directions: *computer vision,* based on object recognition algorithms and *geometric analysis* employing methods developed in GM. Shape analysis consists of finding similarities among objects in terms of shape and analyzing the nature and causes of shape variations. Alternatively, pattern recognition is a category of methods employed to detect differences in shape and pattern for decision-making and binning of specimens while shape analysis focuses on differences that are interpreted biologically in a meaningful way [29].

Modern morphometrics considers the shape as a whole taking into account all the geometrical relationships in the input data. The shape can be numerically encoded resulting in a sequence of numbers, a high dimensional vector, subjected to multivariate analysis that provides the arguments for shape comparisons, assessment of variability, etc. The procedure of shape encoding is therefore of utmost importance. Fidelity in the record of the original shape, shape representation that captures biologically important shape variations and the requirement that individual numerical components of the representation be meaningful on their own, are conditions to be fulfilled in the shape quantitative assessment [30].

The two main methods, landmark-based and outline-based, both preserve the geometrical information. The relative positions between points are preserved, allowing the shape reconstruction from their numerical signature [31, 32]. However, shape and size are both important in characterizing an organism in terms of individual, population, or among-species variability.

To understand GM, an initial definition of shape is needed as Kendall [33] originally formulated it. *Shape is all the geometrical information that remains when location, scale, and rotational effects are filtered out from an object.* In this context, a figure in a plane is a set of points. Two figures have the same shape if mapping the plane on itself (performing translation, rotation, and scaling), those figures are completely superimposed [34].

Intuitively, our understanding of what space represents is dominated by Euclidean spaces but there are many other spaces with different geometric properties. Morphospaces are spaces with different geometries. However, Euclidean space (has the algebraic structure of a vector space representing a phenotypic change) is characterized by stringent relations and properties allowing many algebraic, geometric, and ultimately statistical manipulations. Therefore, no matter which geometry morphospaces display, for computational reasons, a projection in the Euclidean vector space endowed with properties as a norm and inner product is performed.

Classically, distances between points are measured as the Euclidean distances: it implies that measured variables are presented as Cartesian coordinates in the Euclidean vector space. Morphological spaces are mathematical spaces describing and relating the configuration of organisms where the morphological configuration is represented by a point, the dimensionality of these spaces depending on the number of measured variables [35]. Metrics that are employed in shape spaces include Hausdorff distance, strain energy, and Procrustes distance of which most employed is the Procrustes distance.

In the hierarchy of mathematical spaces, topological spaces formalize the relation of the closeness of a point, generalize standard geometric spaces such as lines and planes and contain metric spaces which are topological spaces endowed with the possibility of measuring distances (Riemannian manifold is a metric space).

The current evolution of geometric morphometrics was triggered by the construction of Kendall's space. Kendall shape space is nonlinear and non-Euclidean, is a curved space. In this curved space, each shape is represented by a point, therefore, conventional linear multivariate statistics cannot be applied. The metric in Kendall's space is referred to as Procrustes distance estimated by Generalized Procrustes analysis [36]. The shape space is approximated by a linear tangent space to the shape space where standard multivariate statistics can be performed. The tangent Euclidean space touches Kendall's space at the point corresponding to the average shape (or other reference or consensus shape). The mapping of points of Kendall's shape space onto tangent space is an approximation resembling the mapping on a flat surface of the curved surface of Earth. Because it is a one-to-one correspondence, it is possible to reconstruct the shape of an object corresponding to each point in the shape space or tangent space. However, a limited range of shape variation [37] bound this correspondence.

Kendall's shape space is a mathematical space and it constitutes a Riemannian manifold in which the distance between any two points is defined as the length of the shortest curve connecting the two points [35].

Numerical representations of form (shape and size) employ coordinate data, boundary outlines, or textural aspects resolved through different methods: landmark-based, and outline-based (such as Fourier descriptors or eigenshape analysis) that deliver information on global shape or form aspects. Localized features are approached with wavelet analysis, a completely objective procedure to identify local shape details as changes in curvature along with a biological specimen [38, 39]. Referring to curvature, *landmark-free* methods have recently emerged in GM landscape. From this perspective, landmark-free methods rely on the geometric representation of the shape (2D or 3D) with vertices distributed on a discreet triangular mesh enveloping the shape. To each vertex, a signature is assigned under the premise that points with similar signatures are more likely to correspond. There are several techniques described under this category (see [28, 40], for details) employed mostly in medical and human anatomy research. The novelty and the important perspectives of this category of methods come from the fact that curvature is in the focus and the projection of shapes takes place in the hyperbolic space. Considering only the 2D dimension of apparently plane objects is a simplification since most of the natural shapes, microscopic included are in fact, hyperbolic, or spherical (have curved surfaces). For the time being, projections of complex and folded structures on hyperbolic plane were performed for human brain scans, for comparisons of fos-

sil primate skulls and protein folding. Among the incorporated differential geometry approaches are surface parameterization using Ricci flow method (explores curvature under the topology of different manifolds), projection on one of the standard models of the hyperbolic planes as Poincaré disk and Klein model endowed with hyperbolic metric [41].

In this context, it is useful to introduce several concepts:

(a) *Landmark space*—Space in which landmarks are digitized and plotted. Is a geometric space of m dimensions where the centroid is a single point.
(b) *Configuration space*—Space in which landmark configuration is represented as a point. Is a geometric space with km dimensions (k landmarks, m dimensions), the set of all possible km matrices. A configuration corresponding to a specimen in an array of specimens is a single point within the space.
(c) *Shape space*—Is a non-Euclidean space in which the configurations are plotted after scaling, rotation, and translation. It has fewer features than the original configuration space: one dimension is lost by setting a common scale, m dimensions are lost due to translation and $[m(m-1)]/2$ are lost due to the rotation. For k landmarks, there are $2k-4$ degrees of freedom and $3k-7$ degrees of freedom for 3D landmarks. The shape space is the set of all possible shapes of the object in question. Due to the filtering process, the dimensionality of shape space is reduced. The shape spaces are also, differentiable manifolds.
(d) *Tangent space*—Is the Euclidean approximation of shape space, also a linear space. The procedure consists in modifying the shape vectors from the curved Riemannian subspace (a smooth manifold) to a hyperplane where Euclidean distance can be employed as a distance metric instead of the geodesic employed on the hypersphere. There is an opinion that the tangent projection is simple to apply and pleasing from a mathematical point of view but the net effect from the numerical point of view is minimal [42].
(e) *Form space*—Is the space relating shape to size of different objects of interest [43].

The numerical description of the form, sufficient from a mathematical point of view, is a one-to-one mapping between the computational procedure and the actual morphology [44]. For classification purposes, the form conveys a complete set of information compared to shape alone [45].

Shape determinism is complex and results from the interplay of genetic and epigenetic factors. Epigenetic interactions can extrapolate a local developmental change into widespread morphological variation [46]. For instance, phenotypic plasticity and developmental instability, the later mirrored by the emergence of asymmetries in normally symmetric organisms induced by environmental factors, are epigenetic manifestations [47]. Symmetry is a fundamental feature of body plans at all scales, from microscopic to macroscopic organisms. The random deviation from symmetry can be quantified with simple morphometric measurements such as width and lengths but also using the instruments of GM. The diversity of symmetries, from simple bilateral or radial to complex symmetries, such as reflection symmetry encountered in microscopic *Micrasterias* proliferates in various levels and types of fluctuating asymmetries. The symmetric and asymmetric variations are included in two orthogonal subspaces of the global shape space and are interpreted differently [48].

There are biological objects that do not display a compact shape and cannot be analyzed with morphometric or GM tools: these are the modular branching systems of mycelia [49] and pseudomycelia, growing fungal or bacterial colonies [50, 51]. Branching systems do not display areas where landmarks can be placed or outline to be traced. Neither landmark nor outline based methods provide a quantitative description of textures. Important surface features of spores, spore ornamentation or the architecture of diatoms' frustules is not possible to approach from GM perspective. The irregular shape of objects, textural features, and space-filling differences are studied with fractals. Mandelbrot [20] defined formally fractals: "A fractal is by definition a set for which the Hausdorff-Besicovitch dimension strictly exceeds the topological dimension." An alternative, more comprehensible for nonspecialists definition followed "A fractal is a shape made of parts similar to the whole in some way" [52]. The fractal theory offers methods to describe inherent irregularities in natural objects [53], but not in the strict sense of shape. The core of the fractal theory is the fractal dimension described as a constant parameter for which several models are applied in different contexts to approach shape complexity. In addition, fractals address shapes and configurations that are not Euclidean entirely or partially.

Fractals describe space filling rather than shape, fitting growth, and exploring versus exploiting growth strategies in modular organisms. Two fractal objects may be morphologically different, still have the same fractal dimension. Fractals do not describe shape in the same way as for instance, GM outline-based methods do [54]. From this perspective, fractals are not properly GM algorithms not permitting direct comparison of shapes.

Lindenmayer systems, a shape modeling algorithmic method, define complex objects by successively replacing parts of a simple initial object using a set of rewriting rules or productions [55]. Inspired by fractals and used in modeling the shape of plants, this approach was applied in the study of fungal mycelia [56].

During the last years, progress has been made and fractals were increasingly used in pattern recognition. New algorithms were devised such as multifractals or curvature scale shape fractals [1] converging more to geometric morphometrics in terms of shape configurations quantification. In the field of pattern recognition, the identification of an organism employs some morphological configuration, multifractals use proving to be a powerful tool.

12.3 Geometric Morphometrics' Tools

The geometric morphometric study of microscopic organisms developed in the last decades paralleling studies in the macroscopic domain but most of these studies employed outline-based methods. There are relatively few studies in which landmark-based methods were employed, as for example, in the case of microalgae characterized by complex and intricate shapes, not manageable if the outline is chosen as shape descriptor [57].

12.3.1 Landmark-Based Methods

The most widely used GM methods in biological sciences are landmark-based that employ 2D or 3D Cartesian coordinates of biologically homologous, discrete points, or landmarks placed on organisms or different organs.

It starts with the construction of a set of landmarks employed on each specimen of a collection considered as fixed points of particular shape trait. In morphometric terms, homology refers to points, curves that have consistent biological meaning and can be subjected to multivariate analysis, providing an adequate summary of the shape. Landmarks need to be structurally similar, ideally homologous between individuals [32, 58]. When the object of interest contains curves between landmarks or too few landmarks can be placed, a better choice is using sliding semi-landmarks [59].

The method is effective when is used to compare biological objects that are fundamentally quite similar.

There are several specifications concerning the extraction of images: landmark coordinates are extracted from digital quality images of specimens using software such as ImageJ or tpsDig. Images should include a scale bar and landmarks should be digitized in the same order for all specimens. A specimen with a missing landmark should not be included.

Coordinates (2D or 3D) are recorded but landmarks coordinates are raw data, not suitable for statistical analyses, that must be transformed, usually by standardization for the position, orientation, and scale in order to conform to mathematical space. For the control of these sources of variation several techniques were devised. Bookstein [58] proposed a set of equations to perform the landmarks' alignment. The article where Bookstein proposed these equations marked the starting point of what was called later GM revolution [60]. In this context, he presented a new metric, centroid size (S) important for further GM developments. Now, however, most employed of landmarks/semi-landmarks alignment is Procrustes superimposition (Generalized Procrustes analysis is an analytical procedure for superimposing landmark/semi-landmark configurations to obtain shape variables) [36, 58, 61].

Landmark alignment techniques referred to as Procrustes superimposition are devised to minimize the differences for position, scale, and orientation of the landmarks or semi-landmarks. This superimposition technique largely employed was proposed by Sneath [62] and consists of a succession of alignment operations:

1. Alignment of position (translation): The best point to use to achieve standardization by translation is the mean of all landmarks within each data set, known as the centroid of the data set. The centroid occupies the origin of the common x, y coordinate system.

$$\acute{x} = \sum_{i=1}^{n} \frac{x_i}{n}, \quad \acute{y} = \sum_{i=1}^{n} \frac{y_i}{n} \tag{12.1}$$

   where n stands for the number of landmarks and x, y are coordinates of the landmarks.

2. Alignment of the size (scaling). The goal of the calculations is to remove size differences using the metric devised by McLeod [63], the root of squared centroid size (RCS):

$$\text{RCS} = \sqrt{\sum_{i=1}^{n} \left(x_i - \acute{x}\right)^2 + \left(y_i - \acute{y}\right)^2} \tag{12.2}$$

   The obtained values are used to rigidly scale each landmark data set to a common size, most conventional being RCS = 1.0. Each x and y coordinate value is divided by the obtained RCS (n in the equation stands for the number of landmarks).

3. Alignment of orientation (rotation): Represent the final step in the Procrustes superposition technique. It consists of rigidly rotating the landmark configuration about the centroid to obtain the best fit between landmark positions [62]:

$$\theta = \arctan\left(\frac{\sum_{i=1}^{m} y_{Ti}\, x_{Ri} - x_{Ti}\, y_{Ri}}{\sum_{i=1}^{m} x_{Ti} x_{Ri} + y_{Ti}\, y_{Ri}}\right) \tag{12.3}$$

where T is the target configuration (usually the first configuration in the data set) and R is the configuration being rotated, m is the number of landmarks, θ is the optimal angle through which to rotate R configuration to match T. The process is an iterative search of the optimal rotational alignment.

The effect of Procrustes superposition is seen in PCA plots that show a reduction of shape variance paralleled by better-resolved shape relationships within transformed data sets. The output of Procrustes superimposition is the mean shape or consensus shape (Fig. 12.1). An extension of landmark-based methods for boundary curves consists in the employment of semi-landmarks or sliding landmarks [65]. Semi-landmarks are points arrayed along an outline that captures information about curvature, making possible the study of complex, curved objects with sparse landmarks [66]. The algorithm requires that the whole structure be homologous. There are two alternative computational approaches in sliding semi-landmarks based on core GM procedures: the Procrustes superimposition [36] and thin-plate-spline (TPS) deformations [67]. Procrustes superimpositions convert the initial semi-landmark coordinates in shape coordinates and the calculated Procrustes distances between two specimens (approximated by Euclidean distance) becomes the measure of shape difference between the analyzed shapes [68].

A series of locations along a curve are digitized and an additional step in the Procrustes algorithm is added by sliding the points along vectors tangent to the curve until their positions align as closely as possible with the corresponding curve of a reference (or average) specimen [61]. The sliding of semi-landmarks is an iterative process in three steps: (1) Computation of a sample mean shape and the tangent vectors for each semi-landmark in each specimen, (2) Sliding the landmarks along the tangents to minimize distances either using Procrustes distances or the bending energy to the mean shape, and (3) Placing back the slid semi-landmarks to the nearest point on the curve [17]. There must be an equal number of semi-landmarks across the sample. The method works best on smooth outlines, which is the case of many microscopic features of bacteria or fungi (spores).

After the performed superimposition, the aligned Procrustes shape coordinates describe the location of each specimen in the curved space, Kendall's shape space. Ordination, statistical analyses and shape visualization are performed as the next steps in GM analysis of the shapes of interest. Ordination and visualization are exploratory by nature and the multivariate statistics are employed to assess differences and changes in shape.

Since statistical multivariate analysis cannot be performed in Kendall's space, shape configurations are projected in Euclidean tangent space that touches curved Kendall's space at the point (configuration) of average or other selected reference or consensus shape.

Different ordination and multivariate statistical methods are employed to investigate shape differences and changes, to summarize variation and reduce the dimensionality of data: PCA (Principal Component Analysis) and the similar (RWA) Relative Warp Analysis for dimensionality reduction, MANOVA (Multivariate Analysis of Variance) for testing differences among groups of shapes, PLS (Partial Least Squares) used to identify patterns of covariation between shape and other continuous variables.

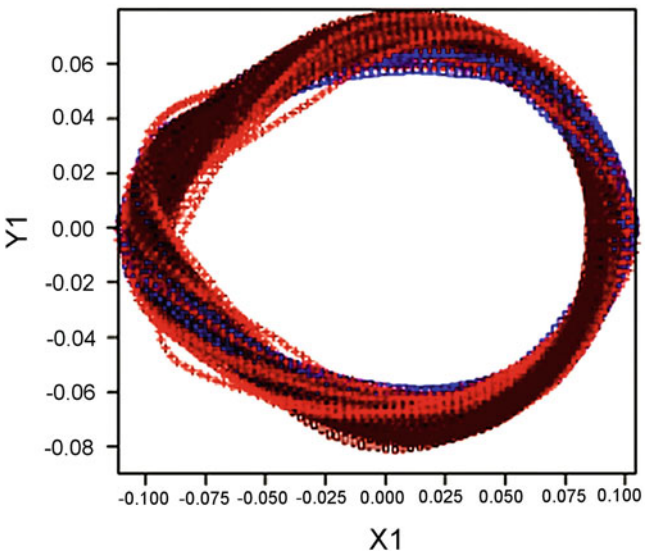

Fig. 12.1 Mean shape (consensus configuration) of *P. plurivora* resulted after Procrustes superposition (MorphoJ software) using semi-landmarks (from [64])

12.3.2 Outline-Based Methods

For 2D representation of objects characterized by a closed and relatively smooth, simple outline, methods based on curve analysis were developed. These methods are based on the assumption that outlines must be considered as a whole. The curve is considered a polygon formed by x, y coordinates of the pixels defining it. Criticism was raised since points on an outline could not be considered homologous between specimens, a fact introducing ambiguity in the shape analysis [65]. Landmarks are considered more definite and less subjected to disagreements about how they should be matched [69]. However, outline and landmark methods are not mutually exclusive and can be combined as it happens in extended eigenshape analysis (ESA) that uses landmark and contour data into an integrated shape analysis [70].

One popular approach for the boundary outline analysis employs Fourier series that are adjusted to some shape descriptor. Fourier series are decompositions of periodic

functions in a sum of more simple trigonometric functions as sine and cosine. Closed outlines can be considered periodic functions from this perspective. This category of methods based on Fourier descriptors describes overall shape mathematically by transforming coordinate information in Fourier descriptors [71]. The functions have frequencies that are integer multiples or harmonics of one another. Lower harmonics provide approximations for coarse-scaled variations in the original periodic function and high-frequency harmonics fit the fine-scale variations [32]. Periodic functions used as descriptors to be transformed employing Fourier series are (1) The distance of any point on the outline to the centroid of the shape, (2) The variation of the tangent angle of any point, and (3) The x, y coordinates on the plane. The corresponding methods are referred to (1) Radius variation, (2) Tangent angle, and (3) Elliptic analysis.

As a general feature, Fourier series are applied to continuous functions but outlines are composed by a finite number of points. Consequently, a discrete equivalent of Fourier series is employed. Several methods derived from the use of Fourier series:

1. *Fourier radius variation* was proposed by Zahn and Roskies [72]: The radius r, taken as a distance from the outline centroid and a given point of the outline can be expressed as a periodic function of the angle θ. The method fails to fit outlines with convexities and concavities, therefore being of limited applicability.
2. *Fourier tangent angle* presented also by Zahn and Roskies [72] fits the cumulative change in the angle of a tangent vector $[\varphi(t)]$ as a function of the cumulative curvilinear distance t along the outline. The methods are also of limited applicability, currently.
3. *Elliptic Fourier analysis* is largely employed and was introduced by Giardina and Kuhl [73], Kuhl and Giardina [31] consisting in a method for fitting separately x and y coordinates of an outline projected on a plane. It has been proven popular among morphometricians as it delivered analyses of curves defined by sets of semi-landmarks [69]. The method does not require equally spaced points along the outline and can fit any type of outline. The coefficients can be made independent of the outline position and normalized for size. Elliptic Fourier functions which are curve-fitting functions are used to transform the data from the spatial domain to frequency domain (generated by parametric formulation).

The Elliptic Fourier parametric equations are of the form:

$$x = f(t) \tag{12.4}$$

$$y = f(t) \tag{12.5}$$

where t stands for the contour of the analyzed object, x and y are the coordinates of contour points.

The Elliptic Fourier equations are the parametric solutions set in the Cartesian coordinate system which allows the separation of boundary contour in x and y components. The contour becomes a sequence of x and y coordinates, in fact, the coordinates of each pixel of the contour t starting from an arbitrary pixel $x(t)$ and $y(t)$ are coordinates of a particle traveling around the contour at a constant speed 1. The variation of x and y coordinates become periodic functions of t that are approximated by Fourier series:

$$x(t) = a_0 + \sum_{n=1}^{N} \left(a_n \cos\frac{2n\pi}{T} + b_n \sin\frac{2n\pi}{T}\right) \tag{12.6}$$

$$y(t) = c_0 + \sum_{n=1}^{N} \left(c_n \cos\frac{2n\pi}{T} + d_n \sin\frac{2n\pi}{T}\right) \tag{12.7}$$

where a, b, c, and d are Fourier coefficients of the nth harmonic, a_0 and c_0 correspond to estimates of the coordinates of the centroid of the original outline (these coefficients are ignored in the following analysis). The coefficients b_n and c_n describe the asymmetry of shapes that can vary from coarse to fine scale. Small values of these coefficients indicate symmetry. N is the maximum number of used harmonic amplitudes, n is the harmonic amplitude, and T is the evaluation angle [74].

The centroids of the contour have as coordinates:

$$\acute{x} = \sum_{p=1}^{P} x_p \tag{12.8}$$

$$\acute{y} = \sum_{p=1}^{P} y_p \tag{12.9}$$

x_p and y_p are the observed contour coordinates ($p = 1, 2, 3 \ldots .P$ or number of pixels).

Elliptic Fourier analysis can be employed to describe any curved, closed outline. Starting with the coordinates of points along the closed curve, EFA decomposes the shape in infinite series of ellipses also named harmonics or modes [31]. The procedure starts from the digital image, the first step is the acquisition of points along a contour: one procedure recommended by the authors of the best known software for Elliptic Fourier analysis (SHAPE) [75] for contour acquisition is the binary image or binary mask method. The boundary of the object contrasted by differently colored background, the chain-coded contour [76] is a sequence of x and y coordinates of ordered points that are measured in a counterclockwise direction from an arbitrary starting point to the pth point.

A finite combination of harmonics is used to reconstruct the shape, usually the number of chosen harmonics must permit the reconstruction of the original shape in detail. Each ellipse represents a certain harmonic and captures

the dominant spatial frequencies within the original shape [77].

There are four coefficients per harmonic, two for x coordinate and two for y coordinate. The first harmonic defines the best fitting ellipse and is used for the normalization of the harmonic coefficients to be invariant to size and rotation. After normalization, the shapes can be individually aligned according to their first fitted ellipse.

$$a_n = \frac{T}{2n^2\pi^2}\sum_{p=1}^{K}\frac{\Delta x_p}{\Delta t_p}\left(\cos\frac{2n\pi t_p}{T} - \cos\frac{2n\pi t_{p-1}}{T}\right) \tag{12.10}$$

$$b_{n=\frac{T}{2n^2\pi^2}\sum_{p=1}^{K}\frac{\Delta x_p}{\Delta t_p}\left(\sin\frac{2n\pi t_p}{T} - \sin\frac{2n\pi t_{p-1}}{T}\right)} \tag{12.11}$$

$$c_n = \frac{T}{2n^2\pi^2}\sum_{p=1}^{K}\frac{\Delta y_p}{\Delta t_p}\left(\cos\frac{2n\pi t_p}{T} - \cos\frac{2n\pi t_{p-1}}{T}\right) \tag{12.12}$$

$$d_n = \frac{T}{2n^2\pi^2}\sum_{p=1}^{K}\frac{\Delta y_p}{\Delta t_p}\left(\sin\frac{2n\pi t_p}{T} - \sin\frac{2n\pi t_{p-1}}{T}\right) \tag{12.13}$$

Each ellipse is represented by the four parameters, the elliptic descriptors related to the major axis, minor axis, angle of rotation corresponding to the long-axis orientation of the ellipse and the angle of the phase corresponding to the position of the first point on the ellipse. The outlines are reconstructed, step by step using an increasing number of harmonics, carried point by point.

The coefficients are not invariant in size, rotation, shift, and starting point of chain coding about the contours, requiring standardization [71]. The resulting elliptic descriptors can be subjected to statistical analysis as variables describing the shape. Fourier coefficients can be treated as independent variables because they satisfy the condition of orthogonality. This permits the assessment of the proportional contribution of each component to the overall variability between specified groups. The property of orthogonality allows the partition of size and shape components [78] meaning that it is possible to separately analyze the contribution of each harmonic to the total form.

For Fourier representations, smooth shapes with low amounts of high-frequency detail will be better reconstructed [30].

The extracted harmonic coefficients are variables to be employed in multivariate statistics and ordination such as PCA that defines the morphological space, MANOVA, (LDA) Linear Discriminant Analysis, hierarchical clustering permitting multiple comparisons among shapes.

One of the disadvantages in using Fourier descriptors resides from the use of frequency domain information (components as amplitude and phase) that do not provide information with respect to where in the spatial domain the frequency component occurs. The method is useful for global aspects of the form but does not provide possibilities for the identification of local aspects [79].

12.3.3 Eigenshape Analysis

Eigenshape analysis (ESA) is a technique used for the reduction of digitized outline shapes into few parameters for multivariate analysis and visualization of shape variation [70, 80]. The procedure is designed to organize as simply as possible a collection of specimens whose shape differences are subtle, complex, and continuous [80], accommodates closed and open contours. The semi-landmark approach as used in eigenshape analysis incorporates curves into landmark-based formalism [14, 66]. The method produces a summary with desirable analytical properties [81] such as mutual independence of the shape indices and a direct graphical portrayal. Although extensively employed in botany, paleontology, zoology, and phylogenetic studies, it was seldom used for the study of microscopic organisms.

The method starts with the extraction of the outline on digital photographs, manually, or automatically.

The coordinate points collected from the outline are converted in angles and in shape φ^* function ZR of Zahn and Roskies [72], the net angular change in direction φ at each step around the perimeter l of the specimen.

$$\varphi^*(t) = \varphi(t) - t \tag{12.14}$$

The representation is invariant to size, translation, and rotation of the object in x, y plane but is sensitive to the location of the starting point and the digitization direction (clockwise or counterclockwise) [82]. The entire curve is interpolated in standard eigenshape analysis in equally spaced points that become the comparison basis across specimens [69]. The name (selected by Lohman) signifies two aspects of the method: (1) the representation of the set of outlines as sets of equivalent shape functions and (2) the assessment of the major directions in shape variation using eigenanalysis. A major difference from EFA resides in the use of a common point of reference during the outline sampling procedure, and by using a constant number of points on the outline, equally spaced. This procedure is introducing a homology of points in a similar manner to landmarks in landmark-based GM [69]. The redescribed semi-landmarks using ZR function (ZR function coefficients) are assembled in a $n \times m$ matrix, m being the number of semi-landmarks and n number of specimens. Correlation or covariance matrix is calculated from a series of m orthogonal eigenvectors (few will con-

centrate the greatest proportion of variance), named also eigenshapes. Eigenvectors define a morphospace [54]. Most of the shape-relevant information is loaded on the first few eigenvectors allowing the regions with pronounced shape variation to attract the eigenvectors in orientation sense [69]. The lengths of eigenshape vectors are proportional to the amount of observed variance across the sample, defining a shape space. Each eigenvector represents a trend of outline shape deformation, with positively and negatively aligned regions.

Principal Components Analysis (PCA) is performed on the covariance matrix of transformed coordinates using the Zahn–Roskies tangent function [72] that is basically, a linear combination of geometric observations analogous to the representation of the shape by Elliptic Fourier decomposition [83]. This consists of the arrangement of a series of *x, y* coordinates into a matrix of a column of vectors or the expression of differences among shapes as a matrix of semi-landmarks [65]. The semi-landmarks that are more variable across the samples, will be more highly weighted.

Outline and landmark techniques are combined in *landmark eigenshape analysis* (also called extended eigenshape analysis) which is considered a very efficient description of the shape. The basics of this technique are the identification of homologous contours bounded by homologous landmarks and to divide these contours in a number of equal length steps that can be represented by their angles in the plane [84]. The landmarks are used to subdivide the outline in topologically equivalent segments [85].

12.3.4 Legendre Polynomials (Orthogonal Polynomial Regression)

It is an outline method used to determine the curved segments of the outline as changes in width function consists of fitting a least-square curve around the outline. The coefficients from orthogonal polynomial regression are used as shape descriptors. The width function is a linear combination of Legendre polynomials of degree n in x_i and each Legendre coefficient c_n is an independent shape descriptor due to orthogonality. The width function can be expressed as an expansion of Legendre polynomial series [86].

$$W(x) = \sum_{n=1}^{N} c_n P_n(x) \tag{12.15}$$

where $W(x)$ is the width function, $P_n x$ is the non-normalized nth Legendre polynomial, and c_n represents n-Legendre coefficients. The coefficients are used as shape descriptors and are endowed with the desirable feature of a direct interpretation of morphological details. The method was recommended for cases when the outline is highly and continuously curved [29].

12.4 Image Acquisition

A critical aspect in shape analysis is image acquisition, especially when it is related to microscopic structures. From *camera lucida* drawings to software toolboxes devised for semi-automatic, automatic, or manual image acquisition, this field has experienced huge leaps forward.

The main problem in microscopic imagery is the simplification of 3D shapes to 2D domain restricted to boundary features. Frequently, there are optical alterations of the specimens (distortions) that induce type I errors (splitting the same species into two different entities) or type II errors (merging species). These limitations were observed in light-transmitted microscopy but also in differential interference contrast and phase-contrast light microscopy. Therefore, high-resolution imaging techniques are recommended as more reliable imaging tools for microscopic organisms [87].

Microscopy imaging techniques include phase contrast, differential interference contrast, scanning microscopy, atomic force, and confocal laser scanning microscopy. Cell's images can be segmented using region-growing and 3D-shape analysis [88]. Images generated in the confines of light microscopy brought at the present-day state of the art, present several important attributes making this sort of imagery particularly suited for GM:

1. The manipulation of the target objects is more precise than in the macroscopic domain due to uniform and controlled light intensity, lack of perspective distortions, and shadowing.
2. The relative simplicity of the overall shape of objects (bacteria, fungi, or diatoms being now in the focus) compared to macroscopic complex anatomy and morphology of macroscopic plants and animals.

The outline-based approaches require some sort of automation in extracting the outline of microscopic objects [89] therefore, considered more tedious. Taking photographs in a different focal plane than the surface plane of the microscopic object (diatom frustules, oomycete sporangia, or fungal spores) is one possible approach in extracting the outline. The outline is directly encoded in a list of *x, y* coordinates of sample points or a list of angles and distances between points [30]. However, it is easier to digitize landmarks and semi-landmarks on the boundary outline of the microscopic objects, the only requirement being the quality of the photograph. Moreover, previously published

images satisfying the quality requirement can be employed [89].

For outline using Elliptic Fourier Analysis, the contour is obtained also from a binary mask (the object of interest is contrasted to the background) and the points on the contour are chain-coded. The method encodes the items' shape at pixel resolution. Prior to registration of outline points, the sample items must be aligned [30]. The subprogram Chain-Coder included in the software SHAPE [75] extracts the contour from digital images by edge detection and stores the information as a chain code. The clearest contrast between object and background is obtained by an appropriate level of thresholding, determined automatically. The chain-coded contours are processed by the subprogram Ch2Nef and the Fourier coefficients are calculated based on stored contour data.

The accuracy of image capture and digitization is estimated using the centroid size of a training set of digitized shapes. Centroid size represents the square root of the sum of squared distances of a set of points on the contour from their centroid in x and y direction. The training set consists in subsamples of captured images in which outlines are repeatedly traced. Repetitions are performed on different days to cover variability induced by the human factor during the digitization process. One way ANOVA on centroids of multiple sampled item is employed to assess the accuracy of imaging and outline or landmarks tracing.

12.5 Visualization of Shape Variation

Visualization of shape changes and variability is situated in the very core of geometric morphometrics [90]. The various methods of visualization communicate more effectively shape information than any numerical output, making GM more appealing than traditional multivariate morphometrics. The possibility to reconstruct shapes from statistical analyses such as principal components, regression, partial least squares, makes possible tracking shape changes, and also shape differences when these features are not detectable after ordinary visual inspection.

For analysis and visualization of shapes using landmark and semi-landmark methods, a key component is Kendall's shape space in which every shape or any physical object occupies a particular point. Every point is projected into a Euclidean tangent space centered on the average shape. Points in tangent space can be related back to actual shapes in the original plane of the landmark coordinates. Vectors in tangent space correspond to shape changes taking into consideration the fact that landmarks vary in space isotropically and non-isotropically (most often). In the transformed space, the differences between and within groups are assessed using Mahalanobis distance that permits computing discriminant functions and Canonical Variate Analysis (CVA) [91]. The importance of shape differences and changes derives from the fact that they link to important processes and structural variability such as ontogenetic development, pathogenicity in bacteria and fungi, pleomorphism, between populations variability, and differences between taxa.

12.5.1 Landmark-Based Methods

The main advantage of landmark coordinates analysis is the relative easiness to draw informative pictures to illustrate the results [92]. Visualization of morphological transformations over the entire form is performed using thin plate splines (TPS), used to obtain models of shape deformation with respect to an average or target shape based on the displacement of all landmarks relative to all others. The TPS function interpolates the inter-landmark space as smoothly as possible by minimizing the integral of second derivatives, a quantity called bending energy. The mathematical model was borrowed from spatial statistics where TPS is employed for the estimation of the value of a property at an un-sampled location based on the values of the property of interest at neighboring locations. In layman terminology, the resulted model shows how the shape of reference specimen must be squeezed or stretched to match the target or average shape as a TPS function makes possible the representation of shapes on deformation grids. D'Arcy Thompson made this type of representation on hand-drawn deformation grids [68]. The TPS deformation grids and warps are visual aids to depict shape differences graphically [93]. The name of these visualization techniques comes from a metaphor of an infinitely thin and large metal plate superimposed on transformed landmark/semi-landmarks configurations, with bending regions that correspond to deformations. Thin plate spline produces deformation grids depicting shape changes with respect to a reference shape.

Mathematically, deformation is a smooth function that maps points in one form to corresponding points in another form (the function goes on without interruptions and is continuously differentiable). The fact that the TPS function is differentiable permits to make interpolations to infer what is happening in inter-landmark regions. However, it is unreasonable to interpolate between distant landmarks or when interpolation spans outside the organismal space if landmarks are positioned on tips of the studied structure, which are drawbacks of the algorithm [92]. This function permits to calculate the relative displacements of the landmarks as compared to a reference shape and these calculations are used to depict shape changes in a variety of graphical

approaches. Usually, the reference shape that best represents the distribution of shapes in a sample is the mean shape [94]. Another reason of caution is the fact that the algorithms used for computing transformation grids such as TPS are based exclusively on geometric and statistical criteria with no biological basis [90]. It expands in the inter-landmark regions, treating the shape globally even if no biological data cover the inter-landmark space.

Deformations are classified as uniform (affine or linear) such as translations, scaling, rotations, compression/dilation, and shear and nonuniform (non-affine, nonlinear) deformations. Uniform deformations preserve the parallelism of lines after deformation meaning that the same change occurs everywhere in the analyzed shape space, while nonuniform deformations do not preserve the parallelism after deformation and influence locally the shape. Real objects subjected to GM analysis show a mixture of uniform and nonuniform deformations. The two components are computed separately.

The components of a thin plate spline use as starting information the distances between landmarks [94]. These are used to calculate an index of bending energy plus the length in Z direction corresponding to deformations changing locally the flatness of the ideal metal plate (spatially local information). Accordingly, the bending energy depends on the spacing between landmarks and the slope of the deformed plate. This energy is minimized in order to obtain a parsimonious description of the change, to smoothen the high values in the Z direction. The derivation of equations corresponding to uniform deformation is devised to find a unit vector that describes the direction of deformation at each landmark due to shear, compression/dilation following the Procrustes [12] superimposition of the deformed shape over the target and undeformed shape.

The nonuniform component is describing the local changes that vary spatially corresponding to small regions of the shape. Thin-plate spline function approximates the observed deformation by a linear combination of the smooth function and the fully described deformations. The nonuniform deformation is decomposed in a series of components (partial warps) at progressively smaller scales and each component (partial warp vector) describes a pattern of landmark displacements based on spacing present in the reference form [60, 67]. The coefficients, partial warp scores, measure the contribution made by a partial warp to the total deformation. The partial warps are obtained by eigenanalysis of the bending energy matrix, unlike principal components analysis (PCA) extracted from covariance/correlation matrices of measurements. There are $k-3$ partial warps for shapes characterized by k landmarks. For instance, partial warp 1 specifies deformations that encompass the entire set of landmarks. The calculation of partial warps precludes the calculation of relative warps.

Thin-plate spline results in a series of coefficients, partial warp scores that can be used in conventional statistical analysis in a similar way with Principal Component scores. The partial scores employ also the Procrustes distances (used in the tangent space). A spline is a convenient tool for visual display and a tool for obtaining transformed variables. Still, it is primarily a graphical display tool [94].

There are various types of graphical visualization of shape changes by landmark displacements: graphs that indicate shifts in landmark positions by lines or arrows utilized at the beginning of GM [60] replaced recently by more sophisticated techniques [90]. More realistic representation uses wireframe graphs with superimposed outline drawings warped using TPS. Another approach is based on heat maps with a color code attached (Jacobian expansion factors): cold colors correspond to areas where target shape contracts and warm colors where target shape expands out of the starting shape [95].

12.5.2 Outline-Based Methods

The Fourier coefficients (descriptors) are reduced in dimensionality by means of Principal Component Analysis (PCA or PC in short) and their scores are used to characterize the shape of the objects subjected to analysis. The effect of each PC is visualized by recalculation of the inverse Fourier descriptors [75, 96]. The procedure as it is included in the software SHAPE [75] requires the calculation of elliptic Fourier coefficients letting the score for a particular principal component be equal to the mean plus and minus two times the standard deviation (the square root of the eigenvalue of the component and the scores of the remaining components are set to zero). The contour shape is reconstructed from the calculated coefficients by the inverse Fourier transformation (Fig. 12.2). The reconstructed contours give a morphological meaning of the variation captured by each important principal component [75].

PCA is generally used to reduce Elliptic Fourier coefficients to a smaller number of independent shape variables. The reduced number of variables can be then subjected to Linear Discriminant Analysis (LDA) to find new axes that would perform a better discrimination and classification.

As eigenshape analysis combines with relative warps analysis, visual representation of shape changes may employ the same thin-plate spline visualization tools (Fig. 12.3). In eigenshape morphospace, shapes are ordinated as points in the planes delimited by principal components (Fig. 12.4).

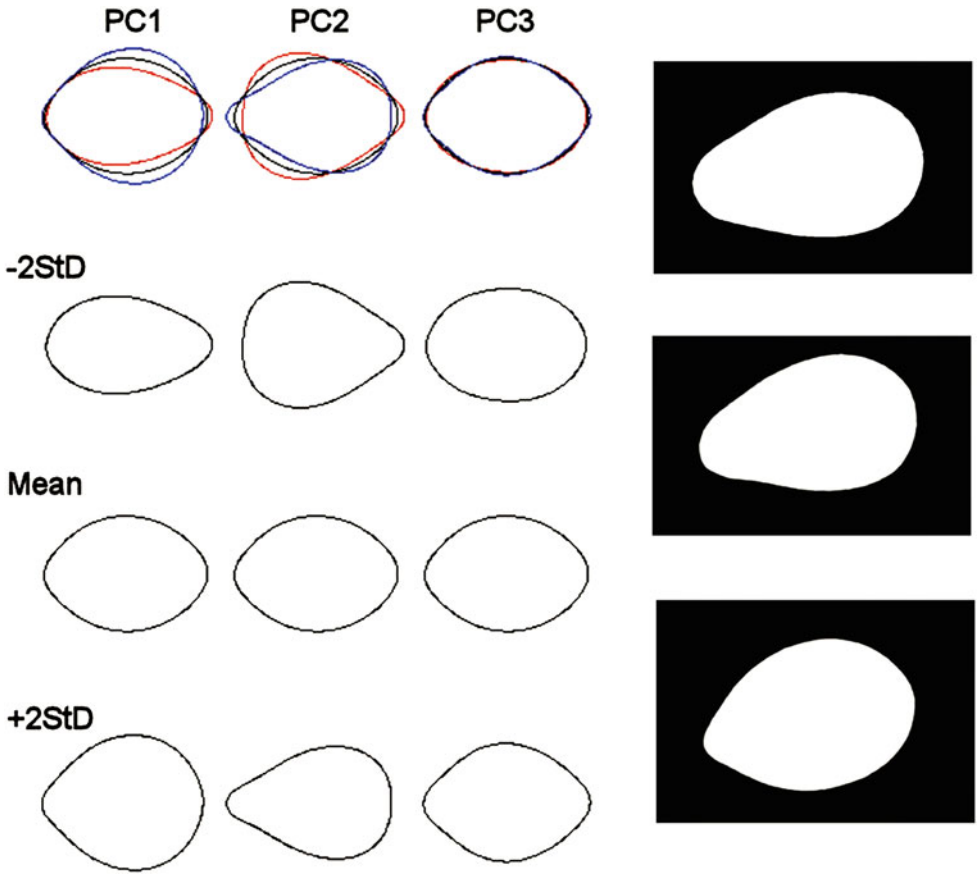

Fig. 12.2 Elliptic Fourier analysis—symmetrical variation using symmetrical group coefficients in *Phytophthora plurivora* sporangia, the effect of principal components 1, 2, and 3, (overlaid mean shape and ±2 standard deviations in the first row). The contour was obtained using a binary mask (from the right panel of the figure)

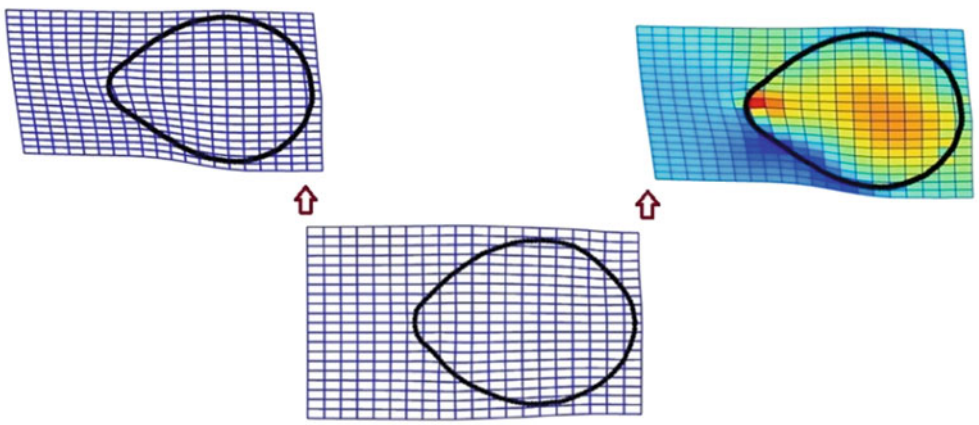

Fig. 12.3 The results of Eigenshape analysis of *Phytophthora plurivora* sporangia can be visualized using thin-plate splines routinely employed in warp analysis. Representation of mean shape in a warped wireframe and individual shape represented in wireframe and using the color map based on Jacobian expansion factors

12.6 Quantification of Shape Variation

The extraction of shape numerical descriptors is only the first step in shape analysis. Multivariate methods applied to shape data reduce the dimensionality to a few independent eigenvectors corresponding to the maximum of shape variation. The choice of the multivariate method used to analyze shape data is of utmost importance for the depiction of shape groups' separation for any of shape variables extrac-

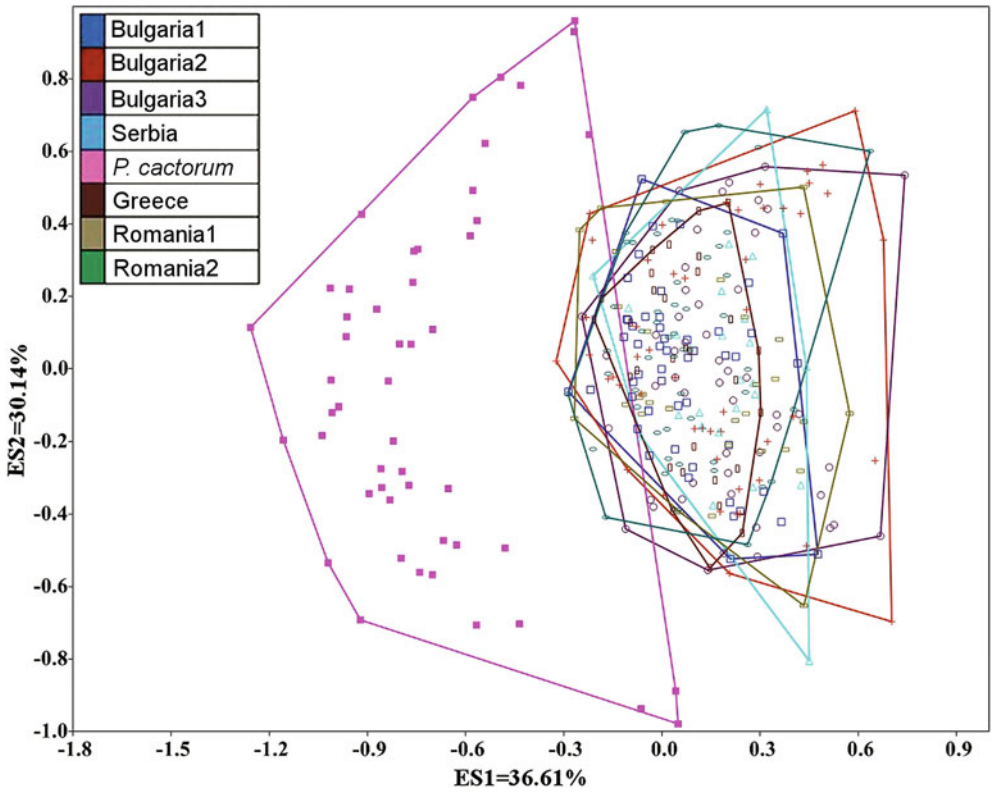

Fig. 12.4 Visualization in Eigenshape analysis of *Phytophthora plurivora* and *Phytophthora cactorum* sporangia. Following PCA, one represents shapes as points in eigenshape morphospace and identifies the variation along individual axes. First eigenshape axis accounts for 36.61% of shape variation and the second eigenshape axis for 30.13% of total shape variation (from [64])

tion methods employed [14]. Therefore, ordination methods are employed to summarize the variation in shape space [97]. Primarily, the assessment of the major directions of the observed shape variation in a data set is performed by eigenanalysis.

The classical and widespread method employed in ordination is Principal Component Analysis that provides a low dimensional projection of the full shape space in a way that the variance of the data is preserved. PCA is employed primarily for dimensionality reduction of shape descriptors. However, the method permits the depiction of total shape variation and, in the case of separation of PCA scores in clusters, shape groups may become evident [86]. Pincus and Theriot [30] considered that PCA of a given shape data set produced an excellent set of numerical descriptors that strike a good balance between the faithfulness of the original shapes and retention of the biologically relevant shape details. Other ordination methods, Canonical Variate Analysis, Multidimensional Scaling, and Correspondence analysis claimed to distort the geometry of the space, are used more in non-landmark shape approaches [35].

Using landmark-based methods, relative warp analysis (RWA) of landmarks may be performed in software PAST [95] and tpsRelw, version 1.53 [98]. If the curves are transformed in a series of semi-landmarks using tpsUtil software [98], Procrustes alignment [34, 36] is used in order to remove the differences due to rotation, scale, and orientation. The transformed data are then subjected to relative warp analysis (RWA) using thin plate splines to visualize the shape deformation of each specimen with respect to consensus shape.

RWA corresponds to a principal component analysis of the covariance matrix of the partial warp scores considered to be at different scales of thin plate splines devised to reduce the dimensionality of data [65]. RWA is performed on the covariance matrix of aligned landmark coordinates. The method ordinates the landmark-based shapes using their mutual similarity and treats the configurations as unified geometric entities, respecting the convention of Kendall shape space. The RW eigenvectors represent a set of displacements of each landmark location across the shape as mediated by nonuniform and uniform shape deformations specified by partial warp scores or weights that serve as variables [99]. PCA ordination on consensus shapes and overall consensus shape (relative warp scores) are performed in order to compare the mean shapes.

Discrimination among groups is one of the central goals when performing a GM study. Group separation is performed

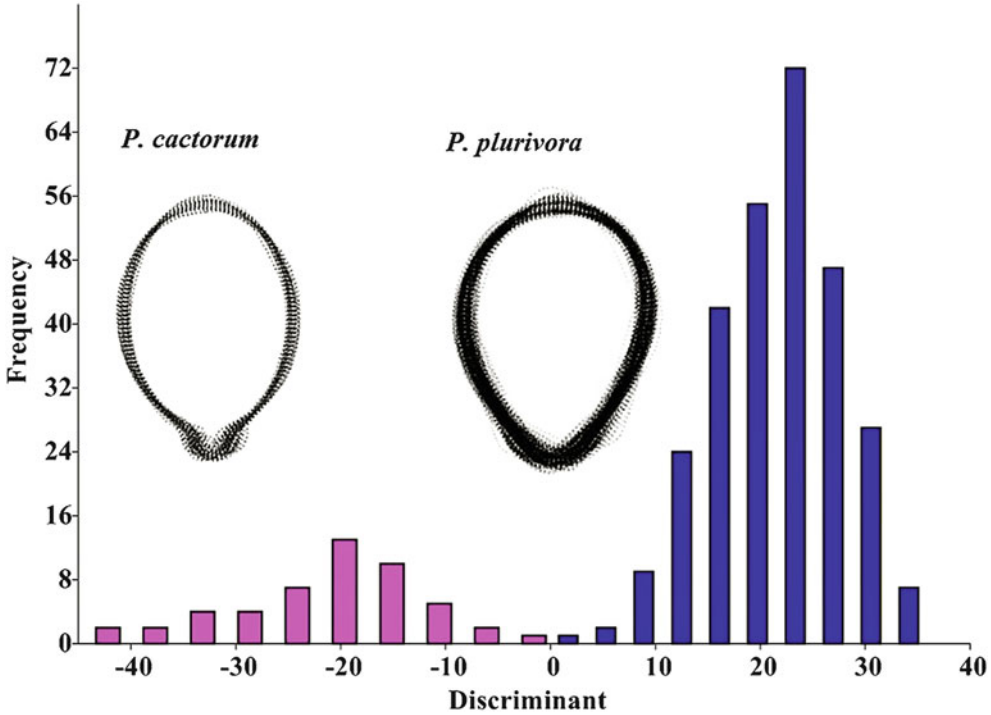

Fig. 12.5 Discriminant analysis permitted the separation of *Phytophthora plurivora* samples from *P. cactorum* based on eigenshape analysis results. Consensus shapes are included in the graphical output (after [64])

using Canonical Variate Analysis, Multivariate Analysis of Variance (MANOVA) and Discriminant Analysis. Canonical Variate Analysis (CVA) maximizes inter-group separation and permits the assignment of objects to groups. Shape variance is partitioned into between and within components variation on ES scores, relative warp (RW) scores, and centroid size, an approach devised by Magrini and Scoppola [100] for better discrimination and separation of shapes. *Discriminant Analysis* permits the cross-validation of shape groups obtained with PCA. The methods are based on Mahalanobis distance that takes into account the correlation among variables. The measurement of the distance between the center of the distribution of all shape descriptors and each individual shape descriptor permits the assignment of each item to the corresponding group [101]. The significance of the result is tested using Wilk's lambda (small values of the statistic are preferred) [102]. The basic idea consists in minimizing the variance within groups and maximizing the variance among all groups (Fig. 12.5). Linear Discriminant Analysis (LDA) was largely employed to Procrustes shape coordinates. LDA seeks a linear combination, the discriminant function that maximizes the ratio of the between-group sum of squares to the within-group sum of squares. It permits the affiliation of a specimen to one of the two compared groups based on its score of this linear combination [103]. It has no biological significance but it plays the role of a decision-making tool in specimens' classifications [45].

CVA (*Canonical Variate Analysis*) is utilized for quantitative discrimination of groups within the shape's morphospace. To perform CVA, the first principal component can be are employed, or the eigenshape or relative warp axes considered as well for shape description as established by Jolliffe's cut level [104] and the normalized centroid size.

Multivariate Analysis of Variance (MANOVA) is generally the first choice in morphometric studies in search of group discrimination, but frequent doubts were expressed on the correctness of the approach because there is a mismatch between the number of employed variables and the degrees of freedom when using semi-landmarks [59]. Therefore, an alternative is to employ the nonparametric alternative of the test, NPMANOVA using the Mahalanobis distance.

Multiple regression of centroid size on the first relative warp axes scores or eigenshape analysis scores can be performed in order to test for an allometric relationship between shape and dimension [105]. The space created by shape and dimensional variables display a particular pattern in terms of variability. Alternatively, allometry can be computed using a multivariate regression of shape coordinates on the centroid size or the logarithm of the centroid size. Significance is tested employing MANOVA or resampling tests [43].

Allometry refers to shape change associated with size differences and can account for a large and statistically significant proportion of morphological variation [16, 106, 107]. The concept was introduced by Huxley in his treatise "Prob-

lems of Relative Growth" (1932), and was based initially on linear measurements. It is expressed as power functions between quantitative traits or as relationships between log-transformed traits.

The shape space can be subdivided into subspaces corresponding to symmetrical and asymmetrical variations, modular versus integral shape subspaces or the geometric scale of variation [67, 74, 108]. A special position has the centroid of a landmark/semi-landmark configuration in terms of significance*: centroid size* is considered in GM as a measure of overall size. By augmenting the landmark coordinates by the natural logarithm of the centroid size, shape space extends to Procrustes form space, a space encompassing shape and size where PCA and statistical analyses can be performed [35, 43].

Independent Components Analysis (ICA) can separate independent signals that have been linearly recombined. ICA operates by finding projections of the data set that are maximally non-Gaussian, according to some normality test. Finding the latent variables that are most likely to mix to create a joint distribution of the data set [30]. It can be applied to any representation of cell shapes. However, the components in ICA are not orthogonal. There were a few cases in which ICA was used in shape analysis, being more employed in computer vision [109].

Partial least squares (PLS), also called singular warps analysis, is a multivariate statistical method devised for the assessment of covariation structure of morphometric and ecological data. It permits the evaluation of the relation between two or more blocks of data [110]. It is based on a form of PCA, extending the regression analysis. PLS employs single value decomposition (SVD) to obtain singular values (square roots of eigenvalues and eigenvectors) of PCA basis matrices. PLS regress two sets of multiple variables against one another. The partial regression coefficients evaluate the correlation between dependent and independent variables [65].

12.7 What Information Conveys the Analysis of Microscopic Imagery?

The GM use has expanded during the last two decades, as important advances in theoretical setting and continuous increase of user-friendly software took place. The range of areas employing GM methodology also increased from paleontology (among the first to apply GM) to zoology, botany, medicine, and archaeology. The interest toward GM in domains studying microorganisms, or analyzing microscopic structures appeared later, and the publication of papers focused on applications of GM at a microscopic scale remained far below other domains such as zoology or medical research. As microscopy advanced hugely during the last decades and microscopic imagery became more sophisticated, few attempts (but notable) were made to analyze the shape of microscopic objects using the rigorous approach of GM.

In microorganisms, microscopic objects by default, the shape is a classification and identification feature and even more, it conveys important information on other aspects. For unicellular structures such as fungal spores or bacterial and yeasts' cells, the shape is correlated with important functions or properties such as adhesion, motility, pathogenicity, and differentiation. In the case of bacteria [7] or dispersal, phylogeny, environmental stress, adhesion to the substrata, motility in the case of fungi [111]. The cell wall is both necessary and sufficient for defining a particular cell shape in bacteria [112]. It can be considered as a repository of the information that flows through the cell-signaling network [113]. In diatoms, the extremely diversified shape of cells protected by a silica shell is fundamentally a closed generalized cylinder [114] and it is the expression of many organizing, competing, and highly regulated processes.

Pathogenic fungi are characterized by high morphological shifts in shape, mostly in dimorphic fungi in which morphotypes are associated with pathogenicity. As a rule, cell shapes evolve as a response to environmental stress [1] and cell shape variability is the manifestation of the alteration of cell wall properties. The analysis of spore or sporangia shapes for instance, using semi-landmarks or other outline-based methods permitted to distinguish statistically distinct populations [30]. Infantino et al. [115] by employing Elliptic Fourier Analysis delivered a classification of the plant pathogenic *Ascochyta lentis* conidial shapes.

In the study of diatoms, the landmark-based methods were employed, for instance in taxonomic, phylogenetic, or ecological contexts [89, 116–118]. The complex, intricate architecture of diatoms' cell wall determining the cell shape is an example of selective advantage in shape evolution. It appears to be important in defense mechanisms against pathogens or predators, and motility. Consequently, shape variability is intimately linked to evolutionary processes and environmental constraints.

From this new perspective, morphotypes could be distinguished based on subtle or latent morphological properties and assigned to different species. For instance, in *Navicula cryptocephala* and *N. trivialis* based on the analysis of different stages of life cycle, GM data permitted to identify a strong strain-specific signal [116]. Using scanning electron microscopy and transmitted light optic microscopy, Beszteri et al. [117] separated morphospecies *Cyclotella meneghiniana* from *C. cryptica* based on combined classical morphometric and landmark data. Sympatric populations of *Reimeria sinuata* and *Gomphonema tergestinum,* characterized by large variations and existence of transitional forms segregated in distinct groups following GM analysis [118].

In other works, authors were interested in discriminations between naturally occurring diatom populations, the correspondence between environmental variables and shapes. They employed to attain these goals, sliding semi-landmarks [89]. In the critical review on the GM use in the study of diatoms, Pappas et al. [29] pointed out that choosing landmarks could become difficult because of the subjective nature of selecting homologous points, despite the variability of studied organisms. Aside from homology fulfillment, the presence of curvatures not covered by landmarks introduced additional sources of error in the interpretation of the results.

In ecological studies, outline methods have been used in diatom research for shape analysis and pattern recognition [29] and employed successfully in taxonomy and classification. Among the first papers on shape analysis of diatom valve outline, Stoemer and Ladewski [86] used orthogonal polynomial regression (Legendre polynomials). From the coordinates of the outline, coefficients from orthogonal polynomial regression were employed as numerical shape descriptors. Outline analysis using Fourier descriptors was another path to follow in diatom shape analysis as in the early work on genus *Tabellaria* [119]. Wishkerman and Hamilton [87] employing Elliptic Fourier Analysis in conjunction with LDA tested whether the methods permitted good discrimination among diatom species, concluding that distinct shapes separated well in shape space. Species similar in shape, however, could not be distinguished using only Fourier descriptors, requiring additional texture or morphometric information [120].

After an extensive search in the published scientific papers, GM in the study of fungal shapes was far less employed compared to other microscopic organisms. Eigenshape analysis in conjunction with relative warps was employed in the study of *Phytophthora plurivora* (Oomycota) sporangia originating from different populations [64]. Fungal spores were studied in the context of image processing techniques using Fourier descriptors [121]. Several early authors have targeted the fractal pattern of mycelia [49, 50, 122–125]. Fractals accommodate branching structures such as mycelia of fungi and filamentous fungi-like organisms as Oomycota or plasmodia of slime molds (Myxomycota) and capture mycelial complexity at the microscopic level. Differences among mycelia were captured in terms of the fractal dimension of normal and virus-infected mycelia of the aggressive pathogen *Cryphonectria parasitica* [126]. Lindenmayer systems were applied to describe the conidiogenesis in *Alternaria* sp. [127]. Other groups of microscopic organisms were addressed in GM studies such as algae from Chlorophyta. Landmark-based methods permitted the assessment of shape variation induced by environmental factors [128].

As landmark-free methods [40] develop and gain popularity for their explanatory power in detecting shape differences in hyperbolic space, as most of the 2D representation refers in fact to hyperbolic or spherical objects, the logic of microscopic analysis of shapes is to enter in the near future in this area of analytic tools. This new approach to the study of shapes explores the curvature under the topology of different manifolds, using projections into one of the standard models of hyperbolic planes such as Poincaré disk or Klein model, endowed with a hyperbolic metric.

12.8 Conclusions

GM analysis in taxonomy and phylogenetics do not substitute molecular analysis but provides extra powerful tools. One must take into consideration the high dimensionality of morphometric data that are difficult to be put into correspondence with genotypes. Future developments will probably focus on methods for the reduction of data dimensionality and selection of significant traits for the explanation of variability taking into consideration the fact that also genetic dimensionality is high. It is expected that analyses of images will increase across many types of organisms at different scales, microscopic included, which implies automate phenotyping, optimization of specimen handling, construction of inclusive databases in connection with handling database software [9].

As the next level in taxonomy will be the automated species identification using technologies such as pattern recognition (using geometric morphometrics set of techniques), machine learning, and artificial intelligence [129, 130]. Automated identification systems are currently used for the identification of insects, Daisy (Digital Automated Identification System [131]), bees (Automatic Bee Identification System-ABIS, [132]), microbial populations (automatic Identification and Characterization of Microbial Populations—AIMS, [133]), or diatom classification [134–136]. Chapter 1 includes a list of projects related to diatom identification.

An increased interest toward the creation of a global database containing digital images useful in GM analyses became obvious [137], as advances in image acquisition and possibilities in acquiring low-cost and still high performing devices also increased. The idea could be easily extended for microscopic imagery, giving a new pace and amplitude to GM studies concerning microorganisms.

In the middle of the unprecedented expansion of molecular methods (various "–omics") in the identification and classification of organisms, the progress made in the field of GM come to add new dimensions to our knowledge on evolution, the connection between shape and function, ecological shape variability, phylogenies, adaptations. Morphological diversity is an important part of biodiversity, trying to find an answer to *why are there so many shapes?*, geometric morphometrics illuminates what Mandelbrot once called

The Geometry of Nature, complex, mostly non-Euclidean, irregular, and unexpected.

Appendix: Software Available

Below is attached a selection of most frequently employed software in GM.

- For Elliptic Fourier Analysis, existing software includes PAST, SHAPE, VsioBioShapeR, SHERPA, Momocs for R [32, 75, 95, 138–140]. *DiaOutline* [87].
- For image processing tools *Image J* and *Fiji* (https://fiji.sc/) are recommended.
- For landmark-based and other outline-based methods, the following software is recommended:
  - *MorphoJ* [140] is devised for landmark-based morphometrics providing also several ordination and statistical tools.
  - PAST—Paleontological Statistics incorporates possibilities to analyze landmark and outline data [95].
  - *Momocs for R* [32].
  - *FracLac for ImageJ* is a module used for fractal analysis and morphology functions [141].
  - Package *tps,* utility programs tpsUtil, tpsDig1, and tpsDig 2w43—for digitization of landmarks and outlines from digital photographs, scanner, or video, tpsSuper—superimposition, unwarping, and averaging, tpsSmallw32—tests for small variation in shape, tpsRegress32—multivariate multiple regression of shape variables on environmental variables, tpsSpline—thin-plate spline visualization, tpsRelw—relative warps analysis, tpsPLS—partial least squares analysis for shapes [98].
  - *Sage* ver. 1.21—Analysis of symmetry and asymmetry [142].
  - *Mace* ver. 1.03—Matrix correlation of geometric data [143].
  - *SemiThinner* ver. 1.02—Conversion of landmark data to semi-landmarks [144–146].

References

1. Backes, A.R., Bruno, M.O., Florindo, J.B.: Shape analysis using fractal dimension: a curvature based approach. Chaos. **22**, 043103 (2012). https://doi.org/10.1063/1.4757226
2. Foote, M.: The evolution of morphological diversity. Annu. Rev. Ecol. Syst. **28**, 129–152 (1997)
3. Van Valen, L.: Morphological variation and width of ecological niche. Am. Nat. **99**(908), 377–390 (1965)
4. Findley, J.S.: Phenetic packing as a measure of faunal diversity. Am. Nat. **107**(956), 580–584 (1973)
5. Ricklefs, R.E., Miles, D.B.: Ecological and Evolutionary Inferences from Morphology: An Ecological Perspective, pp. 13–41 (1994)
6. Hutchinson, G.E.: Homage to Santa Rosalia or why are there so many kinds of animals? Am. Nat. **93**(870), 145–159 (1959)
7. Ursell, T., Lee, T.K., Shiomi, D., Shi, H., Tropini, C., Monds, R.D., Colavi, A., Billings, G., Bhaya-Grossman, I., Broxton, M., Huang, B.E., Niki, H., Huang, K.C.: Rapid, precise quantification of bacterial cellular dimensions across a genomic-scale knockdown library. BMC Biol. **15**, 17 (2017). https://doi.org/10.1186/s1215-017-0348-8
8. Lewontin, R.C.: The Genetic Basis of Evolutionary Change. Columbia University Press, NewYork (1974)
9. Houle, D.: Colloquium paper: Numbering the hairs on your head: the shared challenge and promise of phenomics. Proc. Natl. Acad. Sci. **107**, 1793–1799 (2010). https://doi.org/10.1073/pnas.0906195106
10. Hawksworth, D.L., Sutton, B.C., Ainsworth, G.C.: Ainsworth & Bisby's Dictionary of the Fungi, 7th edn, p. 445. C.M.I., Kew, Surrey (1983)
11. Wang, L., Lin, X.: Morphogenesis in fungal pathogenicity: shape, size, and surface. PLoS Pathog. **8**(12), e1003027 (2012). https://doi.org/10.1371/journal.ppat.1003027
12. Bookstein, F.: Biometrics, biomathematics and the morphometric synthesis. Bull. Math. Biol. **58**(2), 313–365 (1996)
13. Papagianni, M.: Characterization of fungal morphology using digital image analysis techniques. J. Microb. Biochem. Technol. **6**(4), 189–194 (2014). https://doi.org/10.4172/1948-5948.1000142
14. Sheets, D.H., Covino, K.M., Panasiewicz, J.M., Morris, S.R.: Comparison of geometric morphometric outline methods in the discrimination of age-related differences in feather shape. Front. Zool. **3**, 15–26 (2006). https://doi.org/10.1186/1742-9994-3-15
15. Blackith, R., Reyment, R.: Multivariate Morphometrics. Academic Press, New York (1971)
16. Mosimann, J.E.: Size allometry: size and shape variables with characterizations of the lognormal and generalized gamma distributions. J. Am. Stat. Assoc. **65**(330), 930–945 (1970)
17. Mitteroecker, P., Gunz, P.: Advances in geometric morphometrics. Evol. Biol. **36**, 235–247 (2009)
18. Klingenberg, C.P.: Evolution and development of shape: integrating quantitative approaches. Nat. Rev. Genet. **11**(9), 623–635 (2010). https://doi.org/10.1038/nrg2829
19. Cardini, A., Lov, A.: On growth and form in the computer era: from geometric to biological morphometrics. Hystrix. **24**(1), 1–5 (2013). https://doi.org/10.4404/hystrix-24.1-8749
20. Mandelbrot, B.: The fractal geometry of nature. W.H. Freeman, San Francisco (1982)
21. Stanton, D., Horn, M.: Epiphytes as "filter drinkers": life-form changes across a fog gradient. The Bryologist. **116**(1), 34–42 (2013). https://doi.org/10.1639/0007-2745-116.1.034
22. Carlin, M.: Measuring the complexity of non-fractal shapes by a fractal method. Pattern Recogn. Lett. **21**, 1013–1017 (2000)
23. Bruno, O.M., de Oliveira Plotze, R., Falvo, M., de Castro, M.: Fractal dimension applied to plant identification. Inf. Sci. **178**(12), 2722–2733 (2008)
24. Landini, G.: Fractals in microscopy. J. Microsc. **241**(1), 1–8 (2010). https://doi.org/10.1111/j.1365-2818.2010.03454.x
25. Hicks, Y.A., Marshall, D., Rosin, P.L., et al.: A model of diatom shape and texture for analysis, synthesis and identification. Mach. Vis. Appl. **17**, 297–307 (2006). https://doi.org/10.1007/s00138-006-0035-1
26. Macleod, N.: On the use of machine learning in morphometric analysis. Conference paper, pp. 134–171. https://doi.org/10.1142/9789813225701_0008 (2017)
27. Blanco, S., Borrego-Ramos, M., Olenici, A.: Disentangling diatom species complexes: does morphometry suffice? PeerJ. **5**, e4159 (2017). https://doi.org/10.7717/peerj.4159
28. Koehl, P., Hass, J.: Automatic alignment of genus-zero surfaces. IEEE Trans. Pattern Anal. Mach. Intell. **36**(3), (2014). https://doi.org/10.1109/TPAMI.2013.139

29. Pappas, J.L., Kociolek, J.P., Stoemer, E.F.: Quantitative morphometric methods in diatom research. Nova Hedwigia. **143**, 281–306 (2014)
30. Pincus, Z., Theriot, J.A.: Comparison of quantitative methods for cell shape analysis. J. Microsc. **227**(Pt2), 140–157 (2007). https://doi.org/10.1111/j.1365-2818.2007.01799.x
31. Kuhl, F.P., Giardina, C.R.: Elliptic Fourier features of a closed contour. Comp. Graphics. Image Process. **18**, 236–258 (1982)
32. Bonhomme, V., Picq, S., Gaucherel, C., Claude, J.: Momocs: outline analysis using R. J. Stat. Softw. **56**(13), 1–24 (2014)
33. Kendall, D.: The diffusion of shape. Adv. Appl. Probab. **9**, 428–430 (1977)
34. Dryden, I.L., Mardia, K.V.: Statistical Shape Analysis. Wiley, Chichester (1988)
35. Mitteroecker, P., Huttegger, S.M.: The concept of morphospaces in evolutionary and developmental biology: mathematics and metaphors. Biol. Theory. **491**, 54–67 (2009)
36. Rohlf, F.J., Slice, D.E.: Extensions of Procrustes method for the optimal superimposition of landmarks. Syst. Zool. **39**, 40–59 (1991)
37. Marcus, L.F., Hingst-Zaher, E., Zaher, H.: Application of landmark morphometrics to skulls representing the orders of living mammals. Hystrix. **11**(10), 27–47 (2000). https://doi.org/10.4404/hystrix-11.9-4135
38. Lestrel, P.E., Cesar Jr., R.M., Takahashi, O., Kanadawa, E.: A Fourier-wavelet representation of 2D shapes: sexual dimorphism in the Japanese cranial base. Anthropol. Sci. **112**, 3–28 (2004)
39. Lestrel, P.E.: From Elliptic Fourier to wavelets: three decades of boundary morphometrics. In: Lestrel, P.E. (ed.) Biological Shape Analysis: Proceedings of the 4th International Symposium of Biological Shape Analysis, pp. 172–214. World Scientific, Singapore. 1:vi–xi (2017). https://doi.org/10.1142/10562
40. Koehl, P., Hass, J.: Landmark-free geometric methods in biological shape analysis. J. R. Soc. Interface. **12**, 20150795 (2015). https://doi.org/10.1098/rsif.2015.0795
41. Shi, J., Thompson, P.M., Wang, Y.: Hyperbolic Ricci flow and its application in studying lateral ventricle morphometry. In: Yap, P.T., Liu, T., Shen, D., Westin, C.F., Shen, L. (eds.) Multimodal Brain Image Analysis, Lecture Notes in Computer Science, vol. 7509. Springer, Berlin (2012). https://doi.org/10.1007/978-3-642-33530-36
42. Stegmann, B.M., Delgado Gomez, D.: A brief introduction to statistical shape analysis. Informatics and Mathematical Modelling, Technical University of Denmark, DTU. 15 (2002)
43. Mitteroecker, P., Gunz, P., Windhager, S., Schaeffer, K.: A brief review of shape, form, and allometry in geometric morphometrics, with application to human facial morphology. Hystrix. **24**(1), 59–66 (2013). https://doi.org/10.4404/hystrix-24.1-6369
44. Lestrel, P., Kanazawa, E., Wolfe, C.A.: Sexual dimorphism using Fourier analysis; shape differences in the craniofacial complex. Anthropol. Sci. **119**(3), 213–229 (2011). https://doi.org/10.1537/ase.100630/
45. Mitteroecker, P., Bookstein, F.L.: Classification, linear discrimination, and the visualization of selection gradients in modern morphometrics. Evol. Biol. **38**, 100–114 (2011)
46. Hallgrímsson, B., Lieberman, D.E., Liu, W., Ford-Hutchinson, A.F., Jirik, F.R.: Epigenetic interactions and the structure of phenotypic variation in the cranium. Evol. Dev. **9**, 76–91 (2007). https://doi.org/10.1111/j.1525-142X.2006.00139.x
47. Gilbert, S.F., Epel, D.: Ecological Developmental Biology, 2nd edn. Sinauer Associates, Sunderland, MA (2015)
48. Klingenberg, C.P.: Analyzing fluctuating asymmetry with geometric mophometrics: concepts, methods, and applications. Symmetry. **7**, 843–934 (2012). https://doi.org/10.3390/sym7020843
49. Ritz, K., Crawford, J.: Quantification of the fractal nature of colonies of *Trichoderma viride*. Mycol. Res. **94**, 1138–1152 (1990)
50. Obert, M., Pfeifer, P., Sernetz, M.: Microbial growth patterns described by fractal geometry. J. Bacteriol. **172**, 1180–1185 (1990)
51. Matsuyama, T., Matsushima, M.: Fractal Morphogenesis by a bacterial cell population. Crit. Rev. Microbiol. **19**(2), 117–135 (1993). https://doi.org/10.3109/10408419309113526
52. Feder, J.: Fractals. Springer Science & Business Media, p. 11. ISBN 978-1-4899-2124-6 (2013)
53. Li, B.-L.: Fractal dimension. In: El-Shaarawi, Piegorsch, W.W. (eds.) Encyclopedia of Environmentrics, vol. 2, pp. 821–825. Wiley (2002)
54. Krieger, J.D.: Controlling for curvature in the quantification of leaf form. In: Elewa, A.M.T. (ed.) Morphometrics for nonmorphometricians, pp. 27–72. Springer (2010)
55. Prusinkiewicz, P., Hanan, J.: Lindenmayer Systems, Fractals and Plants. Springer, New York (1989)
56. Soddell, F., Seviour, R., Soddel, J.: Using Lindenmayer systems to investigate how filamentous fungi may produce round colonies. In: Stonier, Y. (ed.) Complex Systems. Mechanisms of Adaptation, pp. 61–66. IOS Press, Amsterdam (1994)
57. Neustupa, J., Černá, K., Šťastný, J.: Diversity and morphological disparity of desmid assemblages in Central European peatlands. Hydrobiologia. **630**, 243–256 (2009). https://doi.org/10.1007/s10750-009-9799-4
58. Bookstein, F.L.: Size and shape spaces for landmark data in two dimensions. Stat. Sci. **1**, 181–242 (1986)
59. Webster, M., Sheets, H.D.: A practical introduction to landmark-based geometric morphometrics. In: Alroy, J., Hunt, G. (eds.) Quantitative Methods in Paleontology. Paleontological Society Short Course, pp. 163–188. The Paleontological Society Papers 16 (2010)
60. Rohlf, F.J., Marcus, L.F.: A revolution in morphometrics. Trends Ecol. Evol. **8**, 129–132 (1993)
61. Adams, D.C., Rohlf, F.J., Slice, D.E.: A field comes to age: geometric morphometrics in the 21st century. Hystrix. **24**(1), 7–14 (2013). https://doi.org/10.4404/hystrix-24.1-6283
62. Sneath, P.H.A.: Trend surface analysis of transformation grids. J. Zool. **151**, (1967)
63. MacLeod, N.: Size and shape coordinates. Paleontol. Assoc. Newsl. **69**, 26–36 (2008)
64. Fodor, E., Hâruța, O., Milenković, I., Lyubenova, A., Tziros, G., Keča, N., Slavov, S., Diamandis, S., Kostov, K.: Geometric morphometry of *Phytophthora plurivora* sporangia. Ann. For. Res. **58**(2), 275–294 (2015). https://doi.org/10.15287/afr.2015.411
65. Bookstein, F.L.: Morphometric Tools for Landmark Data: Geometry and Biology. Cambridge University Press, Cambridge (1991)
66. Bookstein, F.L.: Landmark methods for forms without landmarks: localizing group differences in outline shape. Med. Image Anal. **1**, 225–243 (1997)
67. Bookstein, F.L.: Principal warps: thin plate splines and the decomposition of deformations. IEEE Trans. Pattern Anal. Mach. Intell. **11**, 567–585 (1989)
68. Gunz, P., Mitteroecker, P.: Semilandmarks: a methodology for quantifying curves and surfaces. Hystrix. **24**(1), 103–109 (2013). https://doi.org/10.4404/hystrix-23.1-8292
69. MacLeod, N.: Going round the bend: eigenshape analysis I. Paleontol. Assoc. Newsl. **80**, 32–48 (2012)
70. Ray, T.S.: Landmark eigenshape analysis: homologous contours; leaf shape in *Syngonium* (Araceae). Am. J. Bot. **79**(10), 69–76 (1992)

71. Yoshioka, Y., Iwata, H., Ohsawaand, R., Ninomiya, S.: Analysis of petal shape variation of *Primula sieboldii* by Elliptic Fourier descriptors and Principal Component Analysis. Ann. Bot. **94**, 657–664 (2004)
72. Zahn, C.T., Roskies, R.Z.: Fourier descriptors for plane closed curves. IEEE Trans. Comput. **21**(3), 269–281 (1972)
73. Giardina, C.R., Kuhl, F.P.: Accuracy of curve approximation by harmonically related vectors with elliptical loci. Comput. Graphics Image Process. **6**(3), 277–285 (1997)
74. Iwata, H., Ebana, K., Uga, Y., Hayashi, T.: Genomic prediction of biological shape: elliptic Fourier analysis and Kernel partial least squares (PLS) regression applied to grain shape prediction in rice (*Oryza sativa* L.). PLoS One. **10**(3), e0120610 (2015). https://doi.org/10.1371/journal.pone.0120610
75. Iwata, H., Ukai, Y.: SHAPE: a computer program package for quantitative evaluation of biological shapes based on elliptic Fourier descriptors. J. Heredity. **93**(5), 384–385 (2002). https://doi.org/10.1093/jhered/93.5.384
76. Freeman, H.: Computer processing of line drawing images. Comp. Surv. **6**, 57–97 (1974)
77. Schmittbuhl, M., Allenbach, B., Le Minor, J.M., Schaaf, A.: Elliptical descriptors: some simplified morphometric parameters for the quantification of complex outlines. Math. Geol. **35**, 853–871 (2003)
78. Lestrel, P.E., Kimbel, W.H., Prior, F.W., Fleischmann, M.L.: Size and shape of the hominoid distal femur: Fourier analysis. Am. J. Phys. Anthropol. **46**(2), 281–290 (1977)
79. Lestrel, P.E., Cesar Jr., R.M., Takahashi, O., Kanasawa, E.: Sexual dimorphism in the Japanese cranial base: a Fourier-wavelet representation. Am. J. Phys. Anthropol. **128**, 608–622 (2005)
80. Lohman, G.P.: Eigenshape analysis of microfossils. A morphometric method for describing changes in shape. Math. Geol. **15**, 659–672 (1983)
81. MacLeod, N., Rose, K.D.: Inferring locomotor behavior in paleogene mammals via eigenshape analysis. Am. J. Sci. **293**(2), 300–355 (1993). https://doi.org/10.2475/ajs.293A.300
82. Rohlf, F.J.: Relationships among eigenshape analysis, Fourier analysis and analysis of coordinates. Math. Geol. **18**(8), 845–854 (1986)
83. Lestrel, P.E.: Fourier descriptors and their applications in biology. Cambridge University Press, Cambridge (1997)
84. Lohman, G.P., Schweitzer, N.P.: On eigenshape analysis. In: Rohlf, F.J., Bookstein, F. (eds.) Proceedings of the Michigan Morphometrics Workshop, University of Michigan, pp. 147–166 (1990)
85. MacLeod, N.: Generalizing and extending the eigenshape method of shape visualization and analysis. Paleobiology. **25**, 107–138 (1999)
86. Stoermer, E.F., Ladewski, T.B.: Quantitative analysis of shape variation in type and modern populations of *Gomphoneis herculeana*. Nova Hedwigia Beih. **73**, 347–386 (1982)
87. Wishkerman, A., Hamilton, P.B.: Shape outline extraction software (DiaOutline) for elliptic Fourier analysis application in morphometric studies. Appl. Plant Sci. **6**(12), e1204 (2018). https://doi.org/10.1002/aps3.1204
88. Ujihara, Y., Nakamura, M., Miyazaki, H., Weda, S., et al.: Comput. Math. Methods Med. Article ID 381356. (2013). https://doi.org/10.1155/2013/381356
89. Potapova, M., Hamilton, P.B.: Morphological and ecological variation within the *Achnanthidium minutissimum* (Bacillariophyta) species complex. J. Phycol. **42**, 872–866 (2007). https://doi.org/10.1111/j.1529-8817.2007.00332.x
90. Klingenberg, C.P.: Visualization in geometric morphometrics: how to read and how to make graphs showing shape changes. Hystrix Ital. J. Mammal. **24**(1), 25–24 (2013). https://doi.org/10.4404/hystrix-24.1-7891
91. Klingenberg, C.P., Montero, L.D.: Distances and directions in multidimensional shape spaces. Syst. Biol. **54**(4), 678–688 (2005)
92. Zelditch, M.L., Swiderski, D.L., Sheets, H.D., Fink, W.L.: Geometric Morphometrics for Biologists: A Primer. Elsevier/Academic Press, Amsterdam. 443 pp (2004)
93. Oxnard, C., O'Higgins, P.: Biology clearly needs morphometrics. Does morphometrics need biology? Biol. Theory. **4**, 84–89 (2008)
94. MacLeod, N.: Shape models II: the thin plate spline. Paleontol. Assoc. Newsl. **73**, 24–39 (2010)
95. Hammer, Ø., Harper, D.T., Ryan, P.D.: PAST: paleontological statistics software package for education and data analysis. Paleontologia Electronica. http://palaeo-electronica.org. (2001)
96. Rohlf, F.J., Archie, J.W.: A comparison of Fourier methods for the description of the wing shape in mosquitoes (Diptera: Culicidae). Syst. Zool. **33**, 302–317 (1984)
97. Cooke, S.B., Terhune, C.E.: Form, function, and geometric morphometrics. Anat. Rec. **298**(1), 5–28 (2015). https://doi.org/10.1002/1r.23065
98. Rohlf, F.J.: The *tps* series of software. Hystrix. **26**(1), 1–4 (2015). https://doi.org/10.4404/hystrix-26.1-11264
99. MacLeod, N.: Principal & partial warps. Paleontol. Assoc. Newsl. **74**, 35–45 (2010)
100. Magrini, S., Scoppola, A.: Geometric morphometrics as a tool to resolve taxonomic problems: the case of *Ophioglossum* species (ferns). In: Nimis, P.L., Vignes Lebbe, R. (eds.) Tools for Identifying Biodiversity: Progress and Problems, pp. 251–256 (2010)
101. Manly, B.F.J.: Multivariate Statistical Methods: A Primer, 3rd edn. Chapman and Hall, London. 214 pp (2003)
102. Nath, R., Pavur, R.: A new statistic in one way multivariate analysis of variance. Comput. Stat. Data Anal. **2**, 297–315 (1985)
103. Mardia, K.V., Kent, J.T., Bibby, J.M.: Multivariate Analysis. Academic Press, London (1979)
104. Jolliffe, I.T.: Principal Component Analysis. Springer, New York (1986)
105. Klingenberg, C.P.: Size, shape, and form: concepts of allometry in geometric morphometrics. Dev. Genes Evol. **226**(3), 113–137 (2016)
106. Klingenberg, C.P.: Heterochrony and allometry: the analysis of evolutionary change in ontogeny. Biol. Rev. **73**, 79–123 (1998)
107. Viscosi, V., Cardini, A.: Leaf morphology, taxonomy and geometric morphometrics: a simplified protocol for beginners. PLoS One. **6**(10), e25630 (2011)
108. Mitteroecker, P., Bookstein, F.L.: The evolutionary role of modularity and integration in the hominid cranium. Evolution. **62**, 943–958 (2008). https://doi.org/10.1111/j.1558-5646.2008.00321.x
109. Havran, C., Hupet, L., Czyz, J., Lee, J., Vandendorpe, L., Verleysen, M.: Independent component analysis for face identification. In: Conference on Knowledge-Based Intelligent Information and Engineering Systems, Cremona, Italy, pp. 1207–1211 (2002)
110. Rohlf, F.J., Corti, M.: Use of two-block partial least squares to study covariation in shape. Syst. Biol. **49**(4), 740–753 (2000). https://doi.org/10.1080/106351500750049806
111. Calhim, S., Halme, P., Petersen, J.H., Læssøe, T., Bässler, C., Heilman-Clausen, J.: Fungal spore diversity reflects substrate-specific deposition challenges. Sci. Rep. **8**, 53–56 (2018)
112. Holtje, J.V.: Growth of the stress bearing and shape-maintaining murein sacculus of *Escherichia coli*. Microbiol. Mol. Biol. Rev. **62**(1), 181–203 (1998)
113. Rangamani, P., Lipshtat, A., Azeloglu, E.U., Calizo, R.C., Hu, M., Ghassemi, S., Hone, J., Scarlata, S., Neves, S.R., Iyengar, R.: Decoding information in cell shape. Cell. **154**(6), 1356–1369 (2013). https://doi.org/10.1016/j.cell.2013.08.026

114. Round, F.E., Crawford, R.M., Mann, D.G.: The diatoms. Biology and morphology of the genera. Cambridge University Press, Cambridge (1990)
115. Infantino, A., Zaccardelli, M., Costa, C., Ozkilinc, H., Habibi, A., Peever, T.: A new disease of grasspea (*Lathyrus sativus*) caused by *Ascochyta lentis* var. *lathyri*. J. Plant Pathol. **98**(3), 541–548 (2016). https://doi.org/10.4454/JPP.V98I3.008
116. Veselá, J., Neustupa, J., Pichrtová, M., Pouličková, A.: Morphometric study of *Navicula* morphospecies (Bacillariophyta) with respects to diatom life cycle. Fottea. **9**(2), 307–316 (2009). https://doi.org/10.5507/fot.2009.030
117. Beszteri, B., Ács, E., Medlin, L.: Conventional and geometric morphometric studies of valve ultrastructural variation in two closely related *Cyclotella* species (Bacillariophyta). Eur. J. Phycol. **40**, 89–103 (2005). https://doi.org/10.1080/09670260500050026
118. Fránková, M., Poulíčková, A., Neustupa, J., Pichrtová, M., Marvan, P.: Geometric morphometrics a sensitive method to distinguish diatom morphospecies: a case study on the sympatricpopulations of *Reimeria sinuata* and *Gomphonema tergestinum* (Bacillariophyceae) from the River Bečva, Czech Republic. Nova Hedwigia. **88**, 81–95 (2009)
119. Mou, D., Stoermer, E.F.: Separating *Tabellaria* (Bacillariophyceae) shape groups based on Fourier descriptors. J. Phycol. **28**, 386–395 (1992)
120. Sanchez, C., Cristobal, G., Bueno, G.: Diatom identification including life cycle stages through morphological and texture descriptors. PeerJ. **7**, e6770 (2019)
121. Newton, G., Kendrick, B.: Image processing in taxonomy. Sydowia. **42**, 246–272 (1990)
122. Matsuura, S.: Colony of the fungus *Aspergillus oryzae* and self-affine fractal geometry of growth fronts. Fractals. **1**(1), 11–19 (1993). https://doi.org/10.1142/S0218348x93000046
123. Mihail, J.D., Obert, M., Taylor, S., Bruhn, J.N.: The fractal dimension of young colonies of *Microphomina phaseolina* produced from microsclerotia. Mycologia. **86**, 350–236 (1994)
124. Papagiani, M.: Quantification of the fractal nature of mycelia aggregation in *Aspergillus niger* submerged cultures. Microb. Cell. Fact. **5**. http://www.microbialcellfactories.com/content5/1/5 (2006)
125. Golinski, M.R., Boecklen, W.J., Dawe, A.L.: Two-dimensional fractal growth properties of the filamentous fungus *Cryphonectria parasitica*: the effects of hypovirus infections. J. Basic Microbiol. **48**, 426–429 (2008). https://doi.org/10.1002/jobm.200800017
126. Taralova, E.H., Schlecht, J., Barnard, K., Pryor, B.M.: Modelling and visualizing morphology in the fungus *Alternaria*. Fungal Biol. **115**(11), 1163–1173 (2011). https://doi.org/10.1016/j.funbio.2011.08.002
127. Neustupa, J., Hodač, L.: Changes in shape of the coenobial cells of an experimental strain of *Pediastrum duplex* var. *duplex* (*Chlorophyta*) reared at different pH. Preslia, Praha. **77**, 439–452 (2005)
128. Gaston, K.J., O'Neill, M.A.: Automated species identification. Why not? Philos. Trans. R. Soc. Lond. B. **359**, 655–667 (2004)
129. MacLeod, N., Benfield, M., Culverhouse, P.: Time to automate identification. Nature. **467**, 154–155 (2010). https://doi.org/10.1038/467154a
130. Gauld, I.D., O'Neill, M.A., Gaston, K.J.: Driving Miss Daisy: the performance of an automated insect identification system. In: Austin, A.D., Dowton, M. (eds.) Hymenoptera: Evolution, Biodiversity and Biological Control, pp. 303–312. CSIRO, Collingwood, VIC (2000)
131. Arbuckle, T.: Automatic identification of bees' species from images of their wings. In: Proceedings of the 9th International Workshop on Systems, Signals and Image Processing, Manchester, UMIST, pp. 509–511 (2002)
132. Jonker, R., Groben, R., Tarran, G., Medlin, L., Wilkins, M., Garcia, L., Zabala, L., Boddy, L.: Automated identification and characterization of microbial populations using flow cytometry: the AIMS project. Sci. Mar. **64**, 225–234 (2000)
133. Luo, Q., Gao, Y., Luo, J., Chen, C., Liong, J., Yang, C.: Automatic identification of diatoms with circular shape using texture analysis. J. Softw. **6**(3), 428–435 (2011). https://doi.org/10.4304/jsw.6.3.428-435
134. Bueno, G., Deniz, O., Pedraza, A., Ruiz-Santaquiteria, J., Salido, J., Cristóbal, G., Borrego-Ramos, M., Blanco, S.: Automated diatom classification (Part A): a handkrafted feature approaches. Appl. Sci. **7**(8), 753 (2008). https://doi.org/10.3390/app.7080753
135. Pedraza, A., Bueno, G., Deniz, O., Cristóbal, G., Blanco, S., Borrego-Ramos, M.: Automated diatom classification (Part B): a deep learning approach. Appl. Sci. **7**(5), 460 (2017). https://doi.org/10.3390/app7050460
136. Du Buf, H., Bayer, M., Droop, S., Head, R., Juggins, S., Fischer, S., Bunke, H., Wilkinson, M., Roerdink, J., Pech-Pacheco, J., Cristóbal, G., Shahbazka, H., Ciobanu, A.: Diatom identification: a double challenge called ADIAC. In: Proceedings of the International Conference on Image Analysis and Processing, Venice, Italy, 27–29 September, pp. 737–739 (1999)
137. Loy, A., Slice, D.E.: Image data banks and geometric morphometrics. In: Nimis, P.L., Lebbe, R. (eds.) Tools for Identifying Biodiversity. Progress and Problems. ISBN 978-88-88 [Kloster, M., Kauer, G., Beszteri, B.: SHERPA: An image segmentation and outline feature extraction tool for diatoms and other objects. BMC Bioinform. **15**, 218 (2014)]
138. Libungan, L.A., Palsson, S.: ShapeR: An R package to study otolith shape variation among fish populations. PLoS One. **10**, e0121102 (2015)
139. Stela, B., Monleon-Getino, A.: Facilitating the automatic characterization, classification and description of biological images with the VisionBioShape Package for R. Open Access Lib. J. **3**(10), 1–16 (2016)
140. Klingenberg, C.P.: MorphoJ: an integrated software package for geometric morphometrics. Mol. Ecol. Resour. **11**(20), 353–367 (2011). https://doi.org/10.1111/j.1755-0998.2010.02924.x
141. Karperien, A.: User's guide for FracLac v.2.5. School of Community Health, Faculty of Science, Charles Sturt University, Albury-Wodonga, Australia, http://rsb.info.nih.gov/ij/plugins/fraclac/FLHelp/Introduction.htm (2007)
142. Márquez, E.J.: SAGE – Symmetry and Asymmetry in Geometric Data. http://bit.ly/2IkdlQ1 (2014)
143. Márquez, E.J.: MACE – Matrix Correlations for Landmark Data, Version 1.03. http://bit.ly/2IkdlQ1 (2014)
144. Márquez, E.J., Knowles, L.L.: Correlated evolution of multivariate traits: detecting co-divergence across multiple dimensions. J. Evol. Biol. **20**, 2334–2348 (2007)
145. Marquez, E.J.: A statistical framework for testing modularity in multidimensional data. Evolution. **62**, 2688–2708 (2008)
146. Márquez, E.J., Cabeen, R., Woods, R.P., Houle, D.: The measurement of local variation in shape. Evol. Biol. **39**, 419–439 (2012)

Part IV

Applications

Water Quality Assessment

13

A. Goldenberg-Vilar, R. Álvarez-Troncoso, V. Roldán, and Saúl Blanco

Abstract

Diatom metrics methods are becoming important tools for the assessment of environmental conditions in aquatic systems. Diatoms have several advantages as bioindicators: their ubiquitous distribution across world aquatic environments, their ability to integrate multiple water quality features, and the relatively simple and standardized sampling and preparation methods. To date, several diatom indices have been developed, most of which are general pollution indices, especially indicative of eutrophication and organic pollution. This chapter reviews the literature concerning diatom-based analyses for biomonitoring purposes, with a first overview on available methods (microscopy-based, automatic identification, and DNA barcoding), and an account on bioassessment tools using phytobenthos in EU countries, with a special focus on the Spanish experience.

13.1 Introduction

The first tools for ecosystem health diagnosis in rivers were established *ca.* 100 years ago [1], and the use of organisms as indicators of water quality largely originated from Europe, mainly devoted to monitoring organic pollution [2]. Traditionally, water quality assessment has been based on physicochemical analysis, although it has been largely demonstrated that this approach does not provide a temporally integrated picture of the response of ecosystems to impairment [3, 4]. On the contrary, biological monitoring has been proven to be useful especially in running waters, where concentrations can fluctuate notably even within a few hours, reflecting the overall quality status of a river during a certain period [5]. Particularly, changes in species composition reflect variations in water quality in a more integrated manner than mere chemical sampling [6]. In this regard, diatom-based methods are becoming important tools for the assessment of environmental conditions in aquatic systems. Diatoms have several advantages as bioindicators: their ubiquitous distribution across world aquatic environments, their ability to integrate multiple water quality features, and the relatively simple and standardized sampling and preparation methods [7, 8]. Additionally, diatoms exhibit high diversities both locally and regionally, but with comparatively narrow ecological profiles and short generation times, thus responding rapidly to environmental changes [1, 9].

Diatom-based methods are increasingly becoming important tools for assessment of ecological conditions in lotic systems. To date, several diatom indices have been developed, most of which are general pollution indices, especially indicative of eutrophication and organic pollution [10]. The output of these methods is usually a single score that permits rapid assessment of the overall condition of a stream in a manner that is easily understood by nontechnical resource managers [11]. Differences between indices scores are related to the taxonomic spectrum considered, the autecological parameters assigned, and the main environmental stressor that is being monitored [3, 12].

Diatom literature stresses the importance of ion concentration and trophic status as major environmental drivers of diatom distribution in aquatic ecosystems. Available meta-analyses [9, 13] show that diatom communities respond

A. Goldenberg-Vilar (✉)
IHCantabria - Instituto de Hidráulica Ambiental de la Universidad de Cantabria, Santander, Spain

Cimera Estudios Aplicados S.L. Science to Business, Madrid, Spain
e-mail: alejandra.goldenberg@unican.es

R. Álvarez-Troncoso · V. Roldán
Cimera Estudios Aplicados S.L. Science to Business, Madrid, Spain

S. Blanco
Facultad de Ciencias Biológicas y Ambientales, Departamento de Biodiversidad y Gestión Ambiental, Universidad de León, León, Spain

Laboratorio de diatomología y calidad de aguas, Instituto de Investigación de Medio Ambiente, Recursos Naturales y Biodiversidad, León, Spain
e-mail: degsbl@unileon.es

G. Cristóbal et al. (eds.), *Modern Trends in Diatom Identification*, Developments in Applied Phycology 10,
https://doi.org/10.1007/978-3-030-39212-3_13

mainly to chemical variables [5, 10], overriding the effect of physiographical or geographical factors. The results of different diatom-based indices frequently result, however, in contrasting water quality diagnoses. To date, little effort has been done to elucidate the major drivers of diatom indices scores. The sensitivity of diatoms to environmental conditions can make them highly valuable indicators only if the effects of specific factors can be distinguished: while trophic conditions do have an influence on species composition, it is difficult to distinguish specific nutrients causing the effect [14, 15]. For instance, it is important for a diatom metric to discriminate the influence of nutrients from that of organic pollution, in general [16, 17]. Organic pollution is frequently associated with high nutrient concentrations, but under such conditions, nutrients are not necessarily the primary factor influencing community composition [18]. Moreover, naïve use of diatom indices might indicate changing nutrient status when, in fact, it is the degree of acid stress which is fluctuating [8].

Ecological assessment of freshwaters can be accomplished in situ in some cases (e.g., QBR or FHI indices, see Fornells et al. [19] and Pardo et al. [20], respectively) or with a minimal resource investment (e.g., methods using benthic macroinvertebrates). However, the computation of diatom-based metrics requires expensive optical equipment, skilled microscopists, and access to specialized literature. During the last years, several attempts to simplify the protocols have been proposed, either by reducing the number of individuals necessary to provide an accurate result (e.g., [21]) or reducing the taxonomic level of identifications, e.g., genus-based indices [22] of trait-based methods [23]. Two alternative approaches have emerged thanks to the current availability of modern computation facilities, namely computer-assisted automatic identification based on image analysis and DNA barcoding. This chapter presents a brief review of these diatom-based water quality assessment approaches, focusing first on the available methods in current usage for freshwater biomonitoring, and then summarizing the results obtained during the last years, exemplified with field studies carried out in the Iberian Peninsula.

13.2 Sampling and Analytical Protocols

13.2.1 EU Standards

Until the implementation of the Water Framework Directive (WFD), the application of methods based on phytobenthic organisms for ecological monitoring followed the guidance provided in general standard references such as Rice et al. [24]. The basic protocols for the analysis of microscopic slides are inspired in the methods developed for planktonic organisms [25], which in turn are based in the classical references of Utermöhl [26] and Lund et al. [27]. In the case of benthic diatoms, the current EU standard protocols are regulated through the European Norms 13946 [28], which deals with the collection, preservation, and laboratory treatment of samples, and 14407 [29], which covers the identification and quantification of diatoms for samples coming from lotic epilithon. Kelly [30] offers a historical account of the development of these standards. The complete methodology had been previously summarized and made accessible to a general audience in the seminal paper by Kelly et al. [31]. Since then, these norms have been incorporated into the national legislations. In Spain, for instance, Water Authorities have published protocols and guidelines to be followed in river biomonitoring studies (e.g., [32, 33]). European protocols are in general congruent with international standards (mainly ISO 5667, which regulates water quality), except for some minor details (e.g., EN allows the fixation of field samples with formalin, whereas ISO recommends only ethanol or Lugol's solution). The interested reader is referred to Stevenson and Bahls [34] for details on the protocols followed in other countries.

Some authors have presented methodological proposals to either (a) apply the existing standards to other aquatic environments covered by the WFD, or (b) amend certain methodological aspects nod sufficiently detailed in the available protocols. In this regard, Blanco et al. [35] tested some improvements in the treatment of periphyton samples. Noticeably, CEN [29] recommends a systematic scanning of the microscopic slide starting from the coverslip edge. Moss [36] and Battarbee [37] already showed that valves are not randomly distributed due to the effects of water surface tension, which leads to a heterogeneous distribution of the different size classes [38, 39]. Alverson et al. [40] showed also that cell density is usually higher in the central area of the coverslips. It is therefore advisable that the use of random fields rather than "transverses," which is proposed only as an alternative in the European Norm.

Table 13.1 summarizes some protocols and methodological proposals concerning diatom-based biomonitoring and ecological studies available in the literature, arranged chronologically.

13.2.2 Automatic Diatom Identification

Automatic identification of organisms is based on the recognition of shapes of interest based on outline matching against a large reference database. In the case of diatoms, first efforts raised in the late 1990s in the wake of the implementation of the ADIAC (Automatic Diatom Identification And Classification) project, financed by the European MAST (Marine Science and Technology) program. ADIAC involved the creation of large image databases linked to taxonomic and ecological information, together with the development

Table 13.1 Non-exhaustive compilation of available methods dealing with diatom-based biomonitoring and ecological studies

Ref	Fossil	Marine	Freshwater	Genetic	Sampling	Processing	Microscopy	Culture	Forensic	Soil
[41]			•			•				
[42]	•					•				
[43]			•		•					
[37]	•					•				
[148]						•				
[44]						•	•			
[45]			•			•				
[46]	•					•	•			
[47]			•				•			
[48]	•					•				
[49]			•		•					
[50]			•		•					
[51]	•					•				
[52]				•						
[53]			•					•		
[54]				•						
[55]									•	
[56]			•		•					
[57]		•				•				
[58]	•		•		•	•				
[59]				•						
[60]				•						
[61]							•			
[62]			•		•					
[63]			•		•					
[64]		•				•				
[65]								•		
[66]	•						•			
[67]									•	
[68]								•		
[69]									•	
[70]						•	•			
[71]	•					•				
[72]						•			•	
[73]			•		•	•	•			
[74]			•		•					
[75]							•			
[76]							•			
[77]				•						
[78]							•			
[79]										•

of automatic slide-scanning and autofocusing software allowing unsupervised scanning of microscope slides and automatic location of valves [80]. Its main goal was to develop algorithms for an automatic identification of diatoms using image information, both valve shape and ornamentation [81]. *ca.* 6000 images, covering approximately 500 diatom taxa, were acquired, including large test sets which were used for the testing of prototype software packages. The system developed allowed the identification of 37 species with an accuracy of 97% (see the results of this project in Du Buf [82]).

An outstanding improvement of automated classification methods was accomplished in 2014 with SHERPA

software. SHERPA consists of image processing algorithm that allows the identification and measurement of diatom valves and other objects, handling all steps from image segmentation over object identification to feature extraction, and providing interactive functions for reviewing and revising results [83]. By combining SHERPA with slide-scanning microscopes, mass-analyses of diatom cells mounted on permanent slides can be performed [84]. More recently, DiaOutline [85] has been proposed as a tool for valve outline extraction using MATLAB and R to perform elliptic Fourier analysis to identify several diatom taxa. In parallel, other methods based on the morphometric characterization of diatom individuals have been successfully employed for species delimitation. Pappas et al. [86] present a review of the history of usage of morphometric methods of outline shape analysis, pattern recognition, and landmark-based analysis. Particularly, geometric morphometrics, combined with discriminant/classification analysis, is a powerful tool used to disentangle species complexes and compare specimens with type materials (e.g. [87–89], see Chap. 9).

As an attempt to continue ADIAC philosophy with modern computational techniques, AQUALITAS project aims at developing an integrated system based on the development of an open mobile low-cost microscope and advanced image analysis techniques for diatom life cycle and polymorphism modeling as well as standardizing protocols for environmental diagnosis and monitoring (see this volume). In the frame of this project, the characterization of diatom valves by means of local binary patterns together with a log Gabor implementation led to an overall accuracy of 98.11% using bagging decision trees and combinations of descriptors for diatom identification [90]. Besides, the application of convolutional neural networks over a set of 160,000 images reached an overall accuracy of 99% [91]. Applying applies a single neural network (YOLO) over a certain image leads to remarkable results, with an average of 0.84 recall [92].

13.2.3 Diatom DNA Metabarcoding

Modern molecular techniques allow cost-effective a complementary approach to ecosystem health diagnosis, with scope for improved efficiency and reduced analytical error through automation and standardization [93]. In this regard, there is an increasing use of DNA barcoding for water quality monitoring. DNA barcoding has not only improved biomonitoring protocols but has revolutionized also biodiversity studies facilitating the understanding of biogeography, community assembly, and ecological processes [94], allowing to trace the species distribution and ranges in their natural habitats [95]. DNA barcoding is based on the premise that the divergence in small DNA fragments mirrors biological separation of species [96]; this fragment is compared with reference sequences stored in a database to assign an organism name to it [97]. Thus, a good quality reference database is the keystone to any barcoding approach that requires taxonomy assignment [93].

The combination of DNA barcoding with next-generation sequencing (NGS) enables the simultaneous sequencing of DNA from whole communities or "metabarcoding," which leads to species identification from a standardized DNA barcode and high-throughput sequencing (HTS), using DNA reference libraries [98, 99]. This approach has proven a more refined taxon detection than the microscopical approach [99]; for instance, Moniz & Kaczmarska [96] report a 99.5% success rate in separating biologically defined diatom species. Recent attempts to develop taxonomy-free metabarcoding-based biomonitoring protocols for aquatic habitats are showing promising results. For instance, Vasselon et al. [100, 101] found that ecological quality assessment using both molecular and morphology-based (SPI scores) were congruent at the scale of a whole biomonitoring network. In a similar study, 77% of the sampling sites were correctly assigned to their ecological quality status using diatom metabarcoding [102]. In general, the sequence-based technology leads to a higher number of identified diatom taxa in natural samples when compared to light microscopy methods [99].

Despite its successful application, the application of molecular techniques for chromists and, particularly, for eukaryotic microalgae, has still numerous pitfalls and limitations. DNA metabarcoding has thus been subject to criticism in the literature. For instance, it has been demonstrated that DNA barcoding has no discriminating success within species complexes (e.g., [103]), probably as a consequence of low variation rate at the plastid genome level. These authors show that species-rich genera (as in the case of many diatoms) may prove exceptionally difficult to barcode. There are no fast and easy bypasses for systematics and DNA barcoding which can be currently recommended for protistan researchers because automatic species delimitation methods tested proved to be highly dependent in taxon sampling and prone to artifacts [104]. In an extremely diversified group such as diatoms, barcoding therefore has clear limitations and it is inherently incapable of identifying all taxa [105]. For instance, *Frustulia* species cannot be resolved without the use of additional nonmolecular evidences [106]. Besides, maintaining diatom reference databases often implies culturing diatom species, which is a specialized, resource intensive exercise. Actually, as stressed by Rivera et al. [98], differences in molecular and morphology-based environmental diagnoses are due mainly to the incompleteness of the DNA reference libraries. Vasselon

et al. [101] estimate that up to 82% of "morphological" species are not represented in the molecular databases, especially rare taxa occurring in oligotrophic waters [99]. Molecular inventories are also strongly influenced by the DNA extraction method used [100, 107]. In view of these limitations, Kelly et al. [93] recommend in their recent review that the combined use of molecular techniques and "classic" taxonomy since both methods offer alternative views of the river ecosystem status.

13.3 Distribution and Frequency of Diatoms in the Iberian Peninsula

The distribution of diatom communities depends on the species-specific physiological and ecological demands. From the myriad of environmental factors affecting diatom distribution, several studies and scientific reviews [9] highlighted the role of major ion concentrations in both lotic and lentic systems. The primacy of major ion concentrations affecting community composition reflects the fact that water pH is a highly important variable for aquatic biota, regulating many physiological processes, and consequently, water conductivity, alkalinity, or calcium concentration. These environmental variables are highly dependent on river geology, substrate, and physical conditions. Specific diatom assemblages can be found according to the natural differences in river physical features, so to increase the accuracy of anthropogenic impact assessment we may first account for the natural variability among sites. For that purpose, the use of a typology to classify streams (according to their geology, substrate, and physical conditions) has become an accepted part of ecological assessment [108]. The EU Water Framework Directive fixed typology, i.e., "System A" is defined by ecoregions, size based on the catchment area (small 10–100, medium 100–1000, large 1000–10,000, and very large >10,000 km^2), catchment geology (calcareous, siliceous, and organic), and altitude (lowland, <200, mid-altitude 200–800, and high altitude >800 m a.s.l.). Within any given part of the WFD typology, it is assumed that biological communities at undisturbed sites will be broadly similar and will therefore constitute a type-specific biological target. The EU Water Framework Directive also allows each member state to adopt an alternative characterization "System B" with 5 obligatory factors (altitude, latitude, longitude, geology, and size), and an additional 15 optional factors (e.g., distance from river source, mean water depth, and mean substratum composition). No specific categories of value ranges are suggested for each factor in "System B" and the member state is left to decide how many of the optional factors they wish to use. In consequence, a very extensive set of stream types could be defined by individual Member States for each ecoregion within their territorial limits [109].

13.3.1 River Typologies: Siliceous and Calcareous

The general methodology for the establishment of types and reference conditions in Spanish rivers has been regulated by the IPH (Sects. 2.2.1.3 and 2.2.1.4 and Annexes II and III) following a technical proposal by Spanish Research Center CEDEX based on the WFD system B (European Commission report, 2015). The first step in the classification process was to distinguish between the two main biogeographical areas present in the Iberian Peninsula: Eurosiberian area with an oceanic climate and evenly dispersed precipitation through the year, and Mediterranean area, with much lower precipitation volume and dry summers. The variables selected for the classification of river typologies in Spain are specific flow, mean annual flow, average basin slope, altitude and conductivity and GIS modeling has been used for the classification of Spanish River types. As a result, the IPH establishes 32 river types. Additional types have been established by River Basin Authorities (RBAs) (e.g., river types in ES110—this latter still in process) [110].

Although regional classifications of streams have been established throughout the world, little is known about their correspondence with freshwater biota biogeography [111]. Hence, recently researchers began to evaluate the correspondence between ecoregional classifications and biological assemblages. For diatom communities, several approaches have been developed, proving that using biological communities for stream classification greatly reduce the number of river typologies, and thus, simplifying ecological assessment to a few ecologically relevant types [112]. Following a similar methodology developed for the Canadian Diatom Index (IDEC), the Spanish Diatom Index—SDI, and lately iDIAT-ES (Alvarez-Troncoso et al., in prep.) have been developed in 2016 by the Spanish Ministry of Environment. Based on a correspondence analysis (CA) iDIAT-ES developed a chemistry-free index where the position of the sites along the gradient of maximum variance (first axis) is strictly determined by diatom community structure and it is therefore independent of measured environmental variables (Fig. 13.1) (for more information see Sect. 13.4). Based on diatom data at national level comprising 975 sites and around 400 species, the iDIAT-ES resulted in three final river typologies based on catchment geology: siliceous (values for 381 species), calcareous (values for 342), and one for Tinto river (values for 5 species). Diatom community structure according to siliceous and calcareous typologies as defined by the iDIAT-ES with an Ecological Quality Ratio (EQR) higher than 0.8 is represented in Fig. 13.2. Similarly, a predictive diatom-based model to assess the ecological status of streams and rivers of Northern Spain (NORTIDIAT) [113], significantly characterized four different diatom groups with obligatory and optional descriptors of the WFD typology

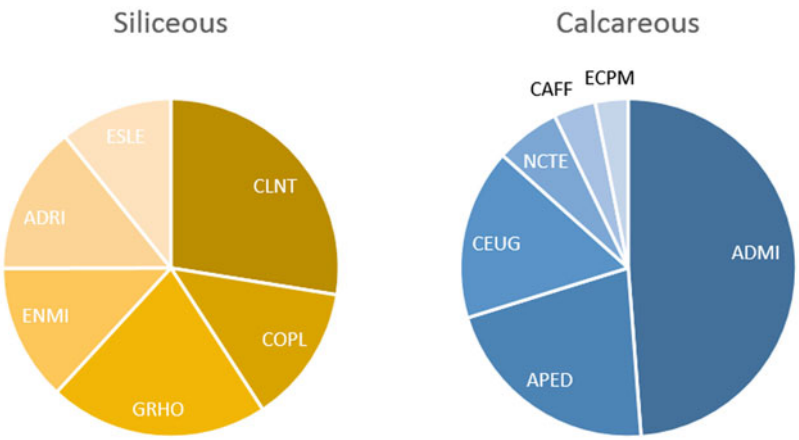

Fig. 13.1 Representative diatom species from siliceous and calcareous typologies. These species show the highest dissimilarity in average abundance between the groups in the same set of samples as used for Fig. 13.2. Abbreviations for calcareous ADMI: *Achnanthidium minutissimum*; APED: *Amphora pediculus*; CEUG: *Cocconeis eug-lypta*; NCTE: *Navicula cryptotenella*; CAFF: *Cymbella affinis*; ECPM: *Encyonopsis minuta*; and for siliceous CLNT: *Cocconeis lineata*; GRHO: *Gomphonema rhombicum*; ADRI: *Achnanthidium rivulare*; COPL: *Cocconeis pseudolineata*; ENMI: *Encyonema minutum*; ESLE: *Encyonema silesiacum*

that corresponded to a four river type's typology B. These four groups represented existing gradients in calcareous geology, catchment size, altitude, and other characteristics of main river types existing in the studied area. The four species group's composition evidenced the correspondence between the diatom assemblages across the N–S and W–E direction, catchment's geology (from 100% siliceous to 100% calcareous) and size (from 2 to 2196 km) and site elevation (from 15 to 1356 m).

13.3.2 Reference Conditions

The assessment of biological quality is based on the degree of deviation from a reference biological population. Biological integrity [114] is measured by comparing a given site with reference ecosystems that lie in similar geomorphological and climatic settings but are not exposed to human impact [115]. Critical to the efficacy of ecological status assessment in rivers is the ability to characterize biological assemblages at reference sites. In Spain many Mediterranean regions, particularly lowland areas, have been substantially modified by human activities [116–118]. The challenge lies in identifying adequate numbers of reference sites within a river type, which ensures the incorporation of the intrinsic variability of environmental conditions within the river type [116].

Over the last decades, numerous bioassessment tools have been developed to evaluate the biological integrity of aquatic ecosystems and to determine the effect of a wide range of stressors on this integrity. Most of these tools are based on the Reference Condition Approach (RCA), where the biological integrity of a site is defined by the "distance" between current conditions and reference condition status [112]. The indices are usually expressed as a value along an alteration gradient (e.g., 0–100) or as an overall statistical difference from reference conditions. To facilitate the interpretation of the biological "distance" of a site from its reference status, the alteration gradient is often divided into classes reflecting qualitative levels of biological integrity. These approaches allow for a rapid and easy overall picture of the ecosystem status and are particularly interesting for water quality managers. Although the creation of biological integrity classes is useful, the approaches used to define the number of classes and the limits between these classes are arbitrary and lack meaningful biological considerations [112]. Indeed, the number of classes is usually arbitrarily determined with widths of either equal proportion (e.g., [3]) or unequal proportion as occurs within the SPI (e.g., [119]), the diatom index currently used in Spain. Indeed, the SPI diatom metric is used as the national classification system for all stream and rivers types in Spain (RD 817/2015), in spite of strong regional differences in the Spanish climate and geomorphological characteristics. A reference value for the SPI is defined for each of the river typologies officially used in Spain under the WFD.

Much of the progress made in the science of ecological assessment emerged from research that advanced our understanding of how the spatial and temporal distributions of freshwater biota are related to naturally occurring environmental features and how those relationships can be most accurately and precisely described and predicted. In that way, similarly than for the definition of river typologies, gradient tools such as iDIAT-ES and NORTIDIAT, also demonstrate their validity for the definition of ecologically relevant referent conditions. In this way, the samples composed of the most

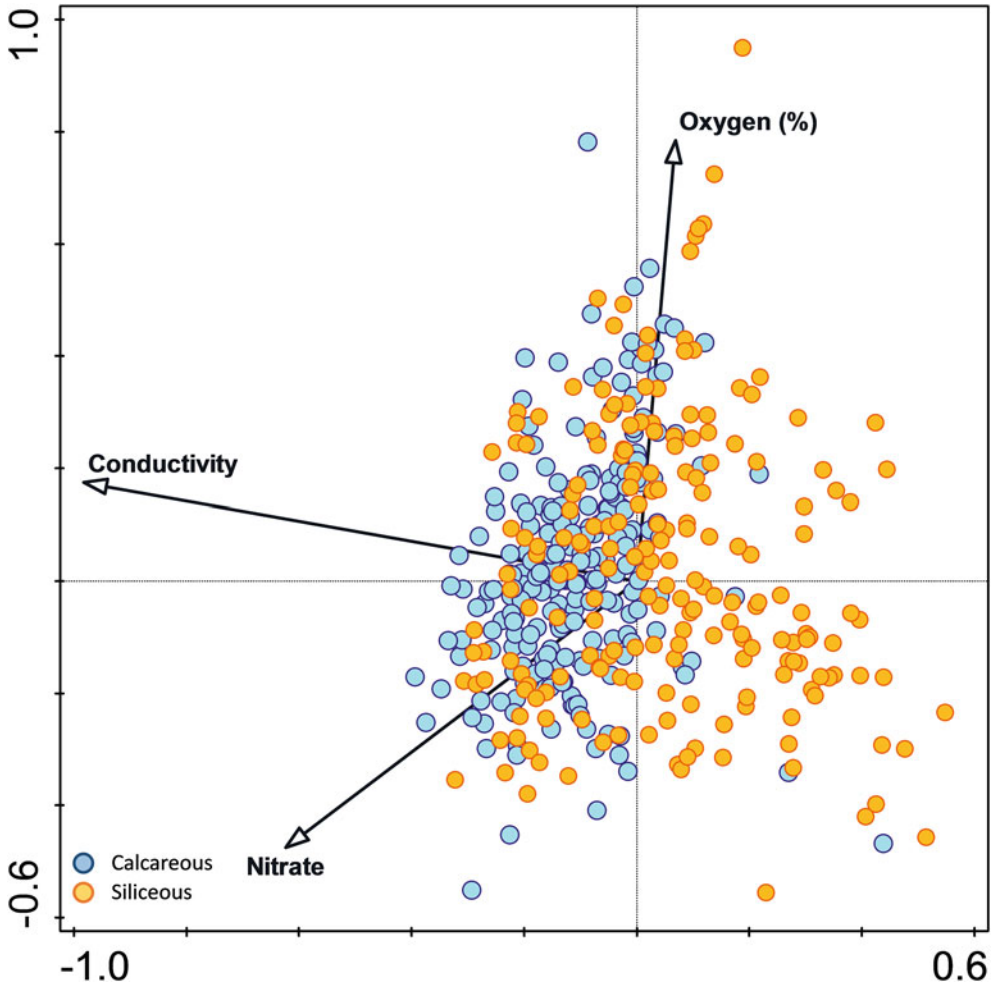

Fig. 13.2 CCA (Canoco 5) of diatom species and environmental variables measured under Spanish routine monitoring programs (Data from the Ministry of Environment MITECO, Spain) divided in siliceous and calcareous typologies. Data span the 31 Spanish River typologies (except Tinto) and 442 sampling locations with EQR > 0.8 collected between 2004–2008. Only significant environmental variables are shown from conductivity, pH, oxygen, biological oxygen demand, nitrate, nitrite, and orthophosphate. Explanatory variables account for 14.74% of the total variation. The cumulative explained variation of first axis is 66.7% and second 85.63% from the total explained variation

different biological communities, compared with reference communities, determine the maximum alteration level. Figures 13.1 and 13.3 show some representative species of the siliceous and calcareous typologies as defined by the iIDIATES in sites under "High" water quality category (EQR > 0.8). The difference from reference communities and similarity with altered communities are used then to assess the degree of alteration of a test site.

The performance of ecological assessments is critically linked to how well we characterize freshwater environments. The knowledge produced from future collaborations between ecologists and watershed scientists coupled with the application of modern modeling techniques will largely determine progress in characterizing and predicting biota-environment relationships and, thus, the accuracy and precision of future ecological assessments [120].

13.4 Diatom-Based Bioassessment Tools

13.4.1 European Autoecological Indexes: SPI, TDI, Rott, and ICM (Intercalibration Common Metric)

The Water Framework Directive (WFD) was declared in 2003 and provides a legal basis for water management in the European Union (EU). The WFD requires that ecological status assessments of rivers and lakes are based on evaluations of phytoplankton, macrophytes and phytobenthos, benthic invertebrates and fish. The objective of the WFD is to protect inland and coastal waters and promote sustainable water use in Europe (Article 1) with "ecological status" used as a benchmark against which progress toward this objective is assessed. Ecological status is defined as "an

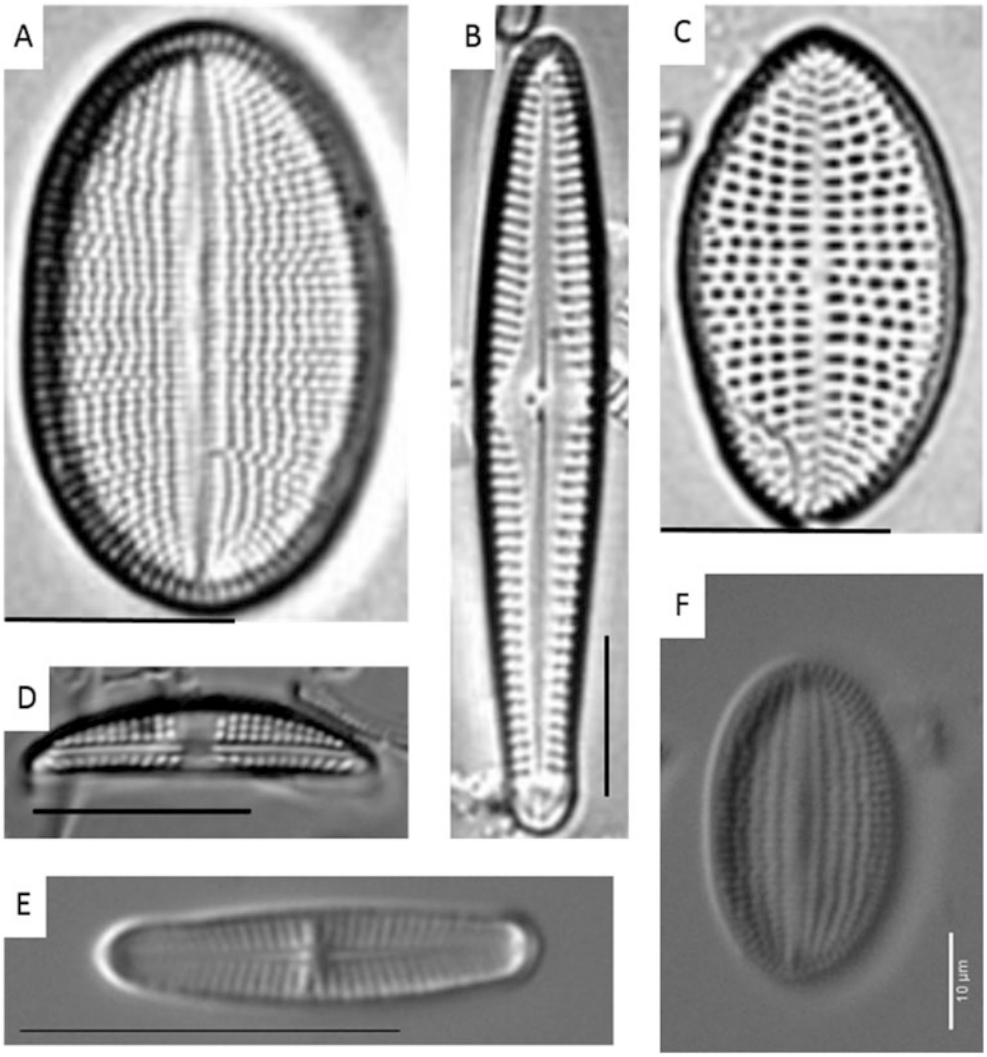

Fig. 13.3 Images of some representative species in each group: Siliceous (**a**—CLNT; **b**—GRHO; **c**—COPL) and calcareous (**d**—APED; **e**—ADMI; **f**—CEUG). Sources (**a**), (**b**) and (**c**): bit.ly/2UDf6fk, (**d**): bit.ly/2KYieCK, (**e**): bit.ly/2DwayBy, (**f**): bit.ly/2UXPjDk. All bars denote 10 µm

expression of the quality of the structure and functioning of aquatic ecosystems associated with surface waters [. . .]" (Article 2). This assumes that a healthy ecosystem is a good indicator that a water body is being exploited in a sustainable manner. Ecological status is a holistic concept, not confined to any single organism group (or "biological quality elements" [BQEs] in the terminology of the WFD); the use of "functioning" in the definition suggests a need to understand both the state of a BQE and its interactions with other BQEs and the catchment. For rivers and lakes, four BQEs are defined, one of which is "macrophytes and phytobenthos," although most member states have treated these as two separate sub-elements, with diatoms frequently employed as representatives of the phytobenthos [121].

Epilithic diatoms have been widely used as efficient indicators for evaluating water quality, considering that they respond quickly to environmental changes, especially organic pollution and eutrophication, with a broad spectrum of tolerance, from oligotrophic to eutrophic conditions [122–124]. Diatoms are one of the key groups of organisms recommended by the WFD for the identification of ecological quality gradients in rivers.

Among the biological methods developed to indicate the trophic level of running waters, the trophic diatom index (TDI) proposed by Kelly and Whitton [125], has been widely used in the European Community, especially after the publication of the Municipal Sewage Treatment Plants policy in 1991. The TDI uses the equation of the weighted average of Zelinka and Marvan [126] to interpret the structure of epilithic diatom biocenoses in terms of nutrient concentrations in rivers, mainly phosphate. However, since 2006 when the intercalibration exercise among geographical areas

in Europe was introduced, the SPI (Specific Polusensibility Index, [127]) was selected for that purpose by the scientific community. This index has been intercalibrated at European level in the different regional groups.

At the beginning of the WFD implementation, those states that have now reported phytobenthos methods, 15 (58%) have chosen to use weighted average metrics developed prior to the WFD, with the SPI (9 states, 35%) being the most commonly employed. The apparent popularity of the SPI, however, disguises many national variants and constitutes a "family" of closely related indices, rather than a wholly consistent approach to ecological status assessment among these states. The use of weighted average metrics as SPI assumes that nutrient or organic pollution is the main pressure encountered within the territory. There is a risk of missing pressures that these indices do not detect [8]. These problems should be overcome by indices based on the actual species expected to be encountered in a particular region and stream type.

Over half of EU states have methods based wholly or partly on weighted average metrics developed before the onset of the WFD, with nine choosing the SPI. Such metrics generally have high correlations with the predominant nutrient or organic pollution gradient and, as such, represent pragmatic solutions to ecological status assessments. However, their widespread use raises questions about what, exactly, "ecological status" means. Strong relationships with chemical pressure gradients may be a mixed blessing as pressure gradients are often composed of several intercorrelated variables, making it difficult to disentangle correlation and causation in the absence of ecophysiological studies of individual species. Moreover, the focus on strong relationships with chemical gradients means that most phytobenthos metrics describe the scale of hazard at a site rather than the risk posed to other trophic levels and to ecosystem services. This first generation of phytobenthos assessment tools may be inadequate when catchment managers need guidance on remediation strategies for particular water bodies. A second generation of assessment tools is needed if the goal is to achieve good ecological status, focusing on the fitness of the phytobenthos as part of aquatic ecosystems, rather than just as indicators of chemical conditions. Diatom indices developed in certain geographic regions are frequently used elsewhere. There are strong evidences that such metrics are less useful when applied in regions other than that where species-environment relationships were originally assessed, showing that species have particular autoecological requirements in different geographic areas. For example, although the SPI index has been developed in France, it has been used in many other European countries under their routine water quality monitoring programs, and it is the recommended diatom index in Spanish rivers [128]. As some authors have already pointed out, there are certain disadvantages when using metrics developed in another region when studying the ecological state of local characteristics [3, 129, 130]. One of the problems detected is an overestimation or, on the contrary, underestimation of the ecological status. The environmental differences from one region to another cause differences in the identity of the species present and also the response of the same species to changes in water quality [31].

In Spain, other diatom indices have been developed like MDIAT [131] that is a multimetric method and DDI [122] that is a method based on specific autoecologies, similar to SPI. During 2016 a new index iDIAT-ES (Álvarez-Troncoso et al., in prep.) was developed for Spain based on ecological distances for the Tagus hydrographic demarcation, the TADI (TAgus Diatom Index) [132].

There are numerous indexes in Europe for calculating trophic conditions in freshwaters ecosystems, and in the last years new diatom indexes have arisen. These indexes were developed independently for both lotic and lentic ecosystems, more often originated from regional datasets, and served mostly as a basis for regional water quality assessments [133]. Some of the indexes have been rescaled under the Diatom Indicator Database that uses a standardized taxonomic diatom list (CEMAGREF taxa list, updated version May 2008).

13.4.1.1 SPI (Specific Pollution Sensitivity Index)

The SPI, Pollution Sensitivity Index [127] has been regarded as one of the most precise indices because it incorporates approximately 2000 species in its database, the largest among all diatom indices [134]. More than 70% of the common species could be found in the SPI list. Most of the variation (82%) in the SPI index is explained by parameters such as conductivity and salt concentration and percentage of urban area, which is consistent with the finding that SPI responds to water quality parameters related to conductivity and eutrophication [134]. These examples support the view that the performance of diatom-based indices in part depends on the degree of overlap between the taxa list in the index development and those that occur in the sampled streams.

Calculation of this index relies on the Zelinka & Marvan [126] formula derived from the saprobic system:

$$\mathrm{SPI} = \frac{\sum A_j v_j i_j}{\sum A_j v_j} \tag{13.1}$$

where A_j is the relative abundance of the species j, v_j is its indicative value ($1 \leq v_j \leq 3$), and i_j its pollution sensitivity ($1 \leq i_j \leq 5$). The values initially falling in the range between 1 and 5 are transformed into values comprised between 1 and 20 in order to make comparisons between the various existing indices easier. Five categories of water quality can be distinguished according to the value of the index: SPI $\geq$ 16: zero pollution or low eutrophication; 13.5 $\leq$ SPI < 16: mod-

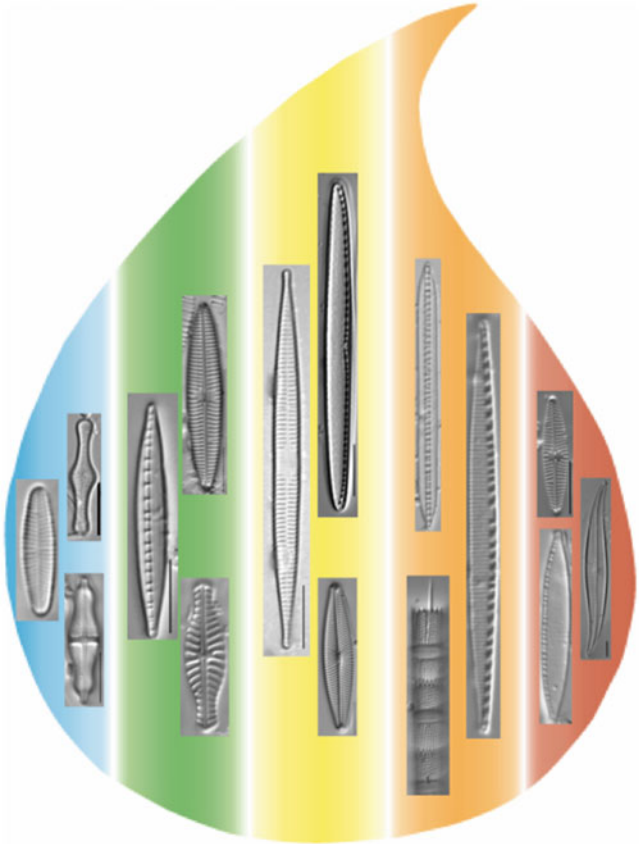

Fig. 13.4 Representative diatom taxa of the different water quality categories recognized in the Water Framework Directive (from left to right: zero, low, moderate, high, and very heavy pollution levels, respectively)

erate eutrophication; $11 \leq \text{SPI} < 13.5$: moderate pollution or heavy eutrophication; $7 \leq \text{SPI} < 11$: high pollution; $\text{SPI} < 7$: very heavy pollution (Fig. 13.4). However, the SPI index has two main obstacles: it requires data at a specific or even intraspecific level, and it is based on constantly changing systematics.

13.4.1.2 TDI (Trophic Diatom Index)

This index was created for monitoring the trophic status of rivers based on diatom composition. It was developed in response to the National Rivers Authority (England & Wales)'s needs under the terms of the Urban Wastewater Treatment Directive of the European Community. TDI represents a useful monitoring tool for site assessments prior to the designation of sensitive areas. It was conceived with the purpose of designing an index to monitor eutrophication in rivers that seemed more appropriate.

The sampling methodology developed to apply this index requires the collection of epilithic diatom samples following the method of Round [135]. The samples are then transported to the laboratory in an icebox and the material is examined alive within 48 h. Afterward, the samples are preserved following the standard instructions for diatom preparation. After the identification, the relationship between taxon and environment is defined by examining graphs summarizing percent count versus Filterable Reactive Phosphorus (FRP for each taxon). "*Sensitivity*" values of between 1 and 5 were assigned to each taxon depending upon the concentration at which taxa were most abundant.

Calculation of the index uses the weighted average equation of Zelinka and Marvan [126]:

$$\text{TDI} = \frac{\sum A_j v_j i_j}{\sum A_j v_j} \tag{13.2}$$

The value of TDI can range from one (very low nutrient concentrations) to five (very high nutrient concentrations). Proportion of valves under each category and its interpretation: <20% total valves belonging to tolerant taxa: free of significant organic pollution; 21–40% total valves belonging to tolerant taxa: some evidence of organic pollution; 41–60% total valves belonging to tolerant taxa: organic pollution likely to contribute significantly to eutrophication of site; >61% total valves belonging to tolerant taxa: site is heavily contaminated with organic pollution.

In conclusion, the TDI represents a useful monitoring tool for site assessments prior to the designation of sensitive areas. Nevertheless, the TDI index will require careful interpretation of the results being aware that its assessment is based on the effect of FRP on diatom community composition.

13.4.1.3 Rott's Index

Rott et al. [130] created an extended database of samples collected in 450 sampling sites in rivers, including approximately 1000 species from 9 different classes of algae. Levels of saprobity and trophy were defined for 650 diatom species. Through his intensive and extensive studies, he created a diatom collection that is housed in the National Institute for Water Research (CSIR) in Pretoria and is used as a reference for research of diatoms in this country [136]. Starting in the last decade, research related to diatoms in South Africa focused on the ecological aspect of the community to assess water quality, and testing was conducted by applying the European indices under South African conditions.

13.4.1.4 ICM (Intercalibration Common Metric)

Intercalibration of methods ensures the comparability of biological elements across similar geographical areas. The WFD requires the national classifications of good ecological status to be harmonized through an intercalibration exercise. Most of the geographical intercalibration groups have finalized Intercalibration results but many Member States

have not joined the group or have not intercalibrated the methods due to some reasons. Those Member States will have to show that their methods are compliant with the WFD normative definitions and that their class boundaries are in line with the results of the intercalibration exercise. Many aspects can influence the outcome of intercalibration: data sampling, treatment methods, taxonomic reliability of databases, choice of metrics for ecological quality status classification, and criteria for selecting reference sites. Harmonization of diatom taxonomy and nomenclature was based on a previous ring test which took place at the European level. Four diatom indices (Indice de Polluosensibilité Spécifique—SPI, Indice Biologique Diatomées—IBD 2007, Intercalibration Common Metric Italy—ICMi and Slovenian Ecological Status assessment system) were intercalibrated using data from six European Mediterranean countries (Cyprus, France, Italy, Portugal, Slovenia, and Spain) [137]. Boundaries between High/Good and Good/Moderate quality classes were harmonized by means of the Intercalibration Common Metric (ICM). Comparability between countries was assured through boundary bias and class agreement. The national boundaries were adjusted when they deviated more than a quarter of a class equivalent (0.25) from the global mean. All national methods correlated well with the ICM, which was sensitive to water quality (negatively correlated to nutrients). *Achnanthidium minutissimum sensu lato* was the most discriminative species of Good ecological status class. *Planothidium frequentissimum, Gomphonema parvulum*, and *Nitzschia palea* were the most contributive to Moderate ecological status class. This intercalibration exercise allowed the establishment of common water quality goals across Mediterranean Europe, which is substantiated with the ICM. The ICM is an index that results from the combination of two widely applied diatom indices, the SPI and Rott's Trophic Index—TI [130].

The SPI accounts for general water quality estimates, low values corresponding to high-pressure levels and low EQRs. The TI measures nutrient load and was adjusted so that high values represented high EQR values.

The ICM is thus defined as:

$$\mathrm{ICM} = \frac{(\mathrm{EQR_{SPI}} + \mathrm{EQR_{TI}})}{2} \tag{13.3}$$

where $\mathrm{EQR_{SPI}}$ = observed value/reference value (This reference value is the median SPI value of reference sites for a national dataset) and $\mathrm{EQR_{TI}}$ = (4 − observed value)/(4 − reference value) (This reference value is the median TI value of reference sites for a national dataset). However, another requisite for intercalibration to proceed was that there should be a significant correlation between the ICM and the national indices, in addition to the ICM response to pressures. Pearson correlation was calculated to estimate the relationship between partner country indices and the ICM, with the criterion that Pearson's correlation coefficient (r) should be equal or higher than 0.5.

From 1031 samples analyzed to define the index, 205 were considered representative of least disturbed and, therefore, used as part of the reference sites in subsequent analyses. Nonsignificant Spearman rank correlations characterized the relationship between diatom data and the environmental pressures in the least disturbed sites. The ICM was responsive to nutrient enrichment, especially ammonia, total phosphorus, and phosphates when considering the entire quality gradient. The ICM proved robust and adequate for intercalibration purposes and reliably reflected national water quality. Intercalibration of diatom assessment methods was attained despite the difficulties encountered during the process, including the taxonomic inconsistencies and different data acquisition due to the robustness of these methods.

13.4.2 Diatom Indexes Developed for the Iberian Peninsula

There are different experiences designing and preparing new indexes for Iberian rivers. They arose from the need of developing more sensitive indicators that are specific for Iberian regions and typologies. The new metrics are based on diatom communities present in the reference conditions of the different Iberian typologies, and thus, provide more sensitive indicators than the ones provided by other European geographical areas [17, 125, 138].

13.4.2.1 Multimetric Index: MDIAT

MDIAT is a diatom multimetric index created as a combination of metric values. The sensitivity of the MDIAT to organic and nutrient stressors supports the use of this index to classify the ecological status of Galician rivers (NW, Spain). This index has been designed only for Galician granitic rivers (NW Spain) and has been intercalibrated at the European level in the Central Baltic Rivers GIG (Geographical Intercalibration Group) due to the need of finding an index that could fit this need. The Northwest of the Iberian Peninsula is influenced by the Atlantic climate, and it is characterized by rainy weather with mild temperatures throughout the year, similar to the rest of Western Europe. The region of Galicia lies in this area of Spain with the Cantabrian Sea to the north and the Atlantic Ocean to the west [131]. The geology is dominated by siliceous rocks: granite in the west and metamorphic rocks in the east.

The selection of diatom indices and metrics for the new index followed the procedure described by Barbour et al.

[139] with some modifications as follows (1) Assessing redundancy, (2) Relation with the physicochemical variables, and (3) Estimating discrimination efficiency. After discrimination and selection of the most suitable indexes, six indexes and two metrics were combined in the multimetric MDIAT. After rescaling, eight rescaled values were summed to the MDIAT. According to the authors, diatom multimetric index (MDIAT) had the highest discriminatory efficiency and highest correlations with the physical–chemical variables of all indices and metrics tested in the NW Spanish region. The new index, the MDIAT has a complex composition that includes newly developed metrics which are more sensitive and specific for Galician oligotrophic waters than the intercalibration index.

In conclusion, MDIAT constitutes a very good tool to evaluate the ecological status of Galician coastal rivers. The multimetric values were better correlated with the physicochemical variables than with the individual indices, integrating the effects of the pressures studied (organic pollution enrichment and eutrophication). The index may be improved and, ideally, further simplified in the future.

13.4.2.2 Autoecological Index: DDI

The goal of this new metric, the Duero Diatom Index (DDI), aimed at monitoring water quality in Duero basin watercourses (NW Spain). DDI was developed as a method of monitoring the integral status of watercourses, in order to realize a comprehensive assessment of water quality in the Duero Basin Rivers. DDI assesses the degree of water pollution as a measure of pH, salinity, organic pollution, and eutrophication, the last being the main factor controlling the distribution of the dominant diatom species in the Duero basin according to Blanco et al. [128]. The authors chose the weighted average method to develop the DDI index since it combines ecological credibility with empirical predictive power and simplicity.

13.4.2.3 Ecological Distance Index: iDIAT-ES

The iDIAT-ES value indicates the distance (or similarity) of each diatom community to their specific community of departure or reference. In this way, a high value represents a site with no or very little impact regarding its reference condition (very similar), while low values represent sites with greater impact due to contamination (low similarity to reference conditions). The weight of each species in the model was obtained by adding the abundances of a species in all the stations for a specific group. The weights of each species were calculated according to the percent of valves of each species in the seasons in which it was present with respect to the total valves of all the species for that set of stations that made up a certain group. The model used to calculate the value of the index of new samples is the formula presented below, based on the work of Lavoie et al. [140] and also on the formula of Zelinka and Marvan [126]:

$$\text{iDIAT.ES} = \frac{\sum_k W_k A_{ik} X_k}{\sum_k W_k A_{ik}} \tag{13.4}$$

where iDIAT-ES is the position of the sample on the main axis and, therefore, its index value, W_k is the weight of the species k, X_k is the value of the species k in the first axis of the CA, and A_{ik} is the abundance of species k in the sample i.

Before calculating the iDIAT-ES index, it is essential to know the river typology that we are studying to choose the right iDIAT-ES group according to the natural conditions of the sampled region. There is an ordination method who allowed to create and designed the iDIAT-ES (Spanish Diatom Index), with values between 0 and 5, where the position of the species of each group is placed over the maximum variation gradient (horizontal axis, X) which it is described by the diatom community composition. A high value of the index (close to 5) represents low impacted or not impacted site, whereas low value of the index means high perturbation or impact in the waterbody. The index represents three different groups corresponding to three ecologically different diatom communities: calcareous, siliceous, and a group for the typology 19 (Río Tinto) that is a very distinctive group in terms of diatom composition. It has been verified that there is a good correlation between the iDIAT-ES index and other indices such as SPI, BDI, CEE, and with other indicators of land uses and physical–chemical variables associated with pollution and pressures of different origin. Therefore, it is considered appropriate to use this new index as a tool for the evaluation of the ecological status in Spanish rivers and also a suitable index for the intercalibration exercise in relation to the rest of European indexes.

The iDIAT-ES has been developed with data from Spanish basins and adapted to the conditions of the Iberian river ecosystems. Its development at the national level has allowed us to consider the particularities of each of the basins and obtain values for each species that are typical of local conditions. Its application is relatively simple given the low number of taxa to be considered, from a database of approximately 18,000 species for the SPI to one of about 400 species for the iDIAT-ES.

13.4.3 Complementary Metrics Based on Diatoms (Growth Forms, Ecological Guilds, Teratologies)

Besides the metrics based on species identities, there are also other diatom metrics that are based on morphological traits such as growth forms, cell sizes, or biovolumes. Functional traits are proxies of adaptation strategies under particular environmental conditions, and life-strategies occupying a

similar niche can be collected in functional groups. Relationships between the abundances of such functional groups such growth forms and nutrients were established in experimental contexts [141, 142] and gave satisfactory results in large-scale studies to assess nutrient and global pollution (e.g., [143]). One of the most used and simplified classifications of diatom functional groups was developed by the ecological guilds published by Passy [144]. Guild refers to a group of species that exploit resources in a similar way, resulting in stronger competition within the guilds than between them. Passy's classification can be regarded as functional, including the way species attached to the substrate, thus how they cope with disturbance (e.g., flow velocity, grazing) and the way they utilize resources. Some of these relationships are proposed for bioassessment tools [139]. Diatom traits are derived from the Irstea database (bit.ly/2XCAe74) for biovolume and pioneer forms, from Kelly et al. [145] for growth forms and from Passy [144] for guilds.

Regarding the teratology, some authors suggested that they should be taken into account in the diatom indexes. By displaying deformities (teratologies) in their siliceous valves, diatoms have the potential to reflect sublethal responses to a wide range of toxic stressors including EU priority substances such as metals and organic compounds (see Chap. 3). Lower percentages of teratology, on the other hand, (<0.5%) [146] are commonly observed in natural diatom assemblages, due to changing environmental conditions. The presence of multiple stressors, however, can significantly increase the proportions of deformed individuals. Diatoms have fast growth rates (from hours to days), and thus respond very quickly to variations in their environment. The observation that valve aberrations are routinely found in extremely contaminated conditions led Coste et al. [147] to include the occurrence and abundance of deformed individuals in the calculation of the biological diatom index BDI. In the BDI, observed deformities were assigned the worst water quality profile, meaning that their presence tends to lower the final water quality score. Further development of teratological-based bioassessment tools have been already emphasized [146] and are under development.

13.5 ID-TAX: Identification Key for Biological Quality Elements Used in Routine Biological Monitoring in Spain

The ID-TAX project started at the beginning of the twenty-first century and it was developed by the Spanish Ministry for the Environment (MITECO) as a tool to standardize taxonomical criteria at national level in compliance with the European Water Framework Directive. The ID-TAX complements other open access tools developed earlier by the Ministry of Environment such as the Tesauro taxonómico (TAXAGUA) and the standard protocols for routine biological monitoring in Spanish water bodies. By the use of these open access tools, water quality assessments based on biological quality elements (BQE) are standard and comparable through the Spanish national territory.

The ID-TAX has developed a system able to classify all taxonomical information available for the BQE used for water quality assessments by the different Spanish water authorities. The results of ID-TAX were published in 2012 as printed books and as online and CD digital applications. The taxonomical information is divided into five sections, one per each BQE: macroinvertebrates, macrophytes, fish, phytobenthos, and phytoplankton. The species identification keys and species detailed information are available per each section. The ID-TAX tool has been developed by taxonomical experts who regularly check the taxonomical information providing an accurate and up to date tool.

The ID-TAX identification key uses the taxonomical information present in Tesauro Taxonómico (TAXAGUA) which has been developed by the Ministry of Environment from 2004 to 2011. The ID-TAX was first published with 1549 taxa from the 25,000 present in TAXAGUA. The number of taxa has been increased since the ID-TAX first review in 2013. The taxa included in the ID-TAX are the ones who have an indicator value for the different ecological indices used for each of the BQE, although some dominant species without indicator value are present as well. The ID-TAX taxonomical information is divided into two parts: a dichotomous key for species identification and a catalog with detailed species information including, morphology, taxonomy, ecology, and the indicator value of each species for their respective ecological index. A digital map with the distribution of species is also available in the web version, located in the GIS and map services of the Spanish Ministry of Environment.

13.6 Conclusions

Diatoms as unicellular eukaryotic algae characterize an organism group which has a number of prominent distinctive features that render diatom analysis as a useful tool for indication of present ecological conditions. Automatic species identification offers a promising tool to identify species complexes with high accuracy aiming at reducing bias in identification assessment. The near-term future of DNA metabarcoding, on the other hand has an enormous potential to boost data acquisition in biodiversity research and water quality assessments worldwide.

To improve the accuracy of water quality assessments based on diatoms, not only the improvements of quantification methods are required but also the development of indices

that reflect climate and geomorphological driven regional variability of diatom assemblages.

The information value of indicators depends largely on how they are developed and calibrated, and more precisely on how well the autoecological requirements of those taxa are quantified. New technologies in diatom species quantification and new regional developed diatom indices anticipate further developments toward this direction.

References

1. Venkatachalapathy, R., Karthikeyan, P.: Application of diatom-based indices for monitoring environmental quality of riverine ecosystems: a review. In: Environmental Management of River Basin Ecosystems, pp. 593–619. Springer (2015)
2. Taylor, J., Prygiel, J., Vosloo, A., Pieter, A., van Rensburg, L.: Can diatom-based pollution indices be used for biomonitoring in South Africa? A case study of the Crocodile West and Marico water management area. Hydrobiologia. **592**(1), 455–464 (2007)
3. Lavoie, I., Campeau, S., Grenier, M., Dillon, P.J.: A diatom-based index for the biological assessment of eastern Canadian rivers: an application of correspondence analysis (CA). Can. J. Fish. Aquat. Sci. **63**(8), 1793–1811 (2006)
4. Rakowska, B., Szczepocka, E.: Demonstration of the Bzura River restoration using diatom indices. Biologia. **66**(3), 411–417 (2011)
5. Blanco, S., Bécares, E., Cauchie, H.-M., Hoffmann, L., Ector, L.: Comparison of biotic indices for water quality diagnosis in the Duero Basin (Spain). Archiv für Hydrobiologie Supplement Large Rivers. **161**, 267–286 (2007)
6. Taylor, J., van Vuuren, M.J., Pieterse, A.: The application and testing of diatom-based indices in the Vaal and Wilge Rivers, South Africa. Water SA. **33**(1), (2007)
7. Feio, M.J., Almeida, S.F., Craveiro, S.C., Calado, A.J.: A comparison between biotic indices and predictive models in stream water quality assessment based on benthic diatom communities. Ecol. Indic. **9**(3), 497–507 (2009)
8. Schneider, S.C., Kahlert, M., Kelly, M.G.: Interactions between pH and nutrients on benthic algae in streams and consequences for ecological status assessment and species richness patterns. Sci. Total Environ. **444**, 73–84 (2013)
9. Soininen, J.: Environmental and spatial control of freshwater diatoms—a review. Diatom Res. **22**(2), 473–490 (2007)
10. Bere, T.: Are diatom-based biotic indices developed in eutrophic, organically enriched waters reliable monitoring metrics in clean waters? Ecol. Indic. **62**, 312–316 (2016)
11. Atazadeh, I., Sharifi, M., Kelly, M.: Evaluation of the Trophic Diatom Index for assessing water quality in River Gharasou, western Iran. Hydrobiologia. **589**(1), 165–173 (2007)
12. Stenger-Kovács, C., Buczko, K., Hajnal, E., Padisák, J.: Epiphytic, littoral diatoms as bioindicators of shallow lake trophic status: Trophic Diatom Index for Lakes (TDIL) developed in Hungary. Hydrobiologia. **589**(1), 141–154 (2007)
13. Blanco, S.: Environmental factors controlling lake diatom communities: a meta-analysis of published data. Biogeosci. Discuss. **11**(11), 15889–15909 (2014)
14. Bate, G., Smailes, P., Adams, J.: A water quality index for use with diatoms in the assessment of rivers. Water SA. **30**(4), 493–498 (2004)
15. Stevenson, R., Pan, Y.: Assessing environmental conditions in rivers and streams with diatoms. In: The Diatoms: Applications for the Environmental and Earth Sciences, pp. 57–85 (1999)
16. Kelly, M.: Use of the trophic diatom index to monitor eutrophication in rivers. Water Res. **32**(1), 236–242 (1998)
17. Kelly, M.: Use of community-based indices to monitor eutrophication in European rivers. Environ. Conserv. **25**(1), 22–29 (1998)
18. Kelly, M., et al.: The Trophic Diatom Index: A User's Manual Revised edition R&D Technical Report E2/TR2. Environment Agency, Bristol (2001)
19. Fornells, N.P., Solà, C., Munné, A.: QBR: un índice rápido para la evaluación de la calidad de los ecosistemas de ribera. Tecnología del Agua. **175**, 20–39 (1998)
20. Pardo, I., et al.: El hábitat de los ríos mediterráneos. Diseño de un índice de diversidad de hábitat. Limnetica. **21**(3–4), 115–133 (2002)
21. Soeprobowati, T.R., Tandjung, S.D., Sutikno, S., Hadisusanto, S., Gell, P.: The minimum number of valves for diatoms identification in Rawapening Lake, Central Java. BIOTROPIA Southeast Asian J. Trop. Biol. **23**(2), 97–100 (2017)
22. Chessman, B., Growns, I., Currey, J., Plunkett-Cole, N.: Predicting diatom communities at the genus level for the rapid biological assessment of rivers. Freshw. Biol. **41**(2), 317–331 (1999)
23. Rimet, F., Bouchez, A.: Life-forms, cell-sizes and ecological guilds of diatoms in European rivers. Knowl. Manag. Aquat. Ecosyst. **406**, 01 (2012)
24. Rice, A., Baird, E., Eaton, R.: Standard methods for examination of water and wastewater. American Public Health Association, Washington, DC (2017)
25. Sournia, A.: Phytoplankton Manual. UNESCO, Paris (1978)
26. Utermöhl, H.: Zur Vervollkommnung der quantitativen Phytoplankton-Methodik: Mit 1 Tabelle und 15 abbildungen im Text und auf 1 Tafel. Internationale Vereinigung für theoretische und angewandte Limnologie: Mitteilungen. **9**(1), 1–38 (1958)
27. Lund, J., Kipling, C., Le Cren, E.: The inverted microscope method of estimating algal numbers and the statistical basis of estimations by counting. Hydrobiologia. **11**(2), 143–170 (1958)
28. CEN: Water quality-Guidance standard for the routine sampling and pretreatment of benthic diatoms from rivers. EN 13946: 2003. Comité Européen de Normalisation, Geneva (2003)
29. CEN: Water Quality–Guidance Standard for the Identification, Enumeration and Interpretation of Benthic Diatom Samples from Running Waters. EN 14407: 2004. Comité Européen de Normalisation, Geneva (2004)
30. Kelly, M.: International and European standards for algal-based monitoring. Oceanol. Hydrobiol. Stud. **1**, 77–81 (2004)
31. Kelly, M., et al.: Recommendations for the routine sampling of diatoms for water quality assessments in Europe. J. Appl. Phycol. **10**(2), 215 (1998)
32. CHD: Metodología para el establecimiento del estado ecológico según la Directiva Marco del Agua. Protocolos de muestreo y análisis para fitobentos (microalgas bentónicas), pp. 1–33. CHD, Zaragoza (2005)
33. Pardo, I., García, L., Delgado, C., Costas, N., Abraín, R.: Protocolos de muestreo de comunidades biológicas acuáticas fluviales en el ámbito de las Confederaciones Hidrográficas del Miño-Sil y Cantábrico. MARM, Madrid (2010)
34. Stevenson, R., Bahls, L.: Periphyton protocols: revision to rapid bioassessment protocols for use in streams and rivers: periphyton, benthic macroinvertebrates and fish. EPA, Washington, DC (1999)
35. Blanco, S., Álvarez, I., Cejudo, C.: A test on different aspects of diatom processing techniques. J. Appl. Phycol. **20**(4), 445–450 (2008)
36. Moss, B., et al.: The estimation of numbers and pigment content in epipelic algal populations. Limnol. Oceanogr. **11**(4), 584–595 (1966)

37. Battarbee, R.W.: A new method for the estimation of absolute microfossil numbers, with reference especially to diatoms. Limnol. Oceanogr. **18**(4), 647–653 (1973)
38. McBride, T.P.: Preparing random distributions of diatom valves on microscope slides. Limnol. Oceanogr. **33**, 1627–1629 (1988)
39. Schrader, H.: Proposal for a standardized method of cleaning diatom-bearing deep-sea and land-exposed marine sediments. Nova Hedwig. Beih. **45**, 403–409 (1973)
40. Alverson, A.J., Manoylov, K.M., Stevenson, R.J.: Laboratory sources of error for algal community attributes during sample preparation and counting. J. Appl. Phycol. **15**(5), 357–369 (2003)
41. Van der Werff, A.: A new method of concentrating and cleaning diatoms and other organisms. Internationale Vereinigung für theoretische und angewandte Limnologie: Verhandlungen. **12**(1), 276–277 (1953)
42. Setty, M.A.P.: Preparation and method of study of fossil diatoms. Micropaleontology. **12**, 511–514 (1966)
43. Brown, S.-D., Austin, A.: A method of collecting periphyton in lentic habitats with procedures for subsequent sample preparation and quantitative assessment. Internationale Revue der gesamten Hydrobiologie und Hydrographie. **56**(4), 557–580 (1971)
44. Ma, J.C.W., Jeffrey, L.M.: Description and comparison of a new cleaning method of diatom frustules for light and electron microscope studies. J. Microsc. **112**(2), 235–238 (1978)
45. Carr, J.M., Hergenrader, G.L., Troelstrup Jr., N.H.: A simple, inexpensive method for cleaning diatoms. Trans. Am. Microsc. Soc. 152–157 (1986)
46. Scherer, R.P.: A new method for the determination of absolute abundance of diatoms and other silt-sized sedimentary particles. J. Paleolimnol. **12**(2), 171–179 (1994)
47. Charles, D.F., Knowles, C., Davis, R.S.: Protocols for the analysis of algal samples collected as part of the US Geological Survey National Water-Quality Assessment Program. Patrick Center for Environmental Research Report, Philadelphia, PA (2002)
48. Rings, A., Lücke, A., Schleser, G.H.: A new method for the quantitative separation of diatom frustules from lake sediments. Limnol. Oceanogr. Methods. **2**(1), 25–34 (2004)
49. Schaumburg, J., Schranz, C., Stelzer, D., Hofmann, G., Gutowski, A., Foerster, J.: Instruction protocol for the ecological assessment of running waters for implementation of the EC Water Framework Directive: macrophytes and phytobenthos. Bavarian Environment Agency, Augsburg (2006)
50. Blanco, S., Becares, E.: Metodo de muestreo de diatomeas epífitas en lagunas para la aplicación de la Directiva Marco del Agua. Tecnología del Agua. **261**, 48–53 (2006)
51. Li, J., Chen, J.: An effective cleaning method for producing pure diatom samples from lake sediments. Earth Environ. **35**(1), 91–96 (2007)
52. Metfies, K., et al.: An optimized protocol for the identification of diatoms, flagellated algae and pathogenic protozoa with phylochips. Mol. Ecol. Notes. **7**(6), 925–936 (2007)
53. Debenest, T., Silvestre, J., Coste, M., Delmas, F., Pinelli, E.: A new cell primo-culture method for freshwater benthic diatom communities. J. Appl. Phycol. **21**(1), 65 (2009)
54. Evans, K.M., Mann, D.G.: A proposed protocol for nomenclaturally effective DNA barcoding of microalgae. Phycologia. **48**(1), 70–74 (2009)
55. Díaz-Palma, P., Alucema, A., Hayashida, G., Maidana, N.: Development and standardization of a microalgae test for determining deaths by drowning. Forensic Sci. Int. **184**(1–3), 37–41 (2009)
56. Fetscher, A.E., Busse, L., Ode, P.R.: Standard operating procedures for collecting stream algae samples and associated physical habitat and chemical data for ambient bioassessments in California. California State Water Resources Control Board Surface Water Ambient Monitoring Program (SWAMP) Bioassessment SOP 2 (2009)
57. Watanabe, T., Kodama, Y., Mayama, S.: Application of a novel cleaning method using low-temperature plasma on tidal flat diatoms with heterovalvy or delicate frustule structure. Proc. Acad. Natl. Sci. Phila. **160**(1), 83–87 (2010)
58. Serieyssol, K., et al.: Diatom fossils in mires: a protocol for extraction, preparation and analysis in palaeoenvironmental studies. Mires Peat. **7**(12), 1–11 (2010)
59. Lang, I., Kaczmarska, I.: A protocol for a single-cell PCR of diatoms from fixed samples: method validation using *Ditylum brightwellii* (T. West) Grunow. Diatom Res. **26**(1), 43–49 (2011)
60. Zoto, G.A., Dillon, D.O., Schlichting Jr., H.E.: A rapid method for clearing diatoms for taxonomic and ecological studies. Phycologia. **12**(1), 69–70 (1973)
61. Friedrichs, L., Maier, M., Hamm, C.: A new method for exact three-dimensional reconstructions of diatom frustules. J. Microsc. **248**(2), 208–217 (2012)
62. Mendes, T., Almeida, S.F., Feio, M.J.: Assessment of rivers using diatoms: effect of substrate and evaluation method. Arch. Hydrobiol. **179**(4), 267–279 (2012)
63. MacDonald, L.A., Balasubramaniam, A.M., Hall, R.I., Wolfe, B.B., Sweetman, J.N.: Developing biomonitoring protocols for shallow Arctic lakes using diatoms and artificial substrate samplers. Hydrobiologia. **683**(1), 231–248 (2012)
64. Vermeulen, S., Lepoint, G., Gobert, S.: Processing samples of benthic marine diatoms from Mediterranean oligotrophic areas. J. Appl. Phycol. **24**(5), 1253–1260 (2012)
65. Gautam, S., Arya, A., Vinayak, V.: Protocol to establish axenic cultures for diatoms of fresh water. Int. J. Sci. Res. **5**(11), 410–418 (2016)
66. Tennant, R.K., et al.: A new flow cytometry method enabling rapid purification of fossil pollen from terrestrial sediments for AMS radiocarbon dating. J. Quat. Sci. **28**(3), 229–236 (2013)
67. Seo, Y., Sato, S., Kuroki, K., Kishida, T.: A simple DNA coprecipitation method for the detection of diatoms in heart blood. Forensic Sci. Int. **232**(1–3), 154–159 (2013)
68. Kimura, K., Tomaru, Y.: A unique method for culturing diatoms on agar plates. Plankton Benthos Res. **8**(1), 46–48 (2013)
69. Zhao, J., et al.: Application of the microwave digestion-vacuum filtration-automated scanning electron microscopy method for diatom detection in the diagnosis of drowning. J. Forensic Legal Med. **33**, 125–128 (2015)
70. Jiang, W., Pan, H., Wang, F., Jiang, M., Deng, X., Li, J.: A rapid sample processing method to observe diatoms via scanning electron microscopy. J. Appl. Phycol. **27**(1), 243–248 (2015)
71. Warnock, J.P., Scherer, R.P.: A revised method for determining the absolute abundance of diatoms. J. Paleolimnol. **53**(1), 157–163 (2015)
72. Wang, H., et al.: A simple digestion method with a Lefort aqua regia solution for diatom extraction. J. Forensic Sci. **60**, S227–S230 (2015)
73. Stancheva, R., Busse, L., Kociolek, J., Sheath, R.: Standard operating procedures for laboratory processing and identification of stream algae. California State Water Resources Control Board Surface Water Ambient Monitoring Program (SWAMP) Bioassessment SOP 0003 (2015)
74. Morin, S., Gómez, N., Tornés, E., Licursi, M., Rosebery, J.: Benthic diatom monitoring and assessment of freshwater environments: standard methods and future challenges. In: Aquatic Biofilms, Ecology, Water Quality and Wastewater Treatment, pp. 111–124 (2016)
75. Ferrara, M.A., De Tommasi, E., Coppola, G., De Stefano, L., Rea, I., Dardano, P.: Diatom valve three-dimensional representation: a new imaging method based on combined microscopies. Int. J. Mol. Sci. **17**(10), 1645 (2016)
76. Mansilla, C., Novais, M.H., Faber, E., Martínez-Martínez, D., De Hosson, J.T.: On the 3D reconstruction of diatom frustules: a

novel method, applications and limitations. J. Appl. Phycol. **28**(2), 1097–1110 (2016)
77. Saba, F., et al.: A rapid and reproducible genomic DNA extraction protocol for sequence-based identification of archaea, bacteria, cyanobacteria, diatoms, fungi and green algae. J. Med. Bacteriol. **5**(3–4), 22–28 (2017)
78. Rojas-Camacho, O., Forero, M.G., Menéndez, J.M.: A tuning method for diatom segmentation techniques. Appl. Sci. **7**(8), 762 (2017)
79. Barragán, C., Wetzel, C.E., Ector, L.: A standard method for the routine sampling of terrestrial diatom communities for soil quality assessment. J. Appl. Phycol. **30**(2), 1095–1113 (2018)
80. Bayer, M., et al.: ADIAC: Using computer vision technology for automatic diatom identification. In: Proceedings of the 16th International Diatom Symposium, Athens, pp. 537–562 (2000)
81. Du Buf, H., et al.: Diatom identification: a double challenge called ADIAC. In: International Conference on Image Analysis and Processing, Venice, pp. 734–739 (1999)
82. Du Buf, H., Bayer, M. (eds.): Automatic diatom identification. World Scientific, Singapore (2002)
83. Kloster, M., Kauer, G., Beszteri, B.: SHERPA: an image segmentation and outline feature extraction tool for diatoms and other objects. BMC Bioinf. **15**(1), 218 (2014)
84. Kloster, M., Esper, O., Kauer, G., Beszteri, B.: Large-scale permanent slide imaging and image analysis for diatom morphometrics. Appl. Sci. **7**(4), 330 (2017)
85. Wishkerman, A., Hamilton, P.B.: Shape outline extraction software (DiaOutline) for elliptic Fourier analysis application in morphometric studies. Appl. Plant Sci. **6**(12), (2018)
86. Pappas, J., Kociolek, P., Stoermer, E.: Quantitative morphometric methods in diatom research. Nova Hedwig. Beih. **143**, 281–306 (2014)
87. Delgado, C., Novais, M.H., Blanco, S., Almeida, S.F.: Examination and comparison of *Fragilaria candidagilae* sp. Nov. with type material of *Fragilaria recapitellata*, *F. capucina*, *F. perminuta*, *F. intermedia* and *F. neointermedia* (Fragilariales, Bacillariophyceae). Phytotaxa. **231**(1), 1–18 (2015)
88. Poulíčková, A., Neustupa, J., Hašler, P., Tomanec, O., Cox, E.J.: A new species, *Navicula lothargeitleri* sp. nov., within the *Navicula cryptocephala* complex (Bacillariophyceae). Phytotaxa. **273**(1), 23–33 (2016)
89. Wengrat, S., Marquardt, G.C., de Campos Bicudo, D., de Mattos Bicudo, C.E., Wetzel, C.E., Ector, L.: Type analysis of *Cymbella schubartii* and two new *Encyonopsis* species (Bacillariophyceae) from southeastern Brazil. Phytotaxa. **221**(3), 247–264 (2015)
90. Bueno, G., Deniz, O., Pedraza, A., et al.: Automated diatom classification (Part A): handcrafted feature approaches. Appl. Sci. **7**(8), 753 (2017)
91. Pedraza, A., Bueno, G., Deniz, O., Cristóbal, G., Blanco, S., Borrego-Ramos, M.: Automated diatom classification (Part B): a deep learning approach. Appl. Sci. **7**(5), 460 (2017)
92. Pedraza, A., et al.: Lights and pitfalls of convolutional neural networks for diatom identification. Optics, Photonics and Digital Technologies for Imaging Applications V, International Society for Optics and Photonics 106790G (2018)
93. Kelly, M., et al., A DNA based Diatom Metabarcoding Approach for Water Framework Directive Classification of Rivers (2018).
94. Malviya, S.: Global Diatom Biodiversity: An Assessment Using Metabarcoding Approach. Ph.D. Dissertation, Paris (2015)
95. Nanjappa, D., Audic, S., Romac, S., Kooistra, W.H., Zingone, A.: Assessment of species diversity and distribution of an ancient diatom lineage using a DNA metabarcoding approach. PLoS One. **9**(8), e103810 (2014)
96. Moniz, M.B.J., Kaczmarska, I.: Barcoding diatoms: is there a good marker? Mol. Ecol. Resour. **9**, 65–74 (2009)
97. Zimmermann, J., Jahn, R., Gemeinholzer, B.: Barcoding diatoms: evaluation of the V4 subregion on the 18S rRNA gene, including new primers and protocols. Org. Divers. Evol. **11**(3), 173 (2011)
98. Rivera, S., Vasselon, V., Jacquet, S., Bouchez, A., Ariztegui, D., Rimet, F.: Metabarcoding of lake benthic diatoms: from structure assemblages to ecological assessment. Hydrobiologia. **807**(1), 37–51 (2018)
99. Zimmermann, J.: DNA barcoding and eDNA barcoding in diatoms. Ph.D. Dissertation, Giessen (2015)
100. Vasselon, V., Domaizon, I., Rimet, F., Kahlert, M., Bouchez, A.: Application of high-throughput sequencing (HTS) metabarcoding to diatom biomonitoring: do DNA extraction methods matter? Freshw. Sci. **36**(1), 162–177 (2017)
101. Vasselon, V., Rimet, F., Tapolczai, K., Bouchez, A.: Assessing ecological status with diatoms DNA metabarcoding: scaling-up on a WFD monitoring network (Mayotte island, France). Ecol. Indic. **82**, 1–12 (2017)
102. Apothéloz-Perret-Gentil, L., Cordonier, A., Straub, F., Iseli, J., Esling, P., Pawlowski, J.: Taxonomy-free molecular diatom index for high-throughput eDNA biomonitoring. Mol. Ecol. Resour. **17**(6), 1231–1242 (2017)
103. Piredda, R., Simeone, M.C., Attimonelli, M., Bellarosa, R., Schirone, B.: Prospects of barcoding the Italian wild dendroflora: oaks reveal severe limitations to tracking species identity. Mol. Ecol. Resour. **11**(1), 72–83 (2011)
104. Hoef-Emden, K.: Pitfalls of establishing DNA barcoding systems in protists: the Cryptophyceae as a test case. PLoS One. **7**(8), e43652 (2012)
105. Fittipaldi, M., Codony, F., Adrados, B., Camper, A.K., Morató, J.: Viable real-time PCR in environmental samples: can all data be interpreted directly? Microb. Ecol. **61**(1), 7–12 (2011)
106. Urbánková, P., Veselá, J.: DNA-barcoding: a case study in the diatom genus *Frustulia* (Bacillariophyceae). Nova Hedwigia. **142**, 147–162 (2013)
107. Khan-Bureau, D., Ector, L., Morales, E.A., Wade, E.J., Lewis, L.A.: Contrasting morphological and DNA barcoding methods for diatom (Bacillariophyta) identification from environmental samples in the Eightmile River in Connecticut. Nova Hedwig. Beih. **146**, 279–302 (2018)
108. Hering, D., Moog, O., Sandin, L., Verdonschot, P.F.: Overview and application of the AQEM assessment system. Hydrobiologia. **516**(1–3), 1–20 (2004)
109. Sandin, L., Verdonschot, P.F.: Stream and river typologies—major results and conclusions from the STAR project. In: The Ecological Status of European Rivers: Evaluation and Intercalibration of Assessment Methods, pp. 33–37. Springer (2006)
110. CEDEX: Directiva 2000/60/CE. Análisis de las características de las demarcaciones. Caracterización de los tipos de ríos y lagos. MARM, Madrid (2004)
111. Tison, J., et al.: Typology of diatom communities and the influence of hydro-ecoregions: a study on the French hydrosystem scale. Water Res. **39**(14), 3177–3188 (2005)
112. Grenier, M., Lavoie, I., Rousseau, A.N., Campeau, S.: Defining ecological thresholds to determine class boundaries in a bioassessment tool: the case of the Eastern Canadian Diatom Index (IDEC). Ecol. Indic. **10**(5), 980–989 (2010)
113. Pardo, I., et al.: A predictive diatom-based model to assess the ecological status of streams and rivers of Northern Spain. Ecol. Indic. **90**, 519–528 (2018)
114. Karr, J.R.: Biological integrity: a long-neglected aspect of water resource management. Ecol. Appl. **1**(1), 66–84 (1991)
115. Leira, M., Sabater, S.: Diatom assemblages distribution in catalan rivers, NE Spain, in relation to chemical and physiographical factors. Water Res. **39**(1), 73–82 (2005)
116. Dallas, H.F.: Ecological status assessment in Mediterranean rivers: complexities and challenges in developing tools for assess-

ing ecological status and defining reference conditions. Hydrobiologia. **719**(1), 483–507 (2013)
117. Munné, A., Prat, N.: Effects of Mediterranean climate annual variability on stream biological quality assessment using macroinvertebrate communities. Ecol. Indic. **11**(2), 651–662 (2011)
118. Sánchez-Montoya, M., et al.: Defining criteria to select reference sites in Mediterranean streams. Hydrobiologia. **619**(1), 39 (2009)
119. Coste, M., Tison, J., Delmas, F.: Flores diatomiques des cours d'eau: proposition de valeurs limites du «Bon État» pour l'IPS et l'IBD. Document de travail–Unité de Recherche Qualité des Eaux–Cemagref, Bordeaux (2004)
120. Hawkins, C.P., Olson, J.R., Hill, R.A.: The reference condition: predicting benchmarks for ecological and water-quality assessments. J. N. Am. Benthol. Soc. **29**(1), 312–343 (2010)
121. Kelly, M.: Data rich, information poor? Phytobenthos assessment and the Water Framework Directive. Eur. J. Phycol. **48**(4), 437–450 (2013)
122. Álvarez-Blanco, I., Blanco, S., Cejudo-Figueiras, C., Bécares, E.: The Duero Diatom Index (DDI) for river water quality assessment in NW Spain: design and validation. Environ. Monit. Assess. **185**(1), 969–981 (2013)
123. Lobo, E.A., Schuch, M., Heinrich, C.G., et al.: Development of the Trophic Water Quality Index (TWQI) for subtropical temperate Brazilian lotic systems. Environ. Monit. Assess. **187**(6), 354 (2015)
124. Rimet, F.: Recent views on river pollution and diatoms. Hydrobiologia. **683**(1), 1–24 (2012)
125. Kelly, M., Whitton, B.A.: Biological monitoring of eutrophication in rivers. Hydrobiologia. **384**(1–3), 55–67 (1998)
126. Zelinka, M.: Zur Prazisierung der biologischen klassifikation der Reinheid fliessender Gewasser. Arch. Hydrobiol. **57**, 389–407 (1961)
127. CEMAGREF: Etude des méthodes biologiques quantitatives d'appréciation de la qualité des eaux. Rapport Division Qualité, Lyon (1982)
128. Blanco, S., et al.: Diatom assemblages and water quality assessment in the Duero Basin (NW Spain). Belg. J. Bot. 39–50 (2008)
129. Potapova, M., Charles, D.F.: Diatom metrics for monitoring eutrophication in rivers of the United States. Ecol. Indic. **7**(1), 48–70 (2007)
130. Rott, E., Pipp, E., Pfister, P.: Diatom methods developed for river quality assessment in Austria and a cross-check against numerical trophic indication methods used in Europe. Algol. Stud. **110**(1), 91–115 (2003)
131. Delgado, C., Pardo, I., García, L.: A multimetric diatom index to assess the ecological status of coastal Galician rivers (NW Spain). Hydrobiologia. **644**(1), 371–384 (2010)
132. Barragán, C.: Desarrollo de un nuevo índice de diatomeas para la evaluación del estado ecológico de los ríos de la Demarcación Hidrográfica del Tajo. In: 18th Conference of the Iberian Association of Limnology (AIL 2016), Tortosa (2016)
133. Besse-Lototskaya, A., Verdonschot, P.F., Coste, M., Van de Vijver, B.: Evaluation of European diatom trophic indices. Ecol. Indic. **11**(2), 456–467 (2011)
134. Descy, J.-P., Coste, M.: A test of methods for assessing water quality based on diatoms. Internationale Vereinigung für theoretische und angewandte Limnologie: Verhandlungen. **24**(4), 2112–2116 (1991)
135. Round, F.: A review and methods for the use of epilithic diatoms for detecting and monitoring changes in river water quality. HMSO Publisher, London (1993)
136. Taylor, J., de la Rey, P.A., van Rensburg, L.: Recommendations for the collection, preparation and enumeration of diatoms from riverine habitats for water quality monitoring in South Africa. Afr. J. Aquat. Sci. **30**(1), 65–75 (2005)
137. Almeida, et al.: Water quality assessment of rivers using diatom metrics across Mediterranean Europe: a methods intercalibration exercise. Sci. Total Environ. **476**, 768–776 (2014)
138. Prygiel, J., et al.: Determination of the biological diatom index (IBD NF T 90–354): results of an intercomparison exercise. J. Appl. Phycol. **14**(1), 27–39 (2002)
139. Barbour, A.M.T., Gerritsen, J., Snyder, B.D., Stribling, J.B.: Rapid bioassessment protocols for use in streams and wadeable rivers: periphyton, benthic macroinvertebrates and fish. EPA, Washington (1998)
140. Lavoie, I., Campeau, S., Zugic-Drakulic, N., Winter, J., Fortin, C.: Using diatoms to monitor stream biological integrity in Eastern Canada: an overview of 10 years of index development and ongoing challenges. Sci. Total Environ. **475**, 187–200 (2014)
141. Hoagland, K.D., Roemer, S.C., Rosowski, J.R.: Colonization and community structure of two periphyton assemblages, with emphasis on the diatoms (Bacillariophyceae). Am. J. Bot. **69**(2), 188–213 (1982)
142. Pringle, C.M.: Nutrient spatial heterogeneity: effects on community structure, physiognomy and diversity of stream algae. Ecology. **71**(3), 905–920 (1990)
143. Berthon, V., Bouchez, A., Rimet, F.: Using diatom life-forms and ecological guilds to assess organic pollution and trophic level in rivers: a case study of rivers in south-eastern France. Hydrobiologia. **673**(1), 259–271 (2011)
144. Passy, S.: Diatom ecological guilds display distinct and predictable behavior along nutrient and disturbance gradients in running waters. Aquat. Bot. **86**(2), 171–178 (2007)
145. Kelly, M., et al., "Common freshwater diatoms of Britain and Ireland: an interactive key", (2005).
146. Lavoie, I., et al.: Diatom teratologies as biomarkers of contamination: are all deformities ecologically meaningful? Ecol. Indic. **82**, 539–550 (2017)
147. Coste, M., Boutry, S., Tison-Rosebery, J., Delmas, F.: Improvements of the Biological Diatom Index (BDI): description and efficiency of the new version (BDI-2006). Ecol. Indic. **9**(4), 621–650 (2009)

Diatoms in Forensic Analysis

14

Eloy Girela-Lopez, Cristina M. Beltran-Aroca, and Herminia García-Mozo

Abstract

Diatoms are single-celled organisms widely distributed in aquatic environments with several applications, such as oil exploration, environmental indications, microbial ecology, or forensic examinations. In this chapter, we analyse forensic applications of diatom analysis, including the usefulness of the test in the diagnosis of drowning, identification of the drowning site, identification of the suspect and information about the time of death. We also address the sample preparation process and review the most used techniques for diatom analysis involving the digestion of tissues from specific organs to study (acid digestion, acid digestion in disorganization can, Soluene-350 digestion, enzymatic digestion, membrane filter methods, and some novel techniques). Finally, we review some protocols in diatom analysis and histological findings in drowning.

14.1 Introduction

Diatoms are single-celled organisms widely distributed in aquatic environments with intricate skeletons. They constitute one of the most abundant and diverse lineages in planktonic, benthic, and terrestrial habitats worldwide, with estimates of up to 200,000 species [1]. The wide range of applications of diatoms includes oil exploration, environmental indications, microbial ecology, and forensic examinations [2, 3]. The use of microalgae in forensic science has been limited; however, its application in certain types of research has been demonstrated so that studies on their taxonomy and ecology are necessary [4].

E. Girela-Lopez (✉) · C. M. Beltran-Aroca · H. García-Mozo
University of Cordoba, Cordoba, Spain
e-mail: ft1gilpe@uco.es

14.1.1 Diatom Test in Drowning

Drowning is the third most common cause of death due to unintentional trauma in the world and accounts for 7% of all deaths related to trauma. It is estimated that 360,000 people die worldwide every year from drowning, making it a major public health problem [5]. Drowning can be considered as a specialized form of asphyxia in which environmental oxygen (air) is displaced by a liquid (usually water), and total or partial immersion of the respiratory orifices has occurred. Many corpses are recovered from the water, but not all have drowned. Of those that have drowned, the pathological proof is often difficult or even impossible to obtain. The diagnosis of drowning on autopsy presents one of the major problems in forensic medicine, especially when there is a delay in recovering the victim [6]. In a routine autopsy, some of the findings include voluminous lungs with increased weight, pleural effusion, froth in the airway, anemia of the spleen, an impression of the ribs on the lateral surface of the lungs, and a marble-like mixed pattern consisting of congestive or emphysemic parts of the lungs [7]. These signs are usually characteristic but not diagnostic since most of them simply indicate that the body has been submerged in water [8]. The human remains found in aquatic contexts are often recovered incomplete and poorly preserved, limiting the opportunities for analysis for identification [9]. In addition, the early onset of putrefaction (especially in warmer waters) not only renders difficult identification of the corpse and evaluation of any lesions present [10], but it also favors such a rapid disappearance of these findings, making it impossible to investigate the circumstances of death [6, 9, 11]. Therefore, it is necessary to standardize methodologies that clarify the facts [11].

Circumstantial data, such as a suicide note or the testimony of an eyewitness, can help to clarify whether a crime, suicide, or accident has occurred [10]. However, Esiyok et al. estimated that, in 69.6% of the cases, there were no eyewitnesses due to the distance from residential areas, so

G. Cristóbal et al. (eds.), *Modern Trends in Diatom Identification*, Developments in Applied Phycology 10,
https://doi.org/10.1007/978-3-030-39212-3_14

the diagnosis of drowning is often based on the exclusion of other causes of death [12].

Thus, to aid in the diagnosis of drowning, several tests have been developed in an attempt to quantify a number of substances from the drowning fluid, which diffuses across the alveolar-capillary membrane into the blood and the tissues during the drowning process, including chemical ion markers, such as strontium, magnesium, and iron concentrations, for evidence of haemodilution and haemoconcentration [13, 14]. Nevertheless, none of the aforementioned tests have high diagnostic predictive value. One of the former tests proposed is the analysis of diatoms. More recently, other tests for the diagnosis of drowning have been proposed, such as bacterioplankton detection by PCR [15], postmortem images [16], or 16S rDNA fragments analysis [17].

Since the first discovery of diatoms in the lungs by Hofmann in 1896 and their diagnostic use by Revenstorf in 1904, the method has been used and improved over the years [6]. Diatom test is based on the presence of diatoms in the water where the drowning likely occurred [4]. The findings indicate when a living person has drowned in diatom-containing water; the inhalation of water causes a high number of diatoms to penetrate the pulmonary alveolar walls and spread through the cardiovascular system, reaching distant organs, such as the liver, spleen, kidneys, and even the bone marrow. If the subject has died previously of a different cause, the absence of a heartbeat will result in the presence of diatoms in the lungs simply by passive diffusion but not in other organs [6]. The diatom test has been considered a "gold standard" test for the diagnosis of drowning by some authors [11].

The test, however, is not without controversy. Some authors [18–20] have questioned its reliability, mainly as a consequence of the high rate of false-positive results in non-drowning deaths due to the ubiquity of diatoms in nature and the possibility of diatoms entering the systemic circulation from atmospheric air, food, and drink [6, 21, 22] and not only from water. There has also been criticism in the opposite direction as a consequence of false negatives (lack of diatom cells in internal organs) attributed to rapid death preventing the penetration of diatoms into the circulation and organs or the drowning occurring in water lacking diatoms [21, 23].

Diatom test for the diagnosis of drowning is widely used in countries in the Northern Hemisphere, mainly in Europe and Asia, but in the Americas (both North and South America), it has not been adopted as a routine procedure in forensic autopsies.

In summary, preliminary qualitative diatom analysis has shown to be a simple and reliable method. It is based on the visual documentation of every diatom or fragment found, with digital images, video or, if available, a scanning electron microscope photograph [21, 24]. However, the final interpretation of the results for the diagnosis of death by drowning must be performed by an expert diatomist. Conversely, recent studies have reported that conventional microscopic identification methods are time-consuming, and there will always be a degree of uncertainty. Therefore, Zhao et al. showed that it is possible to identify the corresponding diatom taxa with the AdvISER-M-PYRO algorithm using the 18S rDNA V7 region and diatom DNA mixtures [25].

14.1.2 Other Applications of Diatoms

As previously stated, qualitative diatom analysis of drowning media and samples of the tissues/organs provide information about the cause of death, as well as very relevant data about the place and time of death [10, 26].

14.1.2.1 Drowning Site

Similarly, diatom analysis has also long been used for ecological mapping in relation to water types and locations. Several studies have considered it as an indicator of the site of drowning [6, 24, 26–29]. It has been suggested that when a corpse rises from the bottom of a drowning site, it usually appears nearby, although a rapid current can transport it a certain distance from the exact place of death [30]. Another issue to consider is when a body is found on land, and no reference body of water is available [29]. Consequently, the presence of differential species spectra and abundance profiles should be evaluated in the medium of drowning [28]. When there is a great diversity of common species from different geographical areas, the least frequent species will be the most useful in determining the drowning site [24, 28, 31]. This effect can hinder the finding of significant differences between different points of the same ecosystem; e.g., Coelho et al. described the sections of a river [31]. Ludes et al. noted a high concordance between taxa recovered in the drowning medium with lung samples if the location of the drowning was known. Otherwise, the coincidence was not as easy to estimate [27]. The most likely causes are environmental variations, such as the mineral content of water, temperature, stratification of the water, acidity, distance from the shore, depth of the sea and the tide [29]. As a result, several studies have suggested that a local diatom database or diatomological map (D-map), including different types of water during different seasons over a period, might be useful in comparisons [27, 30].

Previous studies have reported that the comparison of the diatom species was sufficient to determine the site in cases in which the quantitative analysis was not so obvious [4, 27]. However, more recent research in animals has suggested that adding a statistical method based on the *Kullback–Leibler (KL) distance* of the samples increased the certainty of the diatom qualitative and quantitative combined analysis. The analysis of samples of plankton, fur, stomach, and

lung allowed for verifying the provenance of the samples successfully to determine the site of immersion between different water systems [28].

Horton et al., using a transfer function approach, compared numerically the diatom assemblage in lung or clothing samples with diatoms in all control samples from the water. If the control samples were the most similar to lung or clothing samples according to a *dissimilarity coefficient*, they likely came from the same place that the drowning occurred [32].

14.1.2.2 Suspects

The aquatic community ecology has suggested other applications for diatoms in forensic investigations, as evident in the aforementioned study because strong similarities among lung, clothing, and control samples became relevant evidence in the resolution of a homicide case [32]. Similarly, it was possible to link suspects in assault and attempted homicide cases with a suburban pond where the events occurred by qualitative diatom analysis of sneakers. There were no significant differences in the proportions of the dominant species in any of the samples examined [33]. In both studies, the unique role that diatom ecology played in linking victims and suspects to a common freshwater source was remarkable.

14.1.2.3 Time of Death

In contrast to the terrestrial environment, in aquatic systems, it has been demonstrated that the algal production, in the form of chlorophyll *a,* can be quantified for the estimation of a postmortem submersion interval (PMSI): the time period for which the body was submerged until to time of discovery [34]. Zimmerman and Wallace developed a semiquantitative approach to estimate PMSI using diatom succession and diversity in aquatic habitats. They observed that, as the stages of decomposition progressed, the numbers of diatom species decreased [35]. Recently, a study raised the possibility of estimating the postmortem interval (PMI) and the place where the body was buried using testate amoebae and soil diatoms. This study referred to the influence of a dead body on the soil microfaunal community in nutrient-poor, sandy landscapes [36].

14.2 Sample Preparation: A Review of Techniques for Diatom Analysis in Forensics

Investigation of bodies recovered from water comprises an important proportion of the medicolegal requests. However, the key question of whether the victim died due to "true" drowning can frequently not be easily solved [6, 11]. In certain cases, the traditional postmortem analyses are not sufficient to determine whether the death was caused by drowning. In these cases, the presence of diatoms in the lungs and/or other organs can be crucial to confirm drowning as the potential cause of death. As mentioned above, diatoms are present in the medium in which the possible drowning occurred, and inhalation of water causes penetration of diatoms into the alveolar system and bloodstream and consequently their deposition in the brain, kidneys, and other organs, such as the bone marrow of large bones. After an autopsy, samples of organs are digested with strong acids, and diatom cells are revealed under the microscope. There is also a blood test for diatom content proposed by Yoshioka and Takahashi [37]. In cases in which the victim was already dead before the body was submerged, the transport of diatom cells to various organs is prevented due to lack of circulation.

Diatom analysis in forensics starts with digestion of tissues from the specific organs to study. Analysis of the lungs is mandatory, but usually, other organs are also studied, such as the liver, kidneys, spleen, brain, and even bone marrow from the femur. There are different methods to perform digestion. The most commonly used ones are acid digestion, acid digestion in disorganization can, Soluene-350 digestion, enzymatic digestion, and the membrane filter method [38].

14.2.1 Acid Digestion Method

This method was a revolution in the history of diatom extraction and is accepted worldwide. It is characterized by its low cost and ease of performing and it provides excellent results. Procedures for acid digestion and diatom isolation have varied among authors [6, 10, 39, 40]. Nevertheless, they are basically modifications of the widely reported method of Pollanen [41]. Today, the standardized method could be described as follows: approximately 5–10 g of tissue or part of the specific organ with its major blood vessels are placed in a boiling flask with concentrated HNO_3 (60–70%). Some authors have used HCl and H_2SO_4 to finish diatom extraction [42]. A boiling flask with the tissue is incubated on a hot plate for 24 h and oxidized with H_2O_2 (30%). $K_2Cr_2O_7$ grains can be added to accelerate the process with additional heating for 3 h. Samples are allowed to cool and to sediment for 24–48 h. Then, samples are transferred into graduated tubes and centrifuged at 3000 rpm for 10–20 min. The supernatant is aspirated without disturbing the pellet at the bottom. The samples can be re-centrifugated again up to four times, adding deionized water [40]. From the final sample, a serial of permanent slides is mounted. The final samples are mounted over a coverslip dried on a slide warmer (50–60 °C).

Chandrasiri described a process prior to the addition of HNO_3 for bone marrow samples: boiling them for 12 h

continuously and examining them every hour [43]. Ago et al. recommended the method of acid digestion with fumed HNO_3 and concentrated H_2SO_4 as effective in cases of drowning in water with a low density of plankton, such as bathing water, swimming pools, and the open sea [44]. In contrast, Diaz-Palma et al. tested H_2SO_4 at high concentrations, but it turned out to be more aggressive with a decrease in the number and diversity of species recovered. Eventually, they proposed the combined use of concentrated H_2O_2 (1–2 ml) and 20% HCl (1–2 ml) to achieve optimal digestion and recovery of diatom species, compared to isolated use of these components. In this manner, H_2O_2 at high temperatures acts as an oxidant, eliminating organic material together with a lower concentration of HCl that is less aggressive in a shorter process [45]. Another modified method from the acid digestion method is proposed by Krstic et al., in which 2 g of tissue sample is treated with H_2O_2 for 24 h. After finishing the oxidation process, H_2SO_4 is added in the amount necessary to complete the oxidation of organic matter [10].

14.2.2 Acid Digestion in Disorganization Can

Li et al. [46] developed a new instrument called "can" to improve the acid digestion procedure. This instrument overcame the shortcomings of traditional acid digestion for the destruction of organic material to make diatom identification easier. The can consists of three parts: a can body, an inner cover, and an outer cover. For destruction procedures, the organic material must be filled with Teflon, rendering the instrument corrosion resistant, heat resistant, pressure resistant, and leak proof. Under a strong acid reaction and high-temperature action, organic tissues can be liquefied for the extraction of diatoms. For example, 3 g of the tissue sample is added to 4 ml of strong nitric acid in this instrument. The can must be placed in a dry box at 102 °C for 100 min. Then, the can is cooled, and the post-digestive liquid is placed in a centrifugation tube. After centrifuging with distilled water, the residue obtained is placed on slides for further analysis.

14.2.3 Soluene-350 Method

In the early 1980s, Fukui et al. proposed a new method for extracting diatoms from human organs by destroying tissues. They tested Soluene, Protosol, and NCS, and among these solubilizers, Soluene was reported as the best one for tissue digestion [47]. With this method, the tissue must be cut into small pieces and subsequently homogenized in distilled water. After centrifugation at 18,000 rpm for 10 mm, the precipitate is suspended in 8 vols of Soluene-350 and then incubated at 50 °C for 2 h and subsequently at room temperature overnight. Following centrifugation at 3000 rpm for 60 min, the precipitate is ready to analyze [48].

14.2.4 Enzymatic Digestion

Ludes et al. designed this method of enzymatic digestion for the diagnosis of putrefied bodies. Tissues are treated with both chemical and enzymatic reagents: buffer Tris-HCl (pH 7.5) and proteinase K [49]. For tissue samples, Ludes et al. cut 10 g of each organ with scissors. Samples were rinsed and mixed with 500 ml of 10 mg/ml proteinase K and 100 ml of 0.01 M Tris-HCl buffer (pH 7.5) containing 2% SDS. The mixture was incubated at 50 °C overnight, 500 ml proteinase K was added, and the solution was diluted with 100 ml of distilled water and centrifuged at 3000 rpm for 15 min, after which the upper layer was removed. The sediment was transferred to a slide and examined under the light microscope [49]. Other authors, such as Taylor and Azparren et al., also suggested using proteinase K for the extraction of diatoms from tissue samples of drowned bodies as a more convenient method in terms of rapidity, safety, and environmental protection than chemical testing [50, 51].

14.2.5 Membrane Filter

Funayama et al. introduced this method for the extraction of diatoms from blood samples and tissue material [52]. With this method, filtration was done using a membrane composed of a nitrocellulose type with a pore size of 5 μm. Five milliliters of blood and 10 ml of 5% sodium dodecyl sulfate (SDS) were mixed and stirred slowly. The resulting hemolysate was filtered through a membrane filter 47 mm in diameter. When blood was putrefied or extremely clotted, the pores of the filter became clogged. In these cases, the filter had to be changed with another one. After filtration, the filters were digested with approximately 10 ml of fuming nitric acid for roughly 10 min. After cooling, this solution was diluted 10–20 times with distilled water. This dilution was filtered through another membrane filter measuring 25 mm in diameter, and this filter was dried and observed under a microscope. While treating tissue samples, the residue obtained by nitric acid digestion was diluted with 150–200 ml of distilled water and filtered through a membrane filter 47 mm in diameter. Fatty material remaining on the filter was digested completely with isopropyl alcohol or petroleum ether alternately. This method was considered very useful for solving problems that disturb microscopic observations, i.e., destruction and loss of diatoms and the appearance of inorganic crystals [38].

14.2.6 Novel Techniques

Seo et al. suggested an improvement over the aforementioned techniques since they used the ability of DNA to bind to diatoms for the direct visualization of diatoms by staining of the bound DNA or indirectly through PCR amplification of the bound DNA [53].

Wang et al. used the Lefort aqua regia digestion method, in comparison with the acid digestion method (concentrated HNO_3 plus 30% H_2O_2), obtaining greater digestive capacity ($p < 0.01$) and comparable diatom recovery [54].

Zhao et al. used a microwave digestion system enriched with vacuum filtration and automatic scanning with SEM at 400× magnification (MD-VF-Auto SEM method). A larger number of diatoms were recovered in samples, such as liver or bone marrow, than with the conventional method of acid digestion (HNO_3 and H_2O_2) with a diatom recovery rate of less than 5% [55]. Subsequently, the previous technique was improved with the addition of a method based on filtration through a membrane with pores of smaller diameter than the length of the diatoms [56]. The combination of both techniques improved the detection sensitivity of diatoms in the lungs (100%) and distant organs, such as the liver and kidney (97%), due to membrane filtration (pore size of 0.45 μm) and SEM techniques [57]. This method avoided the loss of diatoms that occurs due to conventional centrifugation and observation by optical microscopy in the laboratory [58, 59]. To improve the accuracy of the test, it was also recommended that the ratio of numbers of diatoms in the lung tissues to those in the drowning medium samples (L/D) be estimated [57].

14.2.7 Suspect Identification Methods

Uitdehaag et al. attempted to link the suspects to the crime scene by investigating possible contact between a garment and the water surface. For the extraction of diatoms from clothes, they compared the dissolving method (DI), the rinsing with ethanol method (RE), and the rinsing with water method (RW). The first two methods were the most recommended [26].

In addition, suspect identification procedures were also performed by Levin et al., analyzing the transfer and persistence of diatoms in common footwear materials. They compared the hydrogen peroxide (30%) digestion method with a novel extraction technique of heating and agitation with distilled water, and the results did not show great differences, either in the average number of diatoms extracted or in the average proportion of fragmented valves. This new technique could be advantageous in avoiding dangerous reactions of peroxide with some types of fabric (leather, rubber, and polyurethane) [60].

14.2.8 Evaluation of Methods for Extracting Diatoms in Tissues

A common recommendation in the reviewed works is that all of the materials (gloves, filters, etc.) and reagents must be carefully treated to avoid contamination. Other materials (surgical instruments, containers, tubes, etc.) should be washed with double distilled water [28, 49, 61] or deionized water and dried in an autoclave [43].

Different works have compared the validity and usefulness of the different digestion methods mentioned above. Ludes et al. compared the chemical digestion method (concentrated HNO_3 and 130% H_2O_2), enzymatic method (proteinase K and SDS 2%), and tissue incineration technique (80 °C for 2 h + 200 °C 8 h + 550 °C 8 h and acid digestion from the ashes) [49]. In the same way, other authors [58, 59, 62] concluded that the method of enzymatic digestion with proteinase K was the most adequate in terms of speed and efficiency since the number of diatoms found was similar to that with the acid digestion method. However, it requires a considerable number of diatoms in the immersion medium, so its sensitivity decreases in closed organs other than the lungs, where the number of diatoms found is much smaller [63]. It is considered a less dangerous and polluting method since it does not require the use of strong acids [24, 62]. Similarly, Ming et al. recovered a higher percentage of marine and freshwater diatoms (91.4% and 85.6%, respectively) with the proteinase K method, although better results were obtained in terms of digestive capacity and dissolution of organic tissues with HNO_3 in the disorganization can, especially in bone marrow [62]. To improve the results, several studies have recommended completing the digestion process with HCl for complete dissolution of the tissue remnants [63] or adding H_2O_2 for the removal of foreign bodies resulting from smoking or air pollution [64].

In the experiments of Ming et al., the demanded times for the different methods to digest the same tissue ranked from the longest to the shortest were as follows: Soluene-350, proteinase K, acid digestion, and acid digestion in the disorganization can. The disorganization can method and acid digestion method digested the tissues more thoroughly than the proteinase K and Soluene-350 methods. For *Cyclotella sp.* and *Cybella sp.* diatoms, the proteinase K method reclaimed the most diatoms, and the acid digestion method reclaimed fewer, while the disorganization can and Soluene-350 methods reclaimed the fewest. For *Navicula sp.*, the majority of diatoms could be extracted using the proteinase K method but only a few diatoms with the other three methods [62].

Different diatoms (in fresh water or seawater) have different resistances to different digestive reagents. As far as the reliability and applicability of the diatom test are concerned, the proteinase K method is the best choice; nevertheless, acid

digestion (nitric acid + hydrogen peroxide) can substitute for it. Sidari et al. reported that the siliceous frustules of seawater diatoms are solubilized by Soluene-350, while those of freshwater diatoms are resistant to the treatment, so Soluene-350 is not recommended to be used for extracting seawater diatoms [48].

14.3 Diatom Analysis

14.3.1 Diatom Identification

For diatom identification, sections 4–6 mm thick from the tissue samples must be obtained and stained. For light microscopy, the usual dyes are haematoxylin and eosin [40]; also, potassium permanganate and oxalic acid are frequently used to discolor the sample [10]. The optical microscope magnification must be 40× for diatom counting and 100× magnification for diatom identification (Fig. 14.1).

Keys for diatoms identification are widely available in books describing each geographic area's main species [65–69], as well as on the web, i.e., https://diatoms.org/; http://www.br.fgov.be/RESEARCH/EDITION/keydiato_BR.html.

Under scanning electron microscopy (SEM), the structure of diatoms remained almost perfect after digestion with proteinase K but it was destroyed to some extent with other methods. Regarding the preparation of diatom slides for SEM analysis, Torre et al. [70], and Torre and Varetto [71] described the treatment of tissue samples: 0.1 M phosphate-buffered solution (pH 7.4) was used to wash the tissue samples, and this solution was fixed in 2.5% glutaraldehyde for approximately 4 h. After a second washing with the same buffer, the samples were dehydrated using graded alcohol series and then dipped in amyl acetate. The completely dried specimens had to be finally gold coated for analysis under the SEM.

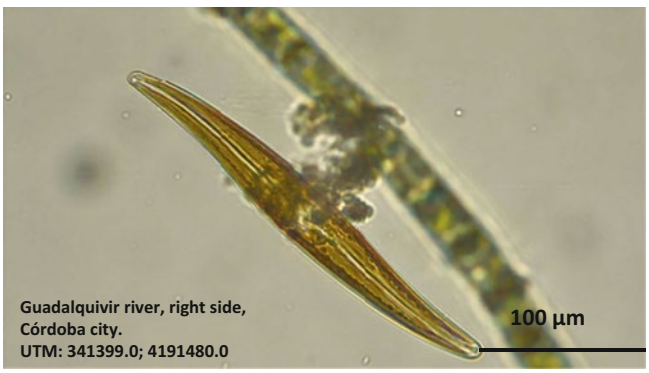

Fig. 14.1 *Gyrosigma attenuatum* (Kütz). Rabenh

14.3.2 Water Analysis

Diatom analysis has been proved to provide supportive evidence of drowning, but the reliability and applicability of quantitative and qualitative diatom analysis in the diagnosis of drowning must be confirmed by the development of a parallel water monitoring system based on algae [27, 72]. The determination of qualitative diatom composition in victims' organs and the surface of the body (or in the environment where the body was found) enables valuable conclusions regarding the possible place of drowning and is sometimes the only valid approach for determining the time of death. Moreover, in suspect drowning cases, during the lifting of the body, a sample of water must be obtained for complete biological and chemical analysis, including diatoms. The qualitative and quantitative diatom results can be compared with those obtained from the corpse to establish a better diagnosis. If this analysis is not performed for any reason, one possibility is to revise the diatom records of the nearest place if they are available from the environmental authorities.

The main reason for what diatoms analyses are performed in environmental studies is their great bioindicator values. The diatom quantity and spectrum changes can indicate eutrophication, organic matter increases, salinity, and acidification [73]. The routine analysis of freshwater sites allows forensic botany to have precise data about the diatom composition from potential death scene sites. The variations in diatoms' quantity and composition are mainly influenced by salinity and nutrients, especially P and N. Other factors involved are light, temperature, pH, current speed, and the substrate [74]. Within benthonic algae, diatoms constitute 90% of the periphyton community. They are highly cosmopolitan species, and their ecological requirements are well known for most abundant species and are all the same in different geographical regions [75]. The main advantage of diatom analyses is their good sampling manipulation and conservation. The silica exoskeleton, the *frustule*, has high resistance to heat, acids, and rot, and their morphological characteristics are the basis of diatoms identification. After cell death, the frustules accumulate in the sediment in the bottom of the river/lake, and they can be analyzed in paleolimnological studies.

In fact, in both Europe and the USA, there are water quality programs that regulate and control the phytobenthos regular analyses in both continental and coastal waters (https://www.epa.gov/, http://ec.europa.eu/environment/water/index_en.htm). The term *phytobenthos* refers to all of the autotrophic organisms living on the bottom of the aquatic ecosystems, including macrophytes (aquatic plants), cyanobacteria, macroalgae, and microalgae,

including diatoms. The term *periphyton* describes the microbiotic community living on submerged substrates (hard mineral substrates, aquatic vegetation, etc.). It includes bacteria, fungi, protozoa, and microalgae. In this last group, diatoms are found, and they can be divided into: *epilithon* diatoms, living on rocks; *epiphyton* diatoms, living on plants; and *epiphelon* diatoms, living on sediments.

In all developed countries, the aforementioned government programs have established routine analyses and protocols to determine the quantity and spectrum of diatoms in each environment. These data can be used and compared with those obtained from potentially drowned corpses to establish possible scenarios and timings. It is necessary to point out that, despite the enormous bibliography about the bioindicator capacity of microalgae, most of the literature, legal directives and manuals have been devoted to diatoms, and information about the rest of the microalgae has been scarce. Regarding the protocols for the detection of diatoms in the routine analyses of water quality programs, the environmental water responsible institutions usually describe in their guidelines and manuals the sampling and analysis methods used by them [76–78]. In general, they establish the main concepts, ranges, limits, and standard methodologies currently used.

There has been a wide range of diatom indices (DIs) proposed by different authors [79]. Among the most used are the IPS [80]; the BDI [81]; the CEE [80]; the LMI [82]; the SLA [83]; the EPI-D [84]; and the ROOT [85]. All of them are based on a combination of the relative abundance and the sensitiveness degree (tolerance) of a given group of selected taxa, usually species. Prygiel and Coste [86] and Kelly et al. [87] described and evaluated many of the DIs, revealing the main premise that each index has been developed to be used in a given geographical area, although some of them have broader validity.

Finally, it is quite important to consider the selection of diatom analysis sampling points, both in the environment and forensic analyses. In each body of water, different environmental administrations have fixed sampling control points at which diatom analyses are performed routinely [76, 77]. In general, in the selection of these control points, the following factors must be considered.

- All of the reference sections of the water body must be represented.
- All of the quality degrees must be represented.
- The diatom control points should coincide as far as possible with the rest of the control points of macroinvertebrates, macrophytes, fish, and physicochemical control points.

For the localization of the points, it is recommended to avoid runoff areas and to choose more than one control point long reference sections.

14.3.2.1 Protocols

In general, the standard protocols for diatom identification in water samples include the following aspects: equipment, sampling, sample conservation, sample treatment, diatom identification, and quality control.

Equipment

The standard equipment for benthonic diatom sampling includes wading boots; latex gloves; a hard brush, knife, and hoe; and a fine net Nytal® or Nylon 20 μm pore light network "*aquascope*" to find adequate subtracts. To keep samples, glass bottles are used (125–150 ml) (for phytoplankton). It is recommended that they be transparent and amber in color. In this way, the light sample is protected, and the color can be appreciated to control for discoloration due to sublimation of the preservative (samples with Lugol). Multiparameter testers with temperature sensors, turbidity, conductivity, pH, and dissolved oxygen are used.

Sampling

For the sampling procedure, it is necessary to use a geographical positioning device (GPS) and a permanent pen or marker (or any other method to label the samples). If labels are used, they must be resistant to moisture. Additional instruments for boat sampling include a boat suitable for local conditions with the appropriate safety equipment.

In general, the sampling frequency in the diatom analyses varies from one to four times per year (coinciding with the four seasons). Nevertheless, recent studies performed on European rivers have indicated that diatom communities can reflect changes in water quality within a period of 60 days, indicating the quality of the two previous months [79]. The general recommendation for routine analyses is to perform them twice per year. In case only one analysis is planned, it should be done during summer.

To determine the optimal sampling time, it must be considered that the response of diatoms to water quality changes is faster in warm waters than in colder ones, so the better seasons in the Northern Hemisphere are spring and summer. Moreover, it is recommended to avoid sampling after a strong rainfall event; in fact, it is better to wait approximately 4 weeks after a thunderstorm [76].

Samples' Conservation

Phytoplankton samples should be submitted as soon as possible to one of the following conservation methods.

Live Samples
Keep the samples alive in the dark and in a refrigerator at between 4 and 10 °C. Proceed to cool them gradually to avoid damage to the cells. If the sample contains a high density of organisms and/or organic matter, it is advisable to dilute the sample with water from the place itself before saving it. The maximum conservation time is 12 h.

Preserved Samples
The most commonly used preservatives are a solution of Lugol (at a rate of 0.5 ml per 100 ml of sample) and formaldehyde (2–4%). All of the fixed samples should be kept protected from light and in a cool place (<15 °C).

Sample Treatment
Samples of water must be centrifuged at 2500 rpm for 15 min and diatoms cleaned by incubation in hydrogen peroxide (130 vol%) at 80 °C for 12 h. The solution obtained must cool at room temperature and be centrifuged a second time (2500 rpm for 15 min). The supernatant is decanted and replaced with diatom-free distilled water. The process is repeated three times until the fluid is transparent with a final spin at 3000 rpm to produce a pellet. After removing the supernatant, the sediment is air dried and mounted in Naphrax. Diatom examination can be performed under a light microscope equipped with an immersion objective or using an SEM.

Diatom Identification
In water sampling identification, it is usually sufficient to use an optical microscope with a magnification of 40× for diatoms due to their treatment has less impact on their shape and color. For water diatom identification, the books and web keys cited above can also be used (Sect. 14.3.1). The use of specific keys depends on each geographic area and whether the sample comes from a river, a lake, a swamp, or the sea. It is recommended, as far as possible, to use diatom keys from bodies of water in geographical areas close to the forensic event. Additionally, it could be very helpful to count one's own collection of pictures from the most frequent diatoms of the area to reduce errors identifying foreign taxa. With pictures, a measurement scale, date, and sampling place should be indicated (see Fig. 14.2).

Quality Control
The treatment and the identification of taxa are the main sources of variability in results [86]. The identification errors could be due to the inexperience of the technician or to the taxonomic difficulties of some taxa. For these reasons, it is necessary to rely on trained personnel. Training courses and proficiency testing programs are required. Intercalibration exercises among laboratories are also recommended.

Fig. 14.2 *Navicula salinarum* Grunow

Sampling data must be recorded individually in databases. Original samples and notes must be saved for at least 5 years. The identification data must indicate the technician and key references. The databases must be revised by another person to avoid transcription errors.

14.4 Histological Findings in Drowning

Diatom testing in the investigation of drowning is based on the theory that diatoms are present in the water where the possible drowning occurred, and that active inhalation of water causes penetration of diatoms into the alveolar system and bloodstream and consequently their dissemination throughout the organism. After the rupture of pulmonary capillaries, small diatoms (e.g., *Melsoira sp., Synedra sp., Cyclotella sp., Stephanodiscus sp., Navicula sp., Nitzschia sp., Amphipleura sp.,* and *Fragilaria sp.*) cross from the pulmonary alveoli into the blood circulation, thereby reaching peripheral organs.

The assumption of the capacity of diatoms to penetrate the alveolo-capillary barrier during drowning was finally addressed by Lunetta et al. [88]. Using scanning (SEM) and transmission electron microscopy (TEM), they investigated the interaction of a natural population of diatoms and a unialgal culture of *Phaeodactylum tricornutum* (PT) with the alveolo-capillary barrier in an experimental model of drowning. The SEM analysis allowed for the identification of several diatom species along the whole airways and their close interactions with the alveolar wall. The TEM analysis was more informative and allowed for precise identification of PT cells in alveolar spaces and detection of their phagocytosis by alveolar macrophages. PT penetrated the pulmonary vessels through the thinnest portions of the alveolo-capillary barrier and through the interstitial spaces and was identified in pulmonary capillaries and venules.

However, there are some other opportunities for diatoms to enter the human organism. There have been indications regarding the possibility of diatoms entering into the systemic circulation from atmospheric air, food, and drink [21]. Despite this mode being theoretically possible, there have been no studies to categorically prove or disprove the possibility of entry of diatom frustules into the systemic circulation via the digestive tract.

In any case, after the autopsy of a presumptive drowning case, samples of different organs are digested with strong acids to clear them of organic material, and diatom cells are revealed under the microscope. The organs more commonly used for diatom studies are the lungs, liver, kidneys, brain, spleen, and bone marrow of large bones. These organs are obtained with caution not to cross-contaminate them with water or fluids from the body, usually including the use of separate sets of surgical instruments for the dissection of external and internal organs, as well as washing thoroughly of all excised tissues with diatom-free deionized water before storage. A minimum of 10 g of tissue without any additive is obtained from every organ and is stored in a refrigerator or freezer depending on the time elapsing until analyses. Diatoms can also be observed in formalin-fixed organs [64]. In this particular research, the authors proceeded to the digestion of the formalin-fixed tissue using proteinase K and incubation with hydrogen peroxide to obtain clearer images of diatoms.

Because of the usual procedure for analyzing diatoms, which entails digestion of the tissue to clear the diatoms, there are no histological findings associated with this type of diagnostic test, which is why there are very few images of diatoms in histological preparations surrounded by tissue (Figs. 14.3 and 14.4), although there are many images of diatoms extracted from different organs after the digestion process (see Figs. 14.5 and 14.6).

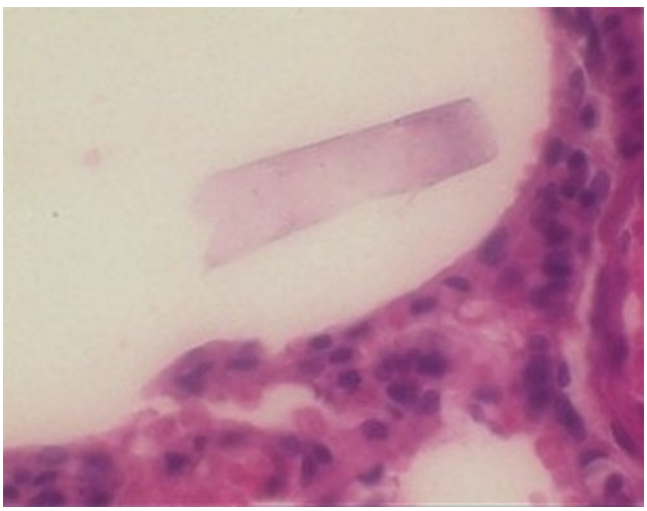

Fig. 14.3 Light microscope photograph of one diatom with rectangular shape (center) in alveolar spaces from a drowned rat (×100)

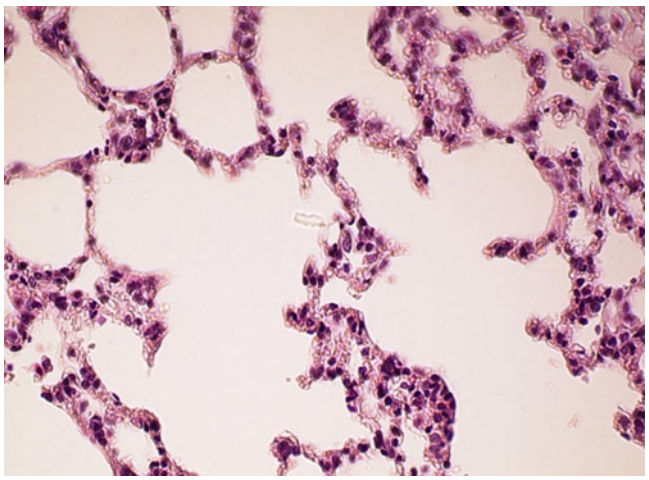

Fig. 14.4 Light microscope photograph of one diatom (center) in alveolar spaces from a drowned rat (×20)

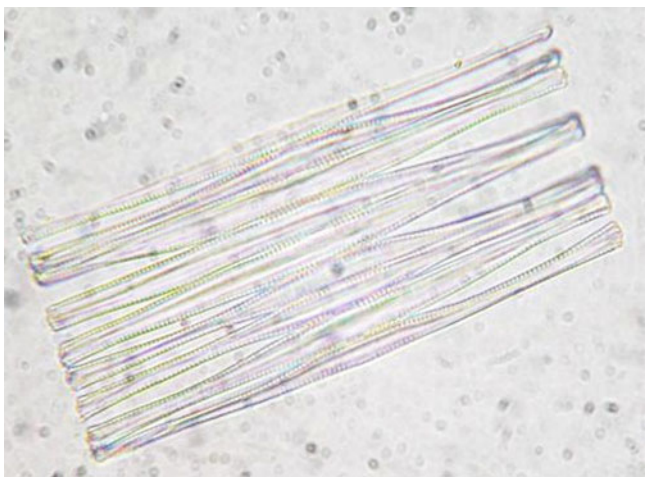

Fig. 14.5 Light microscope photograph of some diatoms (*Fragilaria crotonensis* Kitton) recovered from kidney in drowned human (×100)

Accordingly, what we address in this section are histological findings in drowning. Despite numerous studies, the value of histological investigations into deaths by drowning needs to be considered with caution. As it was previously mentioned, in an autopsy there are no pathognomonic findings to indicate the diagnosis of drowning. The diagnosis is based on the circumstances of the death, plus a variety of nonspecific anatomical findings [89], most of the signs seen in corpses retrieved from water being merely indicative of immersion [6, 8], or alternatively, they can be present also in other causes of death. The histological investigation of drowning-related findings focuses mainly on the lungs and skin. Additionally, histological investigations of injuries and hemorrhages, particularly on the neck and chest wall, have been performed [90].

Fig. 14.6 Light microscope photograph of diatom (*Navicula elegans* W.Smith) recovered from liver in drowned rat (×100)

14.4.1 Skin Histological Findings

Investigations of the epidermis and subepidermal soft tissue were performed mainly to determine the postmortem interval (PMI) in water. Bodies remaining in water give rise to so-called washerwoman's skin: wrinkling and grayish-white discoloration of thick keratin layer areas of the skin without sebaceous glands; i.e., the palms of the hands and soles of the feet.

The following histological signs of water absorption are observed [90]:

- Swelling of the epidermal keratinizing squamous epithelium.
- Detachment of the horny layer.
- Vacuoles appearing in the epithelial cells of the basal germinative layer.
- Cell and nuclear borders of the epidermis gradually disappearing, as with keratohyalin granules.
- With increasing wrinkling, the epidermis detaching from the subepidermal corium.
- The usually thickly layered elastic fibers in subepidermal soft tissue (corium) being affected.

Nevertheless, given the strong variations in water type, temperature, movement, and pollution, as well as variations in victim age and epidermal thickness, histological investigations of the epidermis are unable to make decisive contributions to determining the PMI in water [90].

14.4.2 Lung Histological Findings

In death by drowning, the lungs are the organs most affected by the active inhalation of the drowning medium, most commonly water. From a pathophysiological perspective, death by drowning is asphyxia caused by inhalation of a liquid into the respiratory tract, causing rupture of the pulmonary alveoli and pulmonary capillaries and consequent spread of the drowning medium into the bloodstream. Final strong respiratory efforts lead to the overinflation of lung tissue (emphysema aquosum). White or hemorrhagic oedema fluid (froth) is present in the nostrils, mouth, and airways, which is the usual appearance of the lungs in drowning, also known as "wet lung" or "drowned lung." Some individuals who drown are considered to be victims of "dry drowning." Dry drowning is said to occur in 10–15% of all drownings. Here, the lungs do not have the heavy and oedematous appearance typical of drowning lungs, and the weight of these organs is not increased. Rather, fatal cerebral hypoxia is alleged to be caused by a laryngeal spasm mediated as a vagal reflex with water never entering the lungs. While the aforementioned explanation for dry drowning is interesting, it is a hypothesis and not proven [89].

The following microscopic changes are common in "wet lung" or "drowned lung" [7, 40, 90]:

- Intracellular swelling
- Intra-alveolar oedema
- Emphysema aquosum
- Rupture of terminal air spaces (Fig. 14.7)
- Alveolar dilatation
- Thinning of interalveolar septa
- Congestive pulmonary vessels (Fig. 14.8)
- An inflammatory infiltrate around pulmonary vessels
- A marked increase in alveolar macrophages (Fig. 14.9)

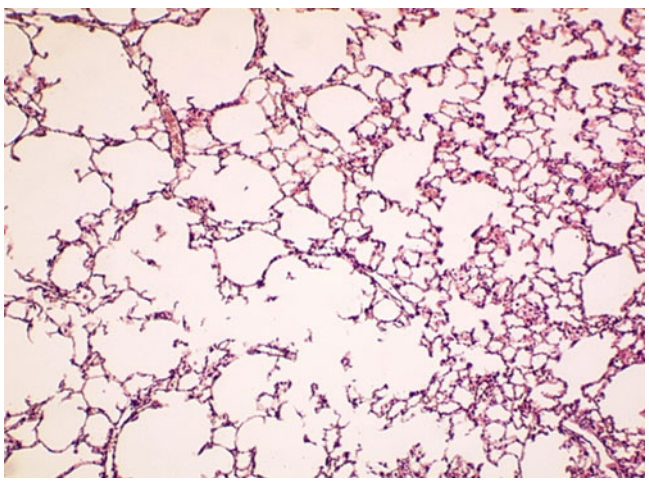

Fig. 14.7 Rupture of terminal air spaces in drowned rat

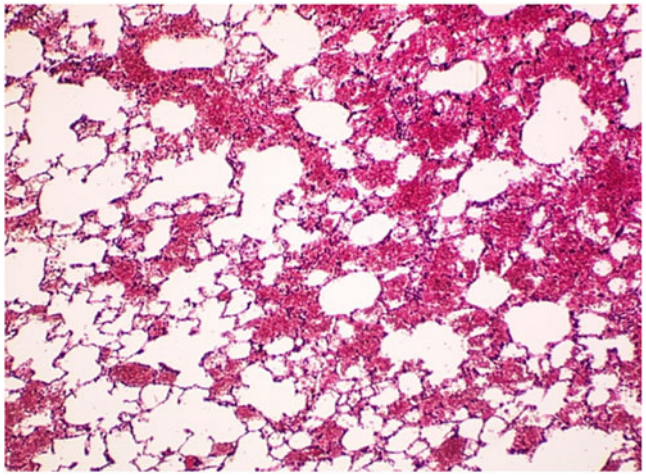

Fig. 14.8 Congestive pulmonary vessels in drowned rat

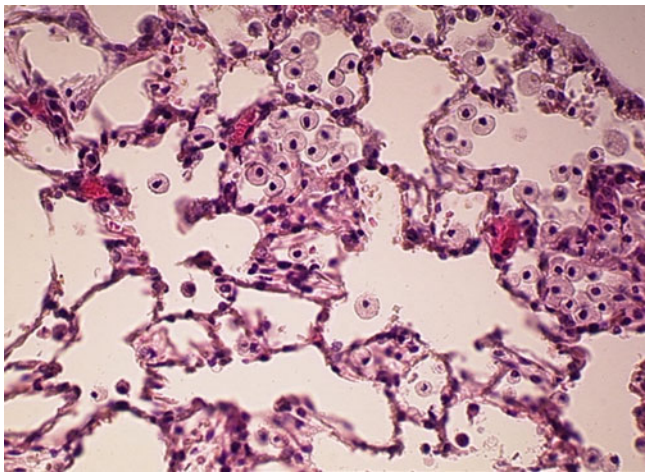

Fig. 14.9 Increase in alveolar macrophages in drowned rat

14.4.3 Muscle Histological Findings

Intramuscular bleeding was reported as the only significant finding in human neck, trunk, and arm muscles in cases of drowning. These hemorrhages have been attributed to agonal convulsions, hypercontraction, and overexertion of the affected muscle groups [91, 92]. Moreover, hemorrhagic changes have been reported in the human sternohyoid during drowning [93]. They are regarded as vital signs because they are likely caused by the extreme strain of the accessory respiratory musculature under strongly forced breathing in the phase of dyspnoea, as well as by the clonicotonic seizures of the subsequent phase of asphyxia under cerebral oxygen deprivation [94]. Nevertheless, the interpretation of hemorrhages in the neck tissues can be controversial. In the absence of trauma in this region, some authors have argued that this bleeding is likely due to hypostasis [91] or the Prinsloo and Gordon artifact (postmortem hemorrhage on the posterior surface of the esophagus) [6].

We started to investigate histological muscle changes during death by drowning after experimental research about diatoms [40], prompted by the unexpected finding of muscle fiber abnormalities in the association of diatoms with drowning in peripheral rat tissue. Our experimental findings in drowned rats [95] indicated that there are histologically evident changes in skeletal muscles after death by drowning. We found scattered evidence of muscle fiber degeneration and muscle fibers containing abnormal deposits of red material and other fibers identified by modified Gomori trichrome staining (MGT) as ragged red (Fig. 14.10). Histochemistry and electron microscopy detected mitochondrial masses, most displaying significant degenerative changes consistent with anoxia (Fig. 14.11). Although not as intense as in the drowning group, similar changes were seen in a group of rats that died of exsanguination, while no alterations were seen in a group of rats that died of cervical dislocation. Microscopic features of these changes suggest two possible mechanisms: intense anoxia, a mechanism common to death by drowning and by exsanguination; and mechanical trauma, found only in death by drowning, linked to intense muscle contractions due to the overstrain involved in forced breathing and in attempting to escape the water. These microscopic changes cannot be considered specific to drowning deaths, but they could help in the diagnosis of drowning, in conjunction with the investigation of the circumstances of death and other complementary tests.

Currently, we are still researching this topic, attempting to prove that these changes also occur in humans by studying histological sections of several muscles (diaphragm, pectoral, and psoas) from three different types of death: drowning, hanging, and sudden cardiac death. In drowning deaths we have observed granular muscle fibers and muscle fibers with basophilic clumps, which correspond to ragged-red fibers by using MGT staining (unpublished results).

14.5 Discussion and Conclusions

14.5.1 Main Controversies of Diatom Test

14.5.1.1 False Positives

The main controversy of this test in the diagnosis of drowning is the lack of specificity due to the finding of diatoms in the different organs of individuals found in water but who died of causes other than drowning [4, 96] This phenomenon occurs because diatoms are very ubiquitous organisms widely distributed in the environment, soil, water supply, food, and even air [6]. Previous research has suggested that the entrance of diatoms into a living organism can occur through different pathways, such as air, drink, or food [10, 21], and they could accumulate in the organs over years [22]. However, further blood dissemination of diatoms to peripheral organs because of inhalation in vivo has been

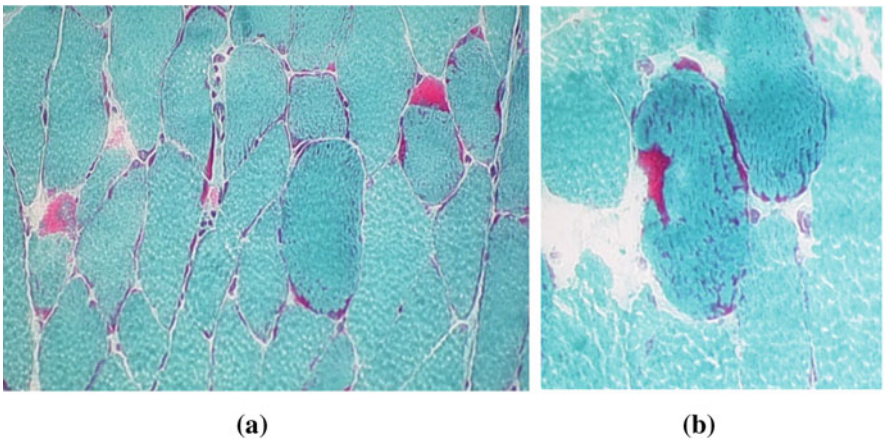

Fig. 14.10 Muscle fibers (Anterior tibial muscle) with reddish clusters (**a**) and a typical ragged-red fiber (**b**). Modified Gomori trichrome staining (MGT)

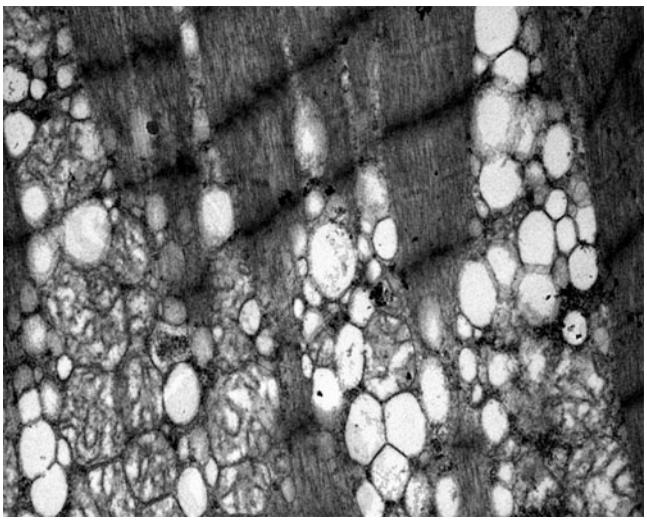

Fig. 14.11 Diaphragm muscle in a drowned rat. Massive accumulation of degenerative mitochondria showing vacuolization and swelling. TEM

considered controversial and unlikely [96]. The ingestion or repeated inhalation of water in swimmers or professional divers [50, 97] and penetration of the transplacental barrier [61] have also been described as possible antemortem contamination source [97]. Furthermore, Yen and Jayaprakash analyzed different cooked foods (chicken, anchovies, fish, and shellfish) and estimated that a person accustomed to eating prawns and cooked clams could ingest approximately 2 million diatoms in a single year [22]. A study performed on not-drowned fish-eating animals (otters) showed diatoms in their organs determining possible antemortem contamination [98]. According to Saukko and Knight, it has not been possible to demonstrate that the diatoms contained in seafood cannot pass through the gastrointestinal barrier, accessing the bloodstream and thus the rest of the tissues and organs [6]. Thus, if this type of food is specifically found in the gastric contents, it is recommended to be cautious when establishing drowning as a cause of death [42].

Similarly, it is well established from a variety of studies that the postmortem penetration by diatoms of a corpse might be due to other circumstances. The prolonged immersion of a body in water favors the advance of putrefactive phenomena in the tissues, allowing for contact between the organs and water and the consequent entrance of diatoms [10]. The decomposition process is very variable depending on several factors, including: "temperature, depth of water, currents, tides, season, dissolved oxygen, sedimentation, geology, salinity, acidity, interactions between chemical and physical processes, and activity of insects and carrion" [99]. Fucci et al. found a small number of diatoms in non-drowned animals with blunt trauma and gunshot injuries [98]. This finding also agrees with Lin et al.'s observation [100], which analyzed sphenoid sinus fluid and lung tissue and demonstrated the presence of a large number of diatoms in corpses that presented stab wounds or an advanced state of decomposition (2 of 100 cases). Di Giancamillo et al. found diatoms in isolated samples from the heart, lungs, skin, and muscle from piglet carcasses immersed in water at different stages of decomposition [101]. Moreover, it was shown that diatoms penetrate the alveolar-capillary barrier in an earlier postmortem period since active transport by pneumonocytes and alveolar macrophages continue to occur for a short period of time, even after death [24]. In this regard, several lines of evidence have also indicated a role for the difference in hydrostatic pressure, along with the relaxation of muscles [27, 100].

Lunetta et al. conducted a series of trials in which they injected a diatom-enriched solution into cadavers that died of causes other than drowning, not finding positive results in closed organs other than the lungs: the brain, kidney, liver, bone marrow, or fluids, such as peritoneal fluid [96]. They also analyzed under standardized methods the diatom content in several organs of 14 non-drowned human bodies and found only 9 diatoms in 6 of the 14 non-drowned bodies, concluding that the issue of potential false-positive tests should not be an a priori impediment to diatom testing

provided that the cutoff value actually considered diagnostic for drowning (20 diatoms per sample) is much higher than these values.

Postmortem contamination during the exhumation of a corpse [61] or of the tissues and organ samples in autopsy could also be potential gateways for diatoms because it is generally accepted that instruments, gloves, paper, water supplies, reagents, and tap water can contain diatoms [21]. However, lack of specificity was denied by Bortolotti et al., who did not find diatoms in the organs of 45 cadavers that died of causes other than drowning [59]. They stated that the occurrence of false positives could be ascribed to contamination during an autopsy, sample collection, and/or sample treatment. Therefore, it is recommended that extreme precautions be taken in the handling of the samples and the cleaning materials used [4, 10, 24, 40, 56, 59, 96].

14.5.1.2 False Negatives

Regarding arguments against diatom testing, another criticism is low sensitivity due to the absence of diatoms detected in subjects who died by drowning [4]. Thus, it has been demonstrated that a rapid death makes difficult or even prevents the entry of diatoms into the circulatory system and organs [10, 21, 100]. Furthermore, in relation to extraction procedures for diatoms in samples, it has also been postulated that very aggressive methods (especially methods of digestion by strong acids or Soluene-350) can destroy the diatoms present in the tissues [10, 11, 40]. In contrast, deficient processing of the sample can result in obscuring the identification and counting of diatoms on microscope slides; thus, adequate enzymatic and chemical digestion (concentrated H_2O_2 + HCl 20%) of the samples is recommended [45, 96]. Another aspect to consider is that diatom examination in the tissues requires a specialized and detailed analysis, so the collaboration of a specialist in algae is required for appropriate results [24, 27].

The amount of tissue also has an influence on sensitivity because, if it is scarce, the concentration of diatoms will be lower and more difficult to detect [49, 56, 96]. Hürlimann et al. recommended 10–20 g of lung tissue (3–4 pieces), 20 ml of blood (without additives) from the left atrium and/or pulmonary vein, 250 g of the right lobe of the liver, 10–15 cm of the femur diaphysis, and 1000 ml of water from the surface of the suspected drowning site [24].

Conversely, negative results have also been related to inadequate sampling far from the site of diatom sedimentation [96]. Lin et al. connected this result to simple sampling from the lower lung lobe—the furthest point that inhaled water can reach [100]. Other circumstances were described by Aghayev et al. in a case of drowning confirmed by autopsy findings, in which a ruptured aorta led to the presence of a small number of diatoms only in lung tissue and blood from the left heart [102].

The most important fact in this regard is the concentration of diatoms in the drowning medium. It has been reported that the diatom test can provide evidence of drowning when there are a considerable number of diatoms in the water that can be disseminated into the bloodstream. Several studies have shown that, if drowning occurs in a medium with few or no diatoms, the concentration of them in the organs will be low or absent [10, 15]. Therefore, a negative result does not exclude the diagnosis of death by aspiration in all cases [21]. In this sense, more recent studies, such as 16S rDNA fragment analysis or bacterioplankton detected by PCR, have been postulated as additional confirmation methods in these cases [15, 17].

It has also been reported that diatom quantification varies according to the location, the tides, the depth, and the salinity of the water, with a greater number in fresh water [11, 40, 62, 100, 103]. Lin et al. found the presence of diatoms in 81.1% of seawater drowning cases, compared to 100% of freshwater cases, with a greater number in the latter [100]. In an experiment performed in rats, smaller sizes and numbers of diatoms were recorded in seawater tissues, compared to river or lake tissues [40]. This phenomenon has been associated with thinner siliceous walls, which render seawater diatoms less resistant to treatments such as acid digestion [40]. Conversely, the size is a determining factor since large freshwater diatoms sink before reaching the sea [103, 104]. Moreover, the number of diatoms less than 20 μm length can be transported to closed organs and bone marrow [24]; therefore, it will be constantly altered by the tides, the state of the river, and the seasonal climatic variations [104]. In this regard, diatom populations also vary seasonally. In the early spring, they expand in fresh water. After this expansion, the live diatoms decrease, but a large number of dead diatoms remain in summer water. In the fall, a second expansion of diatoms occurs and then progressively decreases during the winter months [105].

Death by drowning in treated water, such as spas, swimming pools, or bathtubs, deserves special consideration. It has been reported that the diatom test is unreliable in these waters due to the small number of unicellular algae, making it difficult to detect them [21]. Pollanen et al. highlighted the low sensitivity of diatom testing in their sample drowning series; only 28% of fresh water drownings and 10% of bathtub drownings yielded positive test results [41]. Lin et al. analyzed 10 cases of deaths by drowning in bath water, spas, pools, and a reservoir, in which only 4 cases were found, and 1–3 diatoms in samples of lung tissue and sphenoid sinus fluid were identified. The possibility was proposed that, in the samples in which tap water had been treated, the presence or absence of diatoms would depend on the water purification process [100]. These results are similar to those of Muccino et al., who found diatoms in only 28.6% of drowning victims in bathtubs (4/14) [106]. A previous study suggested that,

when bath water contains a considerable amount of plankton (16.3/100 ml water), diatom testing can be useful in the diagnosis of ambiguous cases of drowning in bathwater deaths. For this purpose, it was considered necessary to examine and compare all pulmonary lobes, at least four distant organs (kidneys, liver, and spleen) and a water sample from the bathtub [44]. In one of the cases with large numbers of diatoms, bathtub water presented a higher concentration (>16.3/100 ml), although less than natural water rich in diatoms. No diatoms were found in the remaining organs. However, drowning was concluded as the cause of death, so it should also be emphasized that careful consideration of the autopsy findings is a prerequisite condition for diagnosis, particularly in cases of death in bath water [44].

14.5.2 Quantitative and Qualitative Analysis

Several lines of evidence suggest that a qualitative and quantitative analysis is necessary in different tissues and drowning media to verify the results [4]. The qualitative and quantitative distributions of the diatoms in the samples will depend on the number of diatoms and the species and dimensions of the diatoms in the drowning medium, as well as the filtration from the lungs to the blood and other tissues [24].

14.5.2.1 Quantitative Analysis

Quantitative criteria are employed to exclude cases of postmortem tissue contamination by algae due to passive transfer of water to the lungs or other organs after death. It is recommended to calculate *diatom density* according to the total number of diatoms per gram of tissue or organ since, in some cases, it is the only reliable differential analysis for the diagnosis of drowning [10]. Uchiyama et al. referred to Hürlimann et al.'s values to establish positive results [15]. *Diatom density* is based on separation values and maximum values in ranges (diatoms by 5 g, depending on the tissue), considering that only the separation values were inaccurate (see Table 14.1) [24].

Subsequently, several authors considered positive samples of organs with at least 10 diatoms per microscope slide [100, 106]. In contrast, Lunetta et al. established that the diagnosis of drowning can be made when more than 20 diatoms/microscope slide is found in the lungs [96]. Ludes et al. considered a positive test with more than 20 diatom frustules/10 g of lung tissue (100 ml of sediment obtained by enzymatic digestion) and more than 5 diatom frustules/10 g of other organs (brain, liver, kidney, bone marrow), but they also recommended a qualitative diatom identification [49, 98].

Zhao et al. used a ratio of the number of diatoms in lung (L) tissue to that in drowning (D) medium samples: the *L/D ratio*. It presents a specificity of 1 with high values (>2), indicating a greater probability of cause of death by drowning than postmortem immersion [56]. Badu et al. established a cutoff value slightly different from other studies because of the smaller mass (3 g) and volume (50 ml) of the sample used. They considered a positive count of 4 diatoms/50 ml in the lungs (specificity: 78%) and 1 diatom/50 ml in the remaining organs (specificity: 100%), finding a very low number of diatoms and only in the lungs in control rats [40].

Table 14.1 Diatom density

Ranges[a]	Separation values[b]	Maximum values[b]
Lungs	200–400	54–108
Liver	10–20	92–184
Kidney	4–8	22–44
Bone marrow	20–40	30–60

Table adapted from Hürlimann et al. [24]
[a]Diatoms/5 g
[b]It should be included all diatom units and fragments

14.5.2.2 Qualitative Analysis

Qualitative analysis is used to verify that diatoms extracted from the organs are not due to exogenous or laboratory contamination. Diatoms vary from location to location, so comparing those found on the victim's clothing or in the organs with those from a body of water might be useful for the location of the place of drowning or even the primary crime scene. A complete taxonomic study requires a comparative study of the diatoms recovered from the tissues/organs of the drowned body and the diatoms present in the water where the body was found [27, 62]. For this purpose, it should be borne in mind that these algae are widely distributed in aquatic environments at the generic level, but at the level of species, they have close tolerances for environmental factors, such as salinity, water temperature, and pH [32]. For example, several diatom species are unique to freshwater and saltwater environments with concentrations affected by inherent water conditions [7]. In addition, the important seasonal climatic variations should be considered, so extensive water sampling is required at the suspected drowning site, at different times and depths [4]. It is recommended to obtain samples in winter, spring, summer, and autumn for more reliable environmental information. If such collection is not possible, winter sampling is the most appropriate [32].

Another significant aspect is the size of the valves since larger ones will only reach the lungs, stomach, and duodenum during drowning, while smaller ones can reach the rest of the organs and bone marrow without difficulty. The presence of very large valves or fragments (>40 μm) in bone marrow could indicate the intake of antemortem diatoms through the gastrointestinal wall or postmortem contamination [24].

Assessment of taxonomic diversity is another factor to consider [4, 27, 62]. A good taxonomic (and quantitative) correspondence between the diatoms extracted from the organs and those from environmental samples allow for establishing with a high probability the diagnosis of drowning [106]. Hürlimann et al. recommended the identification of species for each valve or fragments at the lowest possible identification level, usually the species or variety level. It has been reported that, in samples with large numbers of diatoms (drowning medium, lungs, and stomach content), the identification of 500 valves or diatom fragments is sufficient to characterize a community of diatoms. In samples with low density (blood, liver, kidneys, and bone marrow), all of the valves present on the microscopic slide must be identified [24].

Exogenous contamination with the same type of diatom species involved in drowning is unlikely, although there are wide seasonal and regional variations in the same type of diatom [4]. Pachar and Cameron determined as a positive diagnosis of drowning the presence of a significant number of diatoms but with similar genera greater than a minimum limit established in lungs and closed organs. In cases of a limited number of different diatom species in the control samples recovered at a particular site, any number of diatoms found in submerged bodies, if exceeding this limit, can be considered a positive case of death by drowning [21].

Horton described a case study of a boy who was found floating face down in a pond. The pathologist attributed the death to fresh water drowning and concluded that it was not suspicious. However, the case was reopened because it was thought the drowning might have been homicide by the child's mother. It was suggested that drowning occurred in a domestic bath, and the body was subsequently placed in the pond. Thus, investigators collected 14 samples for diatom analysis from the artificial pond and two samples of sediment from the center of the pond to act as a control in the examination of diatom assemblages associated with three lung tissue samples. The results suggested that two of three lung samples showed a statistically significant relationship to samples from the pond, indicating that the pond was the location of drowning and excluding the mother as a suspect of homicide [107]. Other case studies examples on the use of diatoms or other microalgae have been described in [108].

14.5.3 Conclusions

The autopsy findings in drowning cases are often characteristic but are not pathognomonic, so they must be interpreted in the context of the concrete circumstances of death. Among the several tests proposed for the confirmation of the real cause of death, the diatom method represents one of the most valid for detecting the cause and place of drowning, if conducted properly with the maximal exclusion of possible mistakes.

Contamination should be avoided as much as possible; all the materials (gloves, filters, etc.) and reagents must be carefully treated to avoid contamination. Other materials (surgical instruments, containers, tubes, etc.) should be washed with double distilled water or deionized water and dried in an autoclave. The tissues used should be adequate, obtaining sufficient amounts of the organs, and with caution applied to avoid contaminating them. Lungs should always be assessed for diatoms, together with other closed organs. Alternative, less-harsh extraction techniques (e.g., enzymatic digestion) should be used to analyze seawater diatoms.

Quantitative and qualitative diatom analysis can provide strong evidence of death due to aspiration of water. Analyses of diatom cells in organs should have quantitative figures (i.e., total number of diatom cells per gram tissue or organ) and in some cases are the only reliable differential analyses for final decisions about the diagnosis of drowning, provided that a good taxonomic correspondence exists between the diatoms extracted from the organs and from the environmental samples. A large number of these diatoms must enter into the circulation during the drowning process and reach the closed organs, from whence they can be recovered.

This method provides evidence of drowning only when there is a considerable number of diatoms present in the immersion medium, but a negative result does not exclude death by aspiration of water. When a putrefied body or human remains are found in water, results of diatom testing should be considered unreliable due to potential contamination in these circumstances.

Analysis of diatoms can also be used to assess the place of drowning and to link the suspects to the crime scene by investigating possible contact between a garment and the surface of the water.

Preliminary qualitative diatom analysis can be attempted by nonexperts. However, the definitive qualitative interpretation of the results and therefore the diagnosis of death by aspiration of water, if relying on diatom testing, require the assessment of an expert diatomist.

References

1. Mejdandzic, M., Bosak, S., Nakov, T., Ruck, E., Orlic, S., Gligora Udovic, M., et al.: Morphological diversity and phylogeny of the diatom genus Entomoneis (Bacillariophyta) in marine plankton: six new species from the Adriatic Sea. J. Phycol. **54**(2), 275–298 (2018)
2. Jamali, A.A., Akbari, F., Ghorakhlu, M.M., de la Guardia, M., Yari Khosroushahi, A.: Applications of diatoms as potential microalgae in nanobiotechnology. Bioimpacts. **2**(2), 83–89 (2012)

3. Sackett, O., Petrou, K., Reedy, B., Hill, R., Doblin, M., Beardall, J., et al.: Snapshot prediction of carbon productivity, carbon and protein content in a Southern Ocean diatom using FTIR spectroscopy. ISME J. **10**(2), 416–426 (2016)
4. Pollanen, M.S.: Diatoms and homicide. Forensic Sci. Int. **91**(1), 29–34 (1998)
5. World Health Organization WHO. Drowning. http://www.who.int/news-room/fact-sheets/detail/drowning (2018)
6. Saukko, P., Knight, B.: Immersion deaths. In: Saukko, P., Knight, B. (eds.) Knight's Forensic Pathology, pp. 395–411. Arnold, London (2004)
7. Armstrong, E.J., Erskine, K.L.: Investigation of drowning deaths: a practical review. Acad. Forensic Pathol. **8**(1), 8–43 (2018)
8. Byard, R.W.: Immersion deaths and drowning: issues arising in the investigation of bodies recovered from water. Forensic Sci. Med. Pathol. **11**(3), 323–325 (2015)
9. Gruspier, K.L., Pollanen, M.S.: Limbs found in water: investigation using anthropological analysis and the diatom test. Forensic Sci. Int. **112**(1), 1–9 (2000)
10. Krstic, S., Duma, A., Janevska, B., Levkov, Z., Nikolova, K., Noveska, M.: Diatoms in forensic expertise of drowning–a Macedonian experience. Forensic Sci. Int. **127**(3), 198–203 (2002)
11. Piette, M.H., De Letter, E.A.: Drowning: still a difficult autopsy diagnosis. Forensic Sci. Int. **163**(1–2), 1–9 (2006)
12. Esiyok, B., Balci, Y., Ozbay, M.: Bodies recovered from wells, sewerage systems and pits: what is the cause of death? Ann. Acad. Med. Singap. **35**(8), 547–551 (2006)
13. Azparren, J., de la Rosa, I., Sancho, M.: Biventricular measurement of blood strontium in real cases of drowning. Forensic Sci. Int. **69**(2), 139–148 (1994)
14. Perez-Carceles, M.D., del Pozo, S., Sibon, A., Noguera, J.A., Osuna, E., Vizcaya, M.A., et al.: Serum biochemical markers in drowning: diagnostic efficacy of Strontium and other trace elements. Forensic Sci. Int. **214**(1–3), 159–166 (2012)
15. Uchiyama, T., Kakizaki, E., Kozawa, S., Nishida, S., Imamura, N., Yukawa, N.: A new molecular approach to help conclude drowning as a cause of death: simultaneous detection of eight bacterioplankton species using real-time PCR assays with TaqMan probes. Forensic Sci. Int. **222**(1–3), 11–26 (2012)
16. Filograna, L., Tartaglione, T., Vetrugno, G., Guerra, C., Fileni, A., Bonomo, L.: Freshwater drowning in a child: a case study demonstrating the role of post-mortem computed tomography. Med. Sci. Law. **55**(4), 304–311 (2015)
17. Idota, N., Tsuboi, H., Takaso, M., Tojo, M., Kinebuchi, T., Nakamura, M., et al.: Comparison between temperature gradient gel electrophoresis of bacterial 16S rDNA and diatom test for diagnosis of drowning. J. Forensic Sci. **63**(3), 752–757 (2018)
18. Schellmann, B., Sperl, W.: Diatomeen Nachweis im Knochenmark (Femur) Nichtertrunkener. Z Rechtsmed. **83**, 319–324 (1979)
19. Foged, N.: Diatoms and drowning–once more. Forensic Sci. Int. **21**(2), 153–159 (1983)
20. Peabody, A.J.: Diatoms and drowning–a review. Med. Sci. Law. **20**(4), 254–261 (1980)
21. Pachar, J.V., Cameron, J.M.: The diagnosis of drowning by quantitative and qualitative diatom analysis. Med. Sci. Law. **33**(4), 291–299 (1993)
22. Yen, L.Y., Jayaprakash, P.T.: Prevalence of diatom frustules in non-vegetarian foodstuffs and its implications in interpreting identification of diatom frustules in drowning cases. Forensic Sci. Int. **170**(1), 1–7 (2007)
23. Geertinger, P., Voigt, J.: Death in the bath. A survey of bathtub deaths in Copenhagen, Denmark, and Gothenburg, Sweden, from 1961 to 1969. J. Forensic Med. **17**(4), 136–147 (1970)
24. Hurlimann, J., Feer, P., Elber, F., Niederberger, K., Dirnhofer, R., Wyler, D.: Diatom detection in the diagnosis of death by drowning. Int. J. Legal Med. **114**(1–2), 6–14 (2000)
25. Zhao, Y., Chen, X., Yang, Y., Zhao, X., Zhang, S., Gao, Z., et al.: Potential forensic biogeographic application of diatom colony consistency analysis employing pyrosequencing profiles of the 18S rDNA V7 region. Int. J. Legal Med. (2018)
26. Uitdehaag, S., Dragutinovic, A., Kuiper, I.: Extraction of diatoms from (cotton) clothing for forensic comparisons. Forensic Sci. Int. **200**(1–3), 112–116 (2010)
27. Ludes, B., Coste, M., North, N., Doray, S., Tracqui, A., Kintz, P.: Diatom analysis in victim's tissues as an indicator of the site of drowning. Int. J. Legal Med. **112**(3), 163–166 (1999)
28. Carballeira, R., Vieira, D.N., Febrero-Bande, M., Munoz Barus, J.I.: A valid method to determine the site of drowning. Int. J. Legal Med. **132**(2), 487–497 (2018)
29. Thakar, M.K., Singh, R.: Diatomological mapping of water bodies for the diagnosis of drowning cases. J. Forensic Legal Med. **17**(1), 18–25 (2010)
30. Saini, E., Khanagwal, V.P., Singh, R.: A systematic databasing of diatoms from different geographical localities and sites of Haryana for advancing validation of forensic diatomology. Data Brief. **10**, 63–68 (2017)
31. Coelho, S., Ramos, P., Ribeiro, C., Marques, J., Santos, A.: Contribution to the determination of the place of death by drowning – a study of diatoms' biodiversity in Douro river estuary. J. Forensic Legal Med. **41**, 58–64 (2016)
32. Horton, B.P., Boreham, S., Hillier, C.: The development and application of a diatom-based quantitative reconstruction technique in forensic science. J. Forensic Sci. **51**(3), 643–650 (2006)
33. Siver, P.A., Lord, W.D., McCarthy, D.J.: Forensic Limnology – the use of fresh-water algal community ecology to link suspects to an aquatic crime scene in Southern New-England. J. Forensic Sci. **39**(3), 847–853 (1994)
34. Casamatta, D.A., Verb, R.G.: Algal colonization of submerged carcasses in a mid-order woodland stream. J. Forensic Sci. **45**(6), 1280–1285 (2000)
35. Zimmerman, K.A., Wallace, J.R.: The potential to determine a postmortem submersion interval based on algal/diatom diversity on decomposing mammalian carcasses in brackish ponds in Delaware. J. Forensic Sci. **53**(4), 935–941 (2008)
36. Wanner, M., Betker, E., Shimano, S., Krawczynski, R.: Are soil testate amoebae and diatoms useful for forensics? Forensic Sci. Int. **289**, 223–231 (2018)
37. Yoshioka, N., Takahashi, K.: Demonstration of diatoms in heart blood. Res. Pract. Forensic Med. **29**, 57–61 (1986)
38. Singh, R., Singh, R., Thakar, M.K.: Extraction methods of diatoms-a review. Ind. Internet J. Forensic Med. Toxicol. **4**(2), (2006)
39. Auer, A., Mottonen, M.: Diatoms and drowning. Z. Rechtsmed. **101**(2), 87–98 (1988)
40. Badu, I.K., Girela, E., Beltran, C.M., Ruz-Caracuel, I., Jimena, I.: Diatoms in forensic analysis: a practical approach in rats. Med. Sci. Law. **55**(3), 228–235 (2015)
41. Pollanen, M.S., Cheung, C., Chiasson, D.A.: The diagnostic value of the diatom test for drowning, I. Utility: a retrospective analysis of 771 cases of drowning in Ontario, Canada. J. Forensic Sci. **42**(2), 281–285 (1997)
42. Peabody, A.J.: Diatoms in forensic science. J. Forensic Sci. Soc. **17**(2–3), 81–87 (1978)
43. Chandrasiri, N.: Detection of diatoms in the marrow of thigh bones as evidence of death by drowning. Ceylon Med. J. **46**(4), 145–146 (2001)

44. Ago, K., Hayashi, T., Ago, M., Ogata, M.: The number of diatoms recovered from the lungs and other organs in drowning deaths in bathwater. Legal Med. (Tokyo). **13**(4), 186–190 (2011)
45. Diaz-Palma, P.A., Alucema, A., Hayashida, G., Maidana, N.I.: Development and standardization of a microalgae test for determining deaths by drowning. Forensic Sci. Int. **184**(1–3), 37–41 (2009)
46. Li, Y.G., Hu, C.Y., Wang, C.X., Wang, X.: Development of can for destruction of organic material in use for forensic diatom examination. Forensic Sci. Int. **101**(3), 163–166 (1999)
47. Fukui, Y., Hata, M., Takahashi, S., Matsubara, K.: A new method for detecting diatoms in human organs. Forensic Sci. Int. **16**(1), 67–74 (1980)
48. Sidari, L., Di Nunno, N., Costantinides, F., Melato, M.: Diatom test with Soluene-350 to diagnose drowning in sea water. Forensic Sci. Int. **103**(1), 61–65 (1999)
49. Ludes, B., Quantin, S., Coste, M., Mangin, P.: Application of a simple enzymatic digestion method for diatom detection in the diagnosis of drowning in putrified corpses by diatom analysis. Int. J. Legal Med. **107**(1), 37–41 (1994)
50. Taylor, J.J.: Diatoms and drowning–a cautionary case note. Med. Sci. Law. **34**(1), 78–79 (1994)
51. Azparren, J.E., Vallejo, G., Reyes, E., Herranz, A., Sancho, M.: Study of the diagnostic value of strontium, chloride, haemoglobin and diatoms in immersion cases. Forensic Sci. Int. **91**(2), 123–132 (1998)
52. Funayama, M., Aoki, Y., Sebetan, I.M., Sagisaka, K.: Detection of diatoms in blood by a combination of membrane filtering and chemical digestion. Forensic Sci. Int. **34**(3), 175–182 (1987)
53. Seo, Y., Ichida, D., Sato, S., Kuroki, K., Kishida, T.: An improved method for the diatom test utilizing DNA binding ability of silica. J. Forensic Sci. **59**(3), 779–784 (2014)
54. Wang, H., Liu, Y., Zhao, J., Hu, S., Wang, Y., Liu, C., et al.: A simple digestion method with a Lefort aqua regia solution for diatom extraction. J. Forensic Sci. **60 Suppl 1**, S227–S230 (2015)
55. Zhao, J., Wang, Y., Wang, G., Ma, Y., Shi, H., Wen, J., et al.: Application of the microwave digestion-vacuum filtration-automated scanning electron microscopy method for diatom detection in the diagnosis of drowning. J. Forensic Legal Med. **33**, 125–128 (2015)
56. Zhao, J., Ma, Y., Liu, C., Wen, J., Hu, S., Shi, H., et al.: A quantitative comparison analysis of diatoms in the lung tissues and the drowning medium as an indicator of drowning. J. Forensic Legal Med. **42**, 75–78 (2016)
57. Zhao, J., Liu, C., Bardeesi, A.S.A., Wu, Y., Ma, Y., Hu, S., et al.: The diagnostic value of quantitative assessment of diatom test for drowning: an analysis of 128 water-related death cases using microwave digestion-vacuum filtration-automated scanning electron microscopy. J. Forensic Sci. **62**(6), 1638–1642 (2017)
58. Pachar, J.V., Cameron, J.M.: Submersion cases: a retrospective study–1988-1990. Med. Sci. Law. **32**(1), 15–17 (1992)
59. Bortolotti, F., Del Balzo, G., Calza, R., Valerio, F., Tagliaro, F.: Testing the specificity of the diatom test: search for false-positives. Med. Sci. Law. **51 Suppl 1**, S7–S10 (2011)
60. Levin, E.A., Morgan, R.M., Scott, K.R., Jones, V.J.: The transfer of diatoms from freshwater to footwear materials: an experimental study assessing transfer, persistence, and extraction methods for forensic reconstruction. Sci. Justice. **57**(5), 349–360 (2017)
61. Timperman, J.: Medico-legal problems in death by drowning. Its diagnosis by the diatom method. A study based on investigations carried out in Ghent over a period of 10 years. J. Forensic Med. **16**(2), 45–75 (1969)
62. Ming, M., Meng, X., Wang, E.: Evaluation of four digestive methods for extracting diatoms. Forensic Sci. Int. **170**(1), 29–34 (2007)
63. Kakizaki, E., Yukawa, N.: Simple protocol for extracting diatoms from lung tissues of suspected drowning cases within 3h: first practical application. Forensic Sci. Int. **251**, 179–185 (2015)
64. Takeichi, T., Kitamura, O.: Detection of diatom in formalin-fixed tissue by proteinase K digestion. Forensic Sci. Int. **190**(1-3), 19–23 (2009)
65. Barber, H., Haworth, E.: A Guide to the Morphology of the Diatom Frustule: With a Key to the British Freshwater Genera. Freshwater Biological Association, Ambleside (1981)
66. Cox, E.J.: Identification of Freshwater Diatoms from Live Material, 158 p. Chapman and Hall, London (1996)
67. Gell, P.A.: An Illustrated Key to Common Diatom Genera from Southern Australia, 63 p. Cooperative Research Centre for Freshwater Ecology, Thurgoona, New South Wales (1999)
68. Tomas, C.R.: Identifying Marine Phytoplankton. California Academic Press, San Diego, CA (1997)
69. Blanco Lanza, S., Álvarez Blanco, I., Cejudo Figueiras, C., Bécares Mantecón, E., Ector, L., García Asenjo, C., et al.: Guía de las diatomeas de la cuenca del Duero, 206 p. Confederación Hidrográfica del Duero, Leon (2011)
70. Torre, C., Varetto, L., Tappi, E.: Scanning electron microscopic ultrastructural alterations of the pulmonary alveolus in experimental drowning. J. Forensic Sci. **28**(4), 1008–1012 (1983)
71. Torre, C., Varetto, L.: Scanning electron microscope study of the lung in drowning. J. Forensic Sci. **30**(2), 456–461 (1985)
72. Ludes, B., Coste, M., Tracqui, A., Mangin, P.: Continuous river monitoring of the diatoms in the diagnosis of drowning. J. Forensic Sci. **41**(3), 425–428 (1996)
73. Lobo, E.A., Heinrich, C.G., Schuch, M., Wetzel, C.E., Ector, L.: Diatoms as bioindicators in rivers. River Algae. 245–271 (2016)
74. Rai, S.V., Rajashekhar, M.: Effect of pH, salinity and temperature on the growth of six species of marine phytoplankton. J. Algal Biomass Utln. **5**(4), 55–59 (2014)
75. Lewin, R.A.: The diatoms – biology and morphology of the Genera – Round, F.E. Nature. **346**(6285), 619–620 (1990)
76. Confederación Hidrográfica del Ebro: Metodología para el establecimiento del estado ecológico según la Directiva del Marco del Agua en la Confederación Hidrográfica del Ebro: protocolos de muestreo y análisis para: Fitoplancton, Fitobentos(Microalgas bentónicas), Macrofitos, Invertebrados bentónicos, Ictiofauna, 236 p. Ministerio de Medio Ambiente, Madrid (2007)
77. Smol, J.P., Stoermer, E.F.: The diatoms: applications for the environmental and earth sciences. Cambridge University Press, Cambridge (2010)
78. Fore, L.S., Grafe, C.: Using diatoms to assess the biological condition of large rivers in Idaho (USA). Freshw. Biol. **47**(10), 2015–2037 (2002)
79. Ector, L., Rimet, F.: Using bioindicators to assess rivers in Europe: an overview. In: Lek, S., Scardi, M., Verdonschot, P.F., Descy, J.P., Park, Y.S. (eds.) Modelling Community Structure in Freshwater Ecosystem, pp. 7–19. Springer, Berlin (2005)
80. Descy, J.P., Coste, M. (eds.): A Test of Methods for Assessing Water-Quality Based on Diatoms. Congress of the International Association of Theoretical and Applied Limnology, Munich (2001)
81. Lenoir, A., Coste, M.: Estimation de la qualité des eaux du bassin Rhin-Meuse à l'aide des communautés de diatomées benthiques. Rapport CEMAGREF Bordeaux. Agence de l'Eau Rhin-Meuse, Moulins-lesMetz (1994)
82. Leclercq, L., Maquet, B.: Deux nouveaux indices chimique et diatomique de qualité d'eau courante: application au Samson et à ses affluents (Bassin de la Meuse belge): Comparaison avec d'autres indices chimiques, biocénotiques et diatomiques.

Bruxelles Institut Royal des Sciences Naturelles de Belgique (1987)
83. Sládecek, V.: System of Water Quality from the Biological Point of View. Schweizerbart, Stuttgart (1973)
84. Dell'Uomo, A.: L'indice diatomico di eutrofizzazione/polluzione (EPI-D) nel monitoraggio delle acque correnti: linee guida, 101 p. Agenzia per la protezione dell'ambiente e per i servizi tecnici, Rome (2004)
85. Rott, E., Pipp, E., Pfister, P.: Diatom methods developed for river quality assessment in Austria and a cross-check against numerical trophic indication methods used in Europe. Algol. Stud. **101**(1), 91–115 (2008)
86. Prygiel, J., Coste, M.: Guide méthodologique pour la mise en œuvre de l'Indice Biologique Diatomées NF T 90-354. Bordeaux Agences de l'Eau – Cemagref-Groupement de Bordeaux [cited 2018 October] (2000)
87. Kelly, M.G., Cazaubon, A., Coring, E., Dell'Uomo, A., Ector, L., Goldsmith, B., et al.: Recommendations for the routine sampling of diatoms for water quality assessments in Europe. J. Appl. Phycol. **10**(2), 215–224 (1998)
88. Lunetta, P., Penttila, A., Hallfors, G.: Scanning and transmission electron microscopical evidence of the capacity of diatoms to penetrate the alveolo-capillary barrier in drowning. Int. J. Legal Med. **111**(5), 229–237 (1998)
89. DiMaio, V.J., DiMaio, D.: Forensic Pathology, 2nd edn. CRC Press, Boca Raton, FL (2001)
90. Dettmeyer, R.B.: Histopathology of selected trauma. In: Dettmeyer, R.B. (ed.) Forensic Histopathology: Fundamentals and Perspectives, pp. 37–65. Springer, Heidelberg (2011)
91. Carter, N., Ali, F., Green, M.A.: Problems in the interpretation of hemorrhage into neck musculature in cases of drowning. Am. J. Forensic Med. Pathol. **19**(3), 223–225 (1998)
92. Puschel, K., Schulz, F., Darrmann, I., Tsokos, M.: Macromorphology and histology of intramuscular hemorrhages in cases of drowning. Int. J. Legal Med. **112**(2), 101–106 (1999)
93. Alexander, R.T., Jentzen, J.M.: Neck and scleral hemorrhage in drowning. J. Forensic Sci. **56**(2), 522–525 (2011)
94. Schulz, F., Lach, H., Püschel, K.: Nontraumatic intramuscular hemorrhages associated with death caused by internal diseases. In: Tsokos, M. (ed.) Forensic Pathology Reviews, vol. 5, pp. 129–138. Humana Press, Totowa, NJ (2008)
95. Girela-Lopez, E., Ruz-Caracuel, I., Beltran, C., Jimena, I., Leiva-Cepas, F., Jimenez-Reina, L., et al.: Histological changes in skeletal muscle during death by drowning an experimental study. Am. J. Forensic Med. Pathol. **37**(2), 118–126 (2016)
96. Lunetta, P., Miettinen, A., Spilling, K., Sajantila, A.: False-positive diatom test: a real challenge? A post-mortem study using standardized protocols. Legal Med. (Tokyo). **15**(5), 229–234 (2013)
97. Calder, I.M.: An evaluation of the diatom test in deaths of professional divers. Med. Sci. Law. **24**(1), 41–46 (1984)
98. Fucci, N., Campobasso, C.P., Mastrogiuseppe, L., Puccinelli, C., Marcheggiani, S., Mancini, L., et al.: Diatoms in drowning cases in forensic veterinary context: a preliminary study. Int. J. Legal Med. **131**(6), 1573–1580 (2017)
99. Heaton, V., Lagden, A., Moffatt, C., Simmons, T.: Predicting the postmortem submersion interval for human remains recovered from U.K. waterways. J. Forensic Sci. **55**(2), 302–307 (2010)
100. Lin, C.Y., Yen, W.C., Hsieh, H.M., Tsai, L.C., Huang, T.Y., Huang, C.C., et al.: Diatomological investigation in sphenoid sinus fluid and lung tissue from cases of suspected drowning. Forensic Sci. Int. **244**, 111–115 (2014)
101. Di Giancamillo, A., Giudici, E., Andreola, S., Porta, D., Gibelli, D., Domeneghini, C., et al.: Immersion of piglet carcasses in water–the applicability of microscopic analysis and limits of diatom testing on an animal model. Legal Med. (Tokyo). **12**(1), 13–18 (2010)
102. Aghayev, E., Thali, M.J., Sonnenschein, M., Hurlimann, J., Jackowski, C., Kilchoer, T., et al.: Fatal steamer accident; blunt force injuries and drowning in post-mortem MSCT and MRI. Forensic Sci. Int. **152**(1), 65–71 (2005)
103. Kakizaki, E., Kozawa, S., Matsuda, H., Muraoka, E., Uchiyama, T., Sakai, M., et al.: Freshwater bacterioplankton cultured from liver, kidney and lungs of a decomposed cadaver retrieved from a sandy seashore: possibility of drowning in a river and then floating out to sea. Legal Med. (Tokyo). **12**(4), 195–199 (2010)
104. Kakizaki, E., Kozawa, S., Sakai, M., Yukawa, N.: Numbers, sizes, and types of diatoms around estuaries for a diatom test. Am. J. Forensic Med. Pathol. **32**(3), 269–274 (2011)
105. Miller Coyle, H., Ladd, C., Palmbach, T., Lee, H.C.: The Green Revolution: botanical contributions to forensics and drug enforcement. Croat. Med. J. **42**(3), 340–345 (2001)
106. Muccino, E., Crudele, G.D., Gentile, G., Marchesi, M., Rancati, A., Zoja, R.: Suicide drowning in the non-coastal territory of Milan. Int. J. Legal Med. **129**(4), 777–784 (2015)
107. Horton, B.P.: Diatoms and forensic science. In: Starratt, S. (ed.) Pond Scum to Carbon Sink: Geological and Environmental Applications of the Diatoms, Paleontological Society Short Course, vol. 13, pp. 13–22. Paleontological Society Papers, Knoxville, TN (2007)
108. Hall, D.W., Byrd, J.H.: Forensic Botany. A Practical Guide. Wiley, Oxford (2012)

Benthic Foraminifera and Diatoms as Ecological Indicators

15

Xavier Benito

Abstract

Ecology can be defined as the study of causes that govern the distribution and abundance of organisms and their relation to the environment. Among benthic microorganisms (10 μm–500 mm), diatoms and foraminifera are of great importance in aquatic ecosystems worldwide because (1) their species react in a rapid and sensitive way to environmental changes in water bodies, and (2) they preserve in sediments for a long time due to their shells, which are made of silica (diatoms) or calcium carbonate or cemented detrital material (foraminifera). In shallow coastal ecosystems (coastal lagoons, marshes), these attributes make foraminifera and diatoms extremely valuable for both ecology and geology because modern communities indicate the dynamic transition between terrestrial and marine habitats, and fossil assemblages record past sea-level changes. While many other works provide specific information on the taxonomy, biology, and ecology of foraminifera and diatoms independently, this chapter aims to provide a comprehensive joint perspective of the applications and uses of these two groups of organisms for environmental studies in coastal habitats. Given the ongoing and future threats associated with sea-level rise and water scarcity, and the lack of long-term monitoring data to assess ecosystems' deviation from natural baseline conditions, palaeoecological applications of foraminifera and diatoms are also discussed in the context of environmental and restoration policies.

X. Benito (✉)
National Socio-Environmental Synthesis Center (SESYNC), University of Maryland, College Park, MD, USA
e-mail: xbenitogranell@sesync.org

15.1 Introduction to Benthic Foraminifera and Diatoms: Basic Aspects of Biology and Ecology

Analyses of organisms as indicators of environmental variables that otherwise could not be measured (i.e., proxies; see Glossary) have long been touted as powerful tools since Darwin's "On the origin of the species" [1]. Many studies use proxies to gage spatial and temporal changes in a variety of ecosystems. At land–sea transitional systems, biological indicators are of interest for ecologists because processes are inherently intense and dynamic, allowing them to determine species' response to environmental gradients (natural and/or human-induced). Biological-based proxy studies in transitional systems are also of interest for geologists because fossil records indicate the change of position in palaeocoastlines associated with past sea-level changes. This book chapter focuses on two organismal groups that provide remarkable advantages over most of biological indicators when used together at different scales of spatial and temporal analysis—diatoms (microalgae) and foraminifera (microfauna). On one hand, both diatoms and foraminifera have great potential to leave a fossil record that allows palaeoenvironmental reconstructions. On the other hand, diatom and foraminifera react in a direct and sensitive way to changes in environmental conditions (e.g., water physico-chemistry, substrate type, bathymetry, organic matter, and dissolved oxygen). Moreover, dispersal passive mode dominates on diatoms and foraminifera (although active dispersal over short distances is important for some benthic foraminifera) due to their small body sizes and large population numbers [2, 3] thus leading local environmental controls to override spatial effects associated with potential dispersal constraints [3]. Therefore, well-known autoecological data exist for characterizing the full range of marine and freshwater environments by means of diatoms and foraminifera analysis.

G. Cristóbal et al. (eds.), *Modern Trends in Diatom Identification*, Developments in Applied Phycology 10,
https://doi.org/10.1007/978-3-030-39212-3_15

The importance of shallow coastal ecosystems is based upon the dynamism and high-frequency processes operating at relatively small spatial scales. The complex relationship between riverine and marine systems depends mainly on the fluxes of water, sediment, and energy, all driven by different pulsing events [4]. This dynamism determines one of the principal ecological characteristics of the shallow coastal habitats, namely the extreme fluctuation and interaction of a wide range of parameters used to characterize them (e.g., salinity, nutrients, water levels, and production) [5]. Over geological time scales, and although challenging, the use of dated sediment cores represents a potential record of environmental changes driven by continental and marine processes [6]. In addition, it provides a background to compare natural variability from most recent (post-1850 CE) human impacts [7–9]. For the benthic microorganisms inhabiting these dynamic environments, perhaps no other fossilizable groups such as diatoms and foraminifera (but also ostracoda [10]) are so well documented in terms of their present-day environmental preferences [11, 12].

Foraminifera (unicellular protists, Phylum Foraminifera) and diatoms (unicellular microalgae, Class Bacillariophyceae) are enclosed in a resistant cell wall which is made mainly calcium carbonate ("calcareous" foraminifera, although agglutinated forms made of cemented detrital material are also important; see below) and silica (diatoms). Foraminifera are restricted to marine and coastal environments (oceans, lagoons, marshes, and estuaries), whereas diatoms virtually inhabit every continental, coastal, and marine waters, and often represent a major component of the primary producer communities [13]. Planktonic species live in open ocean environments (diatoms and foraminifera) and continental lakes (diatoms) where usually attain high diversity in the planktonic communities [14]. Benthic diatom communities dominate in coastal habitats in terms of abundance and diversity [11], whereas benthic foraminifera attain higher species diversity with water depth [12].

Most of the foraminifera and diatom taxonomy is based upon cell wall morphology. In foraminifera, wall composition and test morphology, including chamber form and arrangement and shape and position of the aperture are diagnostic characters for species identification, whereas size, shape, and sculpturing of diatom cell walls (called the frustule) are taxonomically diagnostic. Estimations of foraminifera and diatom species number are around 10,000 [15] and 100,000 [16], respectively. However, these numbers may considerably raise in the future by the application of molecular species concepts. Taxonomic classifications of foraminifera and diatoms have advanced since the last two decades so the diagnosis of taxa is shifting from morphology-based to molecular-based approaches [17, 18]. Highly variable species morphologically similar and thus difficult to separate can be even more similar at the molecular level (cryptic and pseudo-cryptic species). This fact minimizes true diversity, endemism, and geographical distribution of foraminifera and diatom communities [19–22]. Thus, no doubt that the impact of molecular classifications will incorporate new perspectives in the ecological and biogeographical assessments of ecosystems that utilize foraminifera and diatoms as bioindicators [23, 24].

Ideally, a good indicator species has a well-defined ecological range, is widespread distributed, and is reliably and easily identified. Not only can different species with different environmental preferences be used as indicators, but also their morphological variability as long as this variability can be unequivocally associated with species responses to environmental fluctuations [25]. Whether foraminifera and diatoms reproduce sexually, asexually, or both, such alternation introduces morphological variation within living populations [17, 26]. Most morphologically high variable foraminifera and diatom species appear to inhabit with high abundances in fluctuating coastal ecosystems, suggesting they have wide ranges of tolerance to multiple environmental parameters [27]. For instance, the foraminifera *Ammonia tepida* (Cushman 1926), *Cribroelphidium selseyense* (Heron-Allen & Earland 1911), and *Quinqueloculina schlumbergeri* (Wiesner, 1923), or the diatoms *Nitzschia inconspicua* Grunow, *Pseudostaurosira geocollegarum* (Witkowski) E.A. Morales, *Planothidium delicatulum* (Kutzing) Round and Bukht. 1996 and small Fragilarioids (Table 15.1). Very few experimental works have attributed changes in environmental variables (e.g., salinity, nutrients) to change in morphological variation of diatoms and foraminifera species shells. Therefore, estimating the ecological indicator value of single individuals or species might be challenging in such ecosystems and so a shift toward a more focused community and functional approaches warrants future studies [13].

15.2 Sampling and Foraminifera Analysis

Below, the standard techniques used to collect and analyze benthic foraminiferal samples are explained. The small size of foraminifera (63 μm–100 mm) and high abundances in small samples (<10 cc) facilitate the sampling and posterior analysis. For a more extended and detailed description of methods and analysis of foraminifera, the reader is referred to [12, 14].

Regardless of the project goals, it is essential that the chosen sampler takes a representative sample avoiding the loss of the sediment surface material (clay, sand, and mud). This is because most of the benthic foraminifera inhabit in the sediment-water interface and/or within the first 1–2 cm of sediment (epifaunal and infaunal taxa) [28]. For samples taken in deeper waters (i.e., nearshore environments, >20 m), Ekman-type dredges are used to seal the sample on

Table 15.1 Diatom and foraminifera taxa distribution in the Ebro Delta habitats (NW Mediterranean)

Environmental variables								
Salinity (ppt)	38.4	38.4	27.9	11.8	6.1	24.1	11.6	52.4
Water depth (m)	14.5	7.2	0.8	0.7	0.8	0.2	0.3	0.03
Sand (%)	34.8	18.5	80.7	55.1	68.5	58.1	33.2	76.3
Organic matter (%)	-	4.9	1.5	4.3	15.2	27.6	48.8	5.8
Dissolved oxygen (mg/L)	-	6.8	7.9	7.5	7.3	5.7	5.6	8.9
PO_4^{3-} - P (µg/L)	-	1.1	2.3	2.4	3.1	4.3	7.3	1.2
NO_3^- - N (µg/L)	-	17.8	23.2	223.1	272.1	32.3	76.3	16.2
Chlorophyll-a (µg/L)	-	2.8	2.9	11.2	11.4	15.1	19.2	4.3
	Offshore	**Nearshore open sea**	**Semi-enclosed bay**	**Brackish coastal lagoons**	**Freshwater coastal lagoons**	***Salicornia* marshes**	***Phragmites* marshes**	**Microbial mats**
Foraminifera								
Ammosphaeroidina sphaeroidiniforme (Brady)								
***Eggerelloides scaber* (Williamson)**		**S**						
Haplophragmoides canariensis (d'Orbigny)								
Reophax subfusiformis Earland, 1933								
Textularia calva Lalicker, 1935								
***Bolivinellina pseudopunctata* (Höglund)**		**S**						
Bulimina aculeata d'Orbigny, 1926								
***Bulimina gibba* Fornasini, 1902**								
Cassidulina laevigata d'Orbigny, 1826								
***Cribroelphidium selseyensis* (Heron-Allen and Earland)**		**S**	**S**					
***Elphidium advenum* (Cushman)**								
Elphidium crispum (Linné) = *Nautilis crispus* Linné, 1758								
Elphidium cf. *flexuosum* (d'Orbigny)								
Elphidium incertum (Williamson)								
Elphidium matagordanum (Kornfeld)								
Elphidium sp.2								
***Gavelinopsis praegeri* (Heron-Allen and Earland)**		**S**						
Nonionoides scaphus (Fitchel and Moll)								
Planorbulina mediterranensis d'Orbigny, 1826								
Reussella aculeata Cushman, 1945								
Uvigerina sp.1								
***Quinqueloculina stelligera* Schlumberger, 1893**								
Triloculina sp.1								
Miliolid undeterminated			**S**					**S**
Asterigerinata sp.1			S					
Bolivina striatula (Cushman)								
Buliminella elegantissima (d'Orbigny)								
Epistominella vitrea Parker, 1953								
***Nonionella atlantica* Cushman, 1947**								
Nonion laevigatum (d'Orbigny)								
***Quinqueloculina jugosa* (Cushman)**		**S**						**S**
***Quinqueloculina seminula* (Linné)**								**S**
***Ammonia beccarii* agg (Linné) (variants included in this taxon)**					**S**			**S**
***Cribroelphidium oceanensis* (d'Orbigny)**					**S**			**S**
***Haynesina germanica* (Ehrenberg)**					**S**			
***Haplophragmoides wilberti* Anderson, 1953**								
***Jadammina macrescens* (Brady)**								**S**
***Trochammina inflata* (Montagu)**							**S**	
***Trichohyalus aguayoi* (Bermudez)**							**S**	

(continued)

Table 15.1 (continued)

Diatoms					
Delphineis surirella (Ehrenberg) Andrews					
Nitzschia coarctata Grunow	S				
Amphora cf. *roettgeri* Lee & Reimer					S
Amphora sp.1					
Mastogloia aquilegiae Grunow					
Mastogloia braunii Grunow					
Navicymbula pusilla (Grunow) Krammer					
Amphora cf. *roettgeri* Lee & Reimer					S
Achnanthes amoena Hustedt					
Achnanthes sp.1					
Amphora sp.5					
Ardissonea crystallina (C. Agardh) Grunow					
Cocconeis cf. *neothumensis* var. *marina* De Stefano, Marino & Mazzella					
Cocconeis peltoides Hustedt					
Cocconeis scutellum Ehrenberg					
Navicula cf. *hansenii* Möller					
Navicula sp.7					
Navicula vimineoides Giffen					
Nitzschia constricta (Kützing) Ralfs					
Nitzschia liebetruthii Rabenhorst					
Nitzschia pararostrata (Lange-Bertalot) Lange-Bertalot					
Planothidium deperditum (Giffen)Witkowski & Lange-Bertalot					
Seminavis robusta Danielidis & Mann					
Seminavis strigosa (Hustedt) Danielidis & Economou-Amilli					
Achnanthes fogedii Hakansson					
Fragilaria atomus Hustedt					
Fragilaria cf. *sopotensis* Witkowski & Lange-Bertalot					
Fragilaria gedanensis Witkowski					
cf. *Fragilaria* sp.1				S	
cf. *Fragilaria* sp.2				S	
Navicula gregaria Donkin					
cf. *Opephora* sp.1					
Pseudostaurosiropsis cf. *geocollegarum* (Witkowski & Lange-Bertalot) E.A.Morales				S	
Pseudostaurosiropsis geocollegarum (Witkowski & Lange-Bertalot) E.A.Morales					
Achnanthes brevipes var. *intermedia* (Kützing) Cleve		S			
Diploneis smithii (Brébisson) Cleve					
Fragilaria cf. *neoelliptica* Witkowski					
Navicula microcari Lange-Bertalot		S			
Navicula perminuta Grunow					
Nitzschia inconspicua Grunow		S			

Gray = species indicators identified using the IndVal method (see main text). S = secondary species. Average values of environmental variables are also shown for each habitat. Foraminifera indicator species highlighted in bold are illustrated in the plates (living and dead tests). See Fig. 15.5 for pictures of the habitats

the seafloor [14]. However, they are not very satisfactory as most of the nearshore and marginal coastal marine sediments are non-cohesive (i.e., sandy-mud), meaning that there may be a loss of material through washing as the sampler is raised through the water column and taken out from the water. For obtaining undisturbed sediments, corers with sealing devices are more appropriate [12]. In the intertidal zone (e.g., marshes), a core tube (Beeker-type sampler) or plastic ring of a certain diameter (ca. 6 cm) is used and pressed down into the sediment so that the top 1–2 cm surface layer is lifted out and collected into a plastic bag (Fig. 15.1a). Ambient water and an equal volume of ethanol to preserve living individuals are added. This sampling is typically repeated 2–3 times to cover spatial variability of the patchy foraminiferal distribution—very common in marginal marine environments like deltas or estuaries as a result of

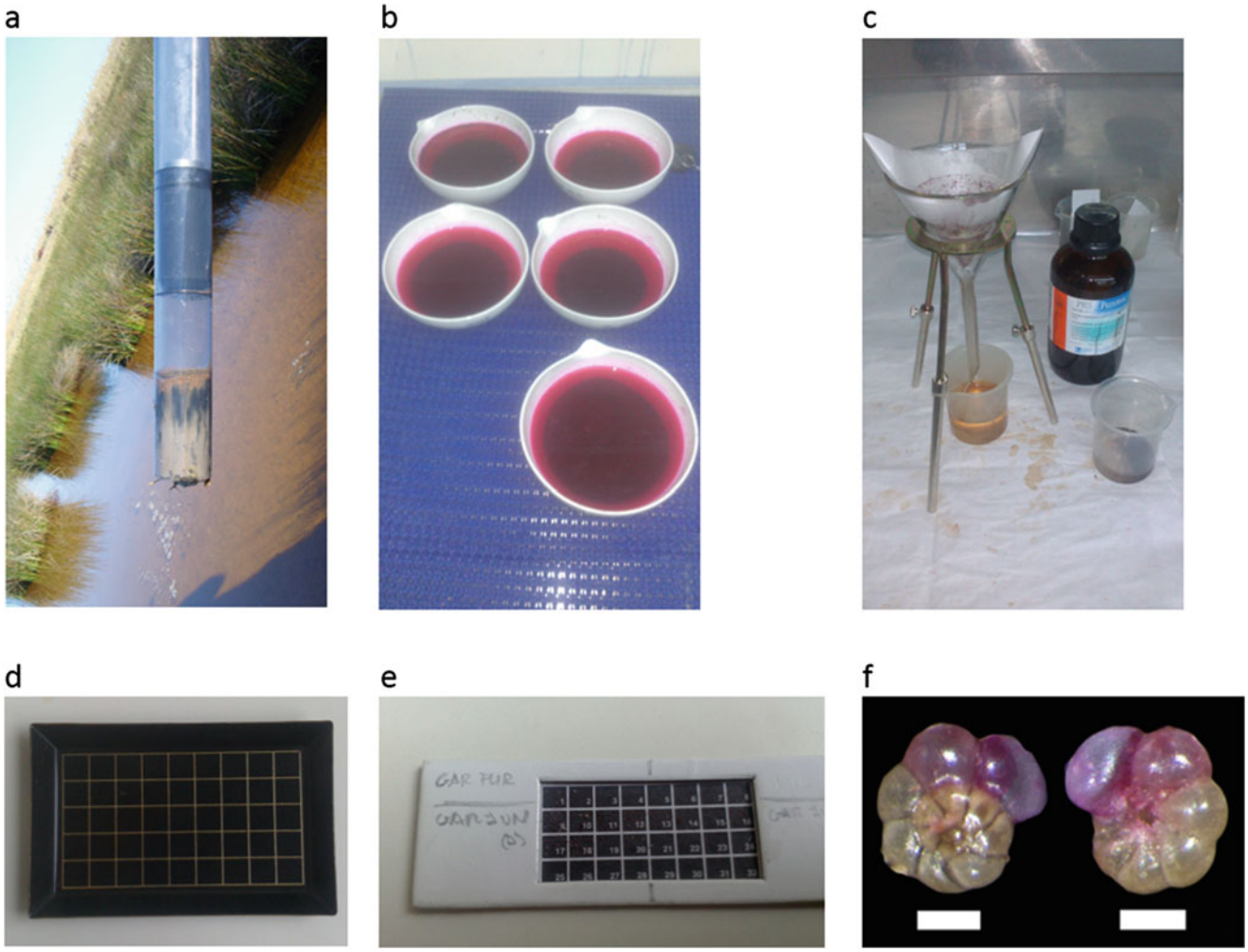

Fig. 15.1 Pictures showing analysis of benthic foraminiferal samples. (**a**) core tube (Beeker-type sampler); (**b**) samples soaked in Rose Bengal to distinguish living foraminifera; (**c**) flotation technique with trichloroethylene; (**d**) container used to pick foraminiferal tests; (**e**) cardboard slide; (**f**) living (Rose Bengal stained) foraminifera

different reproduction pulses among successive years—and the samples are merged for quantitative analysis [29]. It is essential to measure in situ environmental variables such as water depth, salinity, and oxygen, and collect samples for further analysis in the laboratory (e.g., organic matter, sediment type, and nutrients). Finally, it may be necessary to collect time series data in order to cover possible seasonal variability of foraminiferal assemblages [30].

In the laboratory, the methodology used for the analysis of foraminiferal samples is as follows. Each sample is wet sieved through 1 mm and 63 μm sieves (to remove first large organic fragments, then silt and clay). Depending on the type of sediment, samples can be further sieved through 400 and 125 μm sieves. The washed sand fraction retained in the sieve is transferred into a ceramic bowl and an equal volume of Rose Bengal stain was added (1 g Rose Bengal/L deionized water) following Walton's protocol [31]. Rose Bengal stains protoplasm bright red, allowing to identify foraminifera considered to be alive at the time of sampling (i.e., the last few chambers stained) (Fig. 15.1b, f) [32]. It allows distinguishing stained (living) from unstained (dead) individuals [33]. Then, foraminiferal tests are concentrated using a flotation technique with trichloroethylene described in [12] (Fig. 15.1c). Each sample is then gently brushed off into a container to avoid damage of the most fragile tests (Fig. 15.1d). Finally, foraminifera are examined under a binocular stereomicroscope using reflected light, and picking them up into lightly glued cardboard slides with a wet brush (Fig. 15.1e). Taxonomic identifications are made to species level when possible, using different classification schemes depending on the study area. In general, the classification by [15] provides the basis for the generic classification of benthic foraminifera. Identifications for the Mediterranean Sea, including shelf and marginal marine environments, are primarily based on [34–38]. Among others, valuable publications about the Atlantic Ocean species include

[39–42]. Photographs are taken using a digital camera and plates containing representative taxa are digitally mounted using image software.

Because neither single species nor population lives in isolation in nature, but it depends upon species assemblages in the way how they interact with the environment, the analysis of attributes that characterize the assemblage as a whole level of organization is better deemed to be meaningful for ecological assessments. For the case of foraminifera, a set of assemblage metrics is analyzed—the number of living and dead individuals for each sample, the relative abundance of dominant species, the species diversity, the relative abundance of autochthonous and allochthonous species, and proportion of wall types [43].

Analysis of foraminiferal samples is based on counts from living (stained) and dead (unstained) assemblages. Living and dead counts should be treated separately. Whereas living assemblages represent those species in equilibrium with the environment and their variability in space and time, dead assemblages are a result of time-averaged processes from accumulation and mortality of the living ones as well as post-mortem changes (e.g., destruction of tests, transport) [12]. Counting are generally made by picking on representative splits containing approximately 300 tests (dead and alive specimens each), or at least 100 if it was impossible to find 300 for valid statistical analyses [44].

The abundance of living foraminiferal assemblages can be expressed as the absolute numbers of individuals per unit volume, that is, the standing crop [12]. Standing crops are spatially and temporally highly variable in estuarine habitats due to reproduction pulses and patchy distributions [45]. Site-by-species relative abundances (%) matrices are the most used way to represent foraminiferal data. Species relative abundances of living and dead foraminiferal assemblages have been used by several authors to distinguish between autochthonous and allochthonous taxa [46]. In marginal marine environments, for instance, autochthonous species are those with relative abundances >1% and regularly found among the living foraminifera. Species absent in the living assemblages or occurring only occasionally in the live component throughout the year were considered as allochthonous [47]. Therefore, temporal (seasonal, annual) sampling is essential to determine allochthonous and autochthonous species within the region of study. Finally, the numerical relationship between the number of species and the individuals present in an assemblage (diversity) is estimated using the Fisher's alpha index [48] and Shannon index [49], which allows comparing samples of different sizes.

The similarity index of Rogers [50] has long been used in foraminiferal studies to compare the living and dead assemblages from the same sample or to assess seasonal changes for both living and dead assemblages. The index is calculated as follows. For each species present at both assemblages (e.g., living and dead or summer and winter), the lower of the two percentage values is taken and these are summed to give the similarity index, which ranges from 0 to 100%. Similarity values >70% are usually considered to indicate that a given pair of assemblages or samples are very similar [51].

The function of the test explains the ecological and evolutionary success of foraminiferal species. Three main wall types can be found in natural populations (Fig. 15.2). Calcareous foraminifera (i.e., hyaline and porcellaneous) utilize $CaCO_3$ to crystalize their tests with calcite, while agglutinated foraminifera construct their wall of cemented detrital material. Hyaline foraminifera are characterized by near-transparent tests with external pores. In contrast, porcellaneous foraminifera have opaque tests but no external pores due to the distinct structural disposition of the calcite crystals. Agglutinated forms are variable in terms of cemented detrital type material, but generally organic in nature (Fig. 15.2). Agglutinated foraminifera thrive well in waters with no calcium carbonate, whereas hyaline and porcellaneous tests are restricted to brackish-marine waters that contain calcium carbonate, which depends to a great extent on salinity, water depth, and temperature variations [52].

Biotic parameters of benthic foraminiferal assemblages can be used to characterize the terrestrial–marine environmental gradient. Firstly, and despite the difficulty to tease apart the environmental controls of foraminiferal assemblages' distribution due to the spatial and temporal covariation of variables that characterize shallow coastal habitats [53], test composition and abundance typically follow a salinity gradient along with other variables [12]. As salinity, water depth and temperature increase, and agglutinated tests are replaced by hyaline and porcellaneous forms [14], a gradual change is observed all over the world estuaries from agglutinated-dominated assemblages upstream to calcareous-dominated assemblages (hyaline + porcellaneous) downstream [54]. In Mediterranean deltas (nontidal systems), agglutinated species are more abundant in vegetated marsh habitats (*Salicornia*, *Phragmites* spp.), and the hyaline and porcellaneous species in subtidal environments [30] (Fig. 15.3).

Secondly, the diversity of the living assemblages can be used to separate open marine environments (Fisher $\alpha > 5$) from restricted marine environments ($\alpha < 5$). Regardless of the tidal settings (macro, meso, or nontidal) of the studied region, similar diversity patterns have been observed. For instance, [51] found that the diversity of living foraminiferal assemblages increased from the upper (α range = 1–3.5) to the lower parts (α range = 1–4.5) of the Santoña estuary in northern Spain. Murray [46] in a meta-analysis of world tidal estuaries indicates very low values in the upper estuary ($\alpha < 3$) and relatively higher values in the lower estuary

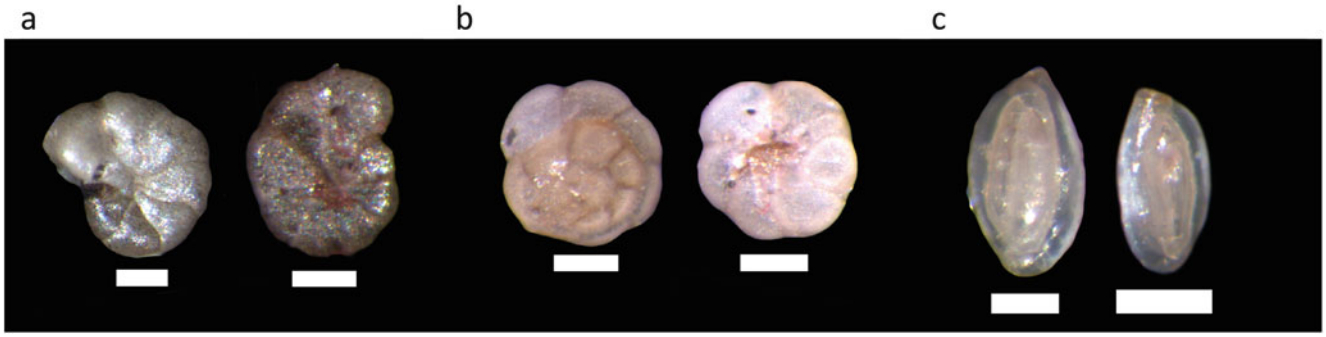

Fig. 15.2 Foraminiferal wall types. (**a**) agglutinated test (*Haplophragmoides wilberti* Anderson, 1953); (**b**) Hyaline test (*Ammonia tepida* Cushman, 1926); (**c**) Porcellaneous test (*Quinqueloculina schlumbergeri* Wiesner, 1923). Scale bar = 100 μm

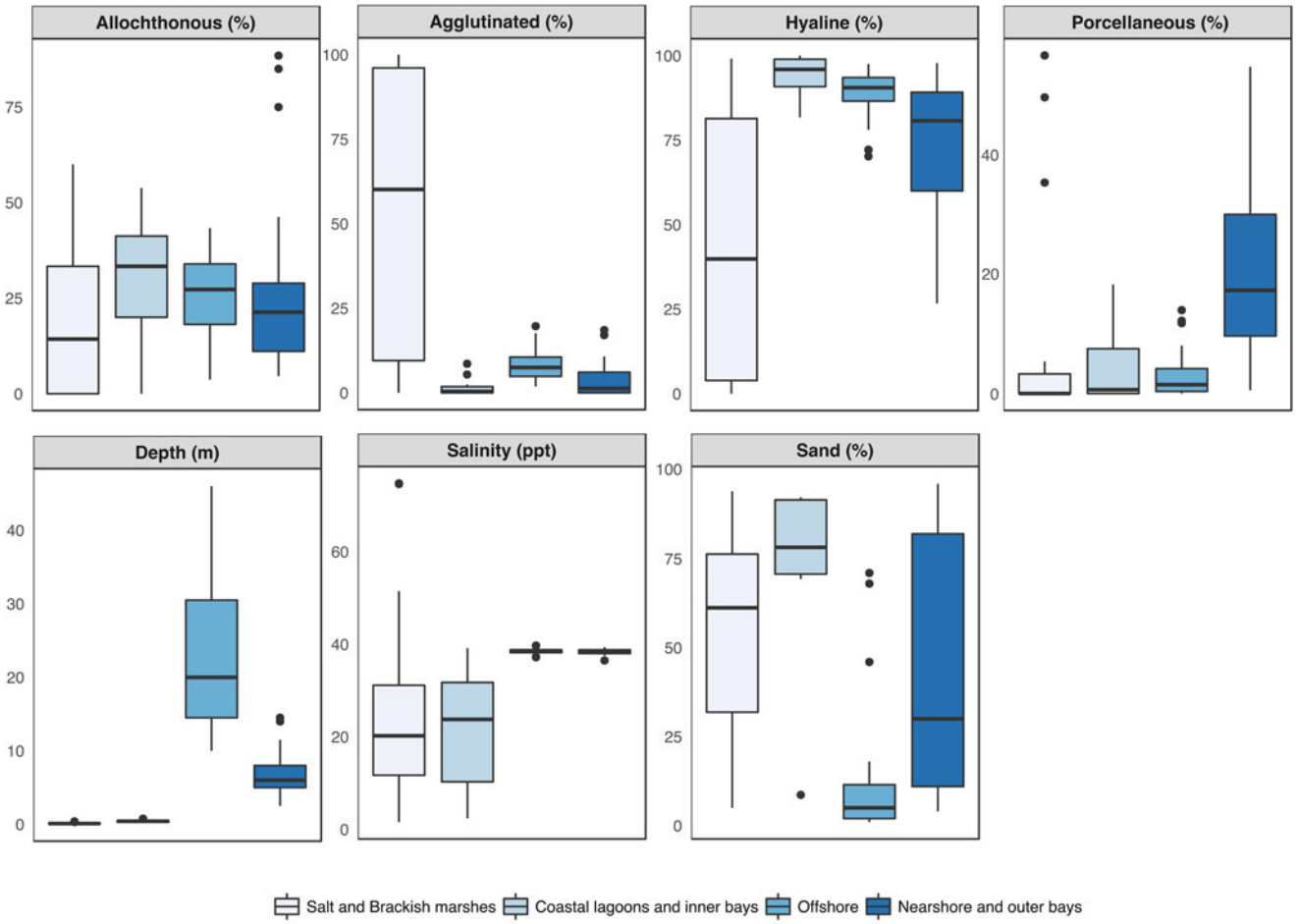

Fig. 15.3 Box plots of measured environmental variables and wall types for the foraminiferal groups of the Ebro Delta (NW Mediterranean) defined by cluster analysis (adapted from [30]). The boxes represent the 25th and 75th percentiles, and the median (middle line inside each box)

(α = 1–5). In a study of the Ebro Delta (NW Mediterranean), a clear shift is observed between the low-diversity habitats (α range = 0.32–6.96) of the deltaic plain (i.e., coastal lagoons and marshes) and the high-diversity habitats (α range = 2.04–16.97) of the open sea (i.e., nearshore and offshore settings) [30]. The wider range of values in the more influenced marine habitats can be explained by the transportation of littoral species that belong to high-diversity assemblages and hence allows a more diverse microfauna to inhabit on the environments closest to the sea (i.e., lower estuaries, shallow bays, and lagoons) [12].

Finally, the similarity between dead and living foraminiferal assemblages across coastal marine environments provide insights about sedimentation processes. In

estuaries and deltas, results showed higher similarity values (65–70%) at the more restricted habitats (upstream estuary, coastal lagoons, and vegetated marshes) compared with the adjacent subtidal marine habitats (around 35%) [30, 51, 55]. Differences between dead and living assemblages can be attributed to living population dynamics, which include taxon-specific reproduction rates and population densities in response to environmental fluctuations and also to transport of dead tests from the open sea [56]. Taphonomy processes associated with test dissolution and fragmentation introduce additional differences between dead and living assemblages. In terms of seasonality, dead assemblages are often more similar between seasons than living assemblages, indicating temporally averaged assemblages which are more useful for the interpretation of palaeoenvironments based on fossil assemblages [30, 32].

15.3 Benthic Foraminifera and Diatoms as Modern and Past Ecological Indicators

The study of the local ecological controls of contemporary distributions of foraminifera and diatoms is key for detailed and precise palaeoenvironmental reconstructions [11, 57]. If a statistically significant relationship exists between species and the variable and habitats of interest, quantitative and qualitative assessments of species-environment relationships can be used as a tool for palaeoenvironmental inferences. For instance, the study of modern analogs relies upon the quantification of similarity (or dissimilarity) measures that identify those modern assemblages most similar to the fossil ones [58]. Another widely used palaeoecological technique is the statistical calibration between selected environmental variables and modern species distributions to infer quantitatively past environmental variables (i.e., the use of transfer functions). Although quantitative reconstructions have been applied in a variety of coastal environments using diatoms [9, 59] and foraminifera [47, 60, 61], this methodology is being contested by the leaders of the field in aquatic palaeoecology [57, 62]. The most important methodological problem derives from attempts to reconstruct variables that are not the primary ecological control of the species (i.e., secondary variables), and from noncausal environmental variables. This might be the case in coastal environments such as deltas, where multiple environmental controls operate both spatially and temporally on species composition and abundance so reconstructing their past environments has proven to be complex [6]. But it is precisely this complexity in reconstructing highly dynamic coastal environments that add interest to this study as they demand a more integrative and complementary approach [63].

A clear example of variables that integrates a combination of ecological processes deemed to be meaningful for coastal palaeoenvironmental reconstructions are salinity and water depth. Confinement and shallowness can be considered surrogates of freshwater-to-marine and water-to-land transitions, respectively—integrative factors indicating not only salinity and water depth gradients but also habitat characteristics such as subaerial wave action, light limitation, habitat instability, food availability, etc.,—all of which influence diatoms and foraminiferal assemblages [12, 48, 64]. Although the depth-related and salinity-related niche of a species varies depending on local physiographic conditions, significant correlations between single variables and foraminiferal and diatoms assemblages have been shown to reflect both the direct and indirect effects of these variables in Mediterranean [30, 65], Atlantic [47, 60], and subtropical [66–68] coastal environments. For the case of water depth, many abiotic (e.g., oxygen, food availability, substrate) and biotic (e.g., competition) factors covary with depth and do determine foraminiferal distributions, especially in nearshore marine waters (<20 m depth) [38] thus producing a bathymetric zonation and allowing estimation of palaeodepth from fossil assemblages [6, 30, 69, 70].

Another method used by aquatic palaeoecologists to reconstruct past environments is the indicator species approach [71]. This analysis produces an indicator value (IndVal, IV) that estimates the association of each taxon with each group [72]. The IV of a given species will be maximal (IV varies between 0 and 100) if all the individuals are found in a single group (high specificity) and they are present in all the samples of that group (high fidelity). The use of diatoms and foraminifera as species indicators of coastal environments is relatively common [9, 30, 65, 73, 74]. However, most diatoms and foraminiferal species inhabiting these ecosystems have been documented as having a broad range of tolerance for a high number of variables; they are able to occupy different environments (eurytopic species) [14, 75]. In this case, the identification of groups of indicator species in combination with individual species' optimum and range of tolerances could better reflect the specific habitats conditions. The reliability of palaeoenvironmental reconstructions can be improved by complementing the strengths of the different statistical techniques used.

Very few studies have applied a combined qualitative (through indicator species analysis) and quantitative (through transfer functions) approach using diatoms and foraminifera to reconstruct coastal environments, where different habitats (e.g., marshes, lagoons, sandflats, and bays) are present in small patches [76]. For the case of the Ebro Delta, quantitative predictions of conductivity and water depth could be inferred using diatoms [65] and foraminifera [30], respectively, but the habitat type would not be necessarily the same.

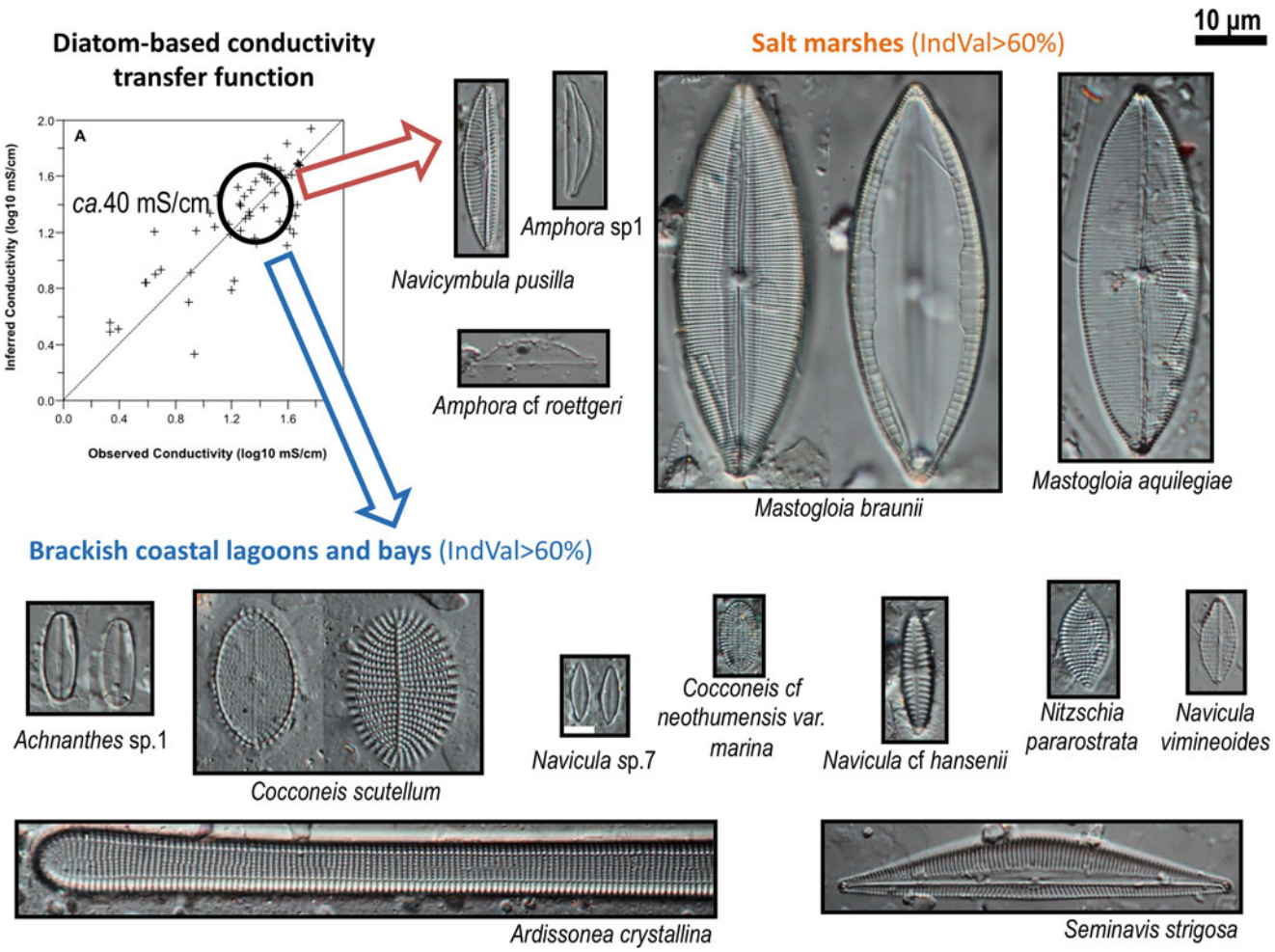

Fig. 15.4 Schematic representation of the complementary analysis by means of diatom species indicator approach (IndVal, [72]) and conductivity-based transfer function. For the same range of conductivity (e.g., 30–40 mS/cm), both salt marshes and coastal lagoons could be possible. Instead, groups of diatom indicator species (IV > 60%) are able to discriminate between them

For instance, for the same range of conductivity (e.g., 30–40 mS/cm), both salt marshes and coastal lagoons could be possible. Instead, groups of diatom indicator species were able to discriminate between them (Fig. 15.4). Likewise, for the same range of water depth (e.g., 2–3 m), foraminifera indicator species can discriminate between two distinct subtidal habitats (i.e., coastal lagoon and nearshore/ outer bay habitats) [64]. Therefore, the use of independent indicators for each habitat type and species' responses to single variables allowed the determination of the extent of marine influence (i.e., from nearshore to deltaic plain environments), as benthic diatoms and foraminifera discriminate between subtidal habitats and marshes, and they separate different types of marshes, from brackish (*Phragmites* marshes with organic-rich sediments) to salt marshes (*Salicornia* and *Juncus* with sandy sediments).

15.4 Multiproxy Analysis

Many studies have analyzed the distribution of foraminifera and diatoms in relation to elevation and salinity in shallow coastal environments. One of the problems with salinity and sea-level reconstructions is that modern ranges of species relative to the variables of interest vary between regions, and a limited number of sites are taken to represent the true indicator value of the species [77]. In addition, for the specific case of Mediterranean coastal habitats, palaeoenvironmental reconstructions have been carried out mainly using data from other areas and using single indicators, either diatoms or foraminifera [69, 78]. To the best of my knowledge, no previous assessment of the qualitative (species indicators) and quantitative (transfer function) statistical validity of the

species-environment relationships has been conducted in coastal wetlands to determine whether the combination of the different groups is more accurate and precise than the indicative value of a single group [77].

A recent study [64] used a multiproxy approach (foraminifera plus diatoms) to compare with the results in which benthic diatom assemblages were used as indicators of the Ebro Delta habitat types [65]. The multiproxy approach applied, first, partial Canonical Correspondence Analysis (CCA) using the most abundant diatom and foraminifera species in the samples and 14 environmental variables to determine the unique contribution of individual variables to microorganisms' distributions. Salinity made the highest unique contribution to explaining the variance of the multiproxy dataset (foraminifera plus diatoms), indicating the ecological importance of this variable in explaining species distributions. Therefore, a transfer function was developed for salinity using the multiproxy dataset. Weighted Averaging (WA) and Weighted Averaging Partial Least Square (WA-PLS) were used as transfer function models. Each model was evaluated on the basis of its predictive ability by calculating three different parameters—correlation between observed and predicted values (r^2), root mean squared error of prediction (RMSEP), and maximum bias [79]. Results reinforced the environmental characterization of habitats (i.e., salt marshes, brackish marshes, brackish coastal lagoons and bays, coastal lagoons with fresher conditions, and nearshore open sea) and salinity prediction (i.e., transfer function) obtained using benthic diatoms solely (Table 15.2). Some previous studies of transitional environments have also investigated whether a combination of different benthic microorganism groups can improve on the environmental information provided by each of them individually (e.g., for foraminifera, diatoms and testate amoebae by [77]; for foraminifera, diatoms and macrophytes by [80]; and for foraminifera and testate amoebae by [81]). The conclusion of those works combining foraminifera and diatoms is very similar to the Ebro Delta—i.e., that combining datasets offer minimal statistical improvement. This may be because foraminiferal microfaunas are less diverse and exhibit lesser compositional changes of their assemblages between sites. Diatoms, on the other hand, have more diverse assemblages than foraminifera and tend to be more compositionally different between sites. Thus, in the Ebro Delta plain, habitats with distinctly different salinities (e.g., salt/brackish versus freshwater) were clearly identified and defined using the diatom assemblages (Table 15.2) but not using foraminifera. This could be explained by the dominance of a few euryhaline foraminiferal species in most of the salt/brackish habitats of the delta, as has been shown in marginal marine environments elsewhere [12, 14].

Benthic foraminifera and diatoms allowed the determination of the extent of marine influence (i.e., from nearshore to deltaic plain environments), they discriminate between subtidal habitats and marshes, and they separate different types of marshes, from brackish (*Phragmites* marshes with organic-rich sediments) to salt marshes (*Salicornia* and *Juncus* with sandy sediments) (Fig. 15.5). The usefulness of one type of indicator or the other, versus a combination of both, should be assessed not only by the amount of environmental information gained but also considering the time needed to obtain it. Foraminifera and diatoms, considered separately, are good indicators of water depth and salinity when regression analyses are applied (i.e., transfer functions), and therefore complementary when analyzed individually. However, there is no information gained about salinity when foraminifera and diatoms are analyzed together (Table 15.2). On the other hand, for the identification and description of the delta plain habitats, diatoms alone discriminated up to five habitat types (i.e., salt marshes, brackish marshes, brackish coastal lagoons and bays, coastal lagoons with fresher conditions, and nearshore open sea) (Table 15.2), while foraminifera detected four (i.e., salt and brackish marshes, coastal lagoons and bays, nearshore open sea, and offshore) [30, 82]. The habitat types recognized when diatom and foraminifera are analyzed together are the same as with diatoms alone. Therefore, since the analysis of benthic foraminifera is more cost-effective (e.g., easier taxonomy and less diverse communities), this group seems to be the most suitable when a coarse-grained habitat reconstruction is all that is required. However, if a finer-grained habitat reconstruction is needed then diatoms should be the proxy to use. Concerning quantitative reconstructions, the choice of the indicator group depends entirely on the parameter one wants to predict (i.e., foraminifera for water depth and diatoms for salinity), and their preservation in the sediment record. Diatoms do not often preserve well in brackish-marine sediments [83, 84], for example, the Ebro Delta sediments in particular [64]. In contrast, benthic foraminifera do preserve well in coastal sediments and are therefore available for palaeoenvironmental reconstructions [6, 69].

15.5 Conclusions and Implications

Shallow coastal marine ecosystems such as deltas are ecologically and economically very important but low elevations make them extremely sensitive to ongoing and future relative sea-level rise (RSLR). The responses of diatom and foraminiferal assemblages to salinity and water depth gradients can be used in conjunction with habitat distribution forecasting models in order to assess the evolution of saltwater intrusion and future habitat changes as a function

Table 15.2 Summary of the multiproxy approach (foraminifera plus diatoms)

Assemblage	Habitat types	Ecological gradients	Overriding variable	Salinity transfer function
Foraminifera plus diatoms	1. Salt marshes 2. Brackish marshes 3. Brackish coastal lagoons and bays 4. Coastal lagoons with fresher conditions 5. Nearshore open sea	Salinity and water depth	Salinity (4.22% unique and independent effects)	$r^2 = 0.63$
Diatoms	1. Salt marshes 2. Brackish marshes 3. Brackish coastal lagoons and bays 4. Coastal lagoons with fresher conditions 5. Nearshore open sea	Salinity and water depth	Conductivity (as proxy of salinity) (4.58% unique and independent effects)	$r^2 = 0.64$

Habitat types were classified using cluster analysis on species distribution (see [62] for further information). Ecological gradients and the overriding variable were determined using partial Canonical Correspondence Analysis (CCA). Salinity transfer function model indicates the best fitted model (r^2) between observed and predicted values based on Weighted Averaging (WA) and Weighted Averaging Partial Least Square (WA-PLS)

Fig. 15.5 The Ebro Delta showing the most characteristic habitats as a representative Mediterranean coastal environment. See Table 15.1 for diatom and foraminifera species indicators for each habitat. Images taken from Google Earth

of scenarios of RLSR and coastal retreat [65, 85]. Ecological impacts associated with saltwater intrusion will prompt economic losses of agricultural crops such as rice paddies [86]. Both scenarios are rather inevitable in low-lying coasts worldwide, where progressive relative sea-level rise could already be implicated in the loss of coastal wetlands and where freshwater supply and sediment load by rivers can be expected to decline due to water resource scarcity [87, 88].

The use of diatoms and foraminifera as modern and past ecological indicators may constitute a quality element to assess water ecosystem conditions. For instance, the Water Framework Directive (WFD) aims to achieve a "good" ecological status of water bodies by assessing the relationship between multiple environmental stressors and aquatic organisms. Although the use of diatoms and foraminifera is not required in the bioassessment of coastal and transitional waters (WFD Appendix V), modern communities have been used as bioindicators variously in coastal ecosystems worldwide. However, caution should be made in coastal environments, where the natural background variability might be obscured with human-induced environmental impacts in terms of shared community species composition of diatoms and foraminifera [73, 89]. Nonetheless, their fossil remains can indicate the extent of deviation from pre-disturbance conditions by distinguishing if low-diversity opportunistic species are the result of natural or anthropogenic stressed conditions [27]. This is an essential component to inform restoration and adaptation programs [7, 8, 90].

Despite the role of microorganisms in ecosystem functioning and structure, they are often neglected in spatial ecology and conservation studies, likely because of their cosmopolitan distributions. However, given the emerged view that also microorganisms show biogeographic patterns, little is known whether or not transitional waters are unique reservoirs of diatom and foraminifera diversity [22, 91]. Diatoms and foraminifera can be more widely and better used to support conservation planning and assessment of ecosystem services. Coastal ecosystems are of paramount importance because they provide more goods and services than other biomes for the same unit area (e.g., productivity, nutrient removal, sediment retention, etc.) [92]. Hence, as more regional studies appear, the perspectives of conservation biology that consider coastal habitat protection may also be applied for microalgae and microfaunas in the context of global environmental change impacts. Criteria such as microbial species richness and aquatic biodiversity are becoming of interest for managers and decision makers, as well as for citizenship [93].

In this chapter, the ecological distribution of benthic diatoms and foraminifera in transitional water ecosystems has been discussed. The high dynamism of such ecosystems is both challenging and attractive for testing multiple ecological and palaeoecological hypothesis on the synergistic effects of human and natural factors. Diatoms and foraminifera can contribute to this approach given their sensitive and quick response to change in water habitat conditions, and their preservation in the sedimentary record. Multiproxy approaches using diatoms and foraminifera are promising to the environmental characterization of the habitats in coastal environments. The recognition of indicator species is complementary to the quantitative transfer functions, since salinity (in the case of diatoms) and water depth (for foraminifera), though very important, are not the only factors structuring the habitats. Here, this has been illustrated for the case of the Ebro Delta as a representative Mediterranean coastal environment. Results can be readily applied to other Mediterranean deltaic areas since they share similar ecogeographic features and socio-environmental issues, with the ultimate goal of providing place-specific, long-term and well-informed management decisions.

Acknowledgments The writing of this manuscript was supported by the National Socio-Environmental Synthesis Center (SESYNC), under funding received from the US NSF DBI-1639145.

Illustration Plates of Foraminifera

Binocular stereomicroscope plates of characteristic foraminiferal taxa from the Ebro Delta habitats (NW Mediterranean). Taxa are arranged by wall structure and alphabetically. Scale bar represents 100 μm (Plates 15.1, 15.2, 15.3, 15.4, 15.5, 15.6, 15.7, 15.8, and 15.9). Adapted from [64]

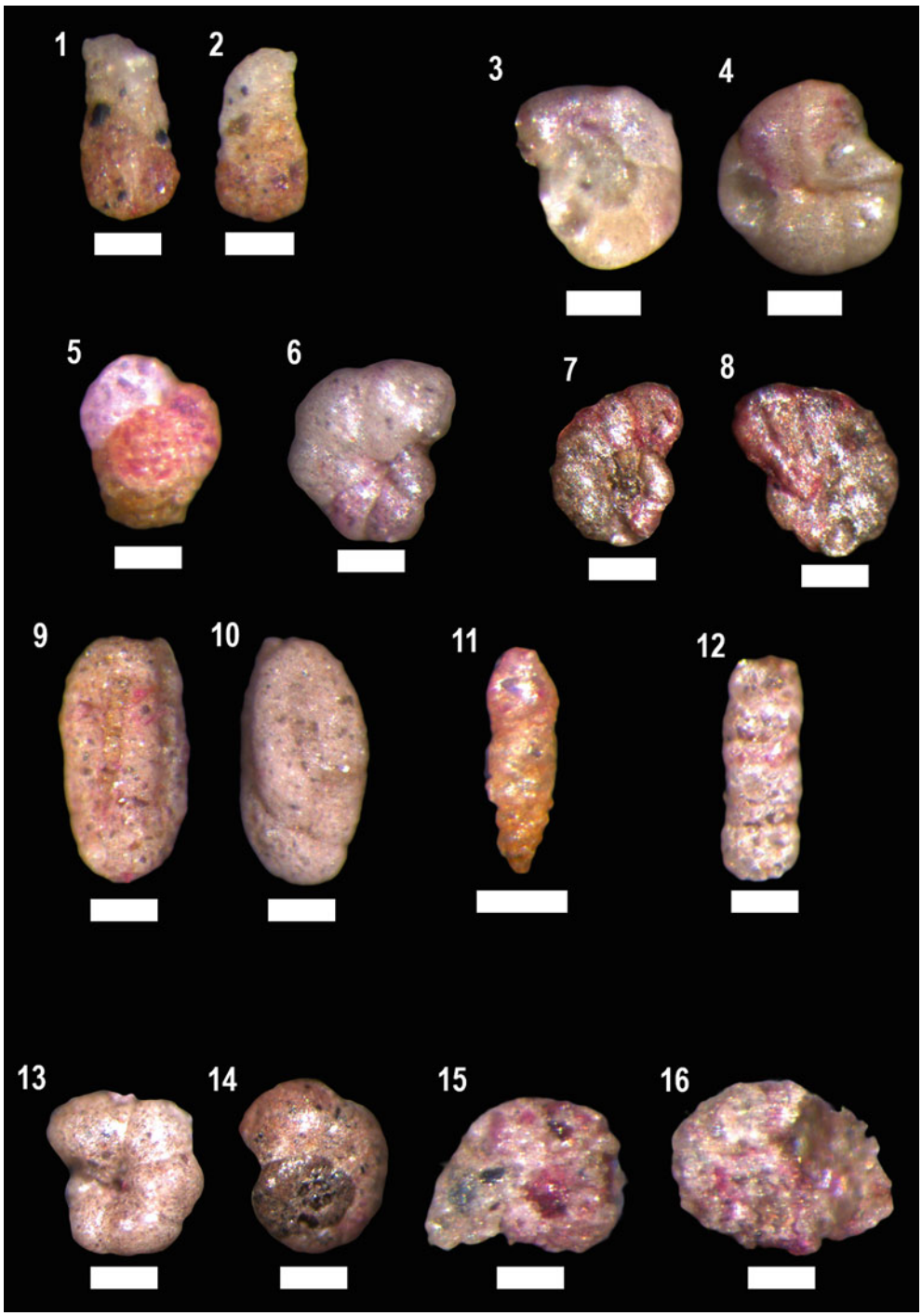

Plate 15.1 Living foraminiferal tests. (**1, 2**) *Ammotium* cf. *morenoi* (Acosta, 1940); (**3, 4**) *Arenoparella mexicana* (Kornfeld, 1931), (**3**)—spiral view, (**4**)—umbilical view; (**5**) *Eggerelloides scaber* (Williamson, 1858); (**6**) *Haplophragmoides wilberti* (Anderson, 1953); (**7, 8**) *Entzia macrescens* (Brady, 1980), (**7**)—spiral view, (**8**)—umbilical view; (**9, 10**) *Miliammina fusca* (Brady, 1980); (**11**) *Nodulina dentaliniformis* (Brady, 1844); (**12**) *Scherochorella moniliformis* (Siddall, 1886); (**13, 14**) *Trochammina inflata* (Montagu, 1808), (**13**)—umbilical view, (**14**)—spiral view; (**15, 16**) Undetermined Textularid

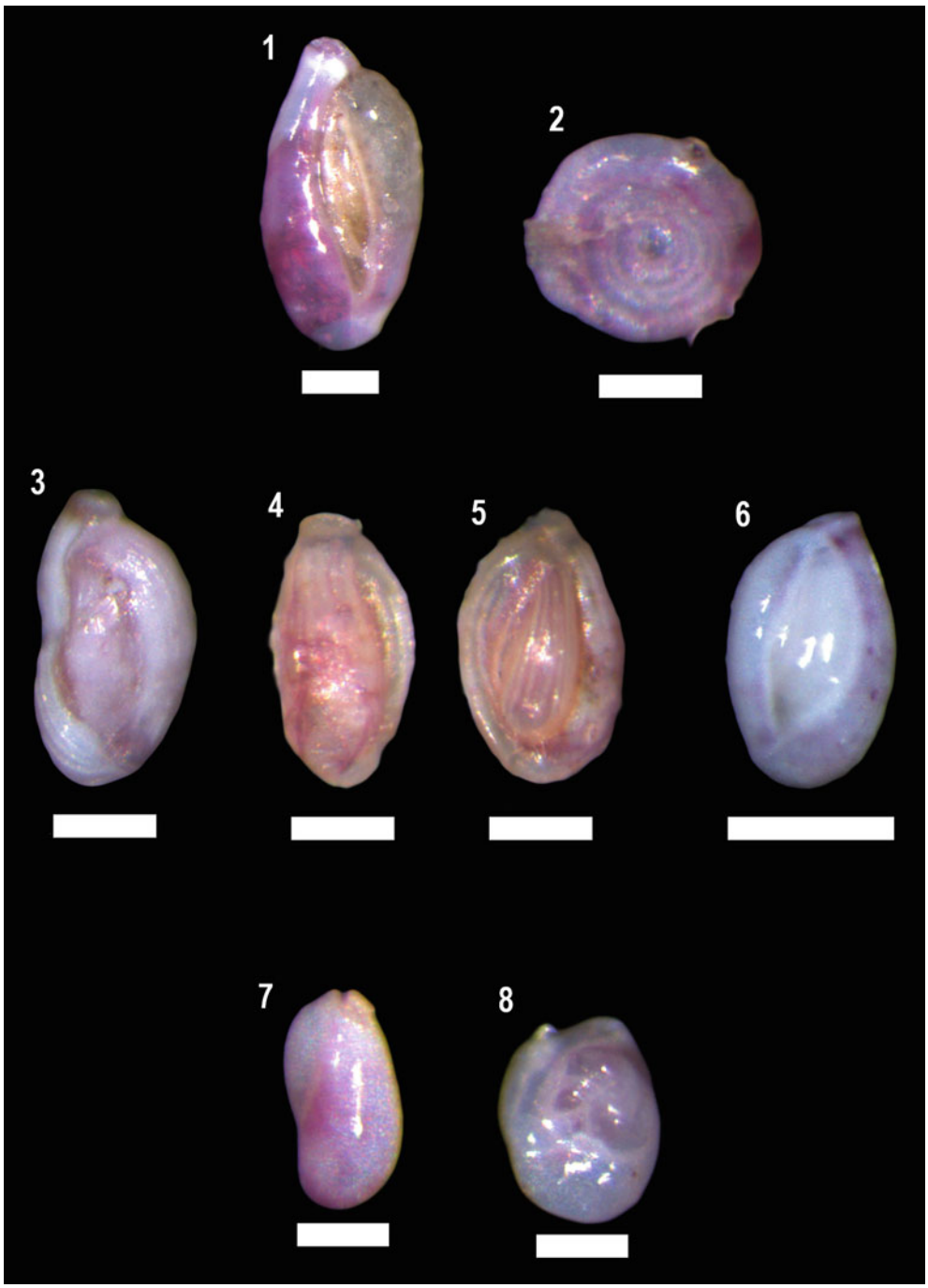

Plate 15.2 Living foraminiferal tests. (**1**) *Adelosina longirostra* (d'Orbigny, 1939); (**2**) *Cornuspira incerta* (d'Orbigny, 1939); (**3–5**) *Quinqueloculina jugosa* (Cushman,1944); (**6**) *Quinqueloculina seminula* (Linneaus, 1758); (**7, 8**) Undetermined Miliolid

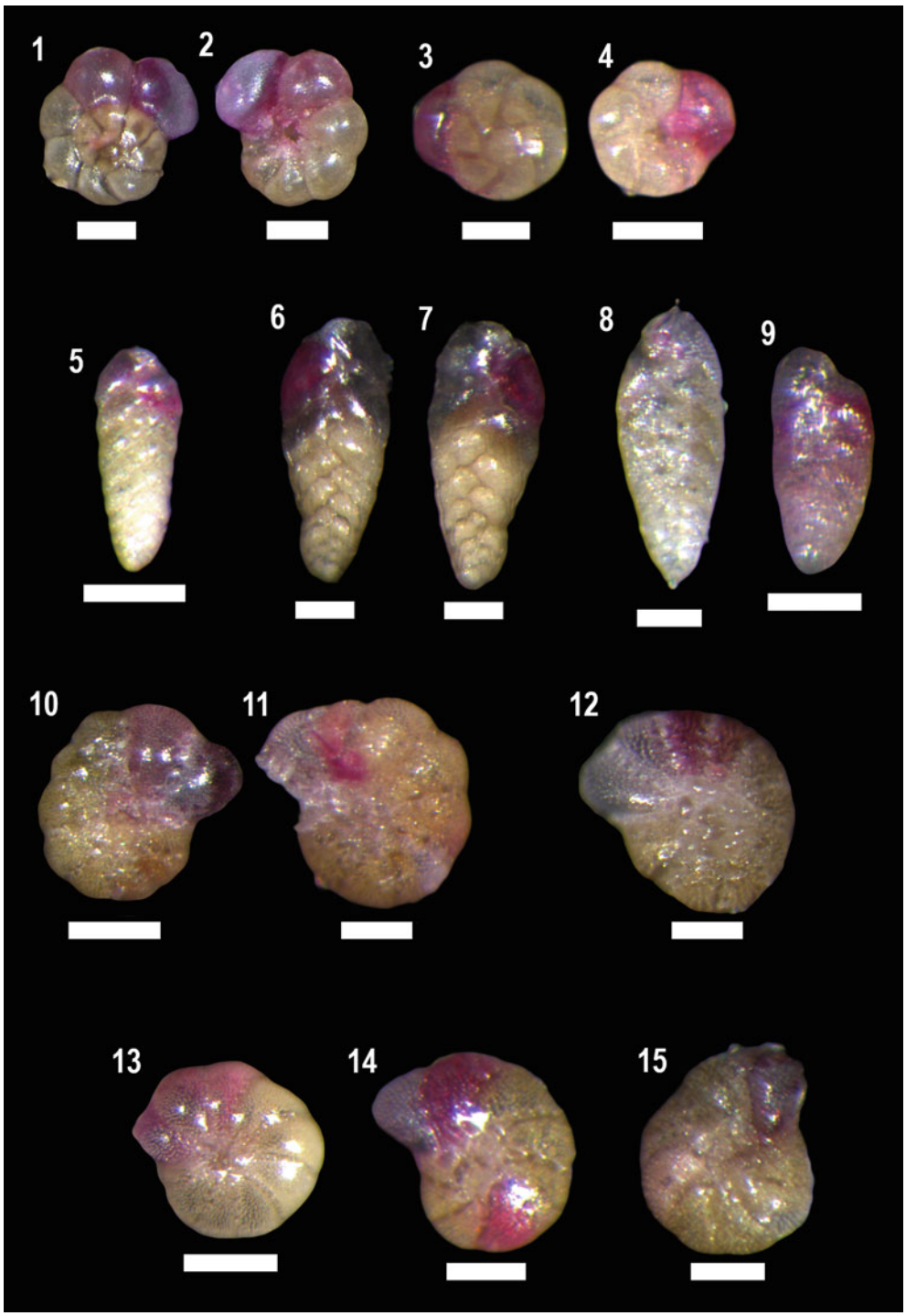

Plate 15.3 Living foraminiferal tests. (**1–4**) *Ammonia tepida* (Cushman, 1926), (**1, 3**)—spiral view, (**2, 4**)—umbilical view; (**5**) *Bolivinellina pseudopunctata* (Höglund, 1947); (**6, 7**) *Bolivina subaenariensis* (Cushman, 1922), (**6, 7**)—general view; (**8**) *Bolivina spathulata* (Williamson, 1858); (**9**) *Bolivina striatula* (Cushman, 1922); (**10, 11**) *Cribroelphidium excavatum* (Terquem, 1875), (**10, 11**)—general view; (**12**) *Elphidium oceanense* (d'Orbigny in Fornasini, 1904); (**13–15**) *Cribroelphidium selseyense* (Heron-Allen and Earland, 1911), (**13**)—general view (*C*. cf. *selseyensis*), (**14, 15**)—general view

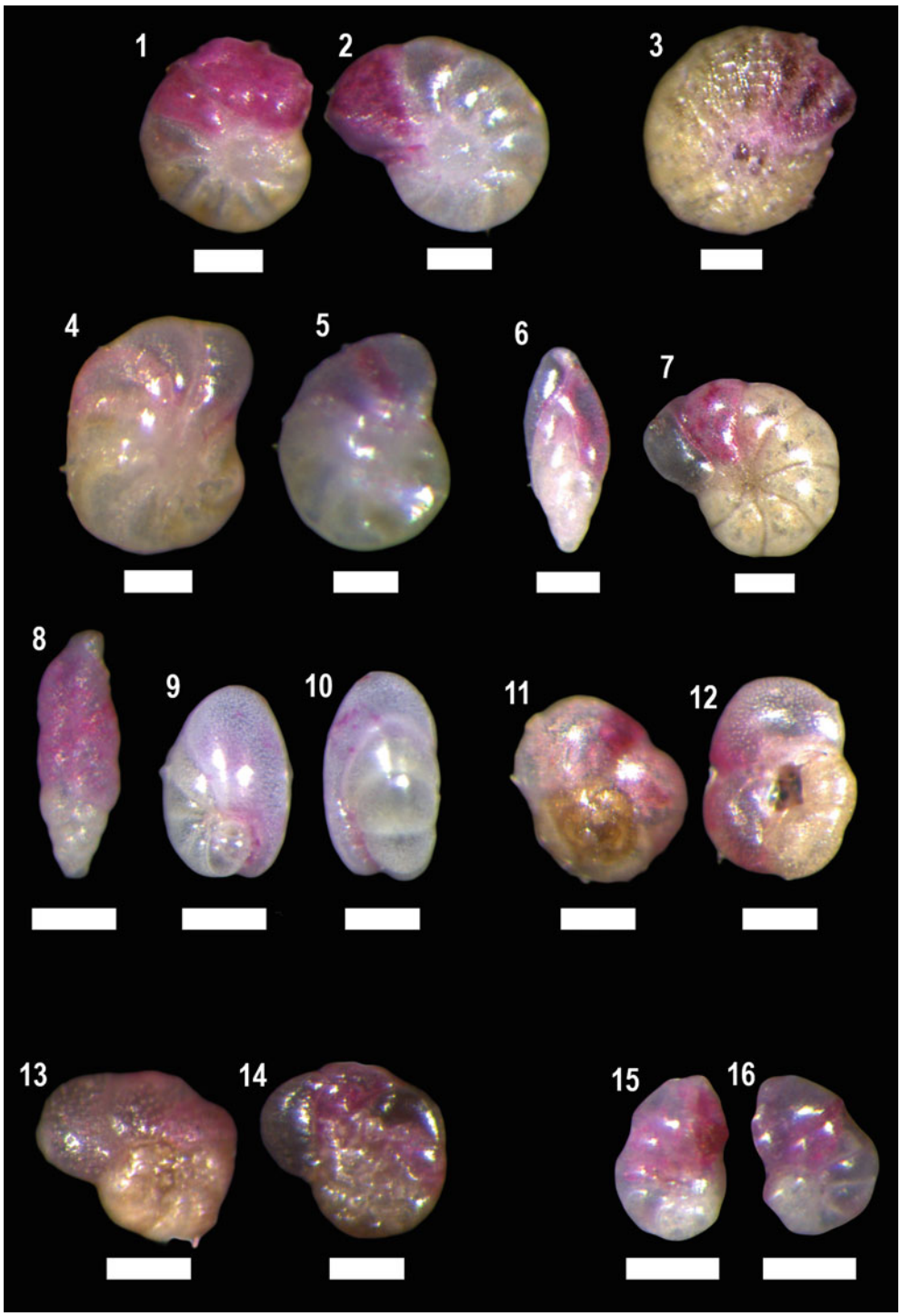

Plate 15.4 Living foraminiferal tests. (**1, 2**) *Cribroelphidium* sp.1, (**1, 2**)—general view; (**3**) *Cribroelphidium williamsoni* (Haynes, 1973); (**4, 5**) *Elphidium advenum* (Cushman, 1922), (**4, 5**)—general view; (**6**) *Stainforthia* cf. *fusiformis* (Williamson, 1858); (**7**) *Haynesina germanica* (Ehrenberg, 1840); (**8**) *Hopkinsina pacifica* (Cushman, 1933); (**9, 10**) *Nonionella opima* (Cushman, 1947), (**9, 10**)—general view; (**11–12**) *Rosalina globularis* (d'Orbigny, 1826), (**11**)—dorsal view, (**12**)—ventral view; (**13, 14**) *Trichohyalus aguayoi* (Bermudez, 1935), (**13**)—spiral view, (**14**)—umbilical view; (**15, 16**) *Pseudononion japonicum* (Asano, 1936), (**15, 16**)—general view

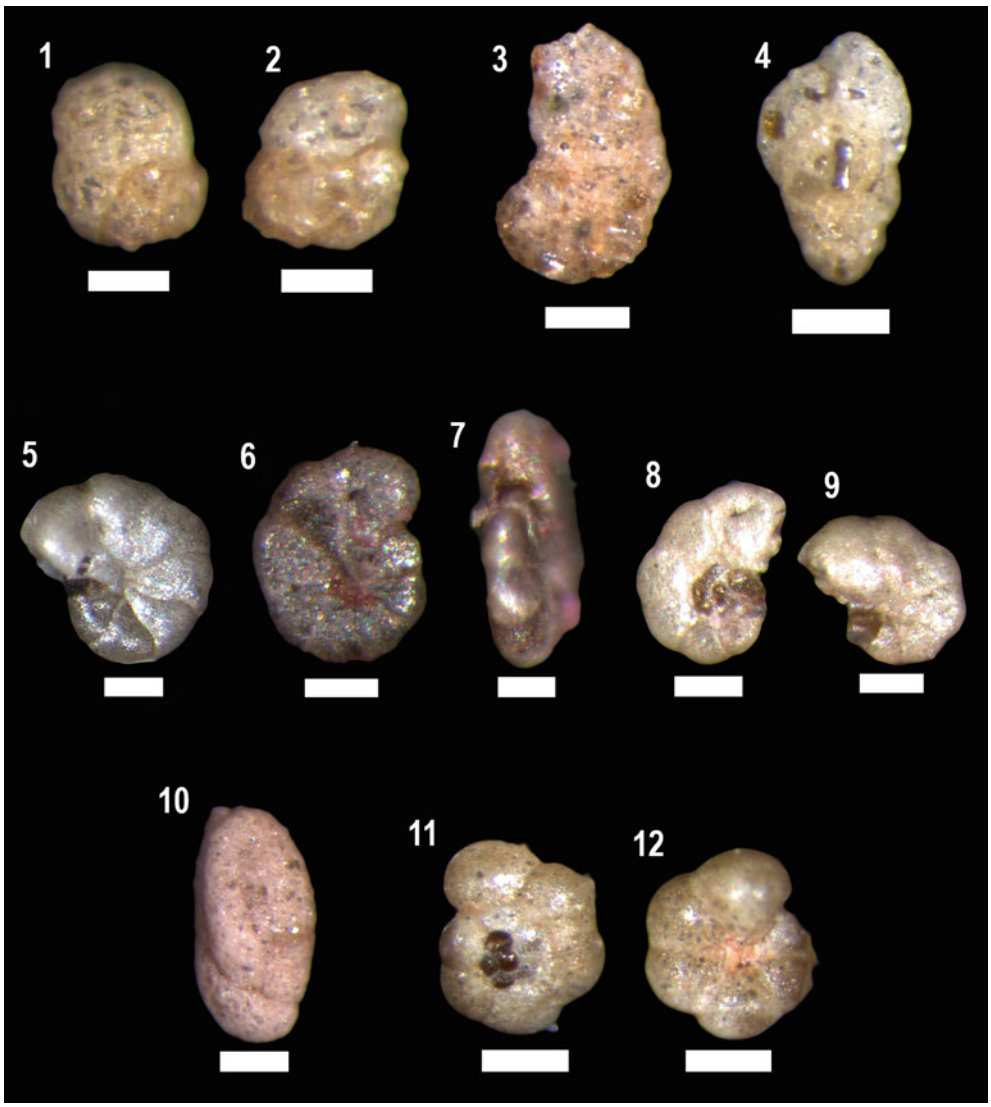

Plate 15.5 Dead foraminiferal tests. (**1, 2**) *Ammosphaeroidina* sp.1, (**1, 2**)—general view; (**3**) *Ammotium* cf. *morenoi* (Acosta, 1940); (**4**) *Eggerelloides scaber* (Williamson, 1858); (**5–7**) *Haplophragmoides wilberti* (Anderson, 1953), (**5, 6**)—general view, (**7**)—edge view; (**8, 9**) *Entzia macrescens* (Brady, 1870), (**8**)—umbilical view, (**9**)—spiral view; (**10**) *Miliammina fusca* (Brady, 1870); (**11, 12**) *Trochammina inflata* (Montagu, 1808), (**11**)—spiral view, (**12**)—umbilical view

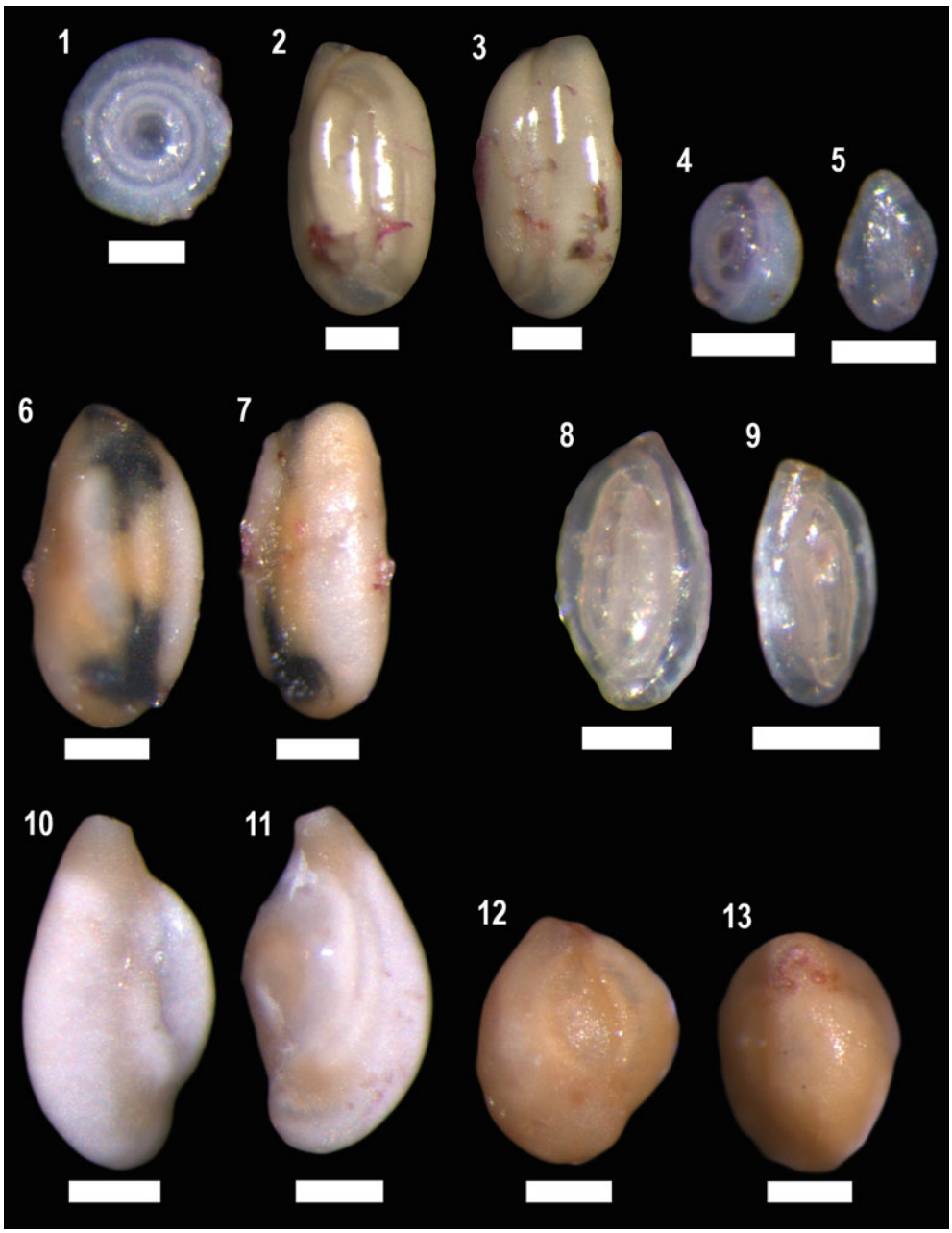

Plate 15.6 Dead foraminiferal tests. (**1**) *Cornuspira incerta* (d'Orbigny, 1939); (**2, 3**) *Quinqueloculina seminula* (Linneaus, 1758), (**4, 5**) Undeterminated Miliolid; (**6, 7**) *Quinqueloculina seminula* (Linneaus, 1758), (**6, 7**)—general view, pyritized test; (**8, 9**) *Quinqueloculina schlumbergeri* Wisner, 1923, (**8**)—general view, (**9**)—oblique view; (**10, 11**) *Adelosina dubia* d'Orbigny in Fornasini, 1905, (**10, 11**) general view; (**12, 13**) *Triloculina* sp. 1, (**12**)—general view, (**13**)—apertural view

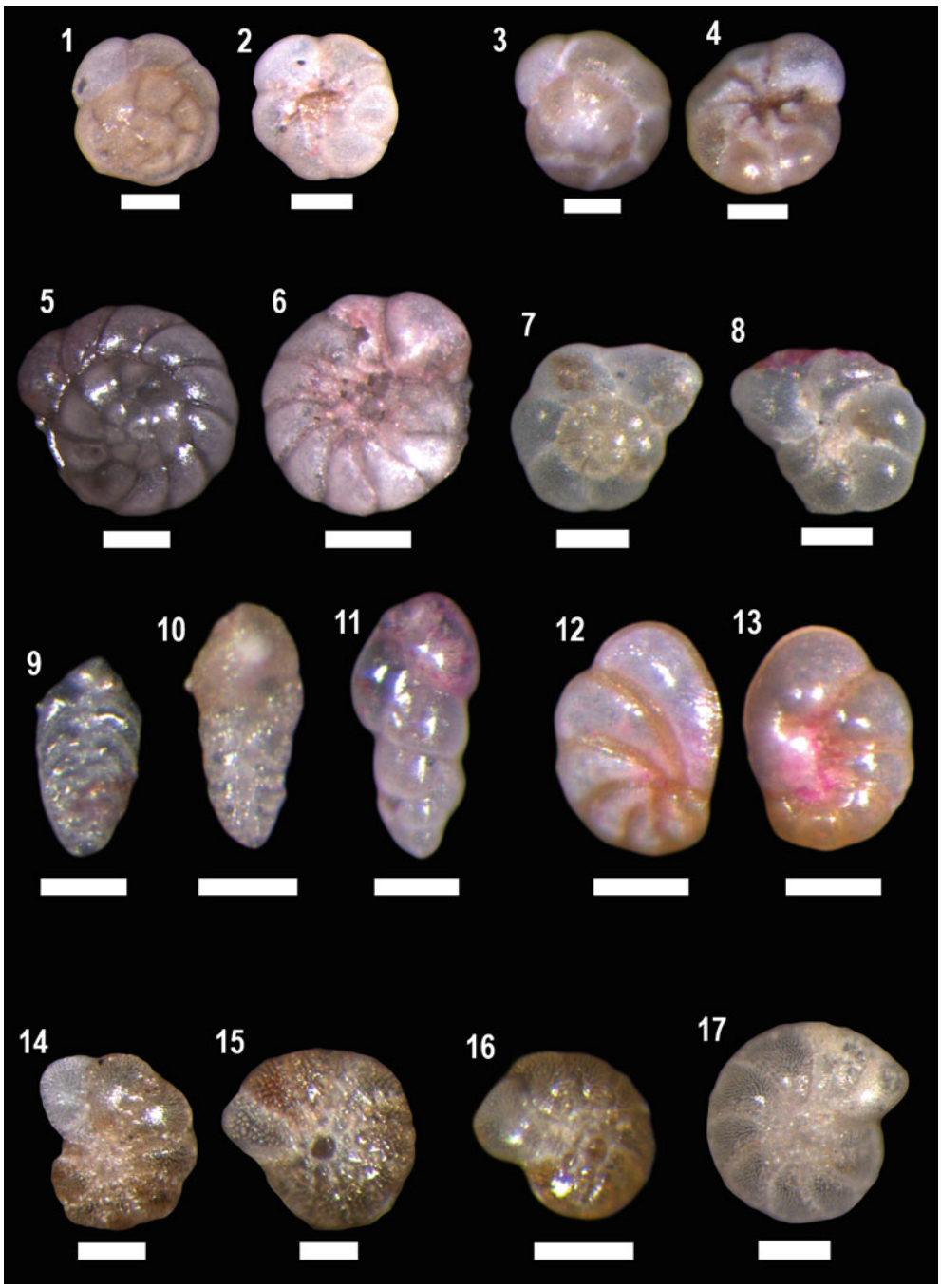

Plate 15.7 Dead foraminiferal tests. (**1–6**) *Ammonia tepida* (Cushman, 1926), (**1, 3**)—*Ammonia tepida,* spiral view, (**2, 4**)—*Ammonia tepida,* umbilical view, (**5**)—*Ammonia beccarii* (Linneaus, 1758), spiral view, (**6**)—*Ammonia beccarii* (Linneaus, 1758), umbilical view; (**7, 8**) *Aubignyna perlucida* (Heron-Allen and Earland, 1913), (**7**)—spiral view, (**8**)—umbilical view; (**9**) *Bolivina dilatata* (Reuss, 1850); (**10**) *Bolivina variabilis* (Williamson, 1859); (**11**) *Bulimina gibba* (Fornasini, 1902); (**12, 13**) *Cancris auricula* (Fichtel and Moll, 1798); (**14**) *Cribroelphidium excavatum* (Terquem, 1875); (**15**) *Elphidium oceanense* (d'Orbigny in Fornasini, 1904); (**16**) *Cribroelphidium* cf. *poeyanum* (d'Orbigny, 1839); (**17**) *Cribroelphidium selseyense* (Heron-Allen and Earland, 1911)

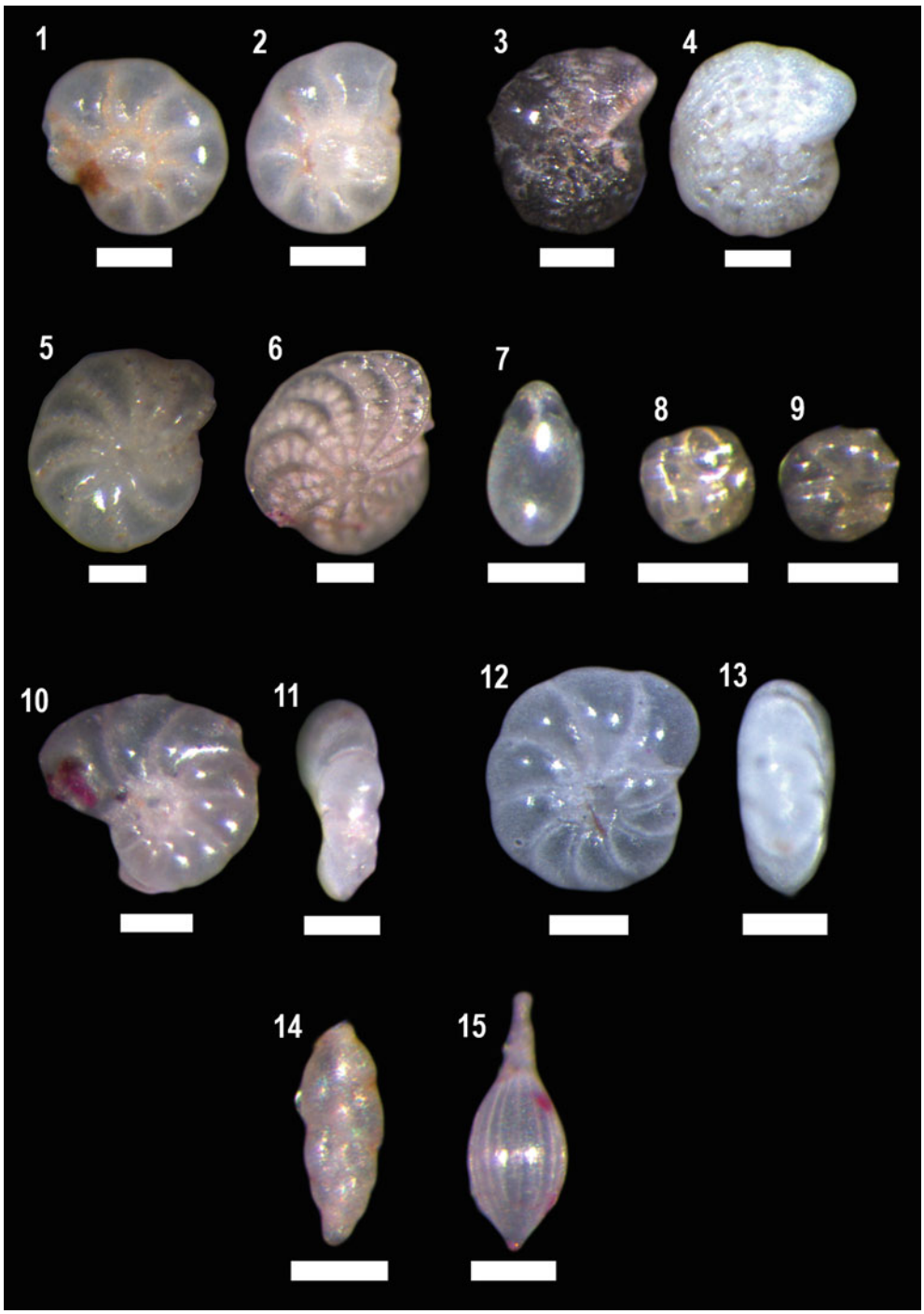

Plate 15.8 Dead foraminiferal tests. (**1, 2**) *Cribroelphidium* sp.1; (**3, 4**) *Cribroelphidium williamsoni* (Haynes, 1973), (**3**)—general view, pyritized test, (**4**)—general view; (**5**) *Elphidium advenum* (Cushman, 1922); (**6**) *Elphidium crispum* (Linneaus, 1758); (**7**) *Fissurina lucida* (Williamson, 1858); (**8, 9**) *Gavelinopsis praegeri* (Heron-Allen and Earland, 1913); (**10, 11**) *Haynesina depressula* (Walker and Jacob, 1798), (**10**)—dorsal view, (**11**)—edge view; (**12, 13**) *Haynesina germanica* (Ehrenberg, 1840), (**12**)—dorsal view, (**13**)—edge view; (**14**) *Hopkinsina pacifica* (Cushman, 1933); (**15**) *Lagena sulcata* (Walter and Jacob, 1798)

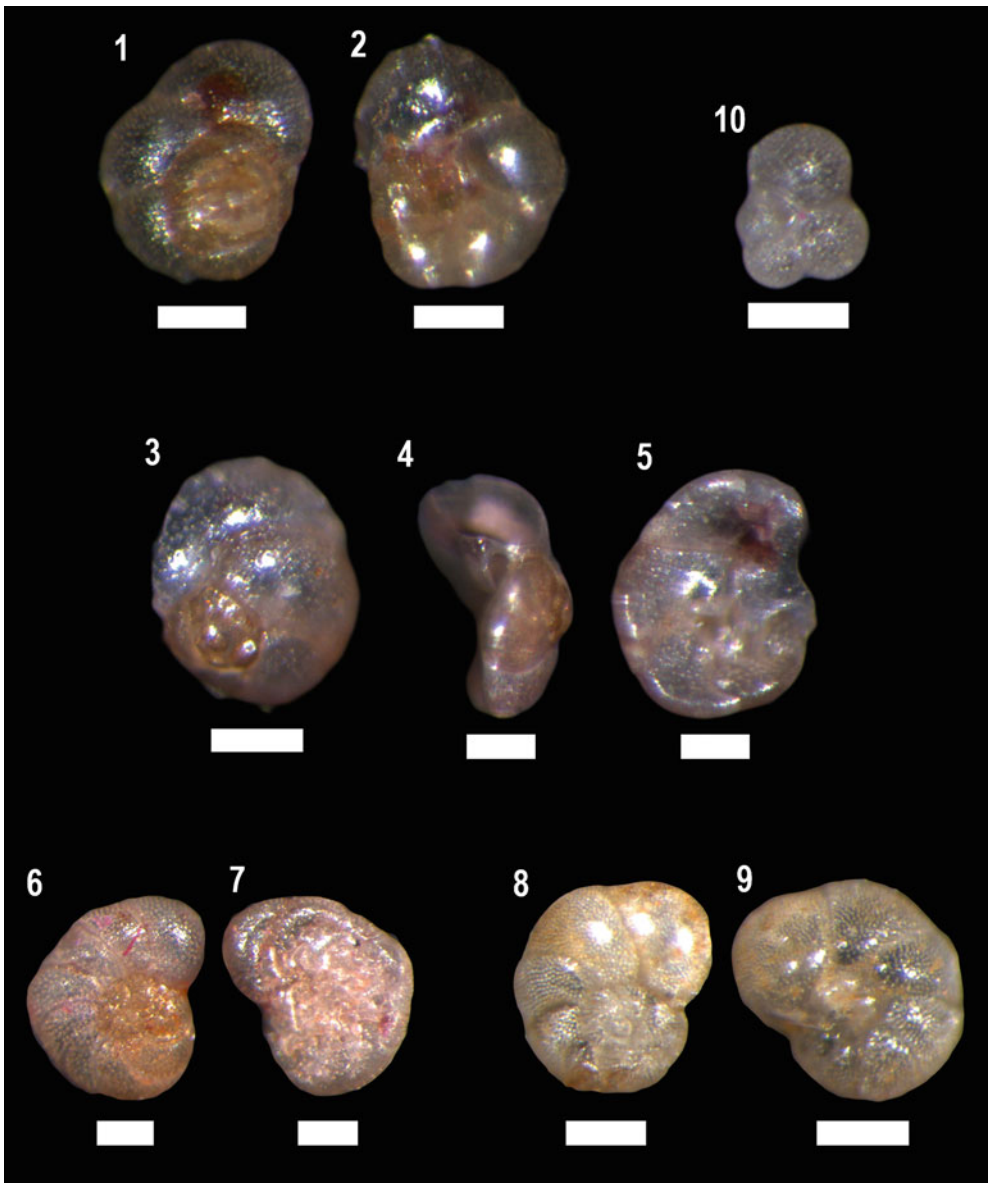

Plate 15.9 Dead foraminiferal tests. (**1, 2**) *Rosalina globularis* (d'Orbigny, 1826), (**1**)—spiral view, (**2**)—umbilical view; (**3–5**) *Rosalina irregularis* (Rhumbler, 1906), (**3**)—spiral view, (**4**)—edge view, (**5**)—umbilical view; (**6, 7**) *Trichohyalus aguayoi* (Bermudez, 1935) (**6**)—spiral view, (**7**)—umbilical view; (**8, 9**) *Valvulineria bradyana* (Fornasini, 1899) (**8**)—spiral view, (**9**)—umbilical view; (**10**) Planktonic form (cf. *Globigerina* sp.)

References

1. Ehrenberg, C.G.: Verbreitung und Einfluss des mikroskopischen Lebens in Süd-und Nord-Amerika. Königlichen Akademie der Wissenschaften, Berlin (1843)
2. Alve, E.: Colonization of new habitats by benthic foraminifera: a review. Earth-Sci. Rev. **46**(1–4), 167–185 (1999)
3. Bie, T., et al.: Body size and dispersal mode as key traits determining metacommunity structure of aquatic organisms. Ecol. Lett. **15**(7), 740–747 (2012)
4. Day, J.W., Psuty, N.P., Perez, B.C.: The role of pulsing events in the functioning of coastal barriers and wetlands: implications for human impact, management and the response to sea level rise. In: Weinstein, M.P., Kreeger, D.A. (eds.) Concepts and Controversies in Tidal Marsh Ecology, pp. 633–659. Springer, Dordrecht (2002)
5. Wetzel, R.G.: Lake and river ecosystems. Limnology. **37**, 490–525 (2001)
6. Cearreta, A., Benito, X., Ibáñez, C., Trobajo, R., Giosan, L.: Holocene palaeoenvironmental evolution of the Ebro Delta (Western Mediterranean Sea): evidence for an early construction based on the benthic foraminiferal record. The Holocene. **26**(9), 1438–1456 (2016)
7. Benito, X., Trobajo, R., Ibáñez, C., Cearreta, A., Brunet, M.: Benthic foraminifera as indicators of habitat change in anthropogenically impacted coastal wetlands of the Ebro Delta (NE Iberian Peninsula). Mar. Pollut. Bull. **101**(1), 163–173 (2015)
8. Wachnicka, A., Collins, L.S., Gaiser, E.E.: Response of diatom assemblages to 130 years of environmental change in Florida bay (USA). J. Paleolimnol. **49**(1), 83–101 (2013)
9. Wachnicka, A., Gaiser, E.E., Boyer, J.: Ecology and distribution of diatoms in Biscayne Bay, Florida (USA): implications for bioassessment and paleoenvironmental studies. Ecol. Indic. **11**(2), 622–632 (2011)
10. Marco-Barba, J., Mesquita-Joanes, F., Miracle, M.R.: Ostracod palaeolimnological analysis reveals drastic historical changes in salinity, eutrophication and biodiversity loss in a coastal Mediterranean lake. The Holocene. **23**(4), 556–567 (2013)
11. Battarbee, R.W., et al.: Diatoms. In: Last, W.M., Smol, J.P., Birks, H.J.B. (eds.) Tracking Environmental Change Using Lake Sediments, pp. 155–202. Springer, London (2002)
12. Murray, J.W.: Ecology and Applications of Benthic Foraminifera. Cambridge University Press, New York (2006)
13. Smol, J.P., Stoermer, E.F.: The Diatoms: Applications for the Environmental and Earth Sciences. Cambridge University Press, Cambridge (2010)
14. Scott, D.B., Medioli, F.S., Schafer, C.T.: Monitoring in Coastal Environments Using Foraminifera and Thecamoebian Indicators. Cambridge University Press, New York (2007)
15. Loeblich Jr., A.R., Tappan, H.: Foraminiferal Genera and Their Classification. Springer, New York (2015)
16. Mann, D.G.: The species concept in diatoms. Phycologia. **38**(6), 437–495 (1999)
17. Hayward, B.W., Holzmann, M., Grenfell, H.R., Pawlowski, J., Triggs, C.M.: Morphological distinction of molecular types in ammonia–towards a taxonomic revision of the world's most commonly misidentified foraminifera. Mar. Micropaleontol. **50**(3–4), 237–271 (2004)
18. Carballeira, R., Trobajo, R., Leira, M., Benito, X., Sato, S., Mann, D.G.: A combined morphological and molecular approach to *Nitzschia varelae* sp. nov., with discussion of symmetry in Bacillariaceae. Eur. J. Phycol. **52**, 342–359 (2017)
19. Sabbe, K., et al.: Six new Actinella (Bacillariophyta) species from Papua New Guinea, Australia and New Zealand: further evidence for widespread diatom endemism in the Australasian region. Eur. J. Phycol. **36**(4), 321–340 (2001)
20. Mann, D.G., Droop, S.J.M.: Biodiversity, biogeography and conservation of diatoms. In: Kristiansen, J. (ed.) Biogeography of Freshwater Algae, pp. 19–32. Springer, London (1996)
21. Pawlowski, J., Lecroq, B.: Short rDNA barcodes for species identification in foraminifera. J. Eukaryot. Microbiol. **57**(2), 197–205 (2010)
22. Murray, J.W.: Living benthic foraminifera: biogeographical distributions and the significance of rare morphospecies. J. Micropalaeontol. **32**(1), 1–58 (2013)
23. Cox, E.J.: Diatom identification in the face of changing species concepts and evidence of phenotypic plasticity. J. Micropalaeontol. **33**, 111–120 (2014)
24. Kociolek, J.P.: A worldwide listing and biogeography of freshwater diatom genera: a phylogenetic perspective. Diatom Res. **33**(4), 509–534 (2019)
25. Cox, E.J.: Morphological variation in widely distributed diatom taxa: taxonomic and ecological implications. In: Marino, D., Montresor, M. (eds.) Proceedings of the 13th International Diatom Symposium, Italy, pp. 335–345. Biopress, Bristol (1995)
26. Trobajo, R., Rovira, L., Mann, D.G., Cox, E.J.: Effects of salinity on growth and on valve morphology of five estuarine diatoms. Phycol. Res. **59**(2), 83–90 (2011)
27. Elliott, M., Quintino, V.: The estuarine quality paradox, environmental homeostasis and the difficulty of detecting anthropogenic stress in naturally stressed areas. Mar. Pollut. Bull. **54**(6), 640–645 (2007)
28. Jorissen, F.J.: Benthic foraminiferal microhabitats below the sediment-water interface. In: Sen Gupta, B.K. (ed.) Modern Foraminifera, pp. 161–179. Springer, Dordrecht (1999)
29. Buzas, M.A., Culver, S.J., Jorissen, F.J.: A statistical evaluation of the microhabitats of living (stained) infaunal benthic foraminifera. Mar. Micropaleontol. **20**(3–4), 311–320 (1993)
30. Benito, X., Trobajo, R., Cearreta, A., Ibáñez, C.: Benthic foraminifera as indicators of habitat in a Mediterranean delta: implications for ecological and palaeoenvironmental studies. Estuar. Coast. Shelf Sci. **180**, 97–113 (2016)
31. Walton, W.R.: Ecology of living benthonic foraminifera, Todos Santos Bay, Baja California. J. Paleontol. **29**(6), 952–1018 (1995)
32. Alve, E., Murray, J.W.: Marginal marine environments of the Skagerrak and Kattegat: a baseline study of living (stained) benthic foraminiferal ecology. Palaeogeogr. Palaeoclimatol. Palaeoecol. **146**(1–4), 171–193 (1999)
33. Bernhard, J.M.: Distinguishing live from dead foraminifera: methods review and proper applications. Micropaleontology. **46**, 38–46 (2000)
34. Colom, G.: Foraminíferos ibéricos: introducción al estudio de las especies bentónicas recientes. Consejo Superior de Investigaciones Científicas, Patronato Juan de la Cierva (1974)
35. Cimerman, F., Langer, M.R.: Mediterranean Foraminifera. Slovenian Academy of Science and Arts and Swiss Academy of Natural Sciences, Ljubljana (1991)
36. Guillem Martínez, J.: Tafonomía, taxonomía y ecología de los foraminíferos de la Albufera de Torreblanca. PhD Thesis, Universitat de Valencia (2007)
37. Milker, Y., Schmiedl, G.: A taxonomic guide to modern benthic shelf foraminifera of the western Mediterranean Sea. Palaeontol. Electron. **15**(2), 1–134 (2012)
38. Jorissen, F.J.: The distribution of benthic foraminifera in the Adriatic Sea. Mar. Micropaleontol. **12**, 21–48 (1987)
39. Murray, J.W.: An Atlas of British Recent Foraminiferids. Elsevier, New York (1971)
40. Cushman, J.A.: The Foraminifera of the Atlantic Ocean, vol. 104. US Government Printing Office, Washington, DC (1918)
41. Cushman, J.A.: A Monograph of the Foraminifera of the North Pacific Ocean, vol. 71. US Government Printing Office, Washington, DC (1910)

42. Brady, B.: Palaeontographical Society Monographs: A Monograph of Carboniferous and *Permian foraminifera*. Palaeontographical Society, London (1876)
43. Phleger, F.B.: Foraminiferal populations and marine marsh processes. Limnol. Oceanogr. **15**(4), 522–534 (1970)
44. Fatela, F., Taborda, R.: Confidence limits of species proportions in microfossil assemblages. Mar. Micropaleontol. **45**(2), 169–174 (2002)
45. Cearreta, A.: Foraminiferal assemblages in the ria of San Vicente de la Barquera (Cantabria, Spain). Rev. Esp. Micropaleontol. **21**(1), 67–80 (1989)
46. Murray, J.W.: Living foraminiferids of tidal marshes; a review. J. Foraminifer. Res. **1**(4), 153–161 (1971)
47. Leorri, E., Cearreta, A.: Quantitative assessment of the salinity gradient within the estuarine systems in the southern Bay of Biscay using benthic foraminifera. Cont. Shelf Res. **29**(9), 1226–1239 (2009)
48. Debenay, J.P., Ba, M., Ly, A., Sy, I.: Les écosystèmes paraliques du Sénégal. Description, répartition des peuplements de foraminifères benthiques. Rev. Paléobiol. **6**(2), 229–255 (1987)
49. Spellerberg, I.F., Fedor, P.J.: A tribute to Claude Shannon (1916–2001) and a plea for more rigorous use of species richness, species diversity and the 'Shannon–Wiener' Index. Glob. Ecol. Biogeogr. **12**(3), 177–179 (2003)
50. Rogers, M.J.: An evaluation of an index of affinity for comparing assemblages in particular for Foraminifera. Palaeontology. **19**(Part 3), 503–515 (1976)
51. Cearreta, A.: Distribution and ecology of benthic foraminifera. Rev. Esp. Paleontol. **3**, 23–38 (1988)
52. Debenay, J.P., Bicchi, E., Goubert, E., Du Châtelet, E.A.: Spatio-temporal distribution of benthic foraminifera in relation to estuarine dynamics (vie estuary, Vendée, W France). Estuar. Coast. Shelf Sci. **67**(1–2), 181–197 (2006)
53. Underwood, G.J., Phillips, J., Saunders, K.: Distribution of estuarine benthic diatom species along salinity and nutrient gradients. Eur. J. Phycol. **33**(2), 173–183 (1998)
54. Weiss, D., Geitzenauer, K., Shaw, F.C.: Foraminifera, diatom and bivalve distribution in recent sediments of the Hudson estuary. Estuar. Coast. Mar. Sci. **7**(4), 393–400 (1978)
55. Rodriguez-Lazaro, J., Pascual, A., García, B.M.: Recent benthic foraminifers as indicators of the sedimentary dynamics of the Tina mayor and Tina Menor estuaries (S Bay of Biscay, N Spain). J. Mar. Syst. **109**, 213–232 (2013)
56. Mendes, I., Dias, J.A., Schönfeld, J., Ferreira, Ó.: Distribution of living benthic foraminifera on the northern gulf of Cadiz continental shelf. J. Foraminifer. Res. **42**(1), 18–38 (2012)
57. Juggins, S.: Quantitative reconstructions in palaeolimnology: new paradigm or sick science? Quat. Sci. Rev. **64**, 20–32 (2013)
58. Birks, H.J.B., Birks, H.H.: Quaternary Palaeoecology. University Park Press, Baltimore, MD (1980)
59. Saunders, K.M., Taffs, K.H.: Palaeoecology: a tool to improve the management of Australian estuaries. J. Environ. Manag. **90**(8), 2730–2736 (2009)
60. Kemp, A.C., Horton, B.P., Culver, S.J.: Distribution of modern salt-marsh foraminifera in the Albemarle–Pamlico estuarine system of North Carolina, USA: implications for sea-level research. Mar. Micropaleontol. **72**(3–4), 222–238 (2009)
61. Leorri, E., Gehrels, W.R., Horton, B.P., Fatela, F., Cearreta, A.: Distribution of foraminifera in salt marshes along the Atlantic coast of SW Europe: tools to reconstruct past sea-level variations. Quat. Int. **221**(1–2), 104–115 (2010)
62. Davidson, T.A., Bennion, H., Reid, M., Sayer, C.D., Whitmore, T.J.: Towards better integration of ecology in palaeoecology: from proxies to indicators, from inference to understanding. J. Paleolimnol. **60**(2), 109–116 (2018)
63. Gaiser, E.E., Rühland, K.: Diatoms as indicators of environmental change in wetlands and peatlands. In: Smol, J., Stoermer, E. (eds.) The Diatoms: Applications for the Environmental and Earth Sciences, 2nd edn, pp. 473–496. Cambridge University Press, Cambridge (2010)
64. Benito, X.: Benthic diatoms and foraminifera as indicators of coastal wetland habitats: application to palaeoenvironmental reconstruction in a mediterranean delta. PhD Thesis, Universitat Rovira I Virgili (2016)
65. Benito, X., Trobajo, R., Ibáñez, C.: Benthic diatoms in a Mediterranean delta: ecological indicators and a conductivity transfer function for paleoenvironmental studies. J. Paleolimnol. **54**(2–3), 171–188 (2015)
66. Wachnicka, A., Gaiser, E.E., Collins, L., Frankovich, T., Boyer, J.: Distribution of diatoms and development of diatom-based models for inferring salinity and nutrient concentrations in Florida bay and adjacent coastal wetlands of South Florida (USA). Estuar. Coasts. **33**(5), 1080–1098 (2010)
67. Gaiser, E.E., Wachnicka, A., Ruiz, P., Tobias, F., Ross, M.: Diatom indicators of ecosystem change in subtropical coastal wetlands. In: Bortone, S.A. (ed.) Estuarine Indicators, vol. 127144. CRC Press, Boca Raton, FL (2005)
68. Saunders, K.M.: A diatom dataset and diatom-salinity inference model for southeast Australian estuaries and coastal lakes. J. Paleolimnol. **46**(4), 525–542 (2011)
69. Rossi, V., Horton, B.P.: The application of a subtidal foraminifera-based transfer function to reconstruct Holocene paleobathymetry of the Po Delta, northern Adriatic Sea. J. Foraminifer. Res. **39**(3), 180–190 (2009)
70. Milker, Y., Schmiedl, G., Betzler, C.: Paleobathymetric history of the Western Mediterranean Sea shelf during the latest glacial period and the Holocene: quantitative reconstructions based on foraminiferal transfer functions. Palaeogeogr. Palaeoclimatol. Palaeoecol. **307**(1–4), 324–338 (2011)
71. Birks, H.J.B.: Numerical tools in palaeolimnology-progress, potentialities, and problems. J. Paleolimnol. **20**, 307–332 (1998)
72. Dufrêne, M., Legendre, P.: Species assemblages and indicator species: the need for a flexible asymmetrical approach. Ecol. Monogr. **67**(3), 345–366 (1997)
73. Rovira, L., Trobajo, R., Ibáñez, C.: The use of diatom assemblages as ecological indicators in highly stratified estuaries and evaluation of existing diatom indices. Mar. Pollut. Bull. **64**(3), 500–511 (2012)
74. Mazzei, V., Gaiser, E.E.: Diatoms as tools for inferring ecotone boundaries in a coastal freshwater wetland threatened by saltwater intrusion. Ecol. Indic. **88**, 190–204 (2018)
75. Trobajo, R., Cox, E.J., Quintana, X.D.: The effects of some environmental variables on the morphology of *Nitzschia frustulum* (Bacillariophyta), in relation its use as a bioindicator. Nova Hedwig. **79**(3–4), 433–445 (2004)
76. Ibañez, C., Curco, A., Day, J.W., Prat, N.: Structure and productivity of microtidal Mediterranean coastal marshes. In: Weinstein, M.P., Kreeger, D.A. (eds.) Concepts and Controversies in Tidal Marsh Ecology, pp. 107–136. Springer, New York (2002)
77. Gehrels, W.R., Roe, H.M., Charman, D.J.: Foraminifera, testate amoebae and diatoms as sea-level indicators in UK saltmarshes: a quantitative multiproxy approach. J. Quat. Sci. Publ. Quat. Res. Assoc. **16**(3), 201–220 (2001)
78. Amorosi, A., Dinelli, E., Rossi, V., Vaiani, S.C., Sacchetto, M.: Late quaternary palaeoenvironmental evolution of the Adriatic coastal plain and the onset of Po River Delta. Palaeogeogr. Palaeoclimatol. Palaeoecol. **268**(1–2), 80–90 (2008)
79. Juggins, S., Birks, H.J.B.: Quantitative environmental reconstructions from biological data. In: Last, W.M., Smol, J.P., Birks, H.J.B. (eds.) Tracking Environmental Change Using Lake Sediments, pp. 431–494. Springer, London (2012)

80. Patterson, R.T., Dalby, A.P., Roe, H.M., Guilbault, J.-P., Hutchinson, I., Clague, J.J.: Relative utility of foraminifera, diatoms and macrophytes as high resolution indicators of paleo-sea level in coastal British Columbia, Canada. Quat. Sci. Rev. **24**(18–19), 2002–2014 (2005)
81. Riveiros, N.V., Babalola, A.O., Boudreau, R.E., Patterson, R.T., Roe, H.M., Doherty, C.: Modern distribution of salt marsh foraminifera and thecamoebians in the Seymour–Belize inlet complex, British Columbia, Canada. Mar. Geol. **242**(1–3), 39–63 (2007)
82. Scrutton, M.E.: The distribution and ecology of recent foraminifera off the Ebro delta. PhD Thesis, University of Bristol, Bristol (1969)
83. Zalat, A., Vildary, S.S.: Environmental change in northern Egyptian Delta lakes during the late Holocene, based on diatom analysis. J. Paleolimnol. **37**(2), 273–299 (2007)
84. Logan, B., Taffs, K.H., Cunningham, L.: Applying paleolimnological techniques in estuaries: a cautionary case study from Moreton Bay, Australia. Mar. Freshw. Res. **61**(9), 1039–1047 (2010)
85. Prado, P., Alcaraz, C., Benito, X., Caiola, N., Ibáñez, C.: Pristine vs. human-altered Ebro Delta habitats display contrasting resilience to RSLR. Sci. Total Environ. **655**, 1376–1386 (2019)
86. Genua-Olmedo, A., Alcaraz, C., Caiola, N., Ibáñez, C.: Sea level rise impacts on rice production: the Ebro Delta as an example. Sci. Total Environ. **571**, 1200–1210 (2016)
87. Nicholls, R.J.: Coastal flooding and wetland loss in the 21st century: changes under the SRES climate and socio-economic scenarios. Glob. Environ. Change. **14**(1), 69–86 (2004)
88. Ibáñez, C., et al.: Basin-scale land use impacts on world deltas: human vs natural forcings. Glob. Planet. Change. **173**, 24–32 (2019)
89. Dijkstra, N., et al.: Baseline benthic foraminiferal assemblages and habitat conditions in a sub-Arctic region of increasing petroleum development. Mar. Environ. Res. **92**, 178–196 (2013)
90. Schönfeld, J., Alve, E., Geslin, E., Jorissen, F., Korsun, S., Spezzaferri, S.: The FOBIMO (FOraminiferal BIo-MOnitoring) initiative—towards a standardised protocol for soft-bottom benthic foraminiferal monitoring studies. Mar. Micropaleontol. **94**, 1–13 (2012)
91. Vyverman, W., et al.: Historical processes constrain patterns in global diatom diversity. Ecology. **88**(8), 1924–1931 (2007)
92. Costanza, R., et al.: The value of the world's ecosystem services and natural capital. Nature. **387**(6630), 253–260 (1997)
93. Casamayor, E.O.: Towards a microbial conservation perspective in High Mountain lakes. In: Catalan, J., Ninot, J.M., Aniz, M.M. (eds.) High Mountain Conservation in a Changing World, pp. 157–180. Springer, Cham (2017)

Glossary

These definitions have been compiled from different sources [1–15].

Abiotic Physical and chemical factors not related to organisms.

Abnormality A deviation from a normal physical condition present in an organism resulting from defective genes or developmental deficiencies.

Acid digestion A process of solving the sample by adding acids and heating until the matrix is fully decomposed.

Allochthonous Occurring outside the place of origin.

Allometry The statistical association between shape and size, refers to any change of shape with size.

Alveolar-capillary membrane A thin tissue layer that occurs between alveolar air and blood in the pulmonary capillaries in the gas exchange area of the lungs. It is used to prevent air bubbles from developing in the blood and blood from reaching the alveoli. The membrane can be permeated by molecular oxygen, CO_2, CO, and many other gasses.

Alveolus A hollow cavity which is an empty space within a body or organism.

Anaglyph Specific type of 3D image, where both semi-images are encoded with different colors (red and cyan) and afterwards superimposed. Viewing of anaglyphs and recognition of spatial effects can be only arranged with red-cyan glasses.

Analyzer Polarizing filter mounted beneath the eyepiece interacting with a polarizer situated beneath the specimen.

Anisotropic diffusion Noise reduction technique without removing significant parts of the image information, such as edges or contours.

Annulus (pl. annuli) Distal striae that are larger and more elongate with more densely spaced pores.

Aperture diaphragm Iris diaphragm situated in the condenser, used for regulating the condenser aperture.

Aperture reduction phase contrast Modification of phase contrast illumination characterized by optional use of the aperture diaphragm for enhancement of the spatial depth.

Apex In pennate diatoms, the poles or ends of the cell.

Apical axis Imaginary line that joins the two ends or apexes of the valve in pennate diatoms, corresponds to the length of the valve.

Apical pore field Group of pores arranged in a pole of the valve, in some genera such as *Gomphonema*, or at both ends of the valve, in many genera of araphid diatoms, or in the genus *Cymbella*. They produce a secretion of mucilage that allows the cell to attach to the substrate.

Aquascope An underwater viewing device used to view underwater organisms often from dry land or from a boat.

Arduino Mega A microcontroller board based on the ATmega2560.

Areola A hole in the basal layer of silica that is repeated regularly, usually obstructed by a thin layer of silica, the velum.

Artificial key An identification key based on whatever characters are easiest to observe and which produces the answer most quickly and reliably. It therefore need not bear any obvious resemblance to the classification to which it corresponds.

Asexual reproduction Any kind of reproduction that does not require the fusion of gametes.

Assemblage Populations of species identified in a sample.

Atrium The upper chamber through which blood enters the heart.

Autochthonous Occurring in the place of origin.

Autecological range Set of environmental factors that enable a species to develop.

Autofocusing (passive) Method to find the best in-focus images based on the number of images (stacks) taken by varying the focus lens position.

Autostereoscopic viewing techniques Specific viewing methods, with the help of which stereo pairs can be inspected and investigated without any optical devices. In general, cross-eyed view can be distinguished from parallel view.

Autotrophic Organism capable of producing complex biological nutrient compounds from basic inorganic sources.

G. Cristóbal et al. (eds.), *Modern Trends in Diatom Identification*, Developments in Applied Phycology 10,
https://doi.org/10.1007/978-3-030-39212-3

Auxospore Specialized cells formed by many diatom species responsible for restoring normal diatom size after successive divisions of mitotic cells.

Average shape of a sample The object with the least squared distances between Procrustes and individual shapes.

Axial light Central light running in or along to the optical axis, used for axial illumination.

Background correction The process to correct/remove acquisition artifacts such as inhomogeneous illumination or dust particles in slide preparations.

Bagging trees (or Random Forest) A method of classification based on constructing a set of decision trees and given by the mode of the classes.

Band-pass filter Only a band of wavelengths being inside of a defined interval can pass through the filter.

Basophilic Staining readily with basic dyes.

Batch processing Programs that are executed with minimum human interaction.

Bending energy The extent of deformation bending between two landmark structures as quantified by the function of thin plate spline.

Benthic Organisms living on or in close attachment to a substrate.

Benthos Biological community inhabiting the bottom of an aquatic ecosystem, or living near it.

Binocular vision This term denotes the inspection of an object with both eyes. Since the optical sensory organs are marked by a mutual distance of about 65 mm, the object is viewed by the left and right eye from slightly different perspectives, producing respective spatial information in the brain.

Binomial Taking two names in taxonomies, in particular those of the genus and species.

Biodiversity In a given habitat, the abundance of plant and animal life.

Biogeography The study of the geographical distribution of animals and plants.

Bioindicator Species whose function or population can reveal the ecological status of the environment.

Biomonitoring Assessment of environmental conditions by means of the use of indicator organisms.

Biota The biological community inhabiting a particular region.

Biotic indices Standardized metrics for the evaluation of any ecological aspect, based on parameters attributable to any organism, at an individual, population, or community level.

Biotic Related to organisms.

Bootstrap Random sampling with replacement în a given population.

Boundary layer The layer of fluid flowing slowly past a surface.

Brightfield Most commonly used illumination based on axial light carried out with transmitted or incident light. Specimens which absorb light are recognized on a bright background.

Bulb "Traditional" light source in microscopy, halogen lamp in most cases, mercury or xenon lamp in special applications.

Cavum Hyaline region on one edge of the central area, the margin on the inside of the valve thickened.

CEC Commission for Economical Community metric.

Central area Hyaline zone in the center of the valve. In some cases it coincides with the central node.

Central dark field Modification of dark field illumination carried out with central (paraxial) transmitted light and lenses interacting with a circular light stop.

Central fissure Extension of the raphe fissure through the nodules, without penetrating the valve wall, at the proximal ends of the raphe.

Central nodule Area separating the two proximal fissures of the raphe, sometimes thicker than the rest of the valve.

Centric A diatom with frustules that pattern symmetrically around a central point (with more than two symmetry planes).

Centroid size The measurement of scale or overall size used in the Procrustes study is the square root of the number of square distances of all landmarks from their joint centroid.

Chain codes Contour descriptors that a sequence of linear segments approximates a boundary. Eight standard line segments constitute the building approximation. The contour code is then the length K of chain V.

Character Set of states that describe some aspect of the organisms to which the character is to be applied.

Chlorophyceae A class of eukaryotic, mostly freshwater, algae that possess chlorophyll a and b and cellulose cell walls.

Cilium A hair like lash or fringe.

Circular oblique lighting (COL) Bright field illumination carried out with concentric oblique light.

Clade A collection of specimens that includes their most recent common predecessor and all of their offspring.

Cladogram A tree diagram used to illustrate phylogenetic relationships.

Classification (taxonomy) Process of defining and naming classes of organisms.

Clogged filters Plugged filters usually obstructed by blood clots in diatom forensic analysis.

Coefficient A number multiplying a function.

Color balance Can be regulated in a color camera in order to adapt the color sensitivity of the sensor to the color temperature and hue of the light source used.

Color filter (absorbing filter) Consists of colorized glass so that defined wave lengths can pass the filter, whereas other incoming wave lengths are absorbed and blocked.

Color temperature [$^\circ K$] The temperature of an ideal black body radiator that radiates color light equal to the light source.

Color It depends on the wavelength of light. Range of visible light: $380\,\text{nm} \leq \lambda \leq 750\,\text{nm}$. Non-visible light: ultraviolet ($\lambda < 380\,\text{nm}$), infrared ($\lambda > 750\,\text{nm}$).

Compensator Transparent and colorless filters used in qualitative polarized light microscopy for induction of additional color contrasts (Lambda compensator, for instance). In quantitative (crystallographic and mineralogical) polarized light microscopy such compensators are used for measurements.

Condenser Lens system used for directing and modulating the illuminating light.

Configuration of landmarks A complete set of registered landmarks for each specimen. Is a distinct sample from homology mapping through pairs of samples, a classified set of points over a whole collection of species that are all homologous.

Confinement Relative to stress gradient from fully marine to either brackish or hypersaline.

Connective Sideways view of the frustule displaying the cingulum and the valve mantles.

Consensus configuration The average configuration of landmark coordinates, computed following Procrustes superimposition, named also Procrustes average or mean shape.

Contrast Enhancement An image-processing filter that increases the contrast of shape or contour borders.

Convolutional Neural Network A class of deep neural networks specialized to analyze visual imagery.

Coordinates A set of values that define a point in geometrical space.

Copula Each of the normally open elements that make up the diatom cingulum and which fit together, thanks to their structure.

Corium The skin's deep inner vascular surface.

Corresponding points Two related points of an object on the left and right semi-image. Corresponding points do usually not occupy the same positions on the left and right image, but are characterized by a so-called deviation.

Costae Thickenings of silica in the valve. Appearing generally as double lines. They most commonly tend to the margins.

Cover slip Thin plane parallel glass plate used for covering the specimen.

Cross-eyed view A specific type of autostereoscopic viewing technique, where the left eye exclusively stares on the right semi-image and the right eye solely inspects the left semi-image. Optimization of this viewing method can be achieved by application of the finger method.

Cryptic Obscured, hidden diversity as a result of similar morphological features.

Curved space Space configured with coordinates and a distance function not proportional to the correct radius power, for example, the space of Kendall.

CVA (Canonical Variate Analysis) Approach in which the group variance is represented relative to the matrix of pooled variance within the group. This considers linear data transformations that optimize variance between groups. The approach is similar to MANOVA (Variance Multivariate Analysis).

Cyanobacteria Prokaryotic phototrophic organisms that occur aş isolated cells or in colonies (e.g., filaments) in diverse habitats; important as phytoplankton.

Dark field Illumination mode showing specimens brightly irradiated on a dark or black background, carried out with transmitted or incident oblique peripheral light. Suited for examination of light absorbing or phase specimens.

Daylight filter Blue filter used for compensation of red hue.

Dead assemblages Foraminiferal fauna lacking alive parts at the time of sampling and thus not stain bright red when Rose Bengal is added in the sample.

Deep learning Machine learning methods based on artificial neural networks.

Deformation grid A standard deformed grid showing the variations in shape between two landmark arrangements.

Depth of a test Number of tests preceding it on a branch in a taxonomic key.

Descriptor A variable (usually numerical) that characterizes an object.

Deviation Physical parameter describing the intensity of the stereoscopic effect. The deviation (d) can be expressed from a numerical point of view through the simple formula. $d = x_l - x_r$, where x_l and x_r, respectively, denote the distances of left and right corresponding point from the right vertical edge of the left and right semi-image.

Diagnosis In botanical nomenclature, a statement of that which in the opinion of its author distinguishes a taxon from other taxa.

Diaphysis A long bone's primary (mid) segment.

Diatomological index Biological index based on diatom communities.

DIC prism Optical component in interference contrast devices used for splitting and re-uniting the illuminating light beams. Synonym: Wollaston prism.

DIC Differential interference contrast. Technique for optical contrast enhancement of phase specimens based on interference of two parallel and polarized light beams separated at a distance lower than the resolution limit.

Diffuser Opaque filter used for achievement of homogeneous fields.

Discriminant function Assign a finding to a specific group in a collection of groups.

Disorganization can Metal container where the digestion of tissues is performed in the forensic diatom analysis.

Dissimilarity coefficient A function that measures the difference between two objects. The diatom assembly in a lung or clothing sample is compared numerically with the diatom assemblies in all other control samples.

Diversity Number of species standardized by sample size.

Dominance The prevalence of a certain species/population in the biotic community due to their ecological or adaptive advantages.

Dominant species Relative to a predominant species in a sample or assemblage.

Dorsal In asymmetrical diatoms, frustular side with a convex margin. The opposite side is the ventral margin.

Double polarizing filters A couple of rotatable polarizing filters used for continuous dimming of illuminating light.

Drowning A severe type of asphyxia in which ambient oxygen (air) has been replaced by a liquid (usually water) and respiratory orifices have been totally or partially submerged.

Dyspnea Difficult, labored, or obstructed breathing. The sense of "not getting enough air." This is a feature usually associated with heart or lung diseases, as well as other forms of asphyxia, such as drowning.

Ecological Quality Ratio (EQR) The proportion between the magnitude of the biological parameter observed for a given surface water body and the value predicted under comparative conditions.

Ecotype A geographic variety of a species which is genotypically adapted to a particular habitat.

Edema Localized enlargement from prolonged watery fluid accumulation in tissues or cells.

Eigenshapes Main elements of an information outline, using curves as relative warps for landmarks.

Eigenvalues In an eigendecomposition of a covariance matrix, the eigenvalues represent the magnitude of the variance of the data along the eigenvectors.

Eigenvectors In an eigendecomposition of a covariance matrix, the eigenvectors represent the directions of the largest variance of the data.

Elliptic Fourier Analysis Process for contour analysis in which variations in x, y, and possibly z coordinates match separately by Fourier analysis as arc length functions.

Emission filter Used in a fluorescence microscope for blocking the excitation light and selecting the emitted light.

Emphysema aquosum Is the term used to describe hyperexpanded and "waterlogged" lungs, and which do not collapse on removal from the body.

Enzymatic digestion A method of dissolving a biological sample by adding digestive enzymes that break down macromolecules into their basic molecules.

Eosin A red fluorescent stain arising from bromine action on fluorescein used for studying cell structures.

Epifaunal Organism living on the surface of the sediment.

Epilithic/Epilithon Growing on stones.

Epipelic Growing on sediments.

Epiphelon Microscopic algae living on sediments.

Epiphenomenon A secondary phenomenon that is a by-product of another phenomenon.

Epiphyton Microscopic algae growing on seaweeds or on aquatic plants.

Epitheca The greater part of the frustule that covers the hypotheca, it consists of the epivalve and the epicingulum.

Epithelium Membrane tissue that covers internal organs and other internal body surfaces.

Eukaryote An organism whose cells contain a nucleus within a membrane.

Eurytopic Species having broad ranges of tolerances for a given environmental factor.

Eutrophic Water body rich in nutrients and subject to eutrophication.

Excitation filter Used in a fluorescence microscope for selecting the excitation light.

Exoskeleton The external structure or shell that covers and maintains most species.

Exposure fusion A technique for blending multiple exposures of the same object into a single image.

Eyepiece Lens system used for post magnification of the intermediate image. Synonym: ocular.

FHI Fluvial Habitat Index for Mediterranean streams.

Fibula Silica bridge between the sides of the raphe channel.

Field diaphragm Iris diaphragm mounted in the illuminating light path, used for regulating the diameter of the illuminating light field.

Filter Plane parallel transparent plate used for colorization or modulation of light.

Fixation Conservation of a biological specimen to preserve the same characteristics shown in the environment.

Fluorescence microscopy Illumination technique used for visualization of fluorescent specimens. The probe examined can be auto-fluorescent or stained with a fluorescent dye. When illuminated with high intensity excitation light of a defined wave length or color, fluorescent specimens emit low intensity fluorescence light of a longer wavelength and different color. This light can be visible when the excitation light is blocked by a so-called emission filter.

Foramen Opening or hole on the outside of the silica wall of the frustule.

Forensic autopsy A battery of studies and procedures carried out on the body to assess the existence of an injury and/or classify any infection that may have caused or led to death.

Form space The space constructed of shapes from which differences due to location and rotation are removed.

Fossil Organism or part of it preserved in the sedimentary archive.

Fourier analysis Periodic function decomposition in a number of basic sinusoidal elements.

Freeman chain code A contour encoding method where each symbol represents the direction of its movement.

Frustule A characteristic siliceous cover of diatoms, with reliefs that allow their taxonomic identification. It is composed of two halves (the thecae) which fit together.

Fultoportula Opening through the valve wall that forms a thin tube into the valve, surrounded by a ring of two to five structures (satellite pores) that penetrate the valve wall.

Fumed HNO3 Pyrogen HNO3, producing heat.

Gamete The male or female reproductive cell that contains half the genetic material of the organism.

Genera Taxonomic groups covering usually more than one species.

Generalized Procrustes analysis An analytical procedure for superimposing landmark/semi-landmark configurations to obtain shape variables.

Genome An organism's complete DNA sequence.

Girdle (or copula) Linking, siliceous bands associated with a valve.

Gradient A relational difference between states.

Graphics Processing Unit (GPU) Specialized electronic circuits with highly parallel structures that are more efficient to process large blocks of data in parallel.

Green filter Used for optimization of gray tones in black and white photomicrography.

Guided filtering A function that performs edge-preserving smoothing on an image based on the contents of a second image, called "guidance image."

Habitat Biotic and abiotic components and their interactions that characterize the environment.

Haloing Special artifact of phase contrast leading to bright or dark margins surrounding the specimen's contours or structures (synonym: halo artifact).

Heavy metal Any metal or metalloid that is known for its potential toxicity to the environment.

Heteropolar Frustules with the valve ends unequal in shape and size.

Heterotrophic Regarding species requiring organic compounds for nutrition; unable to produce food from inorganic substances.

High Dynamic Range A method for reproducing a wider range of dynamic lightness.

Hybridization The action of combining different animal or plant species or varieties and hybridizing.

Hymen A very thin sheet of silica with small circular or elongated perforations covering some areolae in pennate genera.

Hyperplane The vector to which it is orthogonal characterizes a $k-1$ subspace of k dimensional space.

Hyperspace A space characterized by more than three dimensions.

Hypostasis A reddish-purple hue, secondary to gravity, in specific areas of the body due to blood deposition in the small vessels of the dependent regions. Hypostasis is sometimes misinterpreted by people who are not familiar with this process.

Hypotheca The smaller part of the two thecae that constitute the frustule, consisting of the hypovalva and the hypocingulum.

Hypoxia The lack of oxygen triggers a very strong impulse to fix the deficiency.

Identification key Decision tree with inner node characters and terminal node taxon names. Each component corresponds to a character identity on the node from which it originates. The end-user begins at the origin of the tree and tracks the branches relating to the specimen's character state until the name of the taxon is reached.

Identification Method of identifying the taxon to which a species belongs once it has been identified.

Illuminator Assembly for illumination of specimens with incident light (fluorescence microscopy, wafer and industry microscopy).

Image calibration The relationship between number of pixels and a known distance.

Image stack A sequence of images of a transparent object (e.g., a frustule of a diatom) being characterized by a successive displacement of the focus plane. Distances between the focus planes of two succeeding images are usually on the order of several micrometers.

ImageJ An open source image processing program developed by the National Health Institute (NIH) in Java.

Incident light microscopy (epi-illumination) Used for examination of opaque reflecting probes illuminated by axial or oblique concentric or eccentric light. This illumination can be achieved with external light sources or special assemblies consisting of an illuminator and special lenses.

Indicator In environmental contexts, a measurable characteristic of a species, population or community that can be used to assess the ecological status of an ecosystem.

Infaunal Organism living within the sediment.

Infrared cut filter Absorbs infrared light.

Instance segmentation Segmentation technique that identifies each instance of an object in an image.

Intercalibration Process of methodological adjustment that allows to standardize the results of a biotic index at a regional or state scale.

Interference color Interference colors are induced when incoming light is divided into at least two parts having a different optical way and thus a different phase. Diatom frustules appear in various interference colors when illuminated in dark field light.

Interference contrast Technique for optical contrast enhancement of phase specimens based on interference of two parallel and polarized light beams separated at a distance lower than the resolution limit. Synonym: Differential interference contrast, DIC.

Interference filter Multilayer coated glass filter which selects transmitted light by induction of constructive and destructive interference. Wavelengths affected with destructive interference are eliminated and blocked, whereas wavelengths which are in constructive interference are augmented and pass the filter.

Intermediate image Magnified image of the specimen formed by the objective, projected into the tube and observed with the eyepiece.

Interpercentile Range of values situated between two given percentiles in a quantitative variable.

Interspace Space between two fibulae.

Intertidal Coastal habitat covered or uncovered by the sea tides.

Intraspecific Arising or occurring within a species.

IPH Hydrological Planning Instruction for Spanish rivers.

Iris diaphragm Diaphragm of variable diameter used as field diaphragm (situated in the illuminating light path), aperture diaphragm (situated in the condenser), and objective diaphragm (situated in special objectives used for dark field examination).

Isolate Population of organisms that has been obtained in pure cultures.

Isometry A geometric space or transformation which leaves unchanged the distances and angles between points.

Isopolar Frustules with valve ends equal in shape and size.

Keratin A fibrous protein that occurs in the outer layer of the skin and in corneous tissues including fingernails or hair.

Klein model A map and non-conformal model (does nor preserve angles) of the hyperbolic space represented through a unit disk where Euclidean lines are straight.

Köhler illumination Traditional design of illumination in up-to-date light microscopes based on field diaphragm and aperture diaphragm.

Kullback-Leibler distance A measure of how one probability distribution is different from a reference probability distribution. This distance can be used to distinguish the various groups/sites graphically using dendrograms. It's also called relative entropy.

Lamp housing External light source fitted with the microscope, containing a high intensity bulb (halogen, mercury, or xenon lamp, for instance).

Landmark A point of connection within and between populations on each object.

LDA (Linear Discriminant Analysis) A method that provides a linear combination of features that allows to separate two or more objects or classes

LED Light emitting diode.

Lefort aqua regia digestion Digestion performed by a mixture of concentrated nitric and hydrochloric acids. It is a highly corrosive liquid able to attack bones and other resistant tissues in diatom analysis.

Length of a branch Total number of tests leading to a given identification.

Lentic Slow moving water, e.g. ponds and lakes.

Life cycle Collection of stages from the initial cells to the senescent ones that cross the successive generations of each diatom species.

Light Can be described as electromagnetic wave or corpuscle (photon). It is characterized by the wavelength λ [nm] and the frequency ν. Velocity $V = \lambda \times \nu$.

Light source Bulb or LED used for illumination.

Light-dark gradient Brightness gradient on an LM or EM photograph of an opaque object. In the ideal case the light-dark gradient is oriented perpendicular to the image area, so that object depth mapping can be carried out with highest accuracy.

Line Spread Function (LSF) Response of an imaging system to a knife-edge test target.

Lineolae Areolae with an elongated foramen, arranged in longitudinal lines.

Living (stained) assemblages Foraminiferal fauna alive at the time of sampling.

Loading A calculated variable's relationship or covariance with a linear variables combination. For biological description, loadings are used.

Log Gabor filters In the Fourier domain, Gaussian functions moved from the origin to prevent the log-function's singularity.

Long-pass filter Used for blocking wavelengths being shorter or longer than a defined limit.

Lotic Living in actively moving freshwaters, e.g. rivers and streams.

Luminance contrast Axial dark field achieved with mirror lenses or modified glass lenses fitted with a centric light stop.

Lunate Resembling the new moon in shape.

Macroalgae Visible algae, seaweeds.

Macrophages Critical immune cells formed in response to an infection or aggregate damage or dead cells.

Macrophytes Aquatic plants growing in or near water.

Manifold A mathematical space that, on small scale, resembles an Euclidean space of certain dimension.

MANOVA (Multivariate Analysis of Variance) The simultaneous analysis of two or more dependent variables.

Marginal Shallow coastal environment influenced by the continental and the marine depositional realms, generally referring to lagoons, bays, deltas, or marshes.

Mean shape or Procrustes average The average coordinate of the Procrustes's distance.

Metric (Biology) A measure for quantitatively assessing a particular feature of the ecosystem. (Math) A non-negative function of which value is referred to as distance between two points.

Metric space A set of points for which there is a non-negative real number for each pair of points called the distance that is symmetrical and satisfies the inequality of the triangle.

Microalgae Algae 10–50 microns size range; note that here, the prefix "micro" is used indistinctly from microfauna despite the different size ranges of diatoms and foraminifera.

Micromanager An open software package for control of automated microscopes based on ImageJ.

Micrometer Unit of length used for measurements in light microscopy. 1 µm = 0.001 mm.

Micropollutants Pollutants that occur at very low concentrations (µg/L to ng/L) but that induce environmental and health effects, e.g. pesticides, pharmaceuticals, etc.

Modern analogue Fossil species assemblages that occur in modern environments.

Modulation Transfer Function (MTF) The Fourier transform of the LSF.

Monitoring program A monitoring software that tracks and regulates or verifies an ecosystem's health.

Monophyletic A community of organisms (not necessarily different species) that share a common ancestor.

Morphogenesis Differentiation and development of an organism's structure.

Morphological spaces Mathematical spaces describing and relating the configuration of organisms where the morphological configuration is represented by a point.

Morphology The branch of biology that deals with the structure of organisms.

Morphotype A variety of a biological taxon, distinguishable from others by some stable morphological features.

Mosaicking The process to construct a mosaic of images.

MOSFET Metal Oxide Semiconductor Field-Effect Transistor used, e.g., to reduce an LED current.

Mucilage A fluid that builds up in contact with water creating a slimy layer. Generally it is constituted by polysaccharides.

Multifocus fusion A method to create a new image that is focused throughout from a local measure of information content of source images.

Multiproxy Study combining more than one proxy (see proxy).

Nanometer [nm] Unit for defining very short distances and declaring wavelengths. 1 nm = 0.000001 mm.

Narrow band filter (monochromatic filter) Only a very small band of defined wavelengths can pass through the filter.

Nearshore Submerged, close (< 15 m) to the coast.

Neontology Part of the biology which deals with living (recent) organisms, unlike paleontology.

Neural network System architecture in which processors are paired in a way that suggests neuronal connections. Knowledge acquisition is done by trial and error.

Neutral filter (gray filter) Used for lowering the intensity of light without modifying the colorization.

Non-tidal Coastal environment not subject to tidal influence.

Norm Defines a distance function in the normed vector space.

Nosepiece Revolving turret containing a set of different objectives.

Numerical aperture (NA) Indicates the aperture of objectives and condensers ($\leq$0.9 in dry systems, $\geq$0.9 in immersion systems). The "ideal" total magnification (magnification of objective $\times$ magnification of eyepiece) should be higher than 500 $\times$ NA obj. and lower than 1000 $\times$ NA obj.

Nutrient An integral element or compound for growth or species. Nitrogen, phosphorus, and potassium are common nutrients.

Object depth mapping Computer-aided method, where three-dimensional information of a photographed object is produced with the help of image stacks or light-dark gradients. This information is subsequently used for the generation of stereo pairs.

Oblique light Concentric or eccentric light coming from the periphery of field, used for oblique illumination.

Ocellus A thick disc or silica plate that has no characteristics on its rim but is perforated with numerous densely packed pores, areolae or porelli.

Ocular Lens system used for post magnification of the intermediate image. Synonym: eye-piece.

Offshore Submerged, distant (> 15 m) to the coast.

Ordination analysis A generic term for multivariate analysis methods which adapts a multi-dimensional cluster of data points in a way that is typically two-dimensional when projected into lower space.

Organic compound A carbon compound and other element or radical element.

Orthogonal polynomial regression Employing Legendre polynomials, consist in fitting a least-square curve around an outline. From x, y coordinates of the

outline, coefficients derived from orthogonal polynomial regression are used as shape descriptors.

Orthonormal Vectors with length unity, orthogonal pairwise with respect to a matrix P such as matrix of identity. If the rows/columns are orthonormal as an array of vectors, a matrix is orthogonal.

Paleoenvironment Refers to an ancient environment.

Paleolimnological studies Studies referred to reconstruction of inland waters' paleo ecosystems, especially transformations associated with factors such as climate change, human activities, etc.

Parallel view A specific type of autostereoscopic viewing technique, where the left eye exclusively stares on the left semi-image and right eye solely inspects the right semi-image. For a successful realization of the method, the open hand can be used as partition between the visual axes.

Partial Least Squares A multivariate analysis to analyze relationships between two or more sets of variables evaluated on the same individual. This analyzes the covariances of variables between sets.

Partial warp scores Values that characterize each specimen's location within the partial warps space. They represent the rotation around the Procrustes mean configuration.

Partial warps Structures used to describe shifts in form and variability in collection of landmarks.

Patchy distribution Heterogeneous distribution at small, isolated areas.

PCA (Principal Component Analysis) A statistical technique that converts a collection of correlated variables t into a collection of uncorrelated quantities.

PCR Polymerase chain reaction (PCR) is a laboratory procedure used to produce multiple copies of a DNA fragment.

Pennate diatom Diatoms endowed with axial symmetry along a transapical axis.

Pennate A diatom (primary) symmetrical about the apical axis in valve view.

Periphyton Collection of microalgae, heterotrophic bacteria and detritus attached in most aquatic ecosystems to submerged surfaces.

Pervalvar axis Imaginary line that joins the two valves of a frustule, corresponds to the height of the cell.

Phagocytosis System in which phagocytes include microorganisms and cellular debris and digest them.

Phase congruency A measure of feature significance which is robust against illumination and contrast changes.

Phase contrast Illumination technique for examination of low density, so-called phase specimens. Such specimens are optically contrasted so that their density is different from the background.

Phase ring Annular light modulator situated inside of a phase contrast lens, mounted on a phase plate inserted in the objective's back focal plane.

Phenotype Every detectable organism trait arising from a combination of genetic characteristics and environmental conditions.

Phylogenetic With reference to an organism's evolutionary history.

Phylogeny The chain of events that entail the evolution of a species or a taxonomic group of organisms.

Phylum The major taxonomic group of animals and plants. It contains classes.

Phytobenthos Community of photosynthetic organisms, generally microalgae, that live attached to a substrate.

Phytoplankton Microscopic autotrophic forms of plankton.

PLA Polylactic acid biodegradable filament used for 3D printing.

Plankton Microscopic species that drift or float in the ocean or freshwater, whether animal or plant life, consisting mainly of single-cell green algae, diatoms, protozoa, and microinvertebrates.

Plastid Organelle carrying chlorophyll and other pigments in photo-synthesizing species.

Point Spread Function (PSF) Mathematical function that describes the response of an image-forming system to a point source.

Polarized light microscopy Technique for examination of anisotropic specimens by use of polarized illuminating light. The planes of oscillation are different in the illuminating background light and the image forming light that comes from the specimen. Thus, the specimen is contrasted towards the background when examined through a second polarizing filter, called analyzer.

Polarizing filter (polarizer) Light waves passing such a filter remain oscillating only in one defined plane.

Pole A minute passage or opening in diatom valves.

Poles or apices Endings of the apical axis.

Polymorphism Characteristic common in many diatom species by which they acquire different forms, dimensions, and proportions throughout their life cycle.

Pores or areolas Each of the valvar depressions that form the diatom striae.

Poroid Areola that is not markedly sunken on the surface of the basal silica layer of the frustule.

Principal warps Eigenfunctions of the folding energy matrix seen over the original landmark configuration as real twisted surfaces.

Prinsloo and Gordon artifact Hemorrhage on the cervical spine's anterior side, after the trachea and esophagus. It induces the greatest confusion in interpreting neck injuries.

Procrustes distance Distance between two forms considering the landmark configuration is the distance along the surface of the shape space that is not equivalent to the shortest distance in Euclidean space.

Procrustes shape coordinates Landmark shape positions after Procrustes superposition.

Proteinase A enzyme that catalyzes the division of proteins by a process known as proteolysis into smaller peptide fractions and amino acids.

Protist A single-cell organism capable of performing all the necessary functions for its survival. As well, a multicellular organism where a single cell can perform all of the organism's functions as a whole.

Protologue All related to a taxon term, e.g. overview, diagnosis, diagrams, images, references, synonymy, regional details, specimen quotation, discussion, and comments that is required for its publication.

Proxy A tool (geochemistry or species abundance) to infer past environmental conditions for which direct observations are not possible.

Pseudoraphe Hyaline area, without areolae, elongated, arranged between the two apexes of the valve in araphid and monoraphid diatoms.

Psoas Two abdominal and pelvic muscles that stretch the spine and turn the thigh.

Pulmonary alveoli Several of the slim-walled, baglike final expansions of pulmonary bronchioles, alveolar channels, and alveolar sacs through which gas exchange takes place between alveoli and capillaries.

Pulse Width Modulation A method for reducing the average power delivered by an electrical signal by dividing it into discrete parts.

Putrefaction The final phase after death, formed primarily by bacterial enzymes, often anaerobic organisms originating from the intestinal tract, and less frequently by the respiratory tract or an external skin injury.

QBR Index of riparian quality.

Radial symmetry The symmetry property around an axis.

Raphe Groove that runs longitudinally the raphid diatom valve, generally along the transaxial axis, and formed by two raphid branches.

Raphe channel Tube-shaped channel containing the raphe.

Raspberry Pi Zero A single-board low-cost computer with small form factor.

RCNN Region-based Convolutional Neural Network. A technique for deep learning applied to object detection.

Relative warps Main components of a shape distribution in the tangent space (to the shape space of Kendall).

Relief phase contrast Phase contrast carried out with an illuminating light sector instead of concentric light.

RGB Abbreviation of red, green, blue.

RGB intensifiers Interference filters used for selection of red, green, and blue.

Rheinberg illumination Multicolor dark field based on colorized background light and peripheral dark field light filtered at different colors.

Ricci flow An efficient method of curvature that is invariant to rigid movement, scaling, isometry, and conformity.

Rimoportula Opening through the valve wall. Inside the valve is surrounded by two labiate projections.

Rolling ball A mathematical morphology operator for background suppression, especially in the case of inhomogeneous illumination.

Saliency maps A representation by which information stands out relative to its neighbors that is frequently associated with visual attention.

Saprobic Live in an environment that is rich in organic matter but lacks oxygen.

Score Linear combination of variables observed.

Segmentation The process of partitioning a digital image into multiple segments.

Semantic segmentation Segmentation technique that labels each pixel of an image to a category of what is being represented.

Semi-image A single image resulting from the application of stereoscopic techniques. Two semi-images form a stereo pair and may be distinguished by slightly different positions of corresponding points.

Semi-landmarks Points arranged along an outline that capture information about curvature, making possible the study of complex, curved objects with sparse landmarks.

Senescent cell The smallest cells present in a diatom diminution series, formed just before auxo-sporulation.

Sequential Forward Feature Selection Use a subset of features for data approximation by sequentially selecting them.

Sexual reproduction Reproduction that involves the fusion of gametes.

Shade-off Typical artifact of phase contrast leading to artificial differences in brightness of peripheral and central zones in great areas of flat specimens.

Shallowness Relative to shallow water depth.

Shape variables New variables produced for sets of landmarks once the effect of position, orientation, and

scale were removed (transformation of original coordinate values.

Sigmoid S-shaped valves, with both ends curved in opposite directions.

Sigmoid (or logistic) function A mathematical S-shaped function. It has been used as activation function in neural networks.

Silica exoskeleton The external silica structure that supports and protects diatoms' cells.

Skeletal muscle A muscle that is attached to a bone at either or both ends, thereby moving parts of the skeleton. A muscle distinguished by transverse stripes.

Species The largest population of organisms in which any two members of the proper sexes or forms of mating may bear viable offspring, usually through sexual reproduction.

Specimen In botanical nomenclature, a gathering of a single species usually mounted as a single preparation. A specimen may consist of several individuals.

Specimen slide Plane parallel glass plate carrying the specimen.

Sphenoid Butterfly shaped bone at the skull's base.

Sphenoid sinus One of the four paired paranasal sinus that is contained within the body of the sphenoid bone, situated in the middle of the skull, towards the front inside the cranial cavity.

Spine Siliceous projections of the external valvar surface. In some cases, the spines can join cells to each other forming chains.

Stage Platform carrying the specimen or specimen slide.

Standing crop Number of living foraminiferal individuals per unit of volume or surface area.

Stauros Transapically expanded central nodule that may or may not reach the valve margin.

Steeper motor A DC motor which divides the full rotation into the same number of steps.

Stereo pair Pair of two semi-images, which are either placed directly side by side or transformed and arranged to a red-cyan anaglyph. Stereo pairs are the results of both classical and computer-aided stereoscopic techniques.

Stereopsis Scientific term for binocular vision, where an object is viewed by both eyes from slightly different perspectives. This difference, however, is responsible for the generation of three-dimensional information in the human brain.

Stereoscopy Optical technique developed in the sixteenth century, according to which an object is recorded (photographed) from two different perspectives and, therefore, binocular vision of the human eyes is simulated. The resulting semi-images are arranged to a stereo pair or anaglyph and inspected with the help of autostereoscopic viewing techniques or red-cyan glasses.

Sternum An unperforated, and sometimes thickened, silica band carrying the raphe.

Stigmas Perforation in the form of a channel not closed by a velum. Located in the central area of some raphe-bearing diatoms, near the central node or at the proximal ends of the central striae.

Stigmoid Areola more pronounced and differentiated from the rest of the areolae in the valve surface. It is a simple form of stigma where the foramen, the canal, and the alveoli are hardly differentiated from the rest of the areolae of the valve surface.

Stitching The process of combining multiple images with overlapping to generate a panoramic image.

Stria One or several rows of pores or areolae, or even a single alveolus. They can be uniseriate, with a single row of pores; biseriate, with two rows; or multiseriate, with many rows.

Subspecies Various populations of a species varying from one to another by morphological characteristics.

Superimposition The process by which two or more landmark configurations are transformed by removing the differences caused by orientation, scale, and position.

Supervised classifiers Functions that map the extracted features to an output probability of belonging to a given class.

SVD (Singular Value Decomposition) Matrix factorization into a product of three matrices.

Symmetry In mathematics, the property that under a series of transformations something does not alter.

Systematics The study of the diversification of living organisms from a phylogenetic (evolutionary) perspective.

Taxon Any identifiable group of taxonomically related organisms.

Taxonomy Is the practice and science of classification of organisms.

Terminal fissure Extension of the raphe fissure through the nodules, without penetrating the valve wall, at the distal ends of the raphe.

Terminal nodule The thickened area of the silica wall at the distal ends of the raphe.

Theca Each of the two units that form the frustule in a diatom.

Thin-plate spline (TPS) An interpolation function which models the difference between two forms as a smooth deformation that is used to measure deformation grids.

Thresholding The simplest method of image segmentation based on replacing each pixel in an image by a black or white pixel depending on a given threshold.

Time series Repetitive measurements of a variable to identify temporal trends.

Tone mapping An image-processing technique for mapping one set of colors to another in a device (e.g., CRT or LCD) that has more limited dynamic range.

Topological spaces Analytic spaces without metrics yet satisfying several axioms.

Transapical axis The imaginary line orthogonal to the major axis that corresponds to the pennate diatom width of the valve.

Transfer function Regression model that relates proxy-environment relationship quantitatively for a given factor.

Transitional waters Continuum between continental and coastal marine waters.

Transplacental Takes place in or through the placenta.

Trophic species Group of organisms according with their shared feeding position.

Trophic Of or relating to nutrition.

Tube Mechanical connection of objective and eyepiece bridging the distance of both optical components.

Tube lens Facultative lens situated inside of the tube between objective and ocular.

Two-scale decomposition An image decomposition into Base layers (BL) and Detail Layers (DL).

Type specimen The organism that is permanently attached to the name of a taxon.

Unsupervised Classifiers Used to cluster the data without using the ground truth label.

UV cut filter Absorbs ultraviolet light.

Vagal Of or relating to the vagus nerve.

Valve Flat or slightly convex part of the epitheca and hypotheca separated by the valve margin.

Valve face Flat or slightly convex part of the epitheca.

Valve mantle Lateral walls of the valve from the valve margin to the valve edge.

Valvocopula Copula adjacent to the valve, different in structure to the valve and the other copulae.

Variable bright dark field contrast (VBDC) Optical superimposition of a bright field and a dark field image.

Variable interference dark field contrast (VIDC) Optical superimposition of a dark field and an interference contrast image.

Variable interference phase contrast (VIPC) Optical superimposition of a phase contrast and an interference contrast image.

Variable phase bright field contrast (VPBC) Optical superimposition of a bright field and a phase contrast image.

Variable phase dark field contrast (VPDC) Optical superimposition of a dark field and a phase contrast image.

Velum Thin, perforated silica sheet that closes or covers an areola. There are different types of veli, the most complex being the "vola," formed by a network of siliceous bars that project from the edge of the areola towards the center.

Venule A minute vein continuous with a capillary.

Viola-Jones A real-time object detection framework based on the use of Histogram of Oriented Gradient (HOG) features.

Warming filters Red or arrange filters used for compensation of blue hue.

Washerwoman's skin Wrinkling and grayish-white discoloration of thick keratin layer areas of the skin without sebaceous glands as a consequence of long-term permanence under water.

Weighted Least Squares A generalization of ordinary least squares and linear regression.

Wollaston prism Optical component in interference contrast devices (synonym: Wollaston prism) used for splitting and re-uniting the illuminating light beams. Synonym: DIC prism.

YOLO You Only Look Once. A real-time object detector procedure based on Convolutional Neural Networks (CNN).

References

1. Bookstein, F.L., et al.: Morphometrics in Evolutionary Biology: The Geometry of Size and Shape Change with Examples from Fishes, Special publication, vol. 15, 277p. Academy of Natural Sciences of Philadelphia, Philadelphia (1985)
2. Bookstein, F.L.: Biometrics, biomathematics and the morphometric synthesis. Bull. Math. Biol. **58**(2), 313 (1996)
3. Bradbury, S., et al.: RMS Dictionary of Light Microscopy. Oxford University Press and Royal Microscopical Society, Oxford (1989). ISBN 0-19-856413-9
4. Dallwitz, M.J.: A comparison of matrix-based taxonomic identification systems with rule-based systems. In: Proceedings of IFAC Workshop on Expert Systems in Agriculture, pp. 215–218. International Academic Publishers, Beijing (1992)
5. Dallwitz, M.J., Paine, T.A., Zurcher, E.J.: Principles of interactive keys. https://bit.ly/30INHNe (2000)
6. Dryden, I.L., Mardia, K.V.: Statistical Shape Analysis. Wiley, Oxford (2002)
7. Dunn, G., Everitt, B.S.: An Introduction to Mathematical Taxonomy. Dover, New York (1982)
8. Hoyer, C., Chair Technical Committee: ISO 10934-1:2002: Optics and optical instruments – Vocabulary for microscopy – Part 1: Light microscopy. International Organization for Standardization (ISO), Geneva (2002)
9. Gill, D.S.: The Light Microscopist's Diatom Glossary, 2nd edn. (2011). https://bit.ly/2JkfJs3
10. Haralick, R.M., Shapiro, L.G.: Glossary of Computer Vision Terms. Pattern Recogn. **24**, 69–93 (1990)
11. Marcus, L.F., Bello, E., Garcia-Valdecasas, A.: Contributions to Morphometrics. CSIC, Madrid (1993)
12. Pielou, E.C.: The Interpretation of Ecological Data: A Primer on Classification and Ordination. Wiley, New York (1984)
13. Rohlf, F.J.: Fitting curves to outlines. In: Rohlf, F.J., Bookstein, F.J. (eds.) Proceedings of the Michigan Morphometrics Workshop. University of Michigan Museum of Zoology, Ann Arbor (1990)
14. Talent, N., Dickinson, R.B., Dickinson, D.A.: Character selection during interactive taxonomic identification: 'best characters'. Biodivers. Inform. **9**, 1–12 (2014)
15. Zelditch, M.L., Swiderski, D.L., Sheets, H.D.: Geometric Morphometrics for Biologists: A Primer. Academic Press, San Diego (2004)

Index

G. Cristóbal et al. (eds.), *Modern Trends in Diatom Identification*, Developments in Applied Phycology 10,
https://doi.org/10.1007/978-3-030-39212-3